



The hot isostatic processing characteristics of 70/30 cupronickel castings.

KING, S.

Available from the Sheffield Hallam University Research Archive (SHURA) at:

<http://shura.shu.ac.uk/19916/>

A Sheffield Hallam University thesis

This thesis is protected by copyright which belongs to the author.

The content must not be changed in any way or sold commercially in any format or medium without the formal permission of the author.

When referring to this work, full bibliographic details including the author, title, awarding institution and date of the thesis must be given.

Please visit <http://shura.shu.ac.uk/19916/> and <http://shura.shu.ac.uk/information.html> for further details about copyright and re-use permissions.

POLYTECHNIC LIBRARY
POND STREET
SHEFFIELD S1 1WB



Sheffield City Polytechnic Library

REFERENCE ONLY

ProQuest Number: 10697222

All rights reserved

INFORMATION TO ALL USERS

The quality of this reproduction is dependent upon the quality of the copy submitted.

In the unlikely event that the author did not send a complete manuscript and there are missing pages, these will be noted. Also, if material had to be removed, a note will indicate the deletion.



ProQuest 10697222

Published by ProQuest LLC (2017). Copyright of the Dissertation is held by the Author.

All rights reserved.

This work is protected against unauthorized copying under Title 17, United States Code
Microform Edition © ProQuest LLC.

ProQuest LLC.
789 East Eisenhower Parkway
P.O. Box 1346
Ann Arbor, MI 48106 – 1346

**THE HOT ISOSTATIC PROCESSING
CHARACTERISTICS OF 7030 CUPRONICKEL
CASTINGS**

S. King

A thesis submitted in partial fulfilment of the
requirements of
Sheffield Hallam University
for the degree of Doctor of Philosophy

School of Engineering

1992



PREFACE

The work reported in this thesis was carried out at the School of Engineering, Sheffield City Polytechnic between October 1988 and December 1991 whilst the candidate was registered for a higher degree.

The candidate has not during the above period of registration for the CNAAB degree of Ph.D. been registered for any other CNAAB award or for any university degree.

The results presented here are, as far as can be certain, original except where reference has been made to previous work.

A post graduate course was attended at Sheffield City Polytechnic during the above period in the following subjects: Computer Programming / Numerical Analysis and Economics. In addition short courses on Scanning Electron Microscopy Techniques and Thermal Stress Analysis were also attended, both held at Sheffield City Polytechnic.

The author has attended a conference on Isostatic Pressing "ISO4" held at Stratford upon Avon, 5-7 November 1990, and presented a paper entitled "The Hot Isostatic Processing Characteristics Of 70/30 Cupronickel Castings", the paper is shown in Appendix 1.

The author also published a review paper entitled "The Effect Of HIP On Cast Cupronickel Alloys" in the Trades Foundry Journal, 24 February 1989, as shown in Appendix 2.

As a result of this research programme and its findings an addition has been made to the Naval Engineering Standard NES 824 concerning the optimum processing parameters for the recovery of cupronickel castings. The relevant part of the Engineering Standard is shown in Appendix 3.

S. King

January 1992.

ACKNOWLEDGMENTS

The author would like to express her appreciation to Vickers Ship-Building and Engineering Limited for supplying cast NES 824 material, and to the Ministry of Defence Bath, for carrying out quantitative corrosion tests on both cast and hot isostatically processed 70/30 cupronickel. Grateful appreciation is also made to H.I.P Limited for use of their laboratory HIP facilities as well as to Dr. B.A. Rickinson (industrial supervisor) and Dr. L.E. Tidbury for numerous helpful discussions and constant encouragement.

Many thanks to the technicians, administrative staff and lecturing staff of the Department of Metals and Materials Process Engineering for their help and support. Thanks also to Professor D. Tidmarsh for his support.

Grateful thanks are sincerely expressed to Dr. A.J. Fletcher for his interest, guidance and constant encouragement and support throughout the course of this work. Thanks are also expressed to Dr. H. Atkinson (second supervisor) School of Materials, Sheffield University, for numerous helpful discussions.

Finally I would like to pay tribute to my parents, Peter and friends for their patience, support and constant encouragement.

THE HOT ISOSTATIC PROCESSING CHARACTERISTICS

OF 70/30 CUPRONICKEL CASTINGS

by
Susan King

SYNOPSIS

70/30 cupronickel designated in the Naval Engineering Standard NES 824 is associated with high integrity cast components. However this specification restricts the use of welding to recover castings if they are to be wetted by sea water. Hot isostatic pressing is considered to be an alternative recovery process. The mechanisms of pore closure and the processing parameters for successful recovery have been investigated together with their effect on microstructural and mechanical property characteristics. In addition models have been identified which accurately predict pore closure rates in cupronickel castings.

Hot isostatic pressing trials were carried out using processing temperatures within the range 850°C and 1025°C and argon gas pressures of 45MPa to 145MPa. Two time, temperature, pressure procedures were investigated; successive cycles of short duration and single continuous cycles. The investigations were carried out on 70/30 cupronickel (NES 824) specimens that contained artificially introduced porosity in the form of closed internal pores and surface-connected porosity: the latter required encapsulation prior to processing. These investigations have revealed that for the removal of surface-connected porosity, successive cycles of short duration were more effective in closing large pores than a single cycle of the same total duration. In addition elongated pores of small diameter were removed more quickly than pores of equivalent volume porosity but smaller aspect ratio. Shorter recovery times were required for the consolidation of internal porosity in comparison with surface-connected porosity indicating that encapsulation restricts the densification process.

Initially the rate of densification during HIPping was rapid suggesting that plastic flow was occurring. Subsequent densification probably by viscous flow mechanisms occurred at a much lower rate once the sustain conditions had been reached. This fall off in the densification rate applied in particular to encapsulated castings.

The optimum processing conditions for the successful densification of 70/30 cupronickel castings are short sustain times of 45 minutes, a temperature of 950°C and argon gas pressures within the range 83-103MPa.

Hot isostatic processing significantly increases the ductility of 70/30 cupronickel castings without a reduction in strength and has no adverse effects on corrosion resistance.

NOMENCLATURE

A,B	Parameters used in the Standard Linear Solid equation;
a	Average contact area at neck (m^2);
C	Constant;
ρ	Relative density (kg/m^3);
D	Packing density;
Do	Initial relative density;
D _{yield}	Relative density from plastic yielding;
D _c	Critical density at which pores close;
D \cdot	Densification rate (/s);
D _{eff}	Effective diffusion coefficient;
D _L	Lattice diffusion coefficient;
D _{gb}	Grain boundary diffusion coefficient;
δDb	Boundary diffusion coefficient times boundary thickness (m^3/s);
Dv	Volume diffusion coefficient (m^2/s);
E	Youngs Modulus (GPa);
G	Grain diameter (m);
G	Shear modulus (MPa);
k	Boltzmann's constant (J/k);
n	Number of pores in unit volume of material;
P	External pressure (MPa);
P _{eff}	Effective pressure on a neck (MPa);
P _o	Out-gassing pressure (MPa);
P _s	Equivalent pressure caused by surface tension (MPa);
P _i	Gas pressure inside a closed pore (MPa);
R	Particle radius (m);
R'	Radius of unit sphere containing one particle (m);

T	Absolute temperature (K);
t	Time (s);
V	Volume (m^3);
X	Neck radius (m);
Z	Number of contacts per particle;
γ	Surface energy (J/m^2);
ϵ_0, σ_0, n	Creep parameters (s^{-1}, MPa);
Ω	Atomic or molecular volume (m^3);
σ_y	Yield stress (MPa);
Q	Activation energy (kJ/mol);
R	Gas constant (J/mol.K);
ν	Poissons' ratio;
η	Viscosity (GPa.s);
η_∞	Coefficient of viscosity;
τ_c	Critical yield stress (MPa);
n, ϵ	Material constants;
ϵ_{creep}	Creep strain;
$\dot{\epsilon}_{creep}$	Rate of creep strain;
ϵ_p	Plastic strain;
e_{IJ}	Strain tensor;
s_{IJ}	Stress tensor;
ϕ	Material constant used in the Standard Linear Solid equation (s^{-1});
σ	Stress (MPa);
σ^0	Hydrostatic stress (MPa);
ϵ^0	Hydrostatic strain;
$\sigma_{xx})$ $\sigma_{yy})$ $\sigma_{zz})$	Stress in x,y and z directions;

ϵ_{xx})
 ϵ_{yy})
 ϵ_{zz})

Strain in x,y and z directions.

YIELD	Compaction by plastic yielding when the pressure is applied.
V-DIFF1S	Surface-tension driven densification by volume from neck boundary, Stage 1.
B-DIFF1S	Surface-tension driven densification by boundary diffusion from neck boundary, Stage 1.
V-DIFF2S	Surface-tension driven densification by volume diffusion from neck boundary, Stage 2.
B-DIFF2S	Surface-tension driven densification by boundary diffusion from neck boundary, Stage 2.
V-DIFF1	Pressure-driven densification by volume diffusion from neck boundary, Stage 1.
B-DIFF1	Pressure-driven densification by boundary diffusion from neck boundary, Stage 1.
V-DIFF2	Pressure-driven densification by volume diffusion from neck boundary, Stage 2.
B-DIFF2	Pressure-driven densification by boundary diffusion from neck boundary, Stage 2,
PL-CRP1	Pressure-driven densification by power-law creep, Stage 1.
PL-CRP2	Pressure-driven densification by power-law creep, Stage 2.
NH-CRP1	Pressure-driven densification by volume and boundary diffusion from grain boundaries within the particle (Nabarro-Herring Creep), Stage 1.
NH-CRP2	Pressure-driven densification by volume and boundary diffusion from grain boundaries within the particle (Nabarro-Herring Creep), Stage 2.

CONTENTS

	Page Number
1.0 Introduction	16
2.0 Literature Review	
2.1 Development of Copper Alloys for Marine Applications	19
2.2 Nickel-Aluminium Bronzes	20
2.3 Cupronickel Alloys	24
2.4 Characteristics of 70/30 Cupronickel	26
2.4.1 Weldability	
2.4.2 Mechanical Properties	28
2.4.3 Corrosion Performance in Sea Water	29
2.5 Applications of Cast 70/30 Cupronickel	30
2.6 Mechanisms of Corrosion	31
2.6.1 Crevice Corrosion	
2.6.2 Pitting	33
2.6.3 Impingement Attack	34
2.6.4 Cavitation	36
2.6.5 Corrosion Fatigue	38
2.6.6 Stress Corrosion Cracking	39
2.7 Marine Performance of 70/30 Cupronickel	40
2.7.1 General Corrosion	41
2.7.2 Bi-metallic Corrosion	44
2.7.3 Crevice Corrosion	45
2.7.4 Impingement Attack	46
2.7.5 Cavitation Erosion	48
2.7.6 Stress Corrosion Cracking	50
2.7.7 Corrosion Fatigue	50

2.8	Corrosion Resistance of Cupronickel Alloys: Protective Oxide Films	51
2.9	Effect of Alloying Additions on the Corrosion Resistance of Cupronickel Alloys	55
2.10	Hot Ductility of Cupronickel Alloys	59
2.10.1	Effect of Alloying Additions on the Hot Ductility of Cast Cupronickel Alloys	60
2.10.2	Hot Ductility of Wrought 70/30 Cupronickel Alloys	62
2.10.3	Nucleation and Growth of Voids	64
2.11	Sintering	67
2.11.1	Driving Force for Pore Closure	68
2.11.2	Spheroidizing of the Pores	
2.11.3	Mechanisms of Matter Transport	72
2.11.4	Stages of Sintering	76
2.11.5	Theories of Pressure-Less Sintering	77
2.11.6	Theories of pressure Assisted Sintering	82
2.12	Hot Isostatic Pressing	92
2.12.1	Definition of Hot Isostatic Pressing	
2.12.2	Design of a HIPping System	94
2.12.3	Applications of Hot Isostatic Pressing	95
2.12.4	Correction of Casting Faults by HIPping	97
2.12.5	Factors Affecting the Elimination of Casting Defects	99
2.12.6	Shape Change During HIPping	100
2.12.7	The Effect of HIPping Parameters on Density	101
2.12.8	Improvement of Mechanical Properties by HIPping	102

2.13	The Stages of Densification	104
2.13.1	Stage 0 - Powder Packing	105
2.13.2	Stage 1 - Neck Growth	
2.13.3	Stage 3 - Final Densification	106
2.14	Modelling of Densification	106
2.14.1	Stage 1 - Relative Density < 0.92	106
2.14.2	Stage 2 - Relative Density > 0.92	109
2.15	Densification Rate Equations	110
2.15.1	Plastic Yielding	
2.15.2	Volume Diffusion	111
2.15.3	Boundary Diffusion	112
2.15.4	Power Law Creep	
2.16	Hot Isostatic Pressing Maps	113
2.16.1	Applications of HIP Maps	114
2.17	Alternatives to Hot Isostatic Pressing	114
2.17.1	The Ceracon Process	115
2.17.2	Ceracon Process: Pressure Transmitting Media	117
2.18	Classification of Refractory Materials: Potential Pressure Transmitting Media	119
2.18.1	Silica	120
2.18.2	Alumina	121
2.18.3	Zirconium Oxide	121
2.18.4	Silicon Carbide	122
2.18.5	Boron Nitride	122
2.18.6	Boron Carbide	123
2.19	Encapsulation	124

2.20	Particle Sizing and Characterisation	125
2.20.1	Particle Size	126
2.20.2	Particle Size Distribution	127
2.20.3	Particle Shape and Structure	
2.21	Creep and Stress Relaxation	128
2.21.1	Creep	130
2.21.2	Stress Relaxation	131
2.21.3	Plastic Flow and Work Hardening	132
2.21.4	Viscoelastic Stress - Strain Relationships	133
2.21.5	Theoretical Equations Derived for Stress Relaxation and Creep	135
2.21.6	Theoretical Equations Representing Visco-Elastic Processes Derived from The Standard Linear Solid Model	138
2.21.7	Selection of a Mechanical Body to Represent Viscoelastic Behaviour	141
3.0	EXPERIMENTAL PROCEDURES	
3.1	Material Identification	143
3.2	Artificial Porosity Specimens	144
3.3	Encapsulation Techniques	145
3.4	Hot Isostatic Pressing Experiments	146
3.4.1	Laboratory HIP System	146
3.4.2	Hot Isostatic Pressing Experiments	149
3.4.3	Encapsulation Techniques	154
3.4.4	Effect of Thickness of Sand Layer on the Rate of Pore Closure in Encapsulated Specimens	158
3.5	Chemical Interaction between PTM Sands and NES 824	160

3.6	Characterisation of Particles of Refractory Pressure Transmitting Media	160
3.6.1	Sieve Analysis	160
3.6.2	Moisture Content	161
3.6.3	Crushing Strength	161
3.6.4	Compressibility of HIPped Silica Sand	162
3.7	Mechanical Property Evaluations	163
3.8	Hot Tensile Data for 70/30 Cupronickel	166
3.9	Hot Ductility Of 70/30 Cupronickel	168
3.10	Constant Load Ductility Tests	168
3.11	Stress Relaxation Tests	171
3.11.1	Comparison of Calculated and Experimental Stress Relaxation Curves	172
3.11.2	Calculated Creep Curves	173
3.12	Test Procedures for Assessing the Corrosion Performance of 70/30 Cupronickel	174
3.12.1	Salt Spray Tests	174
3.12.2	Sea Water Corrosion Tests	176
3.12.3	Impingement Tests	176
3.13	Modelling of the Pore Closure Rates in 70/30 Cupronickel Castings by HIPping	178
3.13.1	Plastic Yielding	178
3.13.2	Plastic Flow Theory (Pressure Assisted Sintering)	179
3.13.3	HIP Maps	180
4.0	RESULTS	184
4.1	HIPping of NES 824 Castings containing Surface-Connected Porosity	185
4.2	HIPping of NES 824 Castings containing Closed Internal Porosity	189
4.3	Encapsulation Techniques	190
4.3.1	Effect of a Change in the Refractory Pressure Transmitting Medium on the Rate of Pore Closure	191

4.3.2	Investigation into the Out-gassing of Refractory Sands and the Chemical Interaction Between Silica Sands and 70/30 Cupronickel	196
4.4	Compressive Strength Characteristics of Silica Sand	197
4.5	Effect of Pressure Transmitting Medium Thickness on the Rate of Pore Closure of castings containing Surface-Connected Porosity	199
4.6	Change in Pore Shape during HIPping	200
4.7	Mechanical Properties of 70/30 Cupronickel	202
4.7.1	Effect of HIP Temperature on Properties	202
4.7.2	Effect of HIP Time on Properties	203
4.7.3	Effect of Stress Relief on the Mechanical Properties of NES 824 1 - Thermal Simulation of a HIP Treatment 2 - Effect of Stress Relieving HIPped 70/30 Cupronickel	204
4.7.4	Effect of HIPping on the Properties of Recovered Castings 1 - M.O.D Cast Block 2 - HIP Recovered Commercial Castings	206
4.7.5	Hot Ductility of 70/30 Cupronickel	208
4.7.6	Constant Load Ductility Tests	209
4.8	Microstructural Characteristics of 70/30 Cupronickel	210
4.8.1	Effect of the Type of HIP Cycle used to Close Porosity and the Resultant Microstructure	210
4.8.2	Effect of HIP Temperature on the Microstructure of 70/30 Cupronickel	210
4.8.3	Scanning Electron Microscopy of HIPped 70/30 Cupronickel Material	212
4.8.4	Effect of HIP Time on the Microstructure of 70/30 Cupronickel 1 - Grain Size 2 - Segregation	213
4.8.5	Embrittlement of 70/30 Cupronickel at Elevated Temperatures	215
4.8.6	Microstructural Evaluation of a HIP Recovered M.O.D NES 824 Casting	216

4.9	Corrosion Performance of 70/30 Cupronickel	218
4.9.1	Accelerated 5% Salt Spray Tests	219
4.9.2	Substitute Ocean Water Spray Tests	222
4.9.3	Corrosion Performance of 70/30 Cupronickel (NES 824) in Natural Sea water	224
	1 - Full Immersion and Crevice Corrosion	
	2 - Impingement resistance	
4.10	Stress Relaxation Tests	227
4.10.1	Comparison of Calculated and Experimental Stress Relaxation Curves	
4.10.2	Calculation of the Coefficient of Viscosity and other Material Parameters for 70/30 Cupronickel at Elevated Temperatures	228
4.10.3	Calculated Creep Curves for 70/30 Cupronickel	229
4.11	Modelling of Pore Closure Rates in 70/30 Cupronickel by Hot Isostatic Pressing	229
4.11.1	Pore Closure by Plastic Yielding	
4.11.2	Calculation of Pore Closure Rates by the Plastic Flow Theory	231
4.11.3	70/30 Cupronickel Hot Isostatic Pressing Maps	232
5.0	DISCUSSION	234
5.1	Effect of HIP Time on the Pore Closure of 70/30 Cupronickel Castings	
5.2	Effect of HIP Temperature on Pore Closure	238
5.3	Effect of HIP Pressure on Pore Closure	239
5.4	Effect of Pore Geometry on Densification	240
5.5	Effect of Encapsulation Techniques on Pore Closure	241
5.6	Compressive Strength of Silica Sand and its Ability to Resist Densification	246
5.7	Changes in Pore Shape during HIPping	247
5.8	Effect of HIPping on the Material Properties of 70/30 Cupronickel	248

5.8.1	Mechanical Property Evaluations	248
5.8.2	Improvement of Properties by Stress Relieving	252
5.8.3	The Effect of HIPping on the Properties of Recovered NES 824 Castings	
5.8.4	Hot Flow Stress and Ductility of NES 824	255
5.8.5	Constant Load Ductility of NES 824	256
5.9	Corrosion Performance of 70/30 Cupronickel	258
5.10	Modelling of the Pore Closure Rates During Hot Isostatic Processing of 70/30 Cupronickel	263
5.10.1	Pore Closure by Plastic Yielding	
5.10.2	Pore Closure Predicted by the Plastic Flow Theory	268
5.10.3	70/30 Cupronickel Hot Isostatic Pressing Maps	270
6.0	CONCLUSIONS	272
7.0	FURTHER WORK	277
8.0	REFERENCES	
Tables	1 - 61	
Figures	1 - 203	
Appendices	1 - 3	

1.0 INTRODUCTION

Many of the components used in sea water systems, especially those employed in submarines, operate in an extremely severe environment both from a mechanical and a corrosion view point. Not only are the components in contact with a sea water environment, but they also experience the diving depth pressure loading of the submarine and the cyclic loading due to its operation. The high strength cast alloy presently used in HM Ships and Submarines is nickel-aluminium bronze used primarily for its high strength and shock resistance (16). However, in sea water this alloy suffers from excessive preferential phase corrosion at crevices and weld affected areas (13). Owing to these corrosion problems a replacement material is required. That chosen for high integrity cast components in future submarines is a high strength chromium cupronickel, a 70Cu-30Ni alloy containing Cr and Si strengthened by spinodal decomposition (15,20). This alloy is specified in the Naval Engineering Standard NES 824 (24) which restricts the welding of cupronickel if it is to be wetted by sea water, due to the risk of premature corrosion failure. This prevents the use of welding to recover castings containing surface defects and porosity. Thus, there is a need to find an alternative recovery process for castings which are to be used in the next generation of submarines. Hot Isostatic Pressing is a potential alternative.

The use of castings in engineering applications is restricted by the difficulties encountered in producing structural parts of high strength free from defects, such as porosity and microshrinkage. Even if the presence of cavities and internal cracks do not lead to the rejection of castings, they significantly reduce strength, fatigue and creep life in comparison with wrought alloys (154,156, 157,173). Until 1960 there was no economical method of repairing castings containing internal porosity. Repair consisted of cutting out the defective areas and then fill welding with weld metal (158). This process is extremely labour intensive, is often prone to failure at the first attempt, and develops an area of material of nominally different grain size and composition at the surface of the component. Such an area can suffer severe galvanic corrosion in sea water. Hence an alternative method of defect repair is required. Hot isostatic pressing is believed to be such a process.

Hot isostatic pressing is generally associated with the consolidation of powder compacts, so a logical extension of this technology would be to develop it for the removal of defects in Class I cupronickel castings. Hot isostatic pressing has been practised as a recovery process to remove defects from castings since 1970 (34). The process introduces no new material and the structure and properties of the cast material are generally improved (173).

The marine corrosion performance of cupronickel castings has been widely investigated and they have been shown to

possess excellent corrosion resistance. However, the mechanisms of pore closure by hot isostatic pressing had received little attention and the optimum process parameters needed to successfully remove defects from such castings had not been determined. Hence an evaluation of the hot isostatic pressing characteristics of 70/30 cupronickel was required.

The effect of hot isostatic processing variables such as temperature, time, pressure and pressure transmitting medium on the recovery of cupronickel castings containing internal pores and surface-connected porosity are reported. The influence of encapsulation and pore geometry on the rate of pore closure are discussed, together with the comparison of as-cast and hot isostatically pressed 70/30 cupronickel encompassing: corrosion performance, microstructural and mechanical property characteristics.

2.0 LITERATURE REVIEW

2.1 DEVELOPMENT OF COPPER ALLOYS FOR MARINE APPLICATIONS

A material for use in a marine environment is selected by choosing a material having suitable mechanical properties and corrosion resistance for the specialised application. Corrosion resistance is usually the major reason for selecting non-ferrous materials rather than steels, although for some purposes other factors such as electrical conductivity or weight may be important. The highest mechanical properties seldom accompany the best corrosion resistance, and the choice of material usually involves a compromise (1,2).

Pure copper has not been used extensively in marine applications since the use of copper sheathed sailing ships; copper providing a corrosion resistant coating (1-4). The progressive use of copper and its alloys from these early applications through to the development of cupronickel alloys in 1939 are summarised in Table 1.

Copper provides a host of properties from which modern marine alloys are derived (5):

- (i) General corrosion resistance to sea water.
- (ii) Resistance to stress corrosion cracking and crevice corrosion.
- (iii) Resistance to marine biofouling.
- (iv) Excellent ductility and fabrication characteristics.
- (v) High thermal conductivity.

The addition of alloying elements to copper provide:

- (i) Additional strength and corrosion fatigue resistance.
- (ii) Resistance to erosion and impingement attack.
- (iii) Improved resistance to corrosion by both clean and polluted sea water.

The two most favoured copper alloys for marine applications are nickel-aluminium bronze and copper-nickel alloys (6,7).

2.2 NICKEL-ALUMINIUM BRONZE

Aluminium bronze alloys are copper alloys containing 5-17% Al. Alloys containing less than 8.5% Al are single phase, solid solution alloys used only in the wrought form. Alloys containing greater than 8.5% Al can be cast or wrought and have a duplex structure which offers higher strength but with slightly reduced ductility (5). The addition of nickel to these alloys produces a group of alloys known as nickel-aluminium bronzes (NAB), which are used primarily for their high strength and shock resistance. Two of these alloys are specified in BS1400 (8):

- AB2 - A high strength NAB of nominal composition Cu - 9.5% Al, 5% Fe, 5% Ni which is a popular sand casting alloy.
- CMA1 - Cu - 13% Mn, 8% Al, 3% Fe, 3% Ni alloy which has similar properties to AB2 although it is less frequently specified and its main use is for marine propellers (9).

Typical mechanical properties for the alloys listed on the previous page are given in Table 2, and relate to properties attainable in castings of section thickness comparable to test bars of 25mm diameter. The slow cooling of larger castings promotes a coarse microstructure which reduces strength as shown for the AB2 alloy in Table 3. NAB for use in top quality castings is specified in the Naval Engineering Standard NES 747 Part 2 (10).

Cast NAB has a complex microstructure in which individual phases have different chemical compositions depending in part on the cooling rate in different areas of the casting. This microstructure gives rise to a complex corrosion behaviour in sea water (11). The microstructure of NAB includes a kappa (K) phase which has various morphologies (12,13):

- K_I - a rosette form
- K_{II} - a spheroidised precipitate at the grain boundary
- K_{III} - a lathe shaped phase
- K_{IV} - a fine precipitate within the α grains.

Cast metal in clean sea water flowing at up to 4m/s has a low corrosion rate (11). However, preferential phase corrosion of the K phase is initiated under barnacles or other marine fouling settlements, under debris and inherent design crevices such as flange joints and "O" ring seals. A particularly severe form of selective phase corrosion has been found to occur in the heat affected zones (HAZ) of welds (11,13). Although slight compositional differences between the weld metal and the casting may promote this attack, corrosion at the HAZ in the parent cast metal occurs

and is found to be caused by the presence of kappa 3 phase (k_3) in lamellar form, which is distributed throughout the microstructure resulting in creep corrosion fissuring. HAZ corrosion is found in both Metal Inert Gas (MIG) welding and Electron Beam (EB) welds. It has been found that a heat treatment consisting of 6 hours at 675°C has a beneficial effect on the onset of selective phase corrosion of NAB including HAZ corrosion. As of yet no treatment has been found which will prevent it or reduce its rate of progress once started. This heat treatment also gives a measure of stress relief to weld repaired castings and has a beneficial effect on mechanical properties (11). Apart from heat treatment there are two other options for improving the corrosion resistance of NAB castings. One method is to improve the quality of the castings so as to reduce or eliminate the need for weld repair. The other method is to consider external means such as cathodic protection by sacrificial anodes or by water treatment. Laboratory tests have shown that chlorination has a beneficial effect on the corrosion of NAB and several other complex alloys in low velocity sea water (11). Often in marine engineering applications the alloy is unintentionally cathodically protected by electrical coupling to steel structures in close proximity (13).

Although the selective phase corrosion of NAB is a considerable disadvantage the alloy has a low probability of fast fracture so that even with large through thickness defects, failure under internal pressure will occur in a controlled ductile manner resulting in the so called "leak

before break" effect (11). This property is highly desirable for high integrity submarine sea water systems and similar characteristics are sought in possible replacement alloys.

Nickel-aluminium bronzes are used for applications which require high strength and shock resistance as well as resistance to high velocity sea water. However, their high corrosion resistance is due to the formation of a tough protective, self healing surface protective oxide coating, and for this reason they are not recommended for use in abrasive conditions (9). Typical applications of NAB include pump impellers and casings, marine propellers and high duty valves and castings requiring a structural function where strength is important.

Cast NAB has been used in sea water systems of Royal Navy vessels for over 25 years, but the ever increasing operational requirements place more stringent demands on the system, and necessitates the development and use of higher quality materials (14,15). Owing to the inherent corrosion problems associated with NAB its corrosion resistance cannot be improved sufficiently to provide the service life that the Navy now requires. Thus, a replacement material is required which will last the life time of the vessels systems and avoid expensive revalidation and replacement at refit.

2.3 CUPRONICKEL ALLOYS

Wrought Cu-Ni alloys in the same service systems as NAB have provided good service life since 1930 (11,15,16). Thus, it is not surprising that Cu-Ni alloys were examined as replacement materials for NAB. They are potentially attractive, being galvanically compatible with the existing pipe work and provide acceptable mechanical properties and good resistance to biofouling (17). The M.O.D have been investigating cupronickel as a replacement material for NAB since 1970, but it was only with the modernisation of the UK foundry industry and the replacement of fuel fired furnaces with electric furnaces that they became a serious possibility. These improvements allowed faster melt down times and less contamination from furnace atmospheres. This is significant in cupronickel alloys which have a higher melting temperature and are more susceptible to pick up than NAB. Minimisation of contamination, especially by sulphur, is most important in optimising the properties of cupronickels (14,15).

Over the last 20 years several cast cupronickels alloys containing between 10-40% Ni, as listed in Table 4, have been investigated for use in sea water systems. Two main contenders emerged both being based on 70Cu-30Ni:

- (i) 70Cu - 30Ni - Cr - Si (CN1)
- (ii) 70Cu - 30Ni - Nb - Si (CN2)

Alloying Cu-Ni with Nb and Si, alloy (ii), increases the as-cast strength but maximum strength can only be achieved through heat treatment, and it is difficult and sometimes impossible to heat treat large castings. In addition

welding of such alloys may cause reversion to low strength structures in the HAZ (18,19). Thus, prime interest has been shown in the first alloy, an Inco alloy containing 1.6% Cr designated IN768. This alloy has been subjected to investigations to evaluate its welding response, sea water corrosion resistance and foundry characteristics (20). The two cupronickels shown on the previous page are designated under BS1400, as CN1 and CN2. They are both basically Fe bearing 70/30 cupronickels, but they have been strengthened by precipitation hardening which takes place while the casting is cooling in the sand mould. No additional heat treatment is necessary. CN1 relies on the addition of Cr and Si for this hardening, while CN2 has additions of Nb and Si. The small addition of Si improves castability as well as having a strengthening function and corrosion resistance is not impaired (9). Typical mechanical properties of the two alloys (21), are shown in Table 5. Of the two alloys, the Cr containing alloy was eventually chosen as the prime replacement for NAB because it was considered to have better jet-impingement resistance at higher water speeds and better weldability characteristics than the Nb-Si alloy (15,22,23).

The 1.6% Cr alloy was examined in detail and improved by restrictions on impurity level and better production practice and methods. The subsequent alloy was designated in the Naval Engineering Standard, NES 824 Part 1, Issue 1 (24), and selected as the replacement material for NAB (15).

2.4 CHARACTERISTICS OF 70/30 CUPRONICKEL

In general the properties of cast Cu-Ni alloys are evaluated in comparison against NAB, the material it is replacing in marine systems. All data reported for NES 824 is considered in this way.

2.4.1 WELDABILITY

In general cast cupronickel alloys are not as weldable as NAB, and cast NES 824 is no exception. Accumulation of defects and impurities at the grain boundaries in the heat affected zone (HAZ) during welding can lead to intergranular cracking (15). The HAZ cracking has been found to relate to the hot ductility characteristics of the alloy (11,21). Cracking can be influenced by the impurity level, and for this reason impurity tolerances have been tightened in NES 824 Part 1, Issue 2 over the initial issue as shown in Table 6. The low impurity levels are found difficult to achieve by many foundries, and specialised analysis equipment is not always available to determine their levels. Thus, a hot tensile test is also included in Issue 2. At this stage it is only for data collection, but eventually may become an acceptance test and replace detailed impurity analyses as assurance of weldability. The current M.O.D remit is that castings should be weld free. This is to ensure that during the early stages of introduction of the alloy while development is still taking place, only the highest quality castings are used in service. It is hoped that weld repair restrictions on non-wetted surfaces will cease once cast to cast weldability is

demonstrated (15).

Welding trials have been carried out by Inco Alloy Products on behalf of the Procurement Executive Ministry of Defence. Using Metal Inert Gas (MIG) welding techniques and IN732 (the wrought version of the alloy) as the filler wire, sound weld deposits have been produced with excellent ductility. Subsequently a specification outlining the welding requirements was produced, NES 825 (25). The welding wire is marketed by Inco as Monel Alloy 77, the composition of which is specified in NES 825 Issue 2, and shown in Table 7. Although most properties of weld deposits produced by the welding wire are acceptable, investigations have given some indication that the sea water impingement resistance of the weld and associated areas are not as good as the parent casting. The M.O.D believe that this is probably due to low Fe content of the welding wire. Wire with a higher Fe content is currently being investigated, and if successful weld repair on wetted surfaces may be conceivable in the future (26).

2.4.2 MECHANICAL PROPERTIES OF CAST 70/30 CUPRONICKEL

Extensive evaluation of cast Cu-Ni-Cr alloys have been carried out by the M.O.D with consideration of physical, mechanical, fracture and corrosion properties. Typical data are shown in Table 8, taken from the draft new version of Defence Standard 01-2 (Engineering For Naval Applications). As a comparison where possible, equivalent data for NAB are included.

All cast parts produced in 70/30 cupronickel (NES 824) have to undergo strength and soundness evaluations. Thus there is an abundance of cast mechanical property data available. Typical property levels achieved on parts cast at Vickers Ship-building and Engineering Limited (VSEL) are shown in Table 9, together with Youngs Modulus data. This data predicts that strength levels of 305-374 MPa proof stress and 487-584 MPa ultimate tensile strengths are typical of cast NES 824 accompanied by ductilities (% Elongation) within the range 19-24%.

Essentially the cast alloy has high strength, good impact properties and a moderate ductility with a Youngs Modulus of the order of 129-162 GPa. The data supplied by VSEL (27) refers to material produced against NES 824 Part 1 Issue 1 and Issue 2. The material cast in accordance with Issue 2 has lower impurity levels and therefore enhanced mechanical properties. In addition the machinability of NES 824 is similar to that of NAB (15).

2.4.3 CORROSION PERFORMANCE OF

70/30 CUPRONICKEL IN SEA WATER

The corrosion performance of NES 824 together with that of NAB is out-lined in the Defence Standard 01-2 (28). Data taken from this standard are shown in Table 8. In sea water NES 824 has a very good general and crevice corrosion resistance, is resistant to biofouling and also to stress corrosion cracking. In addition, when designing bimetallic couples the alloy can be galvanically treated in a similar manner to 70Cu-30Ni alloy. NES 824 also has good impingement resistance for a copper based alloy, but its upper limit has yet to be defined.

However the cavitation resistance of NES 824 is not as good as that of NAB. This means that NES 824 may not be suitable for pump impellers and the design of pump casings should be avoided due to cavitation (15). At present the Navy is still using NAB for impellers. This section serves to give a brief introduction to the corrosion resistance of NES 824, the particular corrosion properties associated with NES 824 will be discussed in detail in a later section.

2.5 APPLICATIONS OF CAST 70/30 CUPRONICKEL

Naval applications for 70/30 cupronickel include valves, pump casings, pipe fittings and headers (4,5,29). However, due to the emphasis on quality and safety, only high integrity castings are permitted in service. This results in heavy production cost penalties during the initial introduction of the alloy. The price of a NES 824 casting is around 2.5 times that of an equivalent NAB casting (15). However, should on going development prove successful and weld repair be allowed on all surfaces, it is conceivable that the production costs will decrease. In addition the concessional use of Hot Isostatic Pressing (HIPping) to recover castings containing small cavities or microshrinkage (Class I) will also allow some improvement in production costs, especially for large castings.

Other potential applications for 70/30 cupronickel alloy include the off-shore oil industry, desalination plants and fish farming (5,15,30-35). But at the present time it is the 90Cu-10Ni alloy which has wide use in these areas. Prior to use in these areas the resistance of NES 824 to sour environments such as those containing sulphides, as well as its susceptibility to hydrogen embrittlement needs to be considered. Hydrogen embrittlement is frequently caused by the cathodic protection systems used by the off-shore industry to give longer life to steel components. Cupronickel alloys do show a susceptibility to pitting corrosion in the presence of sulphides, but no data is available to compare NES 824 and rank it with respect to other copper based alloys. In addition, its resistance to

hydrogen embrittlement is thought to be very good (15), but this needs to be confirmed. Consequently, until such data becomes available, the possibilities that the cast NES 824 alloy might offer to off-shore oil / gas operators and contractors remain to be fully determined.

2.6 MECHANISMS OF CORROSION

2.6.1 CREVICE CORROSION

Crevice corrosion is often known by alternative names such as differential-aeration and concentration cell corrosion. A general definition of crevice corrosion is the attack which occurs when part of a metal surface is in a shielded environment, compared to the rest of the metal which is exposed to a large volume of electrolyte (36). A unified mechanism of crevice corrosion which applies to almost all commonly encountered situations has been proposed by Fontana and Greene (37) and is summarised below:

Figure 1 shows a schematic diagram of attack by chloride ions upon a passivated metal surface, and indicates the events occurring in a metal / electrolyte system in which a crevice is present.

(i) Initially, the electrolyte is assumed to have a uniform composition and corrosion occurs slowly over the whole of the exposed metal surface, both inside and outside the crevice. During this period normal anode and cathode processes occur, and the generation of positive metal ions is counter balanced electrostatically by the creation of negative hydroxyl ions and is indicated in Figure 1 (a).

(ii) The production of dissolved oxygen results in the diffusion of more oxygen from those electrolyte surfaces which are exposed to the atmosphere. Oxygen is more readily replaced at metal surfaces in the bulk electrolyte than at those within the crevice. Within the crevice this lack of oxygen impedes the cathodic process and the generation of negative hydroxyl ions is diminished within the confined space.

(iii) The production of excess positive ions in the gap causes negative ions from the bulk electrolyte to diffuse into the crevice to minimise the potential energy at this point. In the presence of chlorides, complex ions are formed between chloride, metal ions and water molecules. These undergo hydrolysis producing the corrosion product, and hydrogen ions which reduce the pH, and can be represented by the following simplified equation:



The equation describes a general hydrolysis reaction, in which the role of the chloride ion is extremely complicated, but is conducive to the development of low pH due to its extremely low tendency to associate with hydrogen ions in water. In addition, metals which rely upon the protection of positive films are unstable in chloride environments, and in the active crevice passivity cannot be maintained due to the lack of oxygen available.

(iv) The increase in hydrogen ion concentration accelerates the metal dissolution process, which in turn exacerbates the problem. Attack is also accelerated by the

increase in the chloride concentration within the crevice, since active crevice corrosion cells are autocatalytic, ie. once started they are self sustaining, as indicated in Figure 1 (b). Hence the metal within the crevice is corroding rapidly while the outside is cathodically protected.

2.6.2 PITTING

Pitting is localised corrosion which selectively attacks areas of metal surface where there is:

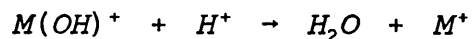
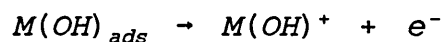
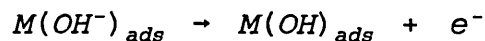
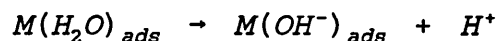
- (i) a surface scratch or other mechanically induced break in an otherwise protective film;
- (ii) an emerging dislocation or slip step caused by applied or residual tensile stresses;
- (iii) a compositional heterogeneity such as an inclusion, segregate or precipitate.

Once a pit forms its propagation mechanisms are very similar to crevice corrosion, and this often causes confusion about the two types of processes (38).

Pitting is distinguishable from crevice corrosion in the initiation phase. Crevice corrosion is initiated by differential concentration of oxygen or ions in the electrolyte, whereas pitting is initiated on flat surfaces entirely by mechanical factors.

The classic description of pitting involves the formation of a pit beneath a drop of water on an iron surface (39), as shown in Figure 2. The consumption of oxygen by the normal cathode reaction in a neutral solution causes an oxygen concentration gradient to be formed within the

electrolyte. The wetted area adjacent to the air / electrolyte interface receives more oxygen by diffusion than the area at the centre of the drop which is at a greater distance from the oxygen supply. The oxygen concentration gradient produced anodically polarises the central region which dissolves:



where, ads indicates absorbed, and implies that the reaction occurs in the solid phase at the solid/liquid interface.

Thus, metal dissolution occurs in the centre of the droplet and reaction of metal ions with hydroxyl ions formed at the edge forms an oxide deposit.

2.6.3 IMPINGEMENT ATTACK

When a fluid flows across a metal surface it can be considered to be a series of parallel layers, each moving at a different velocity. The slowest layer is adjacent to the metal surface where frictional forces and molecular collisions at surface irregularities are greatest, and layer velocity rises to a maximum at some distance into the bulk fluid. This phenomenon is known as laminar flow which has several effects on the rate of corrosion attack; some

of which are beneficial (36):

(i) In a static system an equilibrium is established at the metal surface ie. the cathodic and anodic processes are occurring at the same rate. The ionic distribution in the immediate vicinity of the surface is called the double layer. When the ions from the corroded metal are removed from the system by the flowing electrolyte, equilibrium cannot be established, and in theory, an increased rate of dissolution occurs.

(ii) Due to the replenishment of oxygen differential-aeration cells are minimised and the overall corrosion rate is improved.

(iii) A detrimental effect of increased flow rates is the replenishment of aggressive ions such as chloride or sulphide. However, a high flow rate can be beneficial in systems where a steady concentration of added inhibitor is important to controlling a corrosion process.

(iv) If solid particles are present in the fluid, protective layers may be scoured away and corrosion enhanced. Alternatively, the flow may be sufficient to prevent deposition of silt or dirt which might otherwise cause differential-aeration cells in the crevices beneath.

Such a combination of factors make the effect of flow rate unpredictable, but the most significant effect which results from high flow rates is the break down of the laminar flow and the onset of turbulence. The onset of turbulence can be defined by the use of a Reynolds Number, and at this stage molecules of fluid impinge directly upon the metal and the impact causes mechanical wear. Velocity

is just one of the factors which can cause turbulence; the system geometry also plays an important role in determining whether attack will occur or not. Some factors likely to cause impingement corrosion are listed below:

- (i) a sudden change in the bore direction of a pipe;
- (ii) a badly fitting gasket or joint which introduces a discontinuity in the otherwise smooth metal surface;
- (iii) a crevice which allows liquid flow outside the main body of a fluid;
- (iv) the presence of a corrosion product or other deposit which may disturb the laminar flow.

When moving water flows over copper or copper alloys the turbulence may be sufficient to cause break down of the surface film. This is particularly likely to happen if air bubbles entrained in the water break as they hit the metal surface. The resulting corrosion is characteristic producing clean swept pits often of a horse shoe shape (40).

2.6.4 CAVITATION

Cavitation is a particular form of erosion corrosion caused by the formation and collapse of bubbles of vapour on metal surfaces. This type of corrosion tends to be associated more with components which are driven at high velocity through a fluid, rather than in pipes or tanks where fluid flow occurs across stationary metal surfaces. Thus propellers, impellers and hydraulic turbine gears are the most common instances for encountering corrosion by

cavitation (36).

When the fluid flow over a metal surface becomes sufficiently great, very localised reductions in hydraulic pressure cause the fluid to vaporise and bubbles to nucleate on the metal surface. The same mechanical effect which reduces the pressure also creates pressure increases which cause bubbles to collapse with considerable force. If these forces exceed the elastic limit of the metal, deformation of the surface results; protective films are broken and corrosion ensues. The resultant surface roughening provides improved nucleation sites for new bubble formation and the corrosion process is aggravated. Cavitation failure is associated with the formation of a surface pit. The stress required to produce a pit has been found to be approximately three times the tensile strength of the material (41).

The process of erosion can be broken down into four stages as shown in Figure 3.

(I) INCUBATION

No material loss is detectable but damage to the surface is caused by pitting in a ductile material and cracking in a brittle material, or a combination of both.

(II) ACCELERATION

Material loss begins and the rate of material removal increases. Initially material is removed from localised sites but gradually the removal extends over a large area roughly similar in size to a cavitation zone.

(III) STEADY STATE

The rate of loss of material is almost constant, corresponding to material removal from the whole of the erosion area.

(IV) DECELERATION

Eventually the corrosion rate declines probably because the loss of material is so great that the local flow conditions have changed and reduced the cavitation intensity, or simply that the eroded surface is protected by a layer of stagnant fluid.

Corrosion by cavitation can be controlled by the use of smooth well machined components which offer fewer nucleation sites, and by the use of barriers such as rubber coatings which absorb shock waves, though in severe environments they are less effective. Cathodic protection is also beneficial, since the evolution of hydrogen provides a protective cushion against the damaging forces (37). However, large currents are necessary to produce sufficient hydrogen for adequate protection.

2.6.5 CORROSION FATIGUE

In corrosion fatigue, failure occurs at stresses well below the fatigue limit, and cracks once initiated appear to propagate faster (13). The initiation of fatigue cracks is sometimes a direct consequence of surface pitting induced by corrosion.

2.6.6 STRESS CORROSION CRACKING

The application of a tensile stress to a component which exceeds the yield stress of the material allows plastic deformation to occur, producing a blemish on an otherwise smooth surface. This is known as a slip step, and it is at this site that the material is most vulnerable to initial corrosive attack.

Alloys which rely on thin oxide films for their corrosion protection are especially vulnerable, because the slip step uncovers a microscopic area of bare metal which is highly anodic compared to the surrounding surfaces, as shown schematically in Figure 4. If the metal can repassivate quickly then little danger ensues, but if the passivation time is long enough to allow corrosion at the exposed area to occur, then the criteria for the commencement of stress corrosion cracking has been fulfilled.

The formation of a pit is the usual precursor to stress corrosion cracking and represents the initiation phase. Once a pit has formed, crack growth begins and the propagation phase takes over. This second phase of the process is quantifiable using fracture mechanic techniques (36).

2.7 MARINE CORROSION PERFORMANCE OF CUPRONICKEL ALLOYS

Investigations into the possible use of cupronickel castings for complex components in sea water have been in progress for the last two decades. This has involved the introduction of wrought 70/30 (1%Fe) cupronickel for submarines and 90/10 (1%Fe) cupronickel for surface ships' sea water systems (7,15).

The cast alloy presently used in HM Ships is NAB, which possesses high strength and shock resistance but suffers from preferential phase corrosion at crevices and weld affected zones. Corrosion rates in such areas have been reported to be of the order of 1mm/year (15).

Consequently components require expensive non-destructive evaluation (NDE) and/or replacement at frequent intervals during service life in order to comply with the requirements for maximum corrosion tolerance to be less than 10% of the wall thickness.

Over the last 20 years several cast cupronickel alloys as listed in Table 3, have been investigated for possible use in sea water systems, but the prime interest has been in the INCO alloy IN768 (21). The marine corrosion performance of this alloy has been widely investigated in comparison where possible with NAB. The composition of an IN768 alloy investigated is shown in Table 10. This compositional range was tightened with regards to impurity levels which lead to the development of 70/30 cupronickel strengthened by Cr and Si designated in the Naval Engineering Standard NES 824 (25).

2.7.1 GENERAL CORROSION

Corrosion specimens of IN768 after exposure for one year fully immersed in the sea at Langstone Harbour produced average corrosion rates of 0.02mm/year calculated from weight loss measurement, and the maximum rate of attack estimated from metallographic examination was 0.05mm/year (15).

Corrosion rates for IN768 have also been determined by the use of a corrosion probe inserted in an auxiliary sea water system, approximately 1 metre inboard of the hull valve, down stream of the strainer on a submarine operating in the English Channel and North Atlantic. The initial polarisation admittance (1/polarisation resistance) fell from a value of 18 μ A/mV to a value of 7 μ A/mV after 40 days and remained constant until the probe was removed 50 days later. The steady rate of 7 μ A/mV corresponds to a corrosion rate of 0.05mm/year (16). This value is higher than that obtained in Langstone Harbour, due to the higher flow rate of 3m/s compared with the immersion specimen which was only subjected to tidal flow.

The steady state corrosion rate for IN768 differs from that of cast NAB whose corrosion rate falls with time according to the relationship (16):

$$d = 0.026 t^{0.75}$$

where d = depth of corrosion (mm)

t = time (years).

In addition the operation of a submarine at various diving depths has no measurable effect on the corrosion rate of

IN768, whereas the corrosion rate of NAB tends to fall slightly with increased diving depth.

A list of some metals and alloys commonly used in marine service as condenser tubes in power generating plants and ships are shown in Table 11, which indicates their general corrosion rates in sea water (42). In general the copper-nickel alloys are far superior to the other alloy systems.

Many investigators (15,43-45) have measured the resistance of Cu-Ni alloys to corrosion in sea water by weight loss determinations. Table 12 shows the trend for short term laboratory tests (20 hours duration) carried out in aerated 3% sodium-chloride solution (43). Other results obtained for tests carried out in natural flowing sea water are shown in Figure 5 and Tables 13-15. All the investigations show a similar trend where the rate of corrosion decreases as the nickel content of the alloy increases. In addition results obtained on panels of various Cu-Ni alloys placed in natural sea water flowing at 1.5-3.0ft/s in North Carolina for a duration of 497 days (43) as shown in Figure 5, indicate that increasing the Ni content above 40% significantly lowers the corrosion rate.

The results of other corrosion trials carried out on Cu-Ni tubes (45) subjected to tidal sea water in the Bristol Channel for 3 and 4 years are shown in Tables 14 and 15. During testing all the specimens became covered with thick coatings of oily mud. All the specimens except those of high Cu content (80-100%) acquired growths of marine organisms which stimulated localised corrosion. Even so,

the results still show that increasing the Ni content improves the general corrosion resistance (45).

Differences in marine corrosion performance are related to firstly the influence of alloying elements on the protective corrosion product film and secondly, on the effect of ionic and electronic conductivity. For example Ni coupled with Fe (as a dopant in Cu_2O) provides as extremely protective corrosion product (42).

The service life of cupronickel is not dependent on general corrosion/wastage, since at the normal pH of sea water general corrosion rates are extremely low. Therefore localised corrosion is of extreme importance and is directly dependent on the integrity of the corrosion product and its resistance to localised break down. Break down of the surface protective oxide film (42), can occur due to :

- (i) local pH changes as would occur in crevices or pits causing localised solubility;
- (ii) mechanical removal by abrasion or high fluid shear forces;
- (iii) gas release or bubble impingement causing local removal;
- (iv) penetration by deleterious ions such as chloride or sulphide;
- (v) the presence on the metal surface of foreign substances such as carbon which may also act as pit initiation sites; or
- (vi) the formation of a non-protective film.

2.7.2 BIMETALLIC CORROSION

The short term potential of IN768 in sea water is typical of a 70/30 cupronickel at -0.180V (sce), but on prolonged exposure potential drifts to around -0.100V (sce) as occurs more slowly with other copper alloys (16). This behaviour is attributed to corrosion occurring initially as the cuprous ion Cu^+ and subsequently as the cupric ion Cu^{2+} , producing pseudo anodic passivation as indicated in the polarisation curves shown in Figure 6. These curves were obtained in natural sea water at 20°C under potentiostatic control at a scanning rate of 5mV/min .

The bimetallic corrosion of IN768 when coupled with more noble materials such as stainless steel, high nickel alloys or titanium (ie. IN768 acts as the anode) can have deleterious results due to the possibility of localised pitting associated with the cored dendritic structure of IN768. This type of localised attack is variable depending on the localised cooling rate of the casting and variability between castings. However, in general IN768 would be expected to suffer less anodic corrosion than most Cu alloys due to its ability to passivate readily.

The behaviour of IN768 when coupled to less noble metals would be expected to behave in a similar manner to other copper alloys, as the cathodic polarisation current is dependent on the availability of dissolved oxygen for the cathodic reaction (16).

2.7.3 CREVICE CORROSION

IN768 has a cored dendritic structure, the difference in composition between the matrix and the dendrites being determined by the rate of the cooling of the liquidus (liquid + α) state. The greater the degree of supercooling the more uniform is the resultant structure/composition. If the 70/30 cupronickel is very slowly cooled, the initial dendrite formed will contain 50% Ni (Point A Figure 7), and the nickel rich dendrites will behave as a material having active and passive corrosion states due to film formation. Hence, their corrosion behaviour is akin to that of stainless steel. Such behaviour is typical of 70/30 cupronickel alloys (16). Electron probe examination micro-analysis (EPMA) of four IN768 castings revealed that local Ni contents rarely exceed 40%, and the highest Ni content recorded was 44.5% (46). Similar investigations carried out by RNEC (47) gives the average analysis of the dendrites to be 58.6%Cu and 41.4%Ni, while that of the matrix was 76.2%Cu and 23.7%Ni.

Crevice corrosion tests carried out on IN768 using the INCO castellated nut test and the perspex sandwich jig, and subjected to immersion for one year in Langstone Harbour produced a maximum depth of attack of 0.18mm (48). This compares favourably with NAB where corrosion rates of up to 1.1mm/year due to selective phase corrosion have been determined (13). IN768 has the advantage that such crevice corrosion takes the form of macro pitting which is clearly visible and readily measured, whereas the non-destructive examination (NDE) techniques required to detect selective

phase corrosion of cast NAB are very sophisticated (21).

Crevice corrosion can occur in any occluded areas that constitute a crevice such as blockages, leaking gaskets, cracks and bad geometry. Crevice corrosion occurs by two main mechanisms (36,42):

- (i) Differential aeration cell corrosion where the oxygen depleted area inside the crevice becomes anodic and corrodes rapidly, such corrosion is typical of stainless steels and many high Ni alloys.
- (ii) Metal ion concentration cell corrosion, where the metal surface in contact with a well oxygenated bulk solution becomes anodic, because metal ions build up in the crevice. Metals in contact with their ions become enobled.

Copper alloys are more prone to metal ion concentration cell type crevice corrosion, and flowing solutions tend to aggravate this form of attack. The typical crevice corrosion of some copper based alloys are shown in Table 16, which indicates that 70/30 cupronickel has good resistance to such processes (42).

2.7.4 IMPINGEMENT ATTACK

Impingement attack and pitting corrosion have been observed for many copper base alloys in marine environments.

However, it is not usually a serious problem if the alloy is matched to the environment and service conditions.

Typical pitting rates for copper based alloys are shown in Table 17. In general, those alloys not susceptible to dealloying have extremely low penetration rates and higher

flow velocities tend to reduce their incidence of pitting (42).

Impingement attack of IN768 has been measured using a Modified Brownsdon-Bannister test (49) and submerged jet disc tests (50). A modified Brownsdon-Bannister test involves air at 0.7 bar being forced through a capillary tube 100mm x 0.61mm diameter at a rate of 3.21l/min, to produce a jet impinging on a specimen submerged in sea water. The specimen is clamped at 60° to the jet and the jet-specimen gap is 2mm. These tests carried out for 600 hours on IN768 and 70/30 (1%Fe) cupronickel produced corrosion attack to a depth of 0.03mm ± 0.01mm for both materials (16).

The submerged jet test involves submerging a disc of IN768 in sea water and subjecting it to a jet of sea water at a velocity of 1.7m/s. No attack is experienced unless the potential is at least -100mV (sce) and even at potentials up to 0.0mV the attack is very slight, being observed as an etching of the dendritic structure. Similar tests carried out on 70/30 (1%Fe) cupronickel also failed to cause any significant impingement attack (49).

The impingement resistance of cast 70/30 cupronickel can be enhanced by the addition of 0.2-1.75% Cr. The improved performance is not affected by the addition of Nb, Si or Ti as hardening elements (51). Other investigators found that enhancement occurs over the range 0.3-1.0%Cr (Figure 8), since higher levels of Cr tend to reduce corrosion resistance under less turbulent corrosion conditions (52).

Other investigators observed that impingement resistance of copper based alloys varied with the condition of the material (53). The decrease in impingement resistance after aging at certain temperatures has been attributed to the precipitation from solid solution of elements which can effect the oxidising characteristics of the alloy, and also promote galvanic action between the precipitate and the matrix.

2.7.5 CAVITATION EROSION

Cavitation erosion rates of IN768 and NAB have been compared using two test methods, where local conditions are characterised by a cavitation index and the local velocity:

- (i) ARE HH erosion test (16).
- (ii) Nozzle or long orifice test (54).

The ARE HH erosion test consists of a 25mm diameter cylinder located in the centre of a 47mm square tunnel section. Recirculated water at a constant temperature is pumped through the tunnel and the cylinder acts both as a diverter which promotes cavitation in the minimum cross-section and as the test specimen, since erosion takes place on the down stream face. Pressure and velocity are measured at the entrance of the tunnel and corresponding values for the restriction are calculated using precalibrated flow break down (choking) conditions. Tests are continuous for up to 100 hours and erosion rates are calculated from mass loss measurements.

The nozzle (or long orifice) test (54) uses a sharp edged orifice which has a cylindrical length 4 times its

diameter. A submerged cavitating jet is produced by a large pressure difference across the orifice. Under these conditions flow is choked and depends only on the up stream pressure. Control of the pressure in the test chamber determines the cavitation intensity. The cavitation jet strikes the specimen face placed normal to the flow direction and the resultant erosion is measured by mass loss. Positive location of the specimen allows replacement and, as a result, the determination of cumulative volume loss versus cumulative erosion time is possible.

Results of the cavitation erosion assessment on IN768 and NAB are shown in Figure 9. The cupronickel erodes at a higher rate than NAB in both tests. No comparison can be made between the two tests and neither relates to a particular service application. However, for cast materials with a range of grain sizes the cylinder test is considered to be the most realistic comparison due to the larger eroded area and the value of velocity being closer to those encountered in service conditions.

The dependence of erosion rate on velocity is given by the following relationship (16):

$$\text{Erosion Rate} \propto (\text{Velocity})^n$$

where $n = 3$ to 10 . The "sixth power law" is often used by designers since most test data is available to this value.

2.7.6 STRESS CORROSION CRACKING

This form of attack is extremely rare in marine environments and is usually associated with ammonia or SO₂ contamination. In general copper-nickel alloys, aluminium bronzes and high copper alloys are immune to stress corrosion in clean sea water and contaminated sea water (42,45). Cast NAB has been found to fail by stress corrosion cracking in natural sea water when subjected to slow strain rate tests held at potentials within the range -0.075V to -0.200V (sce), involving strain rates within the range 4×10^{-7} to 10^{-4} mm/s. IN768 subjected to the same test conditions does not show evidence of stress corrosion cracking. Hence, it can be concluded that IN768 is markedly more resistant than NAB to stress corrosion failure in sea water (16).

2.7.7 CORROSION FATIGUE

For sea water systems applications, the interest is in low frequency rather than high frequency corrosion fatigue. Fracture toughness tests (56) have been carried out on precracked plate specimens under trapezoidal wave form loading at 1 and 0.01Hz, the rise: dwell: fall time ratios being 2:3:2. At a frequency of 1Hz IN768 is superior to cast NAB as shown by the crack growth rate versus stress intensity results in Figure 10. At a frequency of 0.01Hz corrosion blunting of the crack occurs preventing fatigue crack propagation. Thus it appears that corrosion fatigue is only likely to arise at higher frequencies and is unlikely to be a problem in sea water systems (16).

Low corrosion fatigue behaviour of high strength cupronickel parent and weldment material was carried out by the M.O.D (57). This involved testing over a range of cyclic loads which gave stress intensities at the tip of a 0.5mm crack from $12-35\text{MN}^{3/2}$. Testing was carried out in natural sea water at a temperature of 20°C . The results obtained are shown in Figure 11, which indicate that the low frequency fatigue crack growth rates reported for the parent material, HAZ and weld material are all contained within a common scatter band. This indicates that corrosion fatigue rates are low and occur at a similar rate regardless of whether the casting has been weld repaired.

2.8 CORROSION RESISTANCE OF CUPRONICKEL ALLOYS:

PROTECTIVE OXIDE FILMS

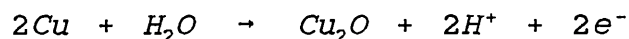
Although the currently used sea water resistant copper alloys have histories which extend over 50 years, the nature of the protective films formed in sea water are still not fully understood. Considerable progress has been made over the last 10-15 years in developing such films, these investigations offer guide lines for improvements to the service performance of existing alloys (58).

The excellent corrosion resistance of cupronickel alloys in sea water is attributed to the growth of the protective corrosion product film which in the classical sense is passive. The uniform formation of this film depends upon the material surface condition; sand blasting produces a more homogeneous surface upon which the film can grow

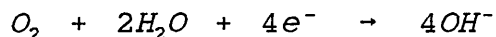
uniformly, producing more consistent corrosion behaviour and hence a longer service life (59). The protective film may require very long times to reach a steady state as shown for 90/10 and 70/30 cupronickel in Figures 12 and 13. In quiet sea water this time span approaches 4 years while in flowing sea water, the corrosion rate continually decreases over a period in excess of 14 years (29). In sea water, the corrosion product formed is predominantly cuprous oxide (Cu_2O) irrespective of the alloy composition (60,61). Often observed in addition to the red-brown Cu_2O is the compound paratacamite ($\text{Cu}_2\text{O}(\text{OH})_3\text{Cl}$), a bulky, green non-protective corrosion product overlaying the Cu_2O . Analysis of films formed on 90/10 cupronickel (60-63) has identified copper, nickel, oxygen and chlorine as the main constituents together with iron which also enters the film early in its formation. Iron and nickel accumulate at the alloy / protective film interface, and the ratios of Cu to Ni in the film are lower than in the alloy.

The morphology, composition and growth kinetics of the passive film have been studied by numerous authors (60-65), and the following reactions describe copper as it corrodes in aerated sea water:

The Anodic Reaction



The Cathodic Reaction



As the Cu_2O corrosion product grows, copper ions and electrons must pass through the film to support the anodic and cathodic half reactions.

Alloying additions of Ni and Fe to copper have been found to improve its corrosion resistance by the incorporation of Ni^{2+} and Fe^{3+} ions into the corrosion product film as "dopants" which alter the defect structure.

Efird (66) has studied the effect of Fe additions on the corrosion resistance and the corrosion product composition for several 90/10 cupronickel alloys in quiet and flowing sea water. For solid solution Fe additions, he concluded that Fe interacts synergistically with Ni, producing Ni enrichment of the corrosion product. For alloys containing a precipitated Fe phase, a significant reduction in nickel enrichment results as shown in Table 18. However, other investigations have indicated that Fe additions are beneficial even in the precipitated form as shown in Figure 14, where 90/10 cupronickel containing over 90% of the Fe in the precipitated form compares favourably with the same alloy in the solution treated condition. In the absence of Fe there is an excess of oxygen and very little Ni present in the cuprous oxide layer. With Fe present Ni enrichment occurs, but the form of the Ni present is dependent upon whether or not the Fe is in solution in the alloy. With Fe in solution there is an excess of Ni in the film present in the un-oxidised state, and the resultant films are brown in colour. With Fe largely out of solution there is an excess of oxygen in the film and the Ni is present as an oxide producing a black

oxide film (66).

Similar results have been reported by Bailey and Berg et al (67,68), where the corrosion product film produced on single phase material is thick and golden-brown in colour. A typical thickness of this film would be $1.5\mu\text{m}$ (69). In contrast precipitated material forms thin green-black films in uncontaminated sea water, the latter films being porous in nature and around $1.18\mu\text{m}$ thick.

When the rate of erosion corrosion of 70/30 cupronickel is relatively low it has been found that the corrosion products formed are yellow-brown in colour and consist of three layers (70):

- (i) The composition of the layer at the metal/oxide interface could not be determined by micro-analysis.
- (ii) The middle layer is rich in Cu, Fe and S.
- (iii) The outer layer is rich in Cu and Ni, with small but significant amounts of Cl and Fe.

The main minerals identified by X-ray diffraction (TEM) were copper-oxide (Cu_2O) and basic copper-chloride ($\text{Cu}_2(\text{OH})_3\text{Cl}$).

In comparison if the rate of erosion corrosion of 70/30 cupronickel is relatively high the adjacent corrosion products formed are black and again consist of three layers as indicated over the page:

- (i) The oxide formed at the metal/film interface once again could not be analysed.
- (ii) The middle layer is rich in Fe with significant amounts of Ni, Cu and S.
- (iii) The outer layer is rich in Cu with small but significant amounts of Cl, Ni and Fe.

The main minerals identified were copper-oxide, basic copper-chloride together with copper-chloride (CuCl), ferric oxide (Fe_2O_3) and a mixed copper-nickel oxide (CuNiO_2) (70).

2.9 EFFECT OF ALLOYING ADDITIONS ON THE CORROSION RESISTANCE OF CUPRONICKEL ALLOYS

2.9.1 NICKEL

Many authors (15,43-45) have measured the corrosion resistance of Cu-Ni alloys to sea water. All investigations show a similar trend where the rate of corrosion decreases as the Ni content of the alloy increases, as indicated in Tables 13 to 15. Increasing the Ni content above 40% significantly lowers the corrosion rate as shown in Figure 5.

2.9.2 CHROMIUM

The versatility of cupronickel alloys for marine services is expanded through controlled additions of Cr in the range 0.5-3.0%. Mechanical properties are affected by the occurrence of spinodal decomposition which acts as a hardening mechanism (71). The yield strength of a Si free 70/30 cupronickel increases with increasing Cr content in a

non-linear manner, attaining a maximum at 3% Cr as shown in Figure 15. The maximum Cr content has been limited to 2.0% due to weldability considerations (20).

The effect of Cr on corrosion properties is not related to the effects of spinodal decomposition, but is best observed under high velocity conditions. Additions of Cr to cupronickel alloys significantly extend the upper limits of the alloys in sea water. Figure 16 indicates a beneficial effect of Cr additions in 70/30 cupronickel at levels as low as 0.2%. Increases in the Cr content further continues to increase impingement resistance at high velocities until a tolerable level of attack is achieved at around 2.0%. Higher levels of Cr are known to increase corrosion in low velocity sea water (72).

2.9.3 IRON AND MANGANESE

The corrosion rate of cupronickel alloys in sea water is reduced by the addition of small amounts of Fe between 0.3 - 1.0%, as shown in Figure 17. However, increasing the Fe content further causes an increase in the corrosion rate (73).

As the amount of Mn present in the alloy increases, smaller additions of Fe are required to achieve the same effect. It has also been stated that the sum of the Fe content plus one fifth of the Mn content should not be less than 0.5%; furthermore, the Mn content should be within the range 0.25-2.0%, and the Fe content 0.3-1.0% (67).

In addition numerous authors (61,64,66,68,69,74-77) have studied the mechanism by which the corrosion product film

protects Cu-Ni alloys and the means by which it is enhanced by the presence of Fe. Alloys containing Fe in solid solution produce a golden-brown film which is highly resistant to impingement. In contrast alloys containing precipitated Fe, produce a thin black film which is protective. The colour changes are associated with changes in magnetic susceptibility which is high in the case of the alloys forming the black film (magnetite) and low for those forming the brown film.

2.9.4 NIOBIUM AND SILICON

These elements are often found in combination in castings for strengthening by age hardening in both cast and wrought cupronickels. Laboratory tests on 70/30 cupronickel containing a singular addition of 1.75% Si show good corrosion resistance to stress corrosion cracking, but exhibit a tendency towards localised corrosion in crevices. Aging has been found to improve the corrosion resistance of the alloy. The addition of up to 0.2% Si has no significant effect on the corrosion resistance of alloys used in quiescent sea water, but marked corrosion occurs in sea water flowing at velocities of 0.5-2ft/s. The addition of 10%Nb restores the corrosion resistance back to the level of localised attack in quiescent sea water (72). Cast alloy IN768 contains 0.3-0.6%Si for strength and weldability, and has better corrosion resistance than other cast Cu-Ni alloys, but is susceptible to shallow cratering attack at low velocities (20).

2.9.5 BERYLLIUM

The addition of Be to Cr modified cupronickel alloys improves the already excellent impingement resistance. Additions of 0.15%Be adversely affect the corrosion resistance in low velocity sea water, while additions of 0.2-0.5%Be improve the corrosion resistance. A harmful effect of Be is the susceptibility to stress corrosion cracking in welds at levels above 0.2% (72).

2.9.6 IMPURITIES

Carbon and phosphorus are classed as impurities in cupronickel and need to be kept to a minimum (below 0.05%) if the alloy is to be welded (15). However, the addition of P at levels of 0.03% has been substituted for Mn without significant effect on corrosion behaviour in sea water (67).

2.10 HOT DUCTILITY OF CUPRONICKEL ALLOYS

Cast high strength cupronickel alloys ($>385\text{MPa}$ 0.2% Proof Stress) have complex compositions and are hardened by precipitation and spinodal mechanisms to give varying combinations of strength and ductility. When fusion welded under constraint, these materials can sustain a form of heat affected zone cracking associated with a lack of ductility at intermediate temperatures of 700-1000K ($427-727^{\circ}\text{C}$) (78), as shown in Figure 18. This variation in ductility with temperature restricts the potential applications of cupronickel material.

Many pure metals exhibit poor ductilities in the temperature range $0.4-0.7T_m$ (where T_m is the absolute melting temperature) over wide ranges of strain rate and grain sizes (79-84). Several authors have proposed mechanisms to explain this minimum ductility: some indicate that it is a basic property of cupronickel alloys (85), while others suggest that it is related to creep type failure associated with grain boundary sliding and cavitation effects resulting in intergranular fracture (81,83). It has also been suggested that failure is due to precipitation embrittlement (86), or is a result of trace impurities (78).

2.10.1 EFFECT OF ALLOYING ADDITIONS ON THE
HOT DUCTILITY OF CAST CUPRONICKEL

(1) IMPURITIES

The effect of impurities on the hot ductility of 70/30 cupronickel has been measured before and after vacuum melting (78). Figure 19 indicates that vacuum melting which reduces impurity levels as shown in Table 19, also produces a significant improvement in ductility. Consequently all work which refers to the effect of alloying additions on hot ductility involves material of high purity.

(2) NICKEL

Increasing the Ni content of the binary alloy has been found to progressively decrease the intermediate temperature ductility from 40% to 10% as the nickel increases from 6% to 30% (78). Figure 20 indicates that fracture in the intermediate temperature region is progressively intergranular in nature as the ductility decreases caused by an increase in the Ni content. It has been suggested that as the Ni content increases recovery processes are delayed thereby affecting ductility (87). Figure 20 also shows that Cu-Ni alloys containing 10-15% Ni have excellent ductility over the temperature range 700-1000K, whereas alloys containing higher Ni contents give inferior results.

(3) **MANGANESE**

Mn is added to cupronickel alloys to aid melt fluidity and to counteract the harmful effect of sulphur impurities, as well as improving strength and weldability if added in sufficient quantity (88). Additions of 0.1% and 5% Mn to a Cu-10Ni alloy have no significant effect on the hot ductility except at test temperatures above 1050K where the ductility of the 5% Mn alloy was slightly reduced with increasing temperature. This was associated with segregation of Mn to grain boundary regions which results in lowering of the melting point of the boundary, thereby indicating that up to 5% Mn can be added to aid melt fluidity without seriously impairing ductility.

(4) **SILICON AND ALUMINIUM**

Si and Al are added to Cu-Ni alloys to provide strengthening by means of precipitation reactions (78). Additions of 5% Al increase the room-temperature strength of the alloy by 50%. Both Si and Al have a deleterious effect on intermediate temperature ductility, particularly Si. Addition of 0.5% Si is sufficient to decrease the hot ductility to unacceptable levels. Addition of 0.1% Al provides adequate ductility whereas higher levels of 5% cause a significant reduction in the intermediate temperature ductility. The poor ductility experienced in a Cu-10Ni-0.5Si alloy over the temperature range 700-1000K suggests that Al is the preferred strengthening addition, and is utilised at the lowest level commensurate with satisfactory strength (78).

(5) **IRON**

Fe additions are made to cupronickel alloys to improve their resistance to impingement corrosion. Adding between 0.1 to 5.0% Fe to a Cu-10Ni alloy reduced the hot ductility of the alloy especially in the intermediate temperature range as shown in Figure 21. Additions of Fe above 2% cause a severe reduction in ductility, which falls to almost zero at Fe levels of 5%. Fe levels should be kept below 1% in order to ensure adequate intermediate temperature ductility (78).

2.10.2 HOT DUCTILITY OF WROUGHT 70/30 CUPRONICKEL

Hot ductility investigated by means of tensile tests conducted over the temperature range 293-1160K with strain rates of $3.3 \times 10^{-4} \text{s}^{-1}$ to $8.33 \times 10^{-2} \text{s}^{-1}$, for specimens with a range of grain sizes, have indicated that the stress-strain curves produced shapes which could be divided into two types, as shown for a Cu-10Ni alloy of $190 \mu\text{m}$ grain size in Figure 22. The first type shows that stress increases uniformly with strain until fracture, whereas in the second type stress quickly reaches a steady state which is maintained until near the fracture strain. The first type of curve predominates at low temperatures and high strain rates, while the second type occurs at high temperatures (81). The variation in the reduction in area at fracture with temperature for various strain rates is shown in Figure 23 for a Cu-30Ni alloy of grain size $125 \mu\text{m}$. All strain rates show a decrease in ductility with increasing temperature until a minimum ductility is

observed (point A). At higher temperatures the ductility increases to reach a maximum (point B), after which it once again decreases (point C). Similar curves have been obtained for other grain sizes and the positions of points A, B and C are given in Table 20. The minimum ductility is independent of grain size and strain rate, but the temperature at which it occurs increases with an increase in strain rate. The maximum ductility decreases slightly with an increase in grain size and strain rate. The fall off in ductility after reaching a maximum varies both with grain size and strain rate (89).

The hot ductility of Cu-30Ni varies in a complex way with grain size and strain rate, but failure always occurs by grain boundary cracking (89). The incidence of grain boundary cracking increases with temperature as the ductility minimum is approached, and no grain boundary migration or recrystallisation occurs. At temperatures between the ductility minimum and maximum cracking occurs but recrystallised grains start to form at grain boundaries and their formation increases with increasing temperature. At temperatures above the ductility maximum the microstructure varies considerably with grain size and strain rate. At low strain rates recrystallisation is reduced but with high strain rates it is most evident in smaller grained material, larger grained material being more susceptible to grain growth.

2.10.3 NUCLEATION AND GROWTH OF VOIDS

The ductility loss and occurrence of a ductility minimum experienced during the plastic deformation of metals in the temperature range $0.4-0.7T_m$ is associated with the onset of intergranular fracture resulting from voids which are nucleated preferentially at grain boundaries. The types of void formation found in the intermediate temperature embrittlement range are known as wedge or W - type voids formed at triple points (79,90), and R - type voids which are round or elliptical in shape (79). Investigations carried out on copper (79) have shown that minimum ductility occurs in the temperature range $350-550^{\circ}\text{C}$, and that ductility loss is roughly proportional to the number of voids nucleated as shown in Figure 24.

2.10.3.1 NUCLEATION AND GROWTH OF WEDGE TYPE VOIDS

W - type voids are nucleated at triple points as illustrated in Figure 25. Triple points act as strain concentration sites since the deformation caused by grain boundary sliding between two adjacent grains must be transmitted through the boundary to a third grain. Cracking occurs when this deformation cannot be accommodated. W - type fracture results in a flat fracture which follows a grain boundary path.

The criterion often used for void nucleation is that cracking occurs when local stresses across a grain boundary exceed the boundary cohesive stress (91):

$$\sigma_s = \left[\frac{12\gamma G}{L} \right]^{1/2}$$

where σ_s = applied shear stress
 γ = energy to make the fracture surface
 G = shear modulus
 L = length of sliding interface

The relationship above is based on the Griffith theory and although errors can arise from any non-elastic deformation it has been found useful in predicting the effects of test variables on metals (79,92). Inclusions at triple points increase the formation of cracks if the binding force between the inclusions and the matrix is low (ie. γ is low) (93). Inclusions with high binding strengths would not be expected to act as nucleation sites (94). γ can also be lowered by the presence of impurities in solution at grain boundaries (79). The mechanisms by which W - type voids grow is uncertain. The most widely accepted growth mechanisms are vacancy condensation and plastic deformation (91,95). Vacancy condensation would probably be the controlling mechanism at high temperatures (faster diffusion) and slower strain rates (longer time). The plastically induced growth would be favoured at lower temperatures and higher strain rates.

2.10.3.2 NUCLEATION AND GROWTH OF ROUND VOIDS

In cavitation, or R - type void formation, fracture results from the linking of voids producing a serrated fracture surface. Cavitation is more important at higher temperatures and lower stresses. The voids tend to nucleate at grain boundaries and often at triple points. Cavitation is not found in pure materials or single crystals and it is widely believed that second phase particles must be present and located at grain boundaries for R - type void formation (79,96). The most widely accepted mechanism for R - type void formation is illustrated in Figure 26. This fracture mechanism relies on stress concentration at a particle and results in decohesion of the grain boundary by shear. Lowering the strain rate (or stress level) generally increases the amount of cavitation (79,97). Decreasing the grain size generally decreases the amount of R - type void formation caused by the shorter relative displacements of the grain boundary.

Both wedge type void formation and cavitation is reduced and ductility reinstated during grain growth or hot working. Thus, when grain boundaries have sufficient mobility to pull away from stress concentration sites or nucleated voids, ductility returns. The growth of R - type voids appears to be analogous to that of W - type voids the controlling mechanisms being dependent on temperature, strain rate and material. In both W and R - type void formation, the addition of a hydrostatic stress of magnitude equal to the yield stress eliminates void

formation and growth. Any voids formed would be healed by sintering or pressure welding (79).

2.11 SINTERING

Sintering is a term generally used by powder metallurgists to describe a process which compresses metal or ceramic particles under the influence of heat to remove porosity and reduce the surface area of the compact, so producing a solid coherent body by welding the particles together (98,99). The decrease in surface energy which accompanies the reduction in surface area is the driving force for the process. The internal surface area of a pore has a specific surface energy per unit area. This occurs because the atoms in the free surface have no neighbours on one side and hence possesses "missing" bonds (100), as shown in Figure 27. The atoms in the surface tend to have a relatively high energy compared to an atom in the interior of the material. Other regions of high energy include areas of disorder such as grain boundaries and dislocations.

The history of sintering has been reviewed by several authors (98,99,101-105); and two principal changes have been found to occur during the sintering process:

- (i) the powder particles weld together and the pores between them become more spherical; and
- (ii) the density of the compact increases.

Although the two changes proceed simultaneously and the driving force for both arises from the excess surface free energy of the powder over that of the bulk material, they

can occur by different mechanisms.

2.11.1 DRIVING FORCE FOR PORE CLOSURE BY SINTERING

The predominant driving force for sintering is the reduction of the surface energy of the powder compact. This is achieved initially by elimination of porosity which commences by spheroidizing of the pores. At this stage the specific surface energy of the pores is greater than that of grain boundary energy. Therefore negligible reduction in the surface energy is achieved by grain growth at this stage.

2.11.2 SPHEROIDIZING OF THE PORES

The first stage of sintering can be considered in terms of a simple model consisting of two spheres of the same radius a (102), as illustrated in Figure 28. The difference between the partially sintered spheres shown in Figure 28 (a) and (b), is that in the case of (a) the centre to centre distance of the spheres does not decrease when the neck is filled to radius x . Whereas in the case of Figure 28 (b) the sphere centres do approach each other. In the first case there will be no overall shrinkage of the system, the material for filling the neck being drawn from the surface of the spheres whose diameters decrease slightly. In the second case the system shrinks and the lense-like area in the neck represents schematically the amount of material which is displaced into the peripheral portions of the neck. In both cases the growth of the neck caused by both viscous or plastic flow, evaporation and

condensation, volume diffusion and surface diffusion decreases the total surface area of the system and hence its total surface energy. This decrease in surface energy of a compact is the motivating force for sintering. The initiator for pore closure by neck growth during sintering, has been expressed as the stress acting on the curved surface of a neck formed between two spheres (102):

$$\sigma = \gamma \left[\left(-\frac{1}{p} \right) + \left(\frac{1}{x} \right) \right] \quad (1)$$

where γ = surface tension of the solid

x = neck radii

p = curvature of the neck.

Although x is small, p is much smaller, so the term on the right hand side of the equation can be omitted; so now:

$$\sigma = - \frac{\gamma}{p} \quad (2)$$

More recent studies (100,106,107) have derived the driving force for pore closure in terms of a pressure P , such that:

$$P = \frac{2\gamma}{r} \quad (3)$$

where γ = the specific energy of the internal surface of the pore

r = radius of curvature of the pore surface.

For a spherical pore, r is the radius of the sphere, but for a more irregularly shaped pore, the surface can be divided into a number of regions with different radii of curvature as shown in Figure 29.

Several important factors have emerged from equation ⁽²⁾: the first is that the driving force required for the removal of small pores is greater than that for the removal of larger pores as will be explained later. In addition, if the pores contain gas the internal pressure of the gas will tend to oppose the driving force for shrinkage, since as the pore shrinks the internal pressure of the gas will rise. The gas may dissolve into the matrix and diffuse into a region of lower pressure such as larger pores or the surface of the compact. Thus, large pores grow at the expense of smaller pores. For an irregular shaped pore matter will tend to be transported to concave regions of small radius of curvature from those where the surface is more gently rounded or convex, as shown in Figure 29. Thus, irregularly shaped pores tend to spheroidize (100). The tendency for the pore to spheroidize is counteracted by the fact that pores tend to be sited at the meeting of two, three or four grains as indicated in Figure 30. The pore geometry is determined by the various interfacial energies involved, such as those between one phase and the pore, one phase and the other for a two phase system, and between grains of one phase (100,101).

For a single phase system of material A, the porosity meets a grain boundary at a fixed dihedral angle (γ) as shown in Figure 31(a), which indicates that the surface energy of the pore γ_s , must balance the grain boundary interfacial energy γ_i which predicts:

$$\cos \frac{\theta}{2} = \frac{\gamma_i}{2\gamma_s} \quad (4)$$

Equation ⁽⁴⁾ can be rewritten to give:

$$2\gamma_s \cos\left(\frac{\theta}{2}\right) = \gamma_i \quad (5)$$

The pore geometry will differ for a multi phase system as shown in Figure 31(b), from which the corresponding resolution of forces show that:

$$\gamma_s \cos \alpha + \gamma_s \cos \beta = \gamma_i \quad (6)$$

where γ_s = surface energy of the pore surface adjoining the A phase

γ_s = surface energy of the pore surface adjoining the B phase

γ_i = grain boundary interfacial energy between phases A and B.

It is energetically favourable for porosity to occupy in order of preference four grain corners, three grain edges, two grain faces and lastly sites in the interior of grains, because the total amount of interface and hence interfacial energy is reduced in ascending order of this list. In addition, the lower the dihedral angle, the more energetically favourable it is for the porosity to remain at a boundary. Hence the last pores to be removed during sintering in the absence of grain boundary migration will be those at four grain corners (100,101). It has been shown by geometrical arguments (103) that at dihedral angles of 60° or less, porosity is found at three grain edges, which produces a structure consisting of two interlinked continuous phases. Whereas the presence of

porosity between grain faces only occurs when the dihedral angle falls to zero.

2.11.3 MECHANISMS OF MATTER TRANSPORT

During sintering of a powder compact, material must flow in order to minimise surface energy and allow the growth of necks between powder particles (101). The mechanisms of matter transport to fill pores are summarised in Figure 32 and the transport paths are identified below:

Mechanism	Transport Path	Source of Matter	Sink
1.	Grain boundary diffusion	Grain boundary	Neck
2.	Lattice diffusion	Grain boundary	Neck
3.	Lattice diffusion	Surface	Neck
4.	Surface diffusion	Surface	Neck
5.	Vapour transport	Surface	Neck
6.	Lattice Diffusion	Dislocation	Neck

Matter can be transported to fill a pore at point A in Figure 32 from a grain boundary between two particles (via the grain boundary itself or the lattice) or from dislocations within the particles (via the lattice). These transport paths correspond with 1, 2 and 6 above, and bring the centres of particles, C and C', closer together. They therefore result in densification. In comparison matter transport paths 3, 4 and 5 do not cause densification because they only involve the transport of matter from one place on the surface of the pore to another, although they can cause neck growth and hence strengthening of the

initial assembly of compacted particles. The net result is a change in shape of the pore but no change in its volume. Figure 32 shows that, as the pore is filled at point A, the length of the neck between the two particles grows. In addition to the transport paths identified on the previous page viscous and plastic flow may occur. Viscous flow is important in the sintering of glasses and other amorphous materials. The occurrence of plastic flow in crystalline materials during sintering, that is the transport of relatively large numbers of atoms by dislocation slip, is controversial (100). For plastic flow to occur, the stresses must be high enough for new dislocations to be generated. During sintering without the application of external pressure plastic flow will probably only occur in the very initial stages of contact formation.

Studies of the mechanisms of sintering have been made by using simple systems which can be treated theoretically and can also be observed in practice, such as that of a sphere of radius r on a plate. In this case it has been shown that the neck radius should obey the law (108,109):

$$\left(\frac{x}{r}\right)^n = \frac{kt}{r^m} \quad (7)$$

where t is time and k is a constant. m and n are also constants which vary with the mechanisms of matter transport as shown over the page:

<u>Mechanism</u>	<u>n</u>	<u>m</u>
viscous or plastic flow	2	1
evaporation/condensation	3	2
bulk diffusion	5	3
surface diffusion	7	4

Thus neck growth can be associated with the first stage of sintering and can be modelled relatively easily. Whereas the theories concerned with the second and third stages of sintering which occur when the porosity is below 15%, are controlled to a significant extent by the grain size of the system and their associated interfacial energies (101).

Apart from path 5 which involves vapour transport, the other paths all involve diffusion, via the pore surface, the grain boundaries or the lattice. Diffusion is thermally activated and the different diffusion paths have different activation energies as shown in Figure 33. The diffusion coefficient D can be described by the following type of equation (110-114):

$$D = D_0 \exp \left(- \frac{Q}{RT} \right) \quad (8)$$

where D_0 = pre-exponential factor

Q = activation energy

R = gas constant

T = absolute temperature.

Figure 33 indicates that the activation energy for surface diffusion is low compared to that of grain boundary and lattice diffusion, the reason for this being that surfaces tend to be regions of high disorder.

At low temperatures surface diffusion dominates, but as the temperature increases grain boundary diffusion predominates to be replaced by lattice diffusion at even higher temperatures. The change from one mechanism to the other depends on the cross-sectional area of the short-circuit paths (ie. grain boundaries and surfaces) available (100). For example, if a material has a large grain size and few internal pores, lattice diffusion will dominate down to relatively low temperatures because the number of short circuit paths is small. Whereas in a material of fine grain size, lattice diffusion will only be prevalent at relatively high temperatures due to the increased grain boundary area. The predominant diffusion path for a system can be predicted by the following equation (100):

$$D_{eff} = (1-F) D_L + FD_{gb} \quad (9)$$

and

$$F = \frac{2\delta}{G}$$

where D_{eff} = effective diffusion coefficient
 D_L = lattice diffusion coefficient
 D_{gb} = grain boundary diffusion coefficient
 F = area fraction of short circuit paths in a plane perpendicular to the direction of diffusion
 δ = grain boundary width
 G = grain size

Therefore, for grain boundary diffusion to predominate

$$FD_{gb} > (1-F) D_L$$

which indicates that the grain size must be small for this process to be significant.

2.11.4 STAGES OF SINTERING

The stages of sintering are described below (100):

STAGE 0: ADHESION

When two particles are placed in contact, interatomic forces draw them together and they deform elastically in the region of contact. In this stage the effect on the volume of porosity is negligible although a neck does form between the two particles.

STAGE 1: DIFFUSION CONTROLLED NECK GROWTH

In this stage, necks between particles grow by diffusion in response to the driving force for reduction in surface energy. As the neck grows, the driving force decreases. During this stage, some pores become 'closed', ie. not connected to the surface and the neck becomes a grain boundary.

STAGE 2: INTERMEDIATE

In this stage necks between particles are enlarged, pore channels close off and pores become spheroidal. There is little force for redistribution of material within pores but there still exists a significant driving force for the removal of pores from the system, and all open porosity disappears.

STAGE 3: FINAL

In the final stage the pores are spherical. Grain boundary migration can occur to minimise grain boundary energy, leaving pores isolated from grain boundary diffusion routes. Removal of such isolated pores is then relatively slow as transport must occur through the lattice. Therefore, if full density is to be achieved, it is important that grain boundary migration is avoided.

The final stages of sintering which involves the closure of isolated pores can be compared to the recovery of 5-16% porosity in 70/30 cupronickel castings. Therefore it is the final stage of sintering which is of particular interest.

2.11.5 THEORIES OF PRESSURE-LESS SINTERING

Theories of the kinetics of densification for the second and third stages of sintering emphasize the significance of grain boundary energy. The important aspects of these models are that pores shrink only when situated on grain boundaries, since they cease to shrink when isolated in the centre of a grain. Thus grain boundaries act as a sink for the vacancies of which the pores are composed, and it is grain boundary diffusion which is the principal mechanism of densification in these stages (98,115-117). Equations developed are of the form:

$$\frac{dP}{dt} = - C \frac{D\gamma v}{l^3 kT} \quad (10)$$

where P = porosity
 t = time
 D = diffusion coefficient
 v = volume of vacancy
 γ = surface energy
 l = measure of grain size
 C = constant
 k = numerical constant

These theories predict that sintering will continue until all porosity is removed in a finite time, although difficulty has been encountered in relating the values of the constants to the geometry of the powder compact.

Earlier sintering models were developed during the period 1940-1950 and proposed that the increase in density during sintering was dependent upon the ability of both amorphous and crystalline solids to deform like viscous fluids, with surface tension as the driving force and self diffusion as the mechanism of deformation. Such a model was developed by Frenkel (118), who predicted that viscosity could be represented by the following equation:

$$\eta = \frac{kT}{D} \Omega_o \quad (11)$$

where η = viscosity
 D = coefficient of self diffusion
 T = absolute temperature
 k = constant
 Ω_o = atomic volume

The mechanism of deformation of solids by viscous flow and the role of diffusion in the deformation of crystalline solids was elucidated further by Shaler (119,120), Nabarro (121) and Herring (122).

From the basis of the theory developed by Frenkel (118), Shuttleworth and Mackenzie (98) proposed a phenomenological theory of sintering by viscous or plastic flow which was to provide the foundation for many of the later theories of hot pressing, as reviewed by Ramqvist (123).

Mackenzie and Shuttleworth's model (98) consists of a body containing a random distribution of pores of uniform size as represented in Figure 34. Each pore of radius r_1 , can be assumed to be surrounded by a spherical shell of incompressible material to a radial distance r_2 . The relative density ρ of the body can be predicted by:

$$\rho = 1 - \left(\frac{r_1}{r_2} \right)^3 \quad (12)$$

The dense non-porous material of the body can be considered homogeneous and isotropic, and may be viscous (Newtonian) or plastic (Bingham body) as indicated in Figure 35. The difference between viscous and plastic flow is evident from this figure which shows that a plastic body has a yield stress τ_c , which must be exceeded before deformation begins. The shearing stress decreases with distance from the pore. Therefore during sintering interaction between individual pores is essential to the densification process, since if the shear stress in any region between the pores falls below the critical shear stress, no flow will occur.

The relationships between density and time derived by Mackenzie and Shuttleworth (98) for viscous and plastic flow under the influence of the surface energy of the pores are as follows:

Viscous flow of the Newtonian type

$$\frac{d\rho}{dt} = C \frac{\gamma^{n^{1/3}}}{\eta} (1-\rho)^{2/3} \rho^{1/3} \quad (13)$$

where ρ = relative density

γ = surface energy

η = viscosity

n = number of pores in unit volume of material

C = constant

and

$$C = \frac{3}{2} \left(\frac{4\pi}{3} \right)^{1/3}$$

Plastic flow of the Bingham type

$$\frac{d\rho}{dt} = \frac{3}{2} \left(\frac{4\pi}{3} \right)^{1/3} \cdot \frac{\gamma^{n^{1/3}}}{\eta_{\infty}} \cdot (1-\rho)^{2/3} \cdot$$

$$\rho^{1/3} \left[1 - a \left(\frac{1}{\rho} - 1 \right)^{1/3} \ln \left(\frac{1}{1-\rho} \right) \right] \quad (14)$$

and

$$a = \sqrt{2} \left(\frac{3}{4\pi} \right)^{1/3} \cdot \frac{\tau_c}{2\gamma\eta^{1/3}}$$

where η_{∞} = coefficient of viscosity

τ_c = yield stress

The theory of Mackenzie and Shuttleworth is based on a model consisting of closed pores in a homogeneous matrix and is valid for the final stages of sintering, where closed pores first appear at porosity levels less than 10%. However, the theory has been shown satisfactory agreement with experimental results for sintering stages even up to 35% porosity, where the pores are associated in the form of channels (123). Since the theory of Mackenzie and Shuttleworth is valid for the final stages of sintering, it is particularly relevant to the study of pore closure in castings containing approximately 10-16% porosity.

Ramqvist (123) found that:

$$n = \left(\frac{1-\rho}{\rho} \right) \frac{3}{4\pi} \frac{1}{r^3}$$

Use of the relationship between the pore radius and the number of pores per unit volume, together with equation⁽¹⁴⁾ allows the rate law for sintering to be rewritten as follows:

$$\left(\frac{d\rho}{dt} \right)_{p-o} = \frac{3}{2} \frac{\gamma}{\eta_{\infty} r} (1-\rho) \left[1 - \frac{\sqrt{2} \tau_c r}{2\gamma} \ln \left(\frac{1}{1-\rho} \right) \right] \quad (15)$$

2.11.6 THEORIES OF PRESSURE ASSISTED SINTERING

During the sintering of a powder compact under the application of an external pressure the initial stage of compaction, probably up to a relative density of 0.85, is a complex process of particle packing, sliding, fragmentation and deformation, and is not likely to yield to a theoretical analysis. The subsequent intermediate (connected porosity) and final (closed porosity) stages both involve a solid matrix with a definite pore system, and should be amenable to theoretical treatment, although only limited success has so far been achieved. A successful pressure-sintering theory would be valuable because:

- (i) it would enable experimental data for a given material to be extrapolated to predict results under changed conditions; and
- (ii) it would enable viscosity or diffusion data to be calculated, and so afford a means of assessing the results of changing the composition of the material being studied (101).

The present survey is restricted to theories which lead to practical densification equations that can be used by those seeking a mathematical fit to experimental data.

During pressure assisted sintering the principal driving force for the closing of pores is the applied hydrostatic pressure instead of the surface tension of the pores.

The total pressure acting on a pore (P) during the compaction of a porous solid body during hot pressing is:

$$P = P_s + P_e - P_i$$

where P_s = effective pressure due to surface tension

P_e = externally applied pressure

P_i = internal pressure in the pores

$P_e \gg P_s$, therefore P_s only becomes effective when the pore is small. If there is any gas contained in the pore, the internal pressure will oppose pore closure since P_i increases with an increase in the density of the component, and can eventually stop densification.

No real contribution to the theory of pressure sintering was made until after the publication of the Mackenzie and Shuttleworth plastic flow theory (98). This theory was extended to cover the application of an externally applied pressure by Murray et al (124), who assumed that the applied pressure was transmitted hydrostatically throughout the specimen. Therefore for pores of equal size, sintering will result in a decrease in their size, but the total number of pores n will remain constant. This assumption implies that the initial powder compact consists of spherical particles of equal size.

The basic equation of Mackenzie and Shuttleworth, equation ⁽¹⁴⁾, could be modified for the effect of external pressure by substituting $2\gamma/r + P$ for the surface tension term $2\gamma/r$, as shown over the page:

$$\frac{d\rho}{dt} = \frac{3}{2} \frac{\gamma}{\eta_{\infty} r} \left(1 + \frac{Pr}{2\gamma}\right) (1-\rho) .$$

$$\left[1 - a \left(\frac{1}{\rho-1} \right)^{1/3} \ln \left(\frac{1}{1-\rho} \right) \right] \quad (16)$$

where

$$a = \frac{\sqrt{2} \tau_c r}{2\gamma \left(1 + \frac{Pr}{2\gamma}\right)} \cdot \left(\frac{\rho}{1-\rho} \right)^{1/3}$$

Equation ⁽¹⁶⁾ can be rearranged as follows (123):

$$\left(\frac{d\rho}{dt} \right)_{P>0} = \left(\frac{d\rho}{dt} \right)_{P=0} + \frac{3P}{4\eta_{\infty}} (1-\rho) \quad (17)$$

Therefore hot pressing increases the sintering rate $(d\rho/dt)_{P=0}$ by the term $3P/4\eta_{\infty} (1-\rho)$.

The external pressure applied during hot pressing is much greater than the pore pressure in the material, and the yield stress, ie.

$$P \gg 2\gamma/r \quad \text{and} \quad P \gg \tau_c$$

Consideration of the above together with the terms in equation⁽¹⁷⁾ indicate that $(d\rho/dt)_{P=0} \ll 3P/4\eta_{\infty}(1-\rho)$, therefore equation⁽¹⁷⁾ can be simplified to produce equation⁽¹⁸⁾. Rewriting the law of hot pressing (124) is:

$$\frac{d\rho}{dt} = \frac{3}{4} \frac{P}{\eta_{\infty}} (1-\rho) \quad (18)$$

or integrated with respect to time:

$$\ln \frac{1-\rho}{1-\rho_0} = - \frac{3}{4} \frac{P}{\eta_{\infty}} t \quad (19)$$

where $\rho = \rho_0$ when $t = 0$

Many investigators have attempted to verify the hot pressing equations (equation⁽¹⁷⁾ and ⁽¹⁸⁾). Table 21 summarises the most important work regarding hot pressing in relation to the theory of Murray et al..

Mangsen et al (125), Vasilos (126) and, Jaeger and Egerton (127) all found good agreement between the Murray formula and experimental data for the hot pressing of Al_2O_3 powder, silica and refractory materials. However Lersmacher and Scholz (128) indicated that the plastic flow theory can describe the early stages of hot pressing but found that deviations occur at longer times and particularly at higher temperatures. They also concluded that the density after long sintering times (eg. 1 hour) does not continuously increase with temperature. Instead there is a maximum density at a specific temperature as illustrated in Figure 36. That a minimum density occurs at a given temperature is related to grain growth during sintering (123).

Many investigators have found that the initial sintering rate during hot pressing is often greater than that predicted by the plastic-flow equation, and that equation⁽¹⁸⁾ would not explain the observed end point density (123,128,129).

McClelland (129), believed that the pressure which is effective in closing the pores would not be equal to the applied external pressure, and that P could not remain constant during hot pressing. On account of the presence of voids which change their size during hot pressing, the

VOL 1

DX 97460. Page count TOTAL 522
Batch number 628

Comments:

INSTITUTION COPY

Institution CNAA (SHEFFIELD CITY POLYTECHNIC)

Thesis by KING, S.

We have assigned this thesis the number given at the top of this sheet.

CNAA has been notified, and will pass the information on to ASLIB on your behalf so that it can be published with the relevant abstract in their *Index to Theses with Abstracts*.

THE BRITISH LIBRARY
DOCUMENT SUPPLY CENTRE

British Thesis Acquisitions

T3-16 B

area through which the pressure is transmitted increases with density. Thus the effective pressure for closing porosity is a function of porosity. McClelland also assumed that the effective area through which the pressure is transmitted is equal to the spherical shell in the Mackenzie and Shuttleworth (98) model, Figure 34, where the pressure is applied on an area consisting of the sum of the shell and the pore. The ratio of the effective area (A_E) to the total area (A_T) (129) is therefore:

$$\frac{A_E}{A_T} = 1 - \left(\frac{r_1^2}{r_2^2} \right) \quad (20)$$

However from the Mackenzie and Shuttleworth model the mean density of a pore plus its associated dense material region equals the density of the compact. Hence:

$$\rho = 1 - \left(\frac{r_1^3}{r_2^3} \right)$$

Therefore using this expression the effective pressure in closing the pore is:

$$P_E = P[1 - (1 - \rho)^{2/3}] \quad (21)$$

Replacing $2\gamma/r_1$ in equation ⁽¹⁵⁾ (123):

$$\frac{d\rho}{dt} = \frac{3P}{4\eta_\infty} (1 - \rho) \cdot \left[\frac{1}{(1 - (1 - \rho)^{2/3})} - \frac{\sqrt{2} \tau_c}{\rho} \ln \left(\frac{1}{1 - \rho} \right) \right] \quad (22)$$

McClland found that during experimental investigations a final density (ρ_f) is reached which is considerably lower than that of the theoretical density. At the final density attained the rate of densification is essentially zero. This can only occur if the term $1/(1-(1-\rho_f)^{2/3})$ is equal to zero. The equation containing the variables which effect the density attainable is shown below:

$$1-(1-\rho_f)^{2/3} \cdot \ln \frac{1}{(1-\rho_f)} = \frac{P}{\sqrt{2} \tau_c} \quad (23)$$

Since τ_c is temperature dependent, the final attainable density is both temperature and pressure dependent. Therefore if the yield stress at temperature is known then the final density can be evaluated. In addition, if the final density at a given pressure is known, then the pressure dependence of the final density can be determined.

In many applications the variation of the final density with temperature is required. Temperature can be varied by the critical yield stress as shown below:

$$\tau_c = A \exp - (Q/RT) \quad (24)$$

where A = constant

Q = activation energy

R = gas constant

T = absolute temperature

Combining equation ⁽²⁴⁾ with equation ⁽²³⁾ predicts an expression for the temperature dependence of the end point density:

$$\frac{1}{T} = \left(\frac{-R}{Q} \right) \cdot (\ln [(1-(1-\rho)^{2/3}) \ln (1-\rho)] + b) \quad (25)$$

Using these equations McClland presented data on the hot pressing of beryllium oxide for pressing conditions of 1200-1700°C, 1000-2000psi and 15-240 minutes.

It must be noted that McClland (129) whilst introducing an effective pressure function disregards one of the basic assumptions of the Mackenzie and Shuttleworth theory (98), which implied a hydrostatic pressure distribution.

Koval'chenko and Samsonov (130) derived an alternative equation from the Mackenzie and Shuttleworth model which is not unlike that derived by Murray et al (equation ¹⁸).

$$\frac{d\rho}{dt} = \frac{\sigma Q}{4\eta_{\infty}} \frac{(3-P)}{(1-2P)} \quad (26)$$

where ρ = relative density

Q = fractional porosity ($Q=1-\rho$)

σ = applied pressure

η = viscosity at infinite strain rate

t = time

Equation ⁽²⁶⁾ was modified to introduce a correction factor for grain growth during sintering (130), as reviewed by Ramqvist (123):

$$\frac{dQ}{dt} = \frac{P}{4\eta_o (1+bt)} \cdot \frac{Q(3-Q)}{1-2Q} \quad (27)$$

where $\eta = \eta_o$ for $t = 0$

or integrated with respect to time:

$$\begin{aligned} \frac{P}{4\eta_o b} \ln (1+bt) &= \ln \frac{(3-Q_o)^{5/3}}{(3-Q)^{5/3}} \cdot \frac{Q_o^{1/3}}{Q^{1/3}} = F(t) \\ (1+bt)^{P/4\eta_o b} &= \frac{(3-Q_o)^{5/3}}{(3-Q)^{5/3}} \cdot \frac{Q_o^{1/3}}{Q^{1/3}} \end{aligned} \quad (28)$$

where $Q = Q_o$ for $t=0$

Q = Fractional porosity ($Q = 1-\rho$)

B = Constant

P = External pressure

Equation ⁽²⁸⁾ has been simplified by Scholz and

Lersmacher (131) to give a form directly comparable with

that of Murray et al (124), equation ⁽¹⁹⁾, which indicates a relationship between two material constants η and ξ :

$$\xi = \frac{4}{3} \eta \frac{(1-aQ)}{Q} \quad (29)$$

where a = constant

Substituting the expression for ξ into the equation derived

by Koval'chenko and Samsonov (130) as shown below:

$$\frac{dQ}{dt} = - \frac{P}{4\eta} \frac{Q(3-Q)}{(1-2Q)}$$

allows the pressure sintering rate law to be rewritten:

$$\frac{dQ}{dt} = - \frac{3P}{4\eta} \frac{(1-Q)Q}{(1-aQ)} \quad (30)$$

or, for $a = 1$

$$\frac{dQ}{dt} = - \frac{3P}{4\eta} Q$$

which agrees with the theory of Murray et al (124), equation (18).

Pressure sintering finds its greatest use with ceramic materials, but unfortunately most ceramics do not deform as viscous or Bingham solids. Attempts to describe the pressure sintering behaviour of materials which deform by vacancy diffusion have been influenced by work by Herring (124), on the diffusional viscosity of polycrystalline solids.

One such model developed is that by Fryer (132,133) which represents the final stage of sintering ie. closed pore sintering:

$$\frac{d}{dt} \left(\frac{P}{\rho} \right) = - z \frac{\sigma D \Omega}{l^2 kT} \left(\frac{P}{\rho} \right)^{5/3} \quad (31)$$

and when integrated with respect to time:

$$\left(\frac{P}{\rho} \right)^{2/3} = \frac{2}{3} \left(\frac{2}{l^2} \right) \frac{D \Omega \sigma t}{kT} + \text{constant}$$

where z is a constant.

This equation was found to work very well with data for the pressure sintering of alumina between relative densities of 0.87 and 0.96. This is really the intermediate range of densities when porosity is continuous, and not the final stage for which the equation was derived. However, there were various errors in the theoretical derivation, and

equation ⁽³¹⁾ can be regarded as being semi-empirical, and is the one of the most useful theories so far developed for describing diffusion controlled sintering (101).

Ramqvist (123) has reviewed the theories of pressure assisted sintering and the models involved are summarised in the form of a flow diagram in Figure 37, which involves models which represent flow mechanisms, diffusion, corrections for grain growth and empirical formulae.

2.12 HOT ISOSTATIC PRESSING

Blaise Pascal (1623-1662), proposed a law to the effect that "pressure applied to a confined fluid at any point is transmitted through the fluid in all directions, and acts upon every part of the confining vessel at right angles to its interior surfaces and equally upon equal areas" (134).

It is the application of Pascal's law that allows powder/particulate matter, contained in a flexible bag or envelope, to be densified under pressure acting through a suitable pressure transmitting medium. The pressure acts equally over the surface of the envelope, which being flexible squeezes the powder uniformly to a compact, whose external geometry is smaller than, but of similar shape to that of the original envelope.

2.12.1 DEFINITION OF ISOSTATIC PRESSING

Figure 38 schematically distinguishes isostatic pressing from unidirectional pressing. In the latter, Figure 38(b) the pressure is applied along a single axis by a ram. The pressure is transmitted by the contact surfaces of the ram and the restraints of the die wall. However, friction exists between the component and the die wall, which contributes to produce non-uniform densification. Isostatic pressing involves no rams or dies and thus eliminates frictional forces. Therefore the pressure is applied uniformly on all surfaces as indicated in Figure 38(a) (100).

Isostatic pressing can be carried out at ambient or elevated temperatures. Compaction of powders at room temperature is known as cold isostatic pressing (CIP), and the powders are further consolidated by a high temperature sintering operation. In contrast the application of pressure at elevated temperatures is referred to as hot isostatic pressing (HIP), and involves the simultaneous application of high temperatures and pressures. Thus HIPping combines the two processes of compaction and sintering in one operation.

The pressure transmitting medium in CIP is usually a fluid such as an oil-water emulsion (ratio of 1:40), and the powder to be compacted is contained within a flexible rubber or polymer bag/envelope. This envelope can either be fixed inside the pressure vessel, or the envelope can be filled with powder external to the vessel, which is then sealed and placed within the vessel for pressing. CIP equipment can be categorized as follows (134):

- (i) fixed bag or dry tooling;
- (ii) wet bag or free mould tooling;

both of which are illustrated in Figure 39.

In comparison the pressure transmitting medium in HIPping is a gas, usually argon or nitrogen.

Hot isostatic pressing is the process used for the recovery of 70/30 cupronickel castings containing shrinkage and microporosity, and the design of a system for this is described in the next section.

2.12.2 DESIGN OF A HOT ISOSTATIC PRESSING SYSTEM

There are two principal types of pressure vessel (100):

- (i) Forged monolithic vessels.
- (ii) Wire wound vessels.

The latter are made by winding high-strength alloy steel wire around a liner, so that the liner is always in a state of compression. A similar wire-winding operation is utilised in the construction of the enclosing yoke assembly as shown schematically in Figure 40.

The HIP system consists of five major components which are listed below (134,136-142) and shown in Figure 41.

- (i) Pressure vessel
- (ii) Internal furnace
- (iii) Gas handling facilities
- (iv) Electrical systems
- (v) Auxiliary systems

The correct design of the pressure vessel including the furnace and the mantle is of great importance to ensure uniformity of temperature, and rapid heating with minimum risk of temperature gradients between the outside and centre of the stock.

HIP systems range in size from 27mm to 1524mm diameter and can be categorized as follows:

- (i) Research equipment: 75-200mm diameter, maximum pressure capability of around 200MPa and temperatures of 2000°C.
- (ii) Production equipment: 250-1400mm diameter, and rated at 2200°C and 200MPa.

Production equipment has typical work-piece volumes of the order of $0.05\text{--}2.5\text{m}^3$, although most HIP systems have a working volume less than 1m^3 (134). Two factors influence the size of the equipment required:

- (i) Capital cost.
- (ii) Productivity (return of investment).

The work-piece volume determines the size and cost of the HIP unit and has a direct effect on the furnace type. High temperature usage (up to 2000°C) also increases costs due to the need for high quality materials which often require complex fabrication techniques. Most high temperature furnaces are constructed from graphite (134).

Productivity depends on the selection of the correct HIP system for specific applications. A well designed and proven system should yield a return investment within five years (134).

2.12.3 APPLICATIONS OF HOT ISOSTATIC PROCESSING

The HIP process was initially developed as a means of diffusion bonding nuclear reactor components, and for the removal of porosity in hard metals. Today HIPped parts are used in a wide range of industrial applications including aerospace, marine and off-shore power generation, together with specialist fields such as automotive, medical, defence, telecommunications and mining (100,134,138,140 and 143). Typical specific applications of HIPping include:

- (1) Forming near net shapes from metal, ceramic and cermet powders.
- (2) Densification of metal and ceramic powder compacts.

- (3) Densification of cemented carbides for the removal of internal flaws (144).
- (4) Diffusion bonding of similar and dissimilar materials (145).
- (5) Producing tool steels, titanium alloys and superalloys which are difficult to fabricate by conventional forming processes (134,146,147).
- (6) Cladding base materials with wear resistant and corrosion resistant materials (148).
- (7) Pressure oxidation of silicon for the semi-conductor industry.
- (8) Hot isostatic pressing impregnation of carbon (HIPIC), which involves mixing carbon fibres and carbonaceous binders such as pitch which are then HIPped to shape.
- (9) Impregnation of a porous structure with molten metal for bearing applications such as porous cast iron impregnated with brass.
- (10) Gas encapsulation: encapsulation of noble gases in a ceramic matrix. This process is used to immobilise radioactive gases such as krypton.
- (11) Sinter hot isostatic pressing (sinter and porosity elimination in one operation) (134,149).
- (12) Correction of casting faults including internal and surface-connected porosity (150-155).

It is this last application which is of interest and will be discussed in detail in the next section.

HOT ISOSTATIC PROCESSING

The use of castings in engineering applications is restricted by the difficulties encountered in producing structural parts of high strength free from defects, such as porosity and microshrinkage. Even if the presence of cavities and internal cracks do not lead to the rejection of castings, they significantly reduce strength, fatigue and creep life in comparison with wrought alloys (154,156,157).

Defects that arise in castings are mainly due to (134,158);

- (i) Non-metallic inclusions as a result of damage during pouring/filling operations.
- (ii) Shrinkage as the material cools through the liquid to solid transition. The last liquid to solidify is often that contained between the dendrite arms, and as the molten metal solidifies it contracts, so producing a cavity as illustrated in Figure 42. Solidification defects found in castings include shrinkage cavities and hot tears.
- (iii) Gaseous defects. Gases such as hydrogen tend to be more soluble in the molten metal than in the solid (100). Therefore as solidification occurs, gas bubbles tend to be formed at the solidification front. If solidification occurs rapidly, there is insufficient time for the gas to escape through the remaining liquid, and pores remain trapped in the solid.

Gas bubbles may also be formed by reaction between the molten metal and the refractory mould material, or the moisture contained within the mould material. Such gaseous

defects give rise to microporosity and blow holes in solidified castings.

The size and number of casting defects can be reduced if good foundry procedures are followed. However, zero porosity in castings is almost impossible to achieve.

Until 1960 there was no economical method of repairing castings containing internal porosity. Repair consisted of cutting out the defective areas and then filling with weld metal (158). Subsequent X-ray penetration examination determined if the repair was successful or not. This process is extremely labour intensive, is often prone to failure at the first attempt, and develops an area of material of nominally different grain size and composition at the surface of the component. Such an area can suffer severe galvanic corrosion in sea water. In addition, the Naval Engineering Standard NES 824 (24) which is applicable to Class I castings, ie. castings which contain less than 5% porosity, restricts the use of weld repair on areas which are to be wetted by sea water. Hence an alternative method of defect repair is required such as HIPping, which has been practised as a recovery process for other metal and alloy castings since 1970 (134). The removal of defects by HIPping introduces no new material, and is rapidly proving cost effective particularly for large cast parts.

2.12.5 FACTORS AFFECTING THE ELIMINATION

OF CASTING DEFECTS

The type of defect present can influence the ability of the HIP process to recover castings. Factors affecting pore removal include (159):

- (1) Free surface endogeneous and exogeneous solidification.
- (2) Oxide films which separate internal surfaces.
- (3) Pores and micro voids filled with insoluble gas.
- (4) Large amounts of surface connected porosity.
- (5) Permeable crack like connections between voids and the high pressure gas medium.
- (6) A high content of brittle non-metallic inclusions.
- (7) Asymmetrical collection of higher volume deficits.
- (8) Formation of unwanted phases during HIPping.
- (9) Need for high quality surface finish and close dimensional tolerances.
- (10) Insufficiently prepared or unclean compressed gas.

Figure 43 illustrates some of the problems encountered during the elimination of pores, of different geometry and variation in location within a casting, in respect to the casting surface.

2.12.6 SHAPE CHANGE DURING HIPPING

When a powder is consolidated by HIPping, the final shape differs from that of the preform in which it was packed (160). The factors which influence this shape change also influence those of a solid-porous body and include:

- (i) Constraint by the preform produces non-uniform densification.
- (ii) Formation of density gradients.

Figure 44 illustrates the effect of density gradients. In Figure 44(b) the surface has densified before the centre, and the dense skin can support a load particularly at its corners. In extreme cases, the inward displacement of the surface is proportional to its distance from the mid planes of the sample. The presence of such density gradients transforms a rectangular bar into a dog bone shape as densification proceeds (Figure 45).

The most common cause of a density front is a temperature gradient. If the pressure is applied to the sample first and the temperature second, a temperature gradient exists through it. It has been found that when the densification rate is greater than a characteristic heat flow time, densification gradients develop and produce large changes in shape (161). Figure 45 shows two identical samples of tool steel, one was heated prior to pressing which gave an almost uniform temperature. The other was heated and pressed simultaneously, producing temperature gradients and a severe shape change.

2.12.7 THE EFFECT OF HOT ISOSTATIC PROCESSING

PARAMETERS ON DENSITY

Densification does not occur under all processing conditions, since void closure is a function of temperature, pressure and time; of these temperature has been discovered to be the most influential since pressure has relatively little effect once above a critical level (162).

2.12.7.1 FORCES PRESENT DURING ISOSTATIC PRESSING AND THEIR INFLUENCE ON VOID CLOSURE DURING DENSIFICATION

There are two driving forces for pore closure during the compaction of a porous solid body subjected to isostatic pressing (113,163,164):

- (i) Surface tension.
- (ii) Externally applied pressure.

The surface tension produces an effective pressure (P_s):

$$P_s = \frac{2\gamma}{r}$$

P_s only becomes effective when the pore is small ($r < 1000$ angstroms).

The total pressure acting on a pore (P) is given by:

$$P = P_s + P_e - P_i$$

2.12.7.2 VOID CLOSURE DURING DENSIFICATION

If the pressure (P) exceeds the yield stress of the material at the HIPping temperature the stresses generated allow densification by instantaneous plastic yielding, dislocation and diffusional creep and by particle sliding (111,163,165).

2.12.8 IMPROVEMENT OF MECHANICAL PROPERTIES BY HOT ISOSTATIC PRESSING

It is well known that the mechanical properties of sand cast metals and alloys are inferior to those of comparable wrought alloys (166). The closure of internal voids during HIPping and the subsequent improvement in mechanical properties is well documented (140,150,151,167), in various metal systems including copper based casting alloys (168), aluminium (169), alloy steels (170), niobium stabilised stainless steel (154,171), 5% Cr die steels (169), carbon steel (172), titanium castings and superalloys (134, 153 and 156).

2.12.8.1 CREEP AND STRESS RUPTURE RESISTANCE

The improvement in stress rupture properties of superalloy castings after HIPping is summarised in Table 22. HIPping significantly reduces the scatter of properties and improves the properties of castings with no detectable defects (134,168).

2.12.8.2 TENSILE STRENGTH AND DUCTILITY

HIPping only marginally improves the proof-stress and ultimate tensile strength of a material, but reduces the scatter in mechanical properties (134,168,173), as shown for Inconel 718 (174) and Rene 120 (175) in Tables 2 and 3 respectively. These results show an improvement in ductility of around 60%.

2.12.8.3 FATIGUE RESISTANCE

Fatigue studies (175) have shown that under both low cycle (0.17Hz) and high cycle (30Hz) fatigue of a titanium alloy, HIPped specimens produce longer fatigue lives as shown in Figures 46 and 47. These results indicate an improvement in the number of cycles to failure for HIPped material compared to unHIPped material at a constant stress.

In addition HIPping increases the fatigue life of steels by 50-70%, and the fatigue life of HIPped material is significantly higher than that obtained on cast material(167,172).

2.12.8.4 OTHER ADVANTAGES OF HOT ISOSTATIC PRESSING

The removal of porosity can influence the weldability of a material, since porous material is difficult and often impossible to weld. Hence HIP can facilitate manufacturing processes and often prevent part rejection (134). In addition HIPping has been reported to improve the corrosion resistance due to the homogenisation of the cast microstructure which reduces the potential sites for galvanic corrosion (176,177).

The specific improvements achieved after HIP vary with the material/alloy, but in general terms the following can be expected (168):

Tensile Strength	-	5 - 15% increase
Yield Strength	-	5 - 10% increase
Ductility (%El)	-	50% increase
Fatigue Life	-	3 - 10 fold increase

Probably more important than any of the above individual improvements is the low degree of data scatter which is characteristic of HIPped castings. This increase in product consistency is crucial from a designers point of view, allowing HIPped castings to be used with increased confidence, and the full performance potential of the material to be approached. Therefore the need to apply a casting factor to designs incorporating cast components is eliminated (168).

2.13 THE STAGES OF DENSIFICATION

The early development of quantitative relationships between density and processing parameters involved the study of sintering of compacted powders.

HIPping is a continuous process and in order to simplify the mechanisms of densification it is convenient to break down the sintering process into three stages as illustrated in Figure 48. The first stage (stage 0) describes the density reached by the packing of the loose powder. The second (stage 1) describes the early phase of densification, while the porosity is still connected. The final stage (stage 2) describes the final densification,

when the residual porosity is in the form of small holes.

2.13.1 STAGE 0 - POWDER PACKING

The initial packing density is dependent on the particle shape, size distribution, and the extent to which surface and frictional forces prevent rearrangement.

An applied pressure (P) causes rearrangements which affect the packing density (D) in the following manner (160):

$$D = A \log P + C$$

where A and C are constants.

2.13.2 STAGE 1 - NECK GROWTH

During this stage necks grow at contact points between particles. The mechanisms which contribute to neck growth are: plastic yielding, creep and diffusion. At high pressures plastic yielding and creep dominate, whilst at lower pressures densification involves various diffusion mechanisms.

The important characteristics in regards to modelling stage 1, are that the necks which form are discrete so they can be treated as being separate. In addition, the porosity is interconnected which allows any gas in the pore to escape and also allows diffusion along grain boundaries.

2.13.3 STAGE 2 - FINAL DENSIFICATION

By this stage the necks have grown until they impinge producing individual spherical pores at a relative density of around 0.92 (180). From a modelling point of view the material can be considered as a solid containing isolated spherical or polyhedral voids connected by grain boundaries. Grain growth may detach the boundaries from the pores or may drag the pores together (160,178). If the grain boundaries are no longer in contact with the pores, the normal diffusion process can no longer cause densification. Hence an applied pressure is required to reduce the size of the pores. Thus, this third stage of sintering/densification can be compared to the pore closure in castings.

2.14 MODELLING OF DENSIFICATION

In this section the geometry of the powder compact and the mechanisms by which it may densify are considered, leading to the development of densification rate equations which will be discussed in this and the following section.

2.14.1 STAGE 1 - RELATIVE DENSITY < 0.92

If it is assumed that the powder particles are spherical and of single size, then the increase in the number of contact neighbours and the growth of the average contact area can be modelled by considering the spherical particles to grow in radius around fixed centres (160,178), as shown in Figure 49. As densification proceeds the degree of overlap of a given particle with its neighbours increases,

so that the contact area between particles grows as shown in Figure 50. It has been shown that the number of neighbours per particle, Z increases in a linear way with relative density D (110):

$$Z = 12 D \quad (32)$$

Z increases from a value of 7.7 at the start of HIPping (assuming random packing for which $D_o = 0.64$) to a value of 12 when full density is reached.

The average area a , of a contact can be approximated by the following equation (178):

$$a = \frac{\pi}{3} \left[\frac{D-D_o}{1-D_o} \right] R^2 \quad (33)$$

where R = Particle radius

D_o = Initial relative density

D = Relative density

Equations for the neck radius x , can also be derived:

$$x = \left(\frac{a}{\pi} \right)^{1/2} = \frac{1}{\sqrt{3}} \left(\frac{D-D_o}{1-D_o} \right)^{1/2} R \quad (34)$$

The total contact area per particle, normalised by the surface area is given by :

$$\frac{aZ}{4\pi R^2} = \frac{D(D-D_o)}{(1-D_o)} \quad (35)$$

In addition the curvature of the neck ρ , is given by:

$$\rho = \frac{x^2}{2(R-x)} \quad (36)$$

or can be approximated by (110):

$$\rho = R(D-D_o) \quad (37)$$

If an external pressure P is applied to the compact with a relative density D , and co-ordination number Z , the average contact force f (106), is given by:

$$f = \frac{4\pi R^2}{ZD} P \quad (38)$$

The contact force produces a contact pressure, P_{eff} , on each particle contact of:

$$P_{eff} = \frac{f}{a} = \frac{4\pi R^2}{aZD} P \quad (39)$$

Combining equation⁽³⁹⁾ with equations^(32 and 33) produces:

$$P_{eff} = \frac{P(1-D_o)}{D^2(D-D_o)} \quad (40)$$

The surface energy γ of the particles provides an additional driving force for densification. However, when the applied pressure P is large, such as during HIPping, the contribution of surface tension can be neglected; but when P is small or absent such as occurs during sintering, the surface energy is the driving force for densification. Therefore during the HIPping experiments carried out on 70/30 cupronickel, densification due to γ can be assumed to be negligible.

2.14.2 STAGE 2 -> 0.92 RELATIVE DENSITY

At relative densities above 0.92 the pores become isolated and are assumed to be spherical, equal in size and evenly distributed. The pore radius r can be obtained by the following equation (113):

$$r = R \left(\frac{1-D}{6D} \right)^{1/3} \quad (41)$$

At this stage the effective pressure P_{eff} is:

$$P_{eff} = P + P_s - P_i \quad (42)$$

The surface energy pressure P_s is found from

$$P_s = \frac{2\gamma}{r} \quad (43)$$

The internal pressure in the pores P_i , increases with density and can eventually stop densification completely.

This internal pressure is given by:

$$P_i = P_o \frac{(1-D_c)D}{(1-D)D_c} \quad (44)$$

where P_o = Out gassing pressure

D_c = Critical density at which the pores close.

2.15 DENSIFICATION RATE EQUATIONS

When a pressure is applied to a powder compact during stage 1 of the densification process, the necks which develop between the particles can grow by plastic yielding, by power law creep or by diffusion (111,165,179 and 180). Therefore in order to model densification and predict a densification rate D' , equations for all the above mechanisms must be involved. Figure 51 schematically illustrates the models on which the densification rate equations are based for stage 1 and stage 2 of densification during HIPping.

2.15.1 PLASTIC YIELDING

(1) STAGE 1

When a pressure is applied to a powder compact it will first deform by plastic yielding. This causes the average contact area a , to grow and the effective pressure (equation³⁹) to fall to the yield stress. This instantaneous yielding occurs prior to densification by time dependent mechanisms. Therefore the densification by time dependent mechanisms starts from the density produced by instantaneous plastic yielding. This starting density is given by (160,178).

$$D_{yield} = \left[\left(\frac{1-D_o}{1.3\sigma_y} \right) P + D_o^3 \right]^{1/3} \quad (45)$$

(2) STAGE 2

The powder compact will only enter the final stage of densification/sintering if the external pressure is high enough to cause yielding of the spherical shell surrounding each pore. If instantaneous yielding causes densification to enter stage 2 of the densification process, then the starting density for time dependent mechanisms is given by:

$$D_{yield} = 1 - \exp \left[\frac{-3P}{2\sigma_y} \right] \quad (46)$$

2.15.2 VOLUME DIFFUSION

In a similar manner to the previously described equations for plastic yielding, densification rate (\dot{D}) equations for time dependent mechanisms during stage 1 and 2 can be predicted (178) as shown below:

(1) STAGE 1

$$\dot{D} = 43C(1-D_o) \frac{D_v}{R_2} \frac{(P-P_o)\Omega}{kT} \quad (47)$$

(2) STAGE 2

$$\dot{D} = 270(1-D)^{1/2} \left[\frac{1-D}{6} \right]^{1/3} \frac{D_v}{R^2} \frac{(P-P_i)\Omega}{kT} \quad (48)$$

2.15.3 BOUNDARY DIFFUSION

(1) STAGE 1

$$D \cdot = 43 C^2 \frac{\delta D_B}{R^3} \frac{(P-P_O) \Omega}{kT} \quad (49)$$

(2) STAGE 2

$$D \cdot = 270 (1-D)^{1/2} \frac{\delta D_B}{R^3} \frac{(P-P_i) \Omega}{kT} \quad (50)$$

2.15.4 POWER LAW CREEP

(1) STAGE 1

$$D \cdot = \frac{3.1}{C^{1/2}} D_{crp} D \left(\frac{C(P-P_O)}{3 \sigma_o D^2} \right)^n \quad (51)$$

(2) STAGE 2

$$D \cdot = 1.5 D_{crp} D (1-D) \left[\frac{1.5}{n} \frac{(P-P_i)}{\sigma_o} \frac{1}{(1-(1-D)^{1/n})} \right]^n \quad (52)$$

where

$$D_v = D_{ov} \exp - \frac{Q_v}{RT}$$

$$\delta D_B = \delta D_{OB} \exp - \frac{Q_B}{RT}$$

$$D_{crp} = 10^{-6} \exp - \frac{Q_{crp}}{RT} \left(\frac{Tm}{T} - 2 \right)$$

$$C = \frac{1-D_o}{D-D_o}$$

$$P_i = \left[\frac{1-D_c}{1-D} \right] \frac{D}{D_c} P_o$$

Nomenclature and units for these equations are shown in Table 25.

2.16 HOT ISOSTATIC PRESSING MAPS

The densification rate equations discussed previously contain all the information required to predict densification during HIPping. However, the equations are not easy to evaluate and because some of the parameters that enter them, particularly material properties such as diffusion coefficients, are uncertain, they are best calibrated against experimental data. This together with the presentation of the results in a useful form is made difficult by the large number of superimposed mechanisms, and the even larger number of variables on which they depend.

This data is most easily assessed in the form of densification or HIP maps as originally developed by Ashby (110,160,178), such as the one shown for copper in Figure 52 (a) and (b).

The densification rate equations have been integrated, summing contributions from each mechanism to predict the density D , after time t at pressure P and temperature T . The diagrams show contours of constant time, indicating the density reached after that time at a given temperature and pressure. The heavy lines block out fields in which a given mechanism is dominant.

Software is available (178), designed for use with IBM XT, AT or equivalent which constructs HIP diagrams using the equations previously described.

The calibration of Ashby's densification rate equations (181), can be carried out using experimental viscosity data which determines the amount of densification due to creep and diffusional mechanisms. This is the same data used to predict pore closure during pressure assisted sintering as derived by Mackenzie and Shuttleworth (98).

2.16.1 APPLICATIONS OF HIP MAPS

The applications of HIP maps include (160,178):

- (1) Calibration of the individual rate equations in order to predict the amount of densification due to creep and diffusion mechanisms.
- (2) Prediction of the effect of change in particle size, initial density or material properties.
- (3) Identification of the conditions necessary to achieve HIPping in a certain time and to a specific density.

2.17 ALTERNATIVES TO HOT ISOSTATIC PRESSING

There are several technologies which are being developed to offer alternatives to hot isostatic pressing (HIPping) for consolidation of powder metal parts. These processes are referred to as pseudo-HIP processes in that they attempt to approximate isostatic pressure distribution using conventional pressing equipment during consolidation. Such pseudo-HIP processes include (182):

- (i) Ceracon process
- (ii) Rapid Omnidirectional Compression (ROC)
- (iii) STAMP process

The process of main interest is the ceracon process because it utilises a granular ceramic medium as the pressure transmitting medium. Thus, it relies on a granular ceramic medium to transfer pressure from an advancing ram of a press to a powder metal preform. The patents rights to the Ceracon process are held by Metal Alloys Inc. It is the type of ceramic medium used at high processing temperatures that is of major interest to the present investigation, but first of all some background on densification by the Ceracon process will be given.

2.17.1 THE CERACON PROCESS

A schematic illustration of the Ceracon process is shown in Figure 53. A porous preform is prepared by either cold pressing, injection moulding, direct sintering or slip casting. The preform is then heated to the temperature for consolidation in a controlled atmosphere. Simultaneously, a ceramic granular medium is heated to the same temperature in a fluidised bed furnace. The heated ceramic grain is charged into a simple ring die and the heated preform is inserted into the hot ceramic as shown in Figure 53.

Alternatively, preform(s) can be loaded into the ceramic grain while cold and heated in place. The preform should be totally surrounded by the ceramic grain, which is the pressure transmitting medium (PTM) (182,183). The heated assembly is transferred to the consolidation press and placed in a die container ring. An axial load is applied

to the ceramic grain by a moving ram. As the axial load is applied to the ceramic grain, the preform experiences both axial and lateral components of force. Densification and deformation of the preform result, with 100% densification being achieved by the selection of the optimum processing variables (184). The cycle time under pressure is a matter of seconds, with the ram being retracted once the desired load has been achieved. Alternatively, a dwell time under load can be accommodated. After consolidation, the ceramic granular medium and fully dense part(s) are separated by the use of a shaker table. The near-net shape part or group of parts can then be finished to final shape and the ceramic grain recycled (182).

Over the last 10 years both the powder metallurgy and ceramic industries have seen a prolific out growth of pseudo-HIP consolidation techniques. For the most part they briefly flourish, dwindle, and in most cases never regain the foothold they once held (185). The Ceracon process however is becoming a prominent contributor to pseudo-HIP technology. Patents for the Ceracon technology date back to 1967 and cover the basic consolidation concept utilising a ceramic grain. More recent patents cover a myriad of improved and modified processes, total production systems, pressure transmitting media and materials processed by the technology (185,187-195).

Several major technical advances have occurred over the past two years which are directly responsible for the phenomenal growth and acceptance of the Ceracon technology.

First and foremost was the development of a totally new PTM (pressure transmitting medium) to replace the older and less effective ceramic grain. This new PTM is a spherical, carbonaceous particle. It has compressive properties such that during consolidation it forms a flexible envelope around the preform, effectively transmitting the axially applied load to the preform surfaces. After consolidation the PTM relaxes and completely detaches itself from the preform.

The ever present problem of ceramic grain fusion during consolidation, and the subsequent need to "break out" the consolidated preform has been totally eliminated with the use of the new carbonaceous medium (185).

The second advance in technology involves improved dimensional control and repeatability of tolerance (185).

2.17.2 CERACON PROCESS: PRESSURE TRANSMITTING MEDIA

Literature published by the Gorham Advanced Metals Institute claims that 21 United States and 14 foreign patents relating to the Ceracon process have been published. A search of the United States Patents Index between 1967 - 1989 has indicated that many of the patents are duplicated and are listed under the same patent number but refer to a separate identity code. In addition the Patent Index is published twice yearly and as a consequence many of the patents dated May - June are reported in the July - December index.

A search of the US Patent Index with respect to the Ceracon process and with particular interest in the ceramic grain and carbonaceous pressure transmitting medium identified

nine patents (186-194) as shown in Table 26. Two of the patents listed: US 3 356 496 December 1967 (186) and US 3 689 259 September 1972 (187), make specific reference to the ceramic grain PTM.

Usable refractory grain materials can be characterised as comprising any of or mixtures of, the ceramics, refractory compounds, carbon and graphite. The term ceramic includes chemically combined metal compounds such as metallic oxides of silicon, aluminium, barium, calcium, magnesium, thorium and zirconium; as well as complex oxides such as combinations of silicon, calcium or magnesium oxides. In addition ceramics encompass metallic sulphates of barium or calcium, aluminates of calcium or magnesium, silicates of aluminium, calcium or zirconium and fluorides such as calcium fluoride. The term refractory compounds includes high melting point inorganic compounds not always characterised as ceramics, including nitrides, borides, carbides, silicides and sulphides of both metals and non-metals (186,187).

A practical size of refractory grain for the Ceracon process has been identified to be in the range 325 - 100 mesh (187). Finer grains grind to dust and do not pack to as high a density as coarser grains. However, coarser grains tend to penetrate more deeply into the surface of the part being consolidated and produce a surface texture which is often difficult to remove. In many cases it is desirable to use controlled mixtures of particle sizes in order to obtain the best total grain characteristics (187).

For the consolidation of iron and similar melting point alloys, fused aluminium oxide grains of less than 100 mesh grain size have been found to produce satisfactory results, since the grains are resistant to self bonding and sintering. However, with many products, the lower hardness and greater deformability of silica at elevated temperatures make it the ideal refractory grain. For very high temperature consolidations such as refractory materials or compounds, it can be advantageous to use materials such as thorium oxide, zirconium oxide, boron carbide or carbon as simple compounds or in combination with other refractory materials, to provide better properties during consolidation than lower melting point refractory grains (187).

2.18 CLASSIFICATION OF REFRACTORY MATERIALS:

POTENTIAL PRESSURE TRANSMITTING MEDIA

Most refractories are ceramic materials made from high melting point oxides such as SiO_2 , Al_2O_3 and MgO . Carbon, carbides, borides and nitrides have also been developed for high temperature applications.

The ability of refractory materials to withstand high temperatures has made them suitable to be selected as potential pressure transmitting mediums (PTM) during the hot isostatic pressing (HIPping) of encapsulated 70/30 cupronickel castings. Consideration has been given to materials which already have proven experience as a PTM in the Ceracon process (186,187). A brief background to some of these refractory materials will be given.

2.18.1 SILICA

There are 15 modifications of silica, the important forms of which are indicated in Figure 54, which shows their ranges of stability and the volume changes occurring on transformation (195,196). The naturally occurring form is α -quartz, which transforms rapidly and reversibly to β -quartz at 573°C, accompanied by a volume change of 1.35%. This volume change is large enough to shatter a piece of the material unless heating past this temperature is carried out very slowly. β -quartz is stable to 867°C but may exist to much higher temperatures, since its conversion to tridymite is slow on account of the considerable degree of atomic reorganisation that must occur during transformation (197). Above 1470°C cristobalite is the stable form of silica, and once again the transformations either from quartz or cristobalite are slow. Cristobalite remains stable to the melting point at 1723°C. Sosman's classification (Figure 54) shows conversion of quartz and tridymite to glass rather than cristobalite at 1450°C and 1680°C.

Cristobalite, when cooled below 1470°C can revert to tridymite, but this reversion is slow and usually metastable cristobalite exists to room-temperature, but with a complex transformation at 275-200°C to a low temperature variety. Similarly, tridymite exists to low temperatures with modifications at 475°C, 210°C, 163°C and 117°C. The volume changes are particularly large at low temperatures and care should be taken to avoid shattering by cooling very slowly from 300-100°C. Similarly during

reheating, care should be taken to avoid spalling and to accommodate any expansion.

The refractoriness of silica is often quoted up to 1710°C and under load initial softening occurs at around 1630-1700°C depending upon the purity of silica.

2.18.2 ALUMINA

Alumina can be obtained from pure bauxite ore which is a mixture of two hydrates; gibbsite ($\text{Al}_2\text{O}_3 \cdot 3\text{H}_2\text{O}$) and diaspore ($\text{Al}_2\text{O}_3 \cdot \text{H}_2\text{O}$), usually associated with a large amount of iron oxide from which it can be easily separated.

Dehydration gives $\alpha\text{-Al}_2\text{O}_3$ (corundum), while heating above 900°C during calcination forms $\gamma\text{-Al}_2\text{O}_3$. Alumina has a melting point of 2015°C which is low compared with those of the other special refractories such as zirconia and silicon carbide. Alumina can be used with confidence up to temperatures around 1900°C (196).

2.18.3 ZIRCONIUM OXIDE

Zirconia melts at 2677°C, and is stable in both oxidising and reducing atmospheres up to 2200°C. Pure zirconia occurs in two modifications with an inversion temperature at about 1000°C (197). Another cubic modification forms which is stable at all temperatures in the presence of lime or magnesia with only a slight reduction in refractoriness. The material is prepared either fully stabilised with approximately 5% CaO or only partially stabilised with slightly different properties. Neither the fully or partially stabilised form has a good spalling resistance, since if the inversion is suppressed the thermal expansion

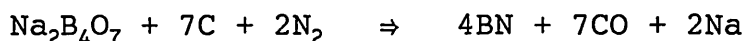
of the material increases.

2.18.4 SILICON CARBIDE

Silicon carbide (SiC) or carborundum is made by fusing together sand, coke and salt in an electric resistance furnace. Part of the product formed is silicon carbide (197). Silicon carbide can be used up to temperatures of 2000°C under favourable conditions but it tends to decompose in air. Silicon carbide is hard and has a good spalling resistance. However, it can be attacked by iron oxide (FeO), and therefore cannot be used in contact with iron or steel at high temperatures (197). For the above reason, silicon carbide may not be suitable as a PTM for the HIPping of encapsulated castings that use mild steel as the capsule material.

2.18.5 BORON NITRIDE

Boron nitride is usually prepared by the action of nitrogen on borax-carbon mixtures at temperatures within the range 1450 - 1650°C (198). The reaction may be represented as:



The mechanical properties of boron nitride are highly directional, because of the preferred orientation of the anisotropic crystals during processing. Boron nitride has a good thermal shock resistance, and is stable in air up to 700°C and oxidises slowly in the range 700-1000°C. It has a low coefficient of friction and boron nitride (hexagonal) has a Mohs hardness of around 2 (198). The hardness of the pyrolytic form is not known, but by analogy with pyrolytic graphite, which it resembles, it would be expected to be

moderately high. This is in direct contrast to cubic boron nitride, which is the hardest synthetic material known (198).

2.18.6 BORON CARBIDE

Limited data is available on boron carbide so the general properties of borides and carbides will be reviewed separately. In general the electrical and thermal conductivities of borides are higher than those of many metals, and they are hard and wear resistant. Borides tend to be brittle at room temperature, but the little data available for high temperature properties indicate they retain (and in some cases improve) mechanical strength at high temperatures combined with a fairly good oxidation resistance. Borides have a low thermal expansion which coupled with good thermal conductivity, suggests a good thermal shock resistance. However, borides are generally inferior to the refractory oxides (198).

Carbides have high melting points but encounter sintering difficulties at the temperatures normally employed. For this reason carbides are usually bonded with 10-60% metal, producing a special class of cermets. This factor alone severely limits their high temperature use, as the bond has a relatively low melting point. A further limitation is their poor oxidation resistance (198).

Therefore, although boron carbide appears to have many beneficial properties as a PTM, the low temperature bonding between the compounds may prevent its use.

2.19 ENCAPSULATION

The need for encapsulation is related to the presence of surface-connected porosity. To remove such porosity a gas tight membrane must be formed around the component prior to hot isostatic processing. The nature of the capsule material is influenced by the following factors (199):

- (i) Possibility of elastic and plastic deformation under pressure and temperature.
- (ii) Possibility of contamination of the material to be HIPped by the capsule material.
- (iii) Possibility of diffusion between the capsule and the component material.
- (iv) Ability of the capsule to withstand evacuation.
- (v) Size of the can and handling restrictions.
- (vi) Geometry of the component to be HIPped. Simple shapes can be easily encapsulated using welded metal tube or sheet. Sealed glass tubes can also be used.

A method for the successful encapsulation of large, complex marine castings has been developed by Infutech Diffusion Bonding Limited (200). Encapsulation of such castings involves the component being placed inside a steel tube or box section which has a sealed end. A siliceous based refractory pressure transmitting medium (PTM) is poured around the casting allowing 12.7-25.4mm clearance between the component and the walls of the capsule. The packed capsule is vibrated in order to obtain a maximum packing density of the PTM. An end-cap containing

a steel evacuation tube is welded on to the top of the capsule allowing the capsule to be evacuated and sealed prior to hot isostatic processing.

Good results have been obtained by the use of this type of encapsulation technique to recover castings containing surface-connected porosity. The appearance of the capsule after HIPping provides an indication of whether or not the HIP cycle has been successful. The appearance of a successfully HIPped capsule includes a flattened evacuation tube, and the top and bottom end-caps will have sunk becoming concave in appearance. In addition the walls of the capsule may show some distortion.

2.20 PARTICLE SIZING AND CHARACTERISATION

The behaviour of metal and refractory powders/particles during processing depends upon the particle size, particle size distribution, particle shape and structure. However, these particle properties cannot be directly translated into values characterising processing behaviour. To do this specific tests need to be carried out such as; tests for flow rate (flowability), apparent density, compactability (compression ratio), green strength and dimensional changes during sintering. The particle size, size distribution, shape and structure can be determined by the methods shown over the page (201):

- (1) Sieving.
- (2) Microscopic sizing.
- (3) Methods based on Stoke's Law:
 - _ the Roller air analyzer
 - the Micromerograph
 - Light and X-ray (Sedigraph) turbidimetry.
- (4) Coulter Counter and Particle Analysis by Light Obscuration.
- (5) Laser Light scattering: the Microtrac particle analyzer.

For particle sizes greater than $44\mu\text{m}$ sieving is by far the most important method. Methods described in (2) - (5) are used for powders with finer particle sizes ie. $< 44\mu\text{m}$. The turbidimetric methods have been developed for very fine refractory metal and refractory compound powders with particle sizes $< 1\mu\text{m}$ to $10\mu\text{m}$.

2.20.1 PARTICLE SIZE

The term particle size must always be defined, since only for spherical powders is there a unique dimension which defines particle size; ie. the diameter of the sphere. For irregular particles, "particle size" will depend upon the method by which the size was measured.

All particle sizing related to encapsulation refractory packing materials was carried out by sieving, therefore this is the only method which will be referred to in detail.

During sieving the powder/particles are shaken through a woven wire screen with square openings. The particle is

defined by the aperture of the sieve which will just retain a given particle. Needle like particles with dimensions in the length direction considerably larger than the sieve aperture may pass through the sieve, if the dimensions perpendicular to the length direction are smaller than the sieve aperture.

2.20.2 PARTICLE SIZE DISTRIBUTION

Particle size distributions for sieve analyses are usually represented in the form of tables or graphs which indicate a relationship between linear or geometric scales and distribution by weight percent frequency, as shown in Figure 55.

2.20.3 PARTICLE SHAPE AND STRUCTURE

The International Standards Organisation have issued a standard number 3252 which gives qualitative descriptions of particle shapes as shown in Figure 56.

acicular	-	needle shaped
angular	-	sharply edged or roughly polyhedral
dendritic	-	branched shape (tree-like)
fibrous	-	regularly or irregularly shaped threads
flaky	-	plate like
granular	-	approximately equi-dimensional but of irregular shape
irregular	-	lacking any symmetry
nodular	-	rounded irregular shape
spheroidal	-	roughly spherical

2.21 CREEP AND STRESS RELAXATION

A material behaves in an elastic manner when there is a linear relationship between the components of stress and strain. In real solids such behaviour is only followed at relatively low temperatures and stress levels. At higher temperatures and stresses a real solid deviates from the idealised elastic behaviour, and shows a more complex relationship between stress and strain which must take into account inelastic behaviour, such as creep, stress relaxation, yielding and work hardening (202-205). It must be remembered that yielding and work hardening also occur at low temperatures.

During the hot isostatic pressing of 70/30 cupronickel castings the high temperatures and pressures involved made it necessary to take creep and stress relaxation into consideration.

In order to predict mathematically the inelastic behaviour of a solid under given thermal and loading conditions, it is necessary to generalise the stress-strain relationship in an approximate manner. There are three types of approaches to such generalisations (204,206):

(i) The most basic studies of this problem make use of the concepts and methods of solid-state physics. In this approach, the microstructure of the material (crystalline, polycrystalline, etc.) is taken into consideration and the approach attempts to predict the mechanical behaviour of materials from this information. Treatments of materials from this view point include work by Cottrell (207) and

Read (208). Ashby also considers this type of view point in the prediction of HIP maps (180).

(ii) It is possible to disregard the microstructure of the material and regard it as a continuum. The general principles of mechanics and thermodynamics as applied to a continuum are then employed to determine the forms of stress-strain relationships which are compatible with the principles.

(iii) The most direct procedure is to assume simple inelastic stress-strain relationships; these define the various ideal inelastic bodies, although they do not represent an actual material they incorporate simple combinations of the different types of inelastic phenomena, such as creep, stress relaxation, plastic flow or work hardening. Tensorial considerations are then employed in the models developed to produce information on the types of viscous processes which exist. This type of analysis has been adopted by Prager and Hedge (209), and Hill (210).

The two principal types of inelastic behaviour (206):

- (i) Viscoelasticity - creep and stress relaxation
 - (ii) Plasticity - plastic flow and work hardening
- will now be discussed in more detail.

2.21.1 CREEP

Many general texts are available on the subject of creep (202-205). This process may be defined as the time-dependent flow of metals under conditions of constant load. The creep behaviour of a material may be assessed by a creep test, which relates strain to four externally modifiable parameters ie. stress, temperature, time and environment. Although creep data can be displayed in various forms, the one which presents most fundamental interest is the curve that relates the strain produced to the time of the test. The shape of the curve depends upon both the stress level and temperature (202) as shown for copper and steel in Figure 57. The four distinct sections of the curve are more clearly illustrated in Figure 58, viz:

- (i) The region of instantaneous strain which occurs on loading.
- (ii) The primary or transient region (Stage I) where the strain rate is continuously decreasing.
- (iii) The secondary or steady state region (Stage II) where the strain rate is constant.
- (iv) The tertiary region (Stage III) where the strain rate increases until fracture occurs.

The occurrence of all these stages together in any one test requires the use of a suitable combination of test conditions. Stress, temperature and time (duration of the test) are the major factors affecting the creep behaviour of a material. Accurate control of these parameters is essential in order to minimise the scatter of results

obtained and gain meaningful evaluations.

2.21.2 STRESS RELAXATION

The process of stress relaxation can be defined as the loss of stress with time at a given deformation (202-205,211).

When a metal or alloy loaded under static, dynamic or creep conditions is prevented from changing its shape, the load it supports decreases with time as shown for steel and copper in Figure 59. The phenomena occurring is called stress relaxation.

In a stress relaxation test the total strain is held constant:

$$\epsilon_P + \epsilon_E = \text{Constant} \quad (53)$$

As the stress supported by the specimen relaxes, the elastic strain also relaxes:

$$\dot{\sigma} = E \times \dot{\epsilon}_E \quad (54)$$

Re-writing equation (53)

$$\dot{\epsilon}_E = - \dot{\epsilon}_P$$

Substituting in equation (54)

$$\dot{\sigma} = - E \times \dot{\epsilon}_P$$

Integrating between limits ϵ_P , ϵ_{P0} and σ , σ^0

$$\epsilon_P - \epsilon_{P0} = \frac{\sigma^0 - \sigma}{E} \quad (55)$$

Thus it may be noted, that during stress relaxation the elastic strain is converted to plastic strain; hence creep occurs under conditions of decreasing stress.

2.21.3 PLASTIC FLOW AND WORK HARDENING

The second important category of inelastic behaviour is that involving plastic flow. This can be explained by considering a specimen in an unstressed state, loaded in simple tension by a load starting at zero and continuously increasing. If the elongation is plotted against the load a curve is produced typical of that shown in Figure 60. If the load is removed at any point before the elastic limit (point Y) is reached the specimen will return to its original length. If the load is increased past point Y, the slope of the stress-strain curve decreases, although a further increase in stress is required to produce additional strain. This increase is ascribed to a phenomena known as work hardening (204). If at point A the load applied to the specimen is reduced, it is found that the slope of the unloading curve is nearly equal to the initial slope of the loading curve. The same is true for the slope of the curve when the specimen is reloaded at point B. If reloading is continued past point C, it has been found experimentally that the stress-strain curve past this point is virtually unchanged by the unloading and reloading process (204). If this experiment is conducted at different temperatures, it is found that the loading and unloading curves obtained are temperature dependent, particularly in regard to the elastic limit and the curve

beyond it.

In this way the phenomena of plastic flow has been investigated intensively from the solid-state physics view point and a semiquantitative theory developed.

2.21.4 VISCOELASTIC STRESS - STRAIN RELATIONSHIPS

Metallic materials subject to loads at elevated temperatures exhibit both elastic and inelastic behaviour, the latter produced by creep and stress relaxation involving intergranular processes or viscous flow of the grain boundaries (204,211). This type of behaviour can be represented by mechanical models as shown in Figure 61 which involves combinations of the following:

- (i) A perfectly elastic spring for elastic deformation.
- (ii) A dashpot consisting of a perforated piston moving in a cylinder containing a viscous liquid for inelastic deformation.

These elements can be combined in different ways so that the model developed behaves in a way that approximates the observed mechanical behaviour of real metals.

The three extensively used models shown in Figure 61 are:

- (i) Maxwell Body - a spring and a dashpot connected in series.
- (ii) Kelvin Body - a spring and a dashpot connected in parallel.
- (iii) Standard Linear Solid - a three element body involving a Maxwell body connected in parallel with a spring.

These models may be considered as either actually representing some of the characteristics of the micro-structure of the material under consideration, or merely as providing a useful analogy for determining appropriate forms of stress-strain relationships.

In terms of stress-strain tensors the following relationships have been derived outlined by Boley and Weiner (204):

Maxwell Body

$$\dot{e}_{IJ} = \frac{\dot{s}_{IJ}}{2G} + \frac{s_{IJ}}{2\eta}$$

KELVIN OR VOIGT BODY

$$2\eta\dot{e}_{IJ} + 2Ge_{IJ} = s_{IJ}$$

STANDARD LINEAR SOLID

$$\dot{e}_{IJ} + \phi e_{IJ} = \frac{\dot{s}_{IJ}}{2G} = \frac{s_{IJ}}{2\eta}$$

In these equations s_{IJ} and e_{IJ} are the deviatoric portions of the stress and strain tensors, G is the shear modulus of the material, η is the coefficient of viscosity and ϕ is a material constant.

STRESS RELAXATION AND CREEP

The relationships between stress and strain obtained from the mechanical models described in section 2.21.4 can be represented in terms of the stress and strain tensors which allows equations for stress relaxation and creep under uniaxial conditions to be derived (204,211,212). Such equations include:

Maxwell Body

Stress Relaxation

$$\frac{\sigma}{\sigma^o} = \exp \left(- \frac{Gt}{\eta} \right) \quad (56)$$

Creep Strain

$$\epsilon_{creep} = \frac{\sigma}{2\eta(1+\nu)} \quad (57)$$

Kelvin Body

Stress Relaxation

$$\sigma = 2G(1+\nu)\epsilon^o \quad (58)$$

Creep Strain

$$\epsilon_{creep} = \frac{\sigma^o}{2G(1+\nu)} \left[1 - \exp \left(- \frac{Gt}{\eta} \right) \right] \quad (59)$$

Standard Linear Solid

Stress Relaxation

$$\frac{\sigma}{\sigma^o} = \left[1 - \frac{2\eta\phi}{E} (1+\nu) \right] \exp\left(-\frac{Gt}{\eta}\right) + \frac{2\eta\phi (1+\nu)}{E} \quad (60)$$

Creep Strain

$$\epsilon_{creep} = \frac{\sigma^o}{E} \left[\frac{E}{2\eta\phi (1+\nu)} - 1 \right] [1 - e^{\phi t}] \quad (61)$$

Consideration of the mechanical models shown in Figure 61 in conjunction with equations ⁽⁵⁶⁻⁶¹⁾ in this section, leads to the following description of the operation of the viscous models in a viscous-elastic situation (204,211):

Maxwell Body

(i) Stress Relaxation

On the sudden application of strain the viscous element is initially zero and the immediate response comes from the elastic behaviour of the spring. With the total strain held constant the subsequent extension of the viscous element causes the load to decrease and the spring to contract.

(ii) Creep

The applied stress is carried directly by the viscous element which gives the subsequent viscous response after the spring has produced an initial elastic strain. Under conditions of constant stress, the relationship between creep strain and time indicate Newtonian flow.

Kelvin Body

(i) Stress Relaxation

This model suggests no stress relaxation occurs because the spring which is in parallel with the dashpot is held at a constant strain, which prevents any movement in the dashpot.

(ii) Creep

From the expression for creep (equation ⁶³), the creep strain increases, at a reducing rate as the time increases. The creep strain approaches a limiting value of $\sigma^0/2G(1+\nu)$ as the time approaches infinity. This is expected from the model, because the spring is restrained by the viscous element during the initial loading, and is then allowed to extend as the viscous element extends.

The Standard Linear solid

The Standard Linear Solid is a three element model that contains the features of both the Kelvin and the Maxwell models. In one arm the spring and dashpot combination allows stress relaxation to occur by the replacement of elastic strain in the spring by viscous strain in the dashpot. However, unlike the Maxwell body, this process is partially restrained by the spring in the other arm of the body (combination shown in Figure 61). Thus, the stress relaxation process essentially ceases at some finite level of stress.

2.21.6 THEORETICAL EQUATIONS REPRESENTING
VISCO-ELASTIC PROCESSES DERIVED FROM
THE STANDARD LINEAR SOLID MODEL

From the Standard Linear Solid model, the relationship between stress and strain in terms of the stress and strain tensors have been suggested by Boley and Weiner (204) to be:

$$\dot{e}_{IJ} + \phi e_{IJ} = \frac{\dot{S}_{IJ}}{2G} + \frac{S_{IJ}}{2\eta}$$

But for uniaxial conditions this equation can be rewritten:

$$\dot{e}_{xx} + \phi e_{xx} = \frac{\dot{S}_{xx}}{2G} + \frac{S_{xx}}{2\eta} \quad (62)$$

The mean stress and strain, and the deviatoric stress and strain tensors are given as:

$$\sigma_m = \frac{\sigma_{IJ}}{3}$$

$$\epsilon_m = \frac{\epsilon_{IJ}}{3}$$

$$S_{IJ} = \sigma_{IJ} - \delta_{IJ} \sigma_m$$

$$e_{IJ} = \epsilon_{IJ} - \delta_{IJ} \epsilon_m$$

For uniaxial conditions the equations shown over the page can be written as:

$$\sigma_m = \frac{\sigma_{xx}}{3} \quad (63)$$

$$\epsilon_m = \frac{(1-2\nu)}{3} \epsilon_{xx} \quad (64)$$

$$S_{xx} = \sigma_{xx} - \sigma_m \quad (65)$$

$$e_{xx} = \epsilon_{xx} - \epsilon_m \quad (66)$$

Equations ⁶⁵ and ⁶⁶ can be rearranged as:

$$S_{xx} = \sigma_{xx} - \frac{\sigma_{xx}}{3} \quad (67)$$

$$e_{xx} = \epsilon_{xx} - \frac{(1-2\nu)}{3} \epsilon_{xx} \quad (68)$$

Similarly,

$$\dot{S}_{xx} = \dot{\sigma}_{xx} - \frac{\dot{\sigma}_{xx}}{3} \quad (69)$$

$$\dot{e}_{xx} = \dot{\epsilon}_{xx} - \frac{(1-2\nu)}{3} \dot{\epsilon}_{xx} \quad (70)$$

By substituting values in equation ⁶², the resulting equation will be:

$$\dot{\epsilon}_{xx} + \phi \epsilon_{xx} = \frac{\dot{\sigma}_{xx}}{2G(1+\nu)} + \frac{\sigma_{xx}}{2\eta(1+\nu)} \quad (71)$$

From the equations referred to in this section Soomro (13) derived two expressions; one for stress relaxation and one for creep strain under uniaxial conditions. The equations derived are as follows:

$$\frac{\sigma^t}{\sigma^o} = (1-A) \text{Exp}(-Bt) + A \quad (72)$$

$$\epsilon_{creep} = \frac{\sigma^o}{E} \left(\frac{1}{A} - 1 \right) [1 - \text{Exp}(-\phi t)] \quad (73)$$

The parameters A and B contain various material properties viz:

$$A = \frac{2\phi\eta(1+\nu)}{E} \quad B = \frac{G}{\eta}$$

The values of the parameters A and B have been chosen to give the best fit with experimental curves. However, both these constants can be determined experimentally by an independent experimental determination of material properties η , E, ν and G whereas ϕ can be revised at will to obtain the required fit.

In the Maxwell body, stress relaxation is represented by a single exponential decay term, which suggests that the stress decays to zero at longer times. Experimental stress relaxation curves obtained for 70/30 cupronickel indicated that stress approaches a positive final value asymptotically. Abbasi (211) and Soomro (212), obtained similar results for 835M30 steel, and discovered it was not possible to fit an expression of the Maxwell type to the experimental stress relaxation curves without varying the ratio G/η with time. Attempts made to model the stress relaxation of 835M30 steel by choosing the best value of G/η produced poor correlation with the experimentally observed behaviour as shown in Figure 62. Furthermore, the use of such G/η ratios in the calculation of creep strains by the means of the Maxwell body gave values that could not be reconciled with experimentally determined creep values (211). Thus, the latter implied that G/η should be constant with time. Therefore, based on the work of Abbasi and Soomro (211,212), the Maxwell model was considered unsuitable as a method by which stress relaxation could be described.

The Kelvin body can also be immediately discarded, because of its inability to predict any stress relaxation.

The Standard linear solid allows the stress relaxation curve to approach a final finite stress level asymptotically. However, the shape of the curve obtained

is dependent upon the values of the two constants η and ϕ , which are part of an exponential constant and an equation constant in the stress-relaxation and creep expressions. They are both dependent upon the type of material and may be made to vary with temperature in order to model the stress relaxation rates pertinent to a specific temperature over a wide range of temperatures. The use of the two constants, allows a much better fit between calculated and experimental curves to be obtained, than is possible with the single factor used in the Maxwell body (211), as shown in Figure 62.

Hence, for these reasons the Standard Linear Solid model has been selected to quantify the viscoelastic effect in 70/30 cupronickel castings during hot isostatic processing.

3.0 EXPERIMENTAL PROCEDURES

Investigation of the hot isostatic processing characteristics of 70/30 cupronickel (NES 824) involved HIP experiments to determine the effect of processing variables such as time, temperature, pressure and pressure transmitting medium on the consolidation of internal and surface-connected pores. Models have also been identified which accurately predict the pore closure rates in castings containing closed internal porosity. In addition the effect of HIPping on as-cast material properties such as strength, ductility, toughness, microstructure and corrosion resistance has been evaluated.

3.1 MATERIAL IDENTIFICATION

All 70/30 cupronickel material used in mechanical property and corrosion evaluations, and in hot isostatic pressing trials involving artificial porosity specimens containing internal and surface-connected pores, was cast material supplied by Vickers-Shipbuilding Limited (VSEL) in accordance with NES 824 Part 1, Issue 1. The test material supplied included:

(i) Four cast weld plates 12.5cm wide x 2.4cm thick x 320cm long which had been stress relieved for 2 hours at 450-500°C followed by cooling in air. The cast identity and chemical composition of the weld plates are given in Table 27 together with the compositional requirements of NES 824.

(ii) Cast mechanical property test bars, melt identification CN 6814/L1 which were subjected to HIPping trials carried out at H.I.P Limited. The chemical analysis of this material is also shown in Table 27.

3.2 ARTIFICIAL POROSITY SPECIMENS

The determination of the optimum processing conditions for the hot isostatic pressing (HIPping) of high strength chromium cupronickel (NES 824), was carried out using artificial porosity specimens. These were cylindrical samples of 70/30 cupronickel 76.2mm long x 12.7mm diameter, cut in half, with hole(s) drilled into the cut faces of known sizes to represent the porosity. When the two halves of the specimen were reassembled in their original position an internal pore was created which was surface-connected ie. the pore was connected to the exterior of the sample at the contact surfaces between the two halves of the specimen. The pore geometries included squat pores of large diameter and elongated pores of small diameter as illustrated in Figure 63 for specimens containing 10% porosity. As the artificial porosity was surface-connected, encapsulation (ie. forming a gas-tight membrane around the component) was required prior to HIPping as shown in Figure 64.

The artificial porosity specimens described so far contain surface connected pores. To make artificial porosity specimens with closed internal pores the two halves of the specimen were joined together by electron beam welding carried out under a vacuum. The pore created was not

surface-connected and HIPping could be carried out without the need for encapsulation. In subsequent text internal closed porosity will be referred to as internal porosity.

3.3 ENCAPSULATION TECHNIQUES

In order to recover castings containing surface-connected porosity they must be encapsulated prior to HIPping. Test pieces involved in mechanical property and corrosion evaluations, together with artificial porosity specimens containing surface-connected porosity used in HIP experiments, were all encapsulated prior to HIP processing. Encapsulation involves the formation of a gas tight membrane around the component.

The method of encapsulation used was similar to that practised by Infutech Diffusion Bonding Limited (200) and involved packing the test specimens in capsules using a pressure transmitting medium (PTM). This PTM must be a refractory material to withstand the high temperatures and pressures involved.

Encapsulation consisted of selecting a mild steel tube of 2-3mm wall thickness, which allowed 15mm clearance between the outer edges of the work piece and the inner wall of the tube. An end-cap (a circular section of sheet material the same size diameter as the tube) was welded to one end of the tube to form a capsule. The test specimen was placed in the capsule and packed with hot refractory particles (to avoid moisture). The capsule was then vibrated to obtain a maximum packing density of the pressure transmitting medium. A second end-cap attached to a 3/8" diameter

vacuum tube was welded to the top of the capsule and the vacuum tube plugged with wire wool to prevent the loss of the PTM during evacuation. The capsule was pressure tested to ensure that the welds were sound, then evacuated and sealed prior to HIPping. A schematic illustration of an encapsulated artificial porosity specimen containing surface-connected porosity is shown in Figure 64.

The refractory pressure transmitting media used during HIPping experiments fell into two categories:

- (i) Refractory sands
- (ii) Alternative refractory compounds such as oxides, carbides, borides and nitrides.

3.4 HOT ISOSTATIC PRESSING EXPERIMENTS

3.4.1 LABORATORY HIP SYSTEM

Research and development is vital to sustain progress and expansion in technological fields, in order to improve the performance of existing materials and to discover new processing routes. For these reasons H.I.P Limited invested in a laboratory HIP system, the ISOHIPPER shown in Figure 65, which was specifically intended for sub-contract research programs.

All the HIP experiments were conducted using the above laboratory system courtesy of H.I.P Limited. The ISOHIPPER offers the design specifications listed over the page:

(i) WORKING VOLUME

75mm diameter by 120mm height when the two zone radiation heating zone is used, or 85mm diameter by 120mm height if the single zone convection heating element is used (radiation heating element removed).

(ii) FURNACE

Constructed from graphite in the design shown in Figure 66, and comprising of two heating elements; radiation and convection. The radiation element is clearly shown and surrounds the charge, while the convection element is situated below the charge.

(iii) TEMPERATURE MONITORING

The charge temperature is monitored by platinum thermocouples (type R) at temperatures up to 1400°C. The furnace temperature is monitored by two tungsten-rhenium thermocouples (type C) which are capable of controlling temperatures of up to 2000°C. These are situated on the outside of the furnace, one at equal height to the convection heating element and the second monitoring temperatures higher up the furnace near the top of the radiation heating element. At processing temperatures above 1400°C the charge couples are removed.

(iv) OPERATING TEMPERATURE RANGES

These are dependent upon the pressure system used:

0 - 2000°C - under argon

0 - 1850°C - under nitrogen

0 - 1250°C - under vacuum.

(v) MAXIMUM PRESSURE CAPABILITY

The pressure is maintained by a dry piston compressor with a maximum discharge pressure capability of 207MPa (30000psi).

(vi) AUXILIARY EQUIPMENT

The laboratory HIP system is fully automated and controlled by a micro-computer.

The operation of a HIP cycle using the laboratory system involved positioning the work piece in the furnace and placing charge thermocouples at the top and bottom of the work piece, to obtain the temperature spread throughout the mass of the component. A hood was placed over the furnace and secured in position. The heating assembly was then charged to the pressure vessel. The pressure vessel was closed and a mantle positioned over the lid of the vessel to comply with safety requirements. The process gas was selected, which was argon for all the HIP experiments carried out on 70/30 cupronickel. A vacuum of the order 200-300mtorr was obtained and the thermocouples re-enabled to ensure that they were in full working order. The furnace was manually purged with argon gas to around 0.34MPa (50psi), the chamber exhausted and then re-evacuated. This chain of events was carried out three times in order to ensure a moisture free chamber under a high quality vacuum. The furnace heating style was selected; convection for working temperatures below 600°C and radiation which utilised both convection and radiation heating elements for working temperatures above 650°C.

Power was coupled to the furnace and checked by observing current flowing in the ammeters. This provided a safety check to ensure furnace elements were operational prior to the HIP cycle being started. The furnace was then switched to automatic and all programming instructions then inputted by the micro-computer. A typical program to control a HIP cycle which involved a sustain time of 45 minutes at a temperature of 950°C with argon gas pressures of 103MPa, involving heating and cooling rates of 15°C/minute and 10°C/minute respectively, is shown in Figure 67. Once the correct cycle parameters had been entered, the HIP cycle was started together with a chart recorder and a data-logger to monitor the temperature and pressure changes during the cycle.

After the cycle had finished the chamber underwent natural let-down to room temperature and 2.07MPa (300psi), the remaining gases were exhausted and the chamber let-down to atmosphere so that the work piece could be removed. After each HIP cycle the pressure vessel was re-evacuated and purged with argon to 2.07MPa to prevent moisture from entering the chamber.

3.4.2 HOT ISOSTATIC PRESSING EXPERIMENTS

The determination of the optimum processing conditions for the HIPping of high strength chromium cupronickel (NES 824) was carried out using artificial porosity specimens which contained either internal porosity or surface-connected pores. The pore geometries included squat pores of large diameter and elongated pores of small diameter (Figure 63).

The specimens that contained surface-connected porosity required encapsulation prior to HIPping. The capsule was evacuated, sealed and together with the specimens containing internal porosity subjected to X-ray penetration examination prior to HIPping. The HIP experiments were conducted within the laboratory HIP system. The specimens were heated at 15°C/minute to the treatment temperature under an argon gas pressure that increased progressively during heating to reach a maximum in the range 41-145MPa. The treatment temperatures selected lay in the range 850-1025°C. Previous work carried out by HIP Limited (173,213) had shown that a temperature of 950°C provided the best combination of strength and ductility for 70/30 cupronickel castings whilst inhibiting grain growth associated with higher HIPping temperatures.

Investigations were undertaken to substantiate the above findings and to determine the optimum HIP temperature with regard to improved mechanical properties. The experiments involved HIPping cast NES 824 material for a period of 4 hours at temperatures of 850°C, 950°C and 1025°C with argon gas pressures of 103MPa. The HIP pressure and sustain time were based on previous experience gained by H.I.P Limited on the HIPping of steel (214). In addition, a comparison was made between the rates of pore closure for three types of treatment at what proved to be the optimum temperature of 950°C:

(i) Type I - Successive 45 Minute HIP Cycles

In type I, pore closure of both internal and surface-connected pores as a consequence of repeated applications of a HIP cycle that involved holding the specimen for 45 minutes at 950°C with a gas pressure of 103MPa. This treatment was designed to allow observation of the stages of pore closure and identification of the densification mechanisms involved. It was thought that increasing the HIP time further might result in complete consolidation of the pores during a single HIP cycle and prevent any meaningful investigations.

The specimens which contained surface-connected porosity were encapsulated, heated and pressurised to the sustain conditions, cooled and removed from their capsule and re-encapsulated with fresh pressure transmitting medium before reapplying the temperature and pressure at the start of the next cycle. Thus each cycle included a heating/pressurisation, a sustain and a cooling stage as illustrated in Figure 68.

(ii) Type II - Continuous HIP Cycle

In type II, pore closure of surface-connected pores occurred when the same temperature and pressure as in (i) were applied as a single continuous cycle for various times from 45 minutes to 12 hours, thus involving only one heating and one cooling stage as shown typically for a 3 hour sustain in Figure 69.

(iii) Type III - Successive Short HIP Cycles

Without Renewed Encapsulation

To separate the effects of the encapsulation process on densification from the effect of the initial heating and holding at temperature and pressure during the first HIP cycle, specimens which contained surface-connected porosity were subjected to repeated cycles as in (i) but without re-encapsulation at the end of each cycle.

In addition to the three types of treatment at 950°C a type IV treatment was applied at 850°C, 950°C and 1025°C as discussed below.

(iv) Type IV - Zero Sustain Time HIP Cycles

The period for which the HIP conditions were held constant is termed the sustain period, and the experiments carried out in (i) indicated that the majority of densification occurred during the first cycle (or within 45 minutes at the sustain conditions). Thus, it was necessary to estimate the amount of densification due to instantaneous plastic yielding and that due to time dependent mechanisms (ie. creep and diffusion). Densification by plastic yielding takes place once the HIP pressure exceeds the yield stress of the material, and should therefore be complete by the time the HIP conditions are reached. Experiments to substantiate this assumption were carried out at temperatures of 850°C, 950°C and 1025°C with argon gas pressures of 103MPa for zero sustain times. An extension of the sustain time to 45 minutes allowed the increase in densification due to time dependent mechanisms

to be identified.

On completion of the constant temperature and pressure stage the specimen was cooled at 10°C/minute until ambient was reached. The dimensions of the pore profile after HIPping were determined by X-ray penetration examination. Pore closure as a result of HIPping was determined by measuring the absolute porosity remaining in the specimen. Quantitative evaluation of the extent of pore closure taking place during each HIP cycle was carried out using Seescan Image Analysis by tracing the pores before and after HIPping, and measuring the change in cross-sectional area of the pore. It was assumed that the change in area of a pore of known volume during HIPping could be equated to the reduced volume, since the reduction in pore size is equal across its radius because the HIPping pressure acts equally and instantaneously on all surfaces.

The next stage of the HIP experiments was to examine the effect of the HIP process on densification. Varying the HIP pressure within the range 41-145MPa (6000-21000psi) allowed the prediction of the optimum processing conditions for maximum densification of NES 824 castings containing internal and surface-connected porosity at a processing temperature of 950°C.

The change in flow stress with temperature within the range 300-1025°C was determined for as-cast 70/30 cupronickel material in order to predict the minimum temperature at which plastic yielding would occur. Comparison of the yield strength at temperature with the

applied HIP pressure during the heating/pressurisation stage of the HIP cycle, allowed the minimum temperature at which plastic yielding would occur in practice to be estimated.

3.4.3 ENCAPSULATION TECHNIQUES

The HIP experiments have indicated that for both un-encapsulated and encapsulated NES 824 castings the initial rate of densification was very rapid (Figure 94 and Figure 85), after which subsequent densification occurred at a much lower rate once the sustain conditions had been reached and held for time periods which exceeded 45 minutes (Figure 87).

Other HIP experiments conducted on encapsulated specimens which contained surface-connected porosity subjected to successive (type III) HIP cycles of short duration without renewal of the packing material prior to each cycle, also showed a similar decline in the densification rate after the first HIP cycle (Figure 92). This indicated that the standard method of encapsulation which uses silica sand as the packing material was in some way impeding pore closure. This reduction in the densification rate needed to be examined further and consideration was given to the possibility that the sand particles were sintering together thus, options for a change in the type of refractory for the densification of 10% and 16% surface-connected pores were examined.

Eleven types of pressure transmitting media were used during encapsulation to identify the optimum refractory PTM, and to ascertain the effect of particle shape and size

on the densification process. The particle sizes of the various refractory materials were determined by sieve analysis, the results of which together with the melting points of the refractory materials are shown in Table 28. The chemical analyses of the refractory sands used as a PTM are shown in Table 29. The refractory pressure transmitting media used in the HIP experiments included:

(i) High Purity Silica Sand

Silica sand is the standard PTM used for the encapsulation of castings prior to HIP processing (200). However, it tends to undergo mechanical locking and partial sintering at the temperatures and pressures associated with HIPping. This desert-based sand is of high purity as shown in Table 29, and is predominantly of a narrow size fraction ($\sim 150\mu\text{m}$). The particles are angular in shape as indicated in Figures 103 and 104.

(ii) Close Fitting Steel Capsule

This type of encapsulation without a refractory packing medium is only suitable for castings of simple geometry. It may be considered as close to the ideal, because once the capsule is sealed it resembles a casting which contains internal pores and behaves in a similar manner during densification by HIPping. Densification can not be interfered with by sintering of refractory particles since there are none present.

(iii) Coarse Tabular Alumina Granules

The high melting point of alumina (2015°C) suggests that sintering will not take place. However, the coarse tabular granules (>355 μ m but <1700 μ m) as shown in Figure 101, were expected to reach a maximum packing density in shorter times for equivalent HIP conditions than fine particles, and thus to impair densification.

(iv) Fine Calcined Alumina Powder

It was thought that the fine calcined powder containing particle sizes within the range 53-75-106 μ m might improve the densification rate, due to their greater resistance to sintering and/or mechanical locking, or by enhanced ease of particle flow under the HIP conditions.

(v) Calcined Alumina And Boron Nitride

Mixtures of these refractory materials in weight ratios of Al₂O₃:BN of 10:1 and 10:3 were used during HIP experiments. The boron nitride had a very fine particle size (<55 μ m) and tended to grind to dust during HIPping. The boron nitride was expected to act as a lubricant and enhance the ability of the refractory particles to transmit the applied load/pressure during the HIP process.

(vi) Zirconium Oxide

Zirconia has a high melting point of 2715°C and would therefore not be expected to undergo sintering at the HIP conditions. The zirconia particles were angular in nature and had particle sizes within the range 75-150 μ m. This oxide material was chosen in order to investigate the effect of changing the type of refractory used as the PTM

on the rate of densification of encapsulated castings.

(vii) Boron Carbide

Boron carbide has a diamond structure of great hardness and a high melting point of 2450°C. This very fine powder (<53-75 μ m) was used to investigate the effect of particle size and change of refractory on the densification rate of encapsulated castings. Boron carbide is hygroscopic and required heating to expel moisture prior to encapsulation. Mixtures of boron carbide and silicon carbide (weight ratio of 3:10) were also examined as a potential refractory PTM.

(viii) Glass

Two types of glass were investigated, a low melting point soda glass (400°C) and a borosilicate glass known commercially as Pyrex which melts around 1680°C. Fragments of glass were packed around the specimen and partially fused in a conventional muffle heat treatment furnace at 1000°C prior to HIPping. In addition investigations were carried out to determine whether evacuation of the capsules which contained fused Pyrex glass was beneficial in regards to densification, and also to provide an indication of the method by which the HIP pressure was transmitted to the test specimen.

(ix) Zone-M-Concrete Sand

This is a water table, 90% quartz aggregate sand chosen because of its particle characteristics. Its particle shape was less angular than the desert sands, as is shown by comparison of Figures 105 and 106 with Figures 103 and 104. The particle size distribution of the zone-M

concrete sand was determined by sieve analysis to be in the range 106-1700 μ m. The particles greater than 355 μ m were of a shell-like nature and were removed. Zone-M-concrete sand was used as a PTM in two forms firstly as an aggregate of particle sizes (106-355 μ m) and secondly as a single particle size sand (150 μ m); in order to investigate the effect of particle shape and size distribution on the rate of densification of encapsulated castings.

(x) Leighton Buzzard Sand

This is a siliceous based (>96% SiO₂) water table sand of single particle size (>355 μ m but <1700 μ m), the particles being of a rounded nature as shown in Figure 109 and 110. This sand was chosen as a comparison against the zone-M-concrete sand in order to compare the effect of large and small rounded particles on the rate of densification of encapsulated castings.

3.4.4 EFFECT OF THICKNESS OF SAND LAYER ON THE RATE OF PORE CLOSURE IN ENCAPSULATED SPECIMENS

The HIP experiments indicated that the standard method of encapsulation which uses silica sand as a packing material impeded pore closure. A study of this reduction in the densification rate was required and in addition to investigating the effect of a change in the refractory medium, two other options were considered:

- (i) changing the capsule diameter, and as a result the thickness of the pressure transmitting medium surrounding the specimen and;
- (ii) changing the diameter of the artificial porosity specimen.

(1) CHANGE IN CAPSULE SIZE

The diameters of the capsules were 22, 40, 50, 63, 75 and 90mm and the capsules contained a standard artificial porosity specimen of 12.7mm diameter (Figure 63). This specimen contained 10% surface-connected porosity. This enabled packing PTM thicknesses of 4.65, 13.65, 18.65, 25.15, 31.15 and 38.65mm to be produced respectively around the specimen.

(2) CHANGE IN SPECIMEN DIAMETER

The diameter of the artificial porosity specimen was increased to 38.4mm while the pore size remained the same, which had the effect of increasing the wall thickness of the specimen from 3.6mm to 16.45mm. This specimen contained 1% surface-connected porosity. The specimens were encapsulated in capsules of 50, 75 and 90mm diameter which produced a PTM packing thickness of 5.8, 18.3 and 25.8mm respectively around the specimen, and provided suitable comparison with the PTM thicknesses investigated in (1).

The encapsulated specimens were evacuated, sealed and subjected to X-ray penetration examination prior to HIP processing. The encapsulated specimens were HIPped for a period of 45 minutes at a temperature of 950°C and argon gas pressures of 103MPa. The encapsulated specimens were once again subjected to X-ray penetration examination and the degree of pore closure deduced, and the effect of PTM thickness and sample diameter/material thickness on the densification rate examined.

3.5 CHEMICAL INTERACTION BETWEEN PTM SANDS AND NES 824

Two cylindrical samples of 70/30 cupronickel 10mm diameter x 20mm long were encapsulated in steel capsules using silica sand and zone-M sand respectively as the packing material. The capsules were evacuated and sealed and subjected to HIPping at a temperature of 950°C for a period of 45 minutes with argon gas pressures of 103MPa. After HIPping the specimens were removed from their capsules and their surfaces cleaned by shot blasting with fine grit followed by ultrasonic cleaning in alcohol. The surface of the specimens was then examined by both optical microscopy and Scanning Electron Microscopy for evidence of out-gassing of the silica based sands during HIPping, and for any sign of inter-reaction between the sands and 70/30 cupronickel. In addition the effect of surface disfigurement by the impression of sand grains was also examined.

3.6 CHARACTERISATION OF PARTICLES OF REFRACTORY PRESSURE TRANSMITTING MEDIA

3.6.1 SIEVE ANALYSIS

The sieves chosen for use in the sieve analysis of refractory particles used as packing materials in the HIP experiments, were taken from a series of sieves specified in BS 410:1976. A set of wire-cloth sieves of 200mm diameter was assembled from the finest to the coarsest in ascending order with apertures of 1.7mm, 355, 150, 106, 90, 75 and 53 μm . A 100g sample of the refractory medium was placed on the top sieve and the sieve

assembly was mechanically shaken for 30 minutes. The predominant particle size was recorded, and if >95% of the particles fell within this range no other measurements were taken. For the zone-M concrete sand the weight of the sand retained by each sieve was recorded. Each fraction as a percentage of the original weight was then calculated.

3.6.2 MOISTURE CONTENT

The moisture contents of the three sands used as a PTM during encapsulation; silica sand, zone-M concrete sand and Leighton Buzzard sand were determined by a standard test method, the "Speedy" moisture tester. The sands were supplied dried so there was no need to dry samples of the sand to a constant weight prior to the test. The "Speedy" moisture tester was then used which involved mixing 6g of sand with 1g of calcium carbonate. The sand and calcium-carbonate reacted and liberated acetylene at a rate which was proportional to the water content of the sand. The percentage moisture content of the sand was read directly from the test apparatus.

3.6.3 CRUSHING STRENGTH

The strength test is a measure of the crushing strength of a sand, and involves producing rammed sand preforms to a standard height of 5.08cm. Preforms of the three PTM sands were produced and their ability to withstand an applied load measured. The load was applied steadily and the crushing strength recorded. This test is sensitive to the moisture content of the sand and a maximum strength is

normally observed at moisture contents of around 2%.

3.6.4 COMPRESSIBILITY OF HIPPED SILICA SAND

A test was devised to measure the load required to cause HIPped sand restrained by a steel capsule to flow.

Silica sand was poured into a 40mm diameter steel capsule and vibrated to obtain a maximum packing density of the refractory particles. The capsule was evacuated and sealed and subjected to HIPping at a temperature of 950°C for a period of 45 minutes and argon gas pressures selected from 41, 62, 83, 103, 124 and 145MPa. The HIPped capsules were sectioned to produce test samples which consisted of either a small ring or a small open ended sample as illustrated in Figure 70. The test samples were subjected to a compression test with a uniaxial directional load applied to the outside of the capsule skin. The load applied was recorded on a voltage output recorder and the maximum load sustained by the test specimens obtained from this data.

The compressibility test provided an indication of the magnitude of the applied load required during HIPping to maintain particle flow as densification proceeds, in order to maintain the transmission of the HIP pressure to the encapsulated part. In addition the test also gives an indication of the compression resistance of silica sand, and how its compressive strength changes with an increase in the HIP pressure.

3.7 MECHANICAL PROPERTY EVALUATIONS

The determinations of yield stress, ultimate tensile strength, ductility (%Elongation) and impact toughness of 70/30 cupronickel (NES 824) in the as-cast and HIPped condition were carried out using standard laboratory equipment: a J.J tensile testing machine and a Charpy impact testing machine. The strength and ductility evaluations were carried out on cylindrical test specimens in accordance with BS500. The Metric A specimen illustrated in Figure 71 is recommended for the testing of cast material. The tapered shoulders of the specimen reduce the build up of stresses at sharp contours and induce fracture to occur within the gauge length of the specimen. The impact toughness specimens were rectangular sections containing a 45° notch as shown in Figure 72, the notch acting as a stress concentrator.

Mechanical property investigations have been carried out on cast 70/30 cupronickel test bars and material taken from weld plates of NES 824 and encompassed:

(i) MECHANICAL PROPERTY EVALUATION - TEST BAR MATERIAL

Determination of the effect of HIPping on the as-cast properties of NES 824. Cast test bars were subjected to hot isostatic processing for a sustain period of 4 hours at temperatures of 850°C, 950°C and 1025°C with argon gas pressures of 103MPa. These investigations were carried out courtesy of H.I.P Limited and lead to the HIP temperature of 950°C being selected as the commercial processing temperature for 70/30 cupronickel (NES 824) (173,213). The HIP pressure and sustain time were based on previous

experience gained from the HIPping of steel (214).

(ii) MECHANICAL PROPERTY EVALUATION - PLATE MATERIAL

A similar investigation to (i), in order to determine the effect of HIPping on the as-cast mechanical and microstructural properties of NES 824 plate material. This investigation was carried out on encapsulated and HIPped sections of NES 824 weld plate material from which Metric A and Charpy impact specimens were machined. The HIP processing conditions included 4 hours at temperatures of 850°C, 950°C and 1025°C and argon gas pressures of 103MPa.

(iii) EFFECT OF HIP TIME ON PROPERTIES

Determination of the effect of HIP time on the mechanical properties of cast NES 824 HIPped at a temperature of 950°C and gas pressures of 103MPa. The HIP time was varied to include 45 minutes, 2, 4 and 6 hours. In addition to investigating the HIP time required to optimise properties at a standard temperature and pressure, the effect of HIP time on the extent of homogenisation (reduction in segregation/coring) of the cast structure was examined, using Scanning Electron Microscopy (SEM) together with quantitative ZAF4 EDAX analysis. The extent of coring can significantly effect the corrosion resistance of these alloys and therefore HIPping was expected to have a beneficial effect.

(iv) HIP RECOVERY OF CAST 70/30 CUPRONICKEL PLATES

Determination of the effect of HIPping to recover cast plate sections of NES 824 which encompassed:

- (a) Class I material which contained <5% porosity; and
 - (b) plates which contained shrinkage and microporosity;
- in order to examine the change in material properties if any, during the closure of the pores. The plates were encapsulated using standard techniques developed by Infutec Diffusion Bonding Limited (200) and HIPped at a temperature of 950°C with argon gas pressures of 103MPa for a sustain period of 4 hours.

(v) HIP RECOVERY OF LARGE CASTING DEFECTS

Determination of the effect of HIPping using standard commercial conditions for 70/30 cupronickel to recover a large casting containing a severe shrinkage defect as illustrated in Figure 73. After encapsulation and HIPping the cast section was cut in half through the original defect, one half of the casting being used in these investigations to compare the mechanical and microstructural properties of HIPped material taken from sound and recovered defect areas. The second half of the casting was used in similar investigations carried out by the Ministry Of Defence.

(vi) THERMAL SIMULATION OF A HIP CYCLE

Investigations carried out by VSEL (215) on material subjected to a thermal simulation of a commercial HIP cycle, that is, heated to the treatment temperature of 950°C at a rate of 10-15°C/minute, holding for a period of

4 hours followed by cooling at a rate of 7-10°C/minute. These investigations revealed that stress relieving material treated in the above manner for 2 hours at 475°C had a beneficial effect in regards to the strength characteristics of 70/30 cupronickel. Thus, it was considered necessary to determine the effect of stress relieving on the properties of NES 824 HIPped under the conditions commercially developed for this material.

3.8 HOT TENSILE DATA FOR 70/30 CUPRONICKEL

The determination of high temperature yield stress and flow stress data for 70/30 cupronickel were carried out on an Instron tensile testing machine. The specimen was mounted in the grips between a load cell and a moving cross head. The load cell was connected to a chart recorder which registered the applied load and the extension in the specimen. The cross head controlled the strain rate which was kept constant at 0.2cm/minute. The testing arrangement is shown in Figure 74, which involved a moveable furnace mounted on the front panel of the machine. The furnace could be moved out of the test zone to allow the insertion of the grips and the specimen assembly, after which the furnace could be returned to its original position. The grips were attached to the load cell and the cross head by universal joints. A resistance wound furnace coupled with a variable transformer was used to raise the specimen temperature. The furnace was packed with Koal Wool at the top and the bottom to prevent heat losses and to control the specimen temperature to the desired accuracy. A

temperature variation of $\pm 3^{\circ}\text{C}$ was observed at a specimen temperature of 950°C , which was within the range specified by BS3500. A chromal-alumel thermocouple was attached to the specimen surface to monitor the specimen temperature. The furnace was calibrated and the relationship between temperature and voltage obtained is shown in Table 30 and Figure 75. In addition to the temperature calibration, the furnace was calibrated to determine the position and extent of its hot zone. The relationship between temperature and distance from the top of the furnace is shown in Figure 76. This enabled the test specimens to be positioned in the furnace between 110-170mm from the top of the furnace, which ensured good temperature control along the gauge length of the test specimen.

A cylindrical test specimen in accordance with BS500 as shown in Figure 77 was selected as a suitable hot tensile specimen, and using the test arrangement described previously tensile tests were carried out within the temperature range $300-1025^{\circ}\text{C}$. The specimen was stabilised at the test temperature and held for 20 minutes prior to the test being carried out. Care was taken to avoid stressing the specimen during the stabilisation period, by adjusting the cross head, so that no load was generated on the specimen at any time.

3.9 HOT DUCTILITY OF 70/30 CUPRONICKEL

The hot ductility of 70/30 cupronickel was found to be difficult to measure because the load-extension curves did not show a well defined point of fracture especially at higher temperatures. Instead the load decreased in stages as shown in Figure 78. Visual examination of the fracture surfaces and the specimens gauge lengths revealed a brittle type fracture with cracks present along the entire gauge length. Close to the fracture surface the cracks had opened up to form voids. Consequently a standardised ductility had to be measured; viz the elongation the specimen underwent prior to necking, that is the extension caused by attaining the maximum stress, as illustrated in Figure 78.

3.10 CONSTANT LOAD DUCTILITY TESTS

During the HIPping of a cast component both the temperature and the HIP pressure are applied simultaneously until the required parameters are reached and sustained. Once the required time has been achieved the pressure is not removed instantaneously but decreases steadily and simultaneously with the fall in temperature. The cooling rate of the HIP unit is 7-10°C/minute and the accompanying pressure reduction is slow. Gas pressures of 55MPa (8000psi) continued to act at temperatures below 800°C as indicated in Figures 79 and 80.

As the casting cools it develops internal stresses due to contraction whilst at the same time it is subjected to an external gas pressure. Thus large stresses are placed on

the casting during cooling which may result in the cracking of commercial cupronickel castings. Therefore it is necessary to investigate the ductility of cupronickel both at HIPping temperatures and at the lower temperatures experienced during cooling.

The author has developed a constant load ductility test in order to simulate the stresses experienced during the cooling stage of the HIP cycle. The test consists of heating tensile specimens in a small resistance wound furnace whilst the specimen is held in the test position between the load cell and the moving cross head of an Instron tensile testing machine, as shown in Figure 74. On reaching the test temperatures which corresponded to the three HIPping temperatures of 850°C, 950°C and 1025°C, the specimen was stressed at a cross head-speed of 0.2cm/minute to just past the yield point of the material. The cross head of the Instron machine was then clamped to keep the specimen stationary. The furnace was switched off and the Koal Wool packing removed allowing the specimen to cool at a rate similar to that of the cooling rate of the HIP unit as shown in Figure 81.

The test specimen was subjected to a complex stress system as it cooled, and was at the same time acted upon by tensile stresses caused by the contraction of the specimens gauge length and the test shackles as they cooled. The specimen was restricted from moving to accommodate these stresses and thus simulated the conditions during a HIP cycle, except that during HIPping the component would be

subjected to compressive rather than tensile stresses. The specimen underwent plastic yielding and creep to alleviate these stresses.

A schematic illustration of a load-extension curve obtained from a constant-load tensile test is shown in Figure 82. This shows that originally the specimen was still at a sufficiently high temperature to adjust to the stresses acting upon it, and experienced stress relaxation due to creep, which was observed as a reduction in load. As the specimen cooled further stress relaxation became more difficult and the specimen was subjected to work hardening, due to the influence of the tensile deformation stresses, and the load-extension curve started to rise. The specimen's extension was accommodated by plastic flow and creep. As the specimen cooled further it became unstable and could no longer support the stresses acting upon it and started to neck at its weakest point, as shown by the reduction in load on the load-extension curve. As the temperature fell below 700-600°C the specimen no longer had the ductility to withstand the test conditions and failure occurred.

3.11 STRESS RELAXATION TESTS

Stress relaxation tests have been carried out on cast 70/30 cupronickel using the test apparatus shown in Figure 74. The test specimen used is in accordance with BS500 and is the same specimen as used in the hot tensile tests (Figure 77). The specimens were placed inside a furnace and mounted in the grips between a load cell and a moving cross head. The cross head controlled the strain rate, which remained constant at 0.2cm/minute. The test specimens were stabilised at the test temperature for 20 minutes prior to testing.

Stress relaxation tests involved the application of the test load (σ^0) which just exceeded the yield stress (σ) of the material at the test temperature. On attaining the test load the strain was held at a constant value. This was achieved by maintaining the cross head at a fixed point during the test. The relationship between load and time was then established from the chart recorder. The stress data obtained was then expressed as a fraction of the initial stress (ie. σ/σ^0), which made it possible to use the data independently of the critical stress level.

The temperature range over which the stress relaxation tests were carried out (400°C to 1025°C) encompassed both the HIPping temperatures of 850°C, 950°C and 1025°C, together with the temperatures encountered during heating to and cooling from the sustain temperature. All the stress relaxation data was recorded for a time of 8 minutes, which allowed, for most test temperatures,

a constant rate of stress relaxation to be reached or approached.

3.11.1 COMPARISON OF CALCULATED AND EXPERIMENTAL STRESS RELAXATION CURVES

The relationship between σ/σ^0 and time obtained from stress relaxation tests at temperatures within the range 400°C to 1025°C is governed by the Standard Linear Solid model as discussed in section 2.21 (201-212). The model states:

$$\frac{\sigma}{\sigma^0} = (1-A) \exp^{-Bt} + A$$

The equation indicates that the value of A lies between 1 and 0.

If $A = 1$, then $\sigma = \sigma^0$ and the behaviour of the material would be the same as that of the Kelvin body; ie. no stress relaxation would occur (211,212).

If $A = 0$, then $\sigma = \sigma^0 \exp^{-Bt}$ which is the same as the equation derived from the Maxwell body (211).

When time becomes infinite, $\sigma/\sigma^0 = A$, which is the limiting stress attained during the stress relaxation test (normally after a period of around 8 minutes).

B is an exponential rate constant which governs the rate of decay and influences the shape of the stress relaxation curve. The Standard Linear Solid model most accurately describes the stress relaxation observed for 70/30 cupronickel material.

The value of A was made equal to the limiting stress observed during the stress relaxation test after around

8 minutes relaxation time. A value of B was then obtained empirically. The values predicted for A also then required minor adjustments to obtain the best fit between the experimental and calculated curves. Hence a set of values of A and B were obtained which were a function of temperature but not time. A and B can be represented by the following equations:

$$A = \frac{2\phi\eta(1+\nu)}{E} \quad B = \frac{G}{\eta}$$

where η = Coefficient of viscosity

G = Shear stress

E = Youngs Modulus

ν = Poisson's ratio

ϕ = material parameter

The material properties G , E , η and ν for 70/30 cupronickel material are only available at room-temperature. NES 824 is a casting alloy and until recently there was no need for elevated temperature data. The equipment required to determine the material data at high temperatures was not available. Therefore all calculated values of η and ϕ will contain a margin of error, dependent upon the unknown relationship between each property and temperature.

3.11.2 CALCULATED CREEP CURVES

The values of A and B obtained from the stress relaxation tests provided a direct measure of the creep strain associated with the stress relaxation process.

Creep strain was obtained from the Standard Linear Solid

model (section 2.21.6):

$$\epsilon_{Creep} = \frac{\sigma^o}{E} \left(\frac{1}{A} - 1 \right) (1 - \exp^{-ABt})$$

In addition, the elastic strain lost during stress relaxation was calculated by substituting σ^{SR}/E into the above equation. The parameter σ^{SR} is the change in stress which occurs during stress relaxation ($\sigma^{SR} = \sigma^o - \sigma^t$). The calculated creep strains will contain a margin of error once again due to the unknown relationship between the material parameters η and ϕ and temperature, since these parameters are used to calculate values for A. In addition the Youngs Modulus of NES 824 material is only known at room-temperature and since all the calculations represent elevated temperature data this is another source of minor error.

3.12 TEST PROCEDURES FOR ASSESSING THE **CORROSION PERFORMANCE OF 70/30 CUPRONICKEL**

3.12.1 SALT SPRAY TESTS

Samples of 70/30 cupronickel in the cast condition and HIPped at temperatures of 850°C, 950°C and 1025°C for sustain periods of 4 hours with argon gas pressures of 103MPa, were subjected to accelerated corrosion tests which involved the use of a spray cabinet and two types of corrosive medium:

- (i) 5% Salt Solution
- (ii) Substitute Ocean Water designated in the ASTM standard D1141-75 (216), the composition of which is shown in Table 31.

It was unfortunate that, due to the lack of material available, the type of test specimens used was different for the as-cast and the HIPped material. The HIPped specimens consisted of small cylindrical bars which had a machined surface finish. These test pieces were prepared from the grips of tensile specimens used in property evaluations. The as-cast specimens were small plate sections taken from weld plate material and polished to a 1200 grit surface finish. It was assumed that the variation in surface finish was slight and would not cause a significant difference in the rate of corrosion attack.

The salt spray test consisted of suspending the material to be tested on a non-corrosive medium such as fine nylon wire, in a sealed cabinet containing the corrosive medium and a nozzle connected to a compressed air supply. The corrosive medium was forced through the nozzle at a pressure of 15psi to cause a fine mist to develop in the cabinet. The spray tests were carried out at room-temperature for a duration of 72 hourly intervals. Seventy-two hours in the spray was equivalent to 4 weeks in a still solution, due to the increased aeration of the spray test.

The weight and surface appearance of the test specimens were recorded before and after testing. Before being weighed the test samples were ultrasonically cleaned in alcohol to remove any salt deposits which were loosely adhering to the specimen's surface. The duration of the salt spray test was extended to 1008 hours (14 x 72 hourly intervals, approximately equal to 12 months in a still

solution) due to the lack of attack which occurred at shorter time periods. The rate of corrosion attack of both as-cast and HIPped 70/30 cupronickel was determined by weight loss measurements.

3.12.2 SEA WATER CORROSION TESTS

Corrosion samples approximately 75mm x 25mm x 4mm were prepared from cast 70/30 cupronickel. One of the samples was hot isostatically pressed at a temperature of 950°C with argon gas pressures of 103MPa (15000psi) for a sustain period of 4 hours. Both the as-cast and HIPped samples were subjected to exposure for one year, fully immersed in the sea at Holton Heath. The rate of corrosion attack was determined from weight loss measurements. These tests were carried out courtesy of the Ministry of Defence, Bath.

3.12.3 IMPINGEMENT TESTS

Cortest (217), were asked to carry out investigations on the behalf of the Ministry of Defence, to assess the corrosion/erosion characteristics of samples of as-cast and HIPped Cu-Ni-Cr alloy (NES 824), together with two control alloys, nickel-aluminium bronze (NES 747) and 70Cu-30Ni (CN107). These alloys were subjected to impingement tests to determine their impingement performance under specified conditions.

From the three alloys to be tested four samples 80 ± 1mm long, 14 ± 1mm wide and 60mm thick were machined. Holes were drilled symmetrically at either end of the sample, 7mm

in diameter and 60mm between centres, as shown in Figure 83. After machining the samples were wet abraded on the impingement face to produce a 240 grit finish, washed, degreased and photographed so that comparisons before and after testing could be made.

The test solution was natural sea water obtained from the Admiralty Research Establishment at Holton Heath, Poole, Dorset. This test solution was maintained at a temperature of $20 \pm 1^{\circ}\text{C}$ and a velocity of 10m/s for the duration of the test, except during water changes. The total test duration was 30 days, and the sea water solution was drained from the test rig every 5 days and replaced with fresh solution. The samples were attached to a pressure chamber which contained impingement jets of 1mm diameter. The distance between the impingement face of each sample and the jet outlet was 5mm. This distance ensured that the velocity of the solution leaving the orifice had not retarded when it hit the surface of the test sample. The test solution was pumped through the pressure chamber leaving the jet orifices at a velocity of 10m/s (7.8psi). After 10 days on test two samples of each material were scratched with a metal probe across their width, the scratch going through the middle of the impingement zone. The depth of the impingement zone was then measured. The two remaining samples were mounted and polished so that the impingement zone could be examined in greater detail. The rate of impingement attack was determined by depth of attack measurements.

3.13 MODELLING OF THE PORE CLOSURE RATES IN
70/30 CUPRONICKEL CASTINGS BY
HOT ISOSTATIC PRESSING

3.13.1 PLASTIC YIELDING

Densification by plastic yielding can be assumed to be instantaneous once the HIP pressure exceeds the yield stress of the material. The density at the start of the time dependent process is considered to be that produced by plastic yielding.

Pore closure by plastic yielding has been predicted by a equation derived by Wilkinson and Ashby (110,165,178), which determines the starting density for time dependent mechanisms.

$$D_{Yield} = \left[\frac{(1-D_o) P}{1.3 \sigma_y} + D_o^3 \right]^{1/3}$$

This equation was referred to in section 2.15 equation ⁽⁴⁵⁾, and has been used to determine the degree of pore closure for 70/30 cupronickel (NES 824) castings containing 10% and 16% porosity at HIP processing temperatures within the range 800-1025°C, together with argon gas pressures of 103MPa. The results obtained have been compared with experimental zero sustain time data obtained on artificial porosity specimens which contained surface-connected porosity and were encapsulated prior to processing.

3.13.2 PRESSURE ASSISTED SINTERING

The driving force for pore closure during sintering is the surface tension of the material (98). For hot pressing there is an additional externally applied pressure (124). Starting from Mackenzie and Shuttleworth's sintering theory (98), Murray et al (124) proposed a hot pressing theory which was the first published theory on pressure assisted sintering. The basic equation derived from these studies as referred to in section 2.11.6 can be represented as follows:

$$\frac{dp}{dt} = \frac{3}{4} \frac{P}{\eta_{\infty}} (1-p)$$

which can be integrated with respect to time:

$$\ln \frac{1-p}{1-p_0} = -\frac{3}{4} \frac{P}{\eta_{\infty}} t$$

The above equation has been used to predict pore closure rates for 70/30 cupronickel castings containing 10% and 16% porosity, HIPped at a temperature of 950°C and argon gas pressures of 103MPa for time intervals within the range 45 minutes to 12 hours.

The pore closure rates predicted have been compared with experimental data obtained on artificial porosity specimens which contained surface-connected porosity and were encapsulated prior to processing.

3.13.3 HOT ISOSTATIC PRESSING MAPS

Hot isostatic pressing maps for 70/30 cupronickel have been constructed for 70/30 cupronickel (NES 824) by the use of software developed by Ashby (178). HIP 6.0 utilises densification rate equations based on current models of sintering and hot pressing as referred to in section 2.13-2.15; these involve plastic yielding, power-law creep, diffusional creep, volume diffusion and grain boundary diffusion. The software package was mainly intended to model the consolidation of powders and is therefore mainly concerned with stages 1 and 2 of the sintering process. However, the closure of voids in 70/30 cupronickel castings predominantly involved stage 3 of the sintering process. Thus, an attempt has been made to assess the accuracy of the software to model the degree of pore closure and predict the densification mechanisms involved for the consolidation of NES 824 containing initial densities of 0.84 and 0.90 Kgm^{-3} (16% and 10% porosity).

A flow chart which summarises the operation of HIP 6.0 is shown in Figure 84. In order to model the densification of NES 824 castings a material file for 70/30 cupronickel had to be created. This requires 41 input parameters, 25 of which are material parameters, while the rest are plotting variables. The plotting variables enable the axis ranges of the HIP maps to be changed. The material variables that can be entered are shown in Table 32 while the plotting variables are shown in Table 33. The material variables describe the properties of the powder: density, melting point, surface energy, elastic, plastic and creep

properties, diffusion coefficients for lattice, boundary, surface diffusion and boundary migration. As can be seen many of these variables are of a sophisticated nature.

70/30 cupronickel is a casting alloy and only limited material data are available other than room temperature properties. Properties at elevated temperatures were determined in earlier investigations, although the accuracy of this data is uncertain.

The accuracy of the HIP maps predicted depends on the accuracy of the material values entered. Nevertheless, if only limited data is available a HIP map can still be constructed since the program has provision for estimating unknown variables. This of course will involve some unspecified loss of accuracy.

Several HIP maps for 70/30 cupronickel have been predicted for the closure of 10% and 16% porosity at a processing temperature of 950°C and argon gas pressures of 103MPa, by varying the degree of material data imputed. The HIP maps drawn include:

Map Type 1. A HIP map based on 6 known material variables with the rest estimated. The material variables inputted included:

- (i) structure (type 1 - metals and alloys)
- (ii) solid density
- (iii) melting point
- (iv) Youngs Modulus at room temperature
- (v) yield stress at room temperature
- (vi) particle radius

The estimated particle radius of $3.5 \times 10^{-5} \text{m}$ was based on data used by Ashby (178) for the prediction of HIP maps for copper. This was the closest composition to 70/30 cupronickel that could be obtained.

Map Type 2. Addition of the atomic/molecular weight to the material parameters used for the HIP map 1.

The atomic weight for NES 824 was calculated viz:

$$\begin{array}{rcl} \text{Atomic Weight} & = & 70\% \text{ Atomic} \quad + \quad 30\% \text{ Atomic} \\ 70\text{Cu}-30\text{Ni} & & \text{Weight Cu} \quad \quad \quad \text{Weight Ni} \end{array}$$

where molecular weight of Cu = 63.546Kg/kmol

 molecular weight of Ni = 558.71Kg/kmol

Map Type 3. Addition of the weighted atomic volume to the material parameters used in map 2.

The molecular volume/atomic volume was calculated viz:

$$\text{Molecular Volume} = \text{Molecular Weight} / \text{Density}$$

where

molecular weight of 70/30 cupronickel = 62.095Kg/kmol

density of 70/30 cupronickel = 8950Kg/m³

Map Type 4. Addition of an estimated grain size for 70/30 cupronickel derived from grain size measurements carried out on NES 824 HIPped at a temperature of 950°C for sustain periods of 45 minutes, 2,4 and 6 hours and gas pressures of 103MPa (Table 48).

The grain diameter inputted was $8.11 \times 10^{-4} \text{m}$ and was made equivalent to the particle radius for the construction of this map.

Map Type 5. For this map the grain diameter was kept constant at $8.11 \times 10^{-4} \text{m}$ but the particle radius was adjusted to half the grain diameter, $4.05 \times 10^{-4} \text{m}$. The other material variables were in accordance with those used for map 4.

The HIP maps constructed for modelling the densification of 70/30 cupronickel with initial densities of 0.90 and 0.84 Kg m^{-3} were examined in order to observe the pore closure mechanisms taking place, and to determine the optimum processing time required for complete consolidation of the pores. The predicted HIP times were then compared with experimental data obtained for the closure of artificial porosity specimens containing both surface-connected and internal porosity.

4.0 RESULTS

The marine corrosion performance of 70/30 cupronickel castings has been widely investigated and they have been shown to possess excellent corrosion resistance. However, the mechanism of pore closure by HIPping had received little attention and the optimum process parameters needed to remove defects from such castings had not been determined. Hence an evaluation of the hot isostatic processing characteristics of 70/30 cupronickel castings was required.

The effect of HIP processing variables such as temperature, time and pressure on the recovery of 70/30 cupronickel castings containing internal voids and surface-connected porosity has been investigated, together with the influence of pore geometry, and the type of pressure transmitting medium used during encapsulation on the rate of pore closure. In addition investigations to compare the properties of as-cast and HIPped material, encompassing: corrosion performance, mechanical properties and microstructural characteristics have been carried out.

On the basis of previous work (173,213,214) HIPping conditions which involved a temperature of 950°C together with argon gas pressures of 103MPa and a sustain period of 4 hours, were considered satisfactory for the removal of defects from 70/30 cupronickel castings. As a result all experiments carried out to assess the effect of HIPping on cast material properties were carried out under these conditions.

The determination of elevated temperature data for cast 70/30 cupronickel including viscosity, yield strength and ductility has allowed the prediction of pore closure rates by the use of visco-elastic and visco-plastic calculations, as well as the use of computer software to predict HIP maps for NES 824 material. Hence pore closure rates predicted from powder metallurgy theories have been compared with experimental rates determined for a porous solid body.

4.1 HIPPING OF NES 824 CASTINGS CONTAINING SURFACE-CONNECTED POROSITY

Figure 85 shows that the level of porosity in encapsulated castings containing surface-connected porosity fell continuously as the number of type I HIP cycles* increased. 16% porosity was completely removed after 4 such cycles, and 10% porosity in the form of an elongated pore after 2 cycles. Reduction in the elongation of the pores (ie. squat pores) inhibited pore closure: this was particularly evident in the case of specimens that initially contained 10% porosity (see Figures 85 and 86). Three type I cycles were required to close squat pores of large diameter, whereas only two cycles were required for the recovery of elongated pores of small diameter.

* Type I- successive 45 minute HIP cycle. Repeated applications of a HIP cycle that involves holding the specimen for 45 minutes at 950°C with argon gas pressures of 103MPa.

Figure 87 shows the corresponding reduction in porosity during the continuous HIPping of specimens containing the more elongated pores. Unlike the situation produced by the successive application of HIP cycles the continuous process (type II HIP cycles*) did not produce a steady reduction in the porosity level. Instead a very large reduction in porosity occurred during the first 45 minutes (which corresponds to the application of a single cycle in Figure 85), but the subsequent rate of porosity removal was low: as much as 8 hours was required to remove 10% porosity, while 4% porosity still remained after the specimen that originally contained 16% porosity had been processed for 12 hours at 950°C.

A heating and cooling stage is inevitable in any HIP process and in the case of successive type I HIP treatments several such cycles are involved. Figure 88 shows the effect on pore closure of heating to and cooling from the working temperature without any sustain period at that temperature (type IV HIP cycle**). The HIPping pressure was attained simultaneously with the maximum temperature. The same figure shows the decrease in porosity achieved by holding for 45 minutes at the sustain temperature and pressure.

*Type II- Continuous HIP Cycle. Temperature and pressure are applied as a single continuous cycle for various times from 45 minutes to 12 hours.

**Type IV - Zero Sustain Time HIP Cycle.

Figures 89 and 90 show the effect of HIPping temperature on the pore closure rate both with and without any sustain period at the maximum temperature. At 950°C (Figure 89), the initial porosity of 5% was reduced to 2.5% by the heating and cooling stage alone and at 1025°C complete pore closure was achieved. No densification occurred during processing at 850°C. Figure 89 also shows the effect of temperature on the reduction of initially 5% volume porosity when the HIPping temperature and pressure were sustained for 45 minutes. In each case (including 850°C) this period at the HIPping temperature produced some densification. At a temperature of 950°C an increase in the sustain period from 0 to 45 minutes reduced the porosity present from 2.5% to 1.25%. Figure 90 shows the corresponding results when the initial level of porosity was 16%. Although some porosity remained after the completion of the HIP cycle even when 1025°C was employed, the general trends were similar to those obtained with the specimens that initially contained 5% porosity.

Figure 91 shows the effect of maximum HIP pressure on the closure of elongated pores containing initially 10% porosity. The results are given in terms of the number of cycles, each of which involved a period of 45 minutes at the HIPping temperature and pressure. An increase in pressure from 41MPa to 145 MPa produced a steady increase in the rate of pore closure. When the pressure used exceeded 103MPa complete pore closure was achieved by the end of the second cycle.

As far as encapsulation is concerned, it is necessary to separate the effects of the encapsulation process from the effect of the initial heating and holding at temperature for the first cycle. Figure 92 shows the effect of subjecting specimens containing 10% initial porosity to repeated cycles (type III*) without re-encapsulation at the end of each. Comparison with Figure 85 shows that the absence of re-encapsulation greatly reduced the densification in the second and subsequent cycles. These results indicate the importance of the use of fresh pressure transmitting medium around the specimen for each cycle. An attempt was made to determine the extent to which encapsulation using refractory particles as a packing medium hinders the densification process, and how a change in the refractory medium effects pore removal, as will be discussed in a later section.

The properties of as-cast 70/30 cupronickel at elevated temperatures are shown in Figure 93. These indicate that a major reduction in both Ultimate Tensile Strength and Yield Stress occurs with the steepest drop in properties at temperatures between 700°C and 800°C. In this region the difference in value between these properties is very small.

*Type III HIP Cycle - successive short HIP cycles (45 minutes sustain) without renewed encapsulation prior to each HIP cycle.

Figure 93 also shows the relationship between the applied pressure in the HIP operation and the temperature during the heating up stage. Although the stress applied in the HIP process was not uniaxial and therefore not directly comparable with the yield stresses it is evident that plastic flow will only occur when the temperature exceeds 800°C. In practice, the temperature at which yielding starts will be even higher because of the compressive isostatic nature of the pressure.

4.2 HIPPING OF NES 824 CASTINGS CONTAINING CLOSED INTERNAL POROSITY

The advantage of HIPping castings containing only internal pores is that they do not have to be encapsulated prior to processing. Figure 94 shows that internal pores of 10% and 16% initial volume porosity can be recovered by a 45 minute HIP cycle (type I) at 950°C, whereas encapsulated specimens required 2 and 4 cycles respectively (Figure 85).

Figure 95 shows the effect on pore closure of heating to and cooling from the working temperature. A 16% internal pore can be recovered by a zero sustain time HIP cycle whereas a 10% pore can be reduced to 1.76% porosity. It is thought that the reduced wall thickness of the 16% porosity specimen allowed the walls of the specimen to collapse and plastic deformation to occur more easily, thus producing an increase in the rate of densification.

Figure 96 shows the effect of HIP temperature on pore closure using successive type I HIP cycles. At temperatures of 950°C and 1025°C a 16% internal pore can be

recovered by one such cycle. In comparison 10% internal porosity can be closed by one such cycle at temperatures of 925°C and above. Lowering the HIP temperature to 900°C allowed a 10% pore to be reduced to 0.18% porosity which can be considered to be sufficiently recovered. A further reduction in the HIP temperature to 850°C and 875°C required in excess of 4 and 5 type I cycles respectively to close 10% porosity. Figure 97 shows the effect of HIP pressure on the closure of internal pores of 10% and 16% initial volume porosity, and indicates that an increase in the HIP pressure from 62MPa to 103MPa produced a steady increase in the rate of densification. When the HIP pressure exceeded 83 MPa recovery of 10% and 16% internal porosity was possible via a 45 minute sustain HIP cycle. Lowering the pressure to 62MPa required 4 such cycles for the recovery of 10% porosity.

4.3 ENCAPSULATION TECHNIQUES

In order to recover castings containing surface-connected porosity they must be encapsulated prior to HIPping. This involves packing the casting in a steel capsule using a pressure transmitting medium (PTM). This medium must be a refractory medium in order to withstand the high temperatures and pressures involved. Sintering of the refractory particles might prevent their use as a PTM. Figure 98 shows that encapsulation via a close fitting steel capsule which required no packing material produced similar pore closure rates during HIPping to those obtained on specimens containing internal porosity (Figure 94).

That is, complete pore closure after one 45 minute HIP cycle (type I) at a temperature of 950°C with argon gas pressures of 103MPa. In comparison, silica sand the standard PTM used during encapsulation, produced slower pore closure rates. This standard technique required 2 type I HIP cycles to recover the same volume porosity as indicated in Figure 85. This suggests that silica sand diminishes the pressure applied to the specimen due to mechanical locking and partial sintering of the refractory particles once they have reached a maximum packing density. Thus a PTM is required which remains fluid at high temperatures and pressures and allows continuing action of the applied load throughout the HIP process.

In order to find an ideal PTM the effect of a change in the refractory medium on the rate of pore closure of castings containing surface-connected porosity needed to be examined.

4.3.1 EFFECT OF A CHANGE IN THE REFRACTORY PRESSURE TRANSMITTING MEDIUM ON THE RATE OF PORE CLOSURE

Eleven materials were chosen as potential packing materials, all of which were of high purity and high melting point, in order to minimise the risk of sintering due to the presence of low melting point impurity phases. The characteristics of the refractory materials including particle size distribution and melting point are given in Table 28. The refractory materials subjected to HIPping trials can be classified into three groups:

- (i) Oxide, boride and carbide powders.
- (ii) Fragmented glass.
- (iii) Refractory sand.

With the exception of the fragmented glass, encapsulation was renewed prior to each type I HIP cycle carried out until pore closure was complete.

4.3.1.1 OXIDE/ BORIDE/ CARBIDE POWDERS

Figure 99 shows that powders of zirconium oxide, calcined alumina and mixtures of calcined alumina and boron-nitride in weight ratios of 10:1 and 10:3, produced pore closure rates similar to those obtained when using silica sand. That is, two successive 45 minute (type I) HIP cycles were required to close a pore of initially 10% surface-connected porosity. An increase in the ratio of boron-nitride to calcined alumina from 1:10 to 3:10 slightly reduced the rate of pore closure as indicated in Table 34, due to the consolidation of the fine powder particles inside the pore. The migration of fine powder particles into the pore during HIPping and the resultant fall in the rate of pore closure was also experienced with powder mixtures of silicon-carbide and boron-carbide (weight ratio of 10:3).

Figure 100 indicates that with boron-carbide acting as the PTM, 3 type I HIP cycles were required to close 10% surface-connected porosity. The mixture of boron-carbide and silicon-carbide reacted chemically both together and with the steel capsule; this made removal of the test specimen from the encapsulation capsule extremely difficult, and it was impossible to remove the consolidated

refractory from inside the pore without machining. This is the reason for the single data point given for this material in Table 34. Figure 99 also shows that coarse particles such as tabular alumina granules, which are typically plate shaped and angular in nature as indicated in Figure 101, restrict densification due to the particles attaining a maximum packing density in shorter HIP times than fine particles. Three type I HIP cycles were required for the recovery of 10% surface-connected porosity when tabular alumina was employed as the encapsulation PTM.

4.3.1.2 FRAGMENTED GLASS

The use of soda glass as a potential PTM for the HIPping of encapsulated castings was not successful, since the glass foamed and reacted with the steel capsule on heating to temperatures associated with HIPping. In comparison, fragments of borosilicate glass commercially known as Pyrex did not bond to or react with the steel capsule, and only partially fused when heated to 1000°C. Subjecting an artificial porosity specimen containing 10% internal porosity encapsulated in an open topped capsule using fused Pyrex glass as the packing material to a type I HIP cycle, produced pore closure rates comparable to those of un-encapsulated samples containing internal porosity (Figures 94 and 95). That is, complete closure of 10% porosity by a single type I HIP cycle. At this stage it was uncertain whether it was the action of the softened glass which transmitted the applied HIP pressure, or whether the partial fusion of the glass allowed the gas to

come into direct contact with the specimen and itself act as the PTM. To clarify this point a specimen containing internal porosity was once again encapsulated using partially fused Pyrex glass as the packing material, but this time the top of the steel capsule was sealed and the capsule evacuated. The results of this trial are shown in Figure 102, and indicate that complete closure of the 10% internal porosity occurred. This suggests that Pyrex glass at HIP processing temperatures above 950°C is sufficiently viscous to transmit the applied pressure.

For comparison a specimen containing 10% surface-connected porosity was encapsulated as above. After being subjected to a type I HIP cycle at 950°C and 103MPa argon gas pressure, the porosity had reduced to 9.05% (Figure 102). The low pore closure rate is probably a result of the fused glass entering the pore and preventing consolidation.

4.3.1.3 REFRACTORY SANDS

The use of alternative refractory materials as the PTM during the HIPping of encapsulated castings indicated that none of the refractory materials described so far offered any advantages over the use of silica sand. The next step was to investigate the use of alternative silica based sands. Generally silica sand is a desert based sand and has angular shaped particles as indicated in Figures 103 and 104. Hence a study of water based sands which possess a more rounded particle morphology was required. The two sands chosen for investigation included a cheap Zone M Concrete sand (90% quartz aggregate sand),

and a more expensive single particle size Leighton Buzzard sand. The chemical analyses and sieve analyses of these two sands are shown in Tables 28 and 29. The Zone M sand had a particle size distribution within the range 106-305 μ m, the most predominant particle size present being around 150 μ m, the latter being used as a single particle size PTM. Zone M sand contains a small proportion of angular shaped particles as shown in Figure 105. However, the overall appearance of the sand was one of a more rounded particle nature as indicated in Figure 106, when compared to desert based silica sand, Figures 103,104. HIPping of artificial porosity specimens encapsulated using the Zone M sand in the form of an aggregate and a single particle size PTM produced closure of 10% porosity by a single type I HIP cycle at a processing temperature of 950°C and argon gas pressures of 103MPa as shown in Table 35 and Figure 107. Figure 108 shows that a pore representing 16% surface-connected porosity can be recovered by 3 and 2 type I HIP cycles when using a Zone M aggregate and single particle size sand respectively. In comparison the use of a coarser single particle size Leighton Buzzard sand which has a particle size within the range >355 μ m <1.7mm, but still has a rounded particle morphology as shown in Figures 109 and 110, required 3 type I HIP cycles to close 10% porosity. A mixture of the Leighton Buzzard sand and the traditional desert based silica sand, 1:1 by weight, slightly increased the ability of the Leighton Buzzard sand to transmit the applied pressure, requiring 2 type I HIP cycles to close 10%

porosity. However this mixture has no advantages over the use of silica sand on its own as the PTM.

4.3.2 INVESTIGATION INTO THE OUT-GASSING OF REFRACTORY SANDS AND THE CHEMICAL INTERACTION BETWEEN SILICA SANDS AND 70/30 CUPRONICKEL

HIPping investigations carried out to determine the effect of encapsulation techniques on the rate of pore closure of specimens containing surface-connected porosity identified Zone M Concrete sand as an alternative PTM to the standard desert based silica sand, since it produced a greater rate of pore closure than the latter. Thus future commercial encapsulation of castings could involve this sand, and for this reason investigations to determine the risk of outgassing or the chemical reaction of either desert based or water table silica sand with NES 824 material was carried out.

Optical and Scanning Electron Microscopy examination of cylindrical samples encapsulated and HIPped using both types of silica sand as the packing material, and HIPped for 45 minutes at a temperature of 950°C with argon gas pressures of 103MPa were carried out. The samples were cleaned via shot blasting and ultrasonic methods prior to investigation. Examination revealed both samples to have a dimpled surface caused by indentation of the sand particles as shown in Figures 111 and 112. The sample packed with Zone M sand had a less prominent surface texture due to the finer particle size of the material (Figure 112). SEM examination of the textured surfaces indicated that the

sample packed in desert based silica sand had particles embedded in its surface as shown in Figure 113. This was even the case after the sample had been cleaned. The removal of the silica particles left behind large angular craters, Figure 114. In comparison the sample packed in Zone M sand was more easily cleaned after HIP processing with the majority of sand particles being removed leaving behind a less severe surface texture as shown in Figure 115.

The appearance of the steel capsules containing both types of silica sand after HIPping were not bloated, so it can be assumed that silica sand does not out-gas during hot isostatic pressing.

In addition SEM examination of the sample surfaces failed to identify any signs of chemical interaction between the NES 824 and silica sand. Therefore it can be assumed that at the temperatures and pressures used to commercially HIP 70/30 cupronickel castings silica sand remains inert.

4.4 COMPRESSIVE STRENGTH CHARACTERISTICS OF SILICA SAND

The results obtained suggest that silica either in the form of a desert based sand or a water table sand appears to be the favoured packing material for use during encapsulation of castings prior to HIPping. However, desert based silica sand impedes the densification of castings due to the mechanical locking of the refractory particles once they have attained a maximum packing density. This suggests that silica sand has a considerable compressive strength even at high temperatures and

pressures.

Typical tests carried out on refractory sands to determine their green strength involve the ability of the sand to hold together in the form of a small cylindrical compact whilst undergoing a crushing load. This type of test when carried out on silica sand, zone M concrete sand and Leighton Buzzard sand produced little information since the sands had no strength while in the form of a compact. This was thought to be due to their low moisture content which was confirmed by carrying out moisture tests using the Speedy Moisture tester. These revealed that the moisture content of all three sands was too low to be accurately measured, the moisture content being less than 0.5%.

The strength of encapsulated and HIPped silica sand (desert based) was investigated by compression tests carried out on two types of test samples as shown in Figure 70. The compressive load at which the sand samples failed to resist deformation was recorded and the results obtained are shown in Table 36. These results indicate that the compressive strength of HIPped silica sand increases with an increase in the HIP pressure, until a critical pressure of around 103MPa is reached. Further increases in the HIP pressure had negligible effect on the compressive strength of the encapsulated sand. These results indicate that at lower HIP pressures silica sand will flow more easily and it might be expected to transmit the applied pressure throughout the densification process. However pore closure rates obtained for HIP pressures in the range 41-83MPa have shown this not to be the case since in excess of 2 type I

HIP cycles were required to close 10% surface-connected at these lower HIP pressures as shown in Figure 91.

4.5 EFFECT OF PTM THICKNESS ON THE RATE OF PORE CLOSURE **OF CASTINGS CONTAINING SURFACE-CONNECTED POROSITY**

The extent to which silica sand restricts densification has been investigated by HIPping specimens containing 1% and 10% surface-connected porosity in steel encapsulation capsules of varying diameter, HIPped at standard conditions of 45 minutes sustain time at a temperature of 950°C with argon gas pressures of 103MPa. The results of these HIP experiments are shown in Table 37, and indicate that the extent of pore closure decreases with an increase in the PTM thickness. Increasing the refractory packing thickness above 13mm significantly reduces the amount of pore closure which takes place. Therefore for maximum consolidation of encapsulated castings the packing material thickness must be kept to a minimum. However, the PTM thickness for a marine casting is often determined by the geometry of the casting since the production of a close fitting capsule is often difficult and involves numerous welded joints which increase the possibility of capsule failure during HIPping. Table 37 shows the effect of sample diameter on the rate of pore closure using PTM thicknesses comparable with those used in earlier investigations. These results indicate that for a constant PTM thickness increasing the sample diameter appears to improve the rate of pore closure. For example a sample of 38.4mm diameter encapsulated with a 18.3mm PTM thickness allowed the initial porosity of 1% to

reduce to 0.35% porosity, an overall pore closure of 65%. In contrast a sample of 12.7mm diameter packed in a capsule allowing a similar PTM thickness of 18.65mm revealed that a 10% pore could be reduced to 4.57% porosity, an overall pore reduction of 45.7%. However several factors will influence the above trend: firstly the volume of the pore will effect the rate of densification since a small pore will consolidate quicker than a pore of larger volume. Secondly any pore situated close to the surface of a casting will densify in a shorter time than a pore a greater distance away from the surface. Thus general trends predicted by the HIPping experiments need to be considered with caution since more than one factor influences the rate of pore closure, and more experiments are required to substantiate which are the most influential.

4.6 CHANGES IN PORE SHAPE DURING HIPPING

The changes in shape of a small diameter elongated pore representing 16% surface-connected porosity in a specimen that was encapsulated and subjected to successive type I HIP cycles at a temperature of 950°C with argon gas pressures of 103MPa are shown in Figure 116. The pore quickly became elliptical in shape and experienced a reduction in diameter but with little overall change in length as observed after 1 and 2 successive 45 minute HIP cycles. Thereafter the rate of consolidation of the blind end of the pore increased relative to that at a position close to the two mating surfaces of the artificial porosity

specimen, producing a tapered pore which underwent complete densification after 4 type I HIP cycles. The inhomogeneous densification of the pore is thought to be related to several factors including pore and sample geometry; the connection of the pore to the surface of the sample, capsule design and the use of silica sand as the PTM. If during HIPping the PTM seeps between the two mating surfaces and into the pore it can hinder densification significantly.

In comparison the unsuccessful closure of internal porosity due to low pressure or temperature shows a variation in the stages of pore consolidation as illustrated in Figure 117, which shows the closure of 10% internal porosity using successive type I HIP cycles at a temperature of 850°C and argon gas pressures of 103MPa. This figure indicates that the walls of the sample collapse quickly due to their reduced wall thickness, while the extreme ends of the pore retain strength and support the applied load so producing a pore which has the shape of a dog bone. In many cases a small residual porosity remains at the extreme ends of the pore, observed as small isolated areas of rounded porosity.

4.7 MECHANICAL PROPERTIES OF 70/30 CUPRONICKEL

The mechanical property evaluations carried out on HIPped 70/30 cupronickel (NES 824) material are considered representative of material which has been cast, encapsulated and HIPped in order to remove surface defects, microporosity and shrinkage cavities.

4.7.1 EFFECT OF HIP TEMPERATURE ON MECHANICAL PROPERTIES

4.7.1.1 70/30 CUPRONICKEL WELD PLATE

Hot isostatic pressing of weld plates, Figure 118, at temperatures of 850°C, 950°C and 1025°C with argon gas pressures of 103MPa sustained for a period of 4 hours had no detrimental effects on the as-cast properties, as shown in Figure 119. The HIP process appears advantageous in that the ductility and toughness of the as-cast material had significantly improved as a consequence of HIPping at temperatures above 850°C. The ductility (% Elongation) of the cast material increased from 16% to 24% after HIPping at 950°C. In addition the Charpy V-notch impact toughness increased from 73 to 126 and 164 Joules after HIPping at temperatures of 950°C and 1025°C respectively. HIPping appeared to have no significant effect on the Yield Stress (YS) of the cast material, but the Ultimate Tensile Strength (UTS) increased considerably with an increase in the HIPping temperature as shown in Table 38.

4.7.1.2 70/30 CUPRONICKEL TEST BAR MATERIAL

The results of the mechanical property evaluations carried out on as-cast and HIPped mechanical property test bars shown in Table 39 (173,213), predict similar trends to those observed in the case of weld plate material as shown by comparison of Figures 119 and 120. Figure 120 shows that HIPping of test bar material improved ductility and produced a slight increase in strength as the HIP temperature was increased from 850°C to 1025°C. The maximum strength was achieved on HIPping at 1025°C, although this higher strength was accompanied by a slight reduction in ductility.

4.7.2 EFFECT OF HIP TIME ON PROPERTIES

The maintenance of the optimum HIP processing conditions which involved a temperature of 950°C and argon gas pressures of 103MPa, and variations in the HIP sustain time to include 45 minutes, 2, 4 and 6 hours indicated that the extension of the HIP time had no significant effect on the strength of HIPped material. However, the Charpy impact toughness reached a maximum of 140 Joules after a HIPping period of 2 hours. Extension of the HIP time further to 4 and 6 hours revealed a slight reduction in toughness as shown in Figure 121.

4.7.3 EFFECT OF STRESS RELIEF ON THE MECHANICAL

PROPERTIES OF 70/30 CUPRONICKEL

Stress relieving cast 70/30 cupronickel had a beneficial effect on both strength and ductility as shown in Table 40. Therefore the next step was to determine whether stress relief would enhance the properties of HIPped material.

4.7.3.1 THERMAL SIMULATION OF A HIP TREATMENT

A mechanical property evaluation was carried out on as-cast 70/30 cupronickel material subjected to a simulated thermal HIP treatment (215), which consisted of: heating at 15°C/minute to 950°C, holding for 4 hours followed by furnace cooling at 8-10°C/minute. The results of these tests showed the cast material to have suffered a slight reduction in strength as indicated in Figure 122. The material was then subjected to a stress relieving treatment: 2 Hours at 475°C, followed by cooling in air, and the strength (UTS) of the material was reinstated above that of the cast material, whilst ductility remained unaffected.

4.7.3.2 EFFECT OF STRESS RELIEF ON HIPPED

70/30 CUPRONICKEL MATERIAL

70/30 cupronickel which had been HIPped at 950°C for 4 hours with argon gas pressures of 103MPa was subjected to a stress relieving treatment which consisted of 2 hours at 475°C followed by cooling in air. This produced a slight reduction in yield stress, but slightly increased the Ultimate Tensile Strength, ductility and Charpy impact

toughness, as shown in Table 41. These results were found to be confusing since the reduction in Yield Stress accompanied by an increase in the Ultimate Tensile Strength could not easily be explained. In addition the increase in ductility would seem unlikely when coupled with the increase in strength. Taking into account the scatter of results it was decided that no benefits could be gained by the stress relief of HIPped material. This assumption was confirmed by HIPping experiments which incorporated the stress relieving treatment into the HIP cycle. This involved cooling from the sustain conditions at a rate of 10°C/minute to 450°C and holding for 2 hours, after which natural cooling was resumed until ambient was reached. A mechanical property evaluation revealed that such a combined HIP and stress relieving treatment produced a slight reduction in the strength and ductility of the HIPped material as shown in Table 41.

4.7.4 THE EFFECT OF HIPPING ON THE PROPERTIES OF RECOVERED CASTINGS

Although the effect of HIPping of sound castings or cast material containing less than 5% porosity has been found to be beneficial, no data was available on HIP recovered castings which contained large shrinkage defects prior to HIPping. Therefore investigation into the effect of using the HIP process for the recovery of large shrinkage defects in commercial castings was necessary, in order to investigate the effect of HIPping on the as-cast properties and microstructural characteristics.

4.7.4.1 M.O.D. CAST BLOCK CONTAINING SHRINKAGE POROSITY

A M.O.D casting containing a severe shrinkage defect as illustrated schematically in Figure 73 was encapsulated and HIPped using standard commercial parameters, which consisted of a temperature of 950°C sustained for a period of 4 hours, with argon gas pressures of 103MPa. Mechanical property investigations which encompassed strength and ductility were carried out on material representing:

- (i) Sound areas of the casting containing < 5% porosity.
- (ii) Recovered material which originally contained the shrinkage defect.
- (iii) Material adjacent to the original defect.

The results are shown in Table 42 and indicate that the Yield Strength of the recovered defect material was relatively unaffected and was comparable with that of the sound material. However, the Ultimate Tensile Strength and ductility (% Elongation) of the material representing

the repaired defect material reduced significantly, falling as low as 391MPa and 6%, compared to 485-516MPa and 16-19% in other areas of the casting.

4.7.4.2 HIP RECOVERED CASTINGS

The low ductility observed in HIP repaired castings especially in material at the original defect site was of special interest, and further investigations were required in order to determine the risks involved with HIPping of NES 824 material.

A worm gear casting containing surface-connected porosity was encapsulated and HIPped using identical conditions to the previous investigations. After this mechanical property evaluations were carried out on sound and recovered defect areas of the casting. The results of this HIPping experiment are shown in Table 43, and reveal that the strength of the recovered casting at the original defect site increased significantly, the 0.2% Proof Stress being increased from 547MPa to 596MPa. In contrast, the sound areas of the casting underwent a slight reduction in strength after HIPping, the 0.2%PS fell from 359MPa to 319MPa. Comparison of the ductility in the as-cast condition (21.0%) and that of the sound HIPped material (21-22%) showed no change. However, the ductility of the HIPped recovered defect area was significantly reduced to 17.5%.

These HIPping experiments carried out to determine the ability of hot isostatic processing to recover casting

defects and its effect on the as-cast properties produced many interesting but conflicting results. Therefore a more controlled experiment was considered necessary and involved the casting of two 70/30 cupronickel test plates. One plate was cast sound whilst the other was cast to deliberately contain shrinkage defects and surface-connected porosity. The two plates were then encapsulated and HIPped using the standard conditions used previously. The test plates were then subjected to a mechanical property evaluation the results of which are shown in Table 44. The results indicate that there is negligible difference in the strength and ductility of sound and HIP repaired material, both showing a significant increase in properties compared to the as-cast material. The strength of the HIP recovered casting increased by 45-58%; while the 0.2%PS increased from 290MPa to 525MPa. Ductility improved by 700%, increasing from 3% to 24%.

4.7.5 HOT DUCTILITY OF 70/30 CUPRONICKEL

The properties of as-cast NES 824 material at elevated temperatures have been investigated by carrying out tensile tests over the temperature range 300-1025°C. The results obtained are given in Table 45, which shows that strength levels (Yield Stress and Ultimate Tensile Strength) decreased with increasing temperature. However the hot strength appeared not to change significantly until temperatures above 500°C were reached. Strength then decreased sharply until a plateau was observed at temperatures between 850-950°C; minimum strength was

observed at the highest test temperature of 1025°C as indicated in Figure 123.

The hot ductility of 70/30 cupronickel was found difficult to measure because the load-extension curves, especially at higher temperatures, did not show a well defined point of fracture, since the load decreased in stages as shown in Figure 78. Consequently a standardised ductility has been measured; viz elongation the specimen undergoes prior to necking, that is the extension caused by attaining the maximum load as also illustrated in Figure 78. The results indicated that ductility reached a maximum at two points, Figure 123, one at low temperatures around 300°C and the other at high temperatures of 1025°C. However a ductility trough was encountered between the temperature range 600-800°C.

4.7.6 CONSTANT LOAD DUCTILITY TESTS

A constant load-ductility test has been developed in order to simulate the stresses experienced during the cooling stage of the HIP cycle. A schematic illustration of a load-extension curve obtained from carrying out a constant load tensile test is shown in Figure 82.

The results of the constant load ductility tests indicated that 70/30 cupronickel undergoes embrittlement leading to failure within the temperature range 600-800°C as shown in Table 46. The same table shows the Yield Stress, maximum load and ductility attained during testing. The ductility of the specimens increased with increasing temperature and

reached a peak around 31%, before decreasing due to embrittlement.

4.8 MICROSTRUCTURAL CHARACTERISTICS OF 70/30 CUPRONICKEL MATERIAL

4.8.1 EFFECT OF THE TYPE OF HIP CYCLE USED TO CLOSE POROSITY ON THE RESULTANT MICROSTRUCTURE

The type of HIP cycles predominantly used to investigate pore closure in artificial porosity specimens included type I and type II HIP cycles.

Microstructural examination of HIP recovered artificial porosity specimens which originally contained 10% surface-connected porosity recovered by either two successive type I cycles at a temperature of 950°C with argon gas pressures of 103MPa, or by a single 8 hour type II HIP cycle, revealed that the resultant microstructure was not dependent on the type of HIP cycle used. Both type I and type II HIP cycles produced plastic deformation and recrystallisation of the worked microstructure followed by grain growth as shown in Figure 124.

4.8.2 EFFECT OF HIP TEMPERATURE ON THE MICROSTRUCTURE OF 70/30 CUPRONICKEL

Previous HIP investigations (173,213) have indicated that the optimum processing temperature for 70/30 cupronickel in regard to improved strength and ductility whilst minimising grain growth is around 950°C. However the effect of HIP temperature on the homogenisation of cupronickel and hence its potential effect on corrosion

performance had not previously been studied.

The effect of HIP temperature on the degree of segregation observed in cast 70/30 cupronickel has been investigated for HIP temperatures of 850°C, 950°C and 1025°C, sustained for a period of 4 hours with argon gas pressures of 103MPa. The investigations involved optical examination and SEM/EDAX quantitative (ZAF4) spot analysis of three areas of the HIPped microstructure representing:

- (i) primary dendrite arms;
- (ii) interface material between the dendrite and the matrix;
- (iii) matrix material.

Optical examination of specimens polished and etched in 10% alcoholic ferric chloride revealed that the grain size of cast cupronickel increased as the HIP temperature increased. Such an observation would be consistent with expectation, although a quantitative measurement of grain size was not possible. The appearance of a section at low magnifications was misleading since the examination of single grains at higher magnifications revealed an accumulation of smaller sub-grains. Thus only a qualitative comparison of a change in grain size with increasing HIP temperature can be made, as shown in Figure 125. This figure also indicates that the extent of segregation appeared to diminish with an increase in the HIP processing temperature.

The results of the SEM/EDAX quantitative spot analyses are shown in Table 47, with the trends for the two major

alloying elements shown in Figure 126, both the table and the figure indicate that HIPping cast 70/30 cupronickel tends to have a slight homogenising effect, and that the effect increases with an increase in the HIP temperature. An increase in the HIP temperature from 850°C to 1025°C reduced the prominence of the nickel dendrites in the microstructure, and the general analysis of the matrix material approached the nominal composition ie. 70%Cu and 30%Ni.

The results of both the optical and quantitative segregation analysis investigations suggest that cast 70/30 cupronickel becomes increasingly homogenised as the HIP temperature increases, ie. coring becomes less extensive.

4.8.3 SCANNING ELECTRON MICROSCOPY OF HIPPED 70/30 CUPRONICKEL MATERIAL

Examination of the tensile fracture surfaces using scanning electron microscopy revealed that specimens subjected to all three HIP temperatures studied (850°C, 950°C and 1025°C) possessed similar structures, a ductile matrix containing large randomly distributed matrix oxides, and small evenly distributed zirconia based particles. The latter were found in the bottom of ductile dimples. This observation suggests that the presence of the zirconia based particles may have initiated tensile fracture. A typical example of the fracture surface of a test bar HIPped at 850°C is shown in Figure 127. The matrix oxides and zirconia based particles are more clearly identified at

higher magnifications as shown in Figures 128 and 129 respectively. Figure 130 shows a back scattered electron image where the zirconia based particles can be more clearly distinguished from the matrix material. Identification of the particles present was carried out by EDAX analysis as shown in Figure 131 which indicates an element peak intensity curve appropriate to zirconium and oxygen.

4.8.4 EFFECT OF HIP TIME ON THE MICROSTRUCTURE OF **70/30 CUPRONICKEL**

Commercial HIP conditions used for the recovery of 70/30 cupronickel castings involve a processing temperature of 950°C held for a period of 4 hours with argon gas pressures of 103MPa. However HIP experiments have shown that 10% to 16% surface-connected and internal porosity can be recovered by shorter HIP times, and that optimum mechanical properties are obtained after a HIP period of 2-4 hours. Until now the effect of HIP temperature on the resultant microstructure and its possible effect on corrosion due to enhanced homogenisation had not been investigated. The effect of HIP time on grain size and segregation has been investigated for sustain periods of 45 minutes, 2,4 and 6 hours.

4.8.4.1 GRAIN SIZE

Mean grain sizes taken from 100 random fields of view of material HIPped for 45 minutes, 2,4 and 6 hours are shown in Table 48. The results indicate that increasing the HIP

time from 45 minutes to 6 hours has no significant effect on the mean grain size of the HIPped material. The mean grain size after being HIPped for 45 minutes is $9.744 \times 10^{-5}\text{m}$ which increases to $2.540 \times 10^{-4}\text{m}$ after being HIPped for 6 hours. The scatter of grain sizes associated with cast material due to variations in cooling rate would account for the marginal differences in grain size observed. Figure 132 allows qualitative comparison of the microstructures observed in 70/30 cupronickel material HIPped for periods of 45 minutes, 2, 4 and 6 hours.

4.8.4.2 SEGREGATION

The effect of increasing the sustain period for material HIPped at a temperature of 950°C with argon gas pressures of 103MPa within the range 45 minutes to 6 hours has been investigated via the use of SEM together with EDAX analysis techniques, which involved quantitative (ZAF4) spot analyses of three areas of the HIPped microstructure:

- (i) centre of a primary dendrite arm;
- (ii) interface between the dendrite and the matrix;
- (iii) matrix material.

The mean nominal analyses of ten such regions of cast and HIPped material are shown in Table 49, in addition the results for the two major alloying elements Cu and Ni are represented graphically in Figure 133. The results indicate that HIPping has a slight homogenising effect on the segregation of the alloying elements, since after HIPping the Ni rich dendrites become less prominent and the Ni and Cu content of the matrix areas becomes closer to the

specification requirements ie. 70%Cu and 30%Ni. However increasing the HIP sustain period from 45 minutes to 6 hours did not enhance the degree of homogenisation, and would therefore have little effect on the corrosion performance of 70/30 cupronickel.

4.8.5 EMBRITTLEMENT OF 70/30 CUPRONICKEL **AT ELEVATED TEMPERATURES**

70/30 cupronickel specimens subjected to both elevated temperature tensile and stress relaxation tests within the temperature range 600-750°C experienced a loss of ductility, and the stress relaxation samples failed to support a load at these temperatures. Standard ductility* falls to as low as 0.04% at a test temperature of 700°C, as shown in Table 45.

Visual examination of the elevated temperature test specimens after testing revealed the appearance of cracks along the gauge length. Typical cracks observed in the polished cross-section of the gauge length are shown in Figure 134. The cracks were initiated at the edges of the specimen and then propagated along grain boundaries as shown in Figures 135 and 136, which represent material stress relieved at temperatures of 700°C and 750°C respectively.

*Standard ductility is measured as the elongation the tensile specimen undergoes prior to necking, that is extension caused by attaining a maximum stress as illustrated in Figure 78.

In addition cracks were initiated at sites of porosity in the cast material, as shown in Figure 137, after which the cracks followed in most instances a grain boundary path. Voids also appeared to have developed at triple points with coalescence along grain boundaries as shown in Figure 138, which revealed a net work of voids and cracks.

4.8.6 MICROSTRUCTURAL EVALUATION OF A HIP RECOVERED **MINISTRY OF DEFENCE NES 824 CASTING**

A M.O.D cast block of NES 824 containing a large shrinkage cavity, the position of which is illustrated in Figure 73, was encapsulated and HIPped using standard commercial HIP conditions. After HIPping two sections of the casting representing sound HIPped material and material which originally contained the shrinkage cavity respectively were surface ground and etched in alcoholic ferric chloride for macro-examination. The macro-structures revealed are shown in Figure 139. The sound material exhibited a coarse equiaxed grain structure, whereas the defect material exhibited a macro appearance similar to that expected for a cast ingot, and contained elongated columnar chill crystals and a fine equiaxed structure in the centre of the material section. The chill crystals which formed during solidification would have originally surrounded the shrinkage cavity which formed due to the unsuccessful feeding of the casting during solidification. During HIPping the application of the high pressures necessary to cause plastic deformation caused the material to become work/strain hardened, which at the high temperatures

involved induced nucleation and recrystallisation to occur. This produced a fine grained microstructure in the region of the HIP recovered casting that originally contained the shrinkage cavity.

The material adjacent to yet below the original shrinkage cavity exhibited a coarse grain size which was larger than that of the sound material. This is thought to be a result of the heat sink which occurs during the casting / solidification process and is not a feature caused by HIPping.

Further slices of material taken from the HIPped casting representing material between the edge of the casting and the recovered defect, were polished and etched. These revealed that the grain size of the casting increased slightly towards the edge, as shown in Figure 140. This was a result of grain growth since the outer edges of the casting would have been subjected to high temperatures for a minimum of 4 hours.

Comparison of mechanical property evaluations carried out on sound and recovered areas revealed the recovered defect areas to be low in ductility as discussed in section 4.7.4.1. Microstructural examination of the same areas of the casting revealed that sound material exhibited extensive coring as shown in Figure 141, together with the presence of precipitates both within the matrix and along grain boundaries as shown in Figures 142 and 143 respectively. In comparison the extent of segregation observed in the defect recovered material was reduced,

Figure 144, and showed a recrystallised grain structure. The presence of twins indicates the degree of deformation sustained in this region of the casting. Precipitates were once again observed at grain boundaries and within the matrix as shown in Figures 145 and 146. The increase in grain boundary surface area due to recrystallisation has increased the number of sites available for precipitation. Thus HIPped recovered material contained an increased amount of precipitate. SEM examination together with EDAX analysis techniques identified the precipitates to be rich in Ni, Zr and Si as shown by the X-ray peak intensity curves in Figure 147. The presence of these intermetallic precipitates is thought to be the cause of the low ductility in HIP recovered defect material.

4.9 CORROSION PERFORMANCE OF 70/30 CUPRONICKEL

Investigations have been carried out to compare the corrosion resistance of 70/30 cupronickel in the as-cast and HIPped condition to three types of corrosive media:

- (i) 5% salt solution;
- (ii) substitute ocean water;
- (iii) sea water.

The corrosion resistance of 70/30 cupronickel to the first two types of medium has been determined with accelerated salt spray tests. In addition the corrosion tests were carried out in flowing sea water and included submerged flow and impingement tests.

4.9.1 ACCELERATED 5% SALT SPRAY TESTS

The amount of corrosive attack which occurred on both as-cast 70/30 cupronickel and material HIPped at temperatures of 850°C, 950°C and 1025°C for a period of 4 hours with argon gas pressures of 103MPa, in a 5% salt spray was negligible. The test duration was 504 hours (7 x 72 hourly intervals), and the small weight losses recorded are shown in Table 50. Due to the lack of corrosion products formed the tests were resumed for a total period of 1008 hours, which is equivalent to 56 weeks immersion in a still salt solution. The weight loss measurements recorded after the extended time on test are also shown in Table 50, and indicate that the weight loss of as-cast specimens was within the range 0.00195g to 0.0022g for specimens of initial weight 8-12g. In comparison HIPped material suffered weight losses of 0.0031g, 0.0031g and 0.0030g for material HIPped at temperatures of 850°C, 950°C and 1025°C respectively for specimens of initial weight 40-45g. Thus there appears to be little difference between the corrosion performance of as-cast and HIPped 70/30 cupronickel in a 5% salt solution, and both appear highly resistant to corrosive attack. The negative weight changes indicate that the small amount of corrosion which occurred was caused by pitting of the surface layers of material.

4.9.1.1 HOT ISOSTATICALLY PRESSED MATERIAL

The appearance of the HIPped corrosion specimens after 504 and 1008 hours on test are shown in Figure 148, which indicates that after extended time on test the degree of tarnishing increased and corrosive pitting became more apparent.

Detailed SEM examination of the specimen surfaces after 504 hours on test revealed isolated areas of pitting as shown in Figure 149, which represented material HIPped at 1025°C. However the pitted appearance is also representative of material HIPped at 850°C and 950°C. SEM examination of the test specimens after 1008 hours on test revealed the majority of the specimens surface to be prone to a small degree of preferential phase corrosion of dendritic regions as shown in Figure 150. In addition isolated areas of more severe corrosion attack were observed as extensive cracking and peeling of the surface layers of material as shown in Figures 151 and 152. These corrosion features are thought to be associated with preferential attack of dendritic regions. Other corrosion features observed included intergranular corrosion and cratering as shown in Figures 153-155. Figure 155 also shows evidence of pitting or removal of precipitates from the matrix (bottom left-hand side of the SEM micrograph). These pits then act as initiation sites for cratering. The SEM micrographs showing the corrosion features identified in HIPped 70/30 cupronickel represent isolated areas of the worst attack examined and are not to be considered representative of the 70/30 cupronickel

performance overall, since very little corrosion was evident. Thus HIPped 70/30 cupronickel is extremely resistant to corrosion attack in a 5% salt solution.

4.9.1.2 AS-CAST MATERIAL

An increase in the test duration from 504 to 1008 hours approximately doubled the weight losses recorded, as shown in Table 50. Even so the extent of corrosion which took place was insignificant. An extension of the test duration resulted in heavy tarnishing of the specimens which produced an etched appearance and outlined the dendritic microstructure as shown in Figure 156. The etched appearance indicated that preferential phase attack of dendritic regions was taking place. Figure 156 also shows that after 1008 hours on test accelerated corrosion of the diagonal cross-section of the specimens had occurred, shown by the presence of a black corrosion product film. This area of advanced formation of the protective corrosion product film was thought to be a result of the sample geometry and the test conditions. The as-cast specimens are plate like and are suspended on a nylon wire by a hole drilled in the corner of the sample. As a consequence during testing the spray condenses on the wire and collects in the hole and over-flows across the diagonal cross-section of the sample. As a result the majority of corrosion occurred around the machined hole as shown in Figure 157. Corrosion features identified on as-cast specimens included cracking and peeling of the surface layers of material, pitting and interdendritic corrosion as

shown in Figures 158 and 159. Apart from the increase in corrosion around the machined hole the remainder of the specimens surface showed little change from its appearance after 504 hours on test. The extent of corrosion which had taken place across the diagonal cross-section of the sample is shown in Figure 160. SEM/EDAX analysis of the protective film produced after 1008 hours on test revealed that it was too thin to be analysed.

4.9.2 SUBSTITUTE OCEAN WATER SPRAY TESTS

Accelerated spray tests were carried out on as-cast 70/30 cupronickel and material HIPped at 850°C, 950°C and 1025°C using substitute ocean water (216) as the corrosive medium, the composition of which is shown in Table 31. The results revealed weight losses of 0.0009g - 0.0013g for cast material after 1008 hours on test. In comparison HIPped material suffered weight losses of 0.0028g, 0.00135g and 0.0034g for material HIPped at temperatures of 850°C, 950°C and 1025°C respectively, as shown in Table 51. These results indicate that there is negligible difference between the corrosion performance of as-cast and HIPped 70/30 cupronickel in substitute ocean water, and that the rate of corrosion is comparable to that experienced in a 5% salt solution.

4.9.2.1 HOT ISOSTATICALLY PRESSED MATERIAL

Visual examination of specimens representing HIPped 70/30 cupronickel material after 1008 hours on test showed no evidence of tarnishing, as shown in Figure 161. SEM examination of the test specimens also revealed little sign of any corrosive attack on specimens representing material HIPped at 850°C and 950°C. The small amount of corrosion observed included pitting and cratering as shown in Figure 162. Corrosion appeared to have occurred preferentially in dendritic regions, Figure 163. These sites then acted as nucleation sites for cratering. The larger weight loss observed in the specimen representing material HIPped at 1025°C appeared to be caused by the erosion of an iron based precipitate situated at the surface of the specimen, since 25% of the specimens surface was covered by an iron oxide deposit (Figure 164). The oxide deposit was identified to be rich in iron by SEM/EDAX analysis as shown by the X-ray intensity peak in Figure 165. Apart from this isolated area of attack very little other corrosion was evident apart from small areas of cratering (Figure 166).

4.9.2.2 AS-CAST MATERIAL

The visual appearance of the as-cast specimens after 1008 hours test duration in a substitute ocean water spray revealed a tarnished or etched appearance (Figure 161). Semi-quantitative ZAF4/EDAX analysis of the corrosion product film revealed it to be rich in nickel, and oxygen with traces of chlorine and carbon as shown in Figure 167.

SEM examination of the as-cast specimens showed that little corrosive attack had occurred, that present being in the form of cracking and peeling of the surface layers of material and cratering (Figures 168 and 169). Figure 170 shows corrosion of areas adjacent to micro-porosity together with erosion of pits caused by the removal of precipitates from the matrix.

4.9.3 CORROSION PERFORMANCE OF 70/30 CUPRONICKEL **(NES 824) TO NATURAL SEA WATER**

4.9.3.1 FULL IMMERSION AND CREVICE CORROSION TESTS

Material representing as-cast NES 824 and material HIPped at a temperature of 950°C for a period of four hours with argon gas pressures of 103MPa has been subjected to full immersion and crevice corrosion tests in the sea at Langstone Harbour. After exposure for one year an assessment of the specimens performance was made. Details of the specimens placed on test, period of exposure and rate of corrosion attack are given in Table 52, the rate of attack was calculated in mm/year. The results reveal that for the standard full immersion specimens a maximum mean depth of attack of 0.0117mm/year and 0.0143mm/year was observed for cast and HIPped material respectively. These results indicate the high corrosion resistance of both cast and HIPped 70/30 cupronickel material. The appearance of the HIPped samples after 12 months immersion is shown in Figure 171, which indicates the presence of a shiny black corrosion product film on one side of the test specimens. It was assumed that the side with the black

oxide coating suffered increased sea water flow across its surface. SEM examination of the corrosion product film revealed it to be etched, making the dendritic microstructure clearly visible as shown in Figure 172. Examination in more detail revealed preferential attack of dendritic regions as shown in Figure 173. SEM / EDAX analysis of these regions confirmed that they were associated with nickel rich areas as shown in Figure 174, which predominantly indicates the presence of nickel oxide. In addition the corrosion product film had undergone cracking which leads to loss of the protective coating, as shown in Figure 175. In comparison SEM examination of the matt side of the immersion specimens revealed the oxide coating to be less well developed. Analysis of the coating showed it still to be of a nickel rich oxide but traces of the matrix material were present. Here copper and chromium were present which indicated that the thickness of the coating was less than that observed previously as shown in Figure 176.

The crevice corrosion trials indicated maximum mean rates of attack to be approximately 0.04mm/year and 0.029mm/year for as-cast and HIPped material respectively as shown in Table 52. The appearance of the HIPped specimens after 6 months on test are shown in Figure 177. The specimens have a matt appearance similar to that observed on one side of the immersion specimens, which had a less well developed corrosion product protective coating. Once again there appears to be very little difference between the corrosion performance of cast and HIPped NES 824.

4.9.3.2 IMPINGEMENT RESISTANCE

Impingement resistance tests were carried out using Cortest's Jig Impingement Rig (217) on four alloys; cast and HIPped (950°C) 70/30 cupronickel (NES 824), nickel-aluminium bronze (NAB) and a 70Cu-30Ni alloy designated CN107. The tests were carried out in recirculating natural sea water for 30 days at a velocity of 10m/s and a temperature of 20°C. The sea water was changed every five days. Ten days into the test half of the test specimens were scratched across their impingement zone. The impingement attack measurements recorded are shown in Table 53. The results show that both cast and HIPped NES 824 material together with the CN107 (70Cu-30Ni) alloy showed no significant impingement attack, although there were signs of superficial attack. Both as-cast and HIPped NES 824 material showed marginal improvement in impingement resistance over the CN107 alloy. In addition the HIPped NES 824 showed a tendency for a further slight increase in impingement resistance over cast material. Small random pitting was observed on the as-cast NES 824 test specimens but this was thought to be associated with porosity. Genuine pitting of both as-cast and HIPped material occurred close to the longitudinal edges of the test specimens. Scratching the samples across their impingement zone appeared to have no effect on their resistance to attack.

In comparison to NES 824 material, NAB suffered impingement attack and formed an annular shaped impingement zone. The CN107 alloy showed signs of superficial attack with slight

random pitting.

4.10 STRESS RELAXATION TESTS

Stress relaxation tests have been carried out on cast 70/30 cupronickel material within the temperature range 400°C - 1025°C, which allowed the relationship between σ/σ^0 and t to be obtained at different test temperatures. The relationships obtained are shown in Figures 178 and 179, and indicate the limiting stress attained during the test or the constant rate of stress relaxation reached after a period of approximately seven minutes.

4.10.1 COMPARISON OF CALCULATED AND EXPERIMENTAL STRESS RELAXATION CURVES

The relationship between σ/σ^0 and time obtained from the stress relaxation tests is governed by the Standard Linear Solid Model, as discussed in section 2.21. The model states:

$$\frac{\sigma}{\sigma^0} = (1-A) \exp^{-Bt} + A$$

where A is the limiting stress attained during the stress relaxation test, and B is an exponential rate constant which governs the rate of decay and influences the shape of the stress relaxation curve. Thus values of A and empirical values of B were adjusted to give the best fit between the experimental and calculated curves as shown for test temperatures of 400-1025°C in Figures 180- 182. The values of A and B determined are shown in Table 54. Figure 183 illustrates how parameters A and B change with

temperature.

4.10.2 CALCULATION OF THE COEFFICIENT OF VISCOSITY
AND OTHER MATERIAL PARAMETERS FOR 70/30
CUPRONICKEL AT ELEVATED TEMPERATURES

Parameters A and B can be represented by the following equations (see section 2.21.6):

$$A = \frac{2\phi\eta (1+\nu)}{E} \qquad B = \frac{G}{\eta}$$

Rearrangement of the above equations allowed values of η and ϕ to be determined. The calculated values contain a margin of error since the material properties included in the above relationships such as G, E and ν are only available for NES 824 at room temperature. The material properties of NES 824 at ambient temperature are shown in Table 55. The margin of error is dependent upon the relationship between each property and temperature. Values for η and ϕ within the temperature range 400-1025°C are shown in Table 54. Figure 184 shows that the viscosity of NES 824 increased with an increase in temperature as would be expected.

4.10.3 CALCULATED CREEP CURVES FOR 70/30 CUPRONICKEL

The values of A and B can provide a direct measure of creep strain via the Standard Linear Solid Model as follows:

$$\epsilon_{creep} = \frac{\sigma^o}{E} \left(\frac{1}{A} - 1 \right) (1 - \exp^{-ABt})$$

In addition the elastic strain lost during stress relaxation can be calculated by substituting σ^{SR}/E into the above equation, where σ^{SR} is the change in stress which occurred during stress relaxation ($\sigma^{SR} = \sigma^o - \sigma^t$). Once again all predicted values will contain a margin of error. Figures 185 and 186 show that both creep strain and elastic strain lost during stress relaxation increased with an increase in temperature.

4.11 MODELLING OF PORE CLOSURE RATES IN 70/30 CUPRONICKEL BY HOT ISOSTATIC PRESSING

4.11.1 PORE CLOSURE BY PLASTIC YIELDING

Values of pore closure by plastic yielding have been predicted via a densification rate equation used by Ashby as discussed in section 2.15:

$$D_{yield} = \left(\frac{(1-D_0)P}{1.3\sigma_y} + D_0^3 \right)^{1/3}$$

This equation has been used to predict the degree of pore closure taking place by plastic yielding during the HIPping of 70/30 cupronickel material of 0.95, 0.90 and 0.84 relative density (ie. containing 5%, 10% and 16% porosity). The HIP processing parameters to be considered include temperatures within the range 850-1025°C and external gas

pressures of 103MPa. The calculated pore closure rates obtained are shown in Table 56 and indicate that at all temperatures studied some degree of pore closure by plastic yielding would take place. In addition the degree of pore closure for any given relative density increased with an increase in the HIPping temperature. Figure 187 compares calculated pore closure rates with experimental data obtained via type IV HIP cycles for 70/30 cupronickel that contained 5% porosity, and indicates that at HIPping temperatures of 950°C or above the difference between calculated and experimental rates is negligible. Figure 188 compares calculated and experimental pore closure rates for the HIPping of 70/30 cupronickel containing 16% porosity, and indicates a lower degree of accuracy between the two sets of data. Calculated pore closure rates indicate that at a HIPping temperature of 1025°C a 16% pore can be fully recovered via densification caused by plastic yielding. However the experimental HIP data indicated that the pore would only be reduced to around half its original size and 7.8% porosity would still be present.

THE PLASTIC FLOW THEORY

The simplified equation for plastic flow during pressure assisted hot pressing (see section 2.11.5) can be represented as follows:

$$\ln \frac{(1-\rho)}{(1-\rho_o)} = -\frac{3}{4} \frac{P}{\eta} t$$

This equation has been used to predict pore closure rates for 70/30 cupronickel specimens containing 10% and 16% porosity by volume. The pore closure rates calculated are for HIP processing parameters which included a temperature of 950°C and external gas pressures of 103MPa. The viscosity of NES 824 at this temperature was determined using stress relaxation experiments and found to be 1594GPa.s (Table 54). The pore closure rates calculated are shown in Tables 57 and 58 for the densification of 10% and 16% initial porosity respectively. Figure 189 compares the calculated pore closure rates with those experimentally determined via type II HIP cycles, and shows that for the closure of a 10% pore the calculated rates are much slower than the experimental ones, although both rates show a similar rate of decay as the sustain period increased. The calculated pore closure rates obtained for a 16% pore indicate that at a temperature of 950°C with external gas pressures of 103MPa a sustain period of >29 hours would be required to recover the pore. In comparison HIP experiments have shown that after a 12 hour sustain period the pore would be reduced to 4%. To reach the same level of porosity a predicted sustain period would be of around

8 hours.

4.11.3 70/30 CUPRONICKEL HOT ISOSTATIC PRESSING MAPS

HIP maps for NES 824 have been constructed by the use of software developed by Ashby (178), HIP 6.0. In order to model the densification of cast NES 824 a material file has to be created. Properties included in this file are shown in Table 32, and plotting variables in Table 33. The greater the number of known material parameters then the greater the degree of accuracy of the predicted HIP map. The material properties of NES 824 used to produce HIP maps type 1-5 are shown in Table 59. These show that the type 1 map only involved a few known basic material parameters, with the rest of the data being estimated from data bases within the software program. The degree of experimental data inputted increased from map type 1 to map type 5 which should produce a consequent increase in accuracy. The estimated properties selected by the HIP data base with map type 5 are shown in Table 60. The software program can produce three basic HIP maps:

- (i) Density - Temperature (fixed pressure).
- (ii) Density - Pressure (fixed temperature).
- (iii) Pressure - Temperature.

All the above HIP maps were produced for NES 824 material of 0.90 and 0.84 relative density processed at a temperature of 950°C and external gas pressure of 103MPa. The pressure - temperature HIP maps are shown for map types 1-4 in Figures 190, 192, 194 and 196 for NES 824 material containing 10% porosity, while Figures 191, 193, 195 and

197 represent NES 824 material containing 16% porosity. The most accurate HIP maps predicted should be those representing map type 5, since these maps were constructed with more experimental data. The density - temperature HIP maps constructed for NES 824 material containing 10% and 16% porosity are shown in Figures 198 and 199. Figures 200 and 201 show the density - pressure relationships, while Figures 202 and 203 show the density - temperature relationships for NES 824 containing 10% and 16% porosity respectively. The pore closure rates predicted by the pressure - temperature HIP maps produced with map types 1-5 for the recovery of NES 824 containing 10% and 16% porosity are summarised in Table 61. The results indicate that apart from map type 3 the rest of the HIP maps predict similar pore closure rates, since an increase in the number of experimental material property variables inputted had relatively little effect on the estimated pore closure rates.

5.0 DISCUSSION

Experiments have been conducted to determine the effect of hot isostatic processing variables such as time, temperature, pressure and pressure transmitting medium on the recovery of 70/30 cupronickel castings containing internal pores and surface-connected porosity. In addition models have been identified which accurately predict the rate of pore closure in NES 824 castings. The experimental results and modelling work will be discussed alongside the influence of encapsulation and pore geometry on densification together with the comparison of the mechanical and microstructural properties of cast and HIPped 70/30 cupronickel material.

5.1 EFFECT OF HIP TIME ON PORE CLOSURE

The results obtained are consistent with a two stage densification process during hot isostatic pressing, involving (i) plastic flow and (ii) viscous flow (creep and diffusion). The results suggest that, initial densification which occurs during the heating / pressurisation stage of the HIP cycle takes place predominantly by plastic flow. Initial pore closure occurs instantaneously when a temperature is reached where the applied pressure exceeds the yield stress of the material, causing plastic deformation to occur. The amount of initial densification taking place has been measured by type IV HIP experiments which involved a zero sustain time. These experiments show that an internal pore of 16% porosity (Figure 95) can be completely recovered by a type IV cycle carried out at a temperature of 950°C and argon

gas pressures of 103MPa. With regards to encapsulated castings containing surface-connected porosity, 2-3% can be recovered by instantaneous plastic deformation irrespective of the starting porosity on attaining conditions of 950°C / 103MPa (Figure 88). The majority of pore closure in specimens containing both internal and surface-connected porosity, occurs within a short period of time (less than 45 minutes for the sample size employed) at the sustain temperature and pressure (Figures 85 and 94). Extending the HIP time from 0 to 45 minutes allows 10% internal porosity to be completely recovered, whereas for an initial pore of 5% surface-connected porosity, the amount of densification taking place can be increased from 2.5% to approximately 5%. Complete pore closure was prevented by sand entering into the pore. Similar results have been obtained for specimens containing 16% surface-connected porosity, where the porosity content was reduced from 16% to 13% and 7% respectively on increasing the HIP sustain time from 0 to 45 minutes (Figure 88). Extending the HIP time further revealed densification to continue at a low rate for encapsulated castings (Figure 87). The fall in the rate of pore closure on extending the HIP time from 45 minutes to 12 hours is thought to be due to the exposure of the refractory pressure-transmitting medium to high temperatures and pressures causing the particles to pack to maximum density and undergo mechanical locking and partial sintering. For pressing to be effective these particles must be able to move under the applied load as densification continues. The locking of the refractory

particles prevents the transmission of the external gas pressure to the casting. Thus pore closure is impeded. Therefore the recovery of large surface-connected pores is best carried out by successive cycles of short duration (type I HIP cycles), with fresh encapsulation prior to each HIP cycle, rather than single cycles of extended time (type II HIP cycles). Single continuous HIP cycles failed to close pores of 16% surface-connected porosity after sustain periods of 10 — 12 hours, whereas 4 type I HIP cycles successfully closed the same volume porosity. The effectiveness of successive type I HIP cycles in relation to type II HIP cycles for the recovery of large pores is thought to be due to several factors: firstly a certain pressure will only reduce the cross-sectional area of a pore by a specific amount determined by the original size of the pore. Furthermore the densification rate during multiple type I HIP cycles decays at a rate which appears to be dependent upon the cross-sectional area of the pore. A pore reduces to approximately half its initial size during each type I HIP cycle, or until the relationship between applied pressure and pore size is above a critical level which allows full densification.

Secondly for castings containing surface-connected porosity, encapsulation techniques involving the use of a pressure transmitting medium hinder the densification process by diminishing the external pressure transmitted to the casting. This subsequently produces a decline in the pore closure rate. The reduction in pore closure rate for encapsulated castings is due to the exposure of angular desert based

silica sand particles to high temperatures and pressures, which causes them to reach an optimum packing density and undergo mechanical locking. The resultant loss of particle flow together with the high compressive strength of the sand diminishes the applied pressure transmitted to the casting, thereby decreasing the rate of pore closure. In some instances the applied pressure is reduced below the critical pressure for densification and no further pore closure is observed until the HIP time is extended above 8 hours (Figure 87). The slight increase in density which occurs after prolonged sustain periods, suggests that for encapsulated castings the initial densification due to plastic flow is followed by a second pore closure mechanism which is time dependent, and can involve both creep and diffusion. This second mechanism has been assumed to be predominantly creep orientated, since it is thought that primary creep could occur during the heating/pressurisation stage of the HIP cycle, and that the second stage of creep, (steady state), could be reached within the first 45 minutes of the sustain period. This assumption is based on experimental data which reveals that the rate of densification gradually falls to zero within 45 minutes at the sustain conditions. Extending the HIP time further from 2 to 12 hours has very little effect on pore closure, except at longer times where a slight increase in the rate of pore closure occurs. This slight increase could be due to tertiary creep or increased diffusion due to the increased time spent at temperature, or could be a feature of experimental data scatter.

It is impossible from the HIP experiments carried out to predict accurately the extent of pore closure taking place due to plastic flow and viscous flow. Hence densification rates have been predicted by the use of pressure-assisted sintering models, and the rates produced compared to experimental HIP data in order to assess the accuracy and reliability of 70/30 cupronickel castings containing both internal and surface-connected porosity, the findings of which are discussed in section 5.10.

5.2 EFFECT OF HIP TEMPERATURE ON PORE CLOSURE

Previous work (173,213) suggests that the optimum HIPping temperature for 70/30 cupronickel is 950°C. At higher temperatures impact toughness and densification due to plastic yielding are increased but considerable grain growth occurs, which is disadvantageous in what is already a relatively coarse grained material. HIP experiments carried out on specimens containing surface-connected porosity and internal porosity confirm both that the optimum processing temperature is 950°C, and that lower temperatures restrict densification due to plastic yielding. For specimens containing surface-connected porosity which are encapsulated prior to HIPping, 850°C is the threshold temperature below which plastic flow is not produced during pressing, and only a limited amount of densification takes place by time dependent mechanisms. This suggests that the HIP pressure of 103MPa does not exceed the yield stress of 70/30 cupronickel at 850°C. Increasing the HIP temperature further indicates that no significant amount of plastic

yielding occurs until a HIP temperature of 900°C has been exceeded (Figures 89 and 90). In contrast, with specimens containing internal porosity the threshold temperature for plastic flow is reduced to below 850°C, since even at this temperature some pore closure occurs (Figure 96). This suggests that it is the encapsulation technique which is restricting densification rather than an incorrect HIP temperature. However, it is not until temperatures of 900°C and 925°C are reached that densification due to plastic yielding becomes significant.

At a temperature of 925°C an internal pore of 10% porosity can be completely recovered by a type I HIP cycle, and at a temperature of 950°C both 10% and 16% internal porosity can be recovered.

Increasing the HIP temperature from 850°C to 1025°C increases the amount of pore closure taking place by both plastic deformation and time dependent mechanisms. Therefore increasing the HIP temperature allows a larger volume of porosity to be removed in constant time.

5.3 EFFECT OF HIP PRESSURE ON PORE CLOSURE

Consideration of the pressure applied during the processing of 70/30 cupronickel encapsulated castings, that is castings containing surface-connected porosity (Figure 91), suggests that a minimum HIP pressure somewhere between 62MPa and 103MPa would be required for HIPping NES 824 at a temperature of 950°C.

The optimum pressure required for the processing of castings containing internal porosity is 103MPa. At this pressure

large pores of up to 16% porosity can be recovered during very short sustain periods (Figure 97).

The optimum HIP processing conditions for the densification of 70/30 cupronickel (NES 824) castings containing 5-16% internal porosity are short sustain times of 45 minutes, at a temperature within the range 875-950°C with argon gas pressures of 62-103MPa. The lower temperature (<900°C) and pressures (<70MPa) are only suitable for the HIP recovery of class I cupronickel castings which contain around 5% porosity. The higher temperatures (>925°C) and pressures (>83MPa) are suitable for the recovery of larger internal defects of 10-16% porosity. The optimum pressure for large pores would be 103MPa. Any higher pressure would be uneconomic.

5.4 EFFECT OF PORE GEOMETRY ON DENSIFICATION

The HIP experiments have highlighted the effect of pore geometry on void recovery as briefly mentioned earlier. Large diameter squat pores require longer HIP times for recovery than do elongated small diameter pores of equal volume porosity (Figures 85 and 86). The reason for this is thought to be associated with the angularity of the casting defect and the wall thickness between the pore and the outer skin of the casting. Long thin pores collapse more readily than larger diameter pores and the presence of angular protrusions such as found in shrinkage cavities aid densification due to regions of high stress. Commercial castings containing large shrinkage voids can be successfully recovered via a 4 hour sustain type II HIP

cycle, whereas a cylindrical pore of 16% porosity is still present although of a reduced nature after a 12 hour period (Figure 87). The presence of stress concentrators caused by an angular pore geometry is assumed to be the cause for this variation in results.

5.5 EFFECT OF ENCAPSULATION TECHNIQUES ON PORE CLOSURE

Encapsulation by the use of a close fitting steel capsule which eliminates the need for a packing medium, allows surface-connected porosity to be closed at similar rates to internal porosity of equal volume (comparison of Figure 94 and 98), that is by one short 45 minute HIP cycle at a temperature of 950°C and argon gas pressures of 103MPa. Thus, the ideal encapsulation technique for castings containing surface-connected porosity would be a close fitting capsule, but in practise this is only suitable for castings of simple geometry.

HIP experiments have shown that for the closure of large surface-connected pores short successive type I HIP cycles are more beneficial than single continuous cycles of extended sustain period (ie. type II HIP cycles). This suggests that the standard refractory pressure transmitting medium silica sand, diminishes the external pressure transmitted to the casting. The reason for this is thought to be due to attainment of a maximum packing density in the refractory particles and partial sintering of these particles when subjected to high temperatures and pressures. This optimum packing density was attained soon after the sustain conditions have been reached. Thus consideration has been

given to the effect of a change in the type of refractory pressure transmitting medium on the densification process. A pressure transmitting medium is required which retains fluid-like characteristics at high temperatures and pressures and allows continuing action of the applied load throughout the HIP process.

An alternative powder consolidation process known as a pseudo-HIP process is the Ceracon process (182), which also utilises a ceramic grain (183) to transfer the applied load to the preform via a moving ram to cause densification. After consolidation, the ceramic grain is removed from the fully dense part by means of a shaker table, after which it is reusable. Such a grain which still flows after processing, would be an ideal pressure-transmitting medium for use during the HIP processing of encapsulated castings. The Gorham Advanced Metals Institute claim that there are 21 US patents and 14 foreign patents relating to the Ceracon process. Two of these: US 3 356 496 December 1967 (186) and US 3 689 259 September 1972 (187) make specific reference to the types of ceramic grain suitable for the consolidation of a range of metals and alloys. It is suggested that a practical grain size for the ceramic grain is 325-100 mesh (187), and that suitable grains include alumina for use with iron and similar melting point alloys. However silica with its lower hardness (195,196) allows greater deformability at elevated temperatures, or for very high temperature consolidation refractory oxides such as thorium oxide, zirconium oxide, boron carbide and carbon are suggested.

The standard pressure-transmitting medium used for the encapsulation of castings containing surface-connected porosity is a desert-based silica sand of particle size 100-355 μm , the particles being angular in nature as would be expected for wind blown particles (Figure 104). This standard pressure transmitting medium allows consolidation of a 10% pore by two successive type I HIP cycles at a temperature of 950°C and argon gas pressures of 103MPa. Unfortunately this pressure transmitting medium is known to impede the densification process. Alternative refractory particles such as calcined alumina, zirconium oxide, and mixtures of calcined alumina and boron-nitride all of which have a higher melting point than silica sand (196-198), should eliminate the possibility of sintering and any restriction of the densification process should then be attributable to particle geometry. The above alternative pressure transmitting media have particle sizes within the range 53-150 μm , and tend to be slightly finer than the silica sand. However in regards to enhancement of the densification process they offer no advantages, since all allow the consolidation of 10% porosity at the same rate as the standard packing material, ie. complete recovery via two successive type I HIP cycles (Figure 99). Thus it appears that restriction of the densification process is due to the particle geometry of the packing material and not the partial sintering of the particles under the sustain conditions. This assumption is substantiated by the fact that coarse particles hinder the densification process even more, since coarse angular tabular alumina particles (355-1700 μm) require

3 successive HIP cycles for the consolidation of a 10% pore (Figure 101). Finer particles such as those represented by boron carbide and mixtures of boron carbide and silicon carbide (9-53 μ m particle size) also reduce the pore closure rate (Figure 100). In addition ultra fine powders are difficult to handle since they migrate into pores during encapsulation and HIPping and thus prevent pore closure. The HIP experimental data shows good agreement with the Ceracon patents in that a practical size of particle for use as the pressure transmitting medium appears to be around 100 μ m. Yet refractory particles of similar size to that suggested as practical diminish the densification process. Therefore, although the size of the particle may be within the suggested range it appears that the particles may be of the wrong geometry.

Sands can be classified into two basic types: desert based and water table sands. The latter have a more rounded particle morphology due to the action of water flow and particle drag along the river bed. Typical water table sands include Zone-M concrete sand and Leighton Buzzard sand (Figures 106 and 110). Zone-M concrete sand is a silica based sand consisting of an aggregate of particle sizes within the range 106-355 μ m, the predominant particle size being around 150 μ m. In comparison the Leighton Buzzard sand is a silica based sand of single particle size, >355 but <1700 μ m.

Encapsulation via the use of Zone-M concrete sand either in the form of an aggregate or a single particle size increases the densification rate of 70/30 cupronickel

castings containing surface-connected porosity, allowing pores of 10% and 16% porosity to be completely recovered via one short 45 minute HIP cycle (Figures 107 and 108). The pore closure rates achieved allow an increase in the densification rate by 50% over rates obtainable via use of the standard packing material. In comparison the larger particle size Leighton Buzzard sand diminishes the densification rate. Thus the Zone-M concrete sand offers densification rates of encapsulated castings which compare favourably with those obtained on castings containing internal porosity and do not require encapsulation. Therefore for improved densification of encapsulated castings the pressure transmitting medium must be ideally one of rounded particle geometry and with a practical handling particle size of around 100-150 μ m.

Another alternative pressure transmitting medium to silica sand which behaves plastically at temperatures associated with HIPping is fused Pyrex glass. At the HIPping temperature of 950°C Pyrex glass is sufficiently viscous to transmit the externally applied pressure, producing similar densification rates to those observed in castings containing internal porosity (Figure 102). However the draw back of this packing medium is that it is potentially hazardous to handle and requires the component to be packed in fragmented glass and heated to 1000°C prior to the HIP cycle in order to fuse the Pyrex glass. In addition this type of pressure transmitting medium can only be used for castings containing porosity which is connected to the surface by very small pores, otherwise the fused glass seeps

into the pores and prevents consolidation.

Silica sand has many advantages over the use of Pyrex glass as a pressure transmitting medium: it is cheap and has no chemical interaction with the 70/30 cupronickel casting or the steel capsule, although the sand particles do become impregnated into the surface of the casting during HIPping, and on removal leave behind a slightly dimpled appearance which can clearly be seen on a machined surface but not on a cast surface (Figures 111 and 112). Any subsequent machining removes this surface texture. In addition silica sand has no out-gassing tendencies at HIP temperatures and pressures involved which eliminates the risk of capsule failure due to bloating.

The optimum requirements for a suitable particulate material to act as a pressure transmitting medium for encapsulated castings appear to be a refractory material of high melting point and purity which remains stable at HIP temperatures and pressures. In addition the particle geometry must be of a rounded nature and ideally possess a particle size within the range 100-150 μ m.

5.6 COMPRESSIVE STRENGTH OF SILICA SAND AND ITS **ABILITY TO RESIST DENSIFICATION**

The compressive strength of HIPped silica sand increases with an increase in the HIP pressure (Table 36). The compressive strength data obtained for encapsulated and HIPped desert based silica sand can only be considered qualitatively due to the variations in packing density,

wall thickness of the steel capsule and weld strength, all of which would influence the trends observed.

An improved and more quantifiable indication of the ability of silica sand to restrict densification is obtained by comparing the densification of castings containing identical pore geometries and porosity of equal volume encapsulated in such a way to vary the thickness of the pressure transmitting medium surrounding the casting (Table 37). Increasing the thickness of the pressure transmitting medium from approximately 6-39mm significantly reduces the rate of pore closure.

Therefore the thickness of the layer of silica sand used as the packing material during encapsulation of cast parts should be kept to below 5-10mm, otherwise low levels of densification can be expected. However in practice the minimum refractory packing thickness is determined by the geometry of the casting.

5.7 CHANGES IN PORE SHAPE DURING HIPPING

Pores of identical size and geometry differ in their modes of collapse during consolidation depending on whether the pore is internal or surface-connected. Surface-connected porosity (Figure 116) becomes elliptical and undergoes a reduction in diameter with little overall change in length during the early stages of densification. Thereafter the blind end of the pore collapses more rapidly than that area of the pore which is surface-connected. The region of porosity connected to the surface of the casting is the last portion to consolidate.

The density gradients acting during the consolidation of the internal pores differ from those influencing the closure of surface-connected porosity. Internal porosity densifies in a manner similar to that of powder compacts as described by Ashby as the dog bone effect (160,161). The outer radii of the pore are able to support a load and the pore is displaced inwards along its length leaving the outer radii almost unchanged, producing a pore similar in shape to a dog bone (Figure 117). These radii are the last regions to consolidate and in many instances it is impossible to achieve 100% densification.

5.8 EFFECT OF HIPPING ON THE MATERIAL PROPERTIES

OF 70/30 CUPRONICKEL

The present investigations have shown that HIPping appears to have a beneficial effect on the properties of NES 824 material, since it reduces the extent of microsegregation (coring) giving improved material homogeneity, thus reducing stresses introduced during casting and improving mechanical properties. However HIPping does have a slight drawback in that it increases the grain size of 70/30 cupronickel material. The grain size increases with an increase in the HIP temperature; for this reason the optimum commercial HIP temperature for NES 824 is 950°C (173).

5.8.1 MECHANICAL PROPERTY EVALUATIONS

HIPping appears to have no detrimental effects on the as-cast properties of 70/30 cupronickel. The process appears advantageous in that the ductility and impact toughness has

significantly improved on HIPping above 850°C (Figure 119). The ductility (% Elongation) and the Charpy (v-notch) impact toughness increase by 66% and 58% respectively on HIPping at 950°C. In addition the Ultimate Tensile Strength increases slightly with an increase in the HIP temperature from 850°C to 1025°C, with maximum strength at 1025°C. However, HIP temperature has little effect on the Yield Stress. The improvements in as-cast properties by HIPping are comparable to trends predicted by earlier investigations (173,213) carried out on mechanical property test bars (Figure 120), which indicate that at the maximum HIP temperature of 1025°C the increase in strength is accompanied by a slight decrease in ductility.

The mechanical properties of sand cast metals and alloys are known to be inferior to wrought material of equivalent grade (166). However the closure of internal voids during HIPping and the subsequent improvement in mechanical properties is becoming increasingly well documented for a wide range of materials (140,150,151,167), including copper based casting alloys (168). In addition HIPping has the ability to significantly reduce the scatter of properties and at the same time enhance the properties of castings containing no detectable defects (134). HIPping can increase the fatigue life of steels by 50-70% (167,172), and the fatigue resistance of HIPped titanium alloys is significantly higher than that of cast material (175), whilst the ductility of superalloys can be increased by around 60% (174,175). The HIP process can also influence the weldability of a material and can facilitate manufacturing

processes preventing part rejection and induce improvements in corrosion resistance due to homogenisation of the cast microstructure which reduces potential sites for galvanic corrosion (176,177). Until now the beneficial effects of HIPping have so far only been reported for powder products, wrought material or castings containing internal porosity. However the use of effective encapsulation techniques allows the same improvements in castings containing both internal and surface-connected porosity as shown by the HIP experiments carried out on 70/30 cupronickel. The HIP experiments carried out on NES 824 material indicate that a HIP temperature of 950°C produces the best combination of strength and ductility whilst inhibiting the grain growth associated with higher HIPping temperatures. The time spent at the sustain conditions involving a HIP temperature of 950°C with argon gas pressures of 103MPa has a negligible effect on the strength (Yield Stress and Ultimate Tensile Strength) of cast NES 824. However impact toughness improves significantly on increasing the HIP time from 45 minutes to 2 hours, although no benefits can be gained by extending the HIP time further (Figure 121).

The use of type I or type II HIP cycles to recover cast samples containing 10-16% surface-connected porosity had no influence on the resultant HIPped microstructure. Both types of cycles allowed plastic flow and subsequent recrystallisation of the worked microstructure as indicated in Figures 124 (i) and (ii).

Previous HIP investigations (173,213) have indicated that the optimum processing temperature for NES 824 that produces the maximum improved strength and ductility whilst simultaneously inhibiting grain growth is around 950°C. Increasing the HIP temperature from 850°C to 1025°C produces a slight increase in grain size, which is accompanied by a reduction in the extent of coring of the cast microstructure (Figure 125). Homogenisation of the microstructure is observed as a reduction in the prominence of the distinctive cast phases; predominantly nickel rich dendrites and a copper rich matrix (Table 47 / Figure 126). The overall matrix analysis becomes closer to the nominal requirements of 70% Cu and 30% Ni as the HIPping temperature increases from 850°C to 1025°C. However when mechanical properties and optimum microstructure coincide the best HIP processing temperature appears to be 950°C (173,213,214).

HIP experiments have indicated that the use of successive short (45 minute) type I HIP cycles at 950°C are more beneficial with respect to pore closure rates than type II cycles of extended duration. However increasing the HIP time from 45 minutes to 6 hours has no significant effect on the HIPped microstructure since the grain size remains unchanged (Table 48). Further, negligible effect is observed with respect to the extent of homogenisation of the cast microstructure (Table 49 / Figure 133).

5.8.2 IMPROVEMENT OF PROPERTIES BY STRESS RELIEVING

The stress relief of cast 70/30 cupronickel material for 2 hours at a temperature of 450-500°C followed by cooling in air has a beneficial effect on both strength and ductility (Table 40). In addition the stress relief of NES 824 which has been subjected to a heat treatment which simulates the thermal HIP cycle (excluding pressure), significantly improves the strength of the material (Figure 122).

However the benefits of stress relief are not transmitted to material subject to the full HIP cycle, since no improvements are gained by stress relieving HIPped NES 824. This is not unexpected since the HIP treatment is carried out at higher temperatures than the stress relaxation treatment and also involves a slow cool at a nominal rate of 7-10°C/minute. Thus the HIP treatment allows far greater potential for homogenisation of the cast microstructure than is obtained by the stress relief process.

5.8.3 THE EFFECT OF HIPPING ON THE PROPERTIES OF RECOVERED NES 824 CASTINGS

The effect of HIPping to recover castings containing shrinkage defects and its effect on the as-cast properties has highlighted many interesting but conflicting results. Many HIP repaired castings maintain the as-cast properties in the originally sound areas of the casting, whilst the recovered defect region has significantly reduced strength and ductility (Table 42). In comparison other HIP repaired castings undergo a reduction in strength of areas of the casting which even prior to HIPping contained no detectable

defects, whilst the recovered defect region exhibits increased strength but reduced ductility (Table 43). The most probable explanation for the loss of strength in sound HIPped material would be experimental data scatter associated with changes in microstructure throughout a casting. In contrast the loss of ductility and strength of an area of a casting which originally contained a casting defect which was HIP recovered is a more serious problem. The reduction in properties is thought to be associated with the formation of Ni, Zr and Si intermetallic precipitates which have been found to be present at grain boundaries or as isolated oxide precipitates within grains (Figures 145 and 146).

The loss of mechanical properties of HIPped defect regions has been associated with the recovery of large shrinkage defects found in castings that would normally have been remelted and cast (Figure 73). However their use in HIP experiments was to produce an indication of the optimum size of casting defect which could be repaired by HIP processing. The closure of such large voids resulted in a considerable changes in the microstructure surrounding the defect, such as recrystallisation of the plastically deformed material (Figure 139). HIP recovery of smaller voids representing 10-16% porosity produced less severe changes in the repaired microstructure although a limited amount of recrystallisation still occurred (Figure 124). The increase in grain boundary surface area as a result of recrystallisation increased the potential sites available for precipitation of Ni, Zr and Si rich oxides which have a tendency to cause embrittlement in

The difference in properties between HIPped sound NES 824 material and HIP recovered defect material could also be influenced by the location of the test material. All sound material represented material taken from the outer edges of the casting, whereas the recovered defect material represented central regions of the casting. Thus the change in microstructure from the edge to the centre of the casting due to a variation in cooling rates would produce a difference in properties which are not influenced by the HIP process. Therefore the effect of a change in microstructure needed to be eliminated. This was achieved by casting two plates of NES 824. One plate was considered to be sound by X-ray penetration examination, whereas the other contained surface-connected shrinkage porosity. The plates were cast under identical conditions. Therefore it can be assumed that the microstructure of the plates are very similar, and that after HIPping an improved quantitative comparison of HIPped sound and defect repaired material could be carried out. The results of these trials together with earlier investigations involving cast test bars (173,213) indicate that HIPping has no detrimental effects on the as-cast properties, and that in general HIPping enhances the ductility and toughness of the casting which is accompanied by a slight increase in strength. These benefits of HIPping are in accordance with the trends observed for other metals by many authors (140,150,151 and 167).

5.8.4 HOT FLOW STRESS AND DUCTILITY OF NES 824

Evaluation of the hot flow stress of cast NES 824 revealed that the hot strength undergoes little change until a temperature of 600°C is exceeded. The yield stress at room-temperature is 351MPa, but falls to 284MPa at 600°C (Table 45). The yield stress at the three HIPping temperatures of 850°C, 950°C and 1025°C are approximately 70, 45 and 20 MPa respectively. Increasing the temperature further causes the strength to decrease sharply until a plateau is observed at temperatures between 850-950°C (Figure 123). Similar trends have been reported by other investigators with significant changes in strength occurring above 700-1000K (78).

The hot ductility of 70/30 cupronickel calculated from the standard ductility measurement referred to in section 3.9, indicates that NES 824 suffers a ductility trough in the temperature range 600-800°C; this range is slightly higher than those reported by other investigators. Positions of ductility minima have been reported for 70/30 cupronickel at both low and high temperatures (89), the positions of which are influenced by grain size and strain rate. Low temperature ductility minima have been observed between 350°C and 650°C, whereas high temperature minima have been observed at temperatures above 887°C (89).

5.8.5 CONSTANT LOAD DUCTILITY OF NES 824

HIPping of commercial 70/30 cupronickel castings has resulted in cracking of cast components(215). Cracking is thought to occur during cooling following HIPping rather than during the sustain period, since as the casting cools it develops internal stresses due to contraction whilst at the same time it is subjected to an external pressure. The pressure applied during HIPping decreases steadily, which is associated with the fall off in temperature (Figures 79 and 80). Thus large strains are placed on the surface material which cannot be accommodated as the casting cools and result in cracking at sharp radii, ports and channels.

The constant load ductility test was developed to simulate the stresses acting on a casting as it cools from the sustain temperature and pressure, and revealed that the ductility of cupronickel falls on cooling through the temperature range 600-700°C causing the test specimens to fracture. This compares closely with the ductility trough experienced during the hot flow stress evaluations (600-800°C). Stress relaxation results also substantiate the temperature embrittlement temperature range since NES 824 cannot support a load which exceeds its yield stress or undergo stress relaxation at temperatures within the range 600-700°C (Figure 178). These results suggest that 70/30 cupronickel (NES 824) material undergoes embrittlement on cooling through the temperature range 600-800°C, and that any subsequent heating or cooling through this critical range should be carried out very slowly in order to prevent cracking.

The ductility loss and occurrence of ductility minima experienced during the plastic deformation of 70/30 cupronickel during tensile testing and stress relaxation tests within the temperature range 600-800°C leads to failure by grain boundary cracking (Figures 135-138). Other authors have reported similar findings (89) and suggest that the incidence of cracking increases with temperature as the ductility minimum is approached. At the ductility minimum no grain boundary migration or recrystallisation occurs as is also shown by the above mentioned figures. Although it has been found that at temperatures above the ductility minimum cracking occurs but recrystallised grains start to form at grain boundaries and their formation increases with increasing temperature (89).

Many metals experience a ductility loss during plastic deformation in the temperature range $0.4-0.7T_m$ due to the onset of intergranular fracture associated with voids which are nucleated at grain boundaries. The types of void formation found in the intermediate temperature embrittlement range are W and R type voids (79,80). W or wedge type voids or cracks are nucleated at triple points and fracture follows a grain boundary path (91,95). In contrast R or cavitation type void formation results from the linking of voids producing a serrated fracture surface (79,96).

The failure of 70/30 cupronickel within the temperature range 600-800°C produced intergranular type fractures. In addition areas of shrinkage porosity were found to be connected by a net work of cracks which followed a grain boundary path

as shown in Figure 138.

5.9 CORROSION PERFORMANCE OF 70/30 CUPRONICKEL

The corrosion performance of cast cupronickel alloys has been widely investigated and they have been shown to possess excellent corrosion resistance (15,16,21, 25, 42-45). There is in contrast very little data available on the corrosion performance of HIPped cupronickel alloys. However, the general opinion of the casting industry is that HIPping would have no detrimental effects on the corrosion performance of NES 824, and HIP processing may even be beneficial due to the partial homogenisation of the cast microstructure.

The corrosion performances of both as-cast and HIPped 70/30 cupronickel (4 Hours/950°C/103MPa) as determined by salt spray tests involving a 5% salt solution and substitute ocean water indicate that there is no appreciable difference between the corrosion behaviour of cast and HIPped material. Both show an extremely high resistance to corrosion after 1008 hours on test as indicated by the small weight losses (Tables 50 and 51). 1008 hours duration in a spray cabinet is equivalent to 56 weeks immersion in a still corrosive medium. Short term laboratory tests carried out by other investigators (43) in aerated 3% sodium chloride solution (Table 12), and long term tests carried out in flowing sea water or natural water (Tables 13-15) (43-45), indicate the high corrosion resistance of cast 70Cu-30Ni cupronickel alloys. All the investigations show a similar trend where the rate of corrosion of cupronickel alloys decreases as

the nickel content of the alloy increases.

Metallographic examination of the NES 824 specimens subjected to short term salt spray tests revealed slight corrosive attack, in the form of preferential phase corrosion of dendritic regions, cracking and peeling of the surface layers of material, pitting and cratering. In addition the formation of the protective corrosion product film was more advanced on the as-cast specimens, although this enhanced protective coating may be associated with the change in specimen geometry for the cast specimens. Examination of the film revealed it to be black although it was too thin to be analysed by SEM / EDAX techniques.

The small weight losses recorded and the lack of a substantial corrosion product indicate the excellent corrosion performance of both as-cast and HIPped 70/30 cupronickel.

The high corrosion resistance of cupronickel alloys in sea water is attributed to the growth of a protective corrosion product film, and the uniform formation of this film is dependent upon the material surface condition. Sand blasting produces a more homogeneous surface upon which the film can grow, thus producing more consistent corrosion behaviour (59). The salt spray test specimens had either a smooth machined finish or a polished (1200 grit) surface finish. This smooth surface would not encourage the formation and growth of the corrosion product film. In sea water the corrosion product formed is predominantly cuprous oxide (Cu_2O) (60,61). It appears that when the

rate of erosion corrosion of 70/30 cupronickel is relatively low the corrosion products formed are yellow-brown in colour and consist of three layers. Analysis of the outer layer shows it to be rich in Cu and Ni with small but significant amounts of Cl and Fe (70). In comparison if the rate of erosion corrosion of 70/30 cupronickel is relatively high the corrosion product formed is black and once again consists of three layers. In this case the outer layer is rich in Cu, with small but significant amounts of Cl, Ni and Fe (70).

Due to the difficulties and caution which must be exercised when using short term salt spray tests to predict long term corrosion behaviour, it was deemed necessary to carry out long term sea water corrosion trials on cast and HIPped NES 824. These trials involved both immersion, crevice and impingement tests. The immersion specimens underwent a depth of attack of 0.0117mm/year and 0.0143mm/year respectively for cast and HIPped material (Table 52).

These corrosion rates compare favourably with those reported for a Inco alloy IN768 (21). The compositional range of IN768 has been tightened in respect to impurity levels, which lead to the development of 70/30 cupronickel strengthened by Cr and Si, and designated in the Naval Engineering Standard NES 824 (25). General corrosion rates of IN768 after one year full immersion in the sea at Langstone Harbour were of the order 0.02mm/year (15).

Crevice corrosion tests carried out on NES 824 revealed rates of attack to be 0.04mm/year and 0.029mm/year for cast

and HIPped material respectively (Table 52). In comparison crevice corrosion tests carried out on IN768 produced maximum depth of attack of 0.18mm (48). This is greater than that experienced by NES 824 in the cast or HIPped condition, but compares favourably with rates observed for nickel aluminium bronze (NAB), where corrosion rates of up to 1.1mm/year due to selective phase corrosion at crevices and weld affected areas have been obtained (13). IN768 has the advantage that such crevice corrosion takes the form of macro pitting which is clearly visible and readily measured, whereas the non-destructive examination techniques required to detect selective phase corrosion of NAB are very sophisticated (21).

Immersion and crevice trials indicate that NES 824 both in the cast and HIPped condition are highly resistant to corrosion and offers improved corrosion performance over IN768. In addition there appears to be a tendency for HIPped material to have a slightly better performance than cast material, although a far greater number of tests would be required to confirm this assumption.

Metallographic examination of the HIPped NES 824 immersion specimens showed the presence of a shiny black corrosion product film (Figure 171). This film has an etching effect making the dendritic microstructure clearly visible (Figure 172). SEM examination together with EDAX techniques analysed the corrosion product film to be rich in Ni, Cu and O₂ (Figure 174). The high proportion of nickel present indicates selective phase corrosion is

taking place. Evidence of this type of corrosion was previously found on specimens subjected to salt spray tests involving a 5% salt solution and substitute ocean water. The analysis of the corrosion product film differs slightly to that identified by other investigators who have found the black corrosion product to be rich in Cu with significant amounts of Cl, Ni and Fe to be present (70). In contrast the corrosion product film developed on NES 824 appears to be rich in Ni.

Impingement attack and pitting corrosion of copper based alloys are known to be low (Table 17). These alloys are not susceptible to dealloying and have extremely low penetration rates. In addition higher flow velocities tend to reduce the incidence to pitting (42).

Impingement resistance tests carried out using the Cortest's Jig Impingement Rig (217) on cupronickel alloys: NES 824 in the cast and HIPped condition, CN107 (70Cu-30Ni) and NAB for a period of 30 days, revealed NES 824 to have a marginally improved resistance to CN107 (Table 53). In addition HIPped NES 824 was found to have an improved resistance to impingement attack when compared with cast material. The cast material was subject to small random pitting which was thought to be associated with the presence of porosity. Similar impingement corrosion investigations on IN768 using a Modified Brownsdon - Bannister test (49) and a submerged jet disc test (50) also failed to produce any significant impingement attack (49). Corrosion attack of 0.02mm - 0.04mm was observed by the first test method.

5.10.1 PORE CLOSURE BY PLASTIC YIELDING

Densification rate equations, as used by Ashby for particulate materials (110,160 and 178) to predict pore closure by plastic yielding (equation 45 section 2.15), have been used to predict the densification of 70/30 cupronickel (NES 824) material during HIP processing. This work shows that for the consolidation of NES 824 castings plastic yielding densification rate equations can only be used with reasonable accuracy at processing temperatures above 900°C. Equation ⁽⁴⁵⁾ fails to predict the lack of plastic flow at lower temperatures observed in practice (Figures 187 and 188). The rate equation suggests that at HIP temperatures within the range 800 - 1250°C some degree of pore closure by plastic yielding should occur, the extent of which increases with an increase in the HIP temperature (Table 56).

At a HIPping temperature of 850°C with argon gas pressures of 103MPa, the use of equation 45 predicts that a pore of initially 5% porosity can be reduced to 2%, whereas experimental HIP data obtained on encapsulated castings containing 5% surface-connected porosity using desert-based silica sand as the pressure transmitting medium indicate that no densification occurs (Figure 187). Nevertheless there is good correlation between experimental and predicted densification at processing temperatures above 900°C. At a HIP temperature of 950°C a 5% pore can be reduced to 2.25%. This compares favourably with the

predicted degree of pore closure, which indicate that a pore of initially 5% porosity can be reduced to 1.9%. Similar trends have been observed with porosity of 16%, although greater discrepancies between experimental and predicted densification occurs at HIP temperatures above 900°C (Figure 188). The plastic yielding rate equation predicts that a pore of initially 16% porosity can be reduced to 4.4%, whereas experimental HIP data obtained on encapsulated castings containing surface-connected porosity indicates that a 16% pore can be reduced to 13.4%. In addition, at a HIP temperature of 1025°C it is predicted that a 16% pore can be fully consolidated, whereas experimental HIP data indicates that the pore can be reduced to 8.4%. Thus it appears that the discrepancy between experimental and predicted densification rates of encapsulated 70/30 cupronickel castings increases as the initial pore size increases. Further investigations using an intermediate pore size of 10% are required to ascertain whether the densification rate is affected by pore size or whether the trends observed are influenced by experimental data scatter.

In comparison good correlation has been observed between predicted and experimental HIP data obtained on 70/30 cupronickel castings containing internal porosity, that is castings which do not require encapsulation prior to HIPping. At a HIP temperature of 950°C with argon gas pressures of 103MPa, the plastic yielding rate equation predicts that a pore of initially 10% porosity can be reduced to 3.3% (Table 56), whereas experimental HIP data

obtained on un-encapsulated castings indicates that a 10% pore can be reduced to around 2% (Figure 95). Similarly, at a HIP temperature of 1025°C experimental HIP data indicates that a pore of initially 16% porosity can be fully consolidated by a type IV HIP cycle, whereas the plastic yielding rate equation predicts that a pore of 16% can be reduced to 4.4%.

Therefore Ashby's rate equation for plastic yielding (160, 178) can be used with confidence to predict pore closure rates for 70/30 cupronickel castings containing internal porosity which are HIPped at a temperature of 950°C. In addition, despite the differences between the experimental and mathematical models, Ashby's plastic yielding rate equation can also be used with reasonable accuracy to predict the pore closure rate of castings containing surface-connected porosity, providing the castings are encapsulated using a close fitting steel capsule. The densification of castings containing up to 5% surface-connected porosity encapsulated using standard techniques involving desert based silica sand as the pressure transmitting medium (PTM) can also be accurately modelled by the rate equation. However the accuracy of the predicted densification rate decreases with an increase in the initial pore size. The results of the HIP experiments also suggest that good correlation would be expected between predicted and experimental densification rates for castings containing surface-connected porosity encapsulated using Zone-M concrete sand as the packing material, since the latter allows densification of 10% porosity at a rate

similar to castings containing an equal volume of internal porosity (Figure 107). However once again as the size of the initial porosity increases so does the difference between experimental and predicted densification rates.

The discrepancy between predicted and experimental pore closure rates at processing temperatures below 900°C with both internal and surface-connected pores, and with 16% surface-connected porosity at processing temperatures within the temperature range 900-1025°C, suggests that the relationship between yield stress and external pressure for compacted powders differs from that of an encapsulated porous solid body. Discrepancy between the predicted and experimental data is probably due to several factors.

Firstly the models are based on the compaction of spherical particles, and the removal of connecting porosity between the particles. This type of consolidation is classed as the stage one: neck growth during the sintering process (111,165,179 and 180). During this stage necks grow at contact points between particles and produce relative densities of < 0.90 (160). In contrast the closure of cylindrical pores of 5-10% porosity from 70/30 cupronickel castings can be considered as stage two of the sintering process. In a powder compact by this stage the necks between particles have grown until they impinge to produce individual spherical pores at a relative density of around 0.92. Thus from a modelling point of view the material can be considered as a solid containing isolated spherical or polyhedral voids connected by grain boundaries. However if grain growth occurs the boundaries may no longer be in

contact with the pores and the normal diffusion process which occurs during sintering can no longer cause densification. Hence an applied pressure is required to reduce the size of the pore (160,178,180). Therefore pressure assisted sintering during the final stage of the sintering process can be compared to the pore closure in castings during HIP processing, since densification proceeds by plastic yielding, power law creep or diffusion (111,165,179,180). Also the densities involved in the recovery of castings by HIPping are more appropriate to stage 3 than the stage 1 model used by the Ashby model. Secondly the experimental yield stress data obtained during hot tensile experiments and used during plastic yielding densification rate calculations is sparse and could therefore be unreliable, although it shows reasonable comparison with other high temperature data recorded for 90/10 and 70/30 cupronickel alloys (78,80,81).

Thirdly encapsulation techniques which involve the use of desert based silica sand as the pressure transmitting medium have been found to restrict significantly the densification process, due to the sand particles attaining a maximum packing density which enables them to become mechanically locked, thus diminishing the external pressure transmitted to the casting.

Due to the good correlation between densification predicted by Ashby's plastic yielding densification rate equation and experimental HIP data for castings containing internal porosity HIPped at processing temperatures above 900°C, it

appears that the discrepancy observed between predicted densification and experimental pore closure rates for castings containing surface-connected porosity could be associated with the need for encapsulation. It is thought that encapsulation using standard techniques hinders the densification process by lowering the applied pressure transmitted to the casting to below the yield stress of NES 824 at the HIP temperature. Thus no further plastic yielding will occur and any further pore closure will take place due to creep and diffusion, that is by time dependent mechanisms. This accounts for the rapid decrease in densification observed in HIP experiments once the HIP sustain period exceeds 45 minutes, and the slow densification observed for HIP times within the range 4 - 12 hours (Figure 87).

5.10.2 PORE CLOSURE PREDICTED BY THE PLASTIC FLOW THEORY

The plastic flow theory developed by Mackenzie and Shuttleworth (98) and modified by Murray et al (124) to cover the application of externally applied pressure has been used to predict the densification of 70/30 cupronickel castings containing surface-connected porosity, which are encapsulated using standard techniques prior to HIP processing. The plastic flow theory assumes that the applied pressure is transmitted hydrostatically and that pores of equal size will decrease in size, but the number of pores will remain constant. Therefore the experimental HIP model involving NES 824 specimens containing single cylindrical pores which are surface-connected, does not

best fit the plastic flow theory. However reasonable agreement has been found between pore closure rates predicted by the law of hot pressing (124) (equation ⁽¹⁹⁾ section 2.11.5) and experimental HIP data obtained on 70/30 cupronickel castings containing 10% and 16% porosity HIPped at a temperature of 950°C for sustain periods which exceed 45 minutes (Figure 189). Equation 19 cannot be used to predict initial densification which occurs once the yield stress has been exceeded by the applied HIP pressure, and the subsequent plastic deformation which occurs within 45 minutes at the sustain temperature and pressure, since the plastic flow theory only involves viscous flow. The reduction in experimental pore closure rates at extended times and the good correlation with predicted densification rates for sustain periods greater than 45 minutes suggests that at extended times the HIP pressure is no longer the driving force for the densification process; pore closure now being driven by surface tension and any internal pressure in the pores (98,100-102). The loss of the externally applied pressure is due to the high compressive strength of silica sand once it has attained a maximum packing density. The sand becomes mechanically locked and opposes the externally applied pressure, thus diminishing the pressure transmitted to the casting such that it is possibly below the yield stress of 70/30 cupronickel at the processing temperature. Thus the densification mechanisms now in operation are time dependent, that is they involve predominantly creep and diffusion (100,101). Densification rates predicted by the plastic flow theory

accurately describe the densification which occurs during the HIPping of encapsulated castings containing surface-connected porosity via type II HIP cycles involving sustain periods greater than 45 minutes.

5.10.3 70/30 CUPRONICKEL HOT ISOSTATIC PRESSING MAPS

The development of HIP maps for 70/30 cupronickel has been achieved by the use of a software program "HIP 6.0" developed by Ashby (178). The program constructs HIP maps using material data stored for a range of pure metals to calculate the densification rate equations involving plastic yielding, volume diffusion, boundary diffusion and power law creep (as described in section 2.15). The program allows HIP maps relating density - pressure, density - temperature and pressure - temperature - density to be constructed for NES 824 (Figures 190 - 201). The pore closure rates predicted by the HIP model accurately describe the densification of cupronickel castings containing internal porosity, predicting that 10% and 16% porosity can be consolidated at a temperature of 950°C with pressures of 103MPa within 4-45 minutes. This compares favourably with experimental HIP data obtained on 70/30 cupronickel castings containing internal porosity, and surface-connected porosity if the castings are encapsulated in a close fitting steel capsule or are encapsulated using Zone-M concrete sand as the packing material. In comparison, the predicted pore closure rates do not compare favourably with experimental densification rates for castings containing surface-connected porosity which are

encapsulated using desert-based silica sand as the pressure transmitting medium. The angular silica particles restrict the densification process during HIPping due to mechanical locking of the particles. The HIP 6.0 software at present is not sufficiently developed to be able to predict the densification of two separate materials such as a ceramic and a metal to be modelled simultaneously.

The above results indicate that from limited material data accurate HIP maps can be predicted for 70/30 cupronickel which compare favourably with experimental HIP data obtained on NES 824 samples containing internal and surface-connected porosity providing the latter is encapsulated using a water table sand as the pressure transmitting medium. Thus it appears that the material data base installed in the software program provides a good estimate of the behaviour of NES 824 at high temperatures and pressures.

Modelling of the densification of 70/30 cupronickel castings containing cylindrical pores was also attempted using finite element analysis. Two systems: Ansys and Pafec were used, the first had limited memory and could not carry out the detailed calculations required. Difficulties were experienced with the second system in regards to entering temperature - stress relationships for a heating and cooling cycle rather than using static conditions. Thus no data of practical use has yet been established by these investigations and further work is required to produce an operational model to simulate the densification of NES 824 castings during HIPping.

6.0 CONCLUSIONS

6.1 The commercial HIP time for the recovery of Class I cupronickel castings can be reduced by 75%, from 4 hours to 1 hour.

6.2 The optimum HIP processing conditions for the densification of 70/30 cupronickel NES 824 castings containing 5-16% internal porosity are short sustain times of 45 minutes, at temperatures within the range 875-950°C and argon gas pressures of 62-103MPa.

6.3 70/30 cupronickel castings containing less than 5% surface-connected porosity encapsulated using standard techniques can be recovered by short HIP cycles using processing conditions of 45 minutes, at 950°C and argon gas pressures of 103MPa.

Successive HIP cycles of short duration appear more effective in reducing porosity contents greater than 10% than extended time single HIP cycles, since the densification rate gradually falls to zero within 45 minutes at the sustain conditions.

6.4 The reduction in pore closure rate of encapsulated castings at extended HIP times is probably due to the exposure of the angular silica particles to high temperatures and pressures, causing them to reach an optimum packing density and undergo mechanical locking. This suggests that the loss of particle flow combined with the high compressive strength of the sand diminishes the applied pressure transmitted to the casting.

- 6.5 For optimum pore closure of encapsulated castings the pressure transmitting medium thickness must be less than 10mm.
- 6.6 Elongated pores of small diameter can be closed in shorter HIP times than pores of equivalent volume porosity but smaller aspect ratio.
- 6.7 The ideal encapsulation technique for the HIP recovery of 70/30 cupronickel castings containing surface-connected porosity is a close fitting steel capsule. 10-16% porosity can be closed by short HIP cycles using processing conditions of 45 minutes at 950°C and argon gas pressures of 103MPa.
- 6.8 The major densification mechanisms occurring during HIPping include plastic deformation and time dependent mechanisms such as creep and diffusion.
- 6.9 Initial densification via plastic deformation occurs when a HIP temperature is reached where the applied pressure exceeds the yield stress. A 16% internal pore can be completely closed by initial densification at a HIP temperature of 950°C, whereas 3-9% pore closure of a surface-connected pore occurs at HIP temperatures of 950°C and 1025°C.
- 6.10 A HIP temperature of 850°C is too low to allow plastic deformation to occur because the yield stress of the material is not exceeded by the standard HIP pressure of 103MPa.

6.11 Particulate materials such as oxides, carbides, borides and nitrides and mixtures of these materials offer no advantages over desert based silica sand as a pressure transmitting medium for encapsulated castings.

6.12 The replacement of desert based silica sand with zone M concrete sand increases the rate of densification of encapsulated cupronickel castings containing surface-connected porosity.

6.13 Desert based silica sand and zone M concrete sand are stable at temperatures and pressures associated with HIPping and have no chemical interaction with NES 824 material.

6.14 A suitable pressure transmitting medium for encapsulated castings is one of high melting point and purity, and has a particle size of 100-150 μ m and a rounded particle morphology.

6.15 HIPping has no detrimental effects on the properties of Class I 70/30 cupronickel (NES 824) castings.

6.16 The ultimate tensile strength increases slightly with an increase in HIPping temperature with maximum strength at 1025°C. This increase in strength is associated with some loss of ductility.

6.17 A HIP temperature of 950°C produces the best combination of strength and ductility whilst inhibiting grain growth associated with higher HIPping temperatures.

6.18 HIPping produces homogenisation and stress relaxation of a casting which should result in improved material isotropy.

6.19 Stress relieving cast 70/30 cupronickel produces a significant increase in both strength and ductility.

As-cast cupronickel subjected to a thermal simulation of a HIP cycle suffers a reduction in strength. The strength levels are retained and improved to levels associated with Class I NES 824 castings on the application of a stress relaxation treatment. However the stress relief of HIPped NES 824 offers no advantages.

6.20 The hot strength of 70/30 cupronickel does not change significantly until temperatures exceed 500°C. The yield strength at the three HIPping temperatures of 850°C, 950°C and 1025°C are approximately 70, 45 and 20MPa respectively.

6.21 70/30 cupronickel suffers a ductility trough between the temperature range 600-800°C. The loss of ductility is associated with the coalescence of voids and subsequent intergranular fracture.

6.22 HIPping has no detrimental effects on the corrosion performance of 70/30 cupronickel in a 5% salt solution, substitute ocean water and natural sea water. The excellent corrosion performance is attributed to the formation of a black oxide corrosion product film.

6.23 Ashby's rate equation for plastic yielding in particulate materials can be used with a high degree of accuracy at HIP temperatures above 900°C to predict the closure of pores in 70/30 cupronickel castings containing:

- (i) 16% internal porosity;
- (ii) 16% surface-connected porosity, encapsulated in a close fitting steel capsule;
- (iii) 5% surface-connected porosity, encapsulated using standard techniques,
- (iv) 10% surface-connected porosity, encapsulated using zone M concrete sand as the pressure transmitting medium.

6.24 The plastic flow theory can be used with reasonable accuracy to predict the densification of 70/30 cupronickel castings which contain surface-connected porosity encapsulated using standard techniques, and are HIPped at a temperature of 950°C and argon gas pressures of 103MPa for sustain periods greater than 45 minutes.

6.25 Hot isostatic pressing maps for 70/30 cupronickel produced using Ashby's HIP 6.0 software accurately predict the densification of castings containing up to 16% internal porosity, together with the densification of castings containing up to 10% surface-connected porosity which are encapsulated using:

- (i) a close fitting steel capsule or;
- (ii) a capsule packed with Zone-M sand either as a single particle size or as an aggregate.

7.0 FURTHER WORK

7.1 Investigate the effect of pore geometry and angularity on the rate of densification of 10-16% surface-connected porosity by successive type I HIP cycles. Substantiate whether large pores close faster than smaller pores due to a reduced wall thickness effect or whether the present experimental results were misinterpreted due to experimental data scatter.

7.2 Investigate the effect of alternative refractory packing materials on the densification rate of encapsulated castings containing surface-connected porosity. A pressure transmitting medium is required which does not impede the densification process during HIPping. Subsequently the aim is to find a pressure transmitting medium which allows the consolidation of encapsulated castings to occur at a similar rate to castings containing internal porosity which do not require encapsulation.

7.3 Investigate the effect of HIPping on the corrosion fatigue of 70/30 cupronickel. Such investigations are currently being carried out by the M.O.D Bath. In addition further corrosion performance investigations encompassing crevice, impingement and submerged tests in natural sea water are required to confirm the trend observed to date, which suggests that HIPping slightly improves the corrosion performance of NES 824 material.

7.4 Investigate in more detail the effect of HIPping commercial 70/30 cupronickel marine castings containing between 5-20% porosity, in order to identify the effect of HIP recovery on the strength, ductility and microstructural characteristics of defect repaired areas. For castings containing severe shrinkage defects an optimum recoverable defect size needs to be determined, such that the recovery of an optimum level of porosity has no detrimental effects on the mechanical or microstructural properties of 70/30 cupronickel material.

7.5 Investigate quantitatively the effect of HIP temperature and time at temperature on the grain size and microsegregation of NES 824 material to substantiate trends observed to date.

7.6 Investigate in detail the cause of embrittlement of NES 824 between the temperature range 600-800°C and thereby explain why cupronickel material cannot undergo stress relaxation at these temperatures. Investigate whether a change in heating or cooling rates can reduce or eliminate the ductility effect observed in this material.

7.7 Investigate whether the plastic yielding densification rate equation can be modified to include a term to account for the presence of a refractory pressure transmitting medium during the densification of encapsulated castings. Assess the accuracy of the predicted data against experimental HIP data.

7.8 Assess the accuracy of the HIP maps produced by the HIP 6.0 software to predict minimum processing parameters in regards to temperature and pressure for the closure of internal porosity in 70/30 cupronickel castings.

7.9 Investigate the possibility of extending the HIP 6.0 software program to model the closure of pores in encapsulated castings containing surface-connected porosity, by taking into account the presence of a second isolated phase such as a refractory packing material.

7.10 Investigate the accuracy of finite element analysis models such as Pafec and Ansys to predict the closure of cylindrical pores of internal porosity in cupronickel material at a temperature of 950°C and applied pressures of 103MPa. In addition investigate the possibility of using such methods to model pore closure throughout the whole HIP treatment, involving heating and pressurisation as well as the degree of closure which occurs at the sustain conditions.

8.0 REFERENCES

1. Bradley J.N., Metallurgical Reviews Vol 17, 81, 1972.
2. Campbell H.S., Ocean Engineering Vol 11, P 387-393, Pergamon Press 1969.
3. Osborn D.H., Sudrabin D.A., Proc National Association of Corrosion Engineers 1969, 24, P 318. Copper Base Alloys: The Logical Choice For Marine Structures and Equipment.
4. Weldron B.A., Anant Narayon S.N., Proc Copper and Its Alloys In The 80's. 3-5 Dec 1981, Bombay, India. "The Developing Uses of Copper - Nickel Alloys In Marine Engineering".
5. Moreton B.B., Proc Copper Alloys In Marine Environments Today And Tomorrow, International Copper Research Association. Paper 1.
6. Hadden P.G., Metals and Materials Engineering July 1988, P 412.
7. Dawson R.J.C., Proc Copper Alloys In Marine Environments Today And Tomorrow. Paper 3. Copper Development Association.
8. BS 1400 : British Standard Institution. Specification for copper alloy ingots and copper alloy and high conductivity copper castings.
9. Mantle E.C., Proc Copper Alloys In Marine Environments Today And Tomorrow. Paper 13. Copper Development Association.
10. Naval Engineering Standard, NES 747 Part 2.
11. Hall K., Mansbridge K.C., Cooper R.E., Proc RYNA Symposium, May 1983, London. "Materials For Submarines".
12. Weill - Couly, Arnaud D., Foundrie Vol 322, P 123-125, 1973.
13. Rowlands J.C., Proc 8th International Congress on Metallic Corrosion, Mainz 6-11 September 1981.
14. Hall B.N., Townsend D.W., Proc Marine Engineering With Copper - Nickel. London, April 1988, Vol 52, P 73.
15. Powell C., Metals And Materials Engineering, December 1990, P 783.
16. Rowlands J.C., Angell B., M.O.D Report, ARE TM (UMM) 88405, March 1988. "The Marine Corrosion Performance Of IN768 Cast High Strength Cupronickel". *

17. Westley Brothers Limited. OEM Design, April 1990. "Cupronickel Alloy".
18. Townsend D.W., Engineering Materials and Design, November 1969.
19. Gilbert P.T., Proc Historical Metals Society Conference University of Aston, Birmingham, September 1984.
20. Ansuini F.J., Badia F.A., Transactions American Foundrymen's Society Vol 78, P 165, 1970.
21. Jones R.L., Rowlands J.C., Proc Copper Alloys In Marine Environments Today And Tomorrow". International Copper Research Association, Paper 17.
22. Anderson D.B., Private Communication. The International Nickel Company Inc. Report on the sea water corrosion resistance of Cr modified cast 70/30 alloys.
23. Gavin S.A., Private Communication. BNF Metals Technology Centre, Wantage.
24. Naval Engineering Standard NES 824 Part 1 Issue 1. Requirements for the Production of High Strength Chromium Cupronickel Sand Castings and Ingots.
25. Naval Engineering Standard NES 825. Requirements for the Production of High Strength Chromium Cupronickel Sand Castings and Ingots.
26. Powell C.A., Copper Development Association Report, March 1990. "Assessment of the Commercial Potential of Cast Cu-Ni-Cr Alloy NES 824".
27. Vickers-Shipbuilding Engineering Limited. Private Communciation.
28. Defence Standard 01-2.
29. Kirk W., Lee T., Lewis R., Proc Copper Alloys In Marine Environments. April 1985, Paper 16. Copper Development Association.
30. Cohen A., Rice La vern, Proc Corrosion 69, Vol 25, P 342, 1969.
31. Schrieber C.F., Osborn O., Rice L., ibid P332.
32. Perry D.A., Proc National Association of Corrosion Engineers. 1969, Vol 25, P 324.
33. Taylor M.D., Proc Corrosion coatings, S. Africa, April-May 1988, 15, (2), 10-12, 14. Metal Abstracts September 1988, 35-1856.

34. Todd B., Proc Copper Alloys In Marine Environmrnts Today And Tomorrow, International Copper Development Association. Paper No 4.
35. Glover T.J., Moreton B.B., Proc UK National Corrosion Conference 1982, 18-16 Nov 1982. "Corrosion and Fouling Resistance of Cu-Ni Alloys In Marine Environments". P 105.
36. Trethewey K.R., Chamberlain J., Corrosion (Book). Longman Scientific and Technical 1988.
37. Fontana M.G., Greene N.D., 1978 Corrosion Engineering (Book). McGraw Hill.
38. Wilde B.E., Proc Localised Corrosion, Nace 1984, P342-352.
39. Evans U.R., The Corrosion and Oxidation of Metals (Book). Edward Arnold 1961.
40. Shrier L.L., Corrosion of Metals and Alloys (Book).
41. Lush P.A., CME October 1987, P 31 "Materials for Minimum Cavitation".
42. Popplewell J., Proc Corrosion 78, 6-10 March 1968, Houston, Texas, Paper 21.
43. La Que F.L., Journal of American Society of Naval Engineers, 1941, Vol 53, 64, P 29.
44. Bassett W.H., Davis C.H., Transactions American Institute Mining and Metallurgical Engineers, Vol 71, P 745, 1925.
45. Friend J.N., Journal of The Institute of Metals Vol 48, No 1, P 109, 1932.
46. Manson J., Irvine J., Parkes J., M.O.D Report ARE TM (UMM) 87408 "Compositional and Microstructural Variations in cast NES 824". *
47. Gosden S.R., Private Communication. "Effect Of Coring On The Corrosion Properties Of IN 768" B.S.c Project RNEC.
48. Rowlands J.C., Proc Localised Corrosion. Williamsburg 1971. "Mechanistic Studies on Localised Corrosion of Copper Based Alloys due to Hydrodynamic Conditions".
49. Brownsdown H.W., Bannister J., Institute Metals Vol 49, P 123, 1932.
50. Lush P.A., Proc 6th European Congress on Metallic Corrosion P137-146, London 1977.

51. Anderson D.B., Efird K.D., Proc 3rd International Congress on Marine Corrosion and Fouling Gaithersburg, Maryland, October 1972, P264.
52. Anderson D.B., Badia F.A., Transactions ASME Vol 95, No 4, P 132.
53. Hall B.N., National Association of Corrosion Engineers Vol 20, P 379t, 1964.
54. Lichtrowicz A., Scott P.J., Proc 5th International Conference on Erosion by Solid and Liquid Impact. Cambridge September 1979.
55. Copper Development Association Publication TN 38. Materials For Sea Water Pipe Line Systems.
56. Hutchings J., Fulmer Research Institute Report R806/2 March 1982. The Corrosion Fatigue Testing of Two Cast Cupronickel Alloys".
57. Galsworthy M.O.D Report ARE TM (UMM) 88406, March 1985. "Preliminary Evaluation Of The Low Frequency Corrosion Fatigue Behaviour Of High Strength Cr - Cupronickel Parent Material And weldment".
58. Gilbert P.T., Proc Corrosion 81. International Corrosion Forum sponsored by the National Association of Corrosion Engineers. April 6-10 1981, Sheraton Centre, Toronto, Ontario, Canada, Paper No 194.
59. Barberry J., Pepin - Donat C., Metallurgie Vol 36, No 11, 1982.
60. North R.F., Pryor M.J., Corrosion Science Vol 10, No 5, 1970.
61. Popplewell J.M., Hart R.J., Ford J.A., Corrosion Science Vol 13, No 4, P 295, 1973.
62. MacDonald D.D., Syrett B.C., Wing S.S., Corrosion Vol 34, No 9, 1978.
63. Krougman J.M., Ijsseling F.P., Proc 4th International Congress on Marine Corrosion and Fouling, Antibes, France, June 1976.
64. Kievits F.J., Ijsseling F.P., Werkstoffe und Korrosion Vol 23, P 1084, 1972.
65. Blundy R.G., Pryor M.J., Corrosion Science Vol 12, No 1, 1972.
66. Efird K.D., Corrosion Vol 33, No 10, P 347, 1977.
67. Bailey G.L., Journal of the Institute of Metals, Vol 79, P 243-292, 1951.

68. Berg P.J., Kievits R.G., de Lange R.L., Proc 2nd International Conference on Marine Corrosion and Fouling, Athens P 95, 1968-9.
69. Drolenga L.J.P., Ijsseling F.P., Kolster B.H., Werkstoffe und Korrosion Vol 34, P 167, 1983.
70. Blacklay E.H., Private Communication. B.S.c Swindon Laboratories, Rotherham.
71. Anderson D.B., Efird K.D., Proc 3rd International Congress on Marine Corrosion and Fouling 1972. "Influence Of Cr On Corrosion Behaviour Of Cu-Ni Alloys In Sea Water".
72. Kirk W.W., International Copper Research Association Report Inc. April 1986. "Evaluation of Alloying Effects On Corrosion Behaviour Of Cu-Ni Alloys In Sea Water".
73. Swartzendruber L.J., Bennett L.H., Scripta Metallurgica Vol 2, P 93-98, 1968. Pergaman Press Inc.
74. Pearson C., British Corrosion Journal Vol 7, P 61-68, March 1972.
75. Kolster B.H., Rodemakers P.L.F, Burggraf J., Potzschke M., 5th International Symposium on Fresh Water From The Sea, P 403, 1976.
76. Ijsseling F.P., Drolenga L.J.P., Kolster B.H., Vander Veer J., British Corrosion Journal Vol 17, No 4, P 162, 1982.
77. Admiral L., Ijsseling F.P., Kolster B.H., British Corrosion Journal Vol 21, No 1, P 33, 1986.
78. Chubb J.P., Billingham J., Hancock P., Dimbylow C., Newcombe G., Journal of Metals Vol 30, 1978.
79. Savage W.F., Nippes E.F., Domby C.W., "Mid-Temperature Embrittlement of Copper". Final Report for INCRA, Project Number 243A, International Copper Research Association 1977.
80. Evans R.W., Jones F.L., Met Technol, 1976, Vol 3, P 494.
81. Jones F.L., Materials Science and Technology, March 1988, P256.
82. Mintz B., Arrowsmith J.M., "Hot Working and Forming Pocesses" Edited C.M. Sellars, G.J Davies, P 99, 1980, London, The Metals Society.
83. Rhines F.M., Wray P.J., Trans ASM, 1961, Vol 54, P 117.

84. Reid B.J., Greenwood J.N., Trans AIME 1958, Vol 212, P 503.
85. Middleton C.J., PhD Thesis, University of Leeds 1971.
86. Lupton D.F., Thompson J.R., Journal of Institute of Metals, Vol 100, P 352, 1972.
87. Chubb J.P., Billingham J., Unpublished work quoted by Chubb et al, Journal of Metals, March 1978, Vol 30, P 20.
88. Guha P., Brown D., Littlewood G., Journal of the Institute of Metals Vol 29, P 148, 1971.
89. Evans R.W., Jones F.L., Metals Technology, Vol 5, P 1, 1978.
90. Williams J.A., Philosophical Magazine Vol 20, P 635, 1969.
91. Stroh A.N., Proc Royal Soc London, A, Vol 223, P 404, 1954.
92. Mclean D., Journal Institute of Metals Vol 85, P 468, 1956-57.
93. Thompson N.B.W., Bell R.L., Journal Institute of Metals Vol 94, P 116, 1956 - 1957.
94. Richinger W.A., Journal Institute Metals Vol 81, P 33, 1952-53.
95. Resnick R., Seigle L., Journal of Metals Vol 85, P 87, 1957-58.
96. Lagarde P., Biscardi M., Grain Boundaries in Engineering Materials (Book). Claitors Publishing Division, Baton Rouge, P367, 1974.
97. Greenwood J.N., Miller D.R., Suiter J.W., Acta Met Vol 2, P 250, 1954.
98. Mackenzie J.K., Shuttleworth R., Proc Royal Physics Society, Vol B62, P 833, 1949.
99. Kuczynski G.C., Proc Powder Met. 18th Sagamore Army Materials Research Conference. Syracuse University Press 1972.
"Fundamentals of Sintering Theory".
100. Atkinson H.V., Rickinson B.A., Hot Isostatic Processing, 1991. Adam Hilger, Bristol.
101. Waldron M.B., Daniel B.L., Sintering (Book). Heyden & Son Ltd. London 1978.

102. Kuczynski G.C., Proc Powder Met. 13-17 June 1960, P 11. "Theory of Solid State Sintering".
103. Smith C.S., Metall Review Vol 9, P 1, 1964.
104. Rhines F.N. Trans American Inst Min Met Eng. Vol 166, P474, 1946.
105. Shaler A.J., Journal of Metals 1949.
106. Fischmeister H.F., Arzt E., Powder Metall Vol26, P 82, 1983.
107. Swinkels F.B., Ashby M.F., Acta Metall Vol 28, P 259, 1981.
108. Kuczynski G.C., Trans AIME Vol 185, P 169, 1949.
109. Herring C., Journal of Applied Physics Vol 21, P 301, 1950.
110. Helle A.S., Easterling K.E., Ashby M.F., Acta Metall Vol 26, P 2163, 1985.
111. Coble R.L., Journal of Applied Physics Vol 41, P 4789, 1970.
112. Johnson D.L., Journal of Applied Physics Vol 40, P 192, 1969.
113. Swinkels F.B., Ashby M.F., Acta Metall Vol 28, P 259, 1981.
114. Arzt E., Ashby M.F., Easterling K.E., Metall Trans A Vol 14A, P 211, 1983.
115. Alexander B.H., Balluffi R.W., Journal of Metals Vol 2, P 1219, 1950.
116. Coble R.L., Journal of Applied Physics Vol 32, P 787, 1961.
117. Johnson D.L., Journal American Ceramics Society Vol 53, P 574, 1970.
118. Frenkel Journal of Applied Physics USSR Vol 9, P 385, 1945.
119. Shaler A.J., Wulff J., Industrial & Eng Chem 1948, Vol 40, P 838.
120. Shaler A.J., Trans Amer Inst Min Met eng Vol 185, P 796, 1949.
121. Nabarro F.R.N., "The Strength of Solids". Vol 60-61, P 75, 1948 London Physical Society.

122. Herring c., Journal Applied Physics Vol 21, P437, 1950.
123. Ramqvist L., Powder Metallurgy, Vol 9, P 1, 1966.
124. Murray P., Rodgers E.P., Williams A.E. Trans Brit Ceramic Society Vol 53, P 474, No 8, 1954.
125. Mangsen G.E., Lambertson W.A., Best B., Journal American Ceramic Society Vol 43, P55, 1960.
126. Vasilos T., Journal American Ceramic Society Vol 43, P 517, 1960.
127. Jaeger R.E., Egerton L., Journal American Ceramic Society Vol 45, P 209, 1962.
128. Lersmacher B., Scholz S., Arch. Eisenhüttenwesen Vol 32, P 421, 1961.
129. McCelland J.D., Proc Powder Metallurgy 13-17 June 1960, P 167. (Academic Press).
130. Koval'chenko M.S., Samsonov G.V., Poroshkovaya Metallurgiya 1961, Vol 1, No 2, P 3-13.
131. Scholz S., Lersmacher B., Arch. Eisenhüttenwesen 1964, Vol 41, P 98.
132. Fryer G.M., Transactions British Ceramic Society Vol 66, P 127, 1967.
133. Fryer G.M., Transactions British Ceramic Society Vol 68, P 185, 1969.
134. James P.J., Isostatic Pressing Technology (Book). Applied Science Publishers, 1983.
135. Freeman A., MPR May 1989, P 360.
"Technical Advice in Hot Isostatic Compaction Equipment".
136. Price P.E., Kohler S.P., HIPping of Metal Powders. Metals Hand Book Vol 7, 9th Edition, Powder Metallurgy P 419-443.
137. Roussos T., Industrial Heating, P 36-37, 1985.
138. Stocksbridge L.J., Lazzaro A.A., Precision Metals, December P 15-16, 1984.
139. Minnebo A., Crum A., "HIP Equipment Design". Proc Int Conf on HIPping of Materials, Antwerp 25-27 April, 1988.
140. Hanes H.D., Seifert D.A., Watts C.R., HIPping Pub No. MCIC-77-34, 1979 Columbus, Ohio, Battelle Memorial Institute.

141. Traff A., Proc 1st Int Conf on Isostatic Pressing, Paper 13, 1978, Loughborough University of Technology.
142. Zimmerman ibid Paper 12.
143. Widmer R., American Society for Metals. Proc High Temperature Alloys. Massachusetts Institute of Technology, 16-18 June 1985.
144. Ermel D., Hack R., Hofmann g., Polhede W., Int Conf on Isostatic Pressing of Materials - Applications and Developments. Antwerp 25-27 April, 1988.
145. Klomp J., Ibid.
146. Lindenmo m., Proc HIP Theories and Applications. Lulea, 1987.
147. Stamberger J., Hribernik B., Jaeger H., ibid.
148. Jarvenpaa M., ibid.
149. Cooper R., Proc Science of Hard Materials, Jackson, Wyoming, August 1981.
150. Widmer R., Int Conf HIPping of Materials. Antwerp 25-27 April, 1988.
151. George J., Eureka June 1984. Innovative Engineering Design. "Treated Castings Match Wrought Components".
152. Rickinson B.A., Proc SCRATA Annual Conference 1985. "HIPping For The Improvement Of castings".
153. Broihanne G., Proc HIPping of Materials. Antwerp 25-27 April 1988.
154. Strode I., Evans D., ibid. Section 4.7.
155. Hannotiau M., Schrijvers J., Sleurs J., ibid.
156. Person C., Ostensson M., Int Cong on HIPping of Materials. Antwerp 25-27 April 1988. (4.13).
157. Strode I., Proc 3rd Int Conf on Isostatic Pressing. London 1986, Vol 1, (37.1-37.11).
158. Poyet P., Cercle Etude Metaux Bull. June-Sept 1984, (6-8), 11.1-11.4.
159. Zeitler H., Scharfenberger W., Munchen, "Correction of Casting Faults". December 1984, Vol 60, P 12.
160. Ashby M.F., Proc Hot Isostatic pressing. Lulea 15-17 June 1987. "The Modelling of Isostatic Pressing".

161. Li W.B., Ashby M.F., Easterling K.E., Acta Metal 1987.
162. Waslelewski G.E., Lindbold N.R., Proc 2nd Int Conf Isostatic Pressing, AIME 1972. MCIC 72-10.
163. Balakrishna Bhat, Arunachalam V.S., Conf on Isostatic Pressing 19-21 Sept 1978. Loughborough University of Technology.
164. Freeman W.R., Met Progress Vol 32, P 112, 1977.
165. Wilkinson D.S., Ashby M.F., Acta Metal Vol 23, P 1277, 1975.
166. Evans E.B., Ebert L.J., Briggs C.W., ASTM 56, 1956, P 979-1020.
167. Larker H.T., Material Science and Engineering Vol 71, P 329-332, 1985.
168. Tidbury I.E., Rickinson B.A., Proc 3rd International Conference on Isostatic Pressing Vol 2, London 10-12 November 1986.
169. Kaysser W.A., Aslan A., Arzt E., Mitkov M., Petzow G., Powder Metallurgy No 1, Vol 31, P 63, 1988.
170. Rickinson B.A., Metals and Materials, February 1985, No 1, Vol 2, P 104-107.
171. Rickinson B.A., Dimbylow C.S., Proc Perspectives in Metallurgical Development, 1884-1984. Sheffield University 1984.
172. Strode I., Bassett M.B., Davies C., Metals Technology Vol 9, P 349-354, Sept 1982.
173. King S., Walker R., Foundry Trades Journal Vol 163, P 97, 1989.
174. Glenn G.M., SAMPE Quarterly 8, 1, 1, 1.
175. Widmer R., Proc 1st Int Conf on Isostatic Pressing, Loughborough University of Technology 1978.
176. Holmes P.D., Proc 2nd Int Isostatic Pressing Conference, Stratford September 1982, Paper 16.
177. Bailey P.G., Schweikert W.H., Superalloys Metallurgy and Manufacture. P 451-465, 1976.
178. Ashby M.F., HIP 6.0. Cambridge University 1990.
179. Wilkinson D.S., Phd. Thesis 1977. "Pressure Sintering". University of Cambridge.

180. Wilkinson D.S., Ashby M.F., 4th Int Round Table on Sintering. 1978 Vol 10, No 2, P 67-76.
181. Tien J.K., Borefkj J.C., Proc Int Conf on Hot Isostatic Pressing. Lulea 15-17 June 1987.
182. Ferguson B.L., Int journal of Powder Metallurgy and Powder Technology. Vol 21, No 3, P 201.
183. Ecer G.M., Sakarcn M., Yeltekin S., Metals Joining Using The Ceracon Process. ASM Paper 8414-001 Nov 84.
184. Raman R.V., Advanced Materials and Processes Vol 4, 1990.
185. Meeks H.S., Proc Hot Isostatic Pressing: Business Oppertunities In The 1990's. 7-8 June 1990, Seattle, Washington.
186. US Patent 3 356 496 December 1967, Hailey R.W., Wheeling Pittsburgh Steel Coroporation.
187. US Patent 3 689 259 September 1972.
188. US Patent 4 518 441 May 1985.
189. US Paent 4 615 208 October 1986.
190. US Patent 4 634 750 January 1987.
191. US Patent 4 645 131 February 1987.
192. US Patent 4 689 008 August 1987.
193. US Patent 4 725 227 February 1988.
194. US Patent 4 758 137 July 1988.
195. Sosman R.B., "The Properties of Silica". American Chemical Society Monograph 1927.
196. Gilchrist J.D., Fuels Furnaces and Refractories (Book). Pergaman Press 1977.
197. Gilchrist J.D., Fuels and Refractories (Book). Pergaman Press 1963.
198. Chesters J.H. Refractories Production and Properties (Book). The Iron and Steel Institute, London.
199. Bukenhout L., Tempels M., Sleurs J., Schrijvers, International Conference on HIPping of Materials, Antwerp, Belgium 25-27 April, 1988.
200. Rickinson B.A., Walker R., Private Communication, Infutec Diffusion Bonding Centre Limited, Chesterfield.

201. Lenel F.V., Powder Metallurgy. Principles and Applications. Metal Powder Industries Federation, Princetown, New Jersey 1980.
202. Drucker D.C., Introduction to Mechanics Of Deformable Solids. Book. McGraw-Hill Book Company, 1967.
203. Pomeroy C.D., Creep of Engineering Materials. Book. Mechanical Engineering Publications Ltd. London 1978.
204. Boley B.A., Weiner J.H., Theory of Thermal Stresses. (Book) John Wiley & Sons Inc., 1960.
205. Fletcher A.J., Thermal Stresses and Strain Generation In Heat Treatment. Elsevier Applied Science 1989.
206. Freudenthal A.M. Inelastic Behaviour of Engineering Metals and Structures. John Wiley & Sons Inc 1950.
207. Cottrell A.H., Dislocations and Plastic Flow in Crystals. Clarendon Press, 1953.
208. Read W.T., Dislocations In Crystals. McGraw-Hill 1953.
209. Prager W., Hodge P.G., Theory Of Plastic Solids. John Wiley & Sons 1951.
210. Hill R., The Mathematical Theory of Plasticity. Oxford, Clarendon Press, 1950.
211. Abbasi F., PhD Thesis Sheffield City Polytechnic, 1983. The Influence Of Visco-Elastic Processes On The generation Of Thermal Stresses In Quenched Low Alloy Steel Plates.
212. Soomro A.B., PhD Thesis Sheffield City Polytechnic, 1986. The Generation Of Thermal Stress And Strain During Quenching.
213. Rickinson B.A., Private Communication H.I.P Limited.
214. Rickinson B.A., Private Communication H.I.P Limited.
215. Pearson J., Private Communication, Vickers-Shipbuilding and Engineering Limited.
216. ASTM Standard D1141-75. Substitute Ocean Water.
217. Cortest Laboratories Limited, Sheffield. Private Communication, Contract Number U 92804-0.

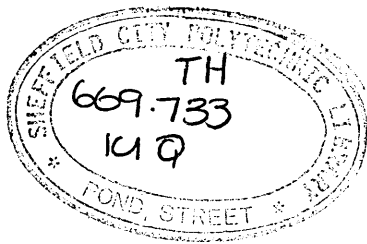
* Available from HMSO.

SHEFFIELD ST 750

000000 000 00 00 00 00 0000000000000000 00 0000

Sheffield City Polytechnic Library

REFERENCE ONLY



Major Developments in Copper Alloys During 1700-1970 (3)

DATE	EVENT
1765	Copper sheet used to sheath wooden British Admiralty Ships.
1801	Paul Revere rolled copper sheet to sheath wooden American Naval Ships.
1860	Development of aluminium bronze.
1870	Brass introduced as a condenser tube material.
1890	First use of Admiralty metal.
1906	First patent issued for Ni-Cu alloys (U.S Patent Number 811,239).
1922	Arsenic found to inhibit dezincification of alpha brass in sea water.
1923	Copper - nickel (70/30) developed for salt water applications.
1925	Copper - nickel (90/10) developed for salt water applications.
1928	First aluminium brass (76Cu 22Zn 2Al) alloys developed in Britain.
1939	Beneficial effects of Fe (approx 0.5%) additions to 70/30 cupronickel determined.
1951	Beneficial effects of Fe (approx 1.2%) additions to 90/10 cupronickel determined.
1968	Development of new IN732 copper - nickel alloy equivalent to or greater than mild steel in as welded condition.

REFIELD CITY POLYTECHNIC LIBRARY

14 Street, Sheffield S1 1WB

0742 532114

0742 532125

Supplier

V.I. 254915

Record No.

Please supply returning form with item reporting within 3 months if unavailable.

V.2-254917

Author

KING, S.

The hot isostatic processing characteristics of 70/30 cupronickel castings

FOR LIBRARY STAFF	
Total cost	
ISBN	669.733 K1Q
Librarian	Class No 08768
New copies: No reqd	Already in stock
Loan Type	Already on order
Reference	In Process
Normal Loan	
Short Loan	
Part time Loan	
Wk Loan	

with the item to be reserved for you please enter Library Ticket No.

--	--	--	--	--	--

Typical Mechanical Properties of Nickel - Aluminum Bronze Alloys (9)

Alloy	Nominal Composition	PS (Nmm ²)	UTS (Nmm ²)	Elongation (%)
AB2	Cu - 9.5 Al, 5 Fe, 5 Ni	250 - 300	640 - 700	13 - 20
CMAI	Cu - 13Mn, 8 Al, 3Fe, 3 Ni	280 - 340	650 - 730	18 - 35

Table 3

Relationship Between Wall Thickness And
Strength Of AB2 Castings (9)

Wall Thickness (mm)	Tensile Strength (Nmm ⁻²)	Elongation (%)
5	708	29
8	662	26
9.5	646	24
19	631	21
38	585	18
76	569	18
152	538	18

Cast High Strength Cupronickel Alloys (16)

MATERIAL	NOMINAL COMPOSITION								TYPICAL MECHANICAL PROPERTIES		
	Ni	Al	Mn	Fe	Si	Cr	+ Others		0.1% PS N/mm ²	UTS N/mm ²	ELONG %
70/30 Cupronickel IN 768	30		0.6	0.7	0.45	1.6	Zr 0.1 Ti 0.05		338	538	21
70/30 Cupronickel + Nb, Si	30		1.2	1.2	0.35	-	Nb 1.3		308	550	20
Lean Cupronickel ex FRI	15	-	10	7	-	-	Co 5		460	660	13
Lean Cupronickel ex Langley 501	14	2	10	5	-	-			276	492	25
Lean Cupronickel ex SMM	13	2.3	1.5	1.0	-	-			425	622	10
Lean Cupronickel ex BNFMR	10	-	1.0	1.5	0.4	-			285	425	21
NAB 348									Min 230 (0.2% Proof)	Min 587	Min 15

Typical Tensile Properties of CN1 and CN2
Cupronickel Alloy Sand Cast Test Bars (9)

Alloy	PS (Nmm ⁻²)	UTS (Nmm ⁻²)	Elongation (%)
CN1	300-320	480-540	18-25
CN2	335 (0.5%)	585	25

Table 6Impurity Levels For NES 824 Part 1 Issue 2 (15)

<u>Impurity</u>	<u>Specified Maximum</u> (Wt%)	<u>Recommended Maximum</u> <u>Target Level</u> (Wt%)
Pb	0.003	0.0015
P	0.005	NS
Bi	0.001	0.0005
S	0.005	0.003
C	0.02	0.006
Co	0.02	NS
B	0.001	NS
Se	NS	0.0005
Te	NS	0.0005
As	NS	0.001
Zn	NS	0.003
	<hr/>	<hr/>
TOTAL IMPURITY	0.05	NS
	<hr/>	<hr/>

(NS = No figure specified in NES)

Chemical Composition Of Welding Wire To NES 825 Issue 2
(15)

(i) Major Elements (Wt%)

<u>Cu</u>	<u>Ni</u>	<u>Cr</u>	<u>Mn</u>	<u>Si</u>	<u>Zr</u>	<u>Ti</u>
Balance	29.0	2.0	1.4	0.2	0.05	0.1
	<u>32.0</u>	<u>2.4</u>	<u>2.0</u>	<u>0.4</u>	<u>0.15</u>	<u>0.2</u>

(ii) Impurity Levels (Wt%)

<u>Fe</u>	<u>Pb</u>	<u>P</u>	<u>S</u>	<u>Bi</u>	<u>C</u>
0.05	0.0015	0.005	0.003	0.0005	0.006
<u>B</u>	<u>Se</u>	<u>Te</u>	<u>As</u>	<u>Zn</u>	<u>Co</u>
0.001	0.0005	0.0005	0.001	0.002	0.001

Properties Of Cast NES 824 And Cast NAB (2,6,7,15,28)

<u>Property</u>	<u>Cu-Ni-Cr</u> (NES 824)	<u>NAB</u> (NES 747)
<u>PHYSICAL PROPERTIES</u>		
Melting Range (°C)	1180 - 1230	1050 - 1080
Density (gcm ⁻³)	8.8	7.6
Thermal Conductivity (WmK ⁻¹)	23	40
Electrical Resistivity (μohm.m)	0.35	0.2
Coefficient of Linear Expansion (μ.strain.k ⁻¹)	18.0 (0 - 250°C)	16.3 (0 - 100°C)
Specific Heat (Jkg ⁻¹ K ⁻¹)	410.3	434
Latent Heat of Fusion (Jkg ⁻¹)	166000 + 2100	---
Magnetic Permeability (μ)	1.01	1.4
<u>MECHANICAL PROPERTIES</u>		
0.2% Proof Stress (MPa)	300 - 320	270
Tensile Strength (MPa)	480 - 540	660
Elongation (%)	18 - 25	15
Reduction of Area (%)	30 - 50	15
Brinell Hardness	170 - 200	160
Modulus of Elasticity (GPa)	139	120
Poissions Ratio	0.3	0.3
<u>FRACTURE TOUGHNESS DATA</u>		
Izod Impact (J)	45 - 60	17
JIC (MJm ⁻²)	0.07	0.05
K _m (MNm ^{-3/2})	59	56
Diameter (mm)	0.054	0.112

Table 8 (continued)

MARINE CORROSION DATA FULL IMMERSION

Corrosion in sea water with reference to SC electrode	-0.18	-0.19
Corrosion Rate (mm/year)	0.02	0.07
Crevice Corrosion (mm/year)	<0.2	0.5
Galvanic Corrosion compatible with:	NAB gun metals	most copper alloys
Form of galvanic attack	general and shallow pits	pitting, and selective phase corrosion
Cavitation Resistance Loss (mm ³ /hr) for velocity 40ms ⁻¹ and cavitation number 0.08	3.2	1.0
Impingement Resistance	>6	4.3
Chloride Stress Corrosion	Resistant	---

JOINING METHODS

arc welding using MIG and TIG, manual metal arc under development.	soldering, gas shielded arc welding. Brazing may give satisfactory results. Oxy-acetylene welding and carbon arc welding should not be practised.
---	--

Table 9

Cast 70/30 Cupronickel Mechanical Property Data (27)

0.2PS (MPa)	UTS (MPa)	Elongation (%)	Hardness (HB)	Youngs Modulus (GPa)
360	549	21	186	147
347	532	24	176	145
360	543	20	171	142
334	515	24	170	139
368	557	21	167	147
349	535	21	172	129
365	545	20	170	133
354	536	20	173	151
372	554	21	183	147
351	539	22	186	143
352	531	23	171	132
374	581	23	181	138
363	549	21	173	139
359	544	20	184	145
357	546	21	186	131
344	529	23	170	140
359	541	21	177	152
355	541	19	179	139
363	553	21	179	153
355	537	20	182	138
351	540	22	182	138
351	533	23	169	150
305	487	23	170	161
335	540	21	181	162
320	510	19	170	141

RANGE

305-374 487-554 19-24 167-186 129-162

-

X

352 539 21 176 144

NES 824 Issue 2 Specification Requirements

300 480 18 -- --
MIN MIN MIN

Composition Of High Strength 70/30 Cupronickel IN768Used For Marine Performance Trials (21)

<u>ELEMENT</u>	<u>IN768</u>
Ni	30.10
Fe	0.60
Mn	0.70
Si	0.49
Nb	---
Cr	1.60
Ti	0.04
Zr	0.11
S	<0.005
P	<0.005
Mg	---
Cu	Balance

Commonly Used Copper Based Alloys And Their
Corrosion Rates In Salt Water (42)

<u>ALLOY</u>	<u>STEADY STATE CORROSION RATE</u> (Mils/year)
Copper (CA 122)	2 - 5
Admiralty (CA 443)	1 - 3
Aluminium Brass (CA 687)	1 - 2
Aluminium Bronze (CA 608)	5 - 2
90/10 (1.4Fe) Cupronickel (CA 706)	0.1 - 0.5
Cu-Ni-Cr (85/15 CA 722)	0.1 - 0.5
70/30 (0.5Fe) Cupronickel (CA 715)	0.1 - 0.5
304 Stainless Steel	0 - 10
316 Stainless Steel	0 - 10
Titanium (Grade 2)	0

Results Of Laboratory Tests On A Copper Nickel SeriesIn Aerated 3% Sodium Chloride (43)

Test Conditions:

Temperature - 86°F
Agitation - specimens moved at a velocity of 13ft/min
Duration - 20 hours

COMPOSITION OF ALLOY	CORROSION RATE (mg/sq.dm/day)
100% Cu	76
70% Cu - 30% Ni	28
55% Cu - 45% Ni	28
30% Cu - 70% Ni	2
100% Ni	2

Corrosion Performance Of Annealed Copper - Nickel Alloys

Results of tests carried out on copper and nickel alloy specimens annealed at 450°C and immersed in a reservoir from which salt water from New York Harbour was pumped through an experimental condenser at atmospheric temperature for 8.5 years. Specimens were cleaned and water was renewed at 6 month intervals (44).

ALLOY COMPOSITION	WEIGHT LOSS (g/sq. inch)
<hr/>	
Copper	0.0122
85% Cu - 15% Ni	0.0112
80% Cu - 20% Ni	0.0110
75% Cu - 24% Ni	0.0104

Results Of Test Bars Exposed At Half Tide level In The
Bristol Channel for 4 Years (45)

Material	Weight Loss After Cleaning (g)	Loss In Tensile Strength After Exposure (%)
Cu	128.1	4.37
Cu (1.75%Ni)	106.3	1.49
Ni	14.8	---

Results Of Test Bars Exposed At Half Tide Level At
Southampton Docks For 3 Years (45)

Material	Weight Loss After Cleaning (g)	Remarks
Cu	3.50	Uniform corrosion, no shell fauna.
98% Cu - 2% Ni	3.90	Uniform corrosion, no shell fauna.
90% Cu - 10% Ni	2.35	No evidence of attack connected with shell fauna.
80% Cu - 20% Ni	1.25	Uniform corrosion, no shell fauna.
55% Cu - 45% Ni	0.20	Traces of attack under shell fauna.
28% Cu - 72% Ni	0.00	Traces of attack under shell fauna.
Ni	0.25	Slight attack under shell fauna.

Relative Crevice Corrosion Of Some
Copper Based Alloys In Sea Water (42)

CORROSION RATE	ALLOY
Excellent	Titanium (low temperatures)
Very Good	90/10 Cupronickel, Aluminium, Bronze
Good	Copper, Aluminium Brass, 70/30 Cupronickel
Fair	Commercial purity Copper, Arsenical
Poor	304, 316 and 400 Stainless Steels

Typical Pitting Rates Of Copper Based Alloys
In Sea Water (42)

ALLOY	PITTING RATE (Mils/year)
Copper (CA 122)	2 - 5
Admiralty (CA 433)	1 - 3
Aluminium Brass	1 - 2
Aluminium Bronze (CA 608)	1 - 2
90/10 (1.4%Fe) Cupronickel	0.5 - 2.0
70/30 (0.5%Fe) Cupronickel	0.5 - 1.0

NB. Velocities >5ft/s usually result in lower pitting rates.

Composition of the Cu₂O Layer from CuNi Alloys Exposed to Flowing Seawater
for Six Months (66)

Alloy Composition wt (%)			Film Composition wt (%)					Molecular Equation
Cu	Ni	Fe Total	Fe ppt	Cu	Ni	Fe	O+	
88	11.8	0.05	0.05	78	2.7	-	19.3	Cu ₂ O(0.1 NiO)(0.9 O)
87	11.6	1.05	0.08	46	27	15	12	Cu ₂ O(0.8 FeO)(0.3 NiO))(1.0 Ni)
86	11.3	1.99	1.84	60	20	4.3	15.7	Cu ₂ O(0.2 FeO)(0.7 NiO)(0.2 O)
69	30.7	0.05	0.05	73	8.4	-	18.6	Cu ₂ O(0.8 NiO)(0.3 O)
69	30.3	0.54	0.02	43	44	2.5	10.5	Cu ₂ O(0.1 FeO)(0.8 NiO)(1.4 Ni)
68	29.6	2.27	0.26	57	27	2.0	14.0	Cu ₂ O(0.1 FeO)(0.9 NiO)(0.1 Ni)

Levels Of Trace Impurity Elements In A 70/30 Cu-Ni Alloy
Before and after Vacuum Remelting (78)

Analysis (ppm)

<u>Mn</u>	<u>Cr</u>	<u>Fe</u>	<u>Sn</u>	<u>Si</u>	<u>S</u>	<u>P</u>	<u>Pb</u>	<u>Bi</u>	<u>Sb</u>	<u>As</u>
-----------	-----------	-----------	-----------	-----------	----------	----------	-----------	-----------	-----------	-----------

(i) 70Cu - 30Ni As Received

<5	<20	<10	<10	100	30	50	24	7	10	90
----	-----	-----	-----	-----	----	----	----	---	----	----

(ii) 70Cu - 30Ni After Vacuum Remelting

<5	<20	<10	10	100	20	50	6	<2	NA	<2
----	-----	-----	----	-----	----	----	---	----	----	----

Positions of Ductility Maxima and Minima (89)

Grain Size	Strain Rate	Point A		Point B		Point C
		\bar{T}	$\frac{R}{A}$	\bar{T}	$\frac{R}{A}$	$\frac{R}{A} \text{ at } 160k$
(μm)	(s^{-1})	(k)	(%)	(k)	(%)	(%)
75	3.33×10^{-4}	790	23	925	78	45
75	8.33×10^{-2}	875	23	1025	74	71
125	3.33×10^{-4}	790	22	925	71	45
125	1.67×10^{-2}	842	22	1005	72	68
125	8.33×10^{-4}	883	22	1025	72	69
205	3.33×10^{-4}	790	23	925	70	38
205	8.33×10^{-2}	875	23	1025	63	59

Summary Of Studies Undertaken To Verify The
Hot Pressing Equation Of Murray et al (123)

AGREEMENT	DISAGREEMENT
Mangesen et al (125)	McCelland (129)
Vasilos (126)	Koval'chenko & Samsonov (130)
Jaeger & Egerton (127)	Scholz (131)
Lersmacher & Scholz (128)	

Improvement of Stress - Rupture Properties of Superalloy Castings by HIPping (134)

Material Condition	Temperature (°C)	Stress (Mpa)	Average Life (Hours)	Elongation (%)	Reduction of Area (%)
IN 738 As-Cast	982	151	19	11.8	21.0
IN 738 HIP	982	151	52.5	20.5	20.6
Rene 77 As-Cast	816	412	77.0	10.0	20.0
	982	151	51.0	19.4	37.0
Rene 77 HIP	816	412	165.0	9.0	18.0
	982	152	68.0	22.0	55.0
IN 792 As-Cast	871	309	175.0	9.2	6.5
IN 792 HIP	871	309	238.0	12.2	22.0

Effect Of HIP On Reducing Scatter Of Tensile Properties
In Cast Inconel 718 (174)

Treatment	0.2PS (MPa)	UTS (MPa)	Elongation (%)	Reduction of Area (%)
As - Cast	869	1007	7.6	13.3
	711	813	2.5	4.9
HIPped	890	1010	16.3	26.2
	827	980	10.1	17.7
As - Cast	852	970	13.9	27.1
	765	861	6.7	15.1
HIPped	865	969	14.9	31.9
	848	882	7.4	19.7

Effect Of HIPping On The Tensile Properties Of Rene 120
(175)

Property	As-cast	HIPped	
		(4 Hours / 1170°C	103MPa) 1204°C
UTS (MPa)	724	703	735
0.2PS (MPa)	582	595	610
Elongation (%)	2.5	4.2	4.2
Reduction of area (%)	1	4.8	4.8

Nomenclature and Units for the Densification Rate Equations
(160)

a	Average contact area at a neck (m^2)
D	Relative density
D_o	Initial relative density (typically 0.64)
D_{yield}	Relative density from plastic yielding
D_c	Relative density at which pores close (around 0.95)
D	Densification rate (/s)
ζD_b	Boundary diffusion coefficient times boundary thickness (m^3/s)
D_v	Volume diffusion coefficient (m^2/s)
f	Fraction of particles with radius R
k	Boltzmann's constant (J/K)
P	External pressure (MPa)
P_{eff}	Effective pressure on a neck (MPa)
P_o	Outgassing pressure (MPa)
R	Particle radius (m)
R'	Radius of unit sphere containing one particle (m)
R_{eff}	Effective particle radius in a distribution (m)
T	Absolute temperature (K)
T_m	Absolute melting temperature (K)
t	Time (s)
V	Volume (m^3)
X	Neck radius (m)
Z	Number of contacts per particle
ϵ_o, σ_o, n	Creep parameters (s^{-1} , MPa)
Ω	Atomic or molecular volume (m^3)
σ_y	Yield strength (MPa)

United States Patent Search 1967 To 1990Pressure Transmitting Media Used In The Ceracon Process

DATE	PATENT NUMBER	DETAILS
DEC 1967	US 3 356 496	Method of Producing High Density Metallic Products
SEPT 1972	US 3 689 259	Method of Consolidating Metallic Bodies
MAY 1985	US 4 518 441	Method of Producing Metal Alloys With High Modulus Of Elasticity
OCT 1986	US 4 615 208	Hydraulic Press Frame
JAN 1987	US 4 634 750	Heating and Handling System for Consolidation System
FEB 1987	US 4 645 131	Powder Filling Method to Produce Fine Powder Sizes
AUG 1987	US 4 689 008	Heating and Handling System for Consolidation System
FEB 1988	US 4 725 227	Heating and Handling System for Consolidation System
JULY 1988	US 4 758 137	Heating and Handling System for Objects

Chemical Composition of As-cast 70/30 Cupronickel Material

(i) Elements

	<u>Cu</u>	<u>Ni</u>	<u>Cr</u>	<u>Fe</u>	<u>Mn</u>	<u>Si</u>	<u>Zr</u>	<u>Ti</u> (Wt %)
Test Bars CN 6814/L1	65.93	30.05	1.86	0.86	0.79	0.27	0.12	0.10
CN 5850/L	65.61	30.40	1.75	0.94	0.75	0.31	0.09	0.12
HS 6946/L1	65.82	30.40	1.78	0.72	0.72	0.31	0.11	0.12
HS 6949/L	65.56	30.78	1.73	0.71	0.68	0.34	0.065	0.11
NES 824		29.00	1.60	0.50	0.50	0.20	0.05	0.03
	Balance	32.00	2.00	1.00	1.00	0.40	0.15	0.15

(ii) Impurities

	<u>Pb</u>	<u>P</u>	<u>S</u>	<u>Bi</u>	<u>C</u>	<u>Co</u>	<u>B</u>
CN 6814/L1	0.003	0.002	0.002	0.0005	0.005	0.018	0.0002
CN 5850/L	0.003	0.002	0.002	0.0005	0.010	0.002	0.0004
HS 6946/L1	0.001	0.002	0.002	0.0005	0.010	0.002	0.0005
HS 6949/L	0.001	0.002	0.002	0.0005	0.011	0.003	0.0005
NES 824	0.005	0.005	0.005	0.001	0.02	0.05	0.001
	MAX	MAX	MAX	MAX	MAX	MAX	MAX

Material Properties Of
Refractory Pressure Transmitting Media

Refractory	Particle Size (μm)	Melting Point ($^{\circ}\text{C}$)
Silica Sand	100 - 355	1610 - 1713
Zone M Concrete Sand Single Particle Size Aggregate	150 106 - 355	
Leighton Buzzard Sand	>355 - <1700	
Tabular Alumina	355 - 1700	2015
Calcined Alumina	53 - 106	
Boron Carbide	9 - 35	2450
Silicon Carbide	<53	
Boron Nitride	<53	
Zirconium Oxide	75 - 150	2715
Soda Glass	Fragments	340 - 430
Borosilicate Glass	Fragments	1680

Chemical Composition Of Refractory Sands

Sand	Chemical Composition (wt%)		
	SiO ₂	Fe ₂ O ₃	Al ₂ O ₃
Silica	99.4	0.054	0.09
Zone M Concrete Sand	90.0		
Leighton Buzzard	>96.0		

Table 30Calibration Of Laboratory Furnace: Temperature - Voltage

Aim Temperature (°C)	Temperature (mV)	Temperature Achieved (°C)	Controller Set Point (mV)	Set Point (°C)
300	11.41	290	11.78	320
400	15.60	397	16.28	420
500	19.85	498	20.56	520
600	24.11	608	25.26	622
700	28.34	702	29.24	718
800	33.30	808	33.66	826
850	34.54	850	34.60	870
950	38.55	950	39.34	965
1025	45.31	1024	42.24	1038

Chemical Composition Of Substitute Ocean Water ASTM D1141

<u>Compound</u>	<u>Concentration</u> (g/l)
NaCl	24.53
MgCl ₂ ·6H ₂ O	5.20
Na ₂ SO ₄	4.09
CaCl ₂	1.16
KCl	0.695
NaHCO ₃	0.201
KBr	0.101
H ₃ BO ₃	0.027
SrCl ₂ ·6H ₂ O	0.025
NaF	0.003
Ba(NO ₃) ₂	0.0000994
Mn(NO ₃) ₂	0.0000340
Cu(NO ₃) ₂	0.0000308
Zn(NO ₃) ₂	0.0000096
Pb(NO ₃) ₂	0.0000066
AgNO ₃	0.00000049

Chlorinity of this substitute ocean water is 19.38.

The pH (after adjustment with 0.1N NaOH solution) is 8.2.

HIP 6.0 Material Variables

Material Property	Units
<u>GENERAL PROPERTIES</u>	
Structure type	--
Solid density	Kg/m ³
Melting point	K
Atomic or molecular weight	Kg/kmol
Weighted atom-volume	m ³ /atom
Surface energy	J/m ²
<u>MECHANICAL PROPERTIES</u>	
Youngs Modulus at room-temperature	GPa
Yield Stress at room-temperature	MPa
Temperature dependence of yield	
Power-law creep exponent	
Reference stress for power-law creep	MPa
Activation energy for power-law creep	KJ/mol
Low temperature to high temperature creep transition temperature	K
Constant C for low temperature creep	
<u>DIFFUSION PROPERTIES</u>	
Pre-exponential for volume diffusion	m ² /s
Activation energy for volume diffusion	KJ/mol
Pre-exponential for boundary diffusion	m ³ /s
Activation energy for boundary diffusion	KJ/mol
<u>GRAIN GROWTH</u>	
Pre-exponential surface diffusion	m ³ /s
Activation energy for surface diffusion	KJ/mol
Pre-exponential boundary mobility	m ³ /s
Activation energy for boundary mobility	KJ/mol
<u>PARTICLE CHARACTERISTICS</u>	
Particle radius	m
Ratio of radii Rmax / Rmean	
Grain diameter in particle	m

HIP 6.0 Plotting variables

Variable	Units
<u>PLOT TYPE AND INITIAL CONDITIONS</u>	
Map type - density / pressure	
- density / temperature	
- temperature / pressure	
Initial relative density	
Initial pore pressure	MPa
<u>FIXED VALUES OF DENSITY / PRESSURE / TIME</u>	
Fixed density	
Fixed pressure	MPa
Fixed Temperature	K
<u>AXIS RANGES - TIME CONTOURS AND PRECISION</u>	
Lower limit of density axis	
Upper limit of density axis	
Lower limit of normalised pressure (P/σ_y)	
Upper limit of normalised pressure	
Lower limit of normalised temperature (T/T_m)	
Upper limit of normalised temperature	
First time contour	s
Multiplier for time contour	
Number of time contours	
Number of program steps	

Table 34

Effect Of A Change In The Refractory Pressure Transmitting
Medium On The Pore Closure Of Surface-Connected Porosity

Initial Porosity (%)	Pressure Transmitting Medium	Number of Type I HIP Cycles	Porosity Closed (%)
10	Close fitting capsule	1	10.00
10	Silica Sand	1	6.03 - 6.49
		2	10.00
10	Calcined Alumina	1	6.60
		2	10.00
10	Tabular Alumina	1	5.51
		2	8.21
		3	10.00
10	Zirconium Oxide	1	6.17
		2	10.00
10	Boron Carbide	1	4.97
		2	8.14
		3	10.00
10	Calcined Alumina + Boron Nitride (10:1)	1	6.62
		2	10.00
10	Calcined Alumina + Boron Nitride (10:3)	1	5.45
		2	10.00
10	Boron Carbide + Silicon carbide (3:10)	1	5.68
10	Fused Pyrex Glass	1	0.95

Table 35

Effect Of A Change In The Refractory Sand Used As A
Pressure Transmitting Medium On The Pore Closure Of
Surface-Connected Porosity

Initial Porosity (%)	Sand	Number of Type I HIP Cycles	Porosity Closed (%)
10	Silica (Desert Based)	1 2	6.03 - 3.97 10.00
10	Zone M Concrete (single particle size)	1	10.00
16		1 2	13.00 16.00
10	Zone M Concrete (aggregate)	1	10.00
16		1 2 3	12.36 15.36 16.00
10	Leighton Buzzard	1 2 3	7.78 8.88 10.00
10	Leighton Buzzard + Silica (50:50)	1	6.00 10.00

Compressive Strength of Desert Based Silica Sand

HIP Details Time/Temperature/Pressure	Maximum Applied Load (MPa)	
	Test 1	Test 2
45 Mins / 950°C / 41MPa	1.42, 1.75	79.6
45 Mins / 950°C / 62MPa	1.96, 2.16	101.0
45 Mins / 950°C / 83MPa	2.74, 2.84	137.8
45 Mins / 950°C / 103MPa	3.61, 4.72	>170.0
45 Mins / 950°C / 124MPa	3.27, 3.91	>170.0
45 Mins / 950°C / 145MPa	3.86, 3.54	>170.0

Table 37Effect Of Pressure Transmitting Medium On The Rate Of
Closure Of Surface - Connected Porosity

Initial Porosity (%)	Capsule Diameter (mm)	Specimen Diameter (mm)	Sand Thickness (mm)	Porosity Closed (%)
1.0	50	38.4	5.8	0.74
1.0	75	38.4	18.3	0.65
1.0	90	38.4	25.8	0.61
10.0	15	12.7	0.0	10.00
10.0	22	12.7	4.65	7.20
10.0	40	12.7	13.65	6.31
10.0	50	12.7	18.65	5.43
10.0	63	12.7	25.15	4.38
10.0	75	12.7	31.15	3.37
10.0	90	12.7	38.65	2.91

Table 38

Effect Of HIP Temperature On The Mechanical Properties
Of 70/30 Cupronickel Weld Plate Material

HIP Temperature (°C)	Yield Stress (MPa)	UTS (MPa)	A (%)	Z (%)	Charpy Impact Toughness (Joules)
As-Cast	300	430	16	74	74,80,90
	315	420	17	55	
	318	440	16	60	
850	320	470	18	60	68,76,80
	320	457	16	52	
	310	470	19	55	
950	288	490	24	56	123,123,126
	280	465	20	47	
	292	498	17	50	
1025	307	490	19	55	160,164,156
	320	484	18	58	
	314	490	23	52	

HIP Conditions: 4 hour sustain period with argon
gas pressures of 103MPa.

Effect Of HIP Temperature On The Mechanical Properties
Of 70/30 Cupronickel Test Bars

HIP Temperature (°C)	0.2% Proof Stress (MPa)	UTS (MPa)	A (%)	Z (%)
850	328	521	26.0	41.8
	327	525	27.5	44.5
	327	525	26.0	34.2
	326	514	18.0	28.5
950	333	537	28.0	43.1
	335	545	26.0	48.5
	333	535	23.5	33.0
	329	537	27.5	47.2
1025	343	552	25.0	36.0
	336	544	24.5	36.0
	334	543	26.0	41.8
	343	501	14.5	23.5

HIP Conditions: 4 hour sustain period with argon
gas pressures of 103MPa.

Table 40

Effect Of Stress Relief On The Mechanical Properties Of
HIPped 70/30 Cupronickel

Material Condition	Yield Stress (MPa)	0.2% PS (MPa)	UTS (MPa)	A (%)	Charpy Impact (Joules)
As-Cast	237	-	509	15	71.2
	234	-	493	13	43.4
Cast +	-	357	541	19	---
Stress	-	342	535	21	---
Relieved					

Stress relief treatment consists of 2 hours at 475°C
followed by cooling in air.

Effect of Stress Relief on the Mechanical Properties
of HIPped 70/30 Cupronickel

Material Condition	Yield Stress (MPa)	UTS (MPa)	Elongation (%)	Impact Toughness (Cv) (Joules)
HIPped	352	487	16	59
	371	506	21	64
HIPped + Stress Relieved	336	528	19	70
	310	528	18	65
HIPped + HIP Stress Relief	297	462	17	66
	294	515	19	60

HIP Conditions: 4 Hours / 950°C / 103MPa

HIP + Stress Relief: As above, cooled at 10°C/minute to 450°C and held at 0.34MPa for 2 Hours followed by cooling at 10°C/minute to ambient.

Mechanical Property Evaluation of a HIPped MOD Casting

Material Identification	Cross Head Speed (mm/min)	YS (Mpa)	UTS (MPa)	Elongation (%)	Reduction of Area (%)	Hardness (HV10)	Charpy Impact (Joule)
Sound	5	310	485	16	45	172	70.5, 7
	20	320	499	16	43		
Defect	5	269	416	6	4	175	-
	20	328	391	13	35		
Adjacent to Defect	5	313	490	19	44	171	-
	20	324	516	17	32		

Table 43Mechanical Property Evaluation of HIP RecoveredWorm Gear Casting

Material Identification	0.2PS (MPa)	UTS (MPa)	Elongation (%)
As-Cast	359	547	21.0
HIPped Sound End 1	322	519	21.3
HIPped Sound End 2	319	519	22.5
HIP Recovered Defect area	380 373	596 600	17.9 17.5

Mechanical Property Evaluation of HIP Recovered
Test Plates Containing Shrinkage Porosity

Material Identification	0.2PS (MPa)	UTS (MPa)	Elongation (%)
As-Cast	110 145	290 290	1 3
HIPped Sound Material (Range of 5 tests)	318-339	495-525	21-24
HIP Recovered Defect Area (Range of 9 tests)	325-336	503-525	20-23

Mechanical Properties of 70/30 Cupronickel
at Elevated Temperatures

Test Temperature (°C)	Yield Stress (MPa)	UTS (MPa)	Ductility (%)
300	319	443	1.00
400	313	449	0.81
500	304	403	0.32
600	284	347	0.12
650	275	305	0.15
	241	293	0.18
700	236	249	0.06
	227	259	0.04
750	163	206	0.14
800	120	144	0.13
850	65	72	0.36
900	40	49	0.47
	54	65	0.37
950	35	51	0.43
	49	56	0.44
1025	17	20	0.61

Constant Load Hot Tensile Data

Test Temperature (°C)	Yield Stress (MPa)	Maximum Load (MPa)	Elongation (%)	Failure Temperature (°C)
850	77	162	28.9	682
950	39 37	58 86	27.0 26.6	600 650
1025	21	71	31.3	750

EFFECT OF HIP TEMPERATURE ON THE QUANTITATIVE SEGREGATION ANALYSIS OF 70/30 CUPRONICKEL

HIP Temperature (°C)	Analysis Area	\bar{x} Normalised Chemical Analysis (Wt.%)								
		Cu	Ni	Cr	Fe	Si	Mn	Ti	Nb	Zr
Cast	Dendrite	52.99	40.90	2.64	1.58	0.44	0.79	0.20	0.14	0.13
	Interface	56.05	38.55	2.36	1.43	0.41	0.84	0.14	0.19	0.15
	Matrix	64.24	31.90	1.56	0.94	0.36	0.74	0.13	0.16	0.07
850 °C	Dendrite	55.33	38.48	2.88	1.64	0.30	0.91	1.22	0.13	0.20
	Interface	56.11	37.76	2.92	1.56	0.36	0.89	0.10	0.16	0.36
	Matrix	69.57	26.54	1.52	0.78	0.31	0.79	0.06	0.21	0.19
950 °C	Dendrite	57.32	36.61	2.85	1.53	0.35	0.99	0.12	0.03	0.19
	Interface	60.84	33.73	2.50	1.24	0.34	0.94	0.11	0.16	0.13
	Matrix	66.48	28.49	1.72	0.94	0.29	0.83	0.07	0.13	0.26
1025 °C	Dendrite	58.09	35.86	3.04	1.41	0.40	0.96	0.12	0.06	0.05
	Interface	61.54	32.96	2.48	1.26	0.34	0.95	0.15	0.14	0.18
	Matrix	69.35	27.58	1.54	0.80	0.28	0.80	0.04	0.07	0.05

Effect of HIP Time on the Mean Grain Size of
70/30 Cupronickel Material

HIP Conditions Time/Temperature/Pressure	Range of Grain Size X100 (mm)	Mean Grain Size (m)
45minutes/950°C/103MPa	8 - 28.5	9.744×10^{-5}
2 Hours/950°C/103MPa	19 - 39.0	2.143×10^{-4}
4 Hours/950°C/103MPa	17 - 41.0	1.766×10^{-4}
6 Hours/950°C/103MPa	4 - 31.0	2.540×10^{-4}

Table 49

EFFECT OF HIP TIME ON THE QUANTITATIVE SEGREGATION ANALYSIS OF 70/30 CUPRONICKEL

HIP Time	Analysis Area	\bar{X} Normalised Chemical Analysis (Wt.%)								
		Cu	Ni	Cr	Fe	Si	Mn	Ti	Nb	Zr
Cast	Dendrite	52.99	40.90	2.64	1.58	0.44	0.79	0.20	0.14	0.13
	Interface	56.05	38.55	2.36	1.42	0.41	0.84	0.14	0.19	0.15
	Matrix	64.24	31.90	1.56	0.94	0.36	0.74	0.13	0.16	0.07
45 mins	Dendrite	57.07	36.92	3.01	1.18	0.40	0.86	0.21	0.16	0.21
	Interface	60.18	34.57	2.63	1.00	0.36	0.83	0.18	0.10	0.14
	Matrix	69.31	27.17	1.57	0.61	0.26	0.72	0.11	0.06	0.19
2 hrs	Dendrite	59.29	34.83	2.72	1.39	0.39	0.88	0.21	0.12	0.18
	Interface	60.70	32.57	2.50	1.25	0.34	0.87	0.19	0.18	0.26
	Matrix	71.25	25.35	1.36	0.74	0.27	0.80	0.09	0.03	0.11
4 hrs	Dendrite	57.32	36.61	2.85	1.53	0.35	0.99	0.12	0.03	0.19
	Interface	60.84	33.73	2.50	1.24	0.34	0.94	0.11	0.17	0.13
	Matrix	66.48	28.49	1.72	0.94	0.29	0.83	0.07	0.13	0.26
6 hrs	Dendrite	56.84	37.05	3.10	1.14	0.39	0.92	0.21	0.17	0.18
	Interface	61.19	33.71	2.56	0.94	0.30	0.85	0.15	0.17	0.15
	Matrix	70.39	26.29	1.39	0.58	0.25	0.69	0.09	0.19	0.14

Corrosion Performance of 70/30 Cupronickel
in a 5% Salt Solution

(i) As-Cast Material

Test Duration (Hours)	Mass Loss (g)		
504	0.0010,	0.0012,	0.00125
1008	0.00195,	0.0021,	0.0022

(ii) Hot Isostatically Pressed Material

Test Duration (Hours)	Mass Loss (g)		
	HIPped:	850°C	950°C 1025°C
504	0.0019	0.00165	0.0013
1008	0.0031	0.0031	0.0030

Corrosion Performance of 70/30 Cupronickel
in Substitute Ocean water

(i) As-Cast material

Test Duration (Hours)	Mass Loss (g)
504	0.0008, 0.0007, 0.0009
1008	0.00125, 0.009, 0.0013

(ii) Hot Isostatically Pressed Material

Test Duration (Hours)	Mass Loss (g)
	HIPped: 850°C 950°C 1025°C
504	0.0004 0.0006 0.0008
1008	0.0008 0.00135 0.0035

Table 52

Casting Description	Specimen Type	Exposure Time Months	Pre Exposure Mass (g)	Post Exposure Mass (g)	Mass loss (g)	* Volume loss cc	Average depth of attack mm/year
As-Cast NES 824 (5.1/4" x 2")	Full Immersion	12	78.7474	78.1860	0.5614	0.0632	0.0117
	Crevice	12	84.2612	83.4230	0.8382	0.0944	approx 0.04
	Full Immersion	12	74.9789	74.7060	0.2729	0.0307	0.0057
	Crevice	12	84.3362	83.8650	0.4712	0.0531	approx 0.023
HIPped NES 824 (350 x 250 x 40 mm) 4 hrs/950°C /103 MPa	Full Immersion	3	77.9789	77.8307	0.1482	0.0167	0.0124
	Crevice	3	83.4010	83.2582	0.1528	0.0172	approx 0.022
	Full Immersion	6	78.9368	78.7655	0.1713	0.0193	0.0143
	Crevice	6	84.0635	83.8600	0.2035	0.0229	approx 0.029
Plate A	Full Immersion	3	79.2726	79.1600	0.1126	0.0127	0.0094
	Crevice	3	83.8382	83.7300	0.1082	0.0122	approx 0.016
	Full Immersion	6	79.1738	79.0620	0.1118	0.0126	0.0093
	Crevice	6	84.2860	84.1750	0.1110	0.0125	approx 0.016
* Specific Gravity determined as 8.88 gm/cc							

Impingement Attack Measurements

Sample No	Diameter of area under attack (mm)		Depth of attack (microns)		Shape of attack in impingement zone
	impingement zone	superficial partial attack	impingement zone	superficial partial attack	
NAB 1	6	28	65	10	Annular " " "
2	4	26	50	10	
3	6	30	85	10	
4	5	28	68	10	
CN 107	-	36	20	20	- - - -
1	-	35	20	20	
2	-	35	20	20	
3	-	38	20	20	
NES 824	-	45	20	20	- - - -
1	-	50	10	10	
2	-	50	10	10	
HIPped 3	-	50	10	10	
4	-	50	10	10	- - - -
NE8 824	-	80	10	10	
CAST 1	-	80	10	10	
2	-	45	10	10	
3	-	80	10	10	
4	-				

Table 54Material parameters of 70/30 cupronickelat Elevated Temperatures

Test Temperature (°C)	σ (MPa)	σ^0 (MPa)	A	B	ϕ $\times 10^{-3}$	η (GPa.s)
400	300	345	0.87	0.010	8.65	5578
500	281	293	0.82	0.0095	7.79	5872
600	184	243	0.80	0.010	8.00	5578
650	184	202	-	-	-	-
700	220	249	-	-	-	-
750	167	198	0.65	0.0175	11.37	3187
800	116	126	0.45	0.015	6.75	3719
850	75	88	0.30	0.015	4.50	3719
900	35	47	0.18	0.025	5.00	2231
950	40	46	0.10	0.035	3.50	1594
1025	26	29	0.08	0.050	4.00	1116

Material Properties of 70/30 Cupronickel at 20°C

PROPERTY	VALUE AT 20°C
Youngs Modulus (E)	152.00 GPa
Shear Modulus (G)	55.78 GPa
Poissons ratio (v)	0.3625

Table 56

Calculated Pore Closure Rates by Plastic Yielding in
Samples of 0.95, 0.90 and 0.84 Relative Density at
Varying Temperatures and 103MPa External Pressure

HIP Temperature (°C)	Yield Stress (MPa)	Initial Density Do	Density after Plastic Yielding Dyield	Pore Closure by Yielding (%)
800	132	0.95	0.961	1.1
		0.90	0.924	2.4
		0.84	0.883	4.3
850	72	0.95	0.970	2.0
		0.90	0.943	4.3
		0.84	0.916	7.6
900	60	0.95	0.974	2.4
		0.90	0.951	5.1
		0.84	0.930	9.0
950	45	0.95	0.981	3.1
		0.90	0.967	6.7
		0.84	0.956	11.6
1025	27	0.95	1.000	5.00
		0.90	1.000	10.00
		0.84	1.000	16.00

Table 57

Pore Closure Rates Predicted Using The Plastic Flow
Theory for the Recovery of NES 824 Castings Containing
10% Porosity at a Temperature of 950°C and External Gas
Pressures of 103MPa

Initial Density	Final Density	Porosity Closed (%)	Predicted Sustain Time
0.90	0.91	1	36 Minutes
0.90	0.92	2	1 Hour 17 Minutes
0.90	0.93	3	2 Hours 2 Minutes
0.90	0.94	4	2 Hours 55 Minutes
0.90	0.95	5	3 Hours 58 Minutes
0.90	0.96	6	5 Hours 15 Minutes
0.90	0.97	7	6 Hours 54 Minutes
0.90	0.98	8	9 Hours 13 Minutes
0.90	0.99	9	13 Hours 11 Minutes
0.90	0.999	9.99	26 Hours 23 Minutes

Pore Closure Rates Predicted By The Plastic FlowTheory for the Recovery of NES 824 CastingsContaining 16% Porosity at Pressing Conditions of950°C and External Pressures of 103MPa

Initial Porosity	Finishing Porosity	Porosity Closed (%)	Predicted Sustain Time
0.84	0.85	1.0	22 Minutes
0.84	0.86	2.0	46 Minutes
0.84	0.87	3.0	1 Hour 11 Minutes
0.84	0.88	4.0	1 Hour 39 Minutes
0.84	0.89	5.0	2 Hours 9 Minutes
0.84	0.90	6.0	2 Hours 42 Minutes
0.84	0.91	7.0	3 Hours 18 Minutes
0.84	0.92	8.0	3 Hours 58 Minutes
0.84	0.93	9.0	4 Hours 44 Minutes
0.84	0.94	10.0	5 Hours 37 Minutes
0.84	0.95	11.0	6 Hours 40 Minutes
0.84	0.96	12.0	7 Hours 57 Minutes
0.84	0.97	13.0	9 Hours 36 Minutes
0.84	0.98	14.0	11 Hours 55 Minutes
0.84	0.99	15.0	15 Hours 53 Minutes
0.84	0.999	15.99	29 hours 5 Minutes

Table 59

Material Parameters used to Increase the Accuracy ofHIP Maps Type 1 - 5

Map Type	Material Parameters	
1	Structure type - 1 (metals & alloys)	
	Solid density	8950 kgm ⁻³
	Melting point	1513 K
	Youngs Modulus at room temperature	152 GPa
	Yield stress at room temperature	300 MPa
	Particle radius	3.5x10 ⁻⁵ m
2	As above plus:	
	Atomic / molecular weight	62.095 kg/kmol
3	As above plus:	
	Weighted atomic volume	1.152x10 ⁻²⁶ m ³ /atom
4	As above plus:	
	Grain diameter	8.11x10 ⁻⁴ m
5	As above plus:	
	Particle radius	4.05x10 ⁻⁴ m

HIP 6.0 Material Properties for Construction of aHIP Map for 70/30 Cupronickel Material**GENERAL PROPERTIES**

1. Structure type	=	1
2. Solid density	=	8950kg/m ³
3. Melting point	=	1513K
4. Atomic or molecular weight	=	62.09kg/kmol
5. Weighted atom-volume	=	1.15x10 ⁻²⁶ m ³ /atom
6. Surface energy	=	13.72J/m ²

MECHANICAL PROPERTIES

7. Youngs Modulus at R.T.	=	152GPa
8. Yield stress at R.T.	=	300MPa
9. T-dependence of yield	=	0.50
10. Power-Law creep exponent	=	4.00
11. Reference stress, Power-Law creep	=	150MPa
12. Activation energy for Power- Law creep	=	226.42kJ/mol
13. Low temperature to high temperature creep transition temperature	=	756.50K
14. C for low temperature creep (Q-ltc = C*Qc)	=	0.65

DIFFUSION PROPERTIES

15. Pre-exponential for volume diffusion	=	1.00x10 ⁻⁴ m ² /s
16. Activation energy for volume diffusion	=	226.42kJ/mol
17. Pre-exponential for boundary diffusion	=	2.26x10 ⁻¹³ m ³ /s
18. Activation energy for boundary diffusion	=	135.85kJ/mol

GRAIN GROWTH

19. Pre-exponential surface diffusion	=	6.77x10 ⁻⁹ m ³ /s
20. Activation energy for surface diffusion	=	226.42kJ/mol
21. Pre-exponential boundary mobility=	=	1.13x10 ⁻¹³ m ³ /s
22. Activation energy for boundary mobility	=	181.14kJ/mol

PARTICLE CHARACTERISTICS

23. Particle radius	=	4.05x10 ⁻⁴ m
---------------------	---	-------------------------

24. Ratio of radii Rmax/Rmean	=	1.5×10^{-2}
25. Grain diameter in particle	=	$3.11 \times 10^{-4} \text{m}$

Table 60 (Continued)

HIP 6.0 Plotting Variables for NES 824 HIP Map

PLOT TYPE AND INITIAL CONDITIONS

26. Map type (1:D/P 2:D/T 3:T/P)	=	1
27. Initial relative density	=	0.84
28. Initial pore pressure	=	0MPa

FIXED VALUES OF D, P AND T

29. Fixed density	=	1.00
30. Fixed pressure	=	103.0MPa
31. Fixed temperature	=	1223K

AXIS RANGES

32. Lower limit, D/DS axis	=	0.80
33. Upper limit, D/DS axis	=	1.00
34. Lower limit, P/SY axis	=	1.00×10^{-3}
35. Upper limit, P/SY axis	=	0.40
36. Lower limit, T/TM axis	=	0.40
37. Upper limit, T/TM axis	=	0.90

TIME CONTOURS

38. First time contour	=	15.00s
39. Multiplier for time contour	=	2
40. Number of time contours	=	10

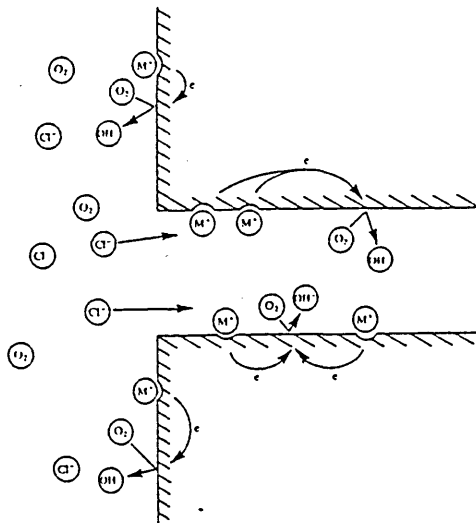
PRECISION

41. Number of program steps	=	180
-----------------------------	---	-----

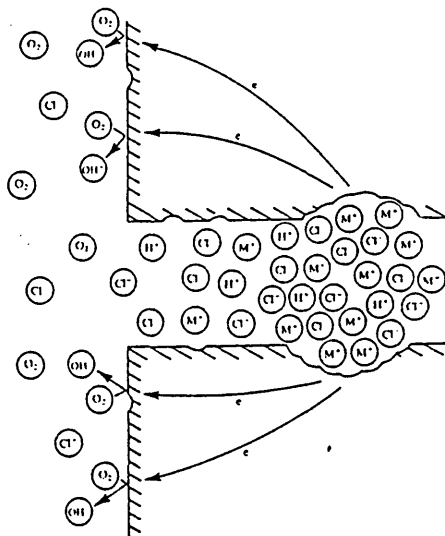
Table 61

Predicted Pore Closure Rates for NES 824 HIP Processed
at a Temperature of 950°C and External Pressures of 103MPa

Map Type	Sustain Period for Complete Densification (Minutes)	
	10% Porosity	16% Porosity
1	4.0	4.0
2	4.0	4.0
3	45.0	45.0
4	4.0	4.0
5	6.0	6.0



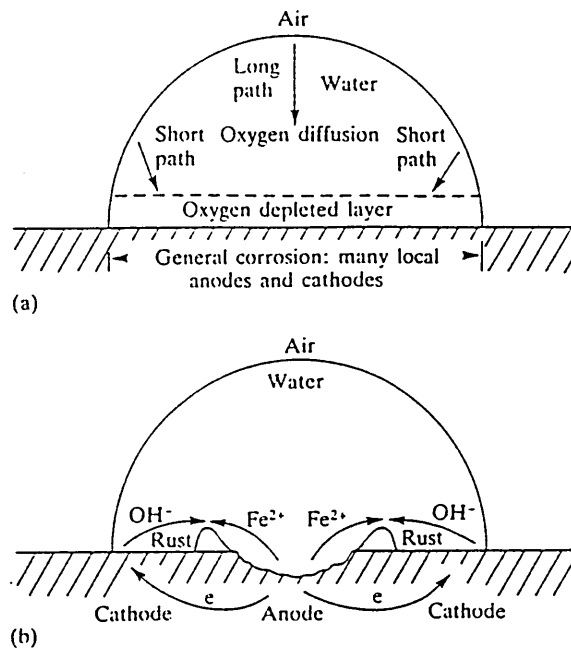
(a)



(b)

The Fontana - Greene mechanism of crevice corrosion (37):

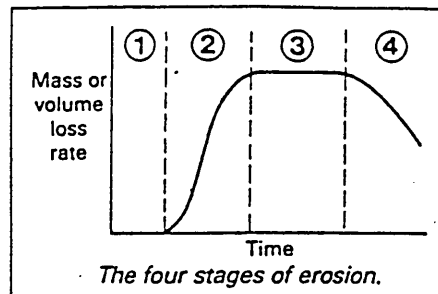
- (a) Initial conditions: corrosion occurs over the whole of the metal surface.
- (b) Final conditions: metal dissolution occurs only inside the crevice where acidity increases, concentration of chloride ion increases, and reaction becomes self sustaining.



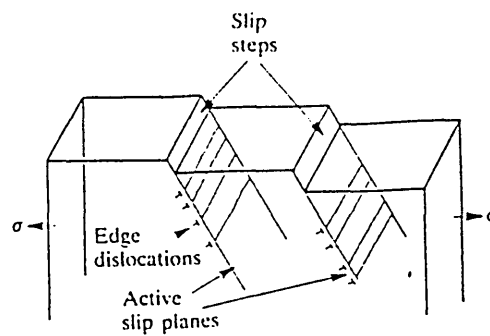
The mechanism of pitting because of differential-aeration beneath a water droplet (39):

- (a) General corrosion over the whole of the wetted metal surface depletes the oxygen levels in the adjacent electrolyte.
- (b) Longer diffusion path for oxygen to reach the central area makes this the anode. Metal dissolution occurs in the centre of the droplet and reaction of metal ions with hydroxyl ions formed at the edge generates a ring of oxide deposit around the corrosion pit.

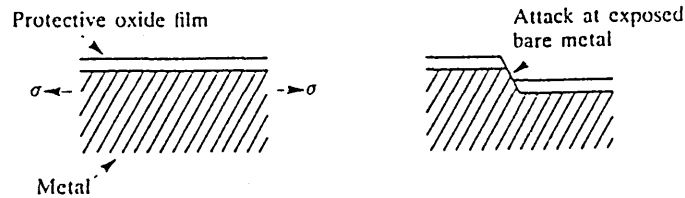
Figure 3



The four stages of cavitaion erosion (41).



(a)



(b)

The role of slip steps in environmental cracking (36).

- (a) The formation of slip steps on the surface of a metal by movement of dislocations along active slip planes under the action of a tensile stress.
- (b) A slip on the surface of a passivated metal creates an active site for the initiation of a stress concentrating pit.

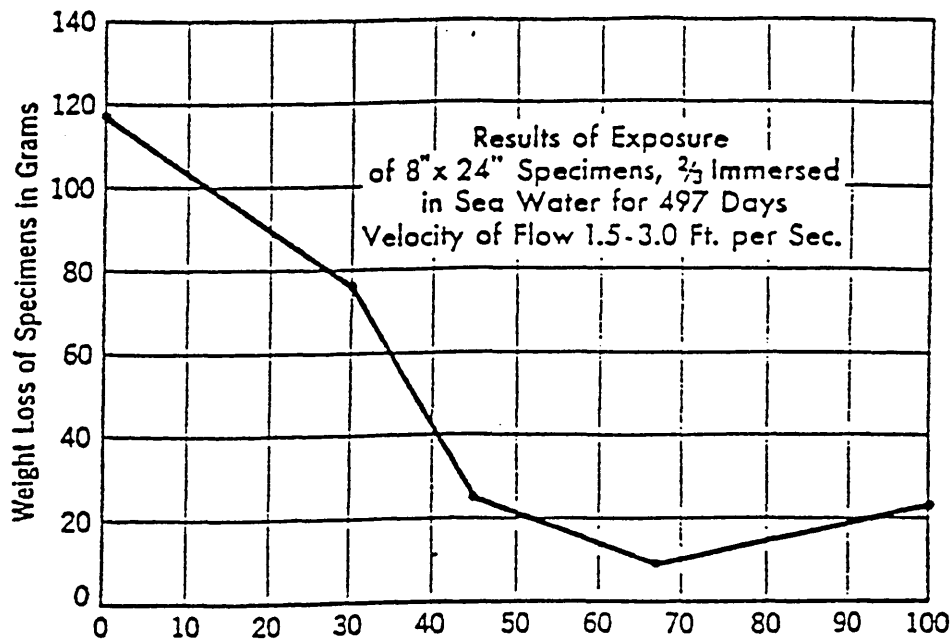
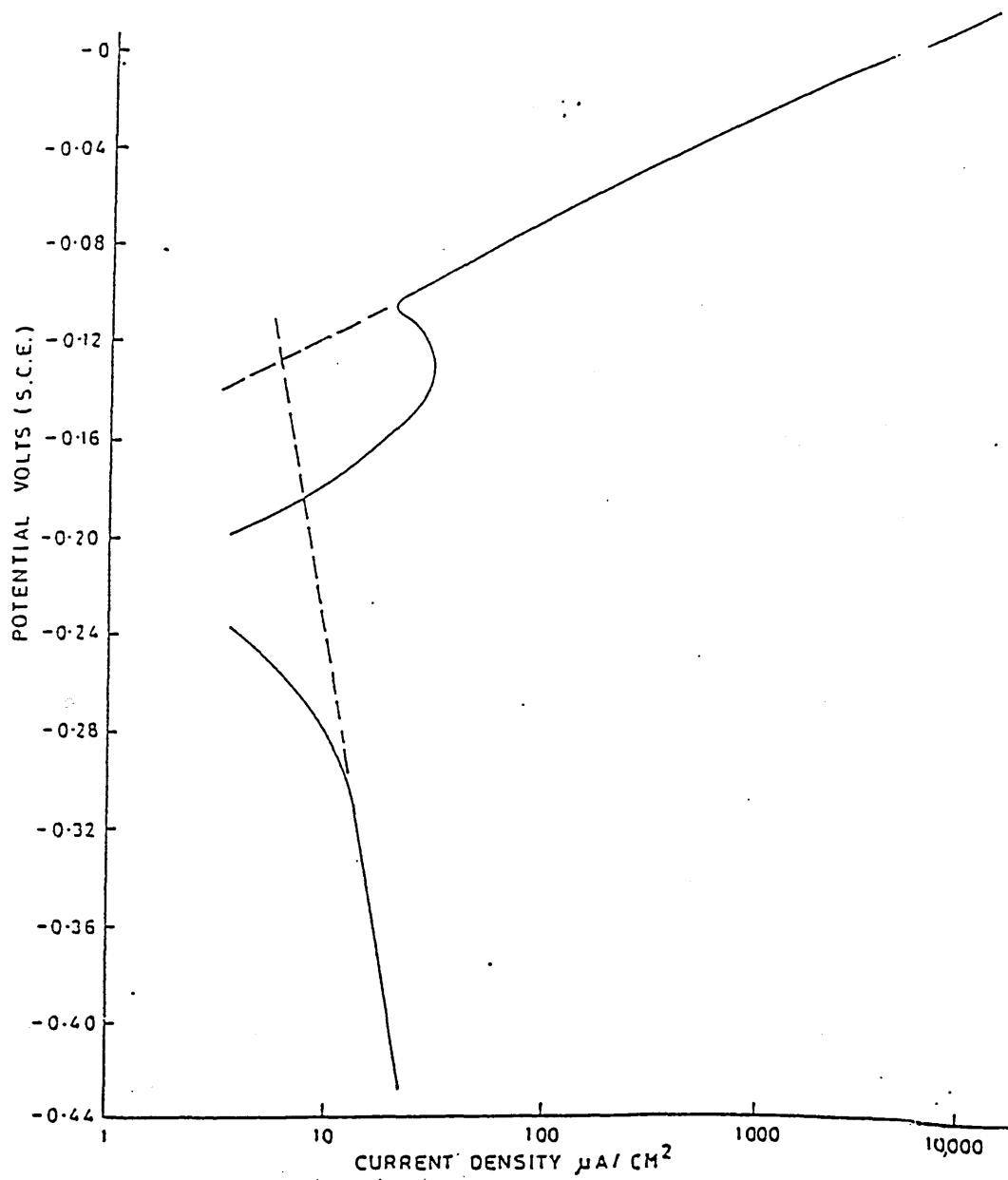


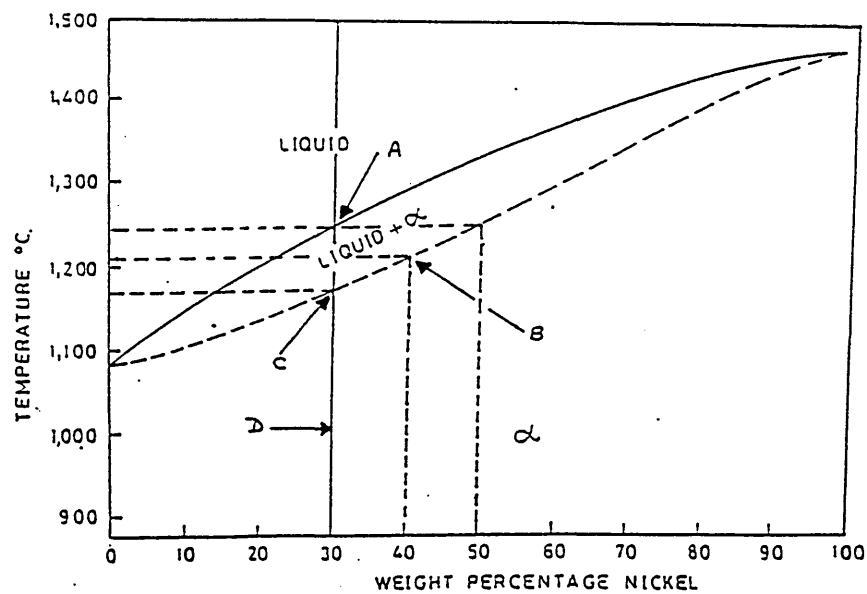
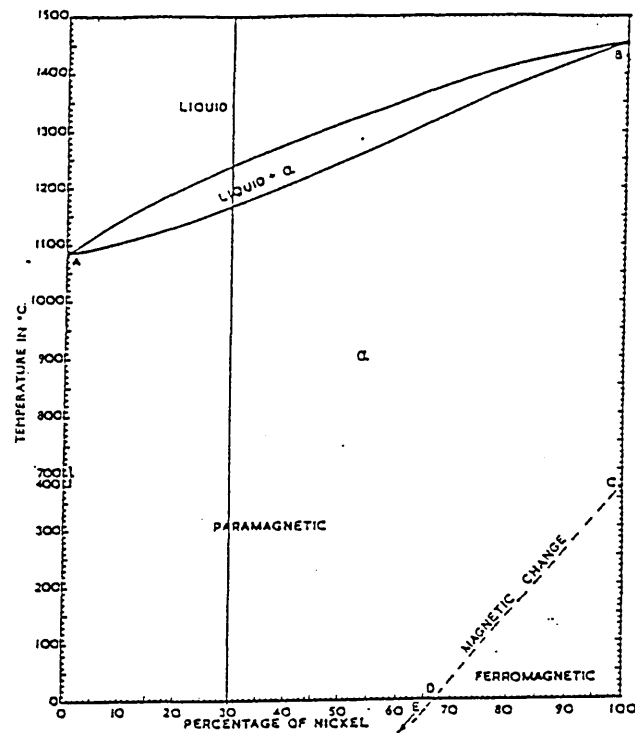
Figure 5

Effect of nickel content on the weight loss of nickel - copper alloys in flowing sea water (43).



Polarisation Curves for IN768 in Sea Water at 20°C (16).

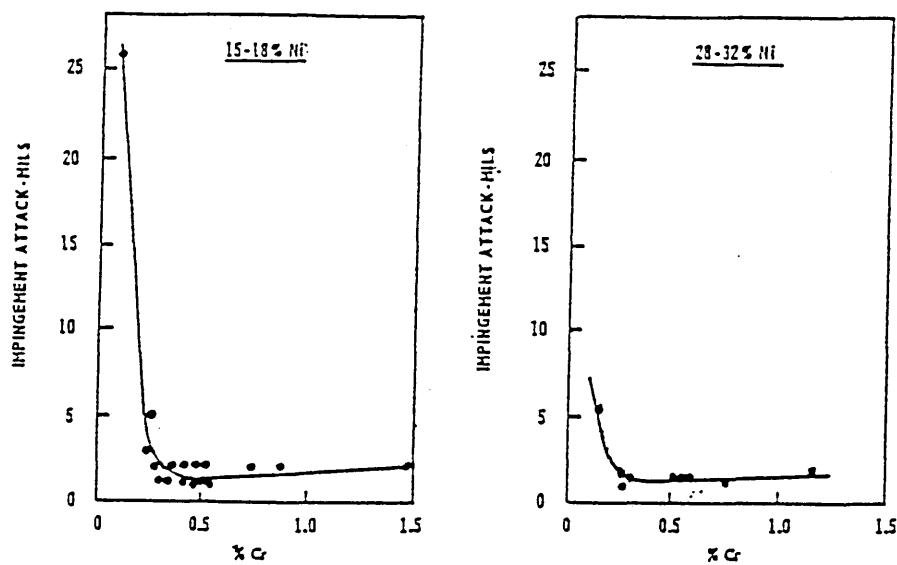
Figure 7



Thermal Equilibrium Diagram for Copper - Nickel

Chemical Composition (wt%)

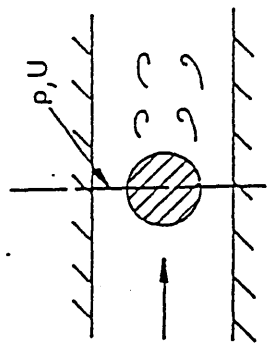
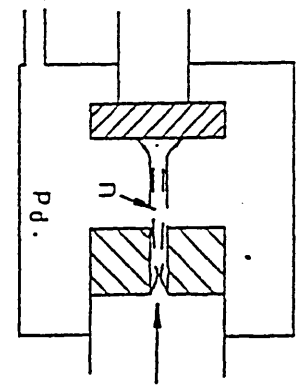
	<u>First to Solidify</u>	<u>Liquid</u>
A	50% Ni	70% Cu 30% Ni
B	40% Ni	80% Cu 20% Ni
C	30% Ni	84% Cu 16% Ni
D	Solid Solution 70% Cu 30% Ni	



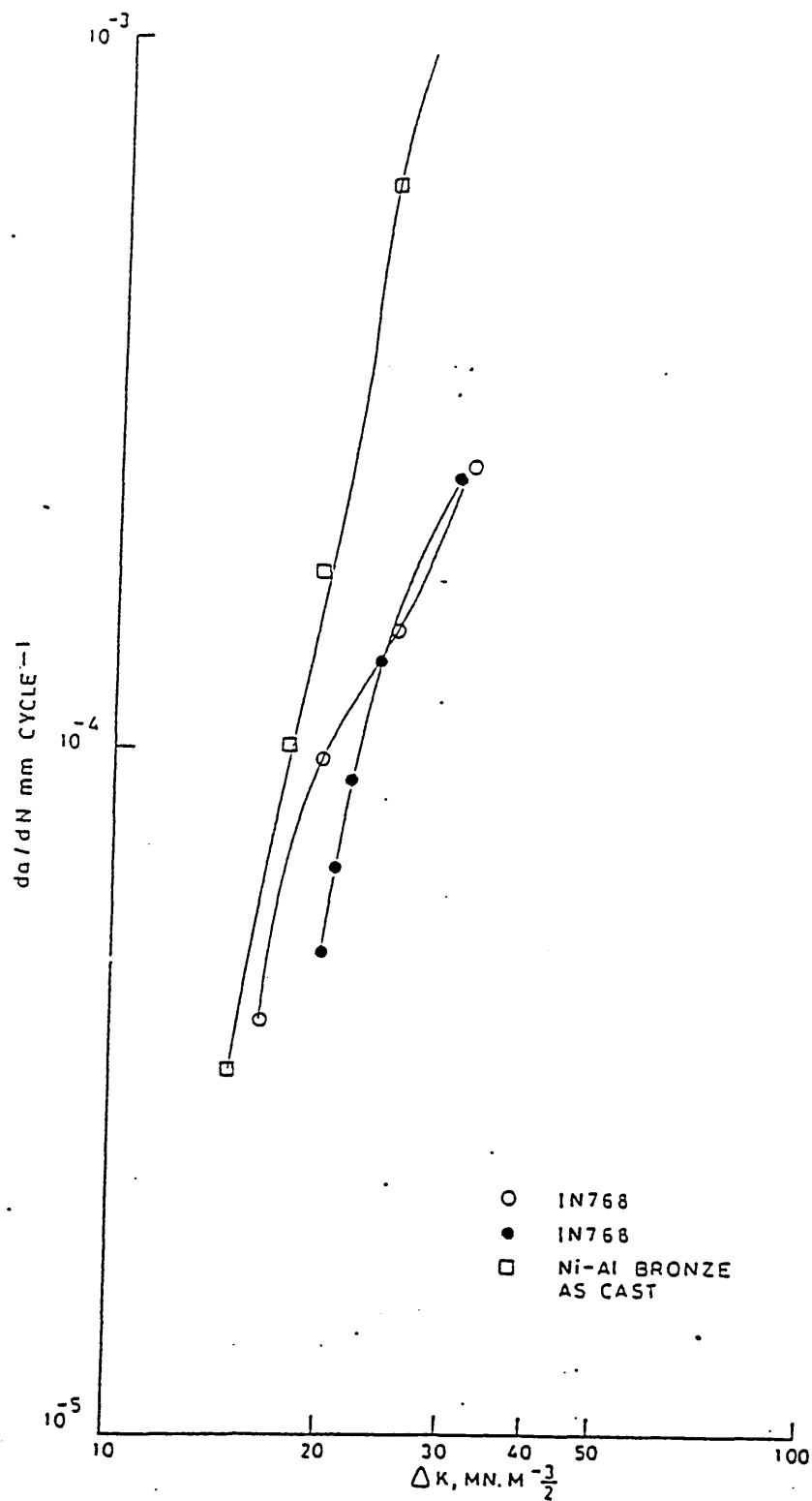
Effect of chromium additions on sea water impingement corrosion resistance of copper-nickel alloys (52).

(Jet velocity 25 FPS / sea water temperature 45-80°F)

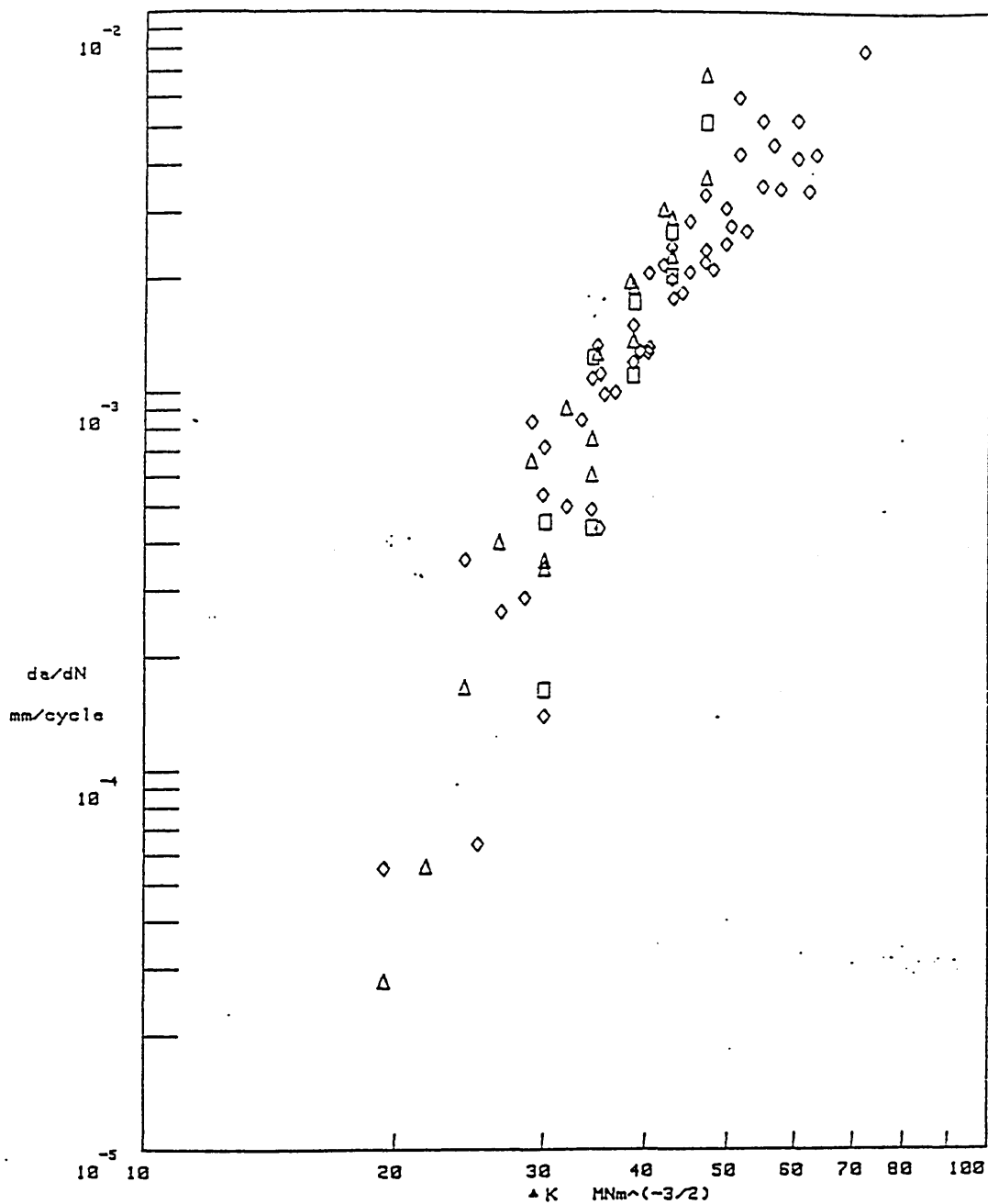
Figure 9

TEST METHOD	CAVITATION NUMBER σ	VELOCITY U m / sec	EROSION RATE mm 3/hr	
			IN768	NAB
<p>CYLINDER 25mm ϕ</p>  <p>APPROX. ERODED AREA mm² 1500</p> <p>NOZZLE 0.3mm ϕ</p>	$\sigma = \frac{P - P_v}{\frac{1}{2} \rho U^2}$ $= 0.08$	40	3.2	1.0
 <p>APPROX. ERODED AREA 20mm²</p>	$\sigma = \frac{P_d - P_v}{\frac{1}{2} \rho U^2}$ $= 0.014$	180	1.5	0.25

Cavitation erosion rates for IN768 and nickel aluminium bronze (16).



Crack growth rate versus stress intensity for IN768 and nickel aluminium bronze in sea water at 1Hz (16).

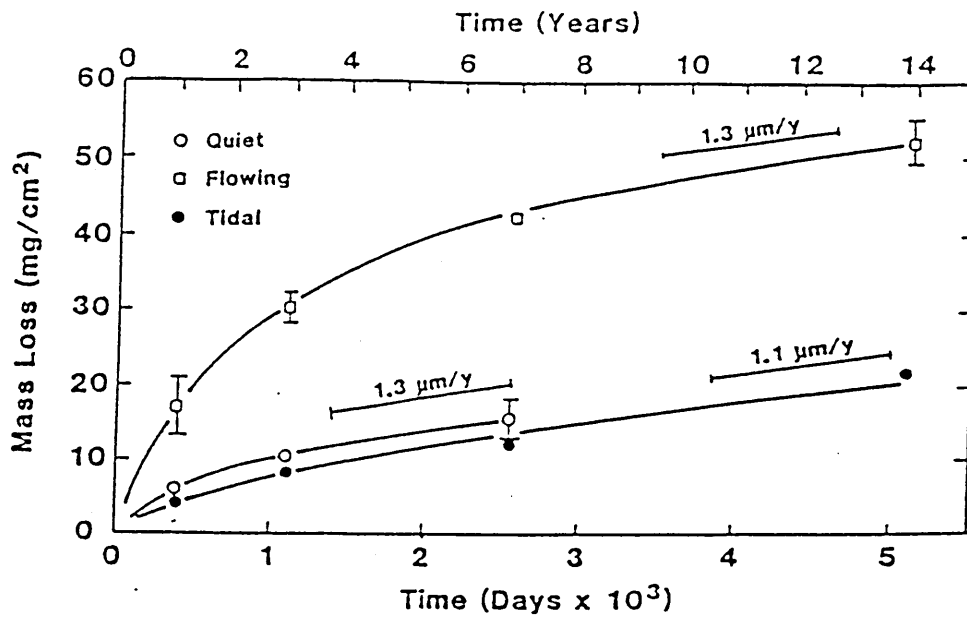


FREQUENCY: 0.008 Hz
WAVEFORM: TRAPEZOIDAL
ENVIRONMENT: SEAWATER
STRESS RATIO: ZERO

PARENT MATERIAL. □
WELD METAL ◇
HAZ △

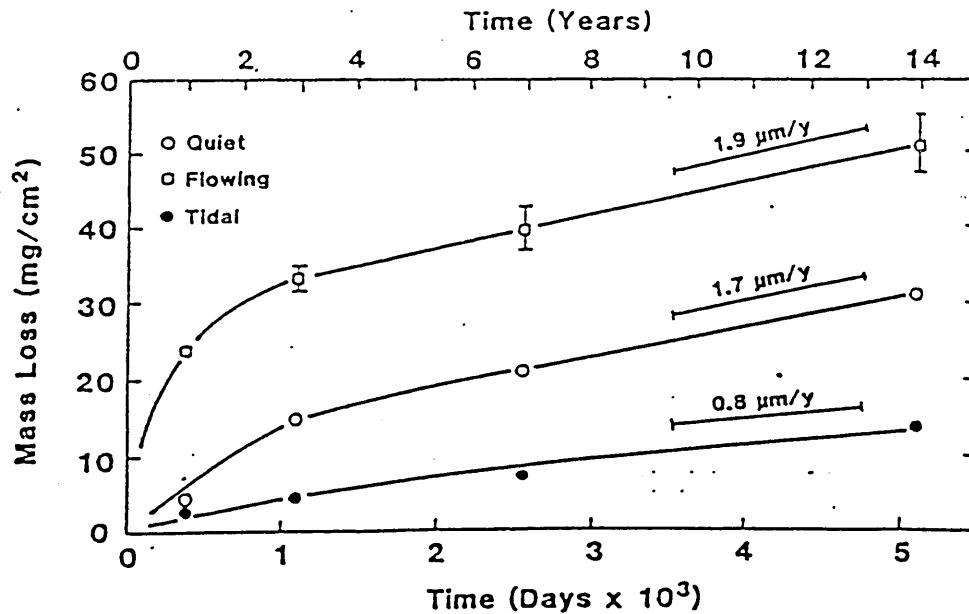
Comparison of fatigue crack growth rates in sea water for high strength cupronickel parent material, weld heat affected zone and weld metal (57).

Figure 12

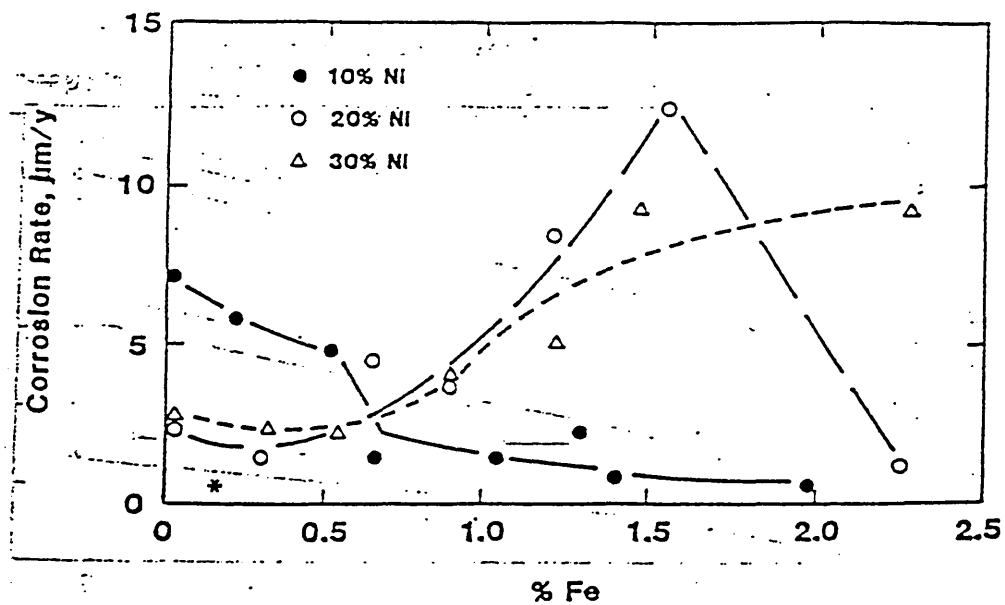


Chronogravimetric curves for 90/10 cupronickel in quiet, flowing and tidal sea water (59).

Figure 13

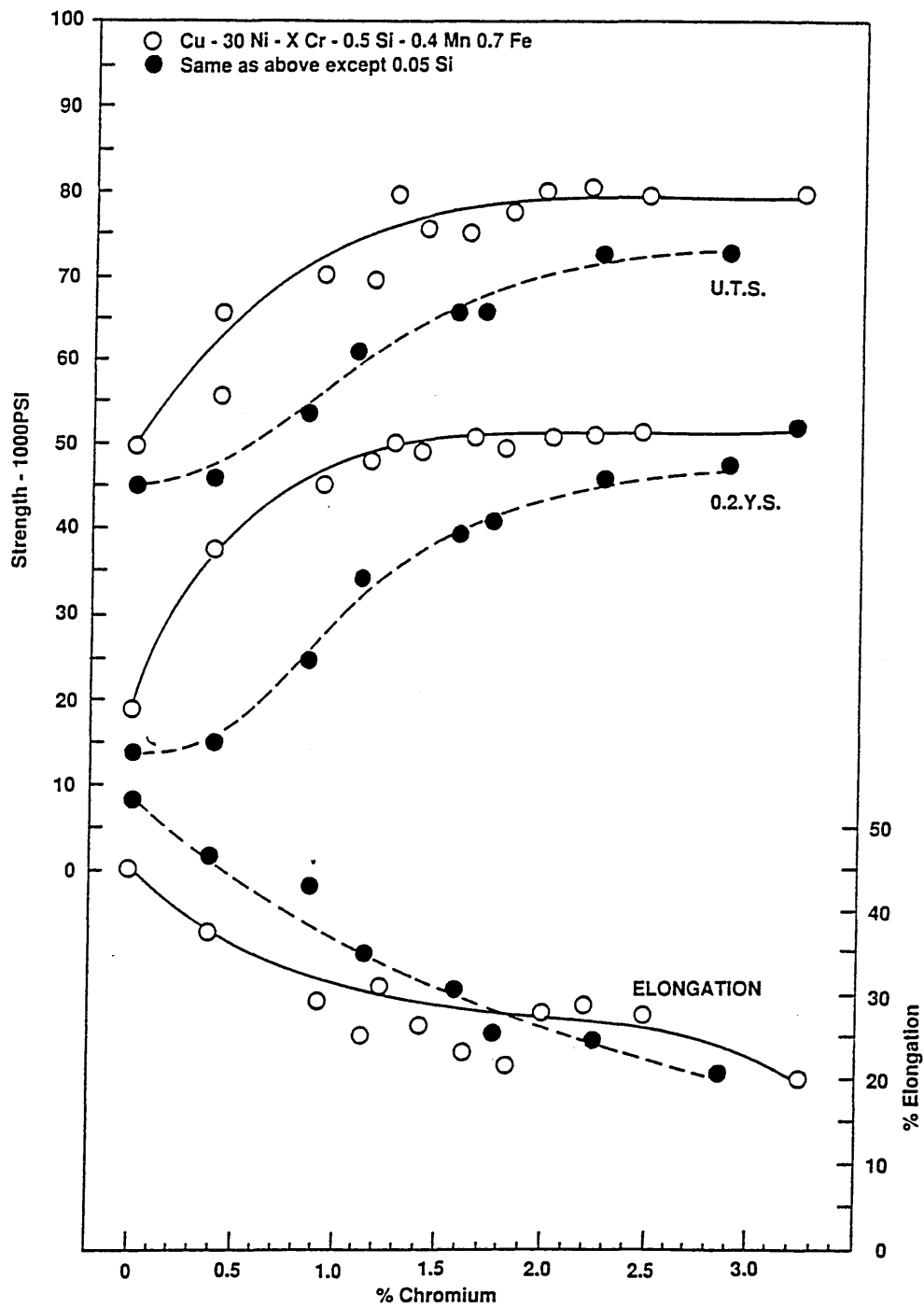


Chronogravimetric curves for 70/30 cupronickel in quiet, flowing and tidal sea water (59).

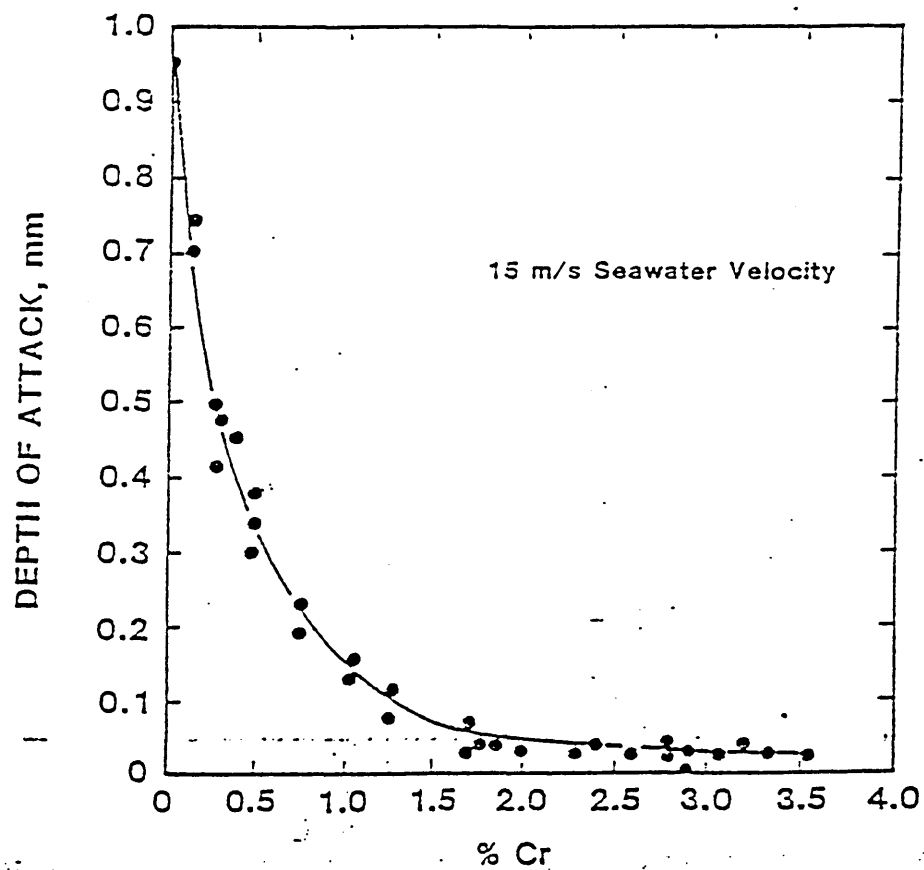


The effect of iron on the flowing sea water corrosion rate of Cu - Ni - Fe alloys after two years exposure (29).

(* = point considering Fe in solution with 1.99% Fe total)

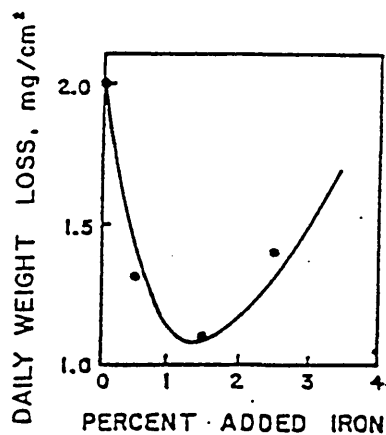


Effect of Cr on as-cast tensile properties of Cu 30% - Ni - Cr - Si alloy (20).

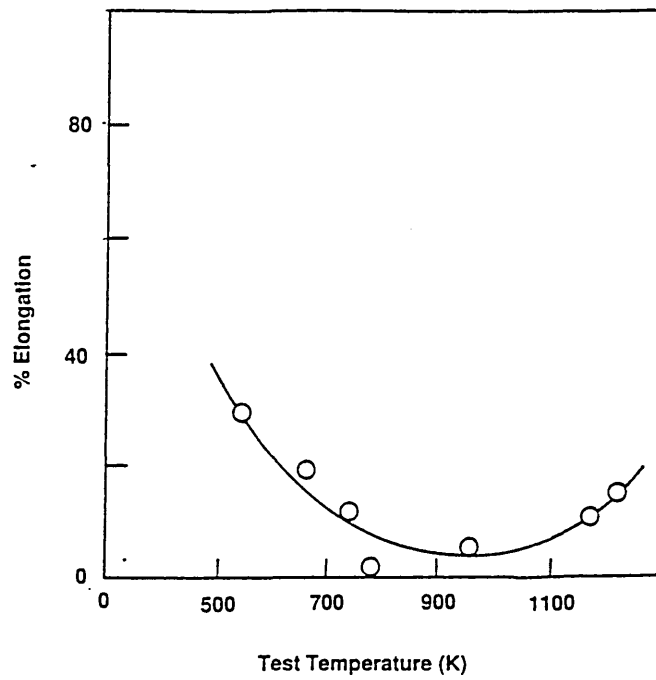


Effect of Cr additions on sea water impingement corrosion of 70/30 cupronickel, test duration 1-2 months (72).

Figure 17

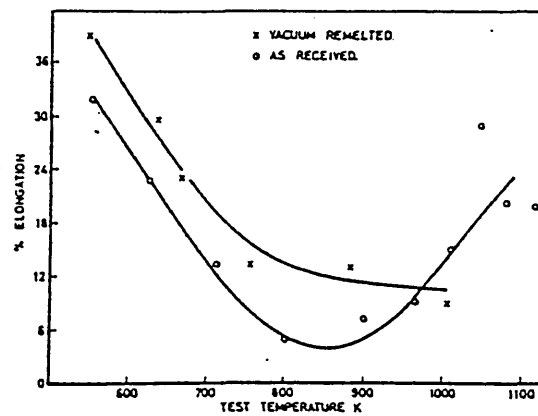


Corrosion rate of 90/10 Cu - Ni alloy as a function of iron additions (78).

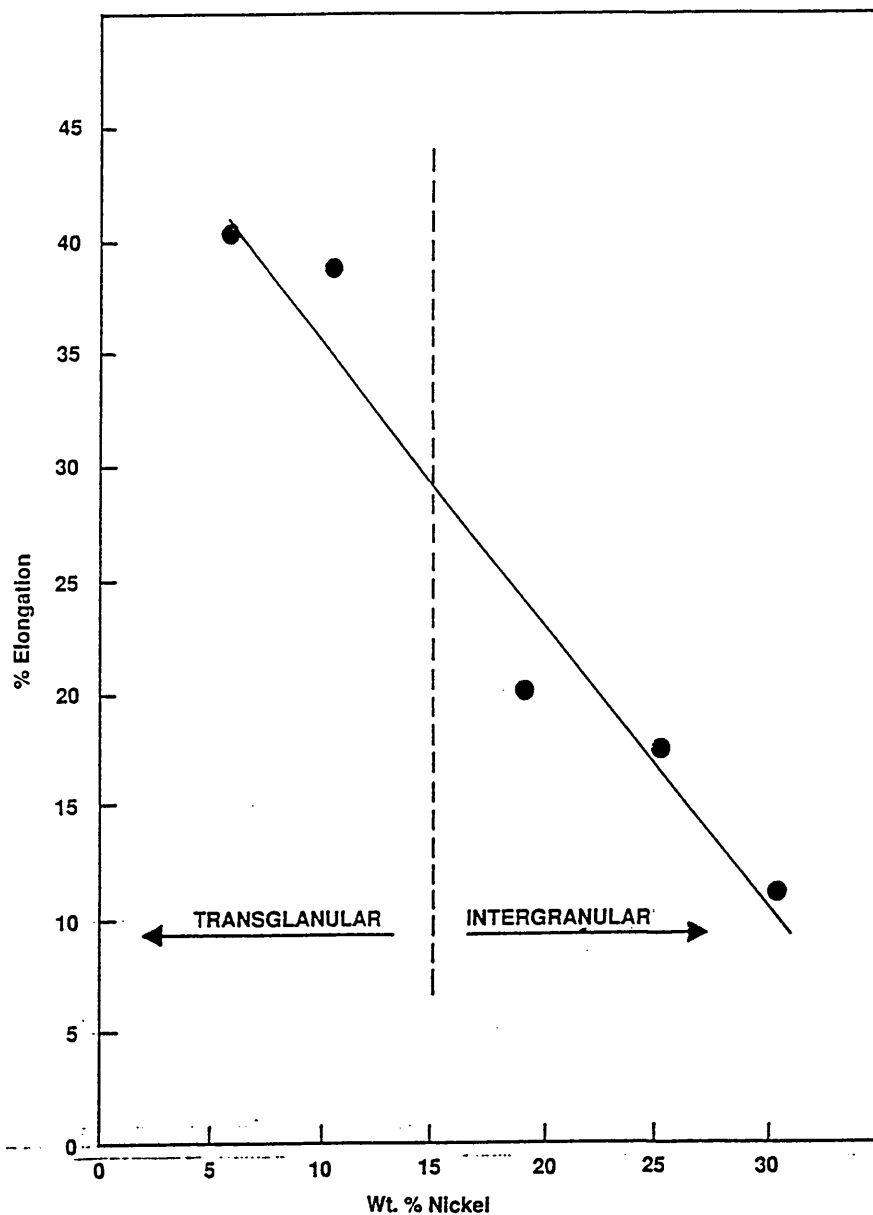


Variation of ductility with temperature for a complex cupronickel alloy (78).

Figure 19

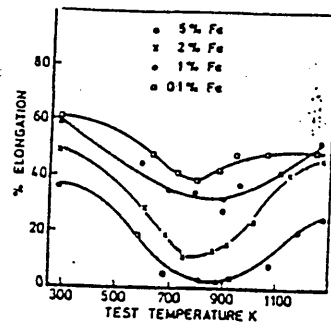


Effect of vacuum remelting on the hot ductility of a copper - 30% nickel alloy (78).



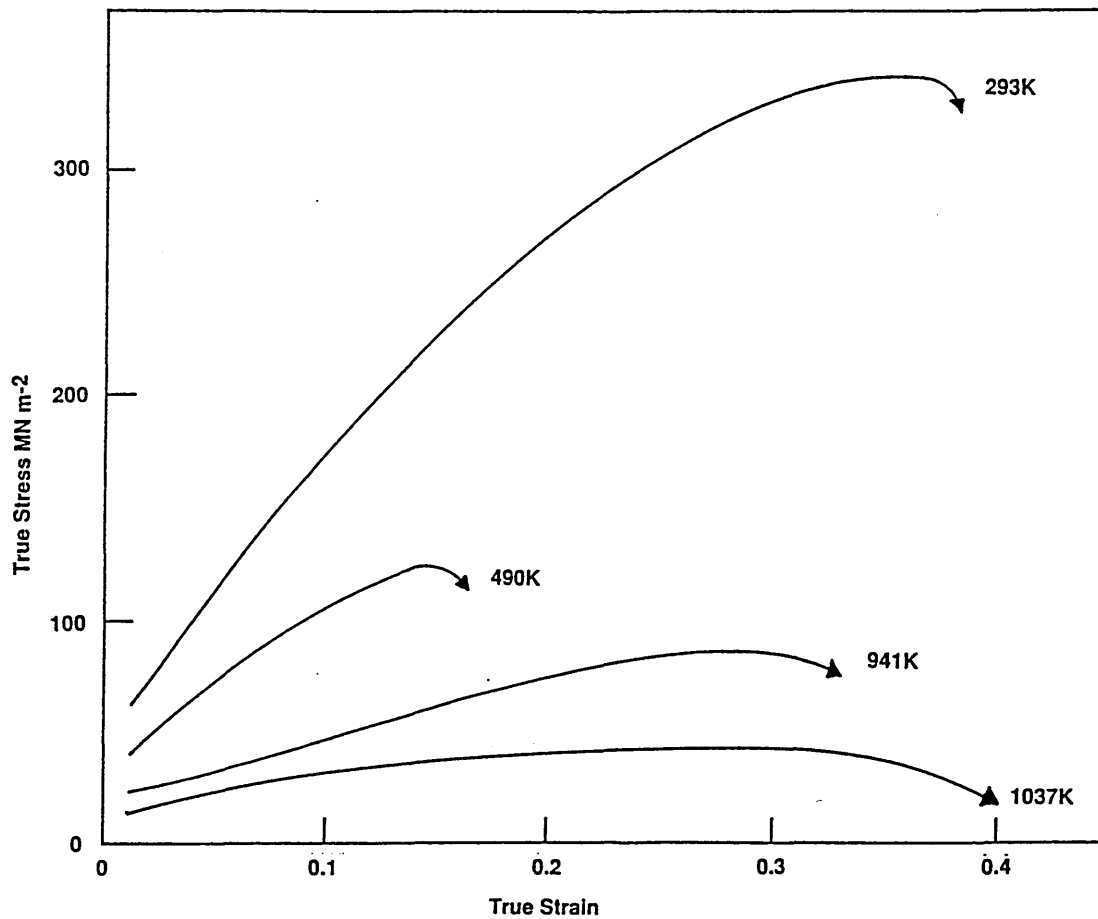
Effect of nickel on the intermediate temperature ductility of binary copper - nickel alloys (78).

Figure 21

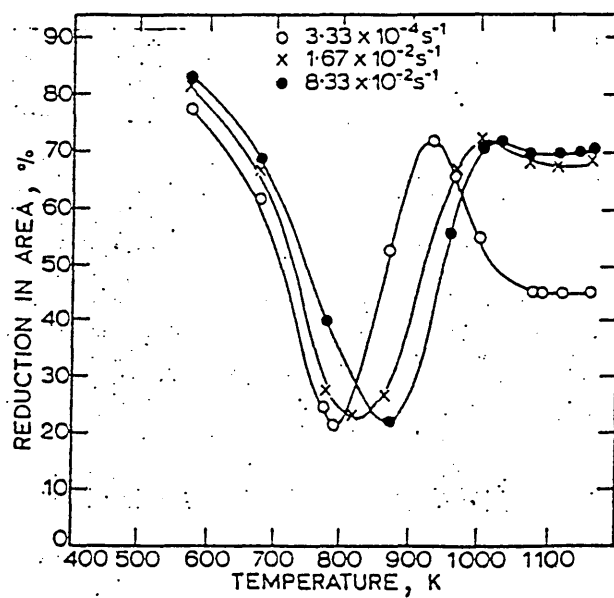


Effect of iron on the hot ductility of a copper - 10% nickel alloy (78).

Figure 22

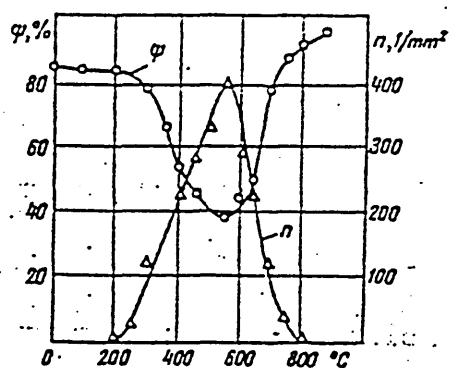


Typical flow curves for Cu - 10% Ni alloy having initial grain size of $190\mu\text{m}$ (81).

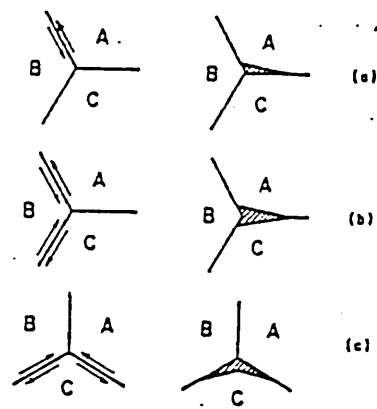


Variation in reduction in area at fracture with temperature and strain rate for Cu-30Ni having a grain size of 125 μm (89).

Figure 24

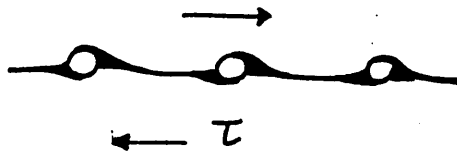


Ductility, ψ , and number of voids, n , as a function of the experimental temperature (79).

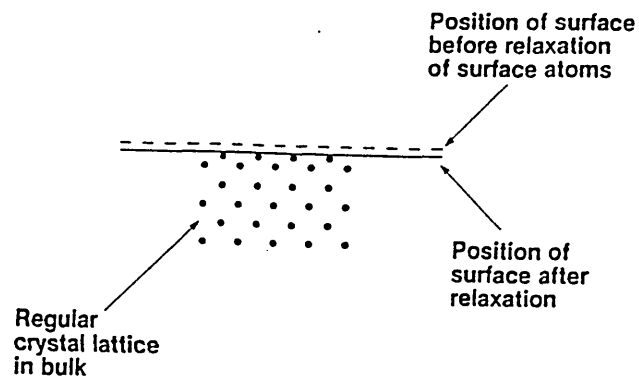


Schematic views at a triple point show three simple means of initiating intercrystalline W-type cracks as a result of grain boundary sliding. The arrows along a grain boundary indicate that this boundary underwent sliding (79).

Figure 26

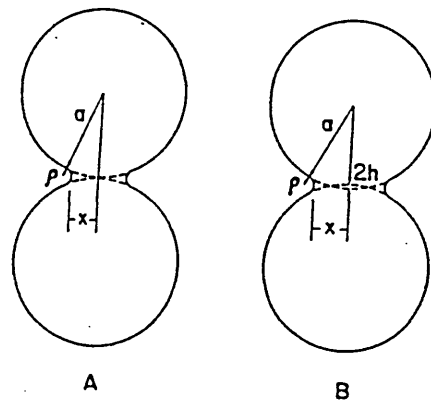


Schematic view of the means of initiating R-type cracks (79).



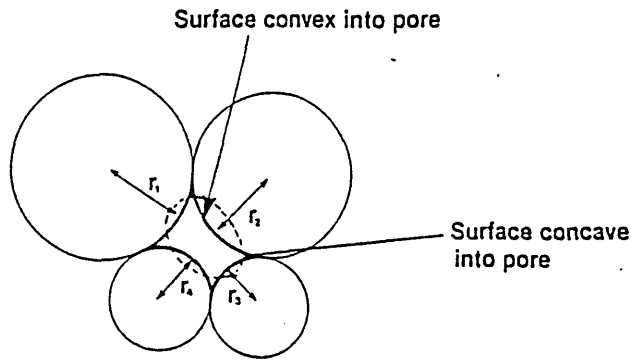
Relaxation of atoms in the surface of a material, leading to disorder in the regular atomic arrangement (100).

Figure 28



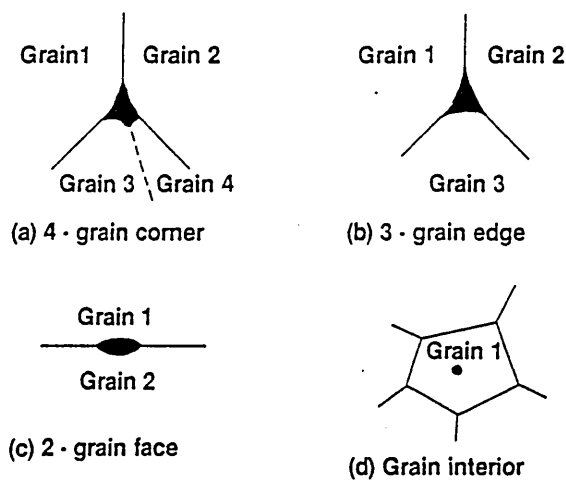
Schematic representation of the contact area between two partially sintered spheres (102):

- (a) Centre to centre distance remains constant.
- (b) Centre to centre distance shrinks.



Pore with varying radii of curvature around the surface:
The broken curve shows the pore surface after some spheroidization has taken place by redistribution of material from convex surfaces to concave (100).

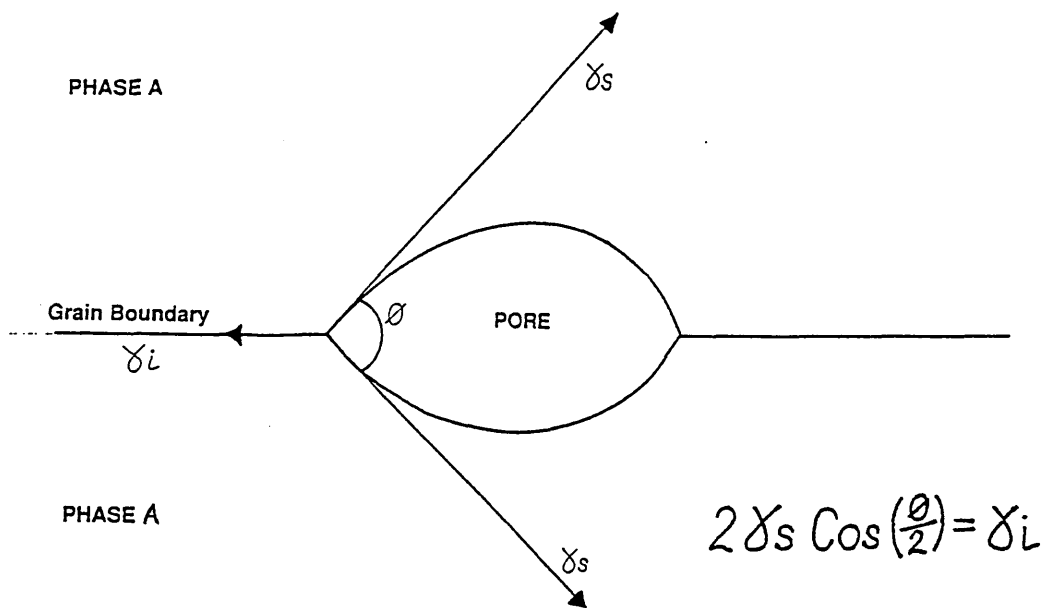
Figure 30



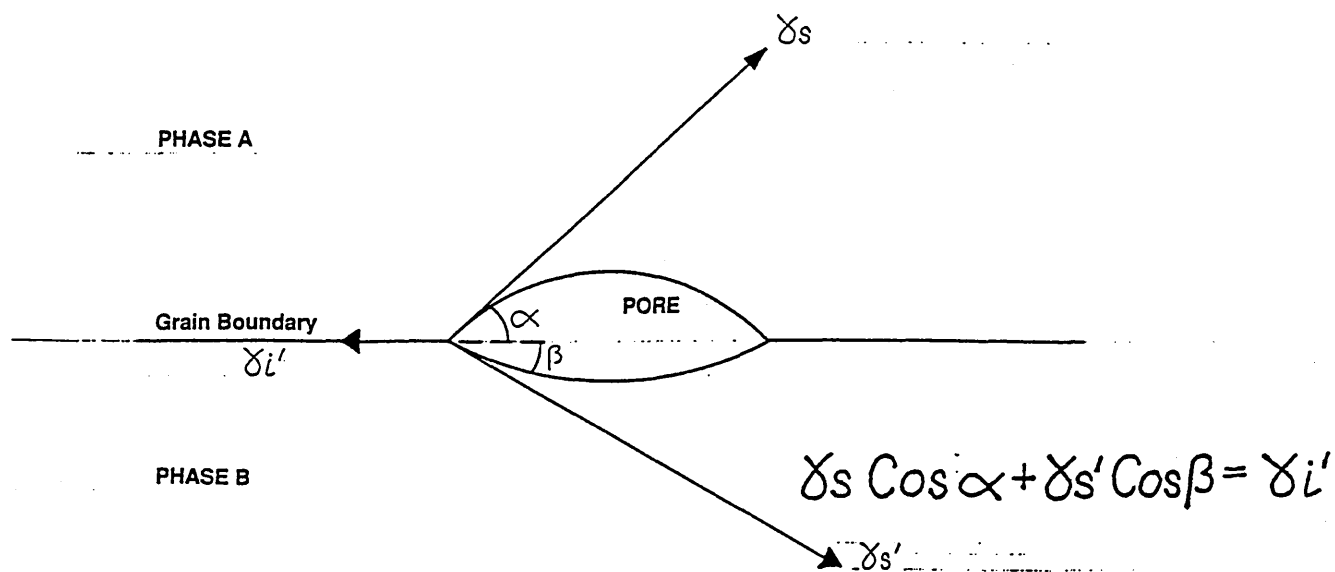
Potential sites for the location of pores (100).

The decreasing order of preference is:

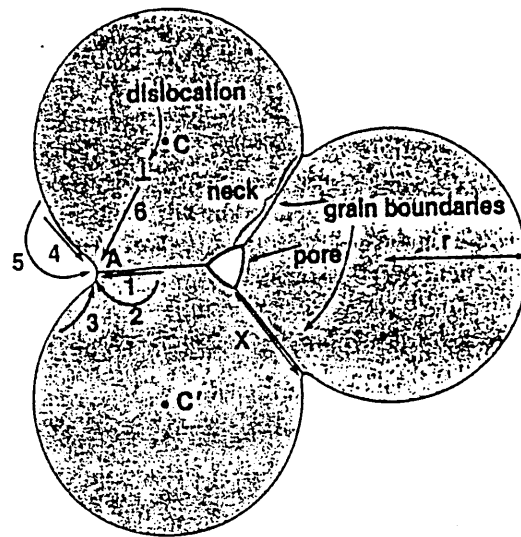
- (a) four grain corner
- (b) three grain edge
- (c) two grain face
- (d) grain interior



(A) Equilibrium configuration at a junction between a grain boundary and a pore in a single-phase material.



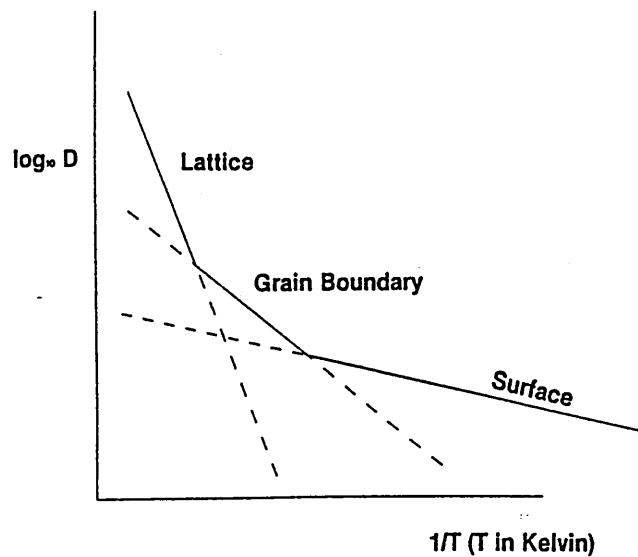
(B) Equilibrium configuration at a junction between a grain boundary and a pore in a two-phase material (100,101)



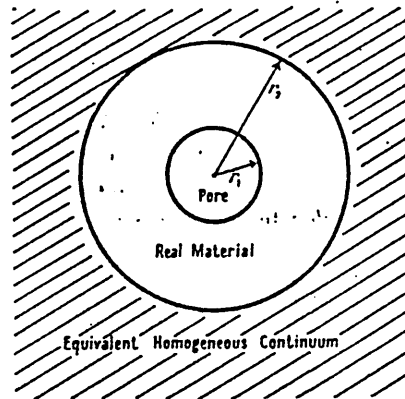
Paths for transport of matter during neck growth in sintering (100).

C and C' = the particle centres
 X = the neck size
 r = particle radius

Figure 33

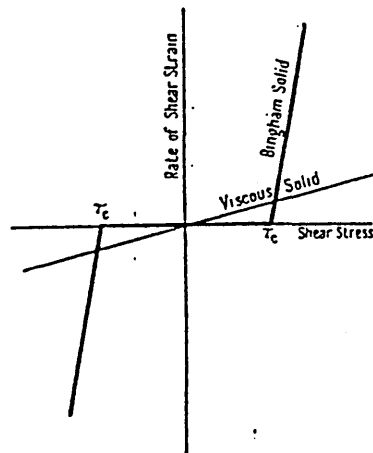


Schematic diagram showing the dependence on temperature for surface, grain boundary and lattice diffusion (100).

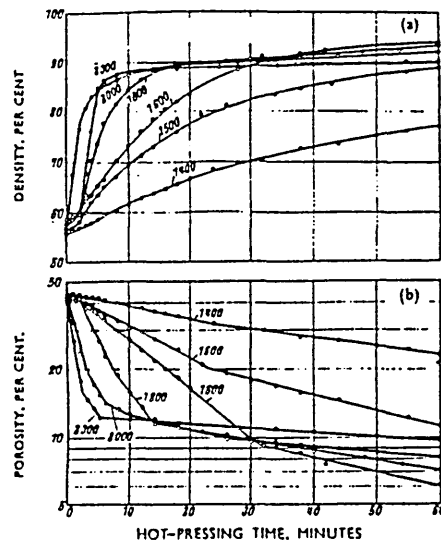


The Mackenzie and Shuttleworth model of viscous or plastic flow (98).

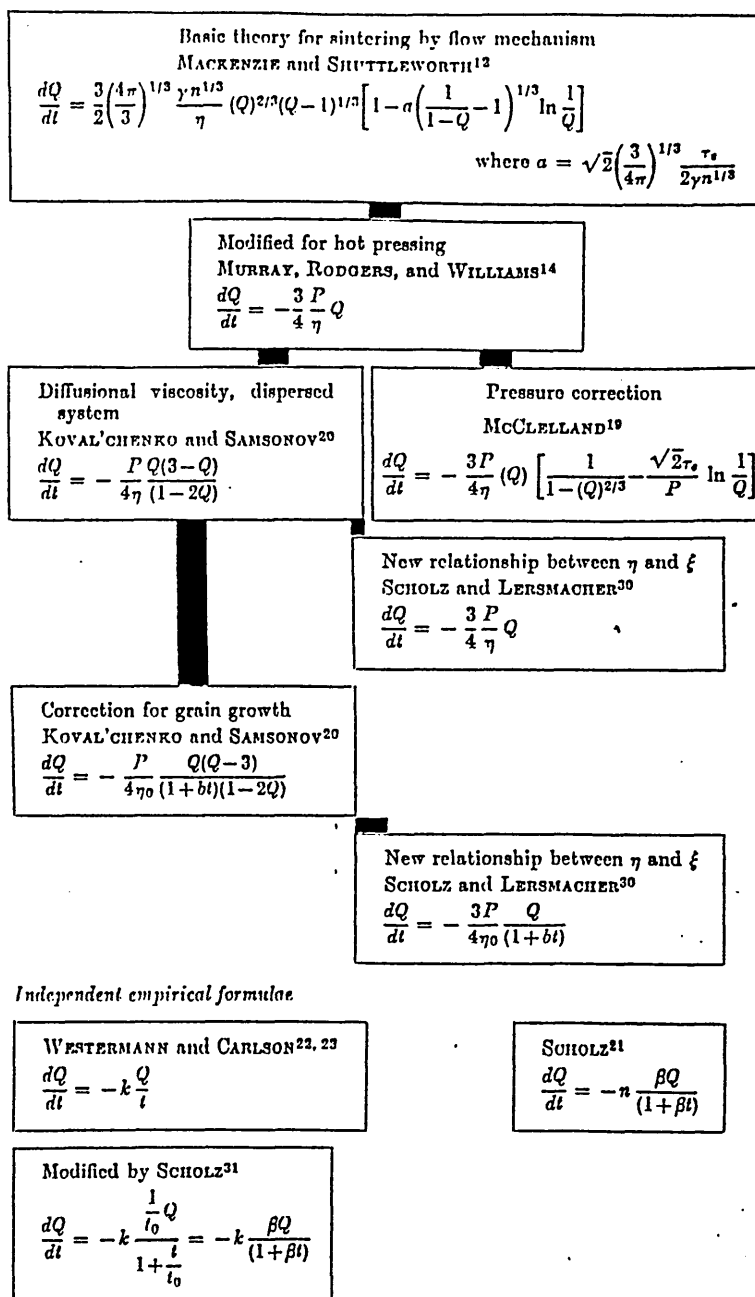
Figure 35



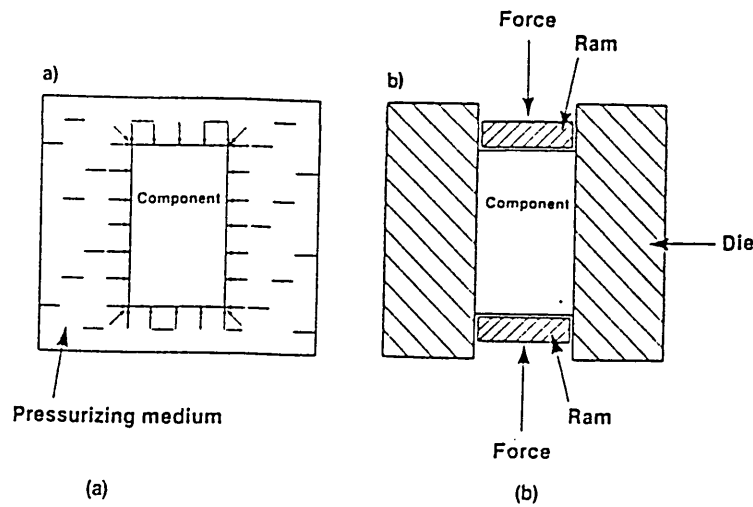
Relationship between rate of shear strain and shear stress for a plastic and viscous body (98).



Relationship between density and time at various sintering temperatures for tantalum carbide (128).

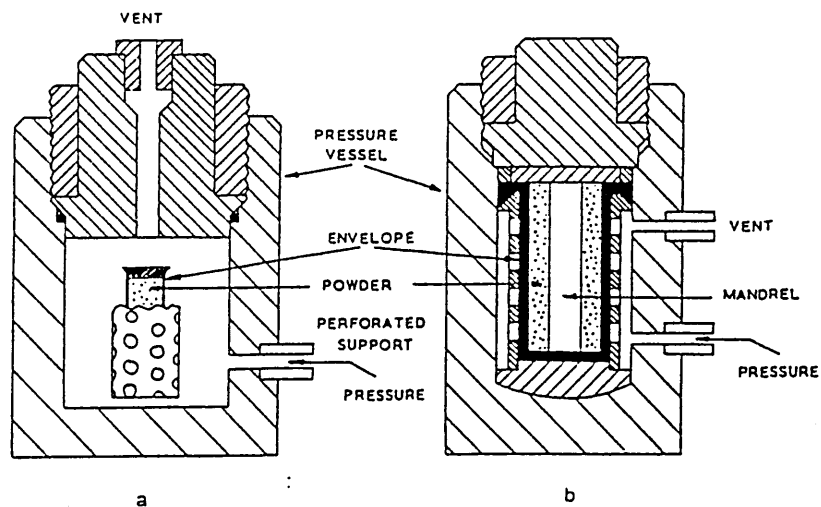


Theoretical equations of hot pressing (123).



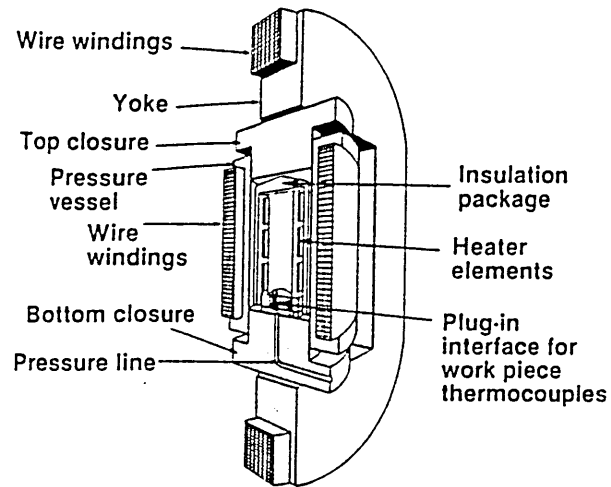
- (a) Isostatic pressing: the forces on the component are equal in all directions.
- (b) Unidirectional pressing: the force is applied in one direction only (100).

Figure 39



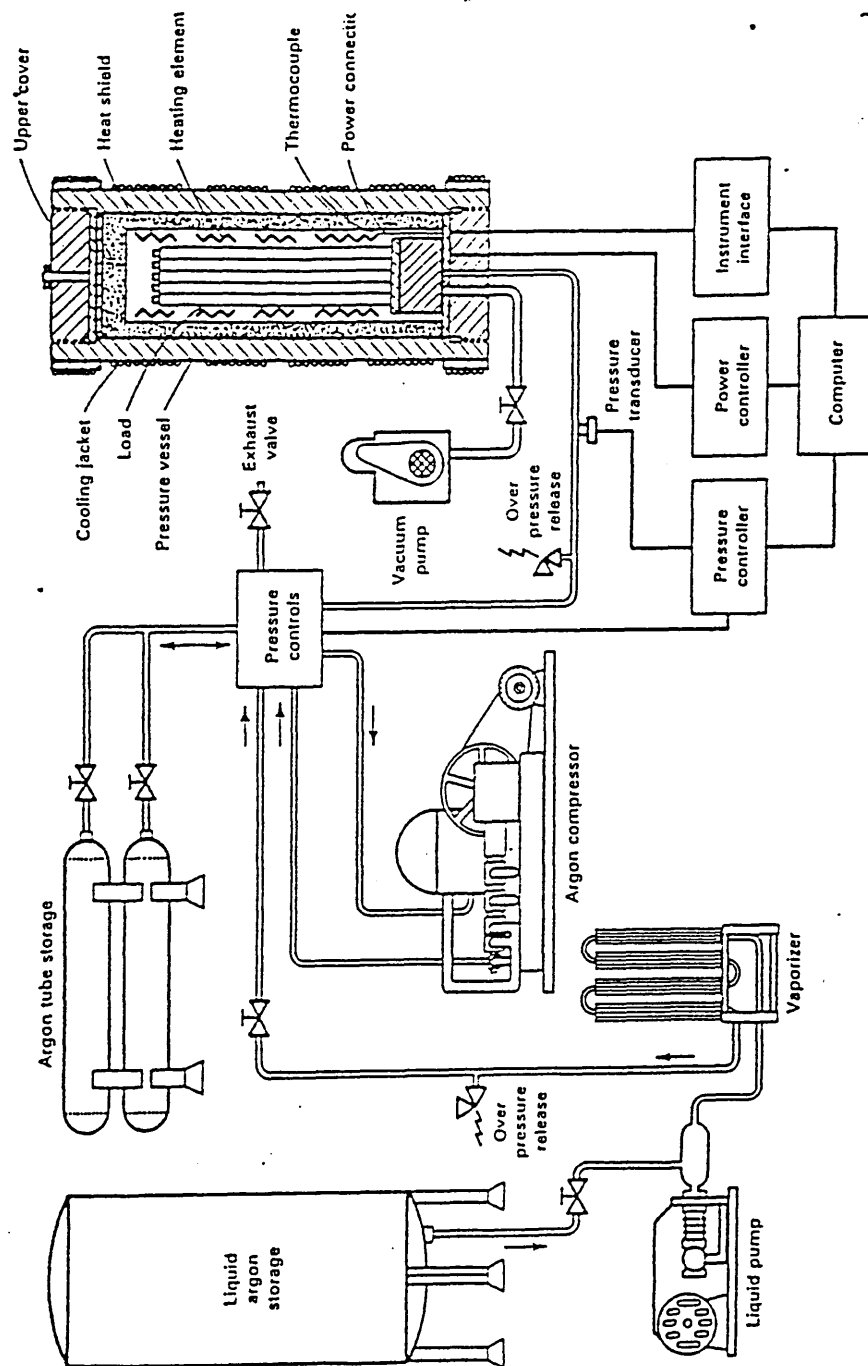
Types of cold isostatic tooling (134):

- (a) Wet bag or free mould tooling.
- (b) Fixed bag or dry tooling.



Schematic illustration showing the design of a hot isostatic pressing system. Components to be processed are placed within the central area and enclosed within the heater - insulation package (170).

Figure 41



Schematic diagram of a hot isostatic processing system (136).

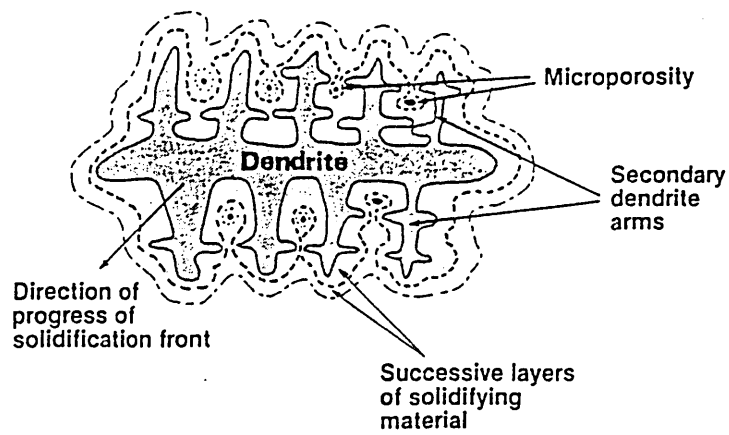
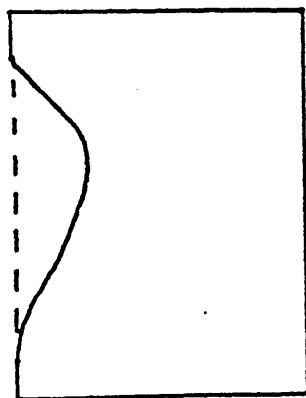
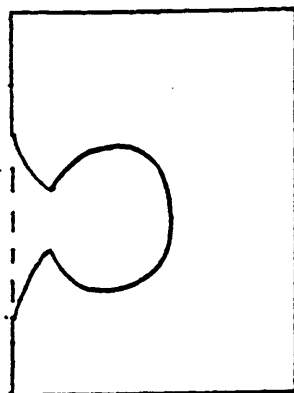


Diagram showing how, as liquid solidifies, porosity forms in the regions between dendrite arms (100).

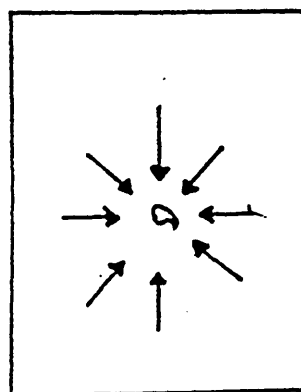
Figure 43



- (A) Pore near to the surface:
material is pressed into the pore space,
the surface becomes rougher.

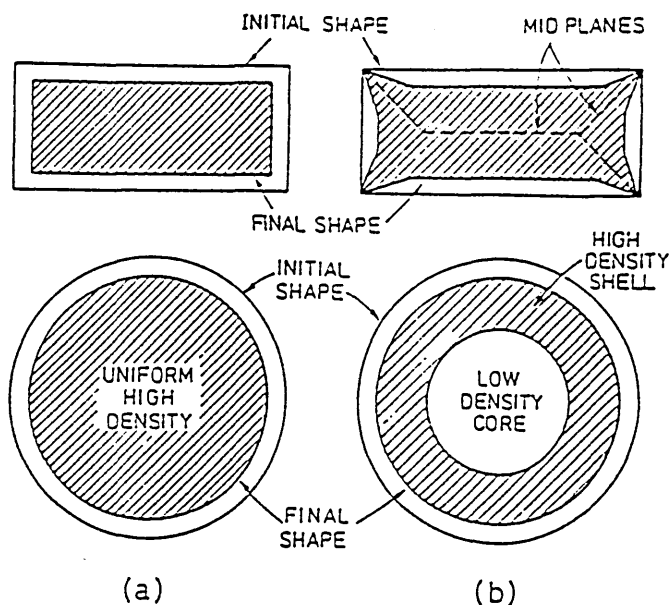


- (B) Pore just below the surface:
the gas pressure bursts the pore covering.



- (C) Pore in the interior of the casting which has
no connection with the surface, can be
successfully eliminated by HIPping.

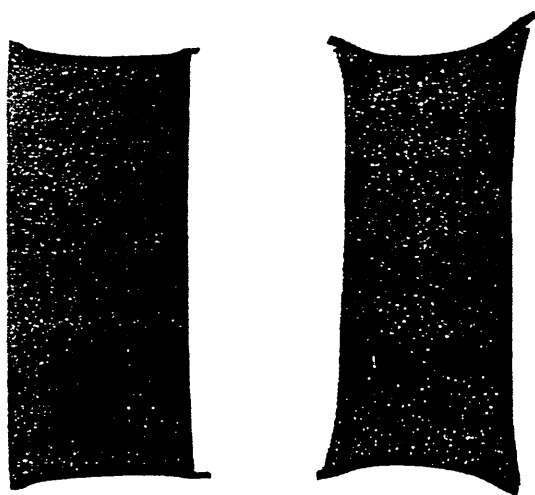
Behaviour of pores during hot isostatic pressing.



Effect of density gradients (160):

- (a) When density is uniform, the final shape is the same as that of the preform.
- (b) When a densification front forms, shape change, density gradients with residual porosity, and internal stresses result.

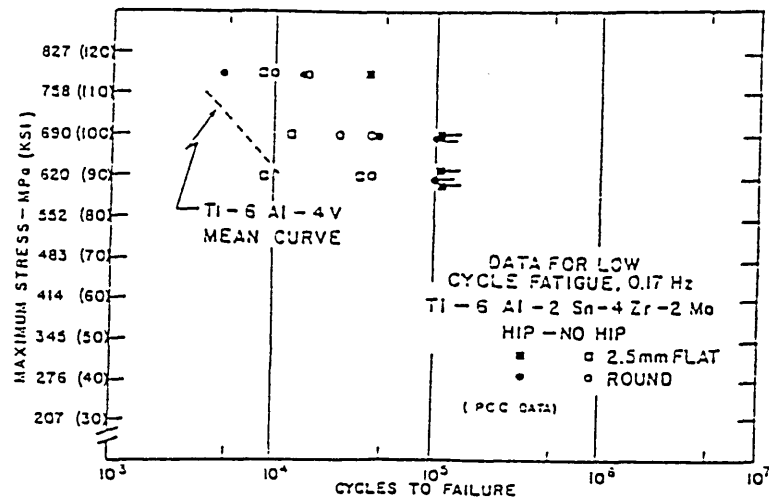
Figure 45



Densification of tool steel samples (160):

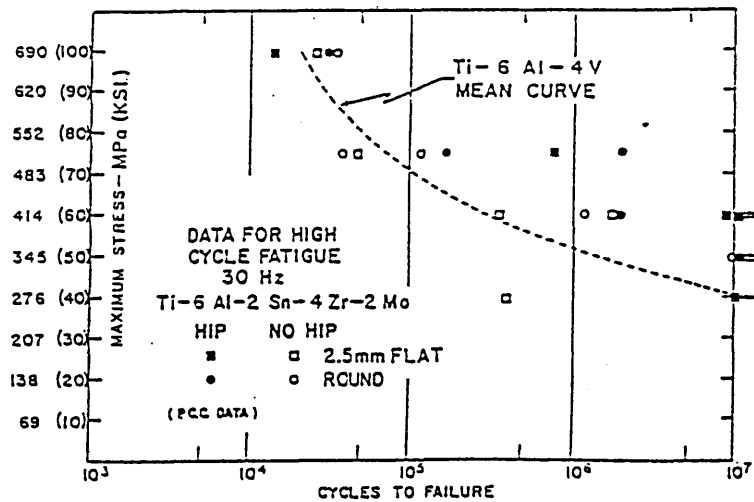
The left hand sample was heated before it was pressed, so that the temperature was uniform during HIPping, producing almost no shape change.

The right hand sample was heated and pressed simultaneously, producing temperature gradients and severe shape change.

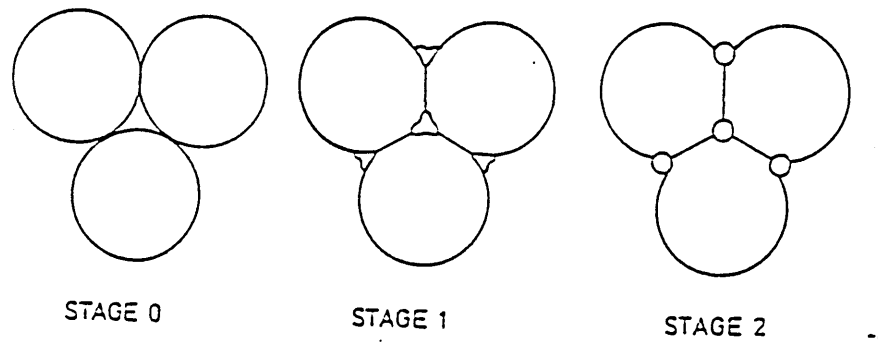


Low cycle fatigue properties of a titanium alloy before and after being HIPped (175).

Figure 47

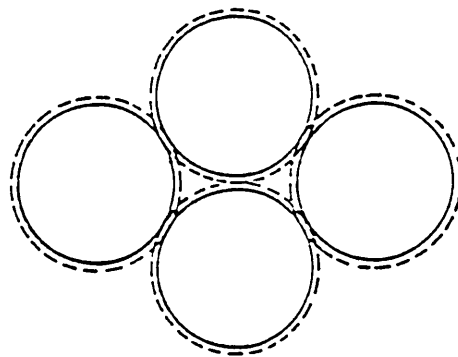


High cycle fatigue properties of a titanium alloy before and after being HIPped (175).



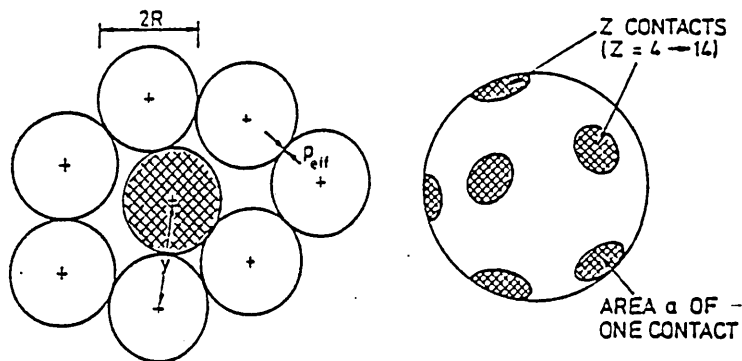
The stages of sintering / densification (160,179).

Figure 49

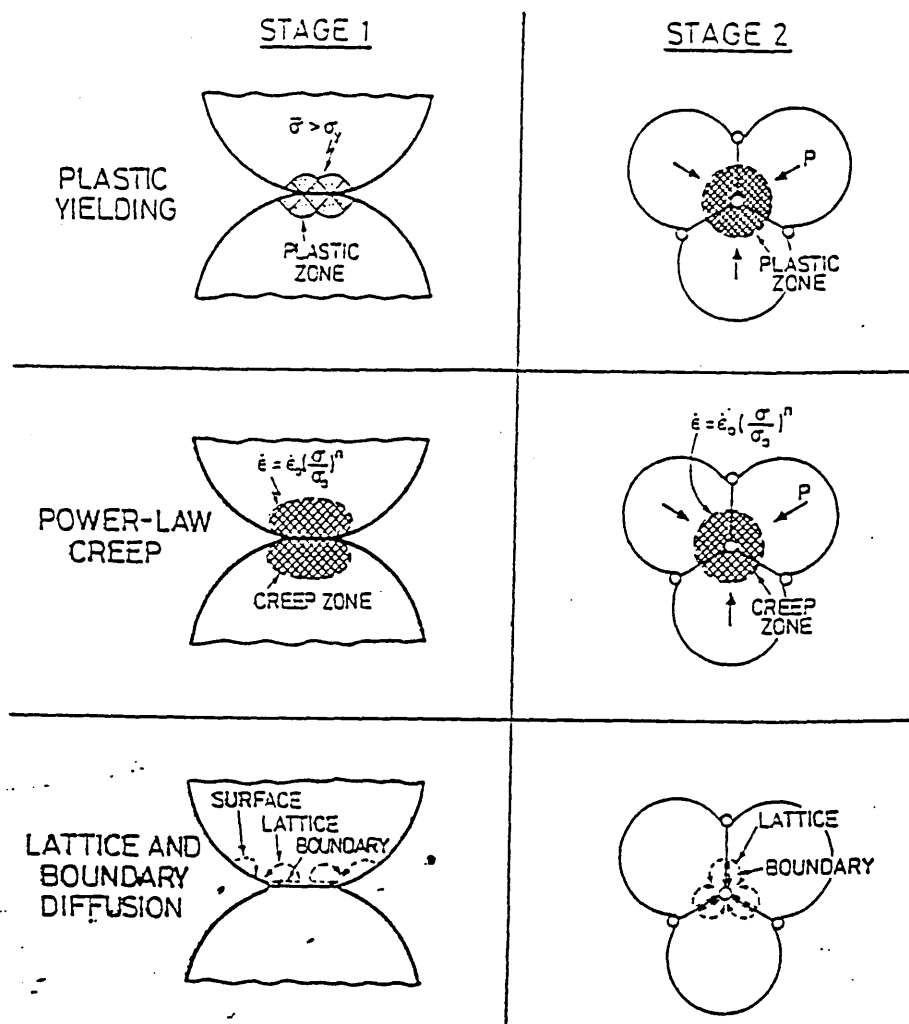


The development of new contacts can be modelled by considering each particle to expand about its centre. Two central particles come into contact as they expand (160).

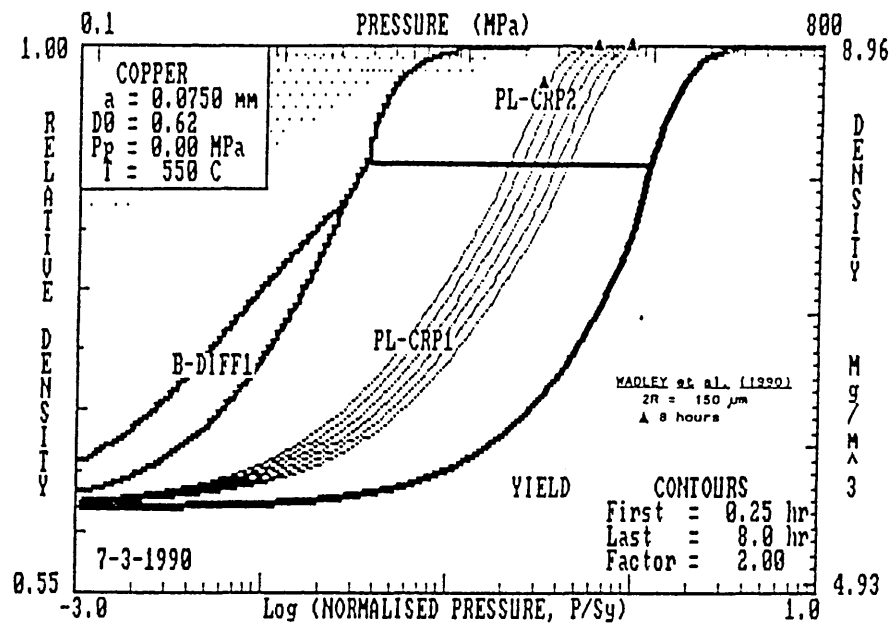
Figure 50



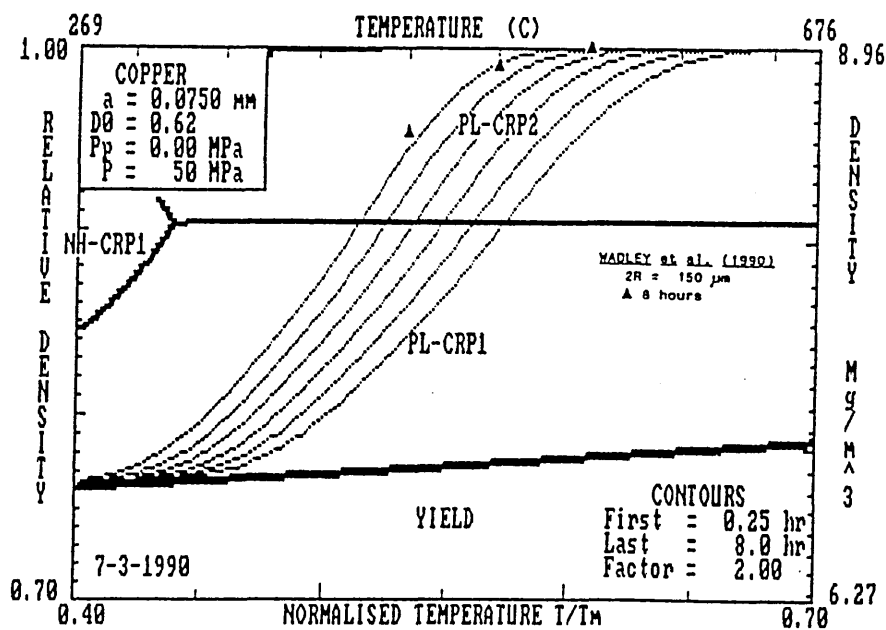
A particle contacts a number Z of its neighbours in small contact areas, a . (160,180).



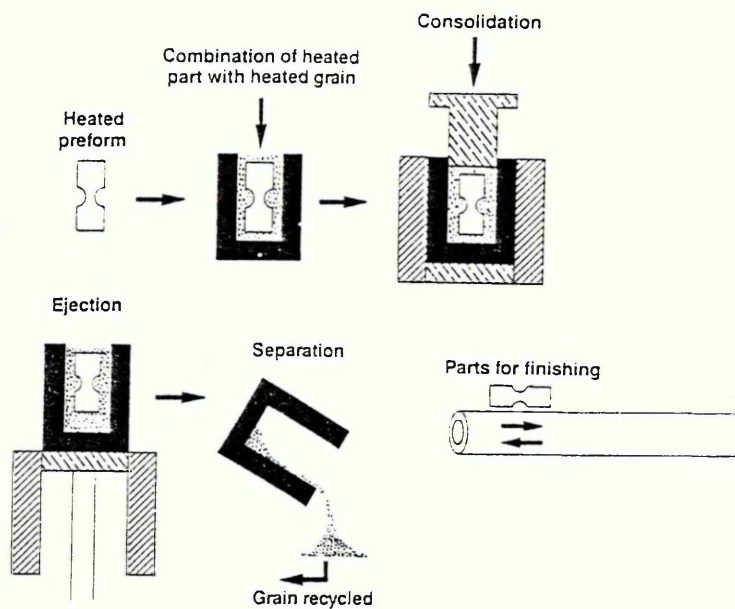
The mechanisms which contribute to stage 1 and stage 2 of densification during hot isostatic pressing (160).



(a) HIP map for HIPping of atomised copper powder, showing the change in density with HIP pressure (180).

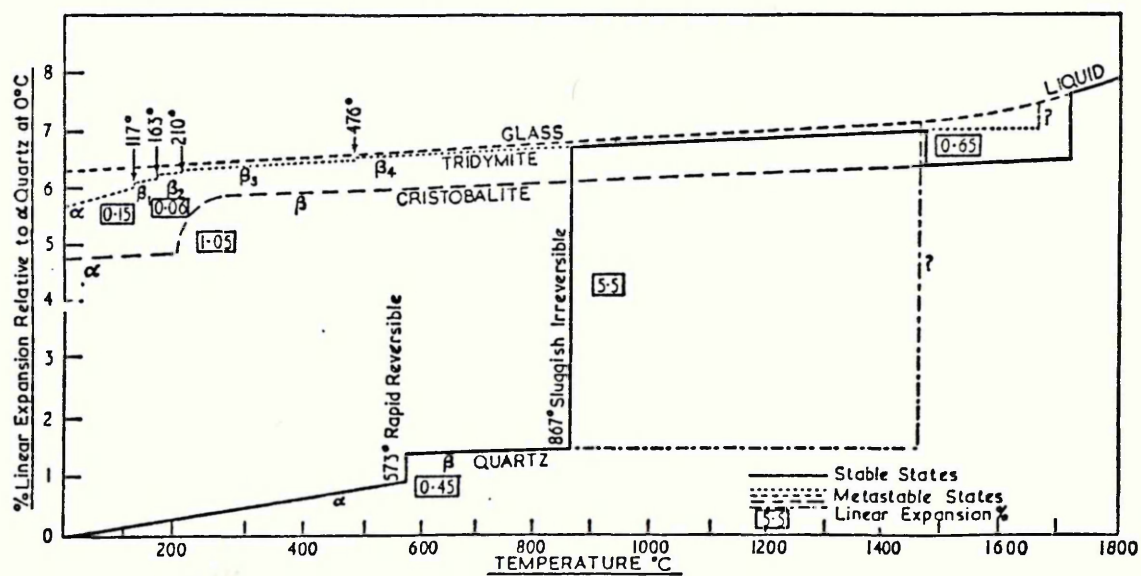


(b) HIPping of atomised copper powder, change in density with temperature (180).



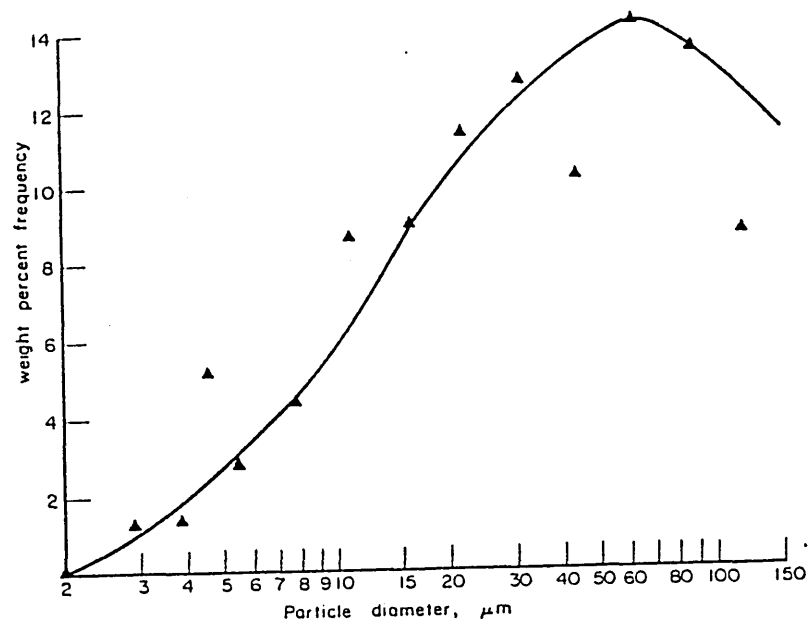
The Ceracon Process (187).

Figure 54



Note: The line for glass probably ought to dip below the tridymite line in the middle range of temperature but has been drawn above it at all points for clarity.

Allotropy in silica and the associated volume changes (197).

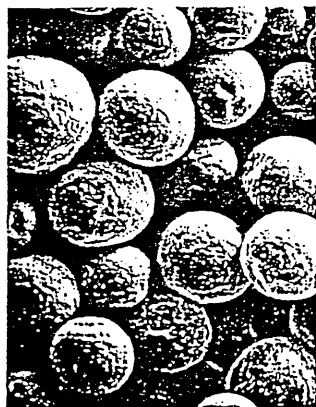


Typical weight frequency plot of particle size distribution of a metal powder (203).

Figure 56

Particle Characteristics - Shape Definition

SPHEROIDAL



GRANULAR



DENDRITIC



NODULAR



FLAKY



ANGULAR



IRREGULAR

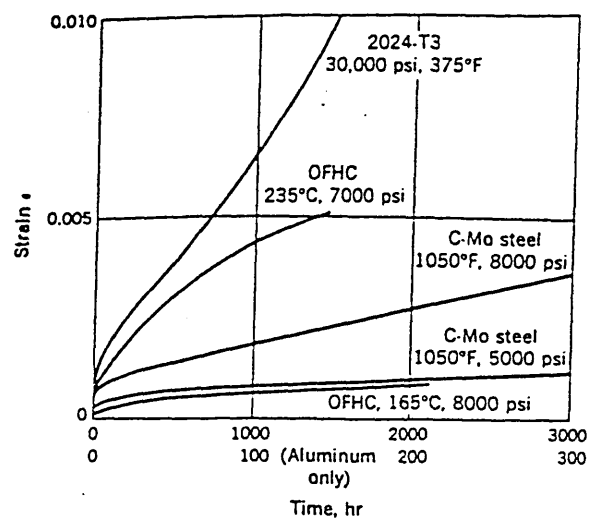


FIBROUS



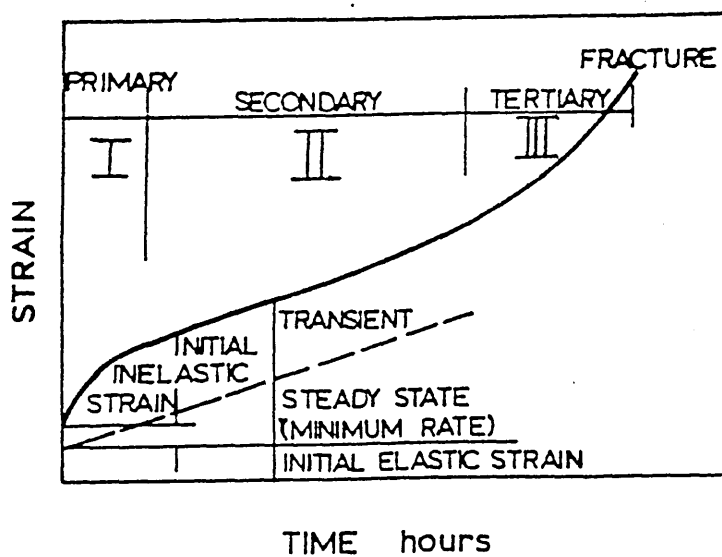
ACICULAR



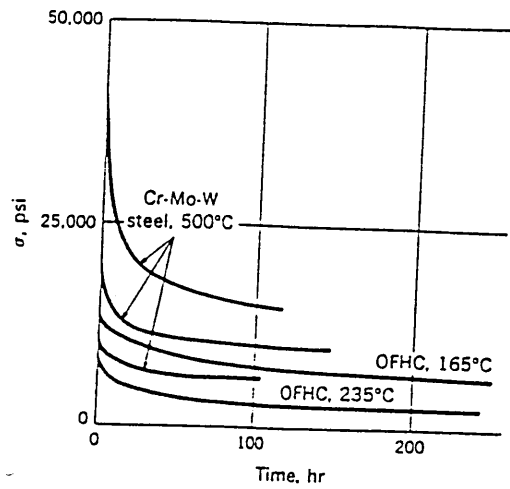


Creep of metals in tension (204).

Figure 58

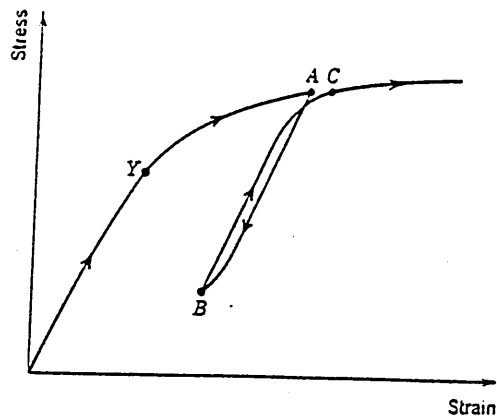


Typical creep curve showing the different stages observed during a creep test (205).

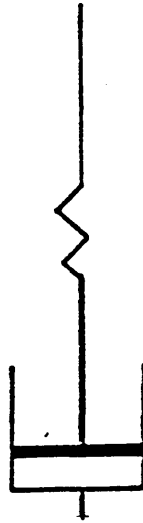


Stress relaxation of metals in tension (204).

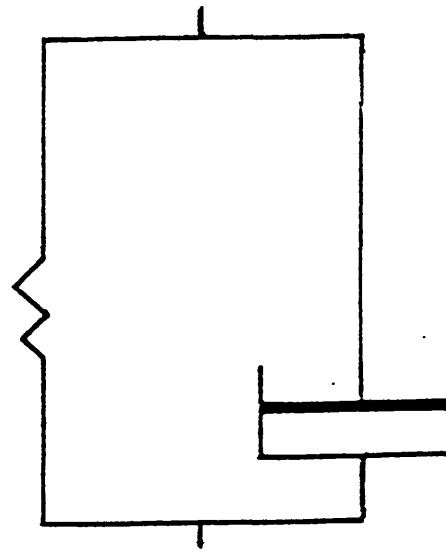
Figure 60



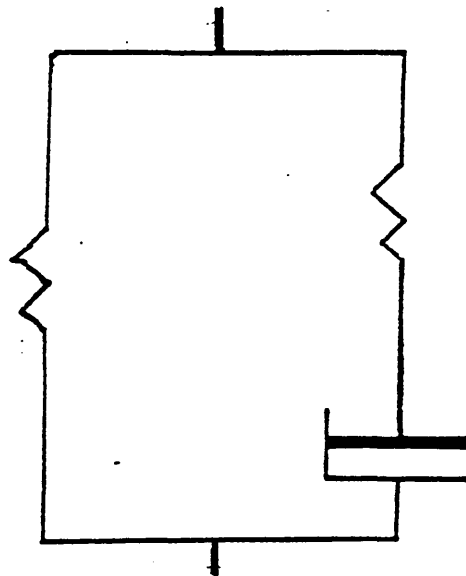
Plastic behaviour in tension test beyond the elastic limit (206).



(a) MAXWELL BODY



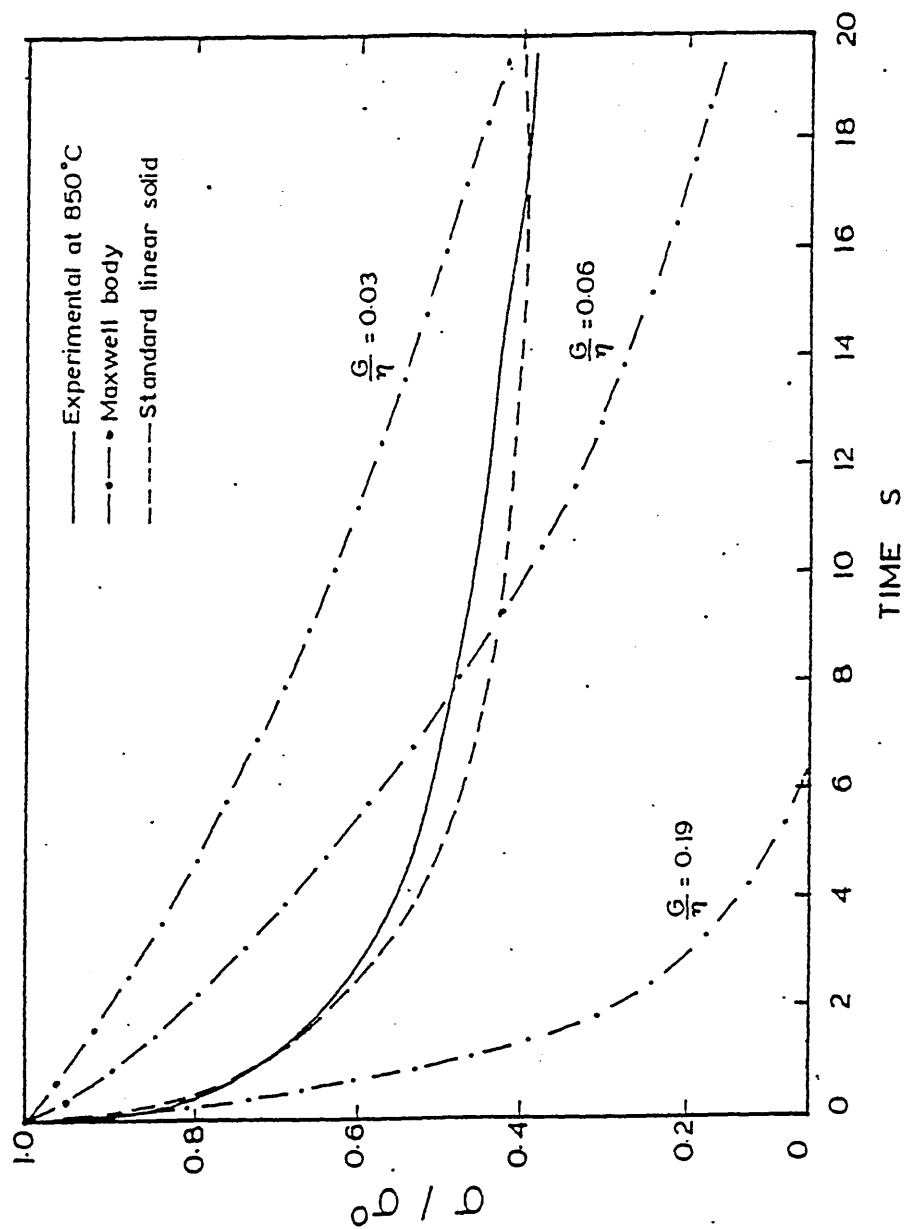
(b) KELVIN BODY



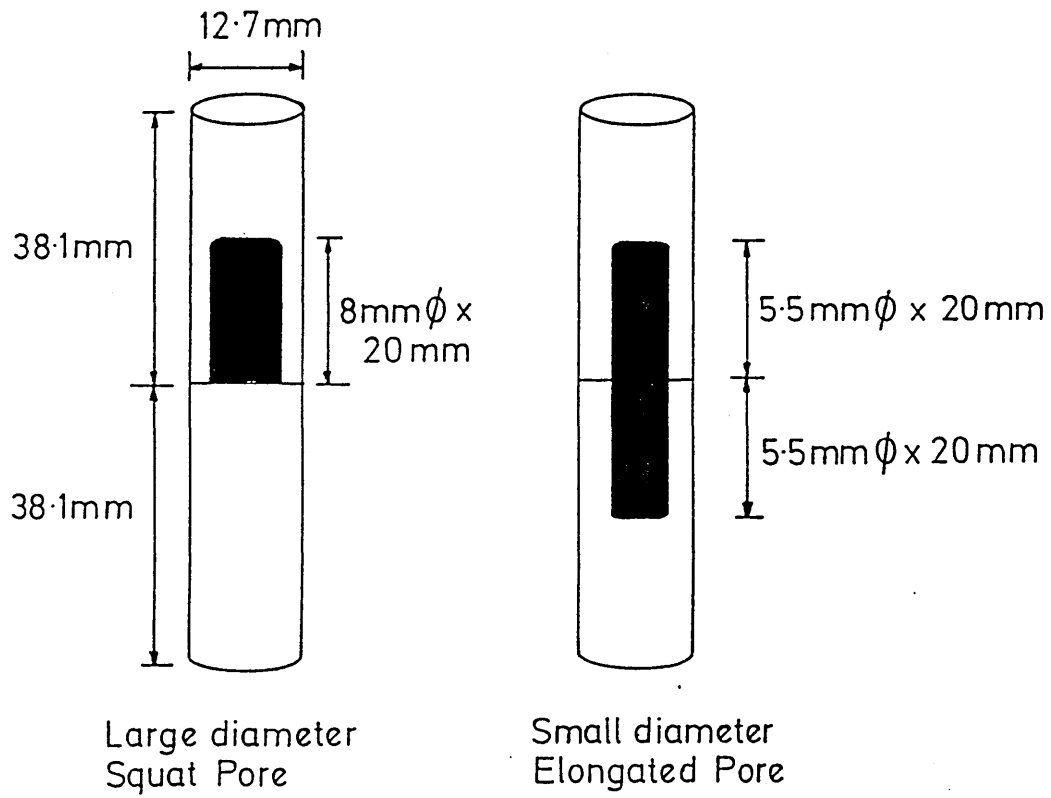
(c) STANDARD LINEAR SOLID

Mechanical models representing the visco-elastic behaviour of materials (214).

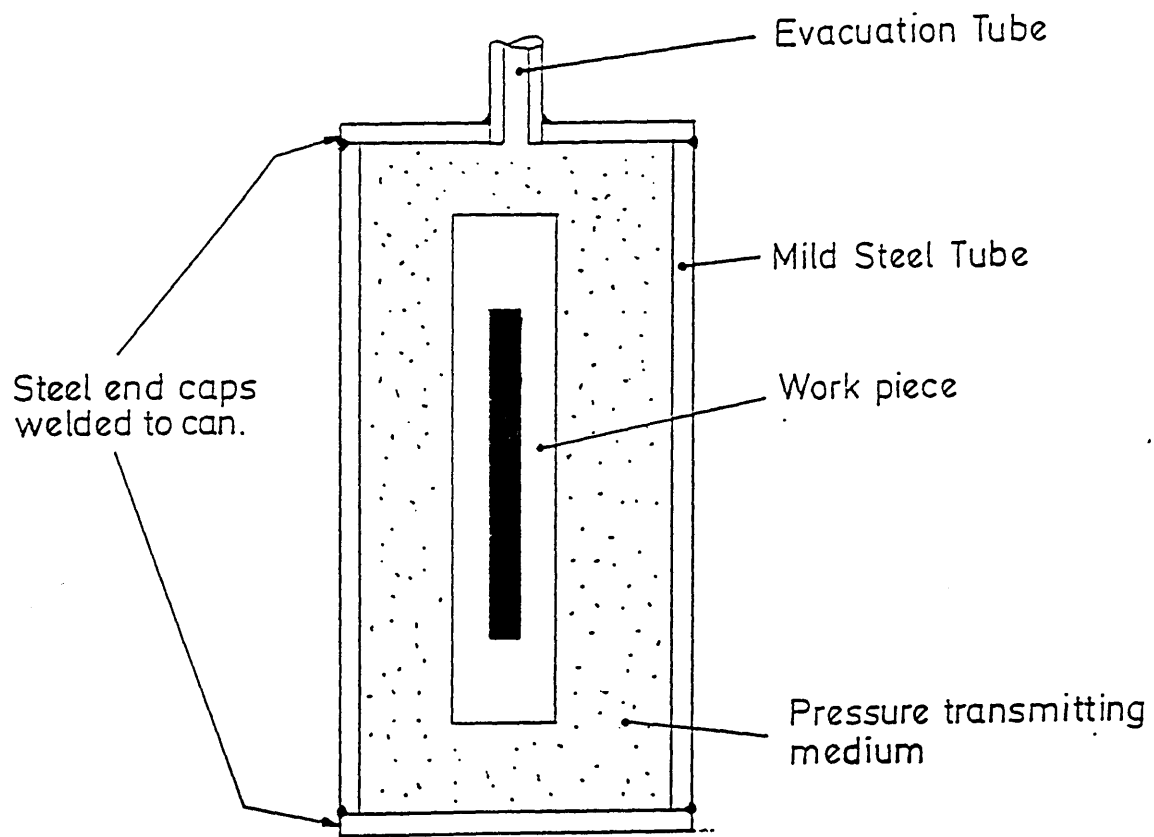
Figure 62



Comparison of predicted stress relaxation behaviour by the Maxwell body and the Standard Linear Solid with the experimental stress relaxation behaviour of 835M30 steel (214).



Pore geometry of artificial porosity specimens containing 10% surface-connected porosity.

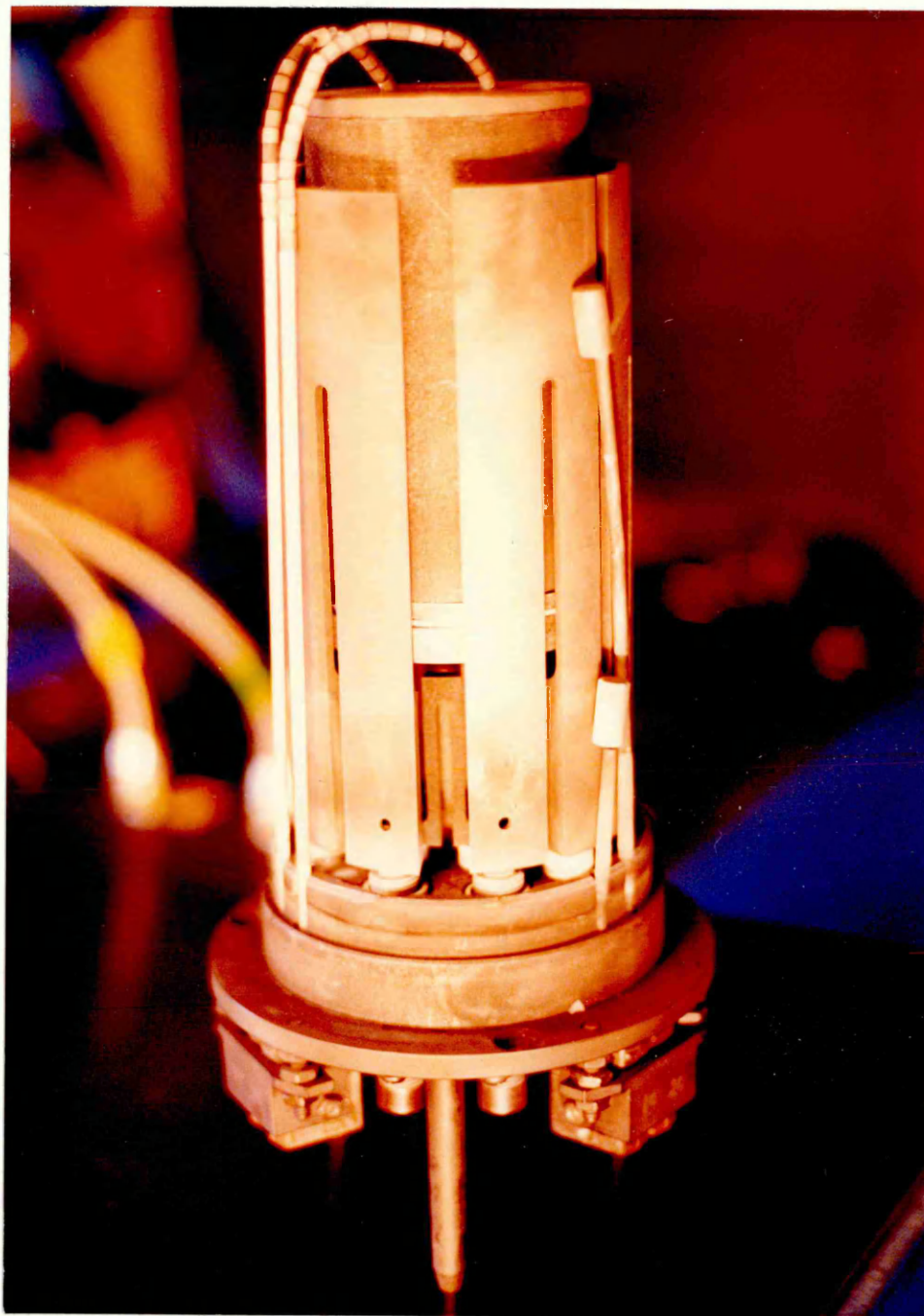


Encapsulation technique for castings containing surface-connected porosity.

Figure 65



Laboratory HIP System - ISOHIPPER
(courtesy of H.I.P Limited)



Furnace arrangement and temperature monitoring system for the laboratory HIP system.

MAX PRESSURE FOR COMPRESSOR	15000
PRESSURE CONTROL TO ATMOSPHERE	

PRESSURISATION STEP	1
HOLD TEMPERATURE	900
TEMPERATURE TOLERANCE	25
TRANSITION TIME	50
HOLD PRESSURE	15000
HOLD TIME	45

LET DOWN STEP	1
NATURAL LET DOWN ON	
HOLD TEMPERATURE	300
TEMPERATURE TOLERANCE	100
TRANSITION TIME	65
HOLD PRESSURE	0
HOLD TIME	1

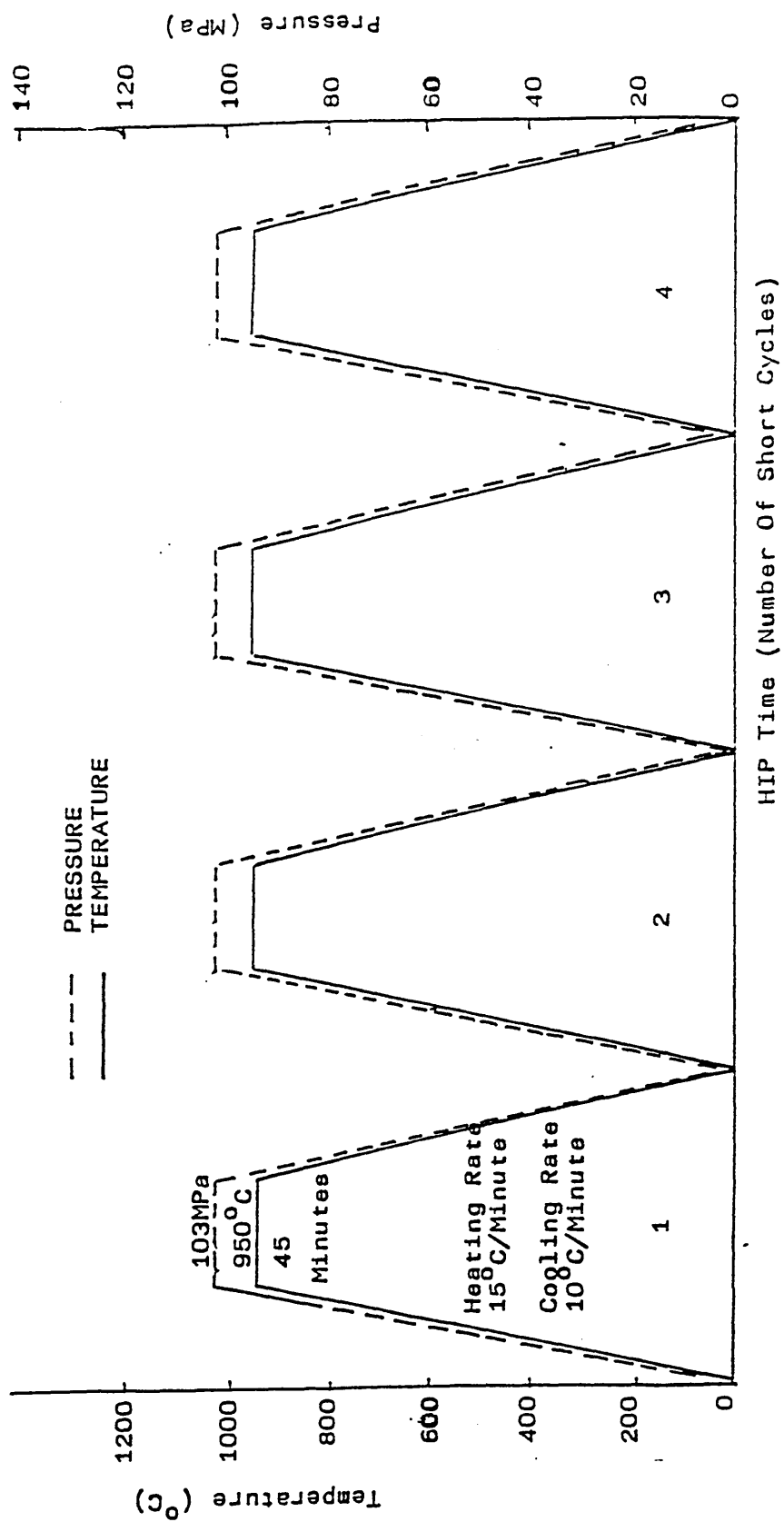
LET DOWN STEP	2
NATURAL LET DOWN ON	
HOLD TEMPERATURE	0
TEMPERATURE TOLERANCE	0
TRANSITION TIME	5
HOLD PRESSURE	0
HOLD TIME	5

LET DOWN STEP	3
NATURAL LET DOWN OFF	
LET DOWN TO ATMOSPHERE	
HOLD TEMPERATURE	0
TEMPERATURE TOLERANCE	0
TRANSITION TIME	0
HOLD PRESSURE	300
HOLD TIME	1

Typical HIP program for HIP parameters of:

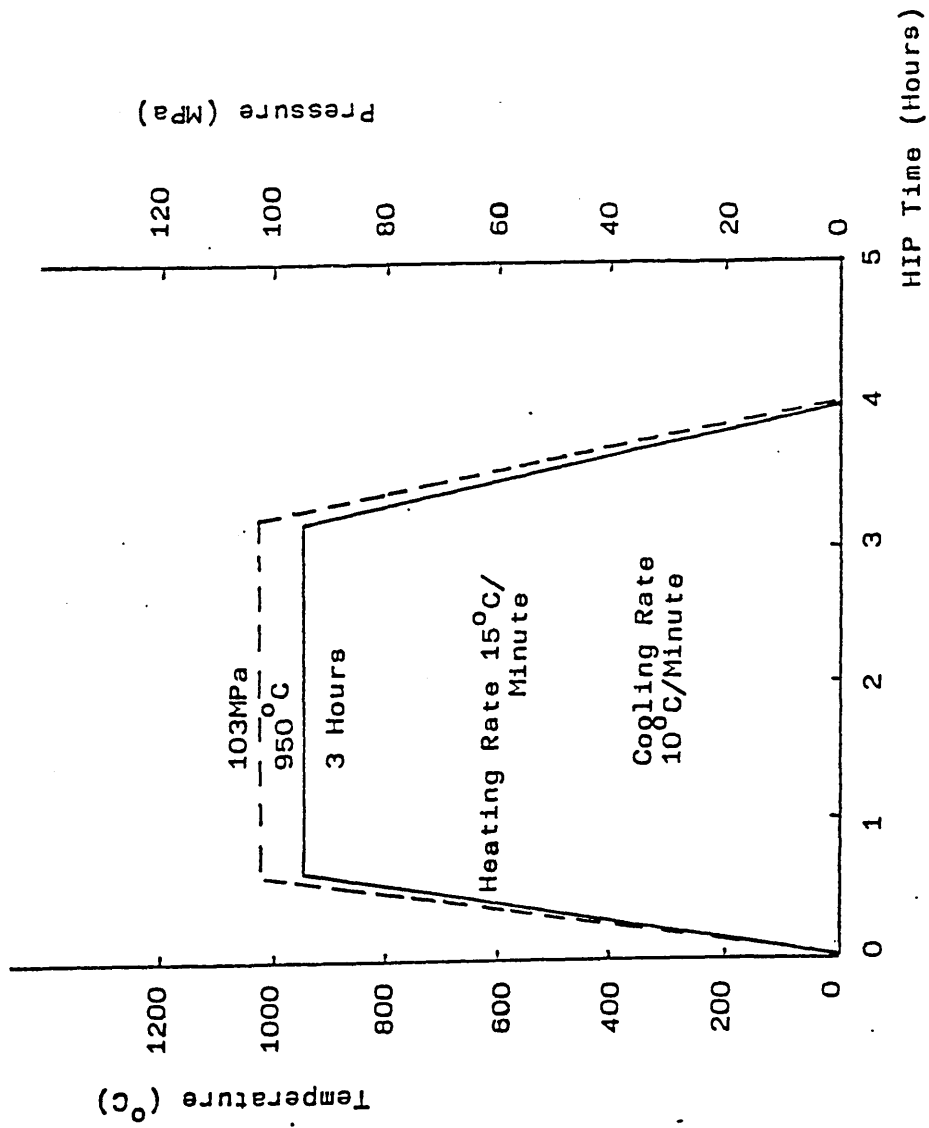
950°C / 103MPa (15000psi) / 45 minutes

Figure 68



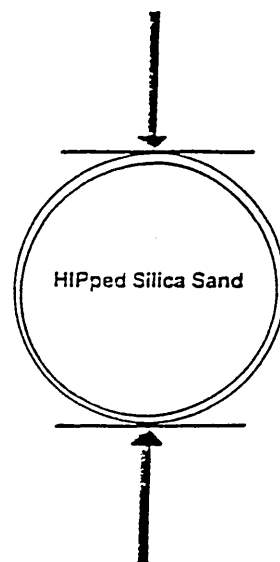
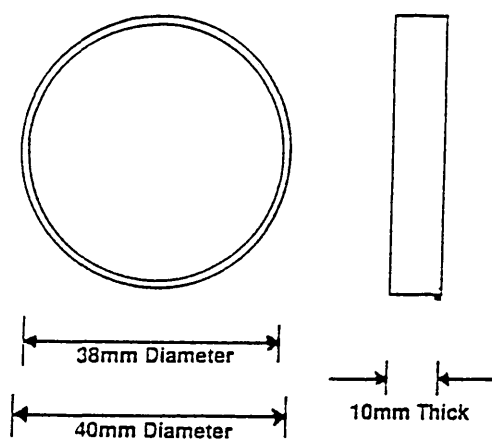
Schematic illustration of 4 successive (Type I) 45 minute HIP cycles.

Figure 69



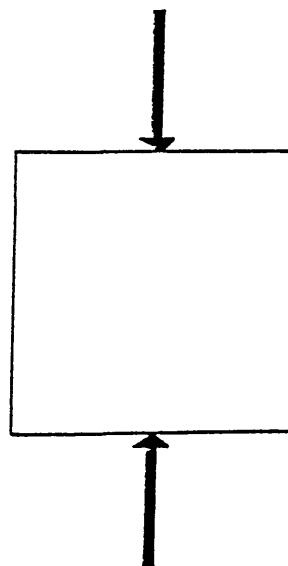
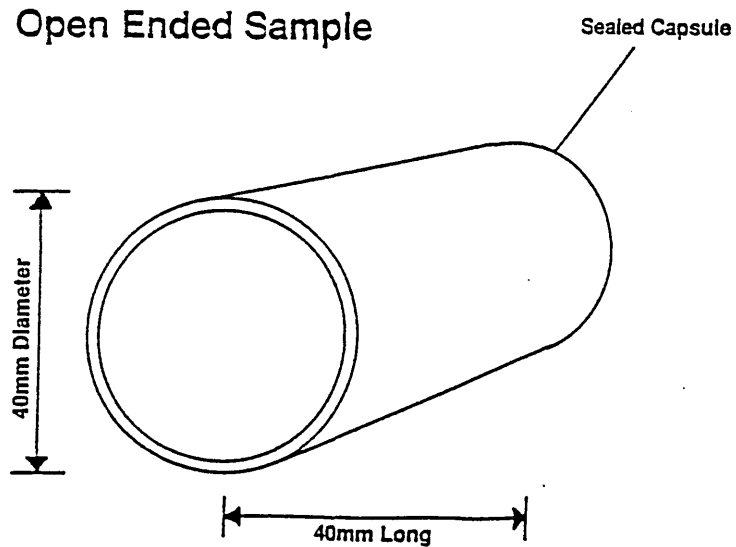
Schematic illustration of a single continuous 3 hour (Type II) HIP cycle.

Ring Sample



Unidirectional
Load Applied

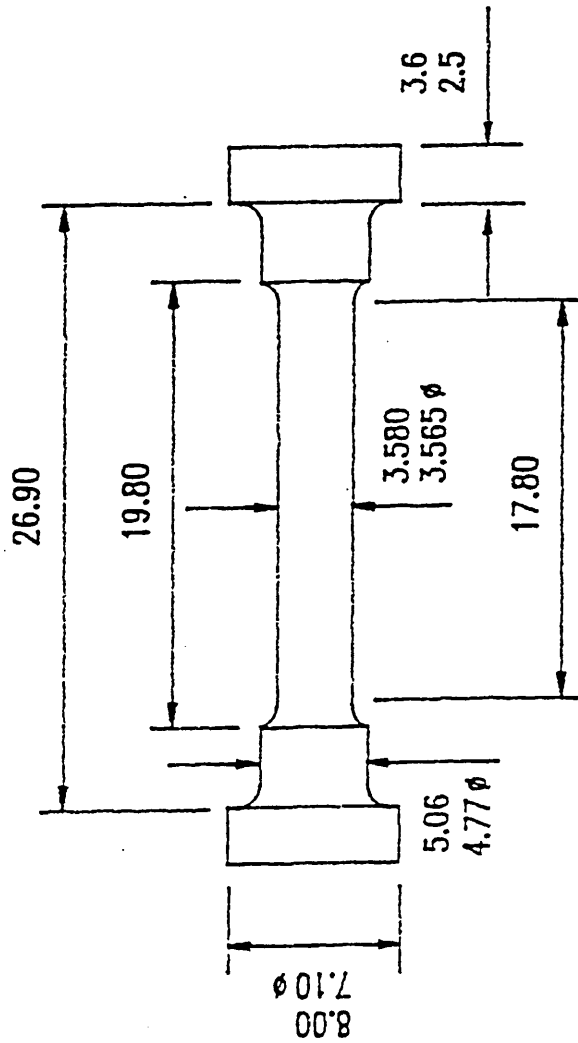
Open Ended Sample



Test specimens used to determine the compressive strength of HIPped desert-based silica sand.

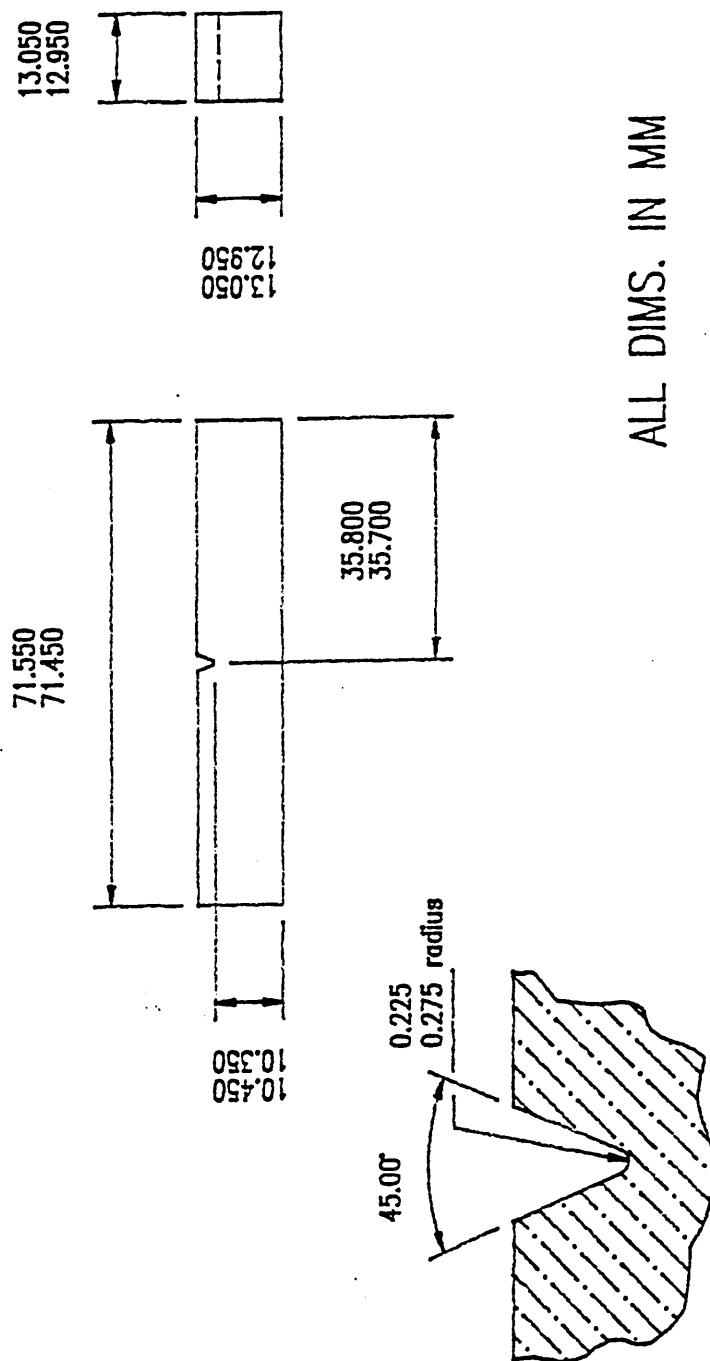
Figure 71

RADII-1mm
AREA sq.mm. 10
THEORETICAL
DIAMETER 3.568



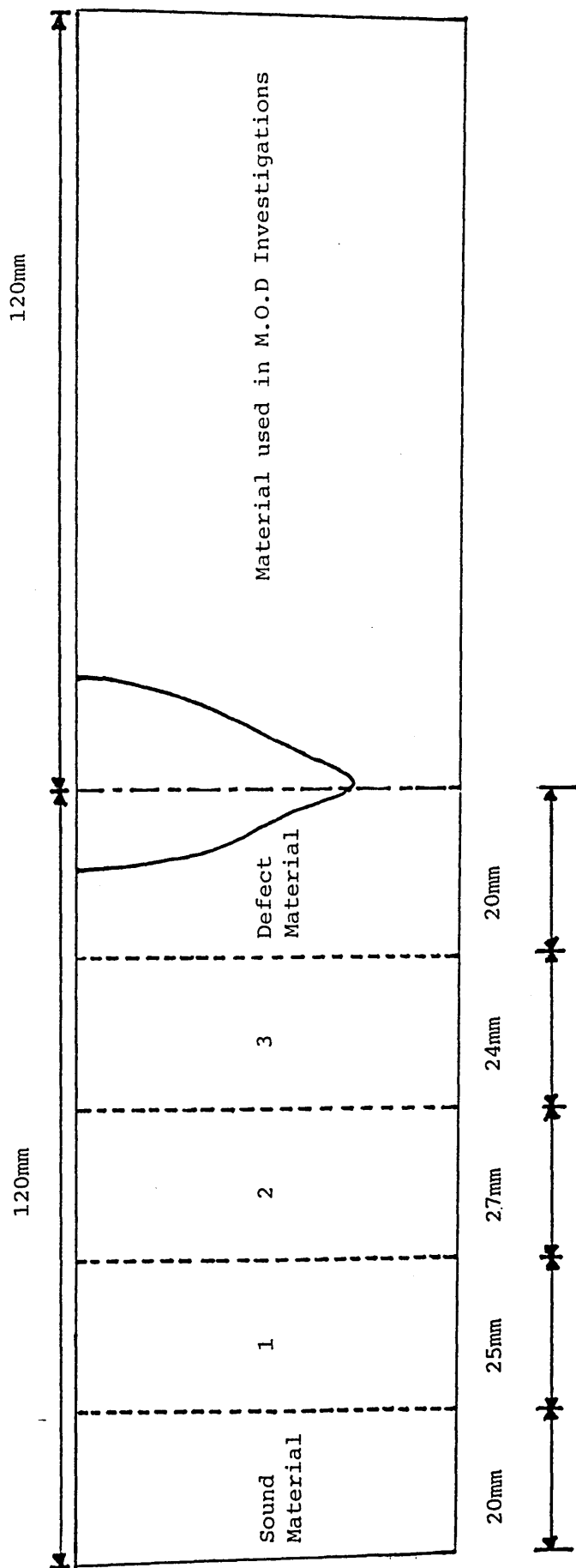
Metric A tensile specimen recommended for the testing of cast metals.

Figure 72

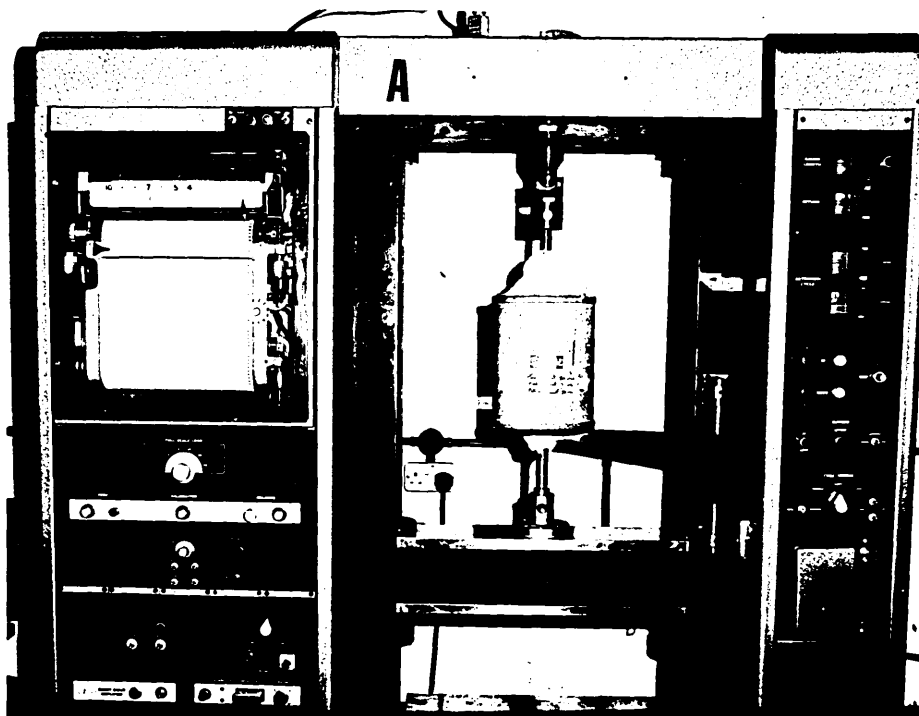


Charpy impact toughness test specimen - 45 ° notch.

Figure 73

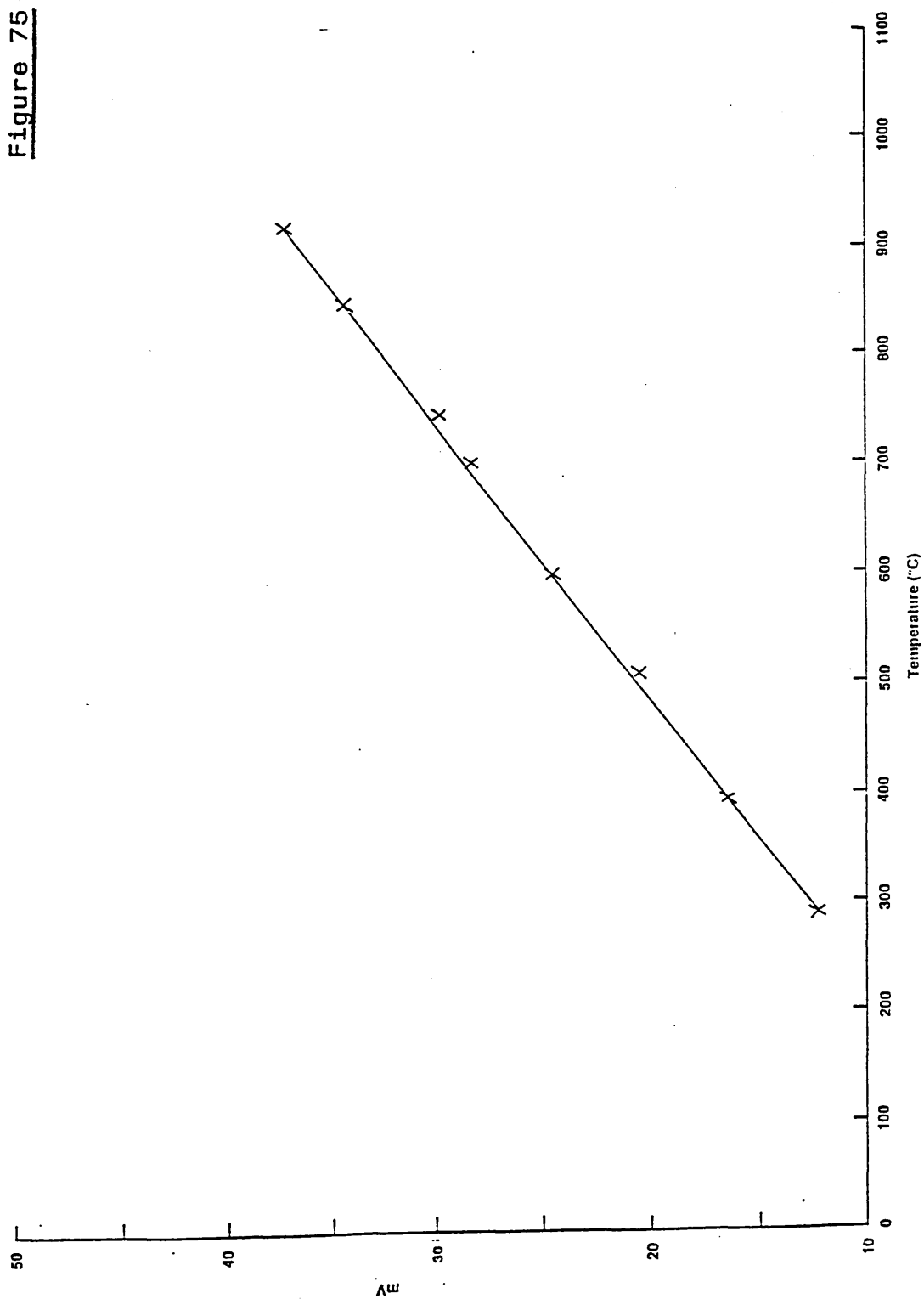


Cut up evaluation of a plate casting which contained a large shrinkage defect prior to HIPping.



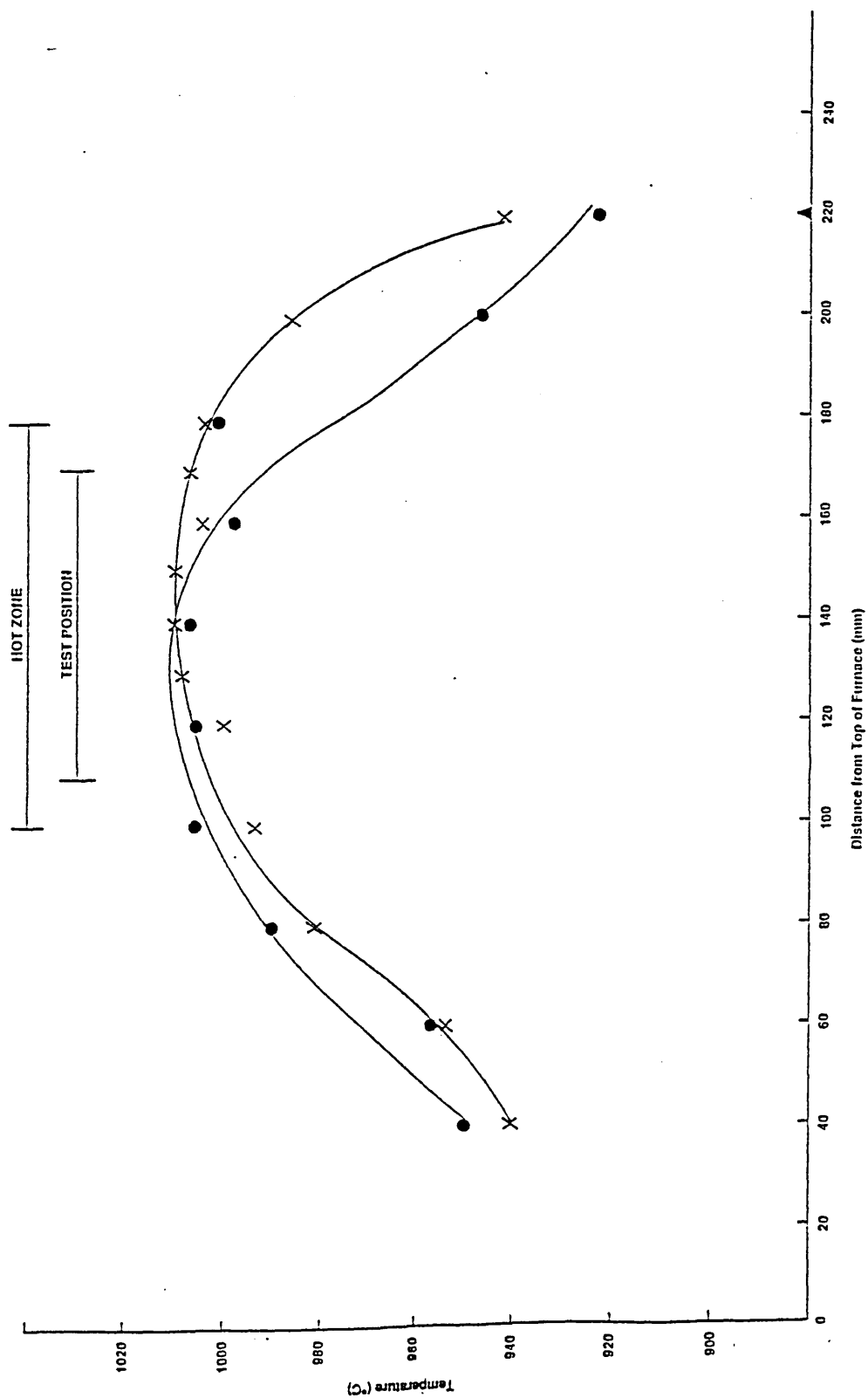
Test apparatus for high temperature stress relaxation, hot ductility and flow stress determinations.

Figure 75



Furnace calibration: relationship between temperature and voltage.

Figure 76



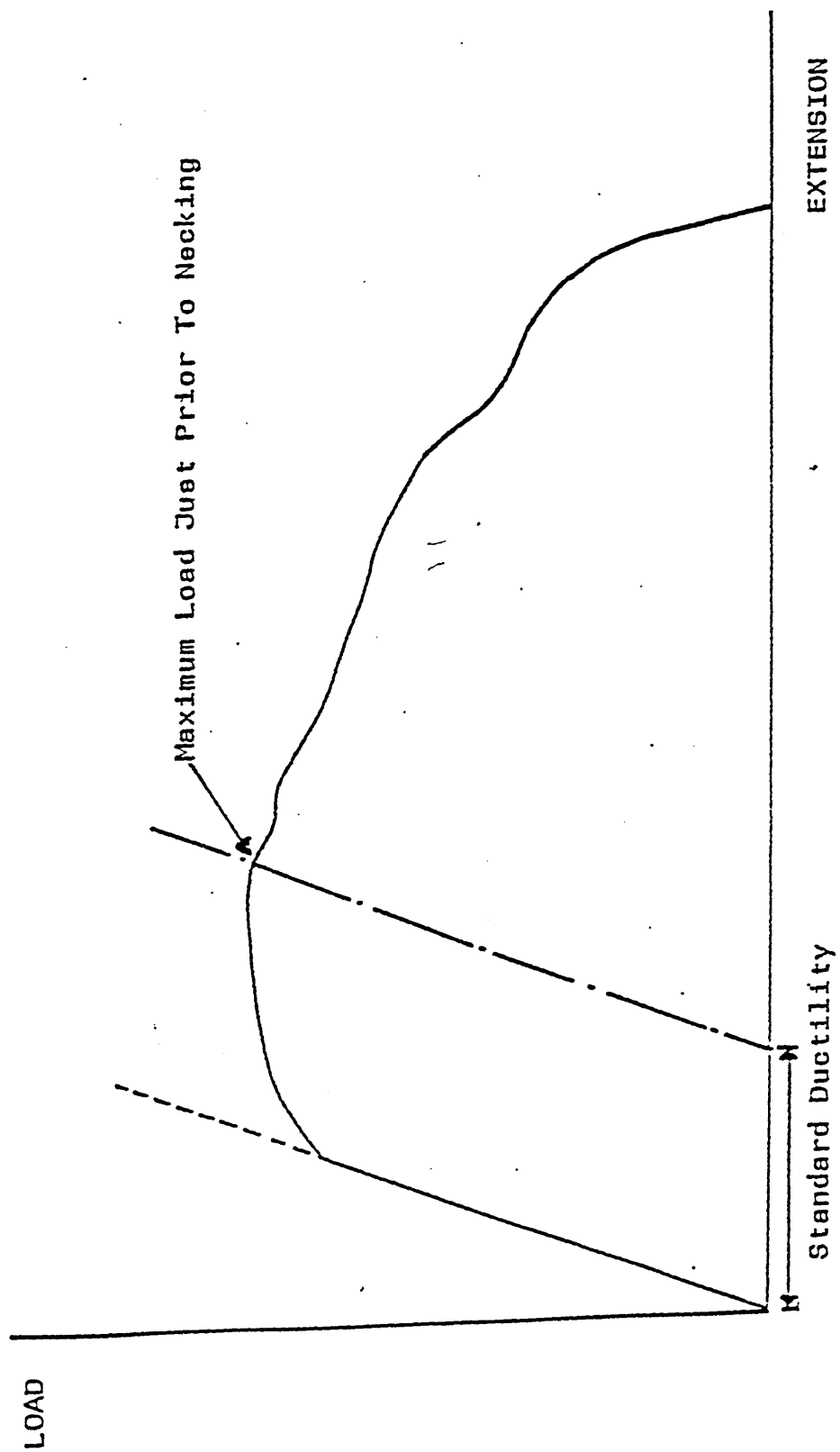
**Calibration of furnace hot zone:
relationship between temperature and distance from the top of the furnace.**

Technical drawing of a mechanical part with the following dimensions and tolerances:

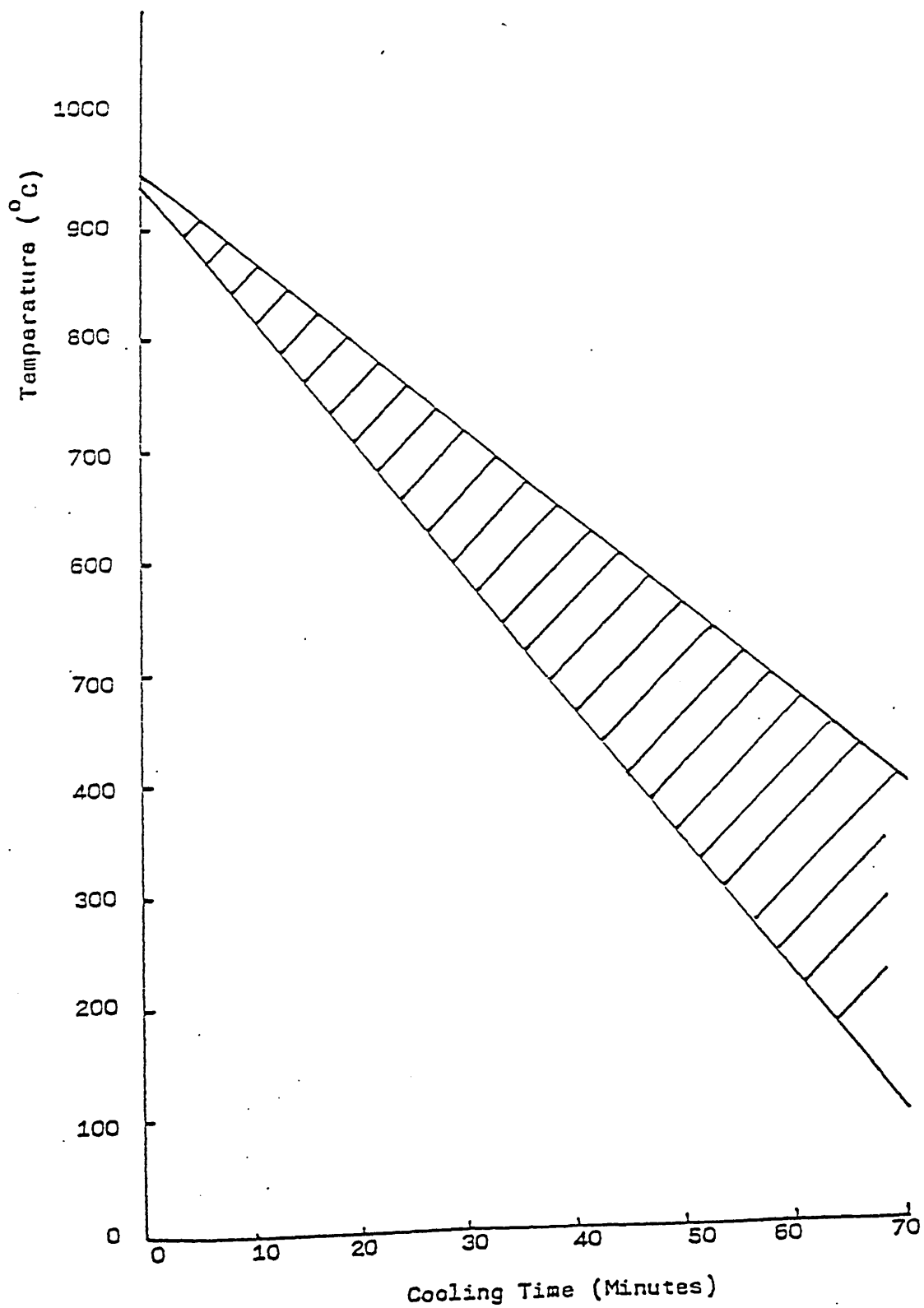
- Overall length: 50.00 $+0.4$ / -0.4
- Distance from left end to first feature: 12.50 $+0.4$ / -0.4
- Distance between features: 25.00 $+0.2$ / -0.2
- Distance from second feature to right end: 4.50 $+0$ / -1
- Feature 1 (Left): R4 $+0.2$ / -0.2
- Feature 2 (Middle): 4.51 ϕ $+0$ / -0.02
- Feature 3 (Right): 60° chamfer, 3.8 ϕ $+0$ / -0.1 , 1.6 ϕ $+0.2$ / -0.1
- Both ends: 0.6 CHAM AT 45°
- Section A-A: 5/16" WHIT (BOTH ENDS)
- Section B-B: 3.8 ϕ $+0$ / -0.1

411

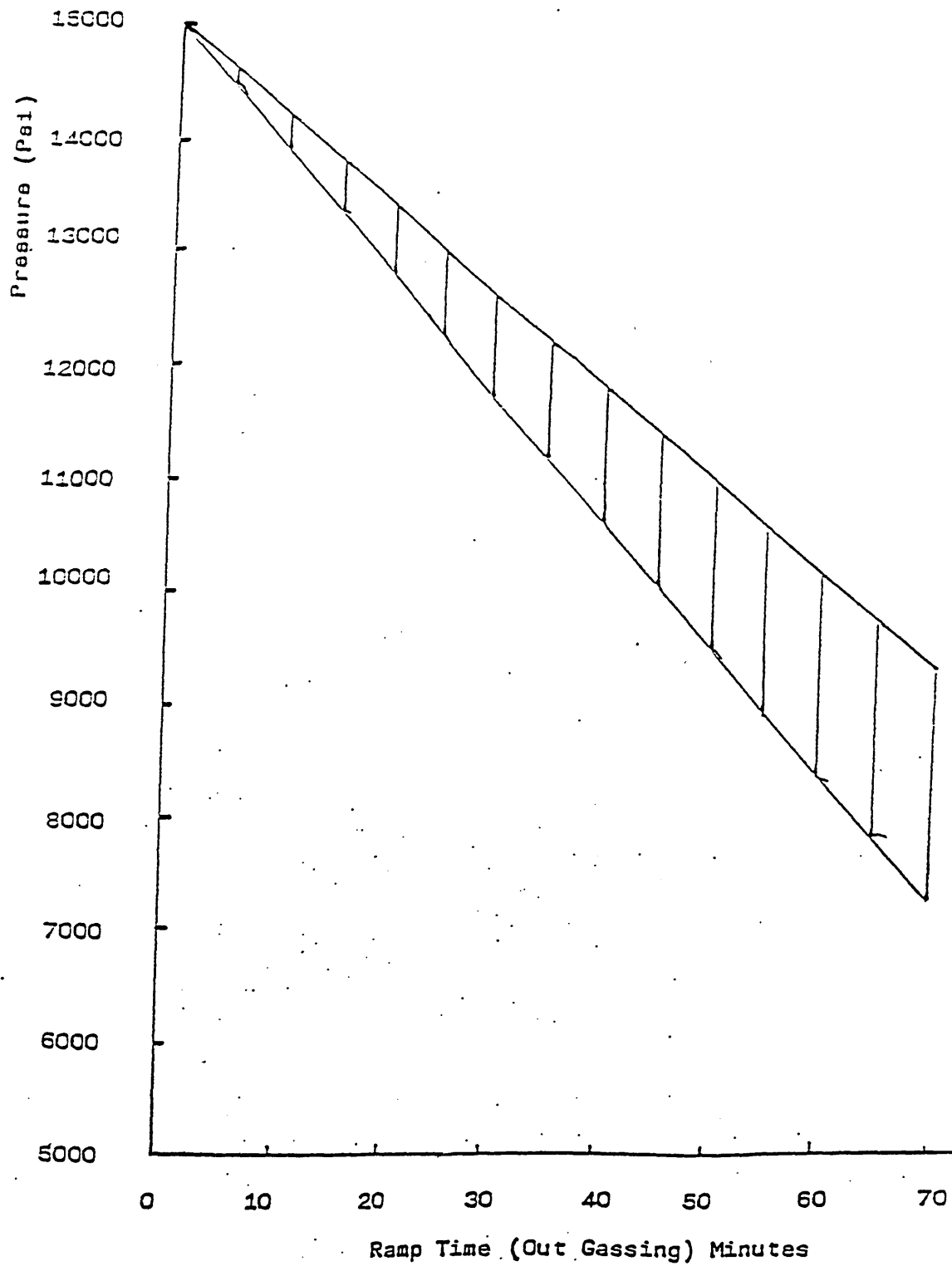
Figure 78



Typical load - extension curve obtained during flow stress evaluations.

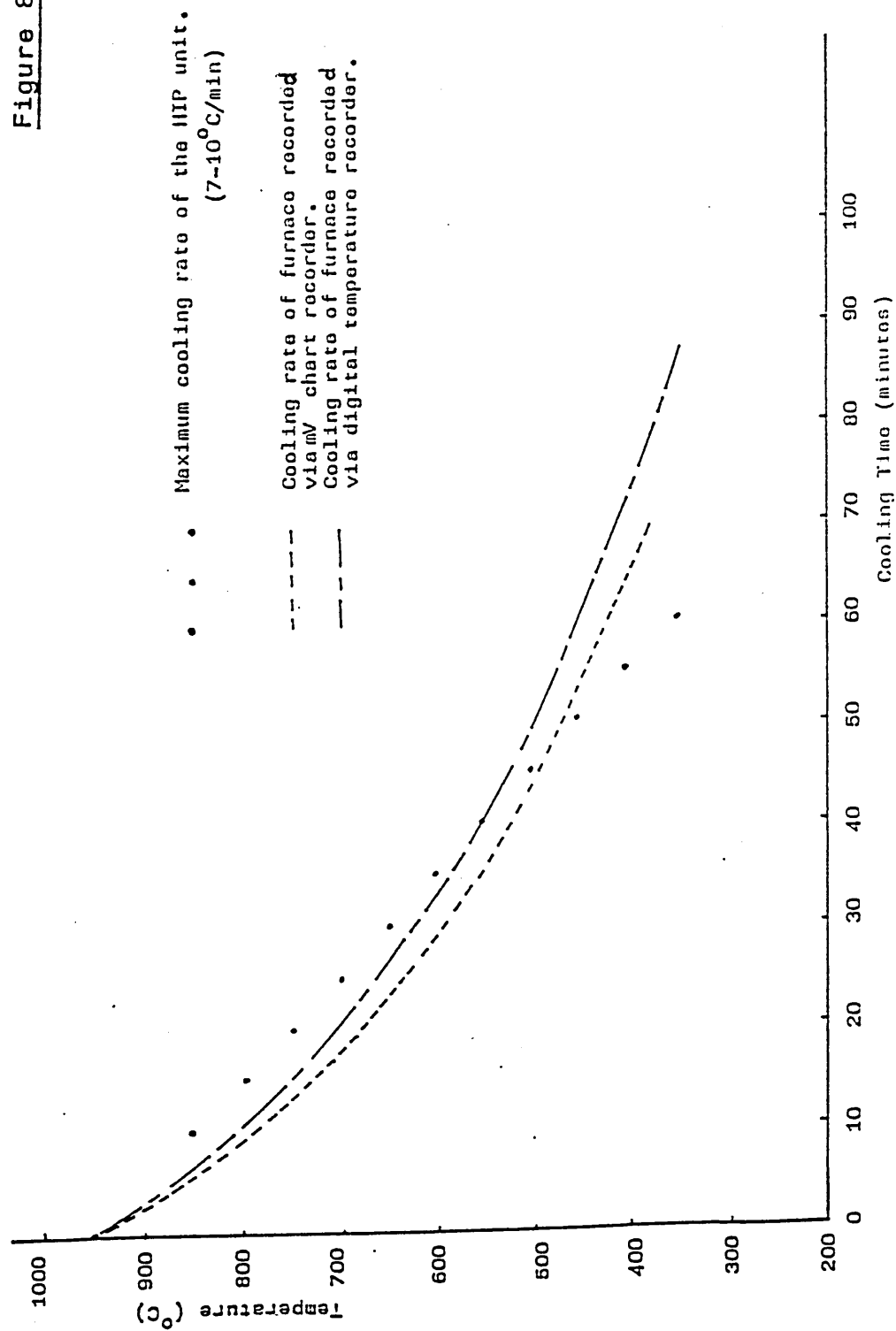


Typical cooling rate used for HIPping experiments



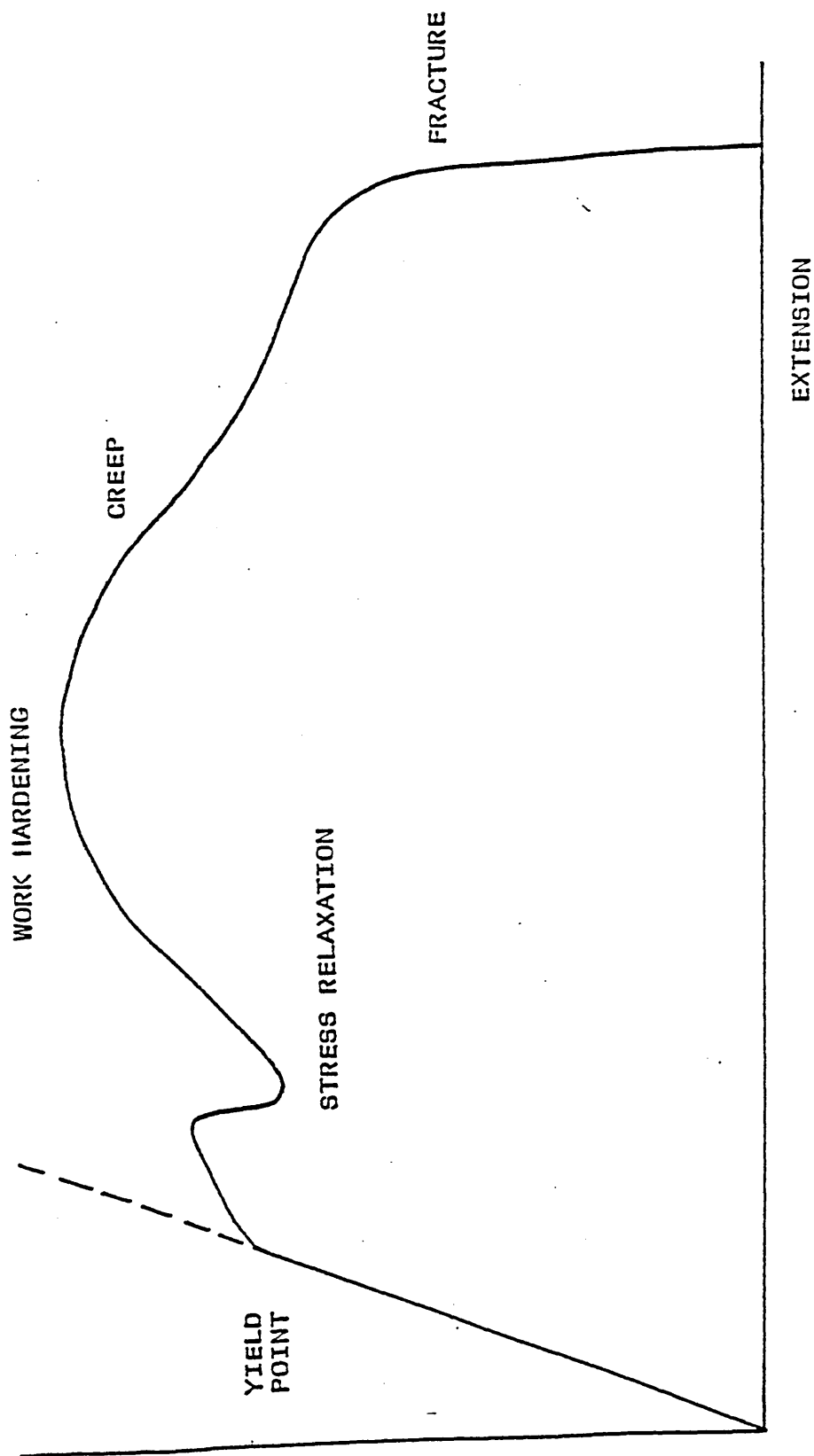
Typical depressurisation (out-gassing) rate used for HIPping experiments.

Figure 81

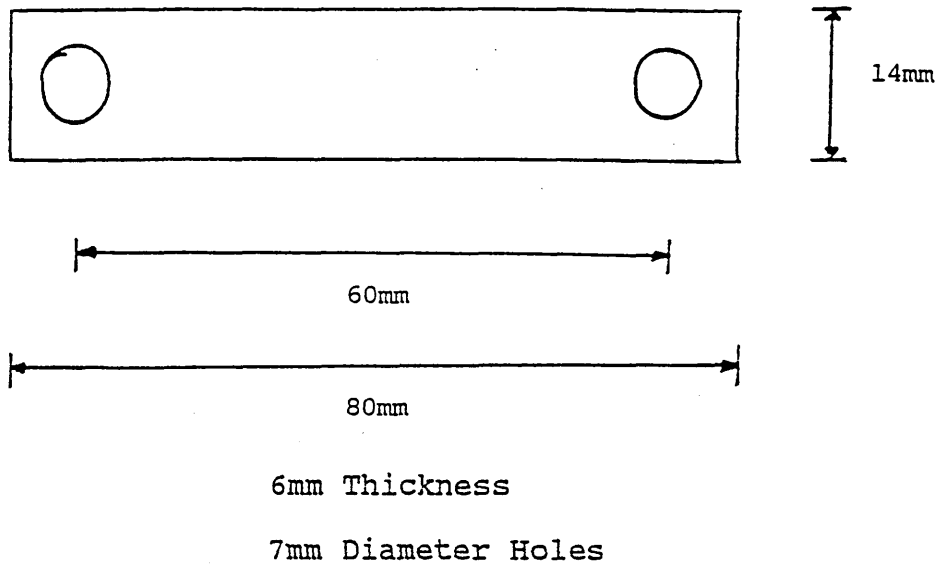


Typical cooling rates of the laboratory HIP system and the furnace used
in constant load ductility tests.

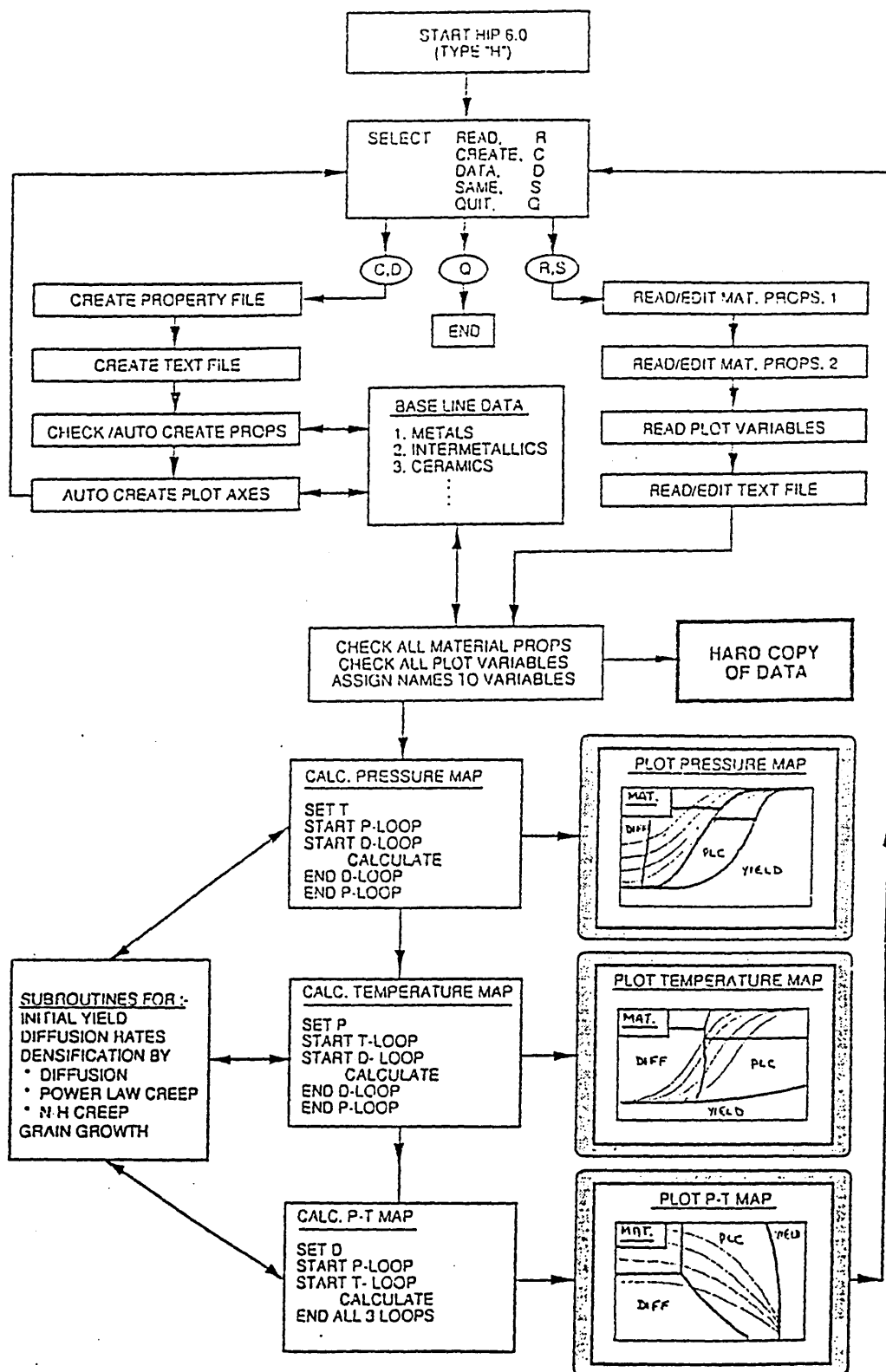
Figure 82



Schematic illustration of a load - extension curve obtained during constant load ductility tests.

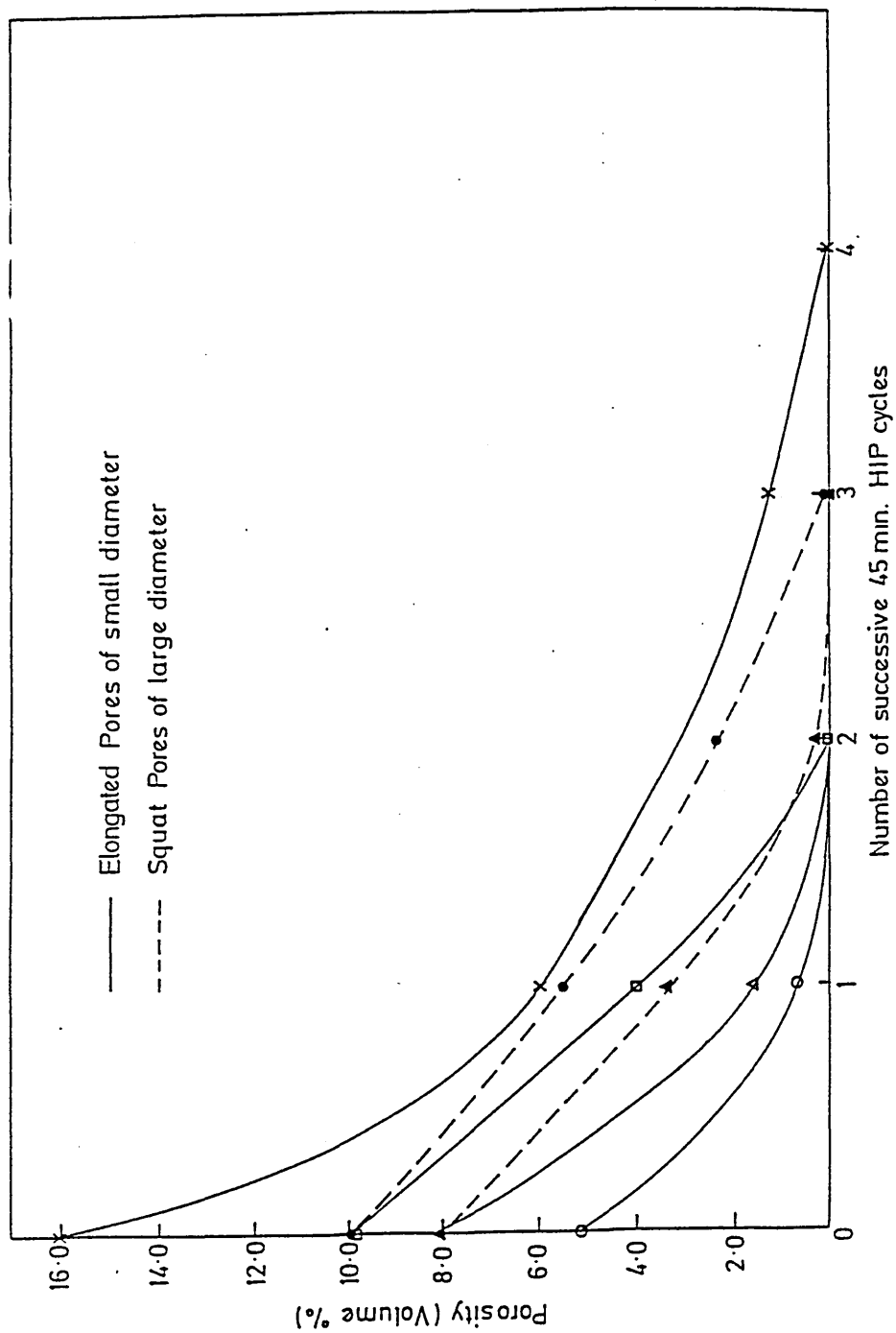


Dimensions of impingement test specimens.

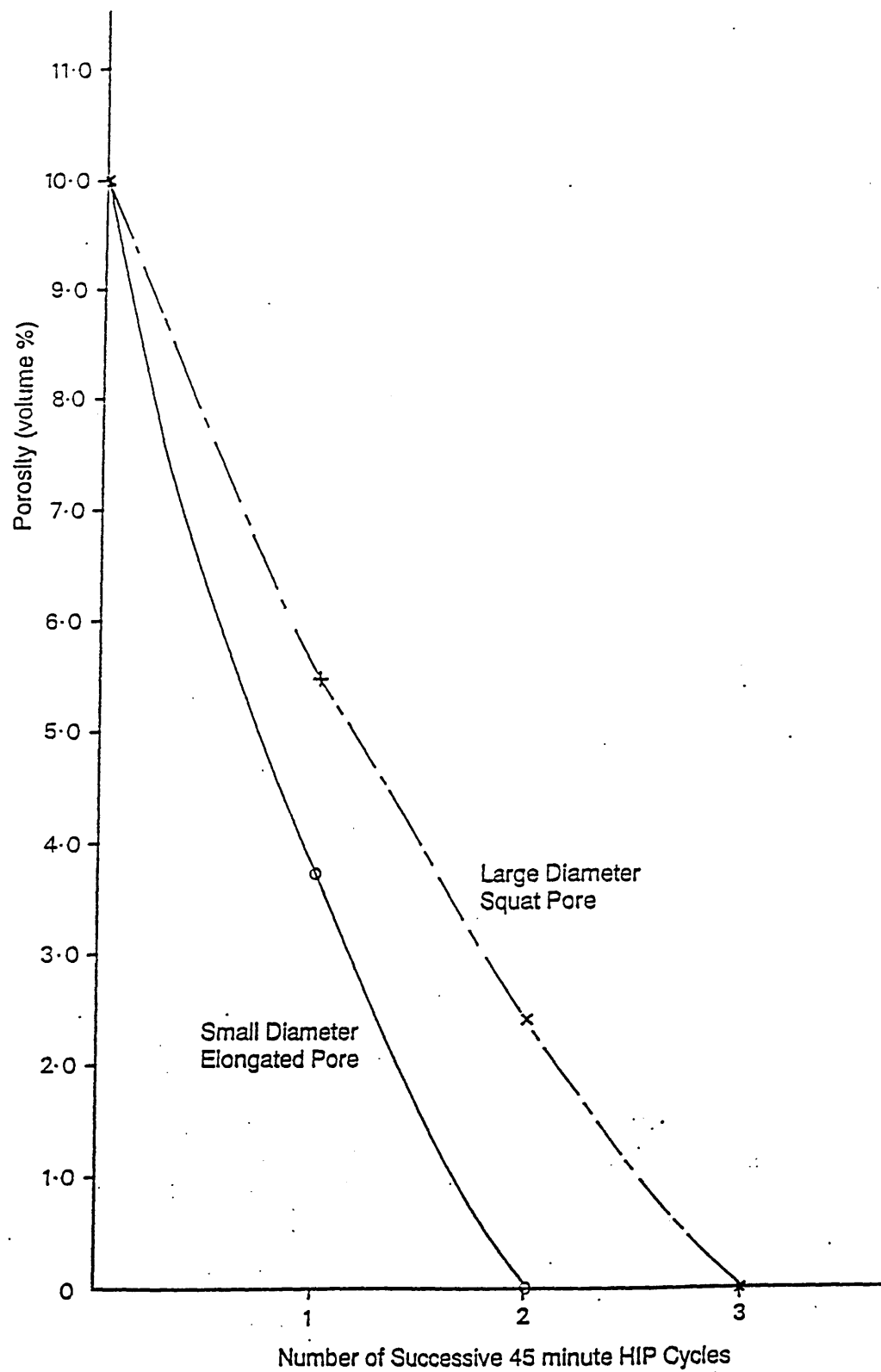


Flow chart rerepresenting operation of HIP 6.0 for the construction of HIP maps (10).

Figure 85

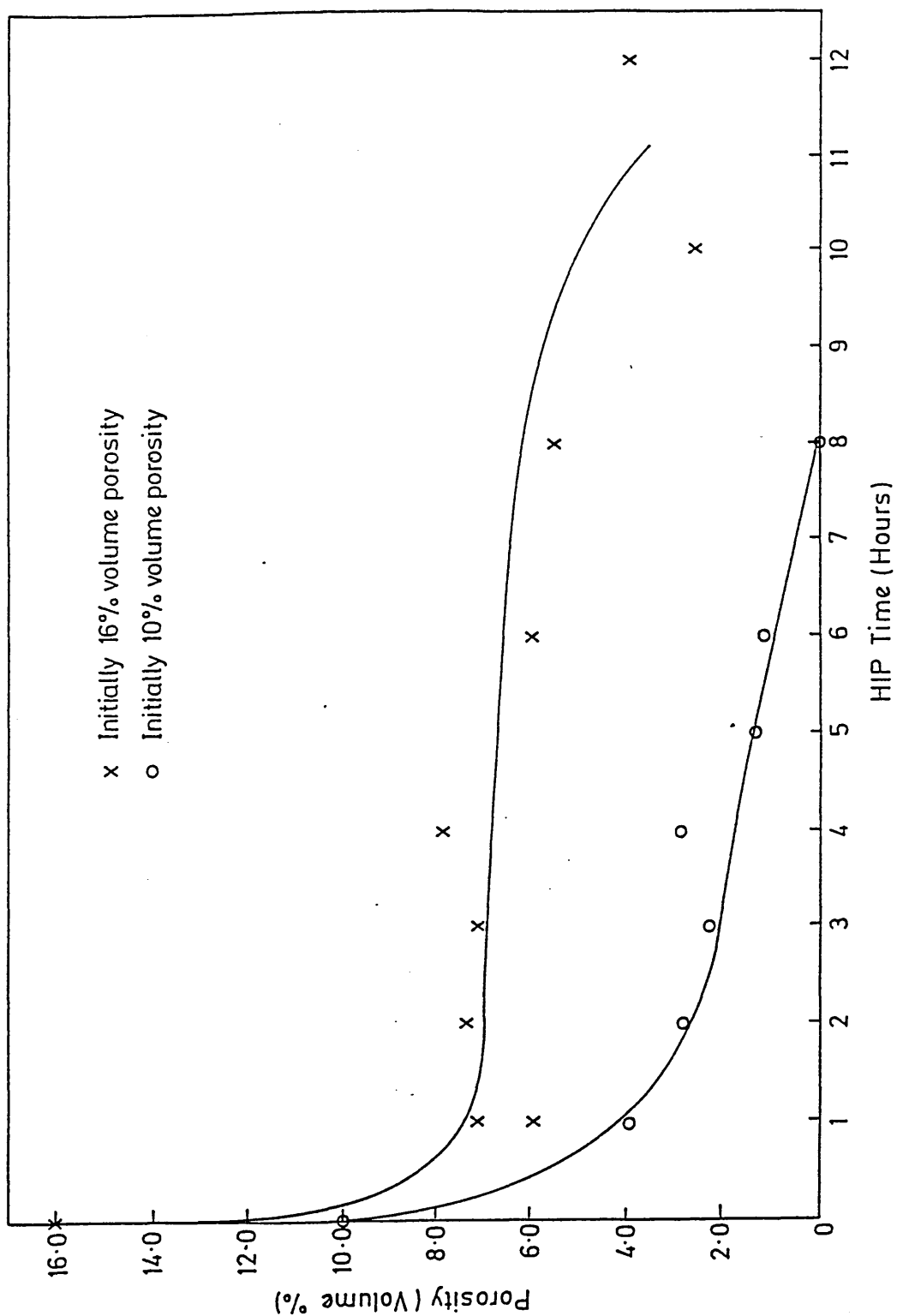


Effect of successive 45 minute (Type I) HIP cycles on the densification of encapsulated artificial porosity specimens containing surface-connected porosity.



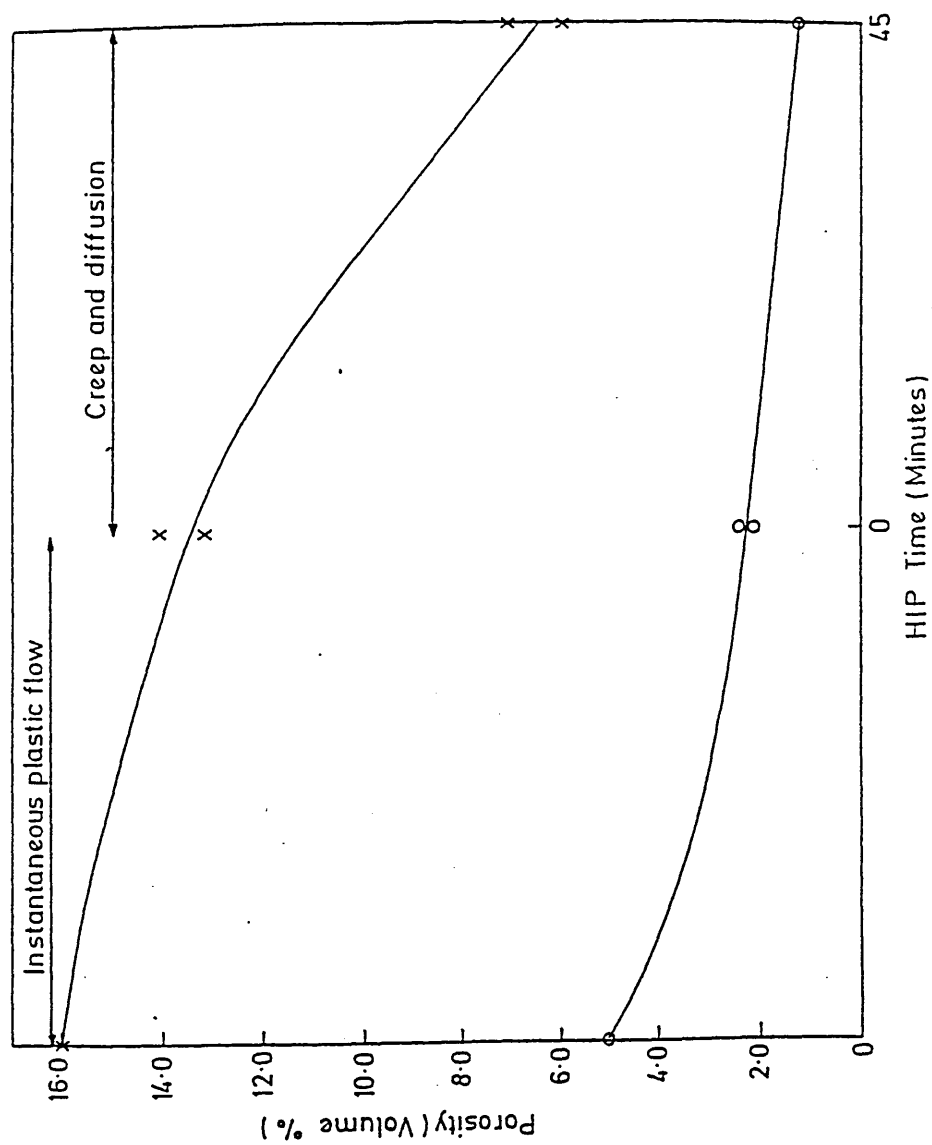
Effect of pore geometry on densification by successive short (Type I) HIP cycles.

Figure 87



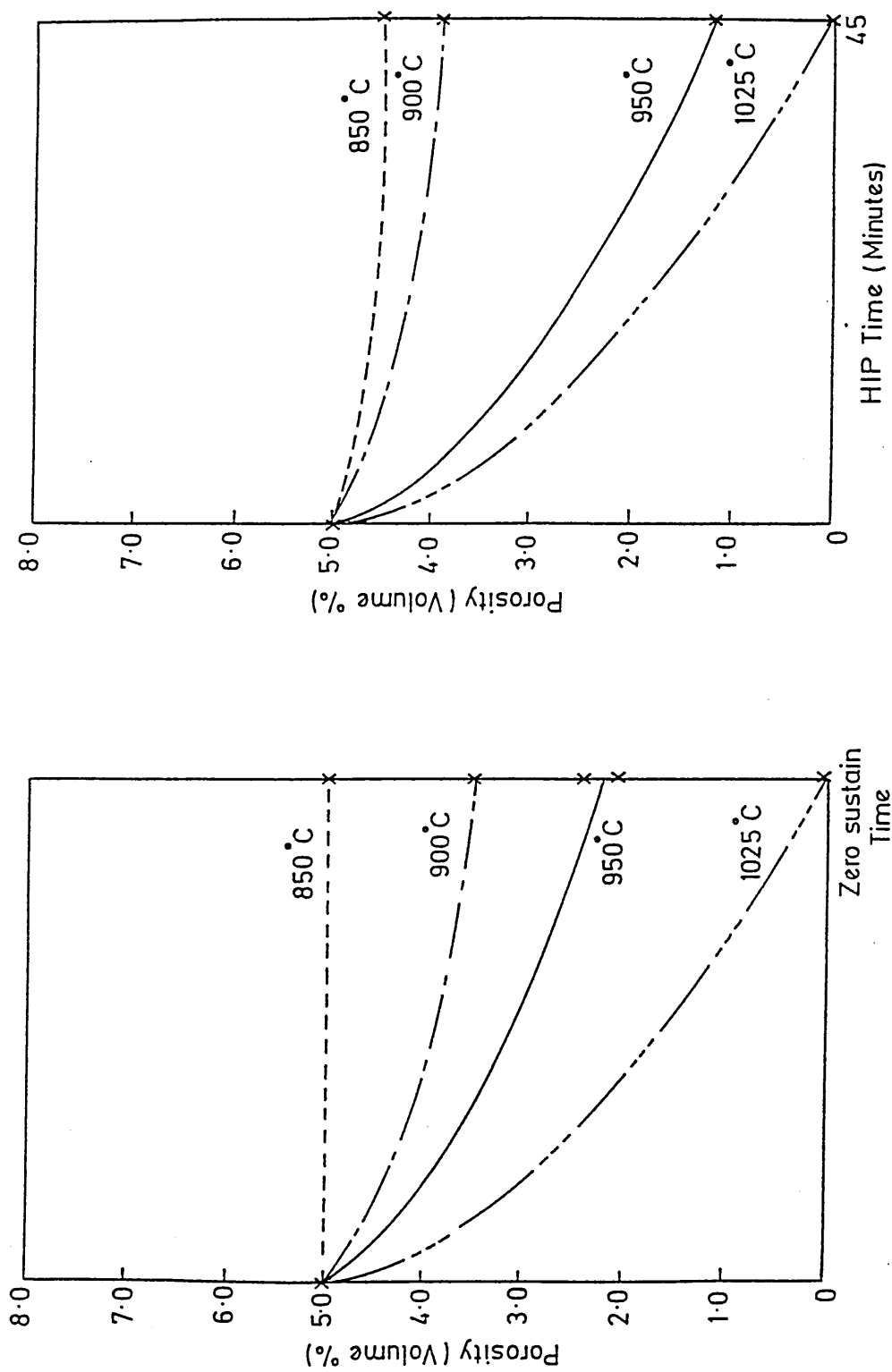
Effect of continuous (Type II) HIP cycles on the closure of elongated pores.

Figure 88



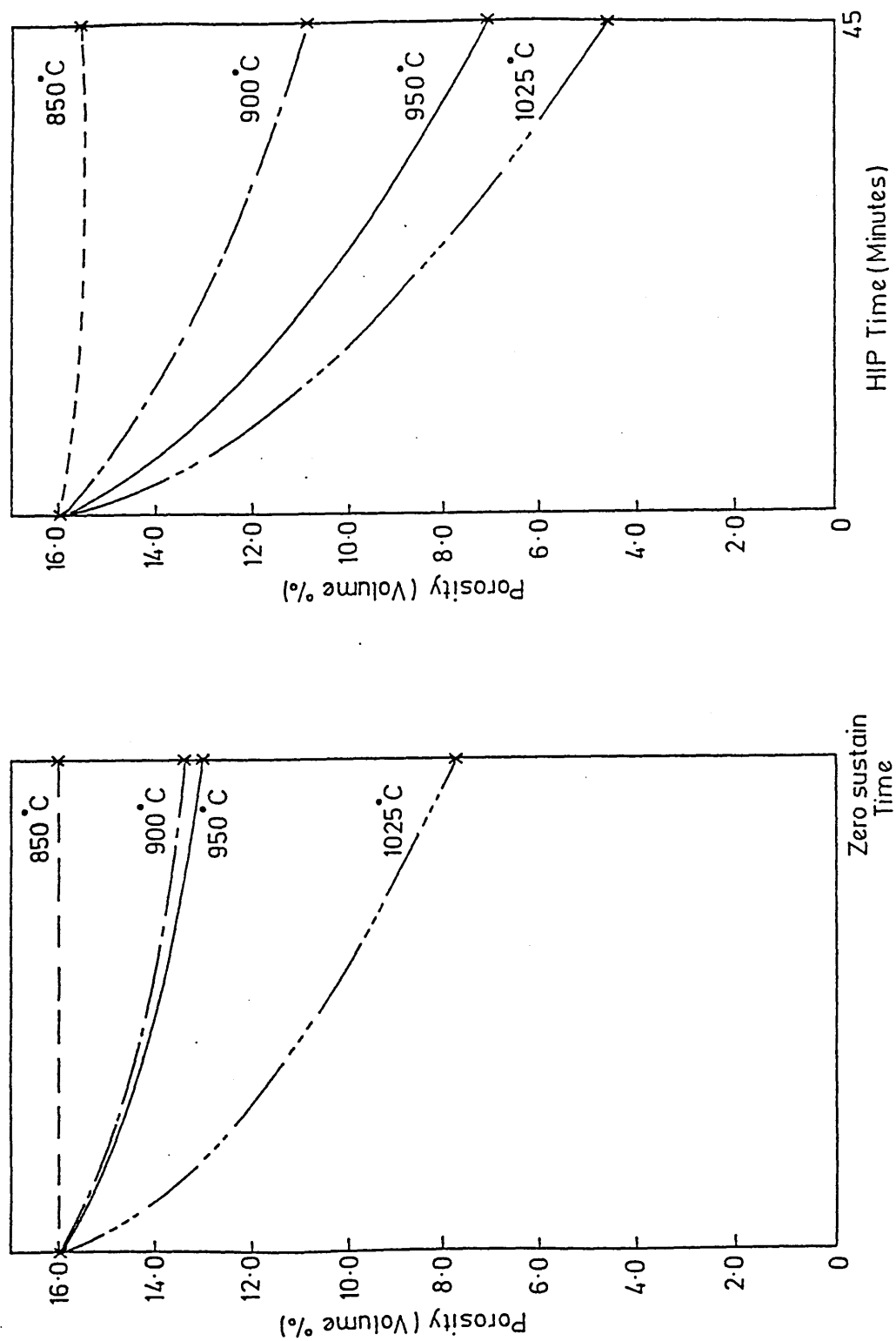
Effect of HIP time on the recovery rate and densification mechanisms of encapsulated artificial porosity specimens containing surface-connected porosity.

Figure 89

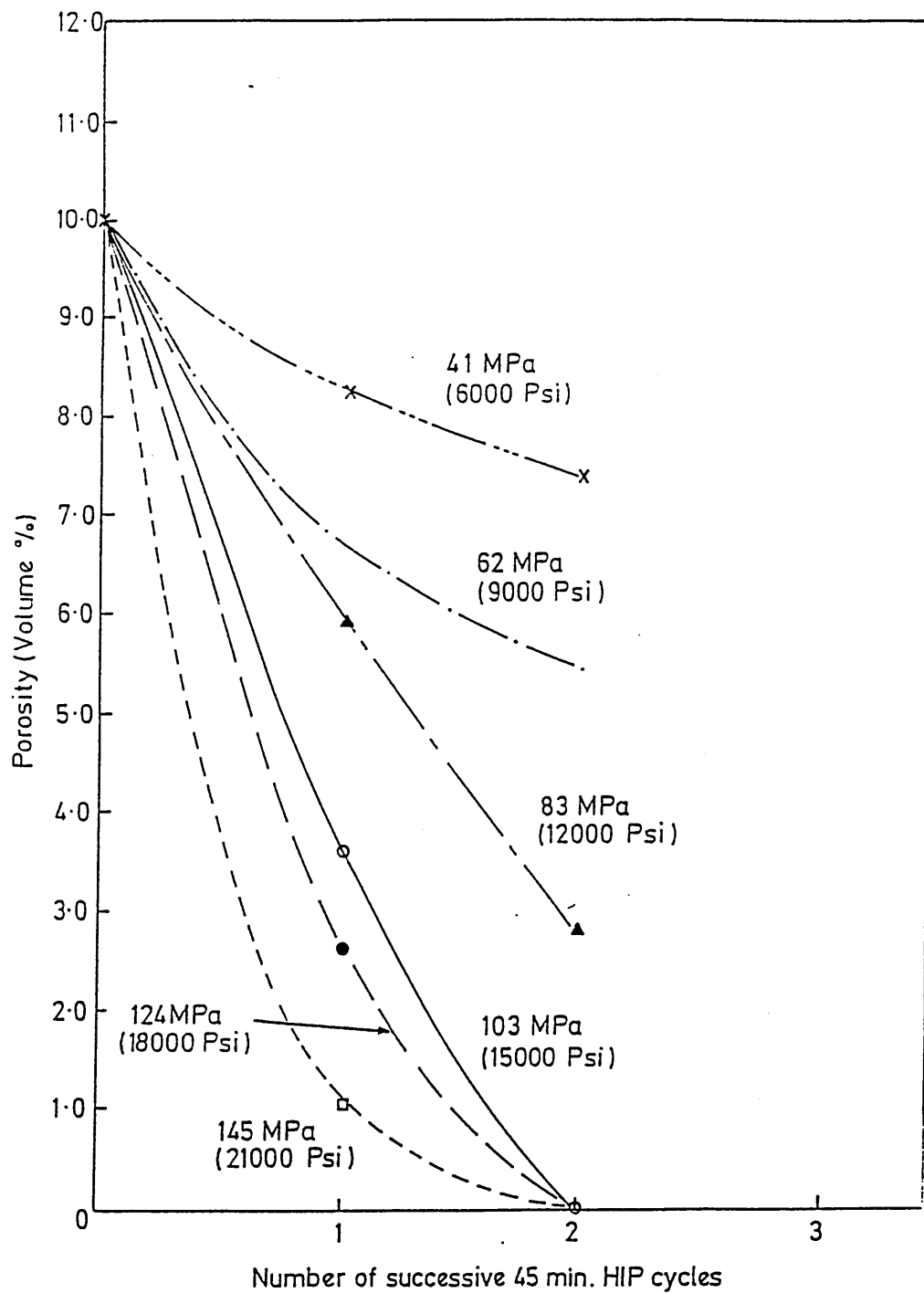


Effect of HIP temperature on the closure of 5% surface-connected porosity.

Figure 90

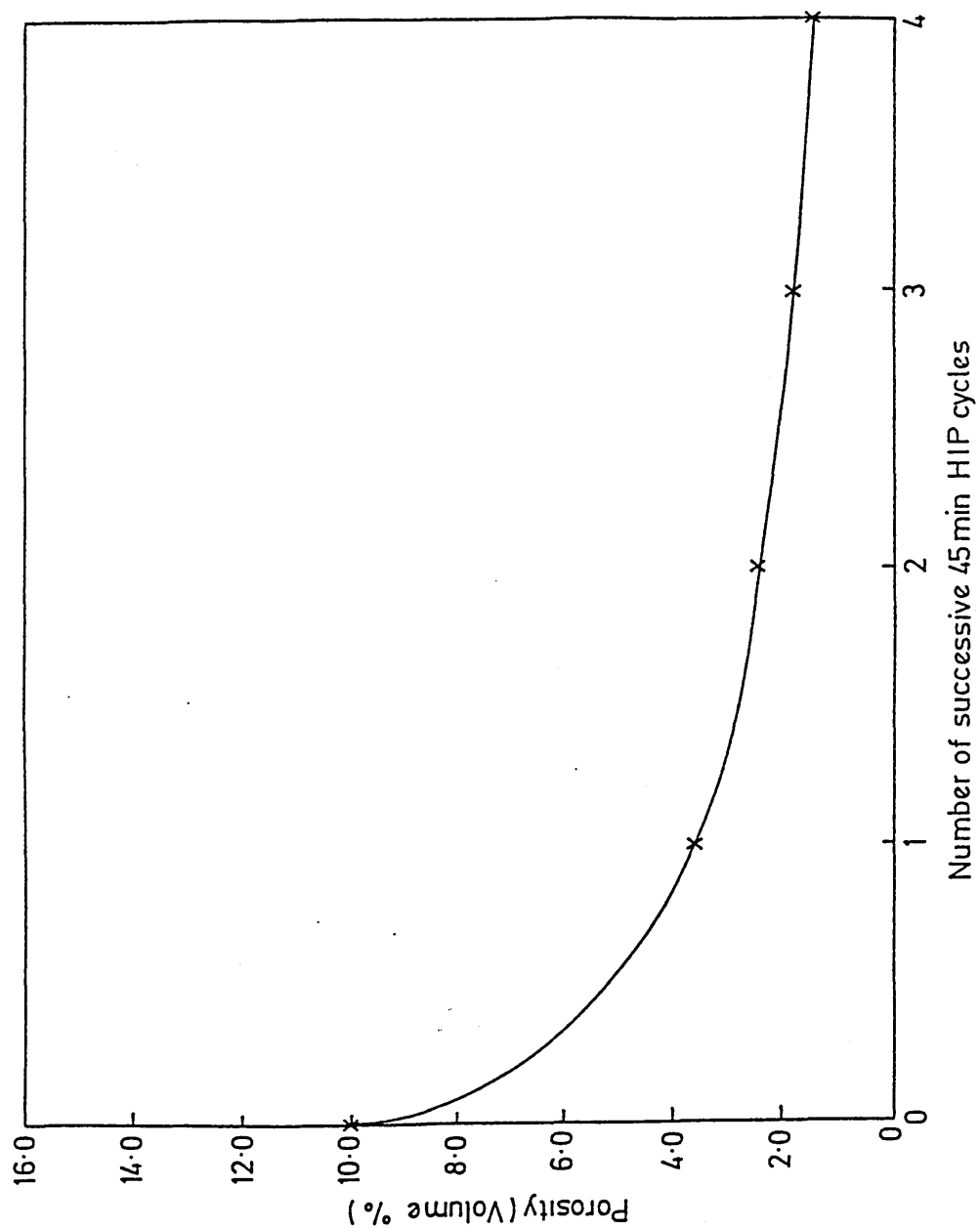


Effect of HIP temperature on the closure of 16% surface-connected porosity.

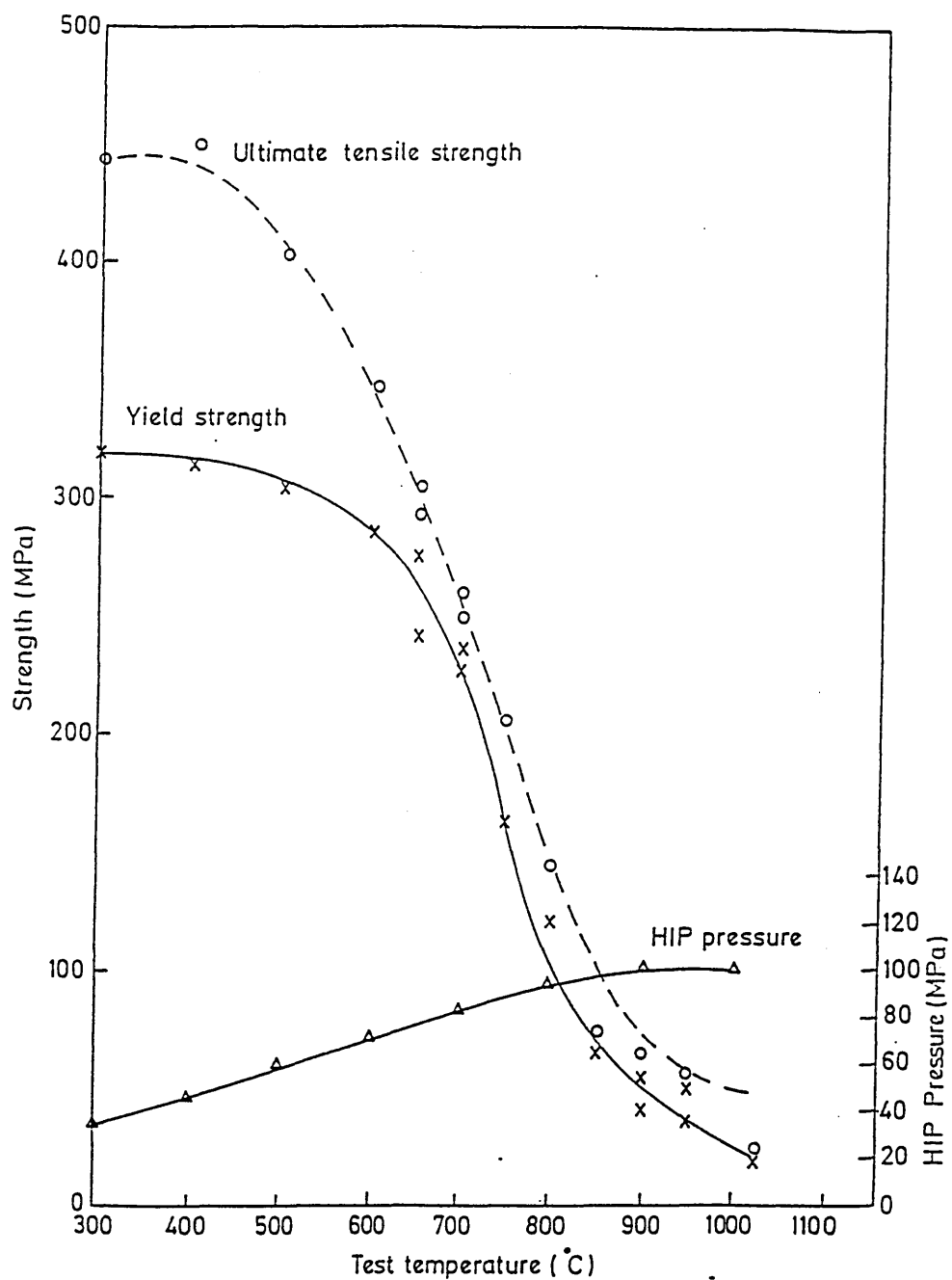


Effect of HIP Pressure on Pore Closure

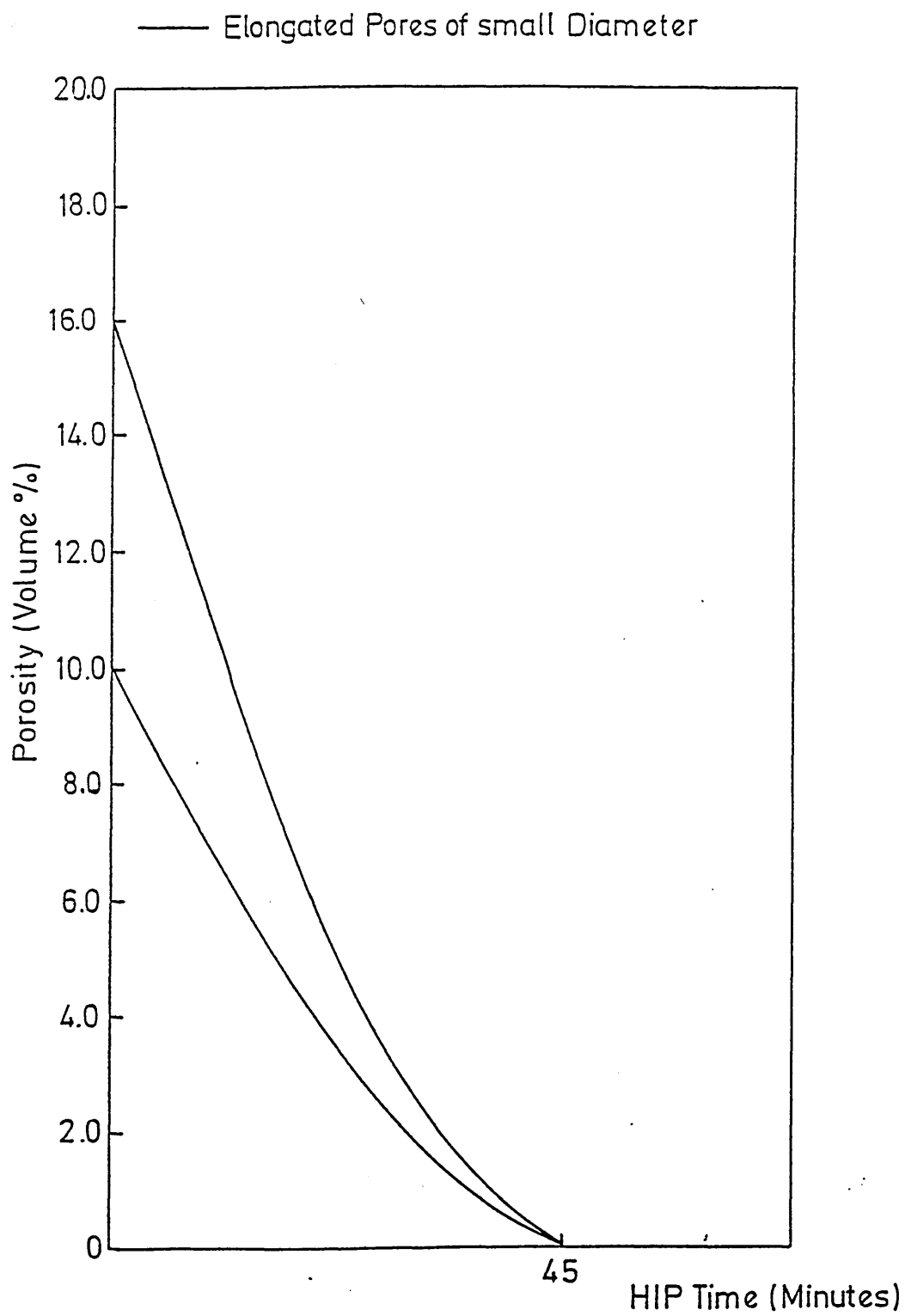
Figure 92



Effect of encapsulation (Type III HIP cycles) on the closure of surface-connected porosity.

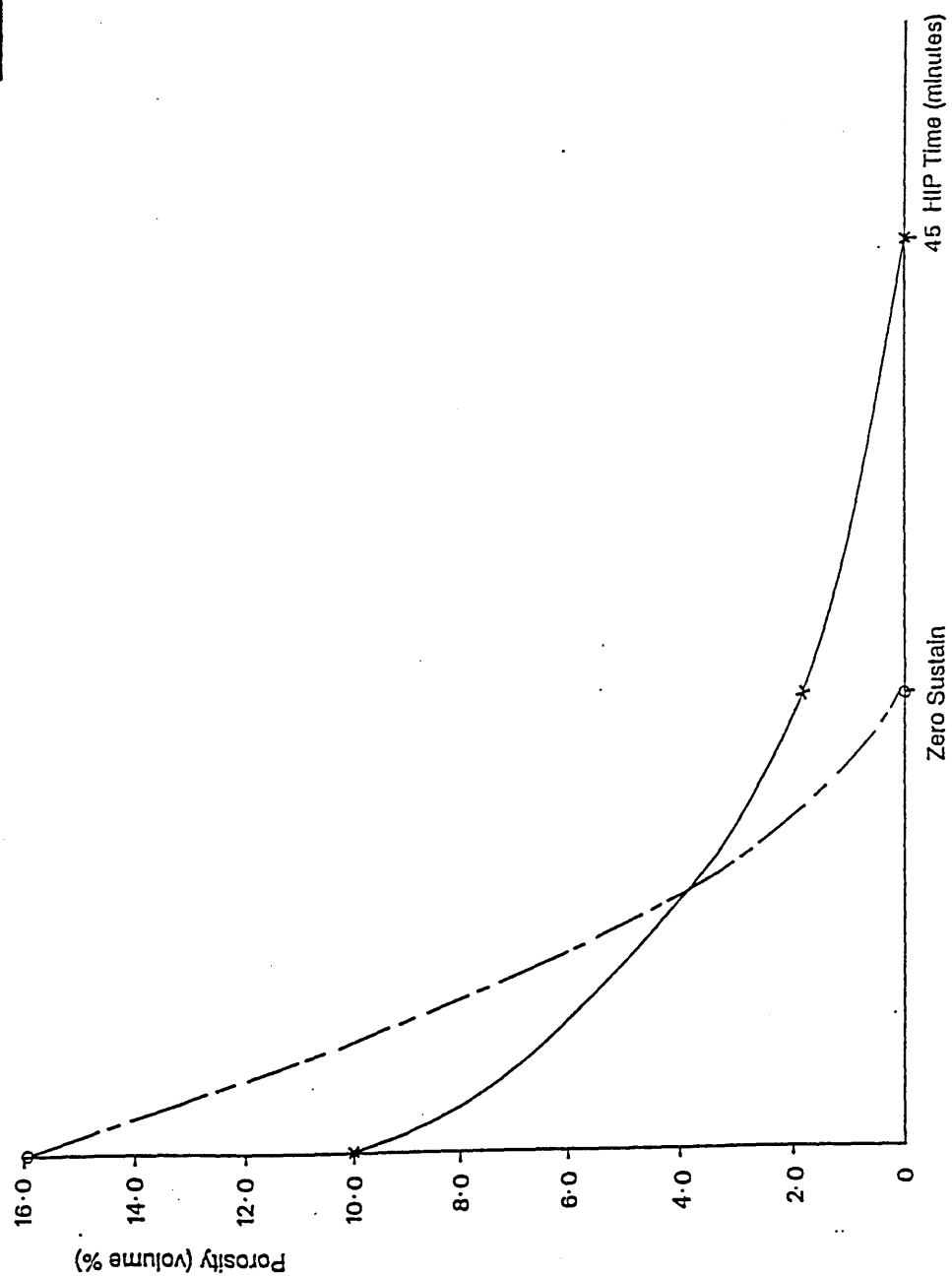


Comparison of the hot strength of 70/30 cupronickel with the pressure applied during a HIP cycle.



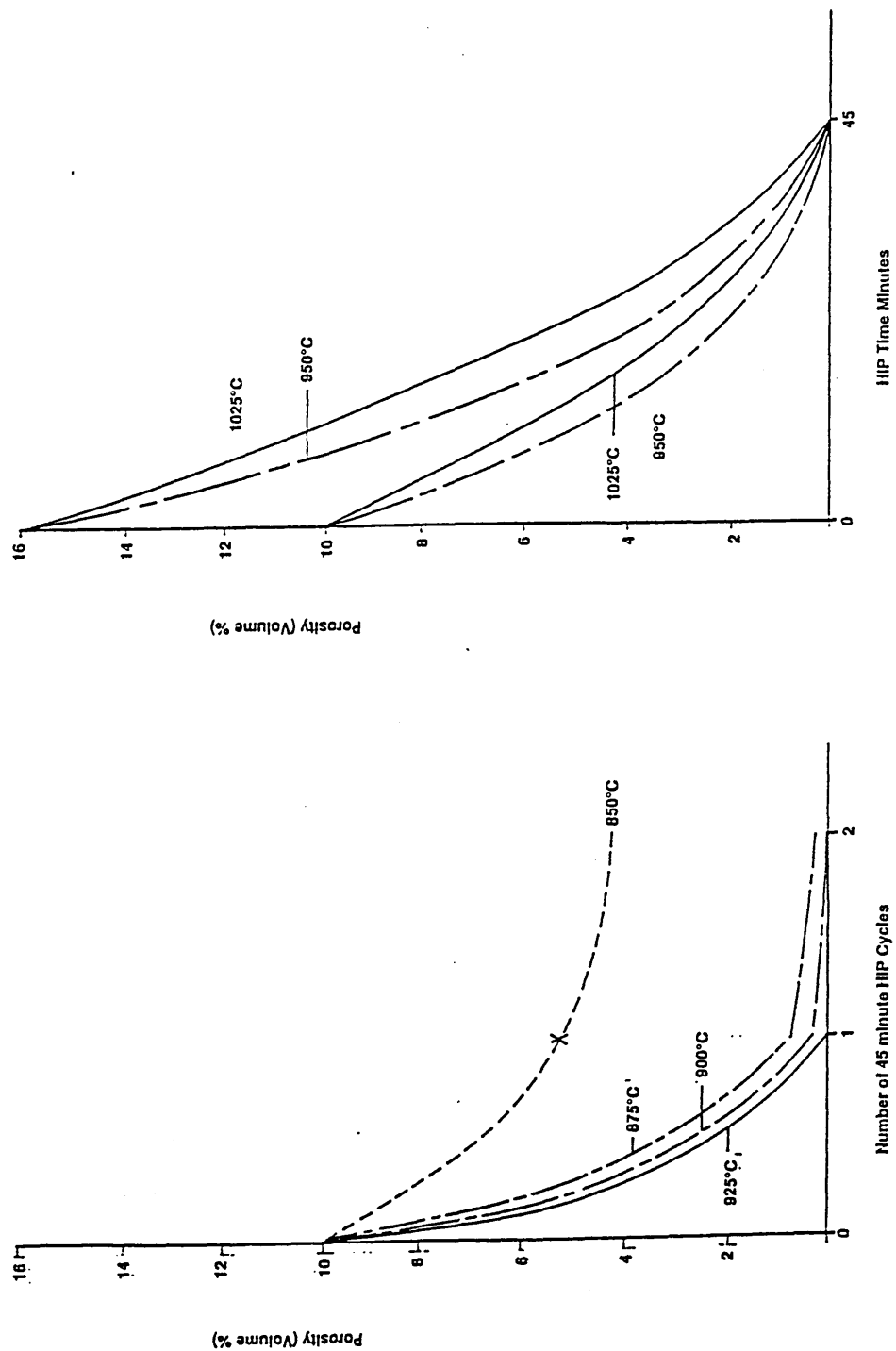
Effect of (Type I) 45 minute HIP cycles on the densification of closed internal porosity.

Figure 95

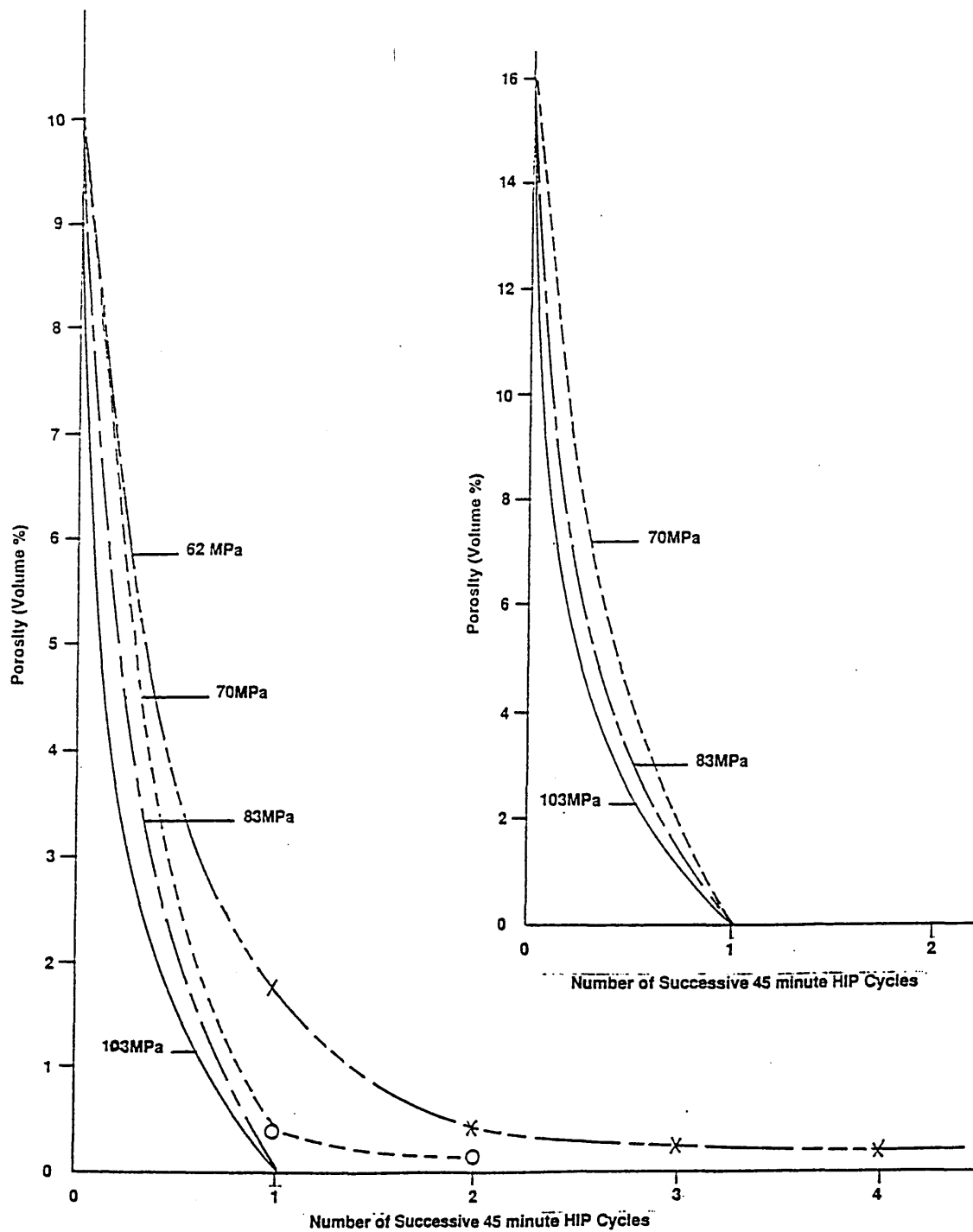


Effect of HIP time on the recovery rate and densification mechanisms for the closure of internal pores.

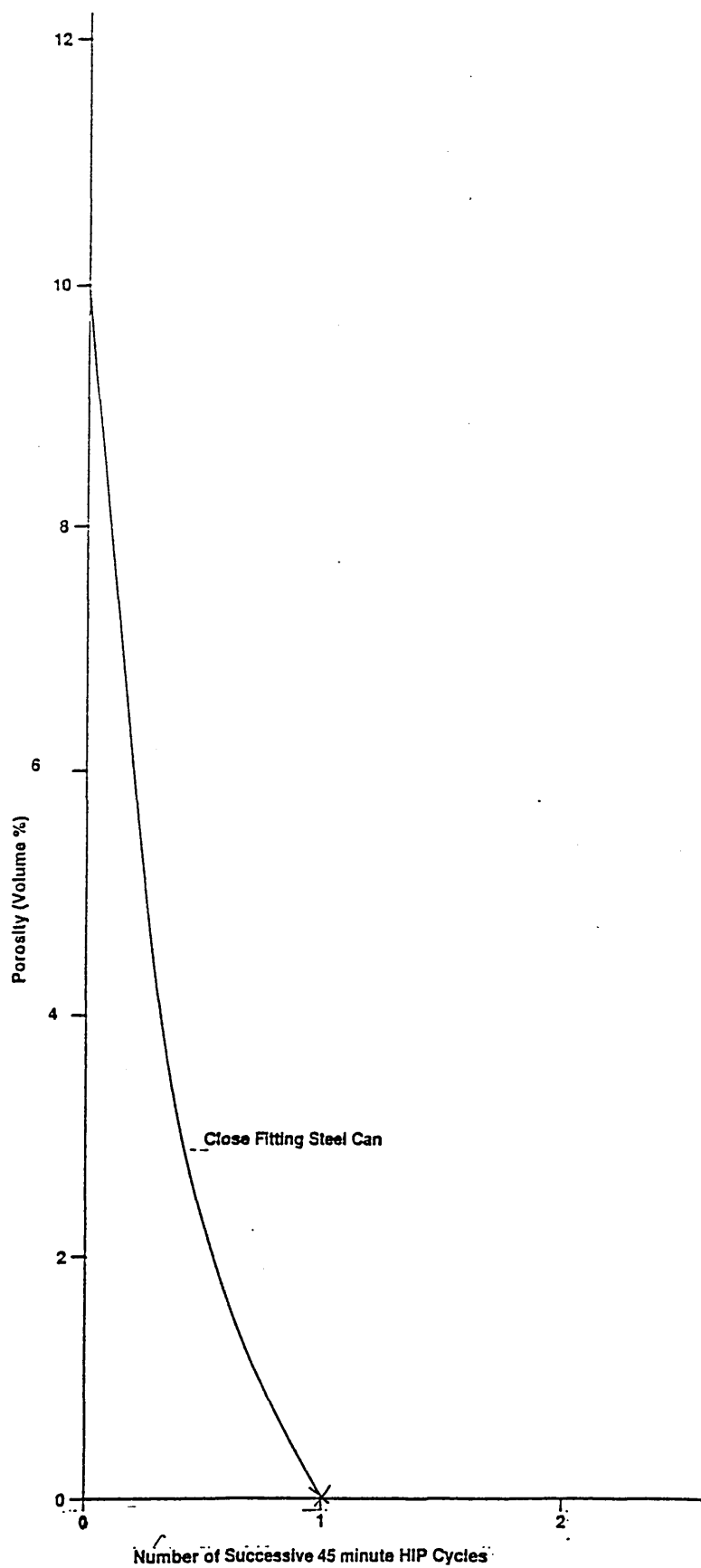
Figure 96



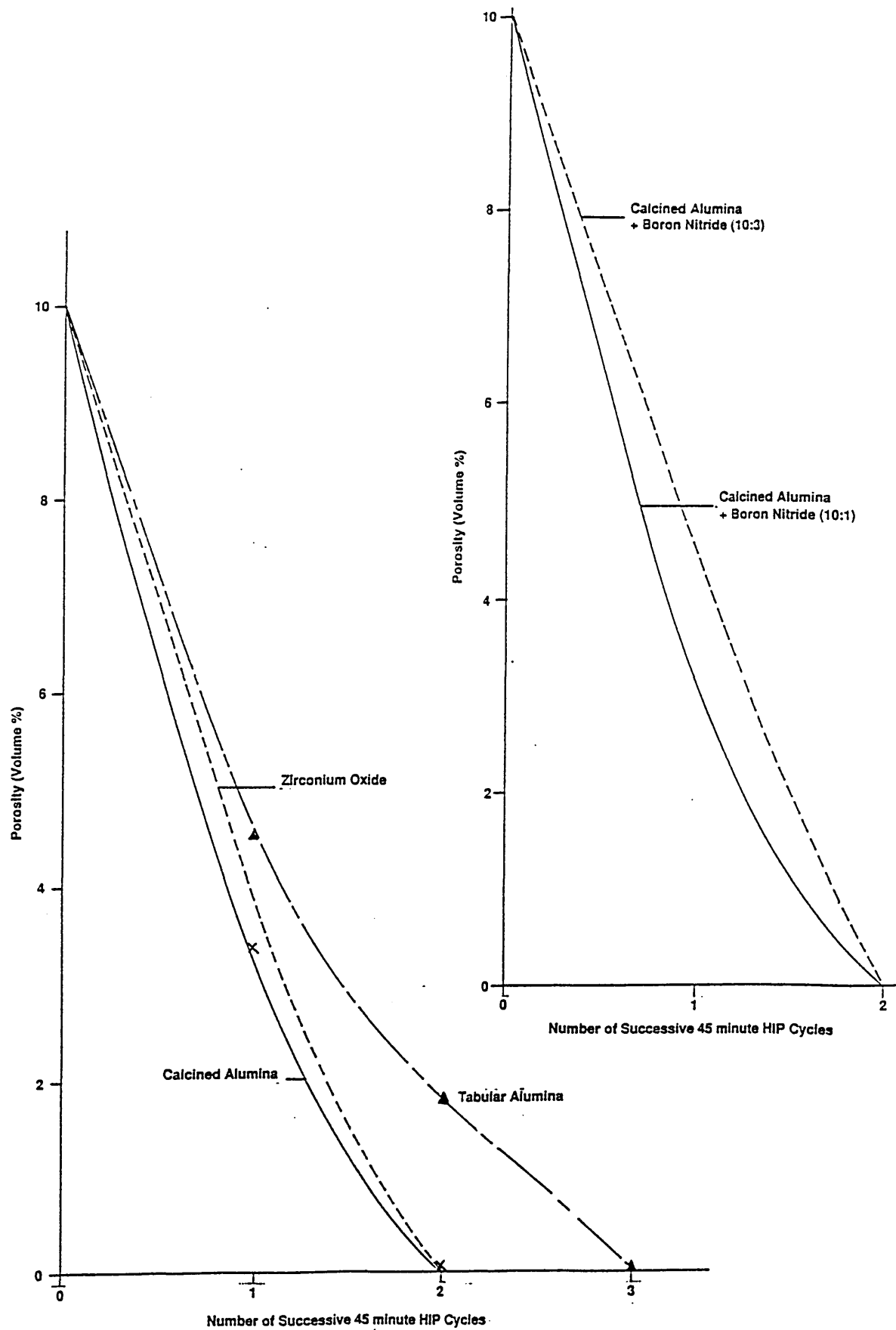
Effect of HIP temperature on the closure of internal pores.



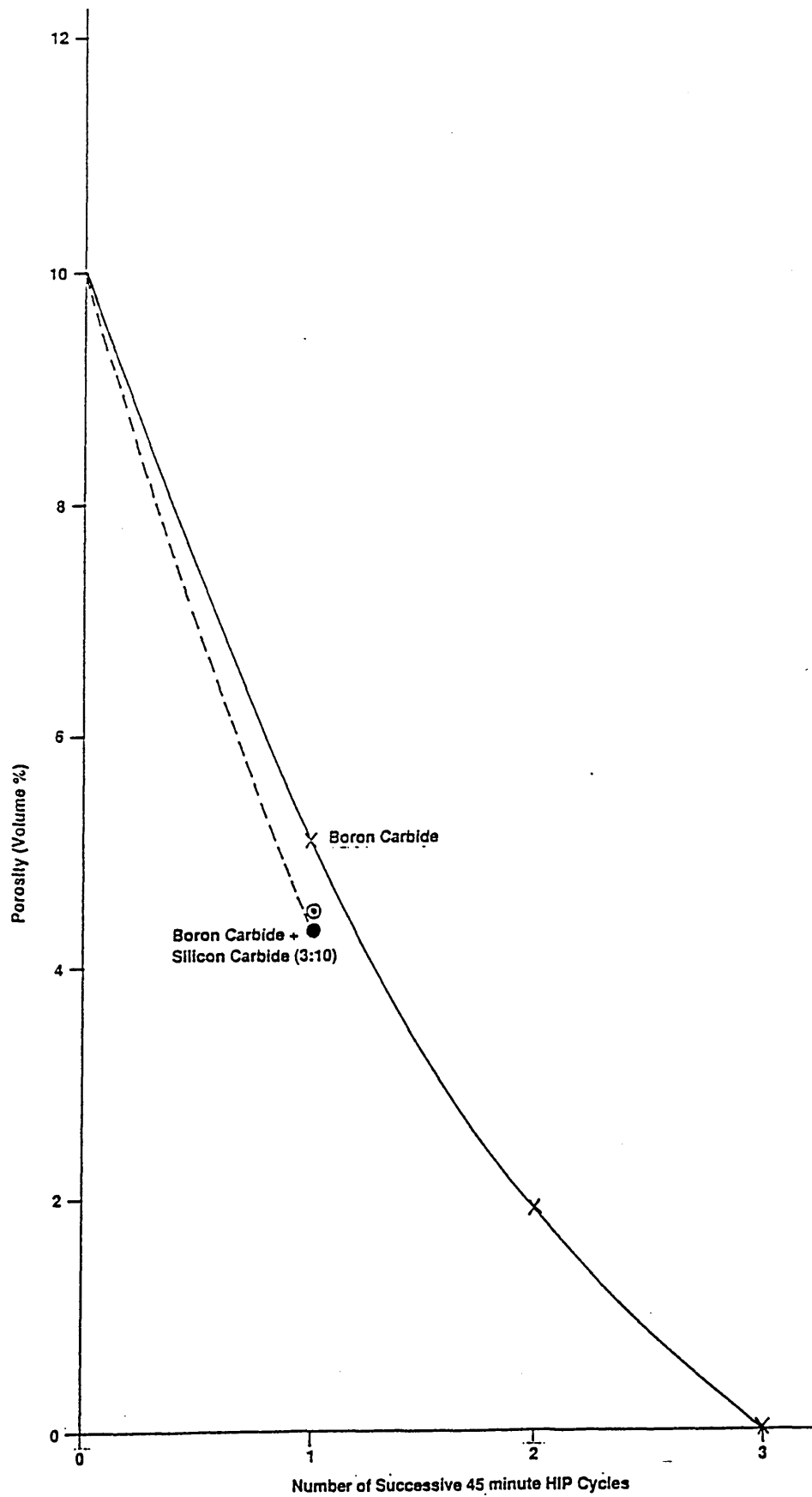
Effect of HIP pressure on the closure of internal porosity.



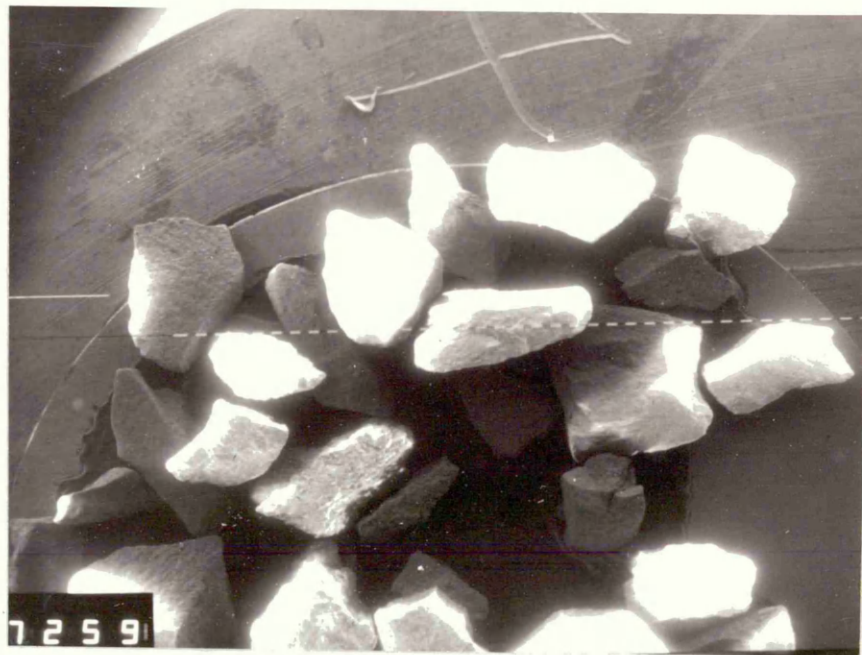
Effect of encapsulation techniques on the rate of pore closure.



Effect of a change in the refractory pressure transmitting media on the rate of porosity closure

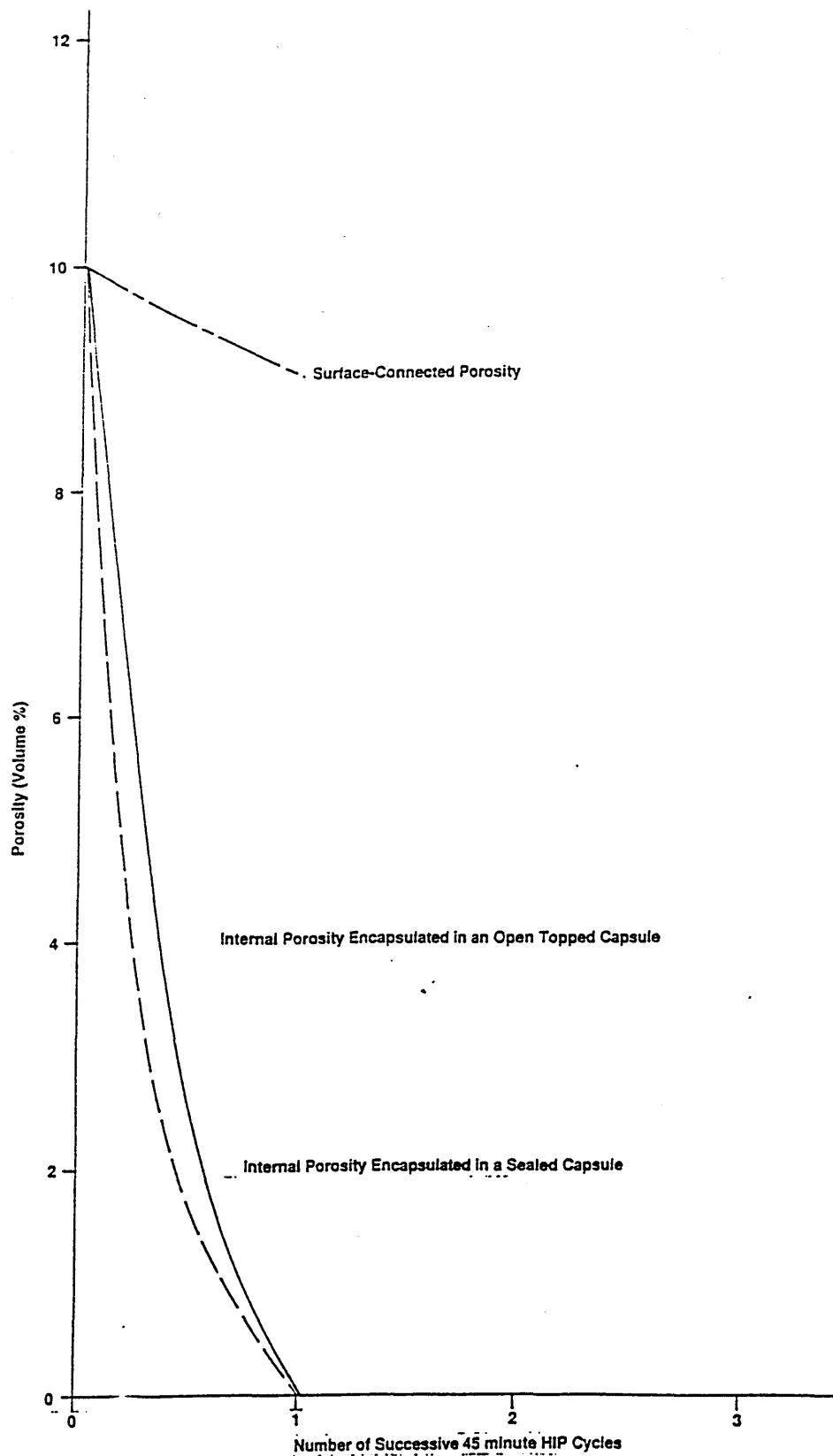


Effect of using carbide powder as the pressure transmitting medium on the rate of pore closure

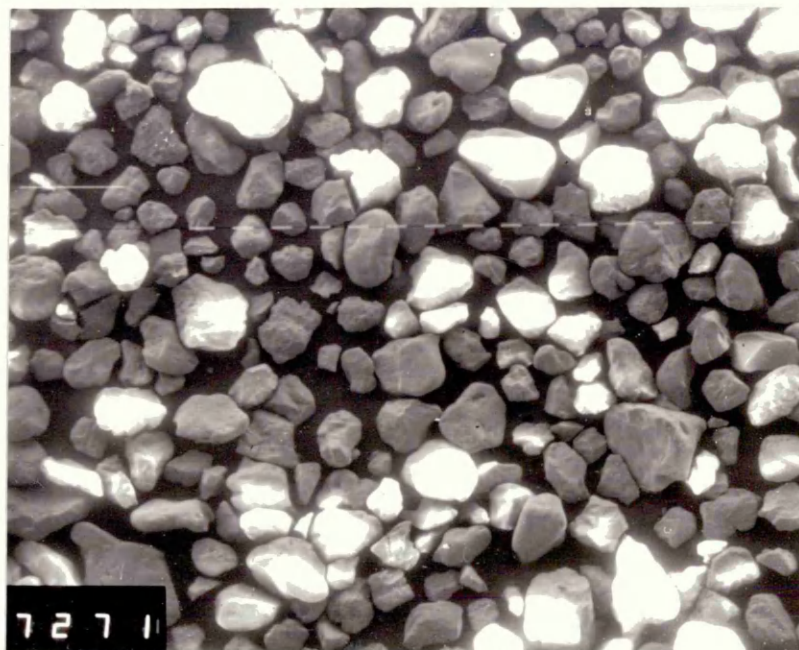


X 9

SEM micrograph showing a general view of tabular alumina particles which indicates their plate like shape and angular features.



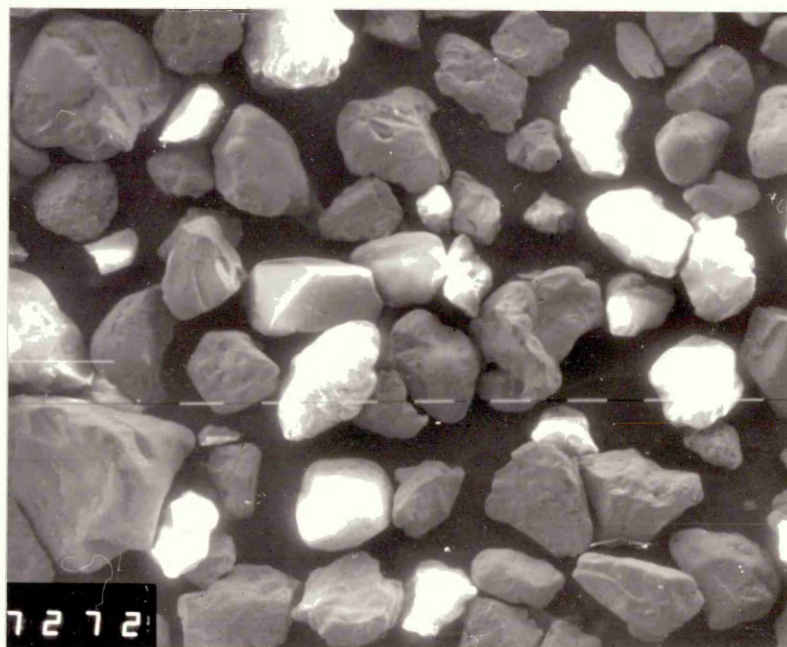
Effect of using fused glass as the pressure transmitting medium on the rate of pore closure.



X 18.75

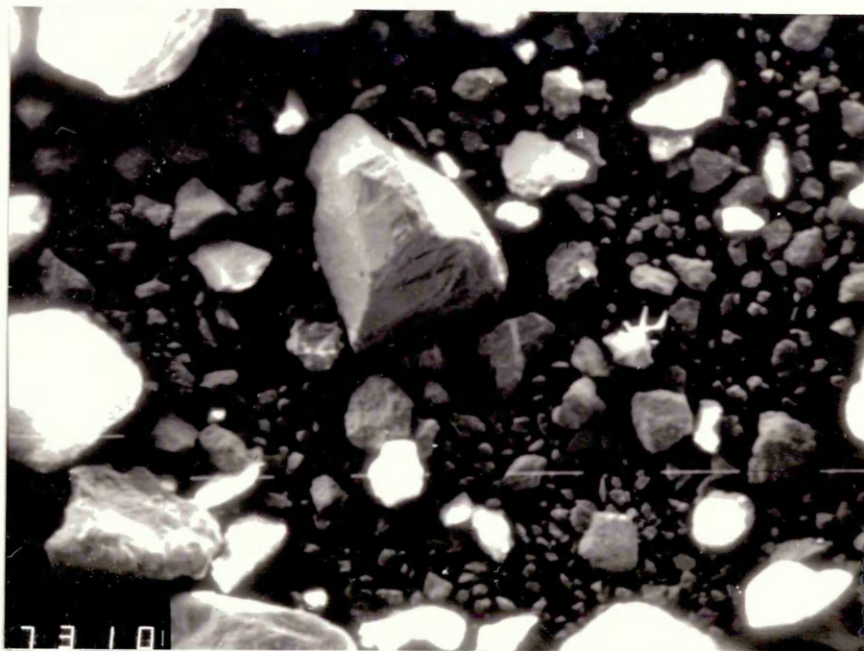
SEM micrograph showing a typical view of desert based silica sand particles which shows their angular characteristics.

Figure 104



X 37.5

Desert based silica sand particles at a higher magnification showing the angular nature of the particles.



X 75

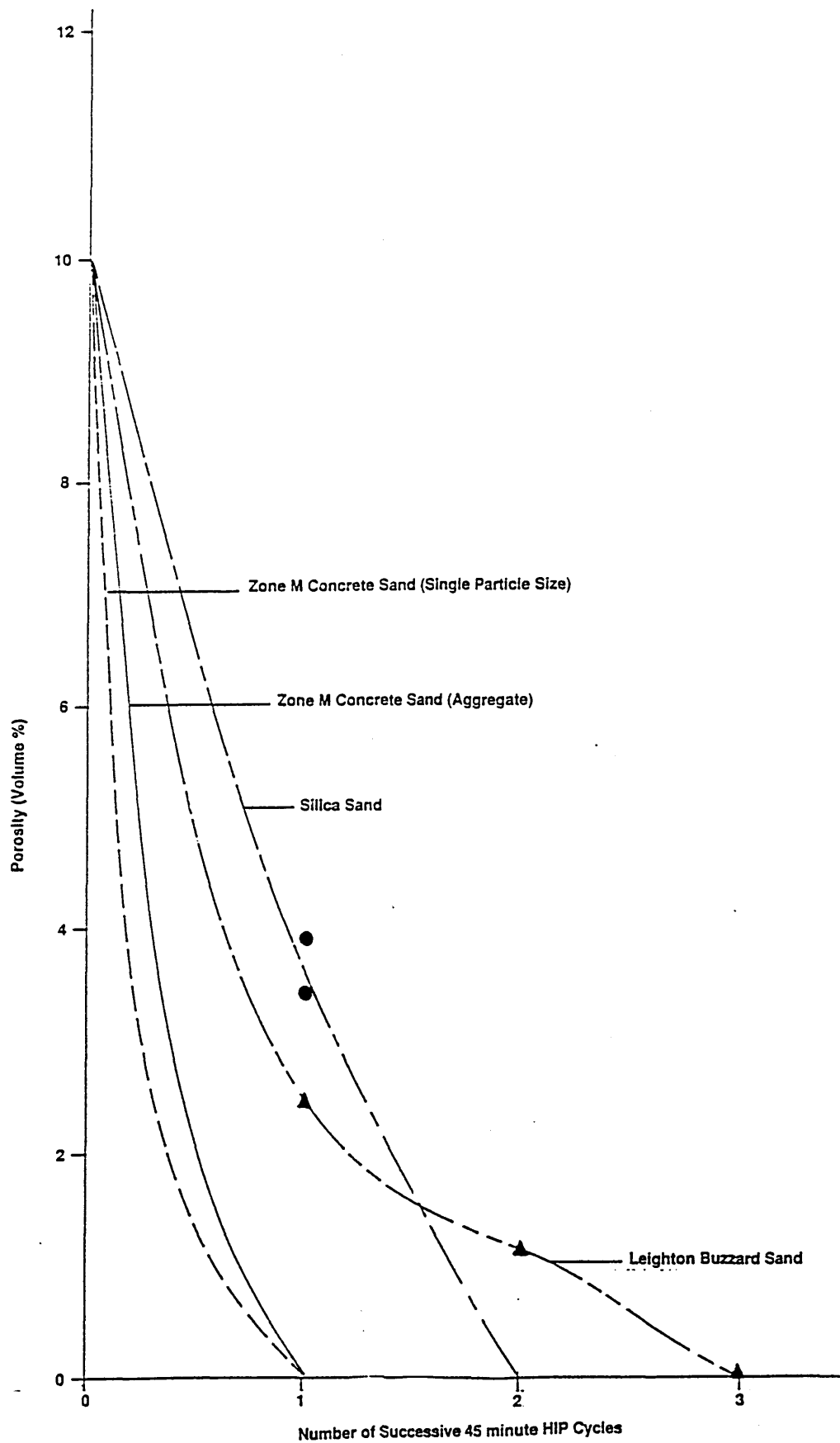
SEM micrograph showing Zone-M concrete sand (water table sand) particles which have a wide distribution of particle sizes $106\text{--}355\mu\text{m}$. The larger particles have a tendency to be angular in nature.

Figure 106

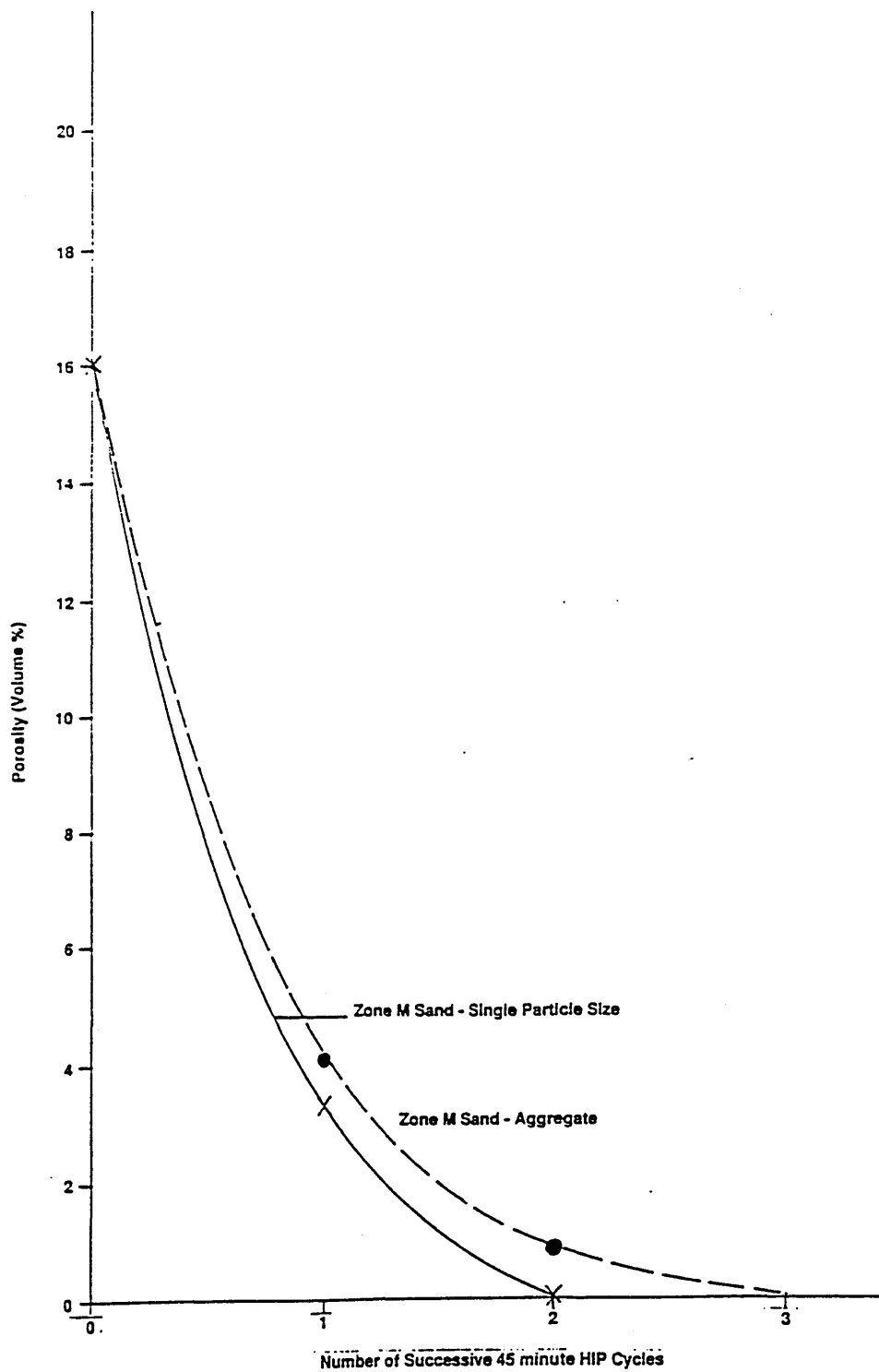


X 47.5

The zone-M concrete sand has a more rounded particle shape as illustrated by the single particle sized grains of $150\mu\text{m}$.



Effect of changing the type of refractory sand used as the pressure transmitting medium on the rate of pore closure.



Effect of changing the type of refractory sand used as a pressure transmitting medium on the closure of large pores.



X 9

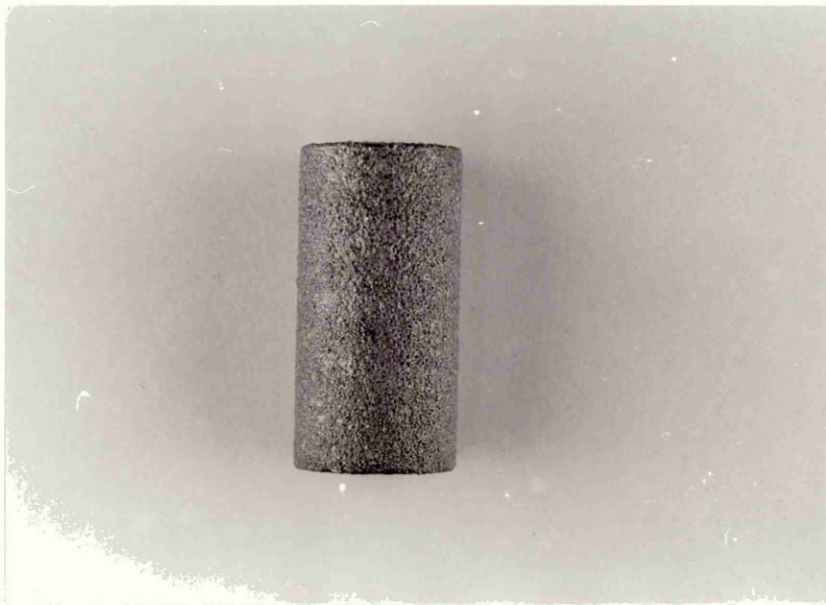
SEM micrograph showing the general appearance of Leighton Buzzard sand particles which are of a single particle size ($>35\mu\text{m}$ $<1.7\text{mm}$).

Figure 110

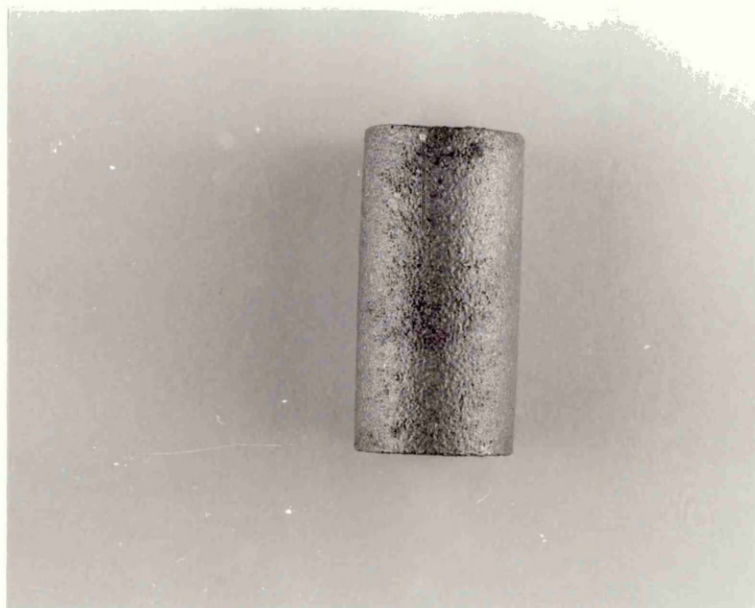


X 37.5

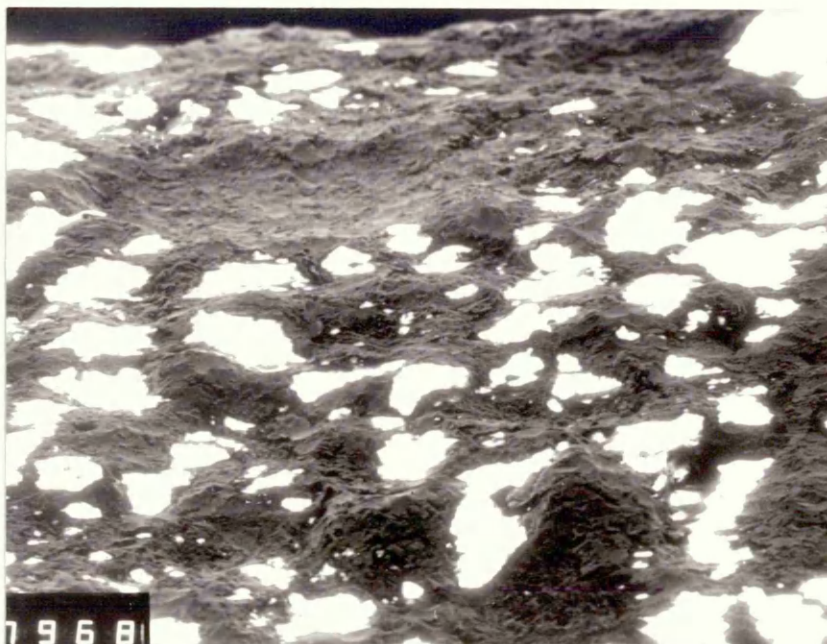
Higher magnification of Leighton Buzzard sand particles showing their rounded particle characteristics.



Photograph showing the surface texture of NES 824 sample HIPped in contact with desert based silica sand, indicating a coarse dimpled surface.



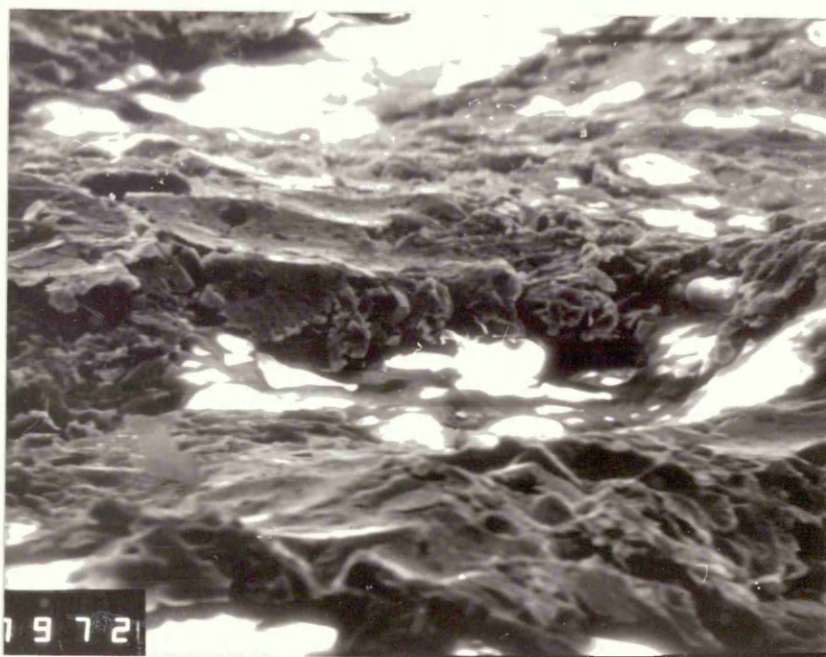
Photograph showing the surface texture of NES 824 sample HIPped in contact with zone-M concrete sand, which indicates that the specimen surface has a dimpled appearance with no visible signs of chemical interaction with the sand.



X 90

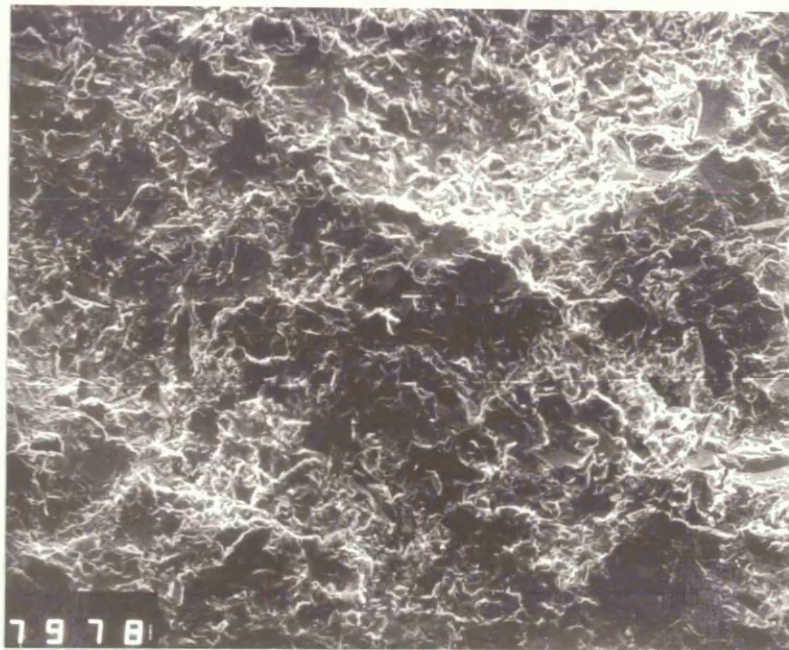
SEM examination identified the angular desert based silica sand still to be embedded in the samples surface after cleaning.

Figure 114



X 680

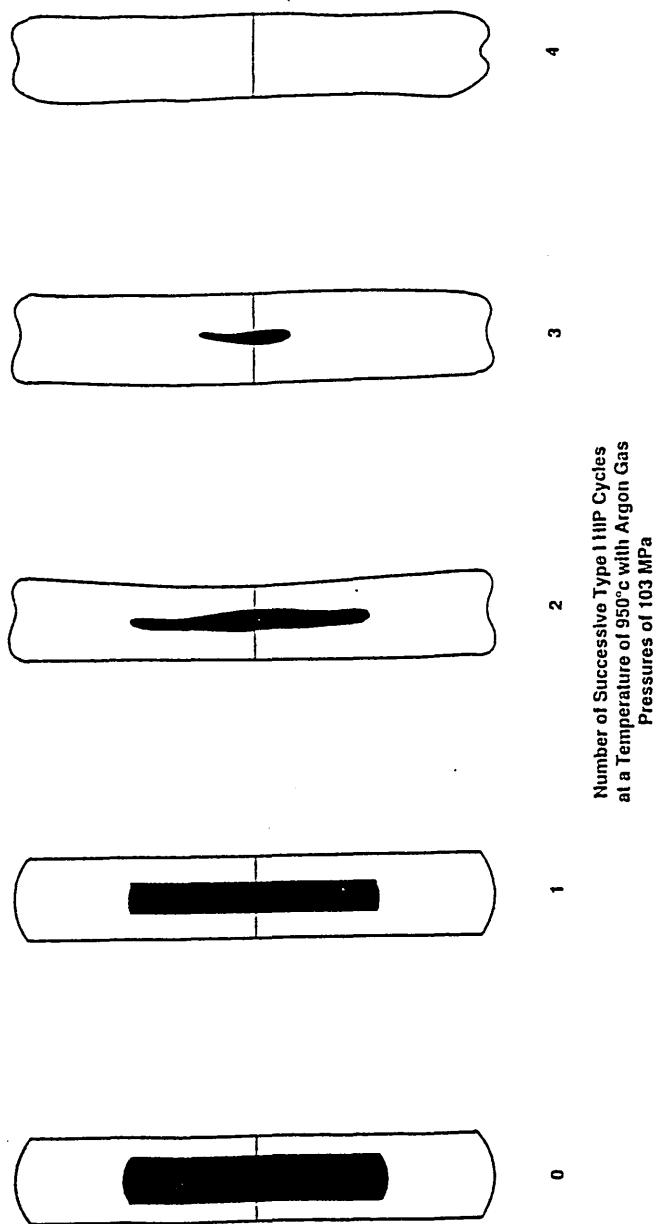
Where the silica particles had been removed a coarse surface texture consisting of angular indentations remained.



X 190

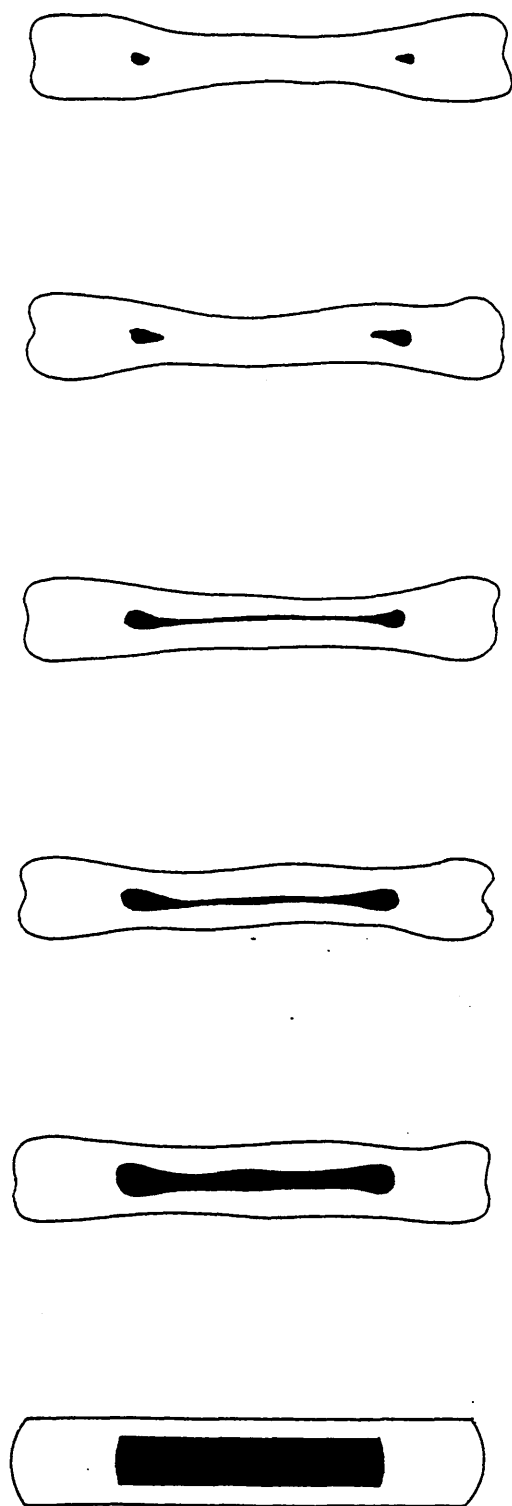
SEM micrograph of NES 824 which has been in contact with zone-M concrete sand during HIPping and then cleaned, exhibits a textured surface of fine dimples and with no adhering sand particles.

Figure 116

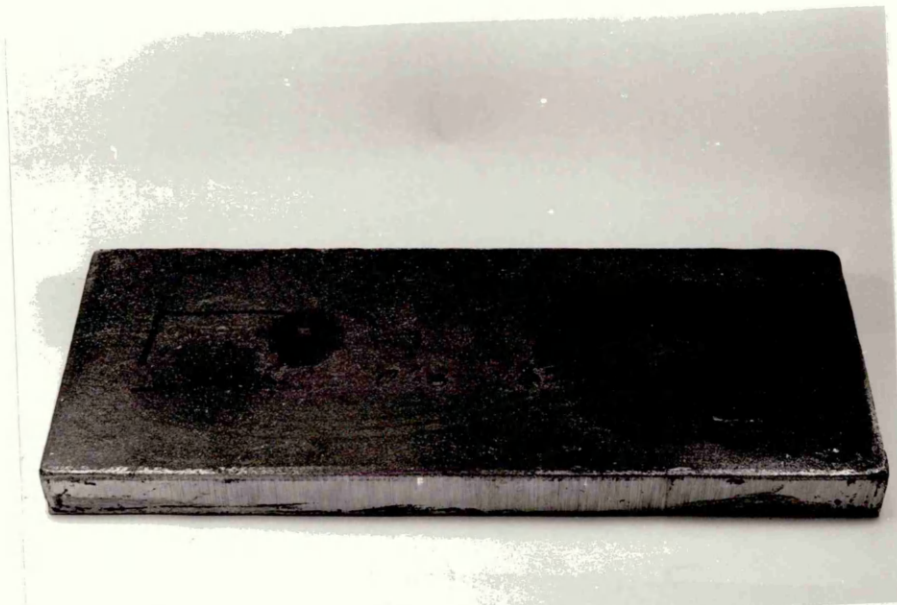


Change in shape of a pore representing 16% surface-connected porosity during successive (Type I) HIP cycles.

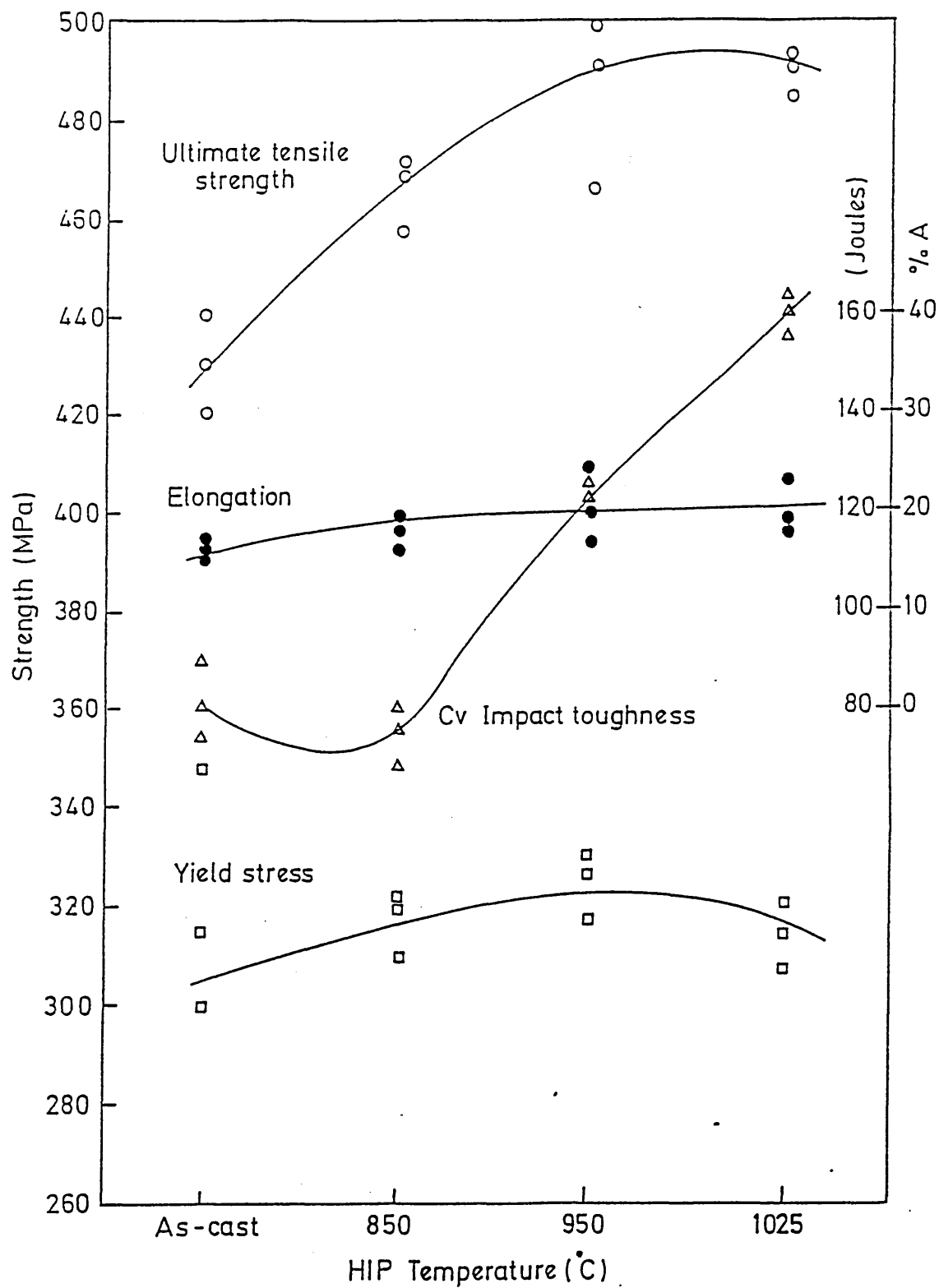
Figure 117



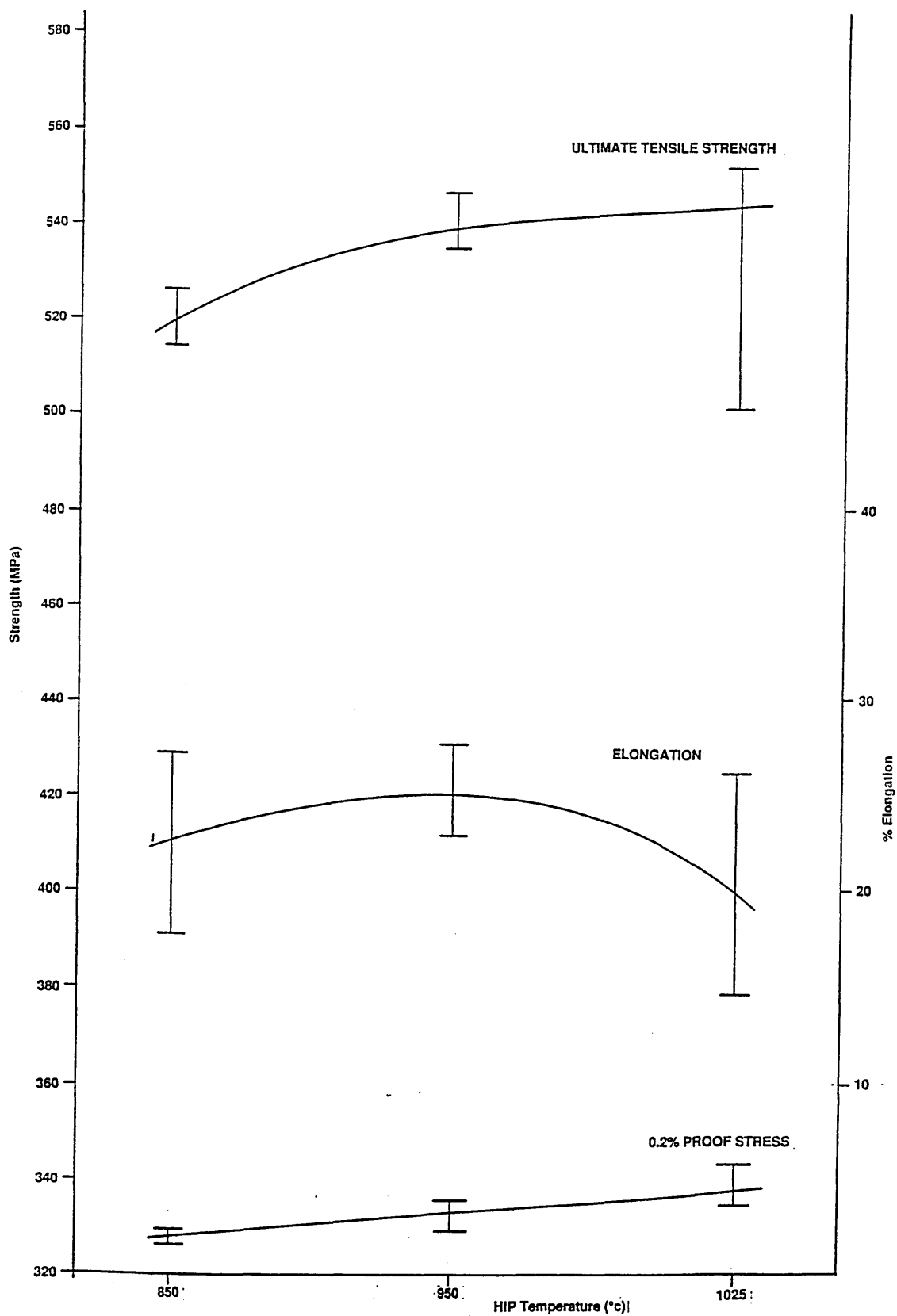
Change in shape of a 10% closed internal pore during HIPping.



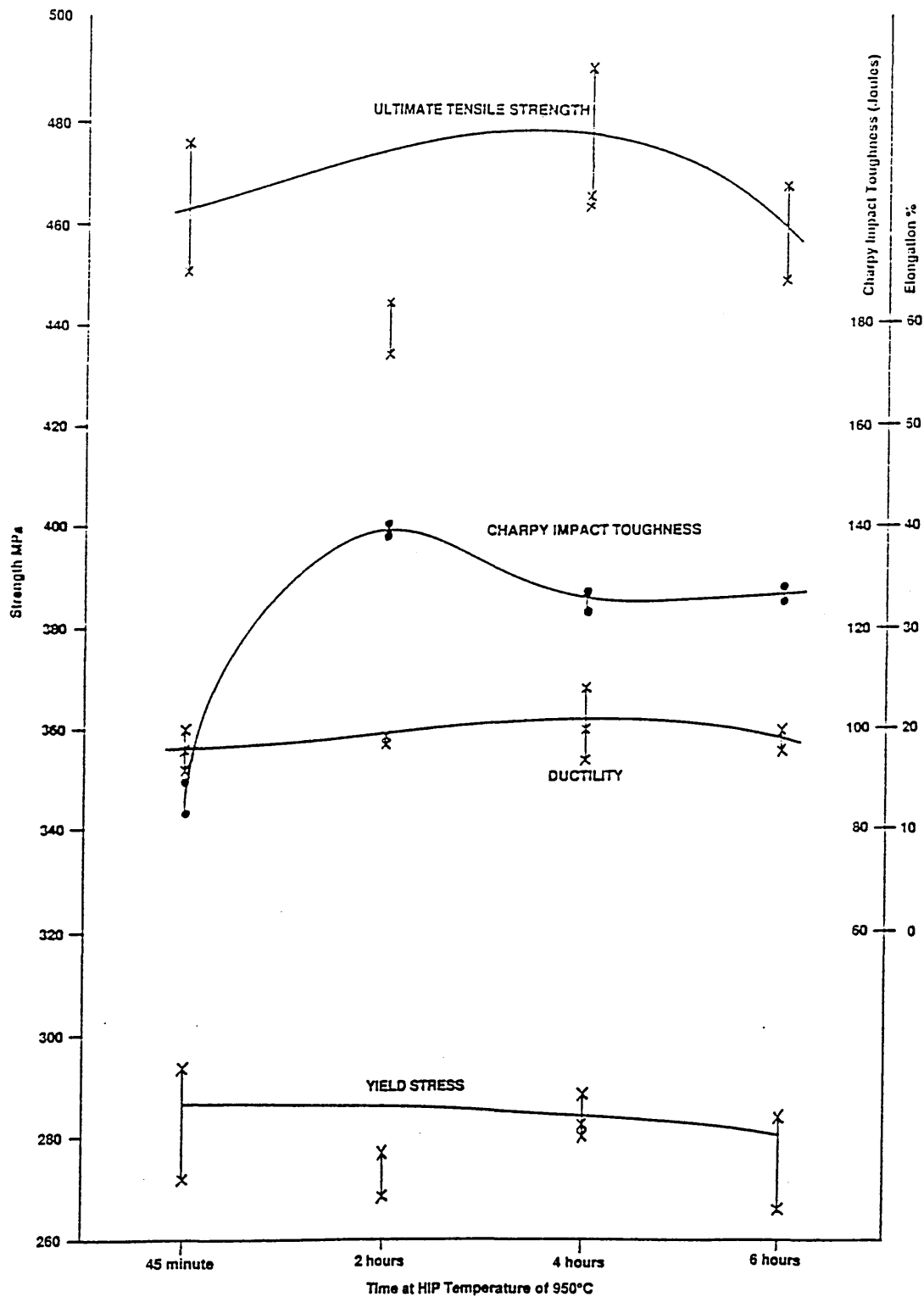
As-Cast NES 824 weld test plate.



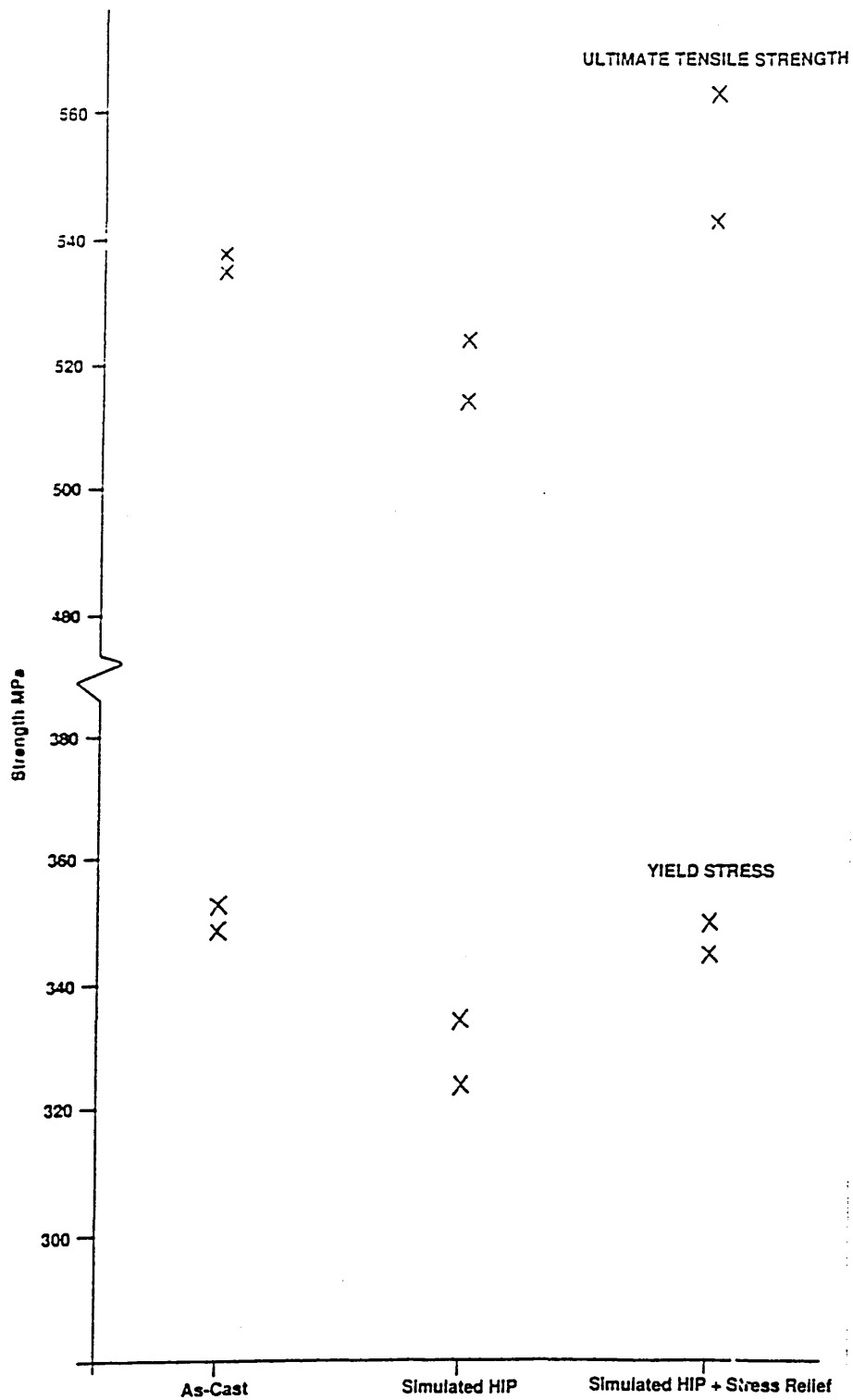
Effect of HIP temperature on the mechanical properties of 70/30 cupronickel weld plate material.



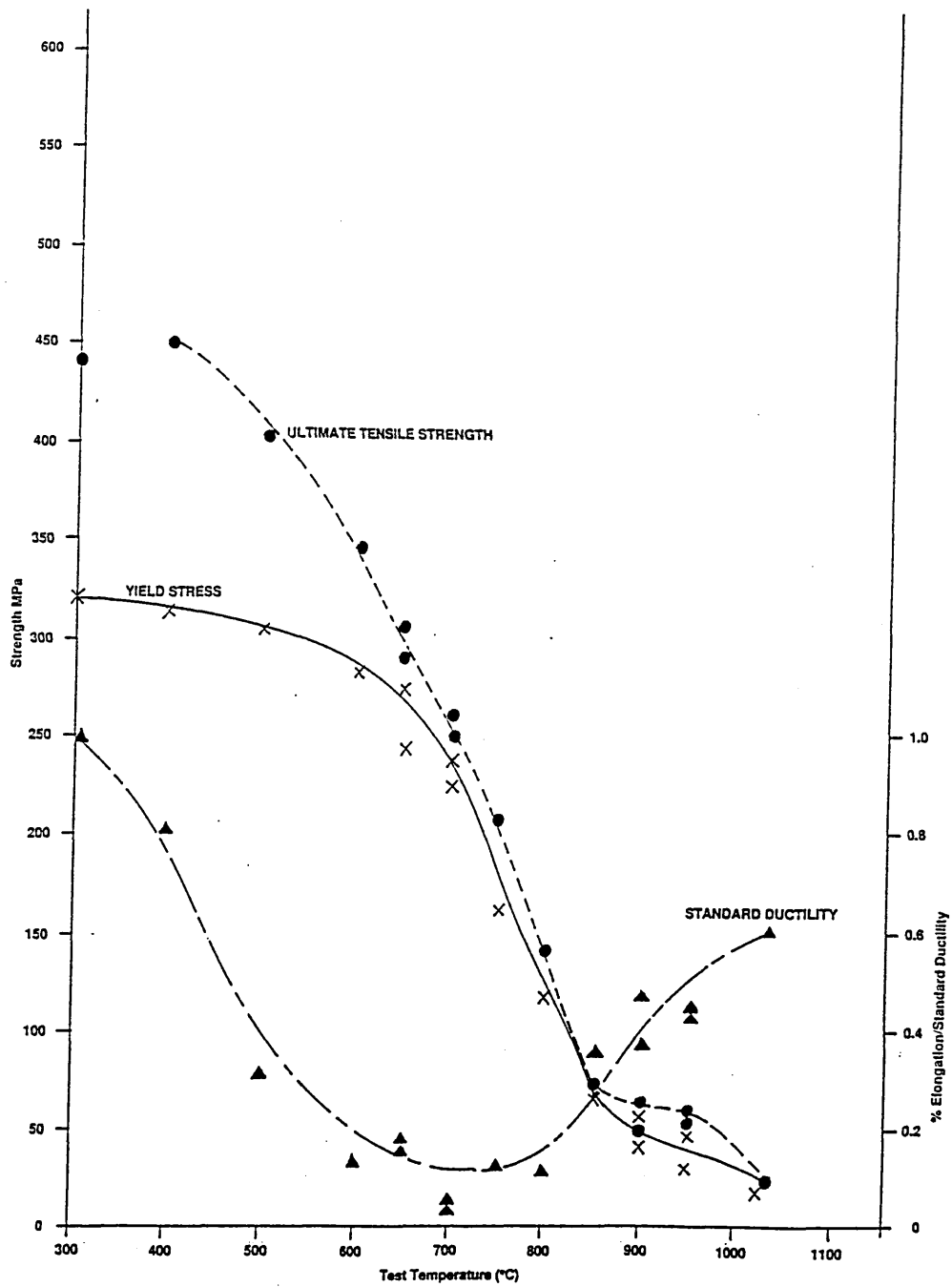
Effect of HIP temperature on the mechanical properties of 70/30 cupronickel test bars.



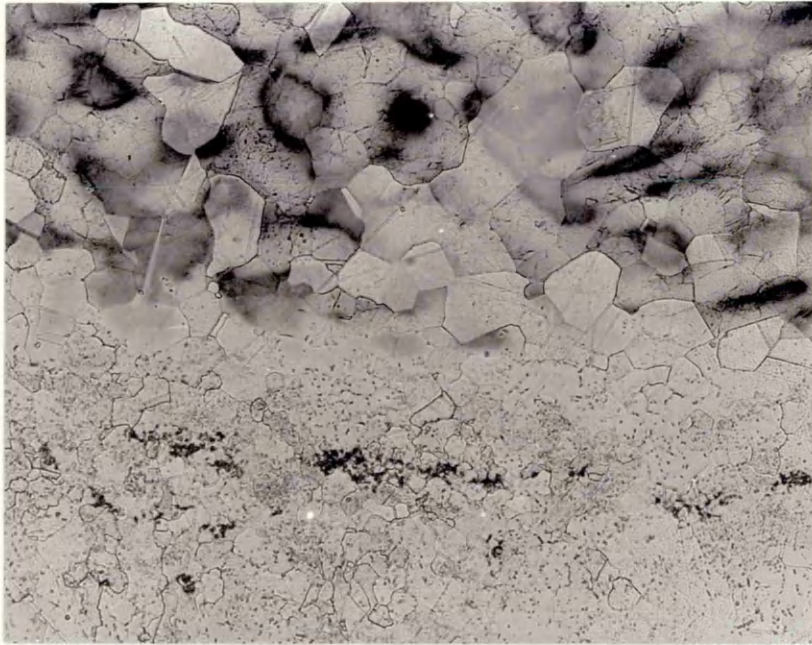
Effect of HIP time on the mechanical properties of 70/30 cupronickel.



Mechanical property data for 70/30 cupronickel subjected to a simulated HIP cycle heat treatment.

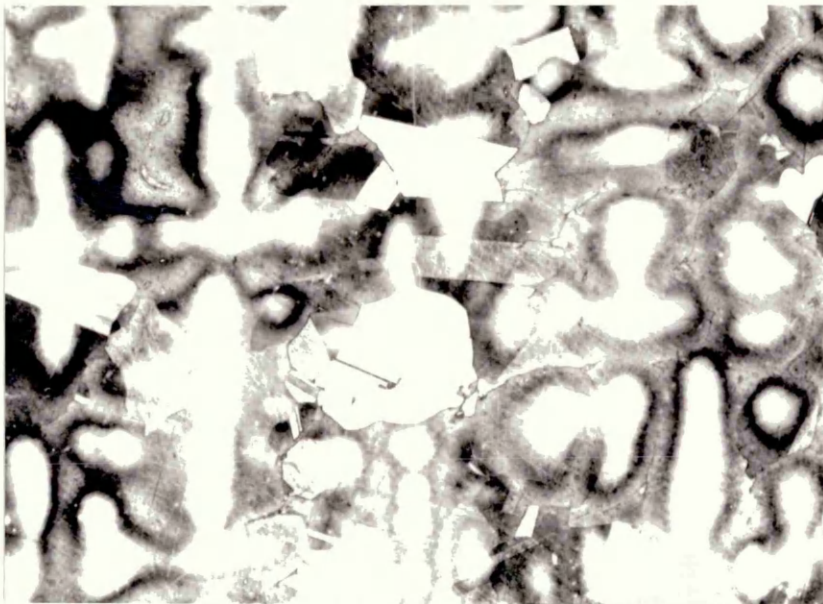


Hot tensile data for 70/30 cupronickel.



(i)

X 758



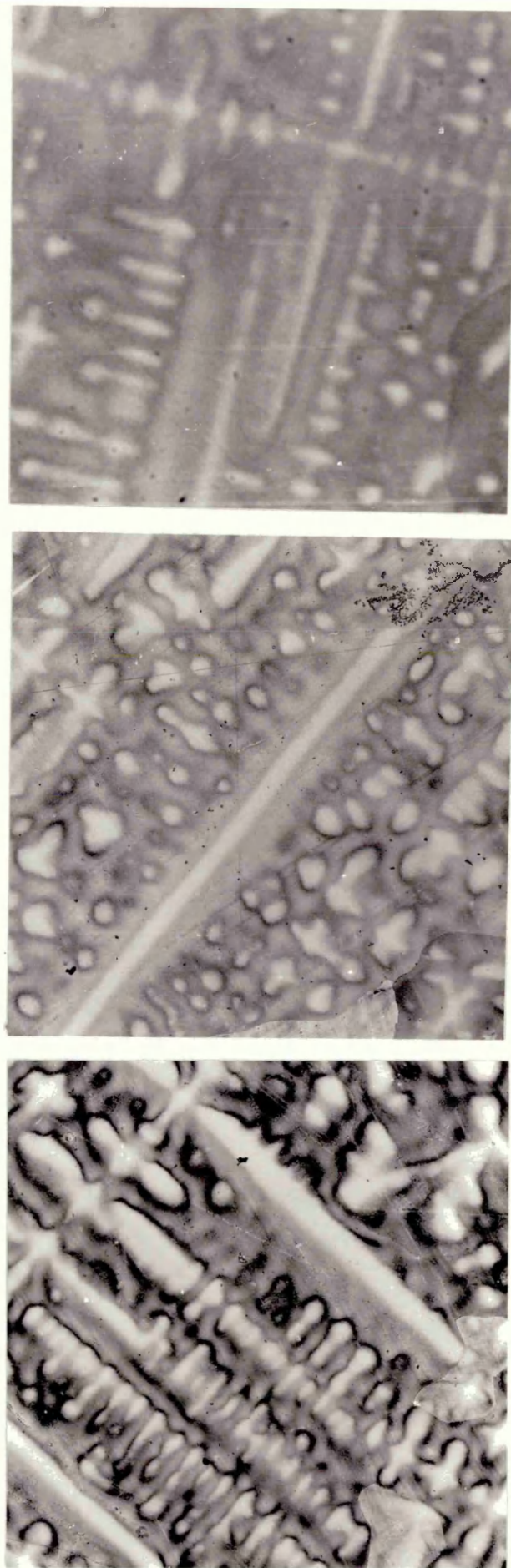
(ii)

X 758

Recrystallisation of plastically deformed material during the closure of 10% surface-connected porosity via:

- (i) 2 successive 45 minute (Type I HIP) cycles
- (ii) 8 hour sustain (Type II HIP) cycle

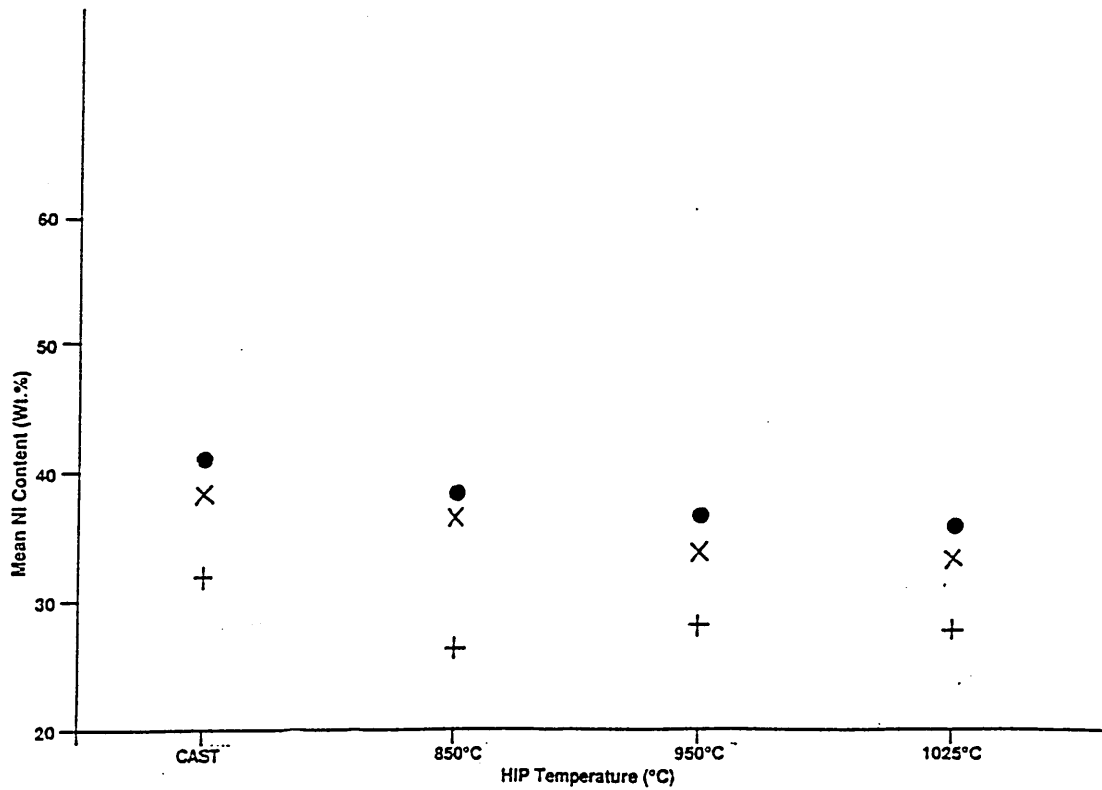
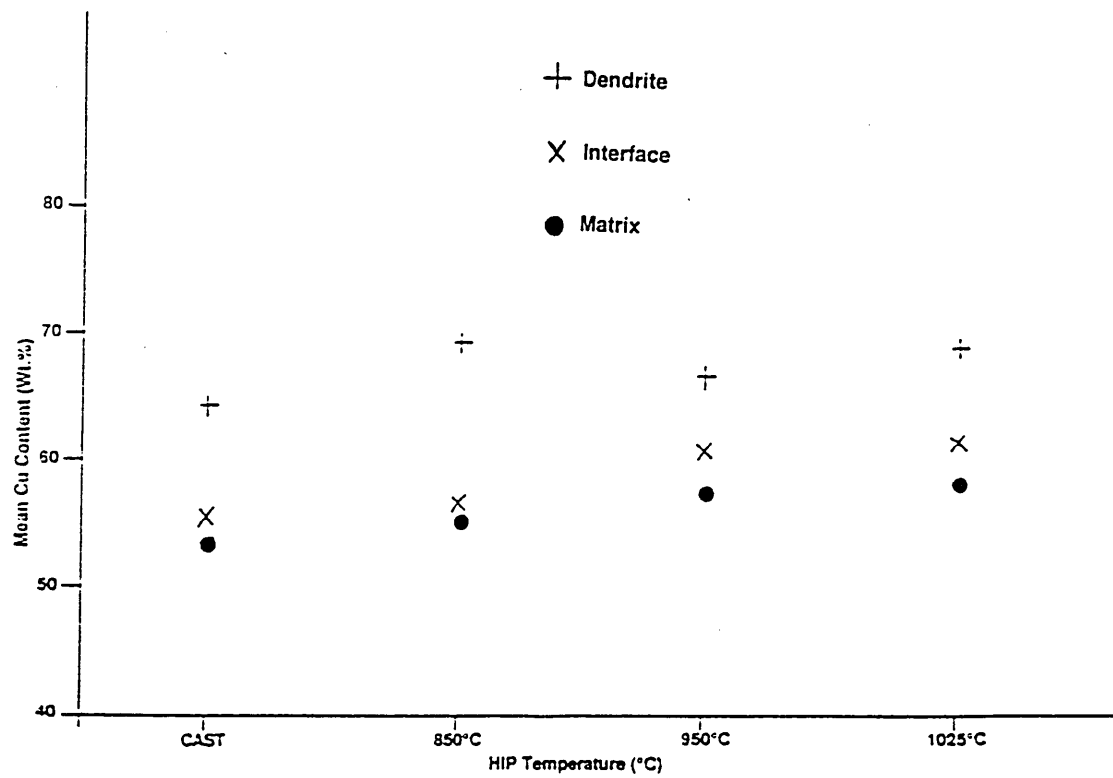
Figure 125
Effect of HIP Temperature on the Homogenisation of Cast 70/30 Cupronickel



(1) X110 (2) X110 (3) X110

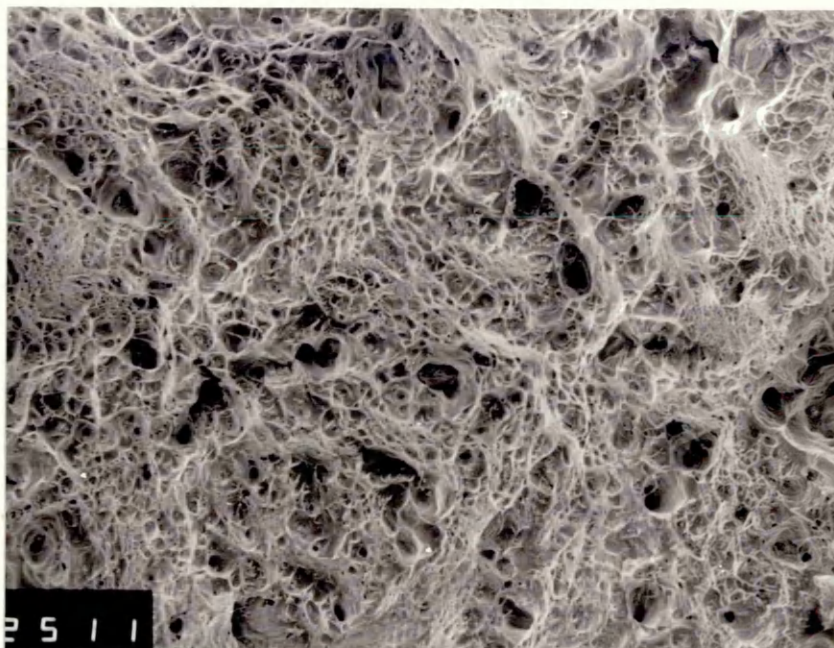
NES 824 etched in 10% alcoholic ferric chloride representing:

- (1) HIPped at 850°C / 4 Hours / 103MPa
- (2) HIPped at 950°C / 4 Hours / 103MPa
- (3) HIPped at 1025°C / 4 Hours / 103MPa



Effect of HIP temperature on the segregation of the two major alloying elements in 70/30 cupronickel.

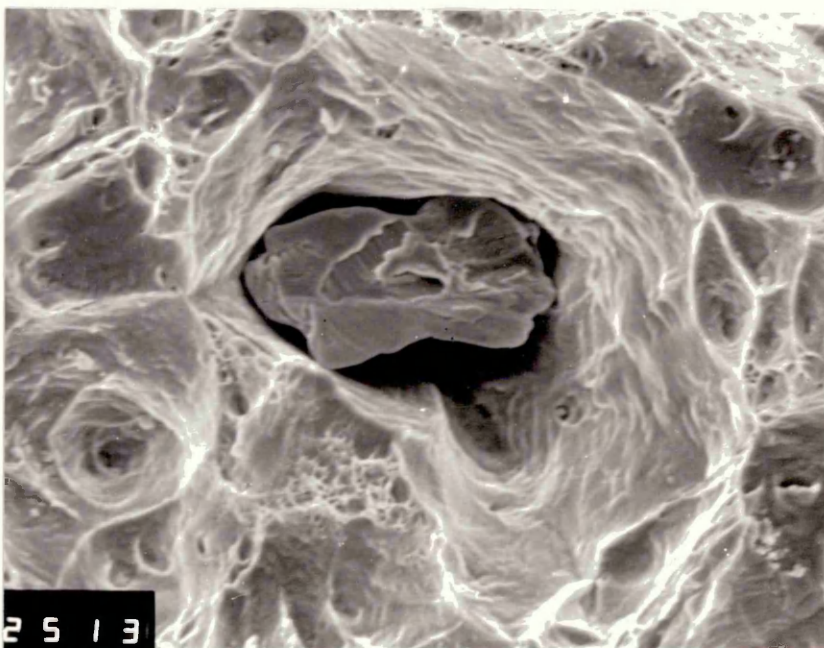
Figure 127



X 100

SEM typical fracture appearance of a NES 824 test bar fractured at 850°C.

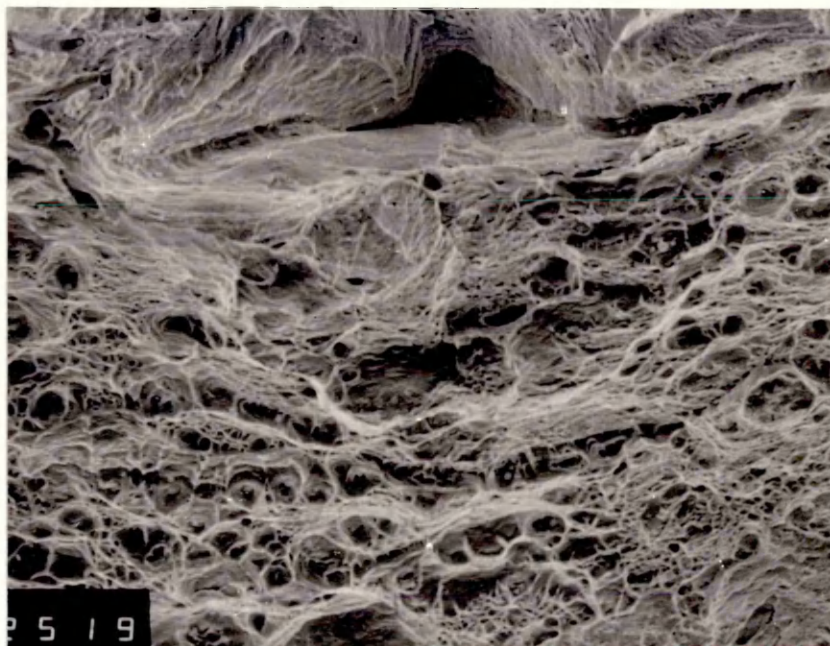
Figure 128



X 450

SEM micrograph showing a large randomly distributed martix oxide in HIPped NES 824 material.

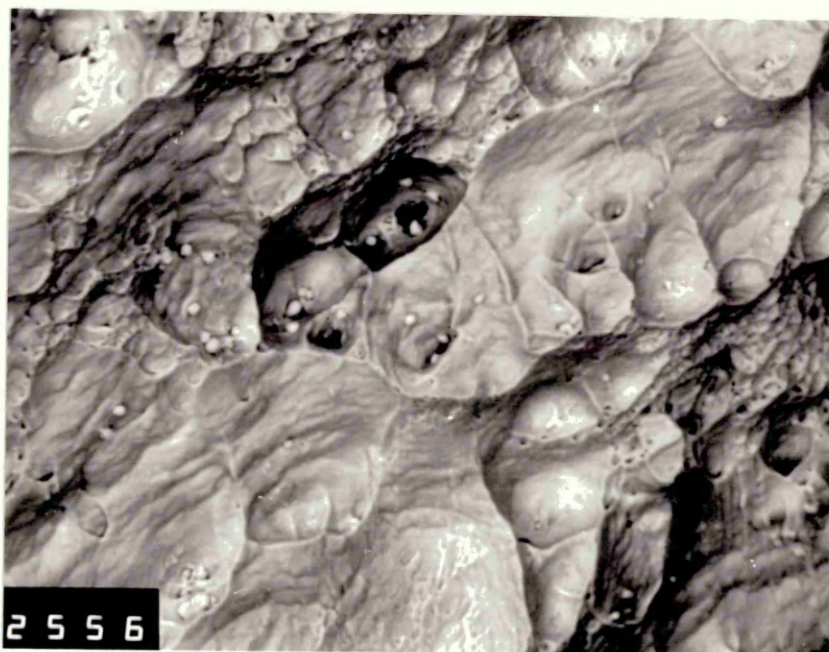
Figure 129



X 450

SEM micrograph showing small evenly distributed zirconia based particles in HIPped NES 824 material.

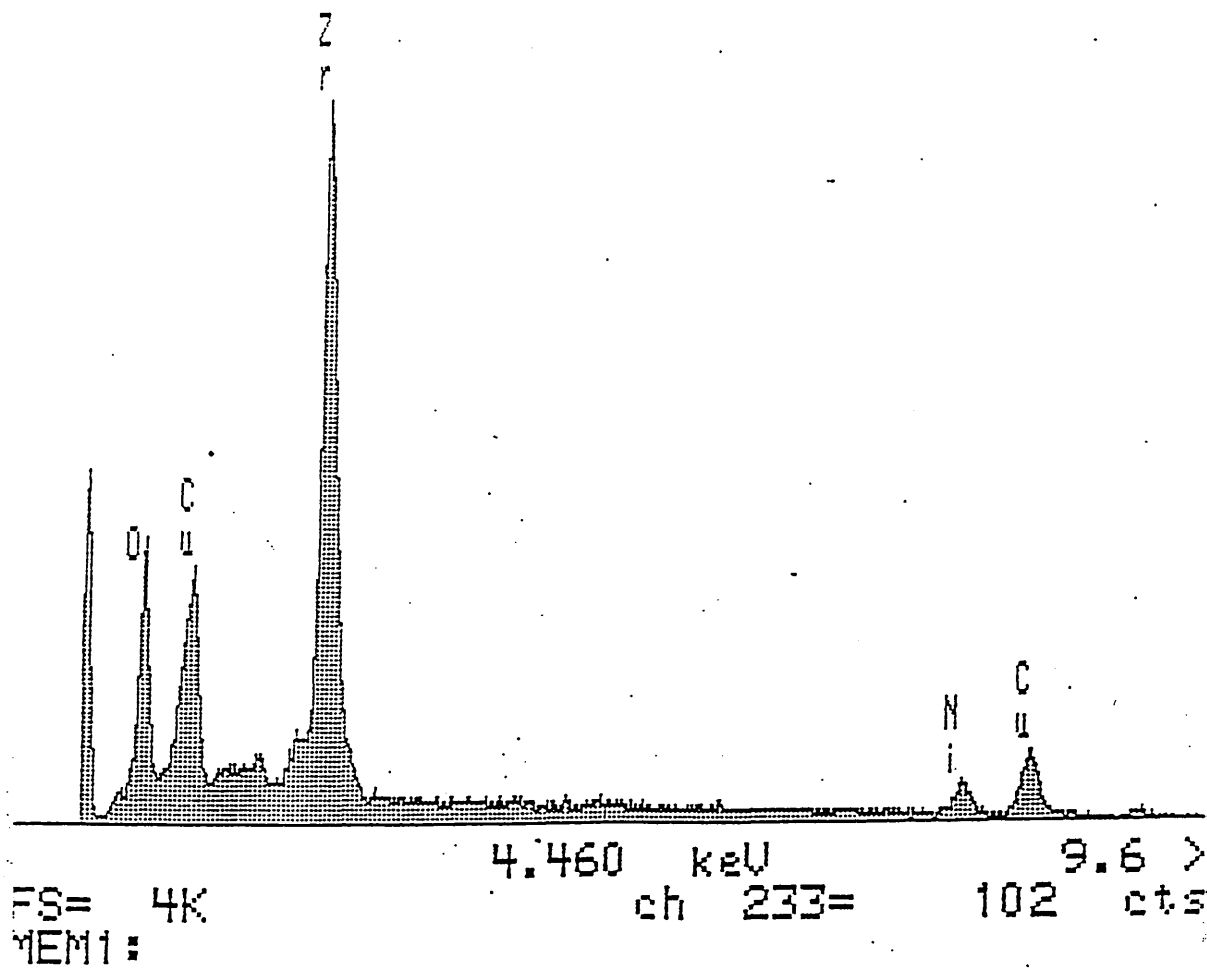
Figure 130



X 500

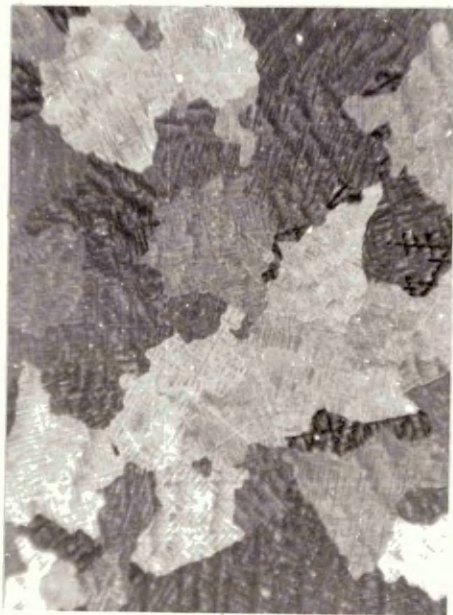
SEM back scattered electron image of zirconia based particles found in NES 824 matrix material.

X-RAY: 0 - 20 keV
Live: 44s Preset: 100s Remaining: 56s
Real: 55s 20% Dead



Edax Analysis - peak intensity curves showing the presence of zirconia rich particles.

Figure 132
Effect of HIP Time on the Microstructure of NES 824 HIPped at 950°C / 103MPa



45 Minutes



X110

2 Hours

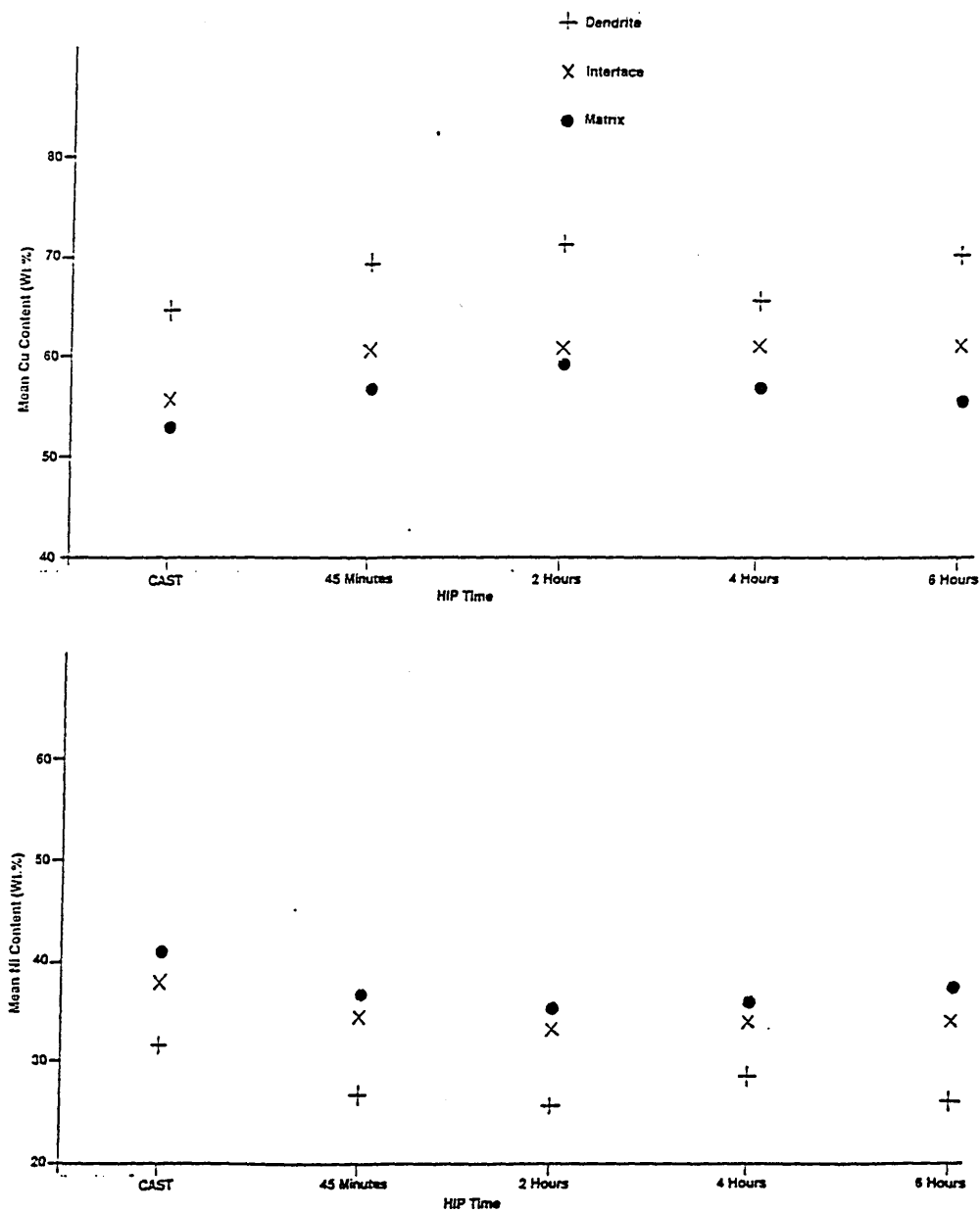


4 Hours

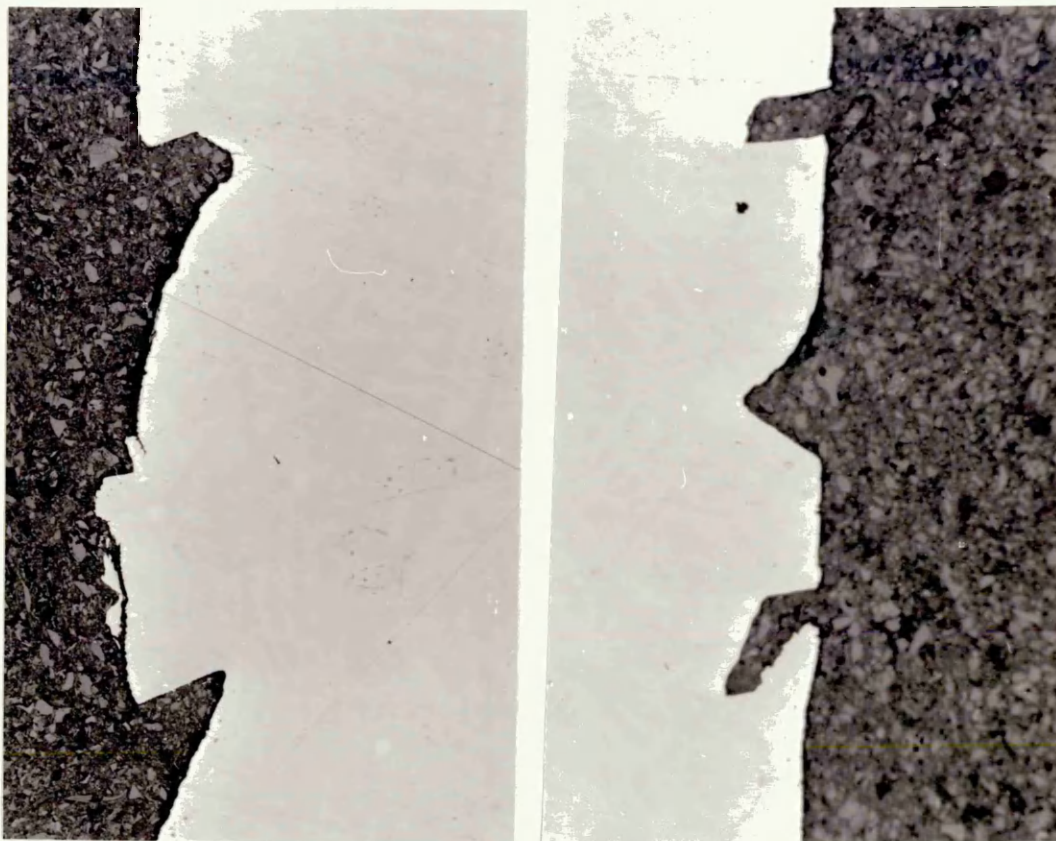


6 Hours

(Etched in 10% alcoholic ferric chloride)



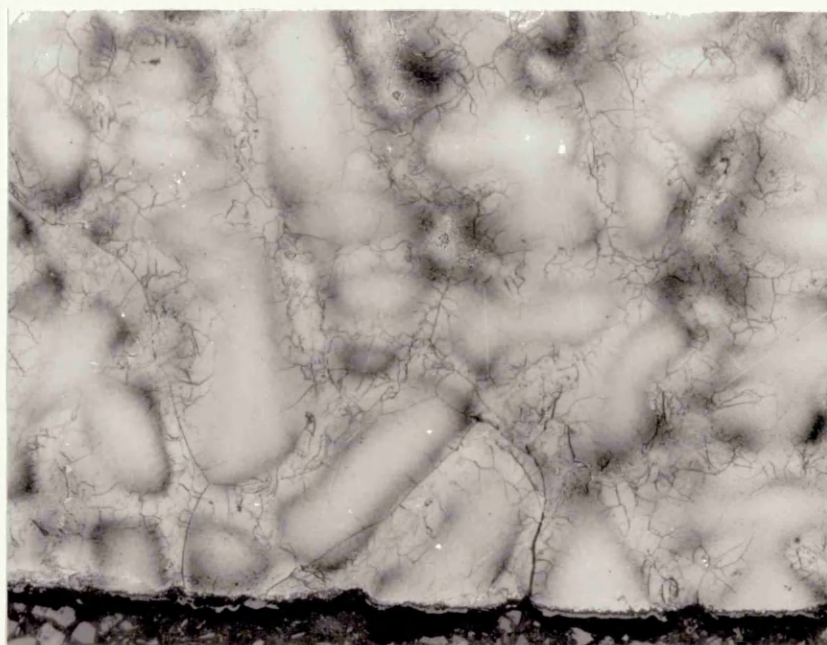
Effect of HIP time on the segregation of the two major alloying elements in 70/30 cupronickel.



X 166.5

Cracks along the gauge length of as-cast NES 824 specimen stress relieved at 700°C.

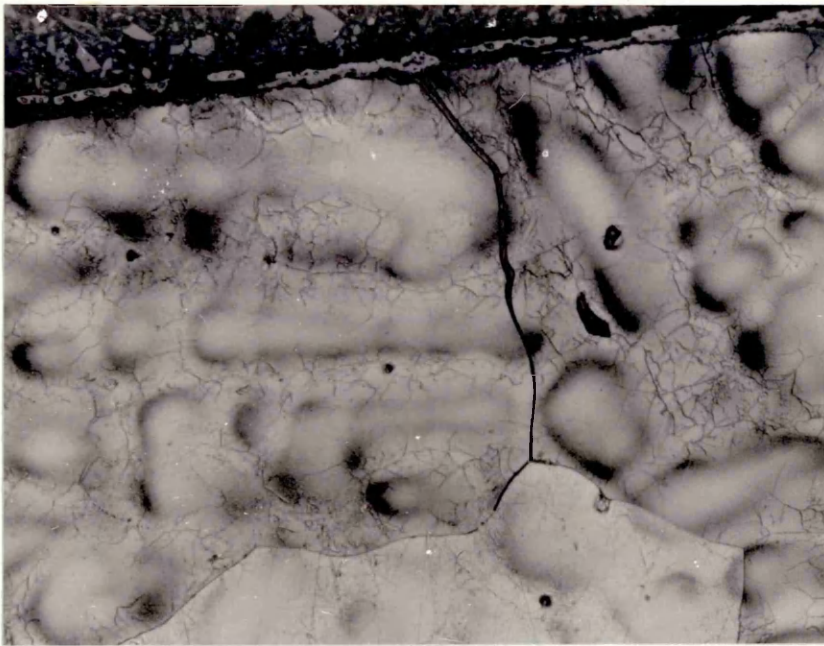
Figure 135



X 666

Net work of cracks observed in a NES 824 specimen stress relieved at 700°C.

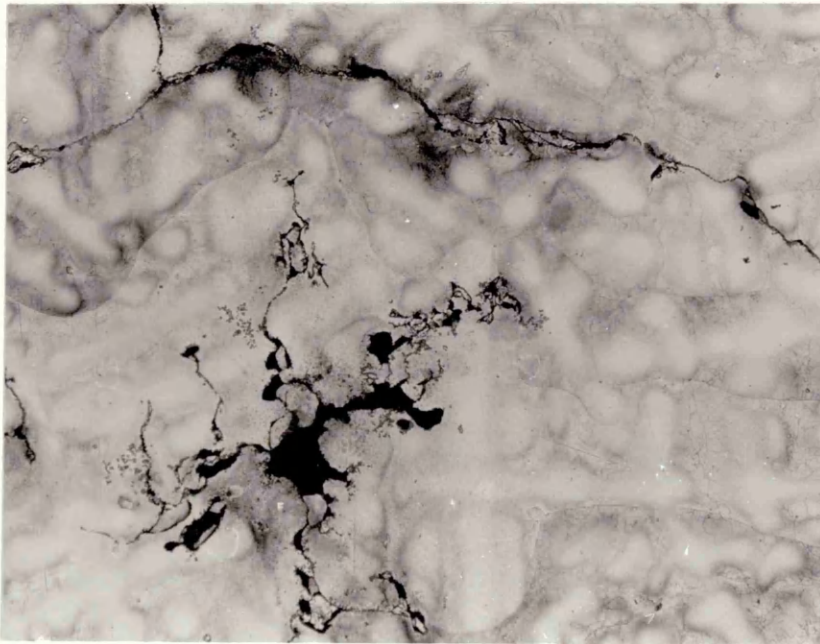
Figure 136



X 166.5

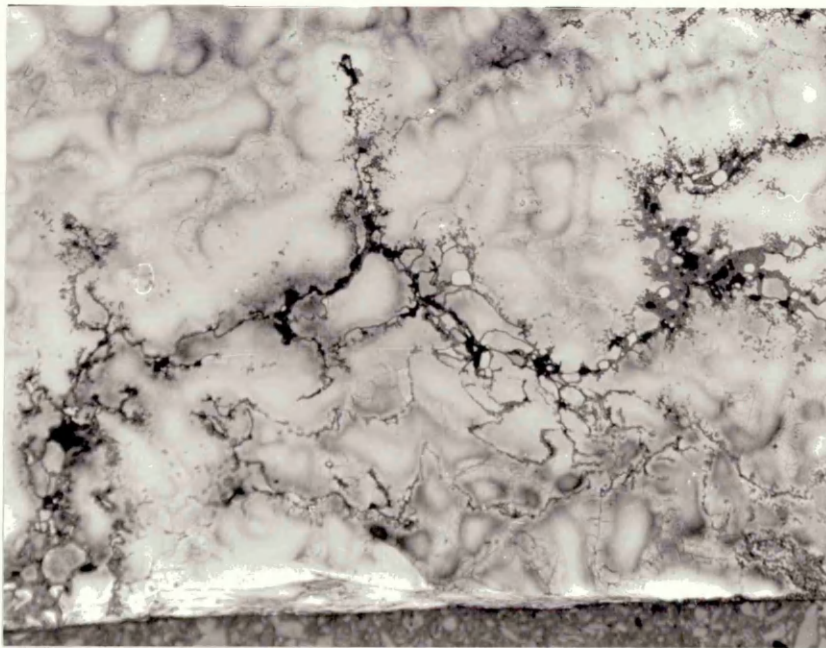
Specimen stress relieved at 750°C showing that cracks initiate at the sample edge and propagate along grain boundaries.

Figure 137



X 333

Cracks initiate at sites of porosity in the cast material. The cracks then grow and propagate along grain boundaries.



X 333

Coalescence of voids along grain boundaries.

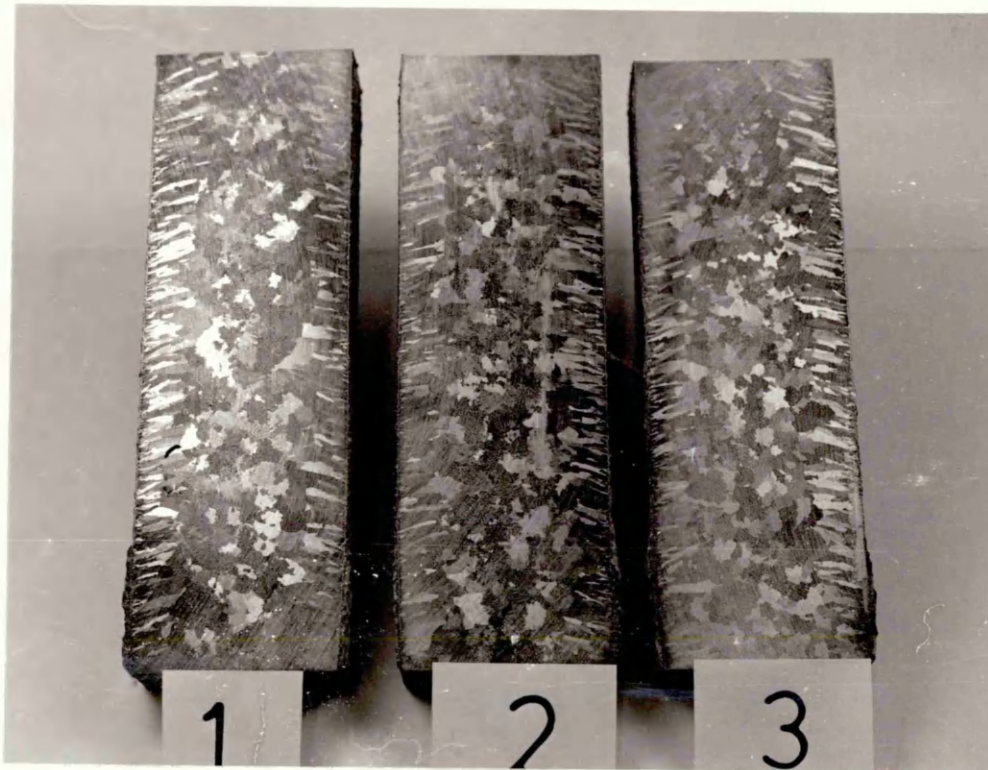


(i)

(ii)

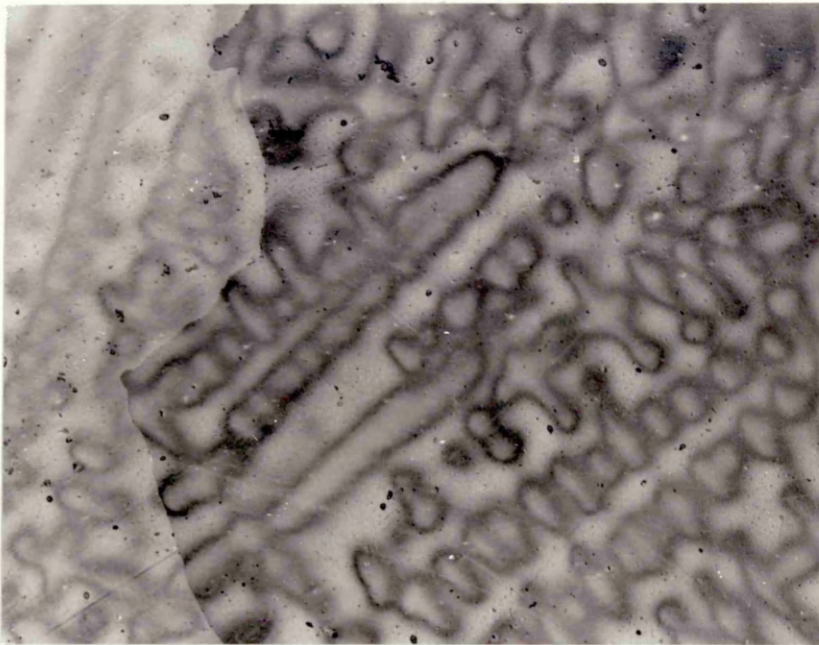
Macro-structure of sections taken from a HIP recovered M.O.D NES 824 casting etched in alcoholic ferric chloride representing:

- (i) Recovered defect material (area originally containing shrinkage cavity).
- (ii) Sound material.



Slices of NES 824 material taken from a M.O.D cast block representing material adjacent to the edge of the casting (identified 1) to that adjacent to the recovered defect material (3).

The macro-structures reveal that the grain size increases slightly as the edge of the casting is approached.



X 150

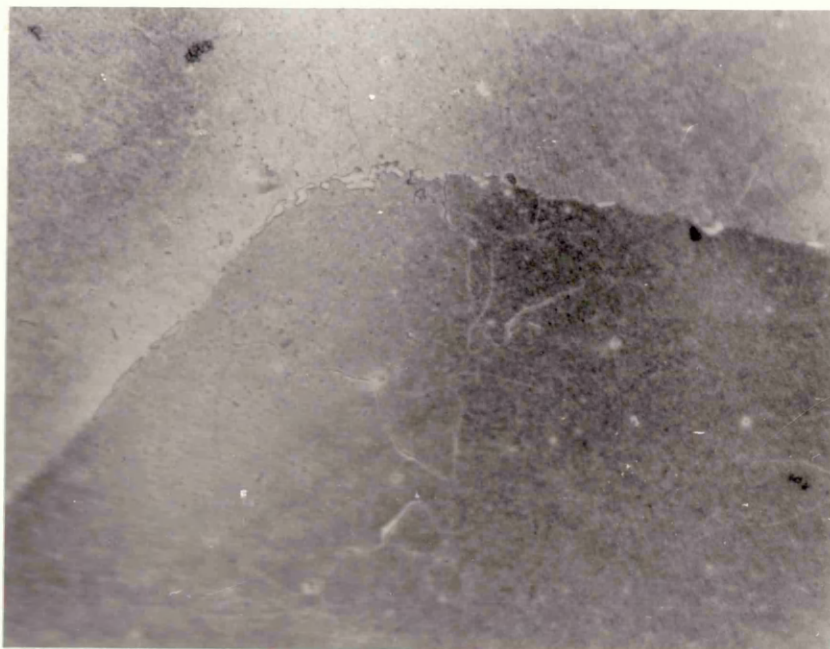
Sound HIPped NES 824 material shows a coarse grain size and extensive coring.

Figure 142



X 15000

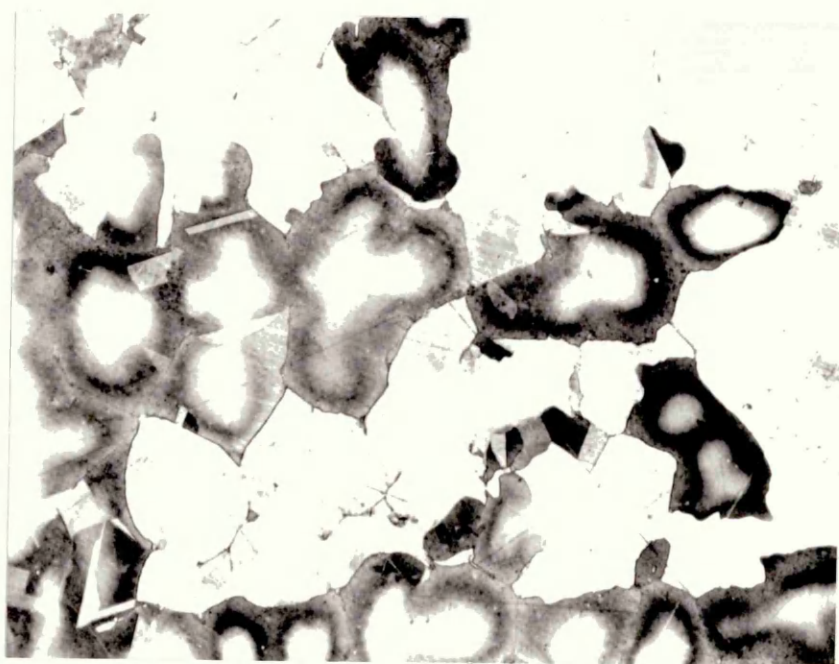
Oxide precipitates rich in Ni, Zr and Si within the matrix of the sound HIPped material.



X 15000

Precipitates located at grain boundaries within HIPped sound material.

Figure 144



X 150

Segregation in the defect material was found to be reduced after HIPping accompanied by a partially recrystallised grain structure.



X 3300

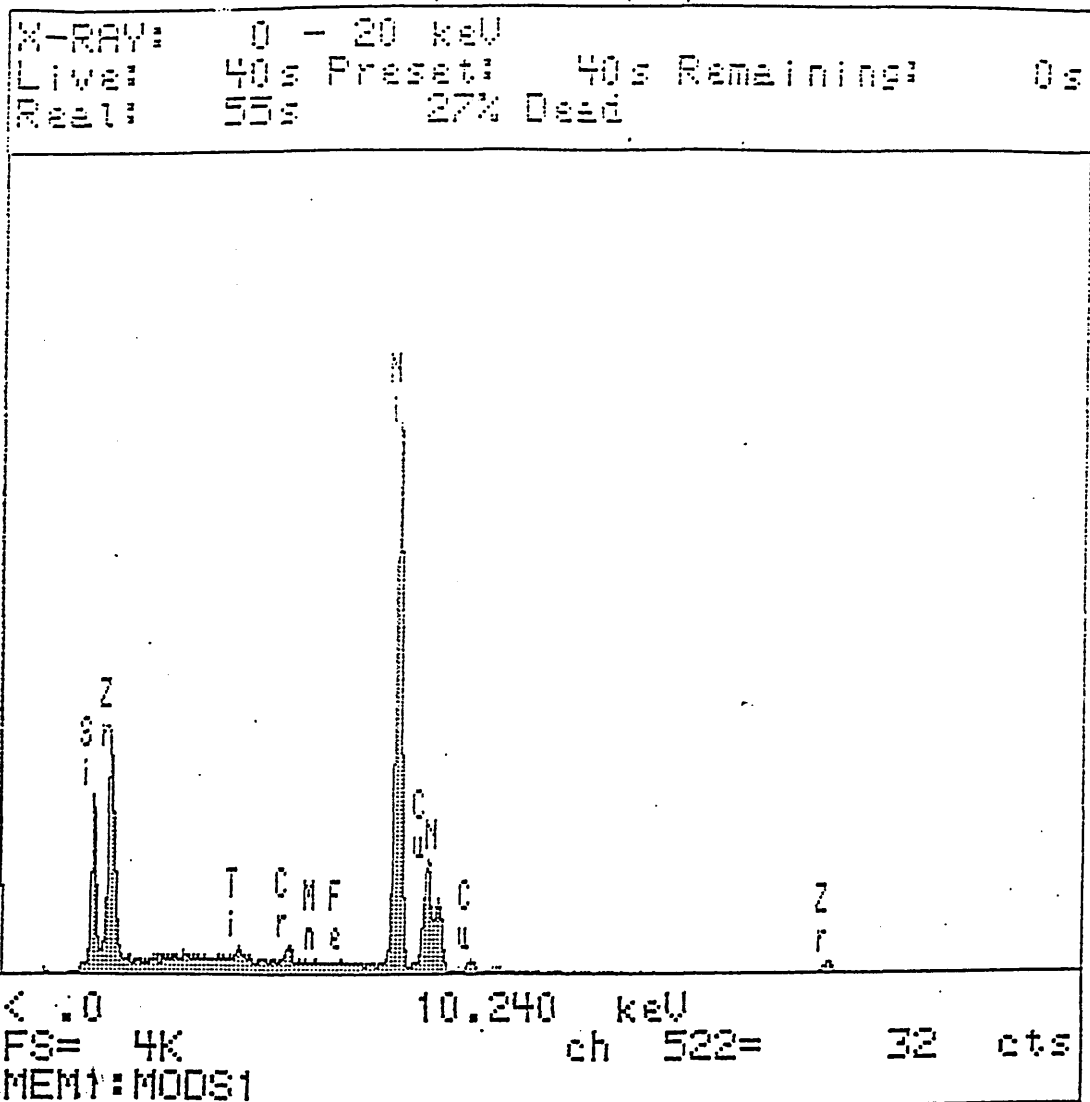
Grain boundary precipitation in HIP recovered defect material.

Figure 146

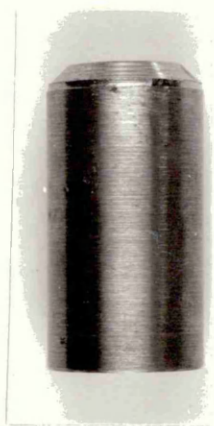


X 3000

Precipitate rich in Zr, Si and O found within the HIP recovered defect material.



X-Ray peak intensity curves indicate the presence of precipitates rich in Ni, Zr and Si.



HIPPed 850°C

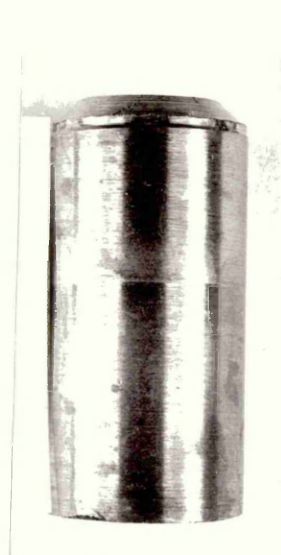


HIPPed 950°C

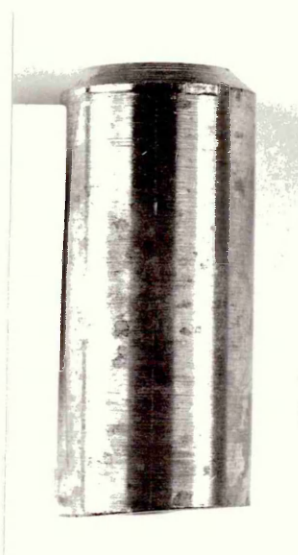


HIPPed 1025°C

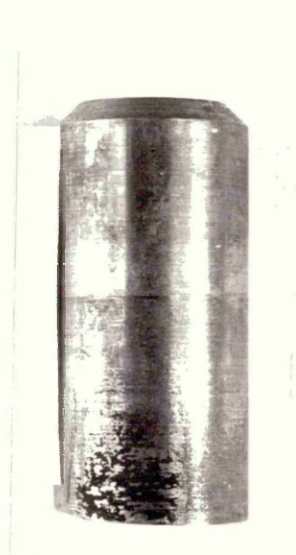
504 Hours Test Duration



HIPPed 850°C



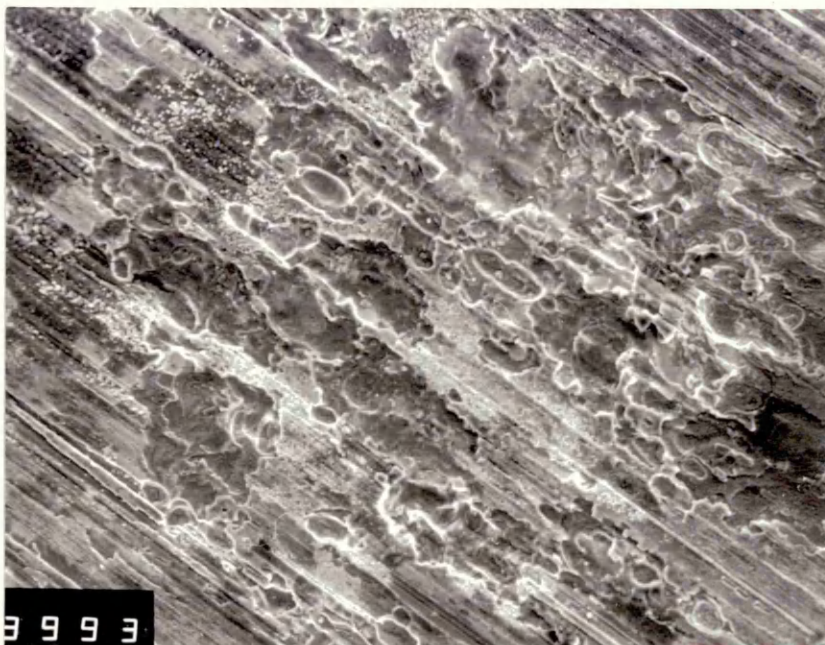
HIPPed 950°C



HIPPed 1025°C

1008 Hours Test Duration

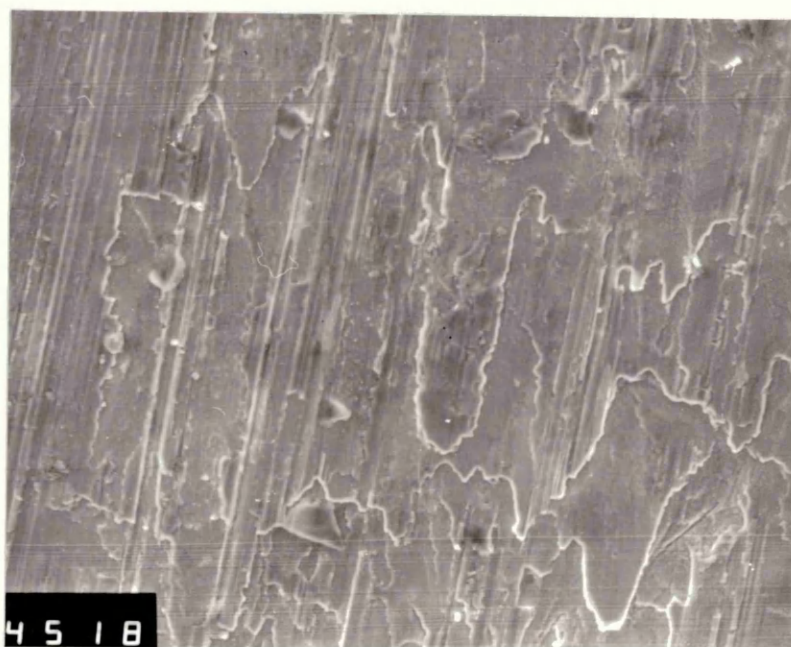
Appearance of HIPPed 70/30 cupronickel corrosion specimens after 504 and 1008 hours duration in a 5% salt spray.



X 180

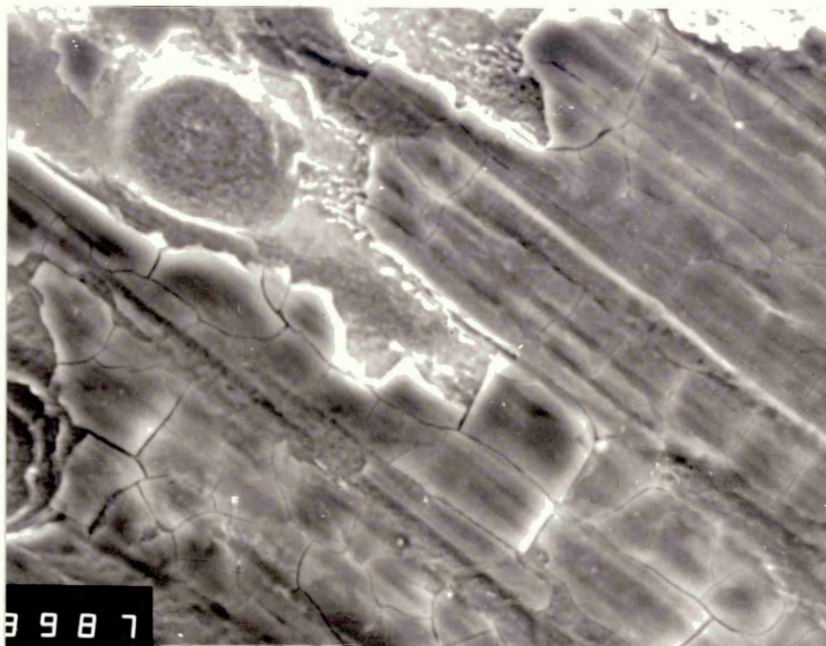
Isolated area of corrosive pitting on NES 824 material HIPped at 1025°C. The pitted appearance is also representative of material HIPped at 850°C and 950°C after 504 hours on test in a 5% salt solution.

Figure 150



X 180

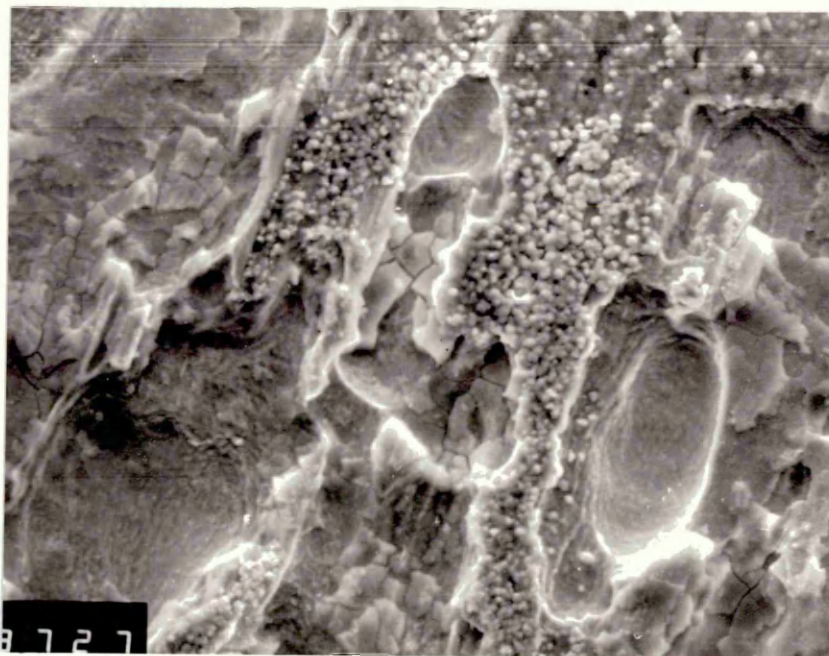
After 1008 hours on test the majority of the specimens surface appears to be prone to a small degree of intergranular corrosion.



X 720

Cracking of the surface layers of material causing them to peel away.

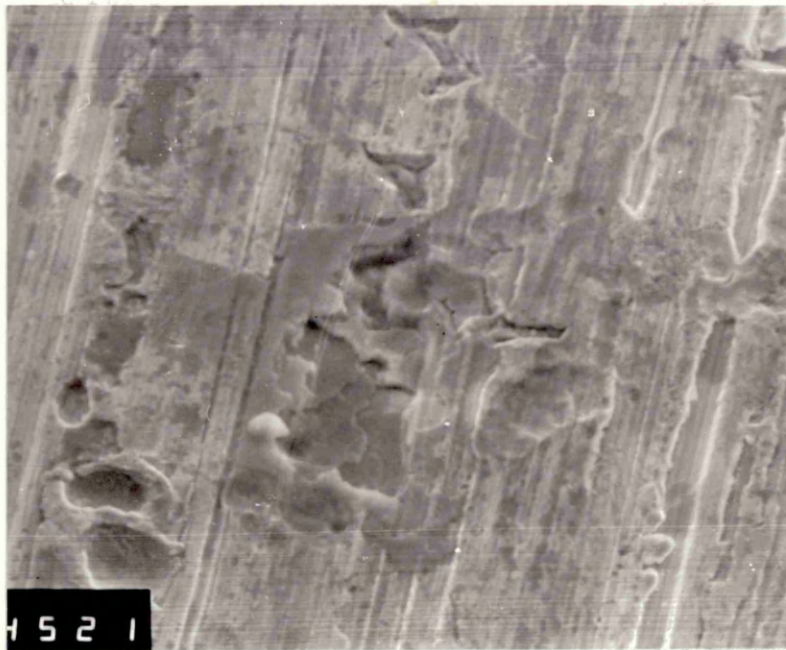
Figure 152



X 680

Preferential phase corrosion at dendritic regions occurring as surface cracking and cratering of newly exposed areas.

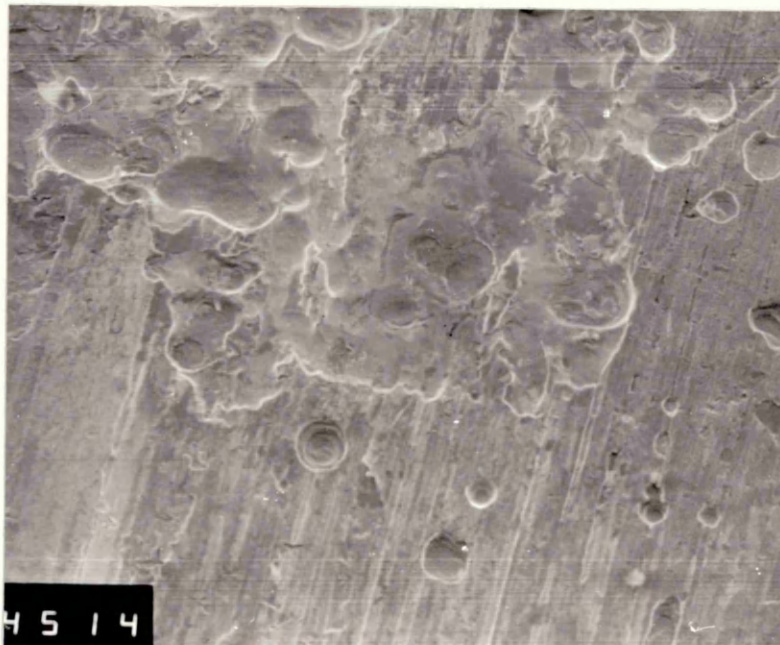
Figure 153



X 680

Corrosive attack of HIPped material after 1008 hours on test took the form of craters, pits and peeling of the surface layers of material.

Figure 154



X 170

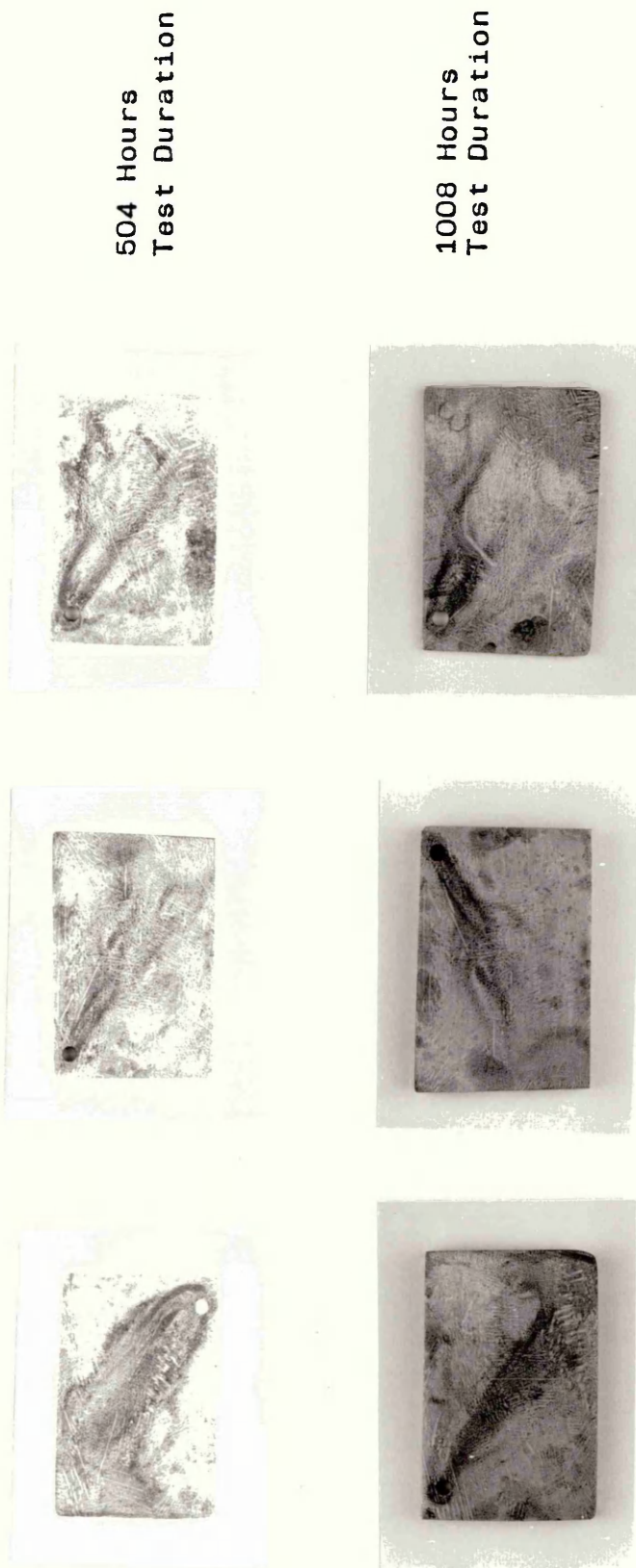
Corrosive attack of HIPped material by cratering.



X 640

Corrosive pitting and cratering of HIPped material
subjected to a 5% salt slution.

Figure 156

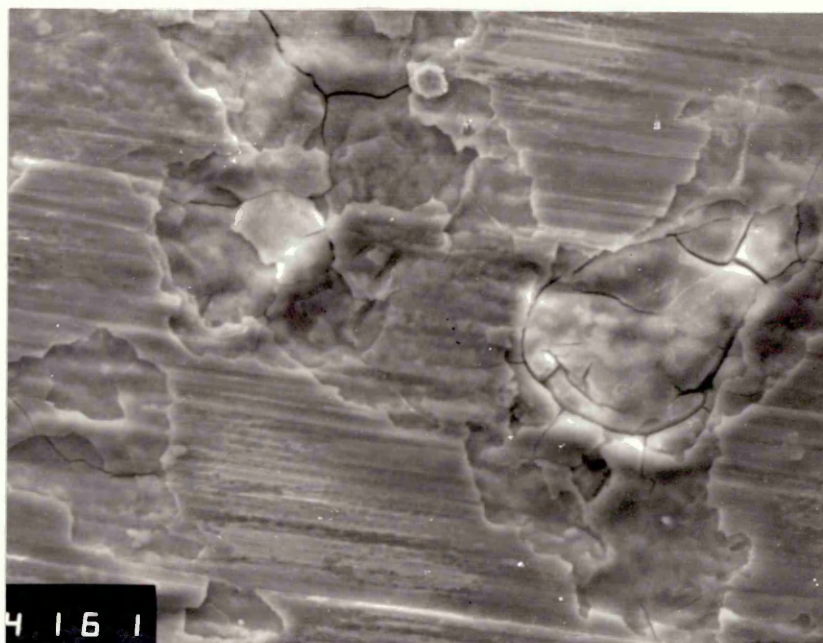


Appearance of as-cast 70/30 cupronickel specimens after 504 and 1008 hours duration in a 5% salt spray solution.



X 190

The majority of corrosion taking place on as-cast specimens after 1008 hours on test in a 5% salt solution was situated around the machined hole.

Figure 158

X 600

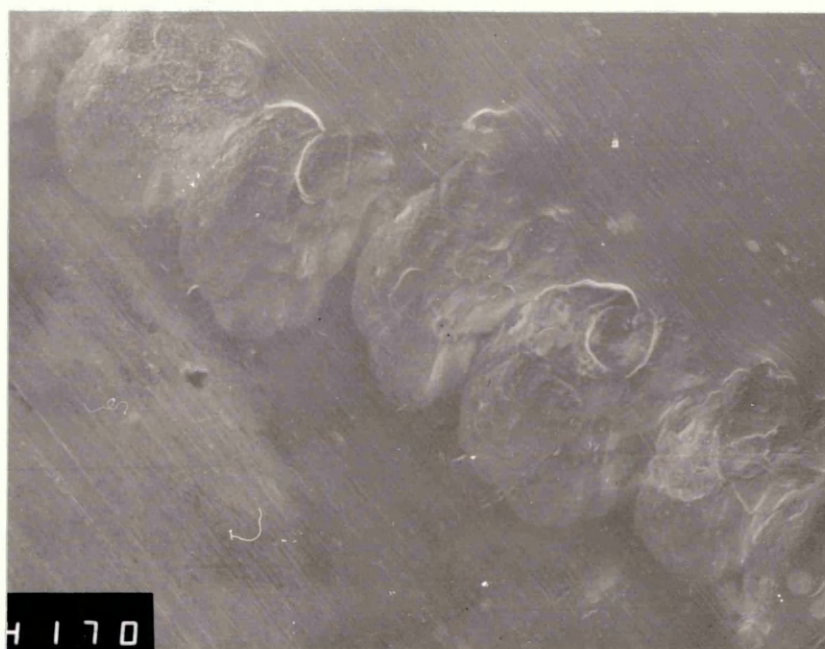
Cracking and removal of the surface layers of as-cast material after 1008 hours in a 5% salt solution.



X 180

Intergranular or interdendritic corrosion of as-cast material subjected to a 5% salt solution.

Figure 160



X 160

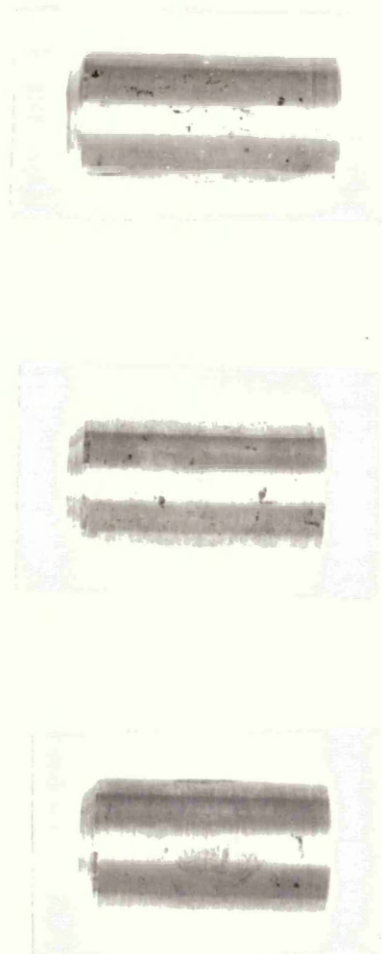
As-cast material showing intergranular corrosion across the diagonal cross-section of the test specimen.

Figure 161

As-Cast



HIPped

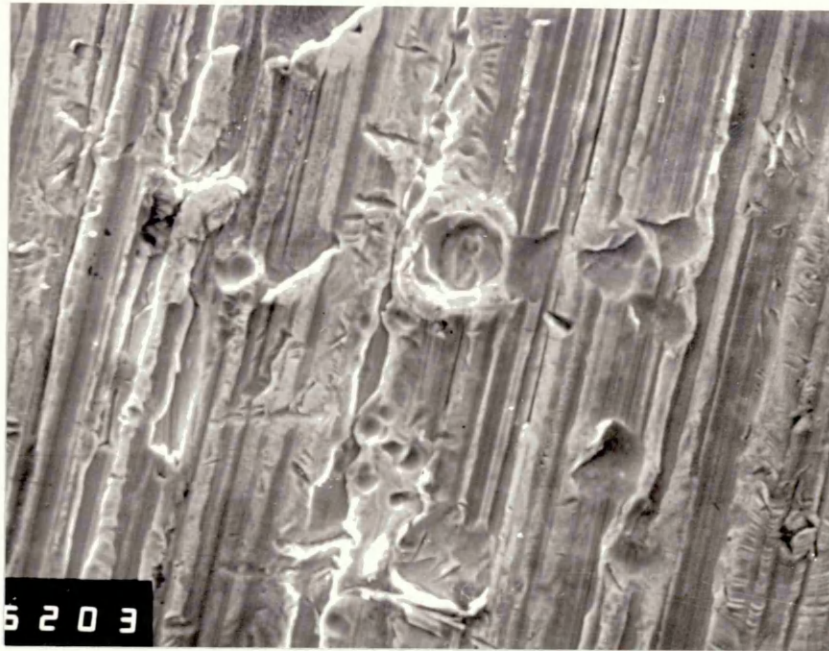


HIPping Temperature: 850°C

950°C

1025°C

Appearance of as-cast and HIPped 70/30 cupronickel after 1008 hours duration in a substitute ocean water spray.



X 162

Corrosive pitting and cratering typical of that observed in 70/30 cupronickel HIPped at 850°C and 950°C.

Figure 163



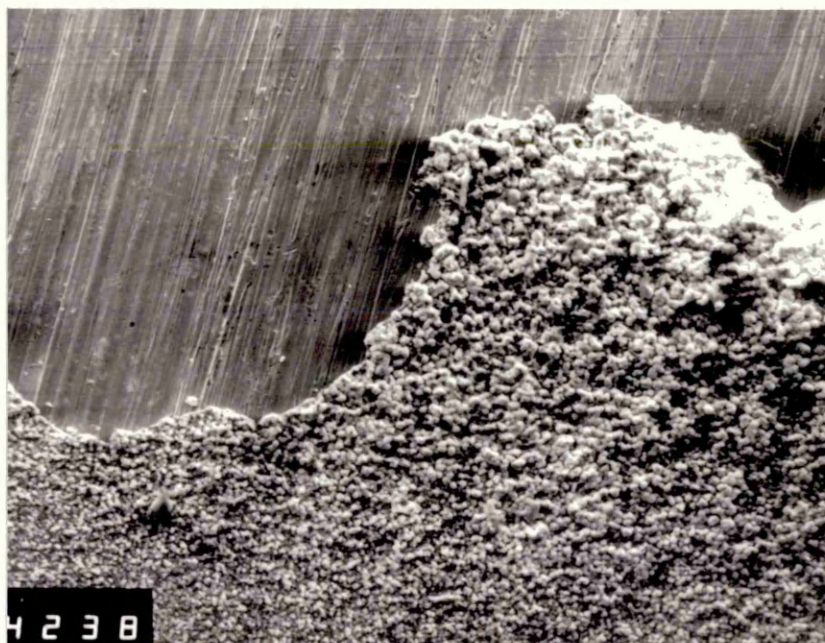
X 1120

Corrosion appears to take place as preferential attack of dendritic regions. These sites then nucleate corrosion craters.

(i)

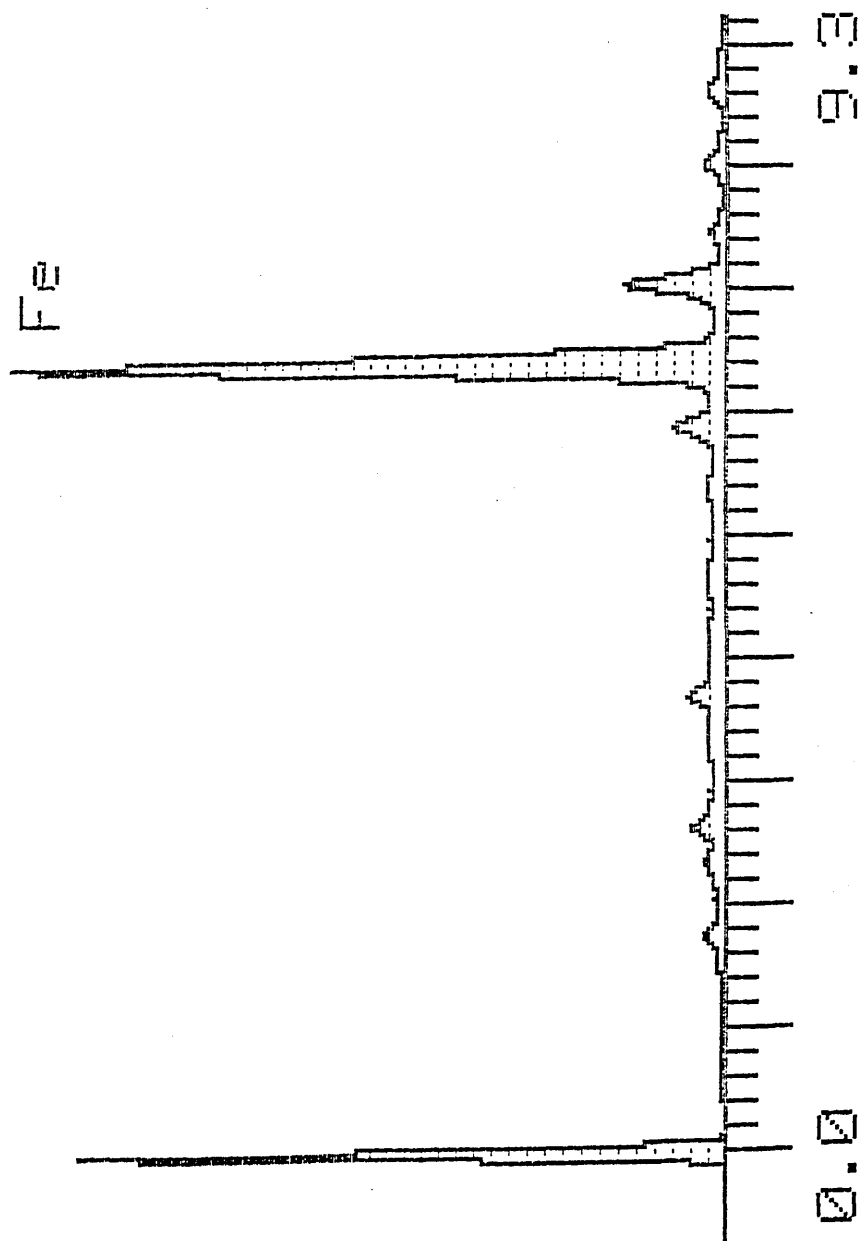


(ii)

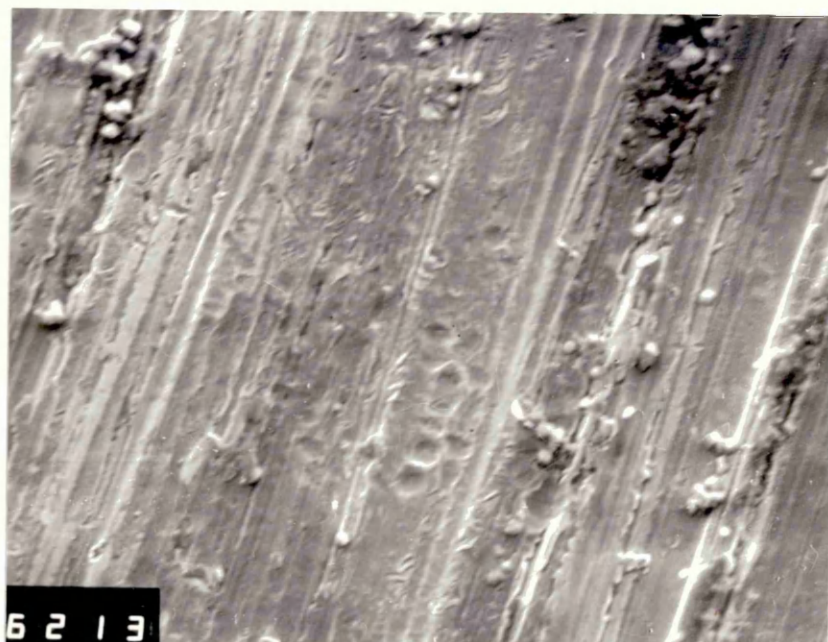


Visual (i) and SEM (ii) examination of a specimen representing 70/30 cupronickel HIPped at 1025°C. 25% of the specimens surface was covered by an oxide deposit identified by ZAF4/EDAX analysis to be iron oxide (Figure 165).

Figure 165

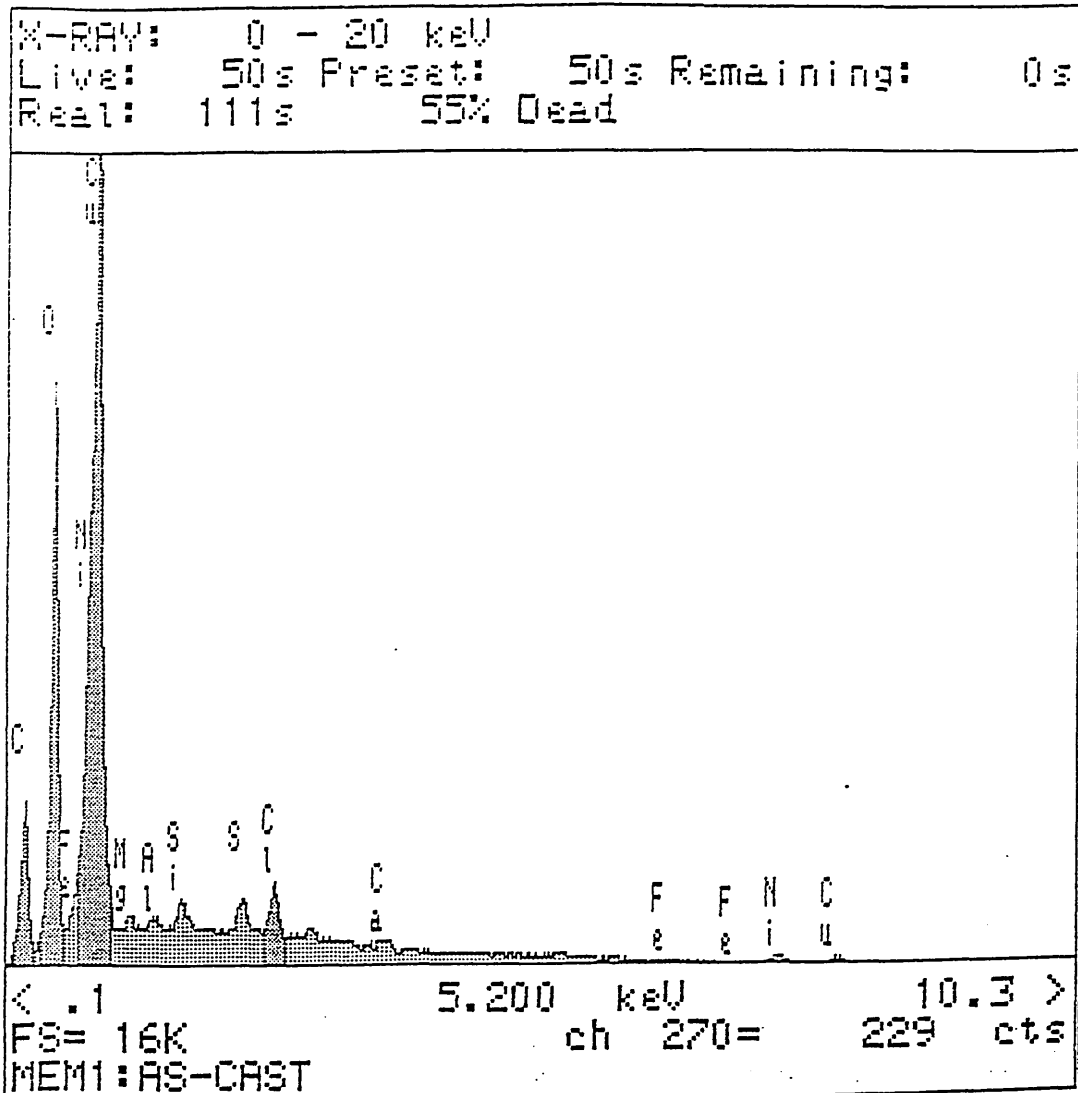


EDAX analysis of oxide deposit found on specimen representing NES 824 HIPped at 1025°C

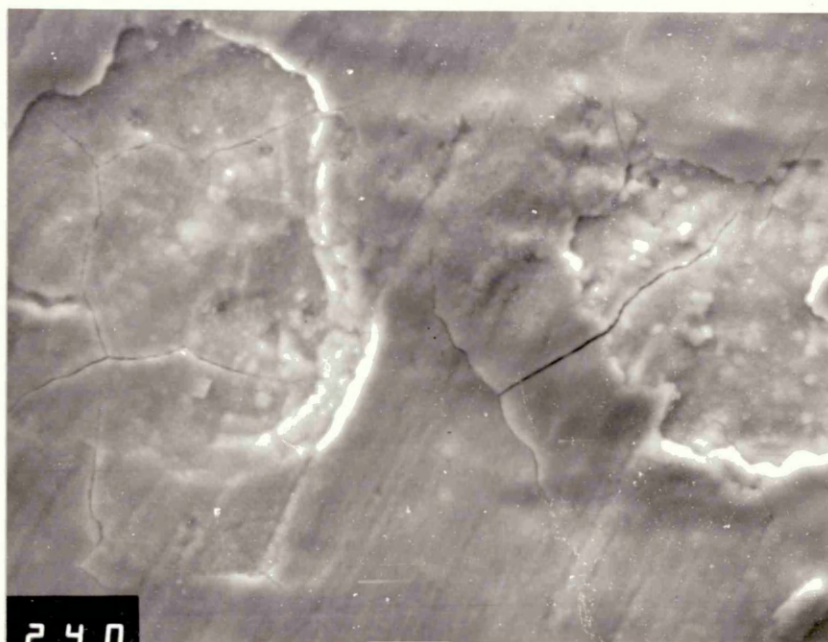


X 320

Apart from the iron-oxide deposit very little other corrosive attack was observed apart from cratering of material HIPped at 1025°C.



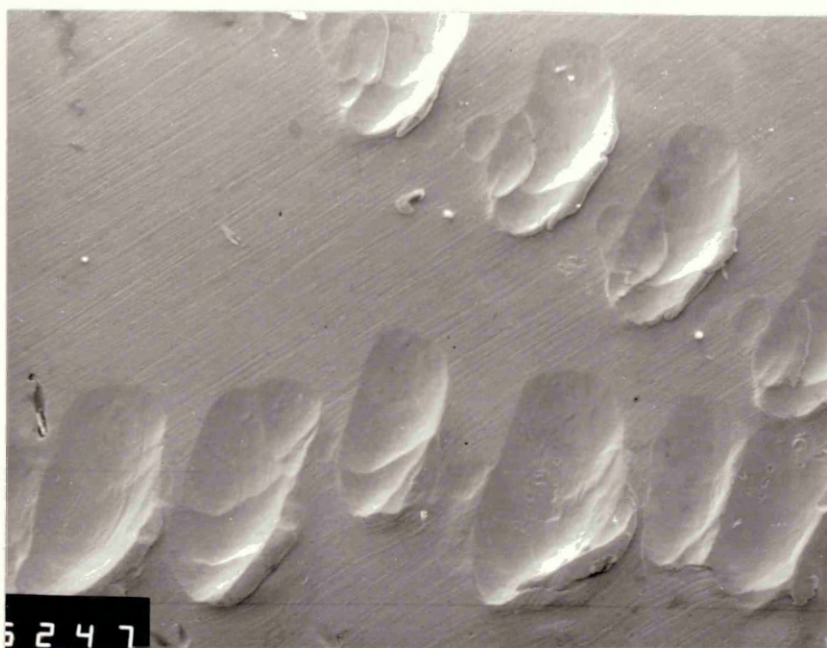
ZAF4/EDAX analysis of the protective corrosion product formed on as-cast material after 1008 hours duration in substitute ocean water, shows the oxide layer to be rich in chlorine, carbon, copper and nickel.



X 720

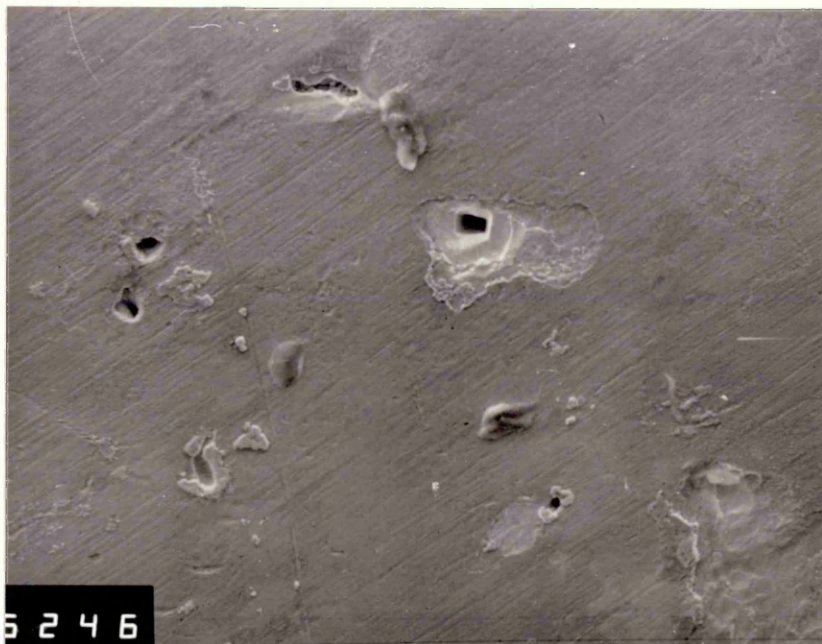
Cracking and peeling of the surface layers of as-cast 70/30 cupronickel after 1008 hours in a substitute ocean water spray.

Figure 169



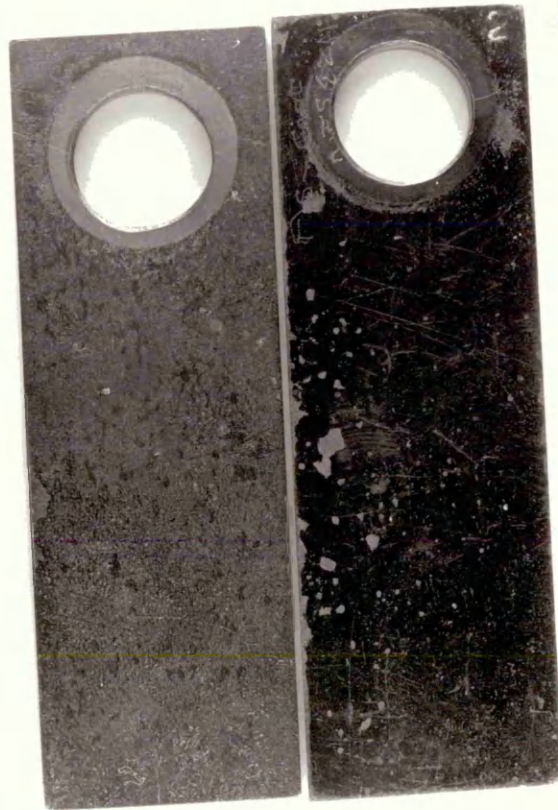
X 90

Corrosion craters observed on the surface of as-cast material subjected to a substitute ocean water spray.



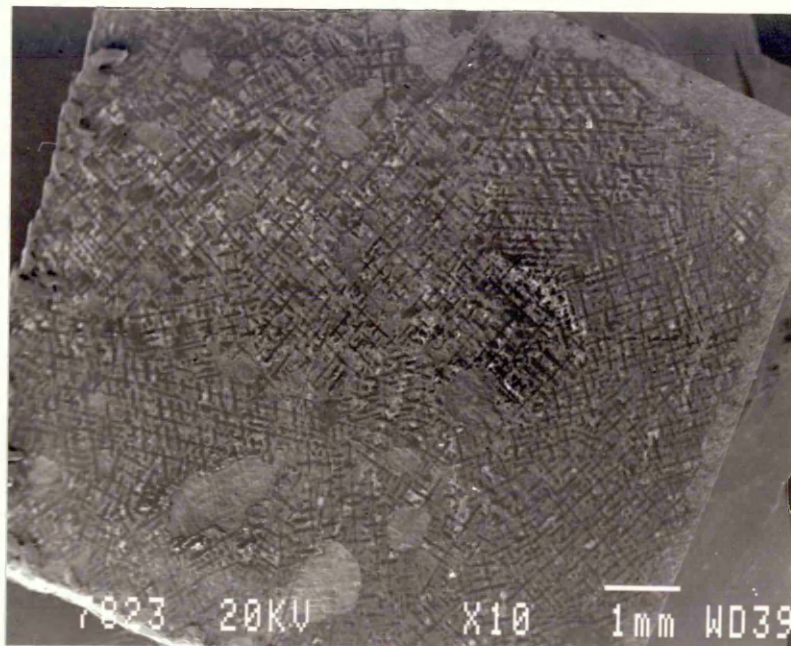
X 180

Corrosion of as-cast 70/30 cupronickel occurs around sites of shrinkage and micro-porosity together with the erosion of pits caused by the removal of precipitates from the matrix.



Appearance of HIPped NES 824 samples after 12 months immersion in the sea at Langstone Harbour. One side contains a shiny black oxide coating whilst the under side of the specimen reveals a matt coating which is less well developed.

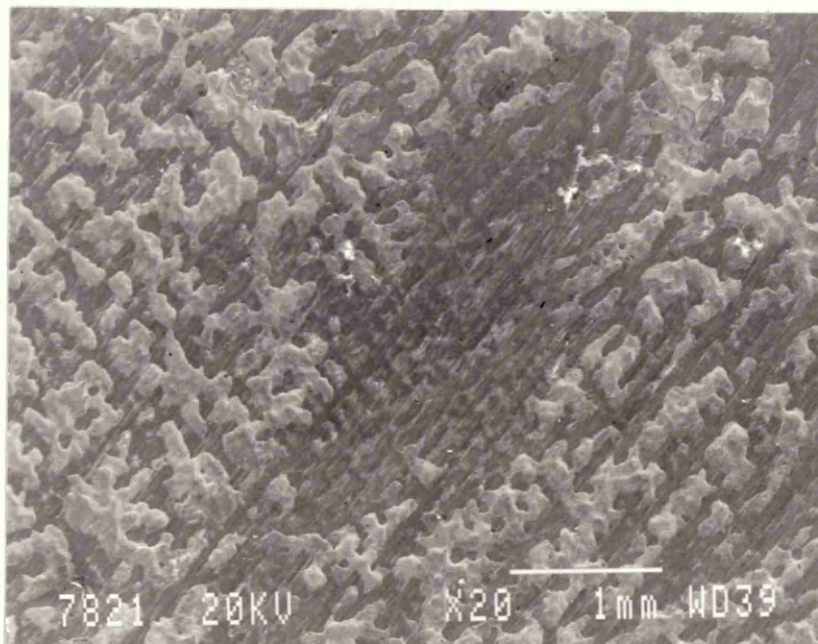
Figure 172



X 10

SEM examination of the shiny black corrosion product film revealed that it etched the matrix material revealing the dendritic structure.

Figure 173

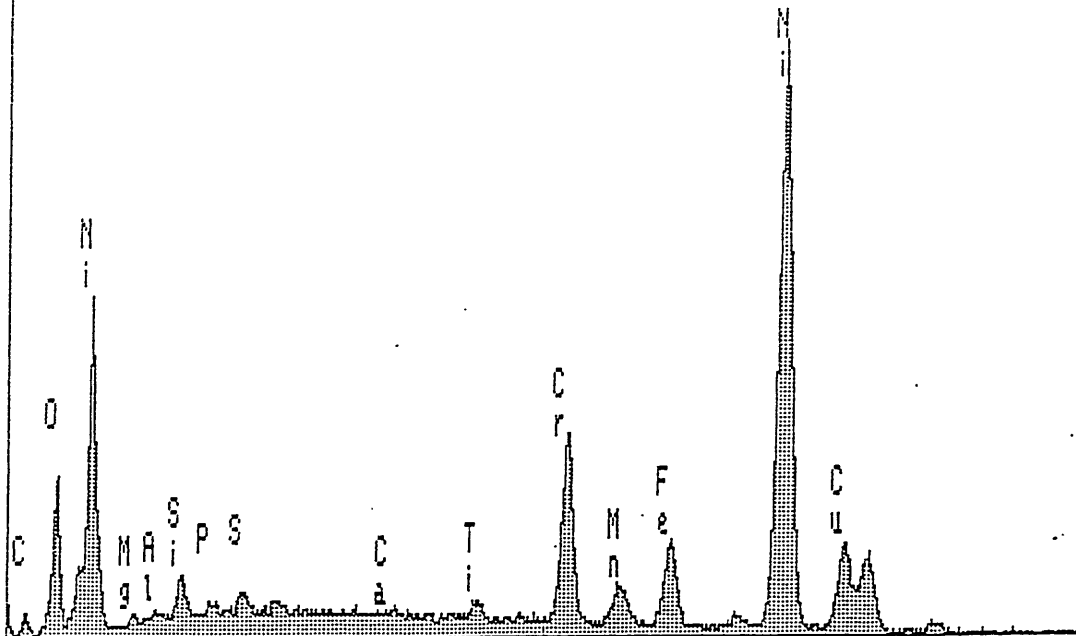


X 20

Preferential attack of dendritic regions. Nickel rich regions form a protective film in preference to the copper matrix.

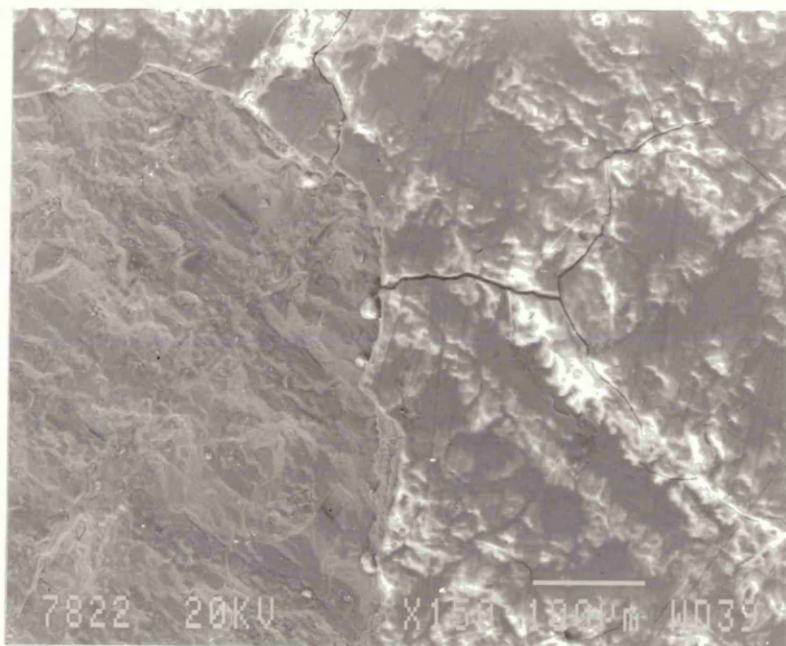
X-RAY: 0 - 20 keV
Live: 50s Preset: 50s Remaining: 0s
Real: 64s 22% Dead

20KV MES 824



< .1 5.200 keV 10.3 >
FS= 4K ch 270= 116 cts
MEM1:SHINY BLACK COATING

X-ray intensity peaks reveal the corrosion product to be rich in nickel and oxygen.

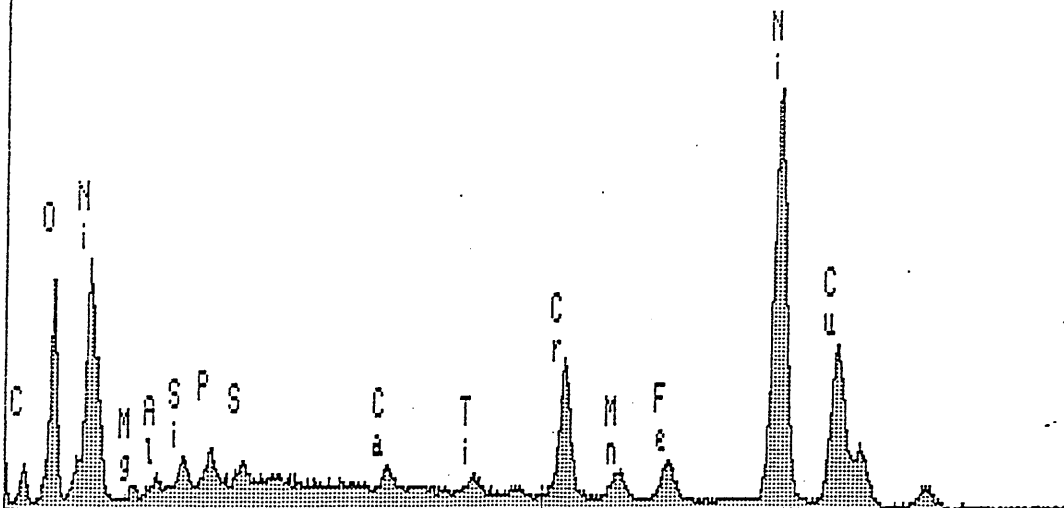


X 150

Cracking of the corrosion product film and subsequent loss of surface protection.

X-RAY: 0 - 20 keV
Live: 50s Preset: 50s Remaining: 0s
Real: 64s 22% Dead

20KV NES 824



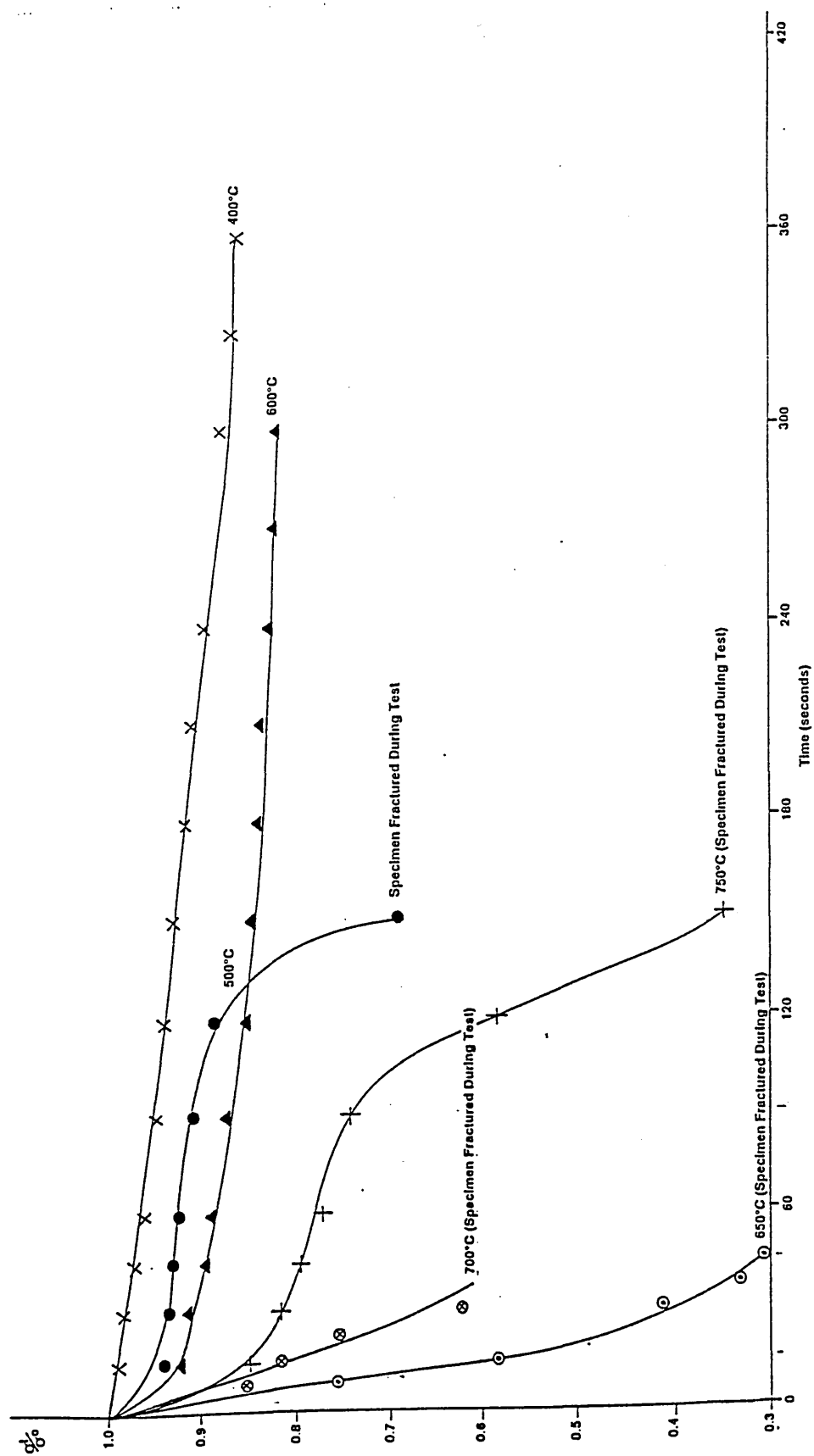
< .1 5.200 keV 10.3 >
FS= 4K ch 270= 128 cts
MEM1:MATT OXIDE COATING

EDAX analysis of the matt oxide coating showing it to be of reduced thickness due to the pick up of the matrix elements which were not identifiable during analysis of the shiny black coating.



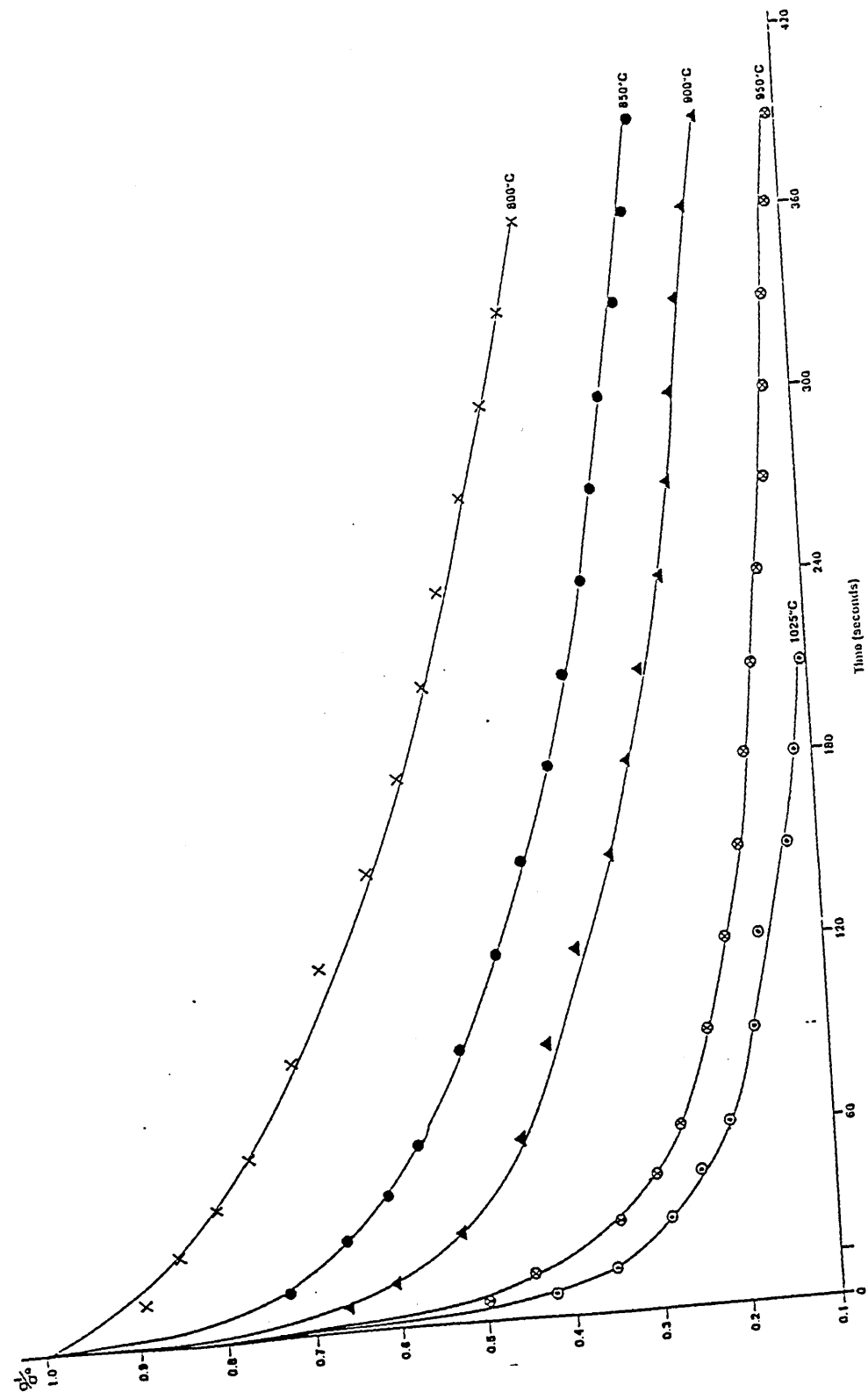
The matt appearance of HIPped NES 824 crevice corrosion specimens after 6 months on test revealed a partially developed corrosion product film.

Figure 178



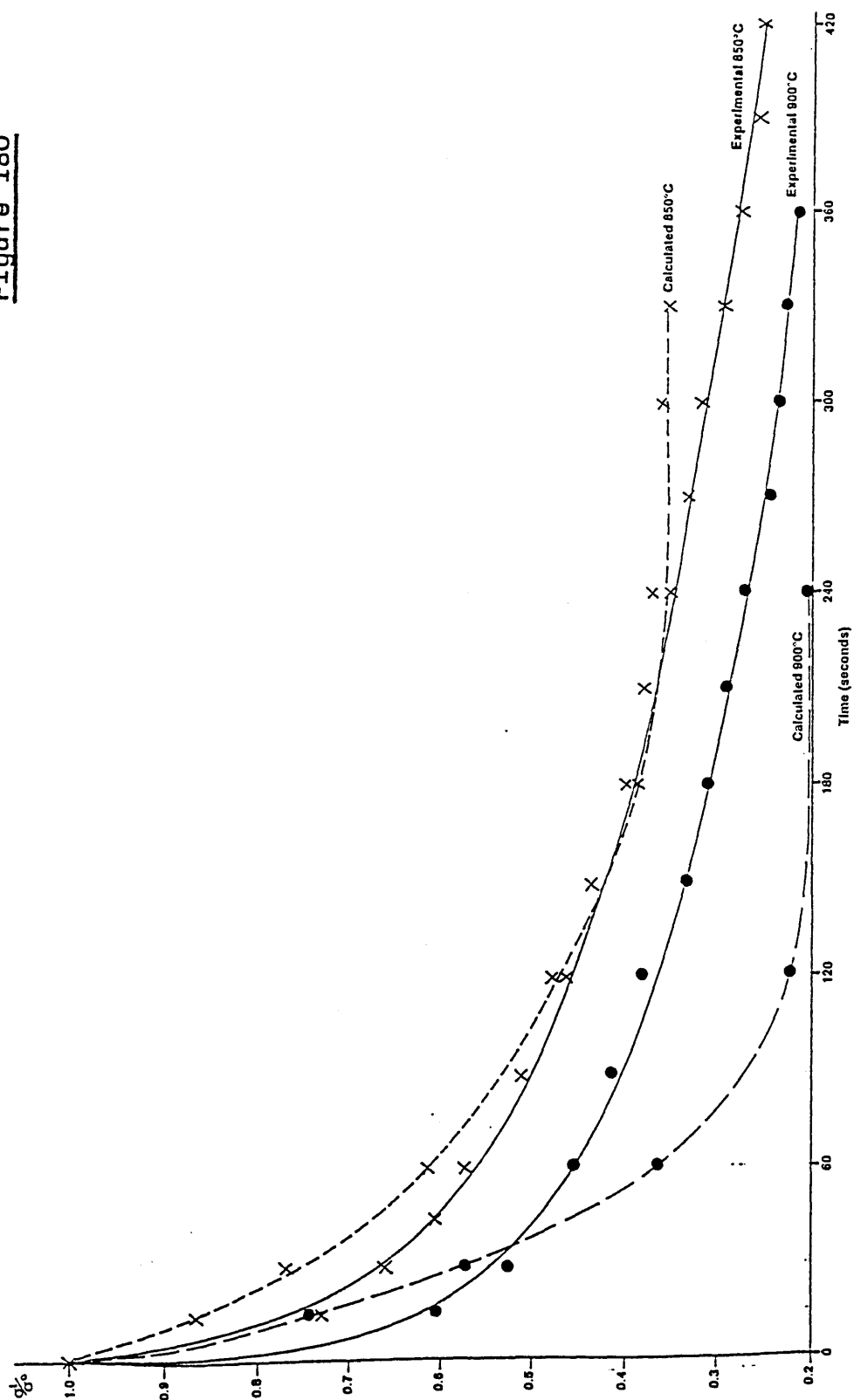
Stress relaxation curves for 70/30 cupronickel at temperatures within the range 400-750°C.

Figure 179



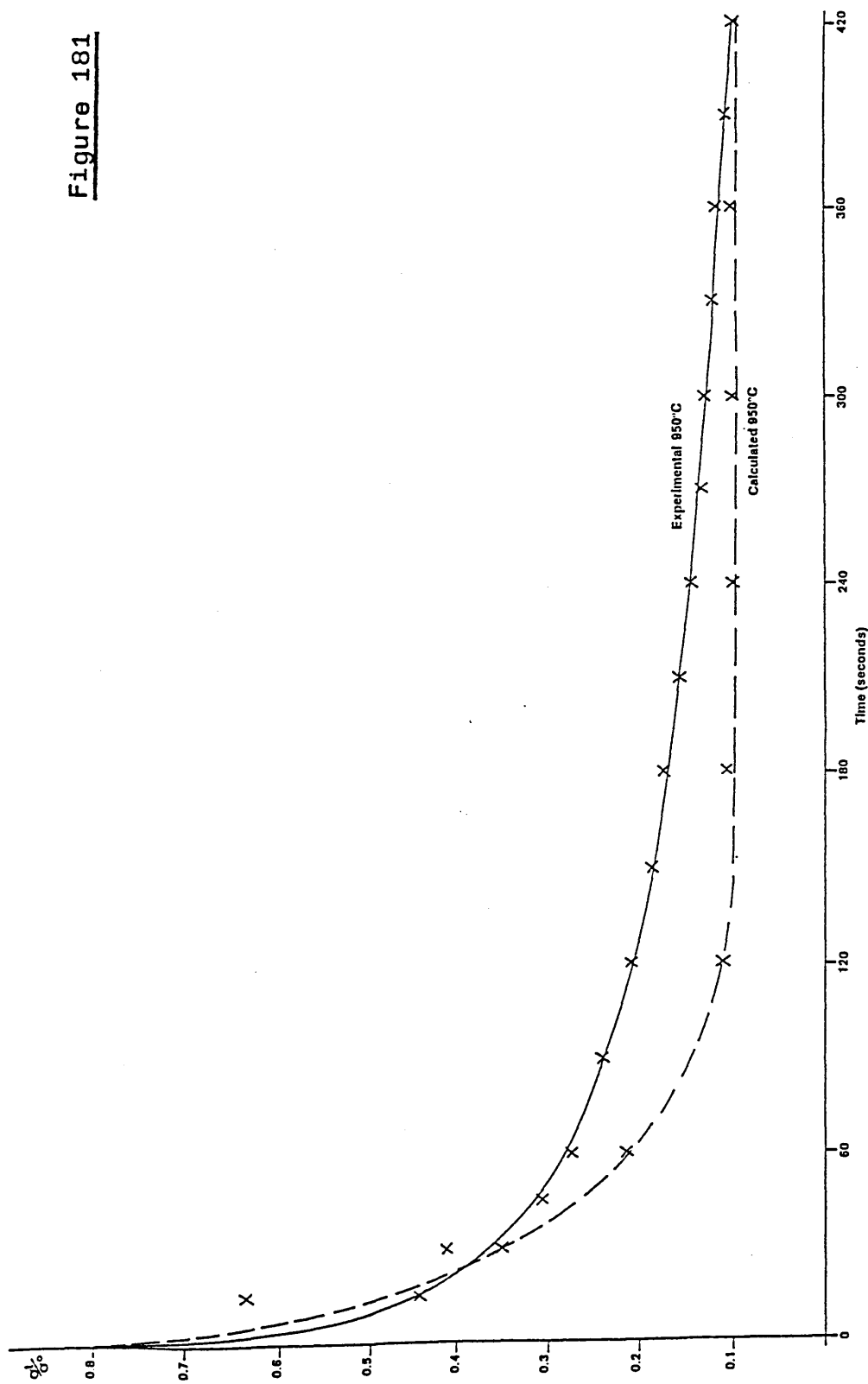
Stress relaxation curves for 70/30 cupronickel at temperatures within the range 800-1025°C.

Figure 180



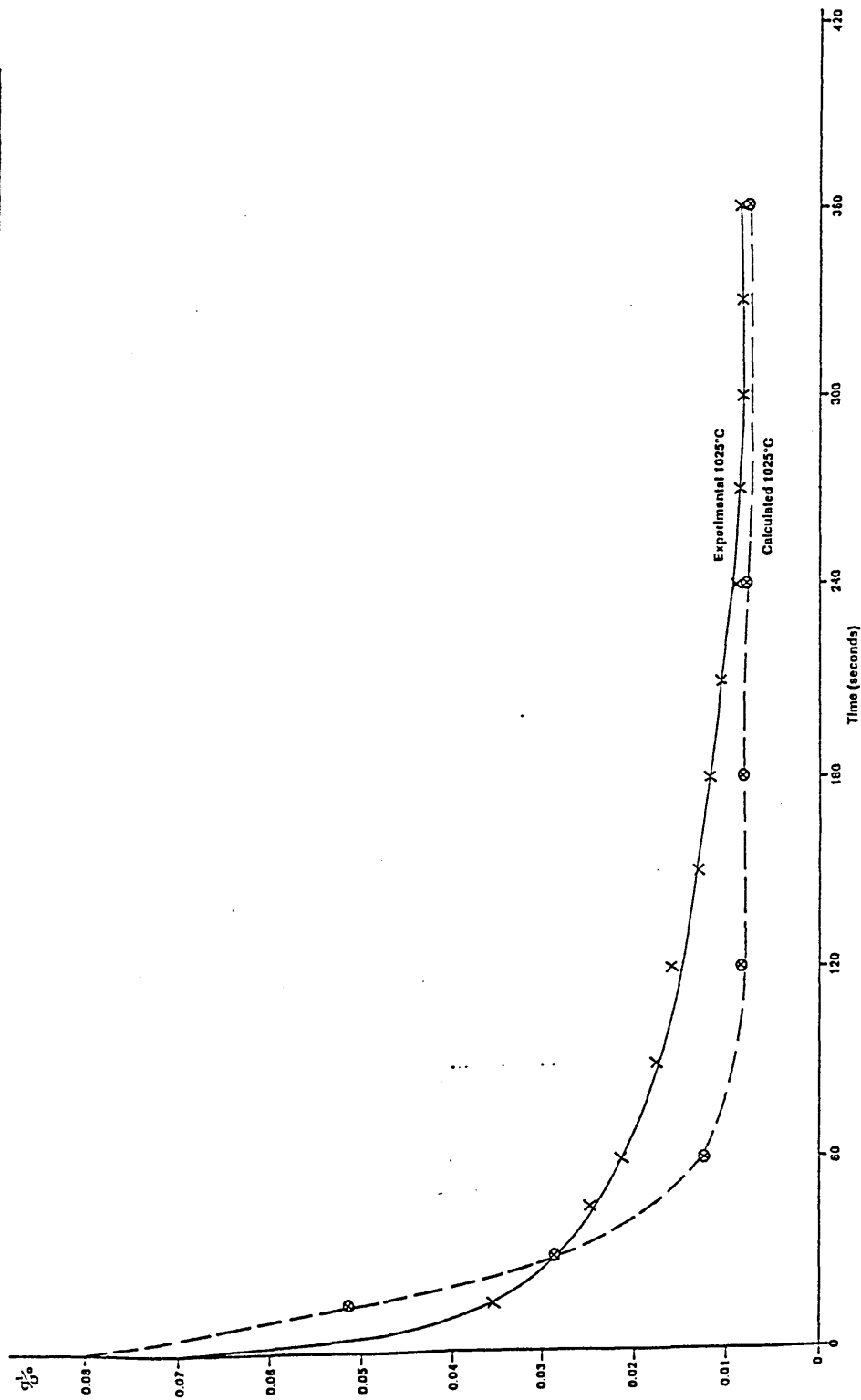
Comparison of experimental and calculated stress relaxation curves for 70/30 cupronickel at elevated temperatures of 850°C and 900°C.

Figure 181



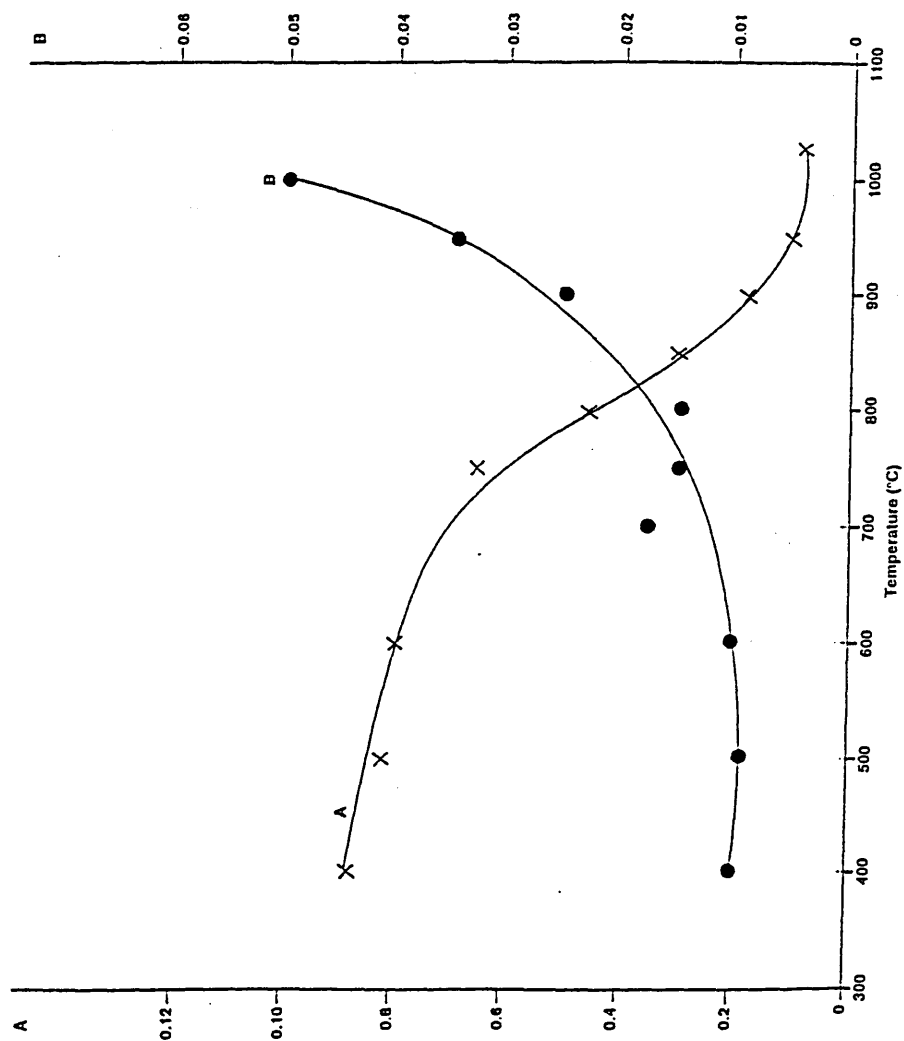
Comparison of experimental and calculated stress relaxation curves
for 70/30 cupronickel material at 950°C.

Figure 182



Comparison of experimental and calculated stress relaxation curves
for 70/30 cupronickel material at 1025°C.

Figure 183

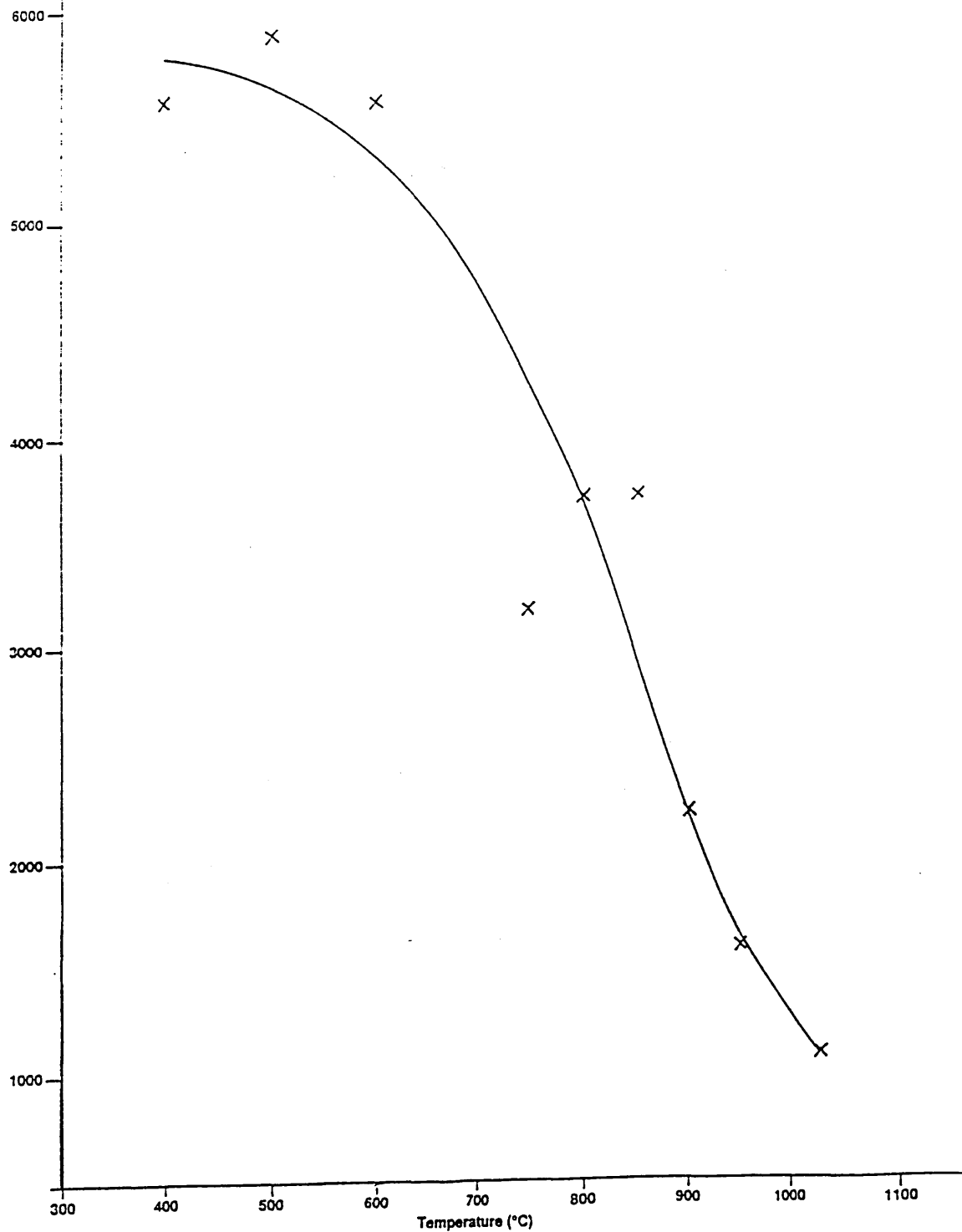


Change in stress relaxation parameters A and B with temperature.

Viscosity

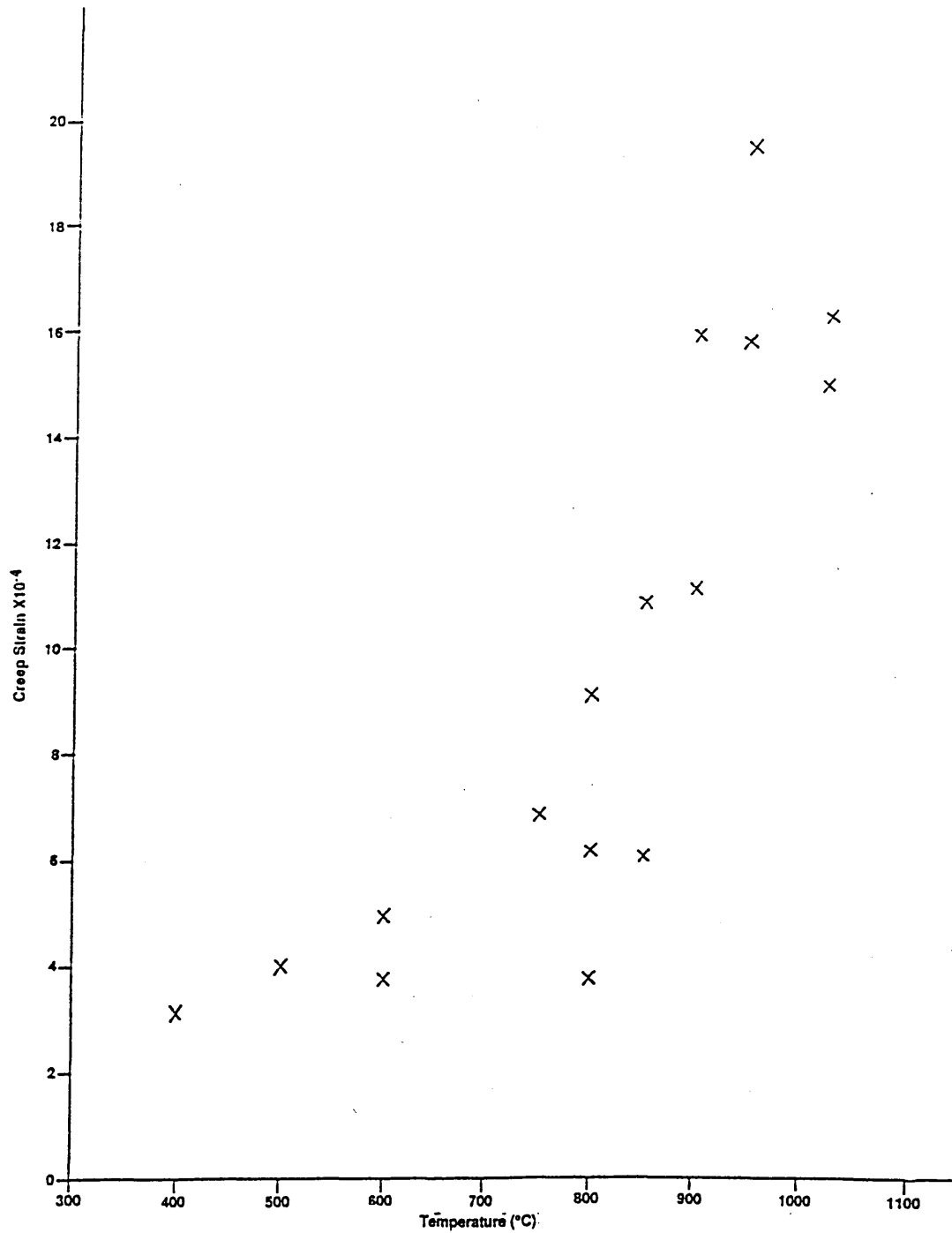


(GPa.s)



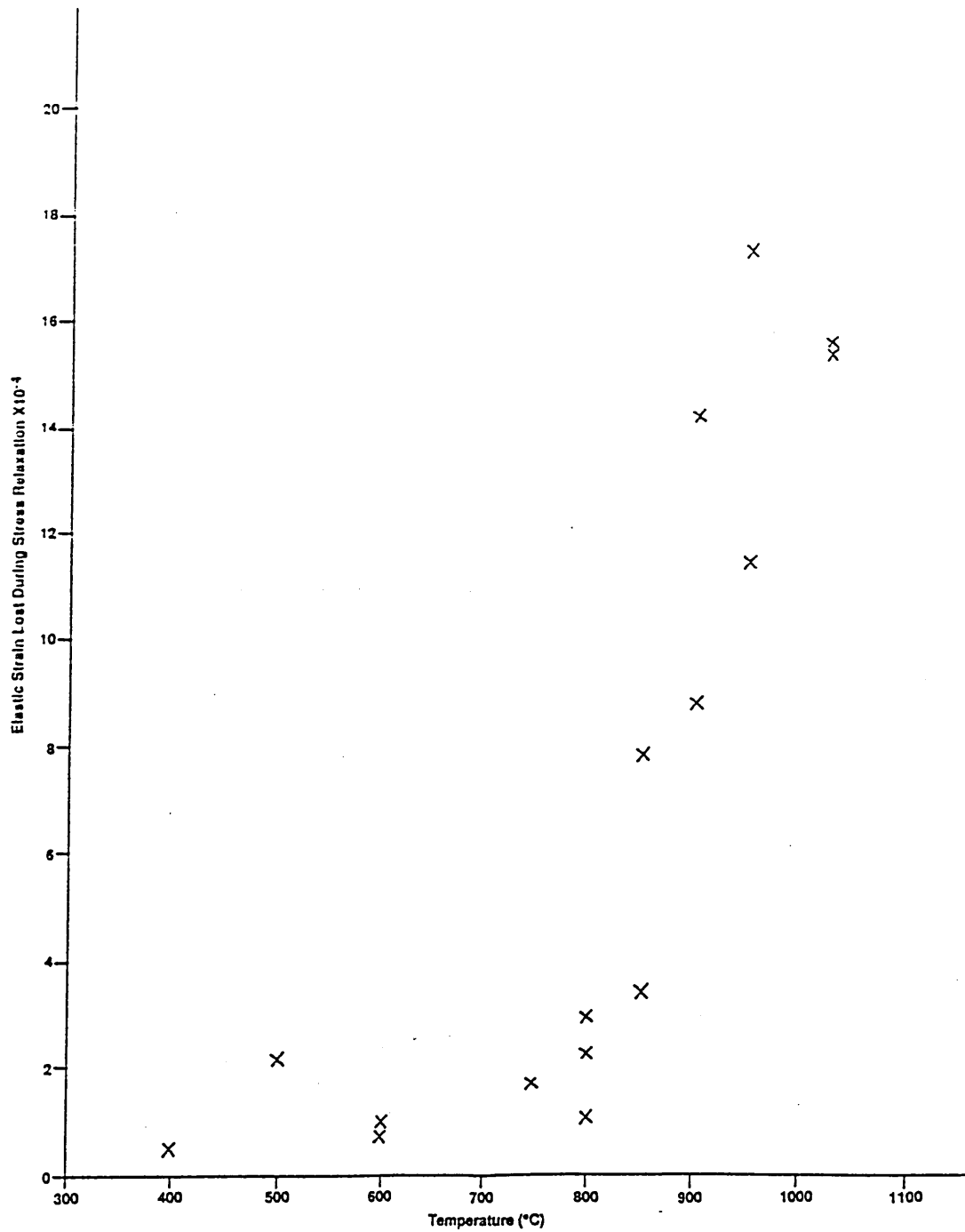
Change in viscosity of 70/30 cupronickel with temperature.

$$\epsilon_{creep} = \frac{\sigma^0}{E} \left(\frac{1}{A} - 1 \right) (1 - \exp^{-ABt})$$



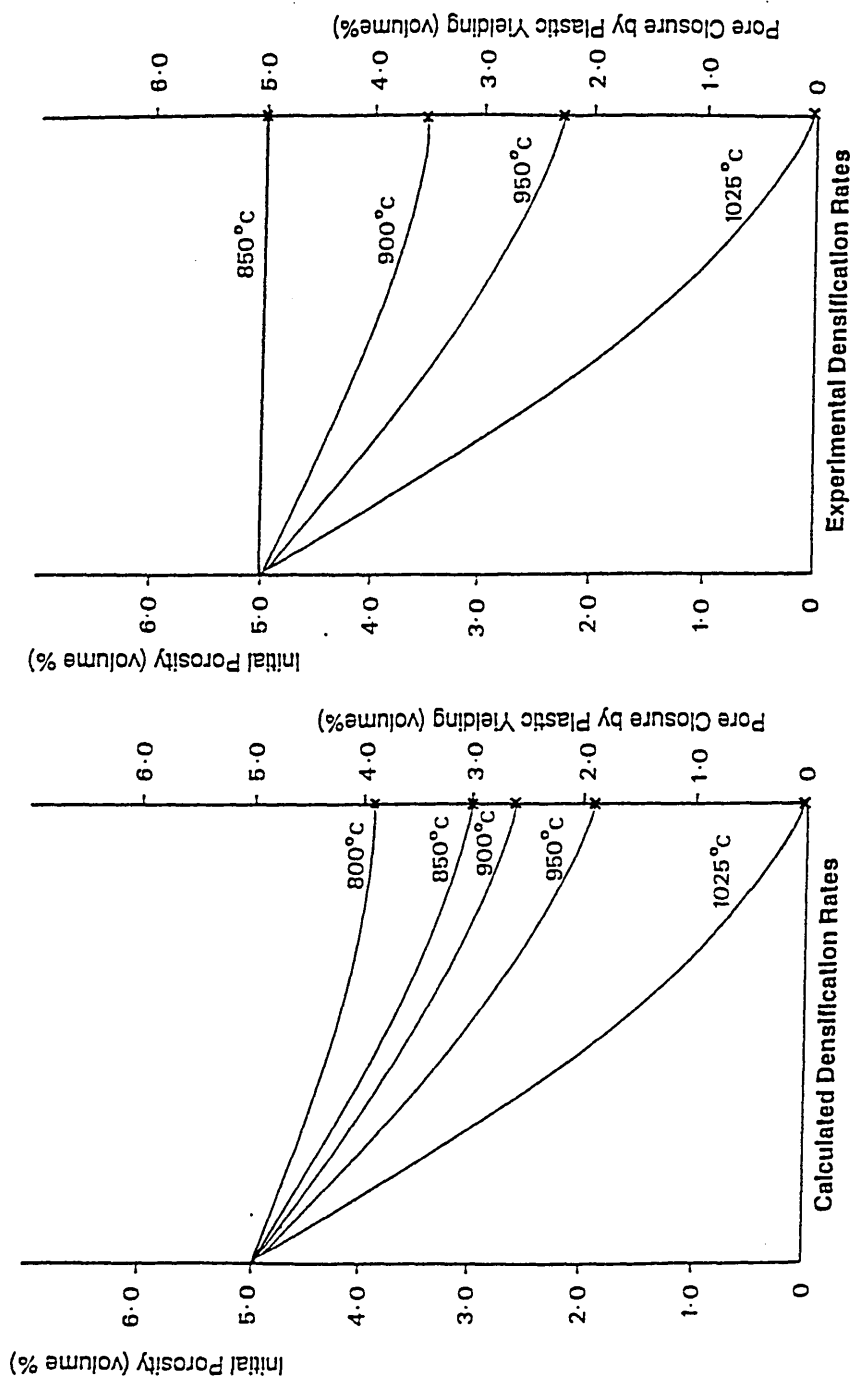
Creep strain at temperature:
The Standard Linear Solid Model.

$$\epsilon_{SR} = \frac{\sigma^{SR}}{E} \left(\frac{1}{A} - 1 \right) (1 - (\exp^{-ABt}))$$



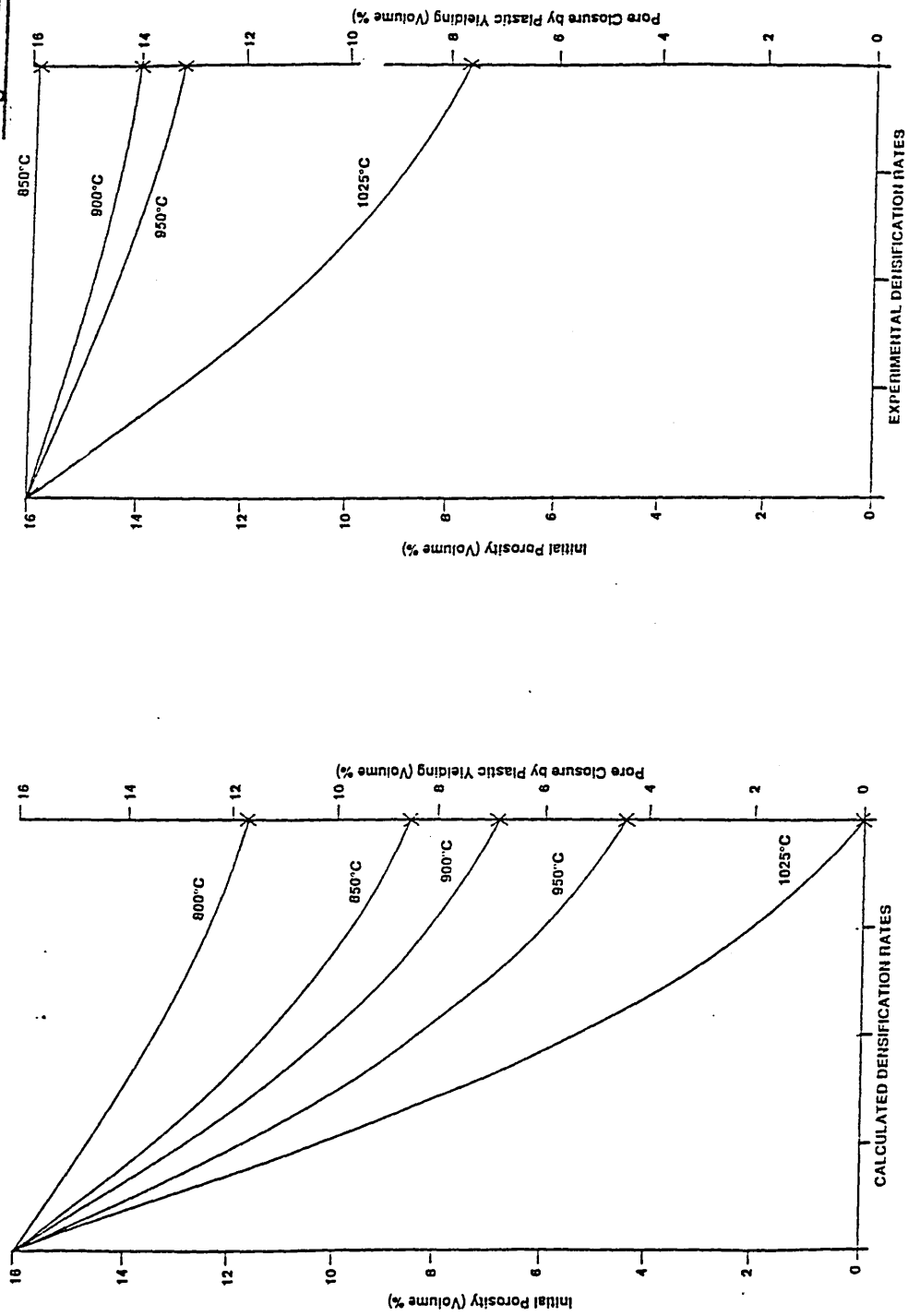
Effect of temperature on the elastic strain lost during stress relaxation of 70/30 cupronickel.

Figure 187



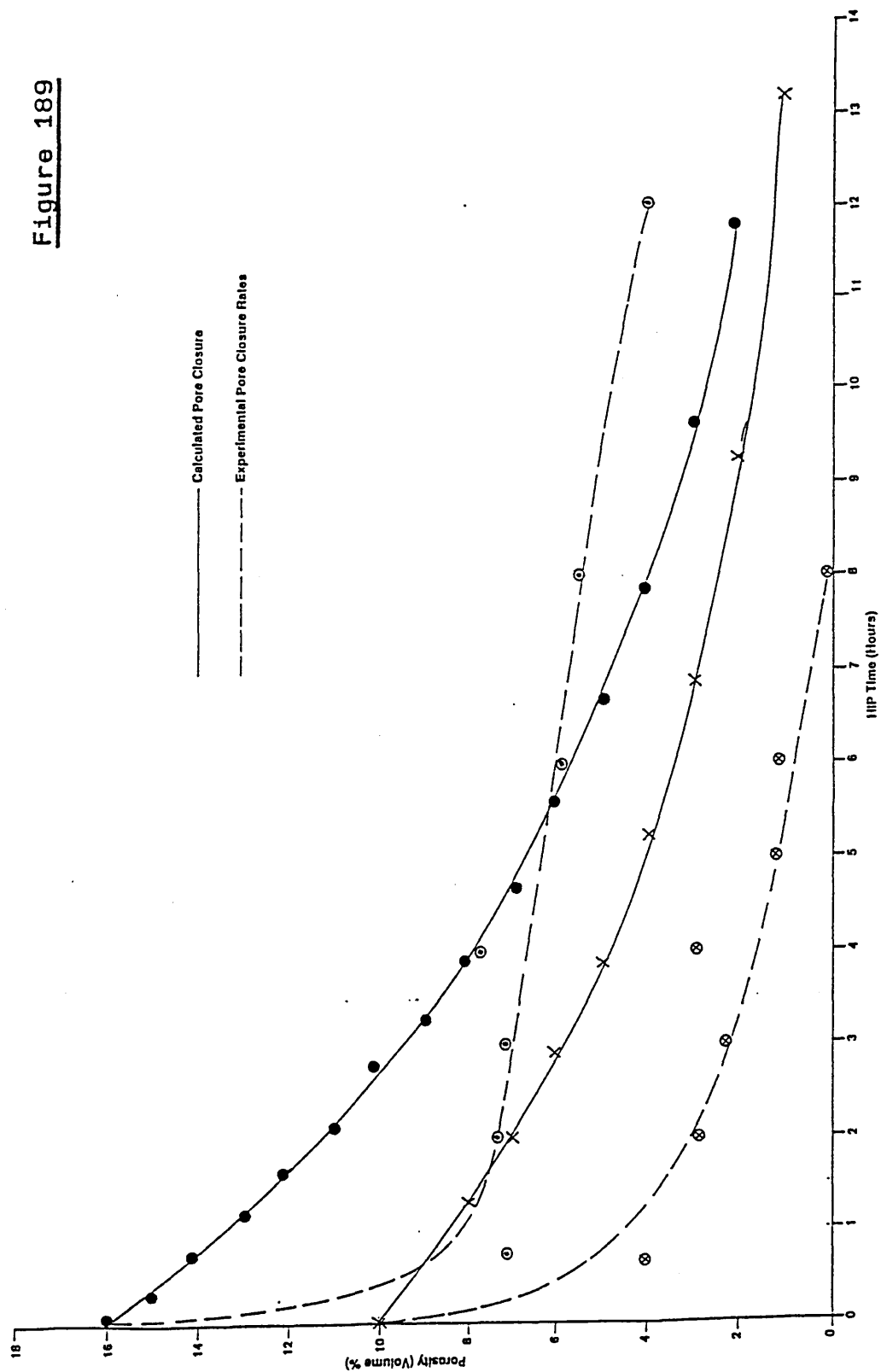
Comparison of calculated and experimental densification rates by plastic yielding of samples containing 5% porosity at external pressures of 103MPa.

Figure 188



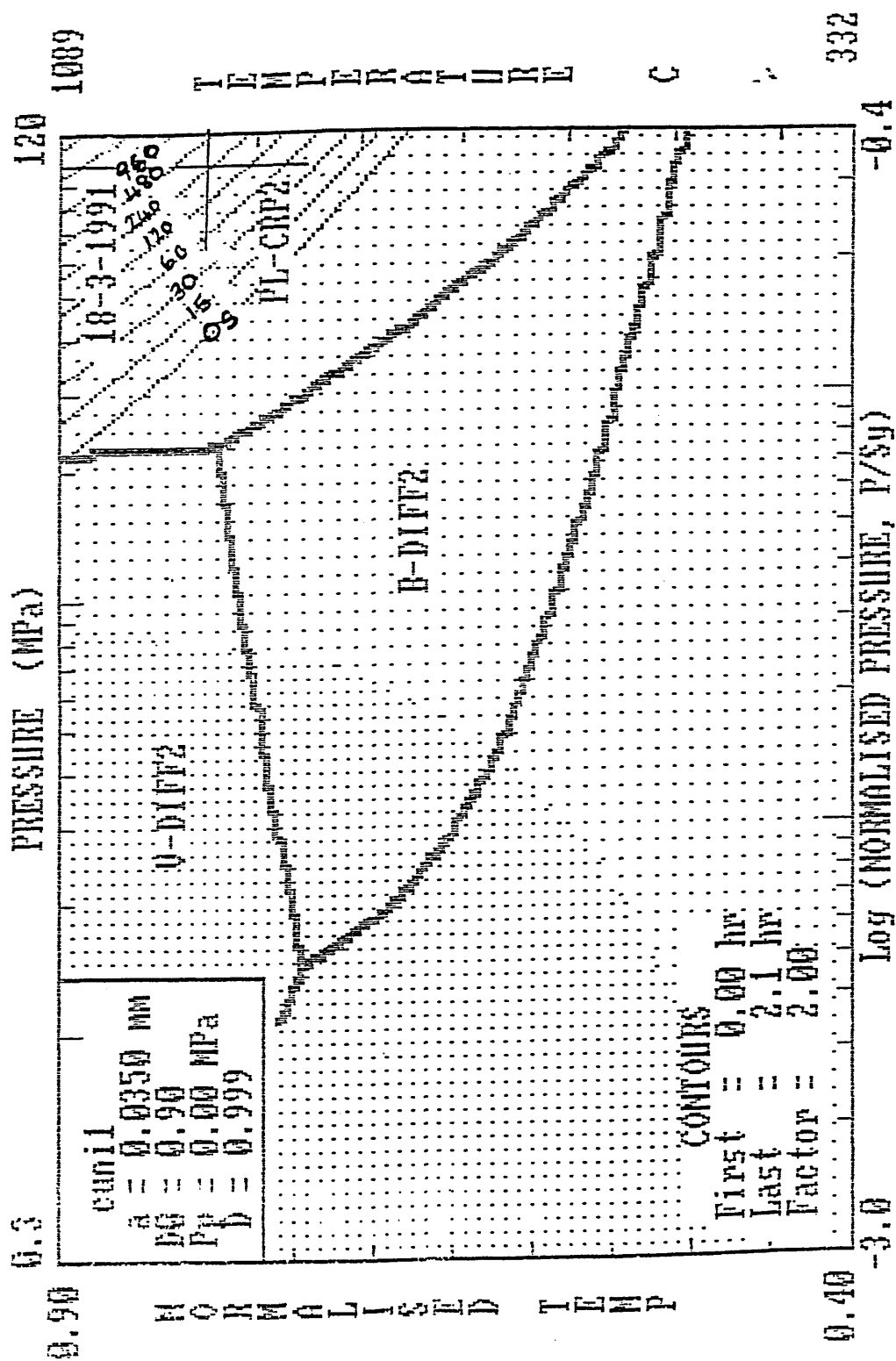
Comparison of calculated and experimental densification rates by plastic yielding of samples containing 16% porosity at external pressures of 103MPa.

Figure 189



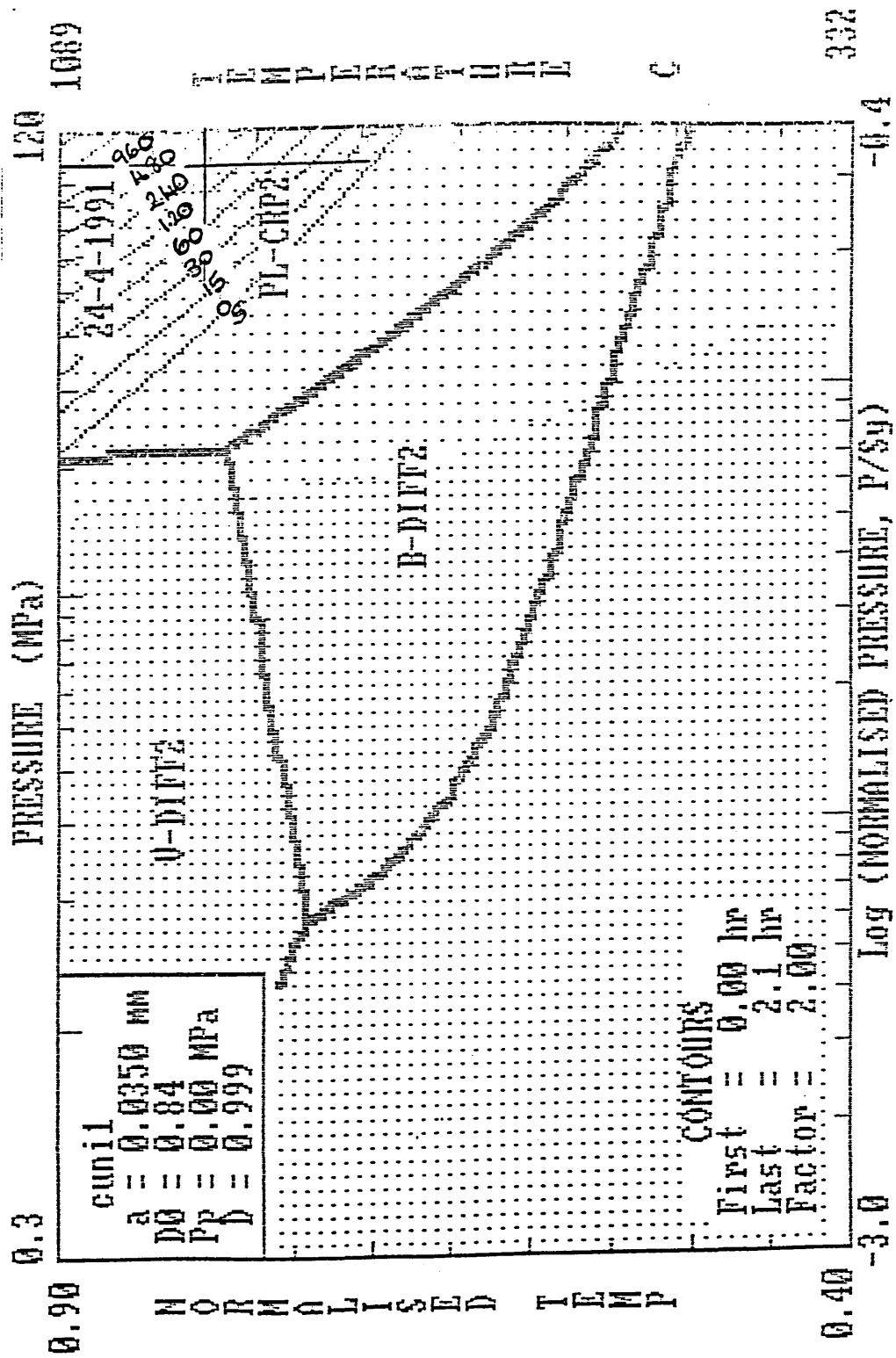
Comparison of calculated and experimental pore closure rates for densification influenced by time dependent mechanisms.

Figure 190



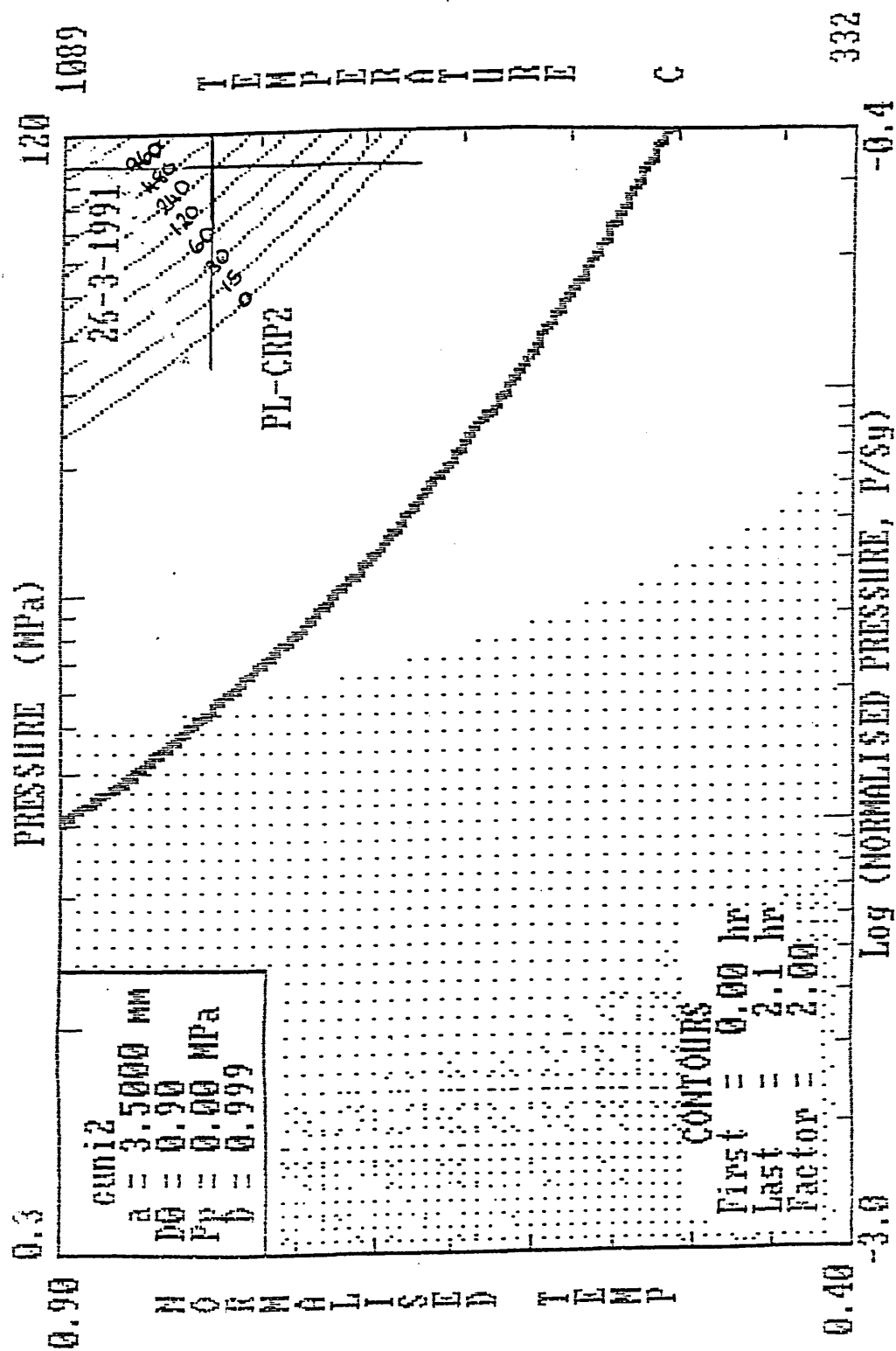
Pressure - temperature HIP map for 70/30 cupronickel:
closure of 10% porosity map type 1.

Figure 191



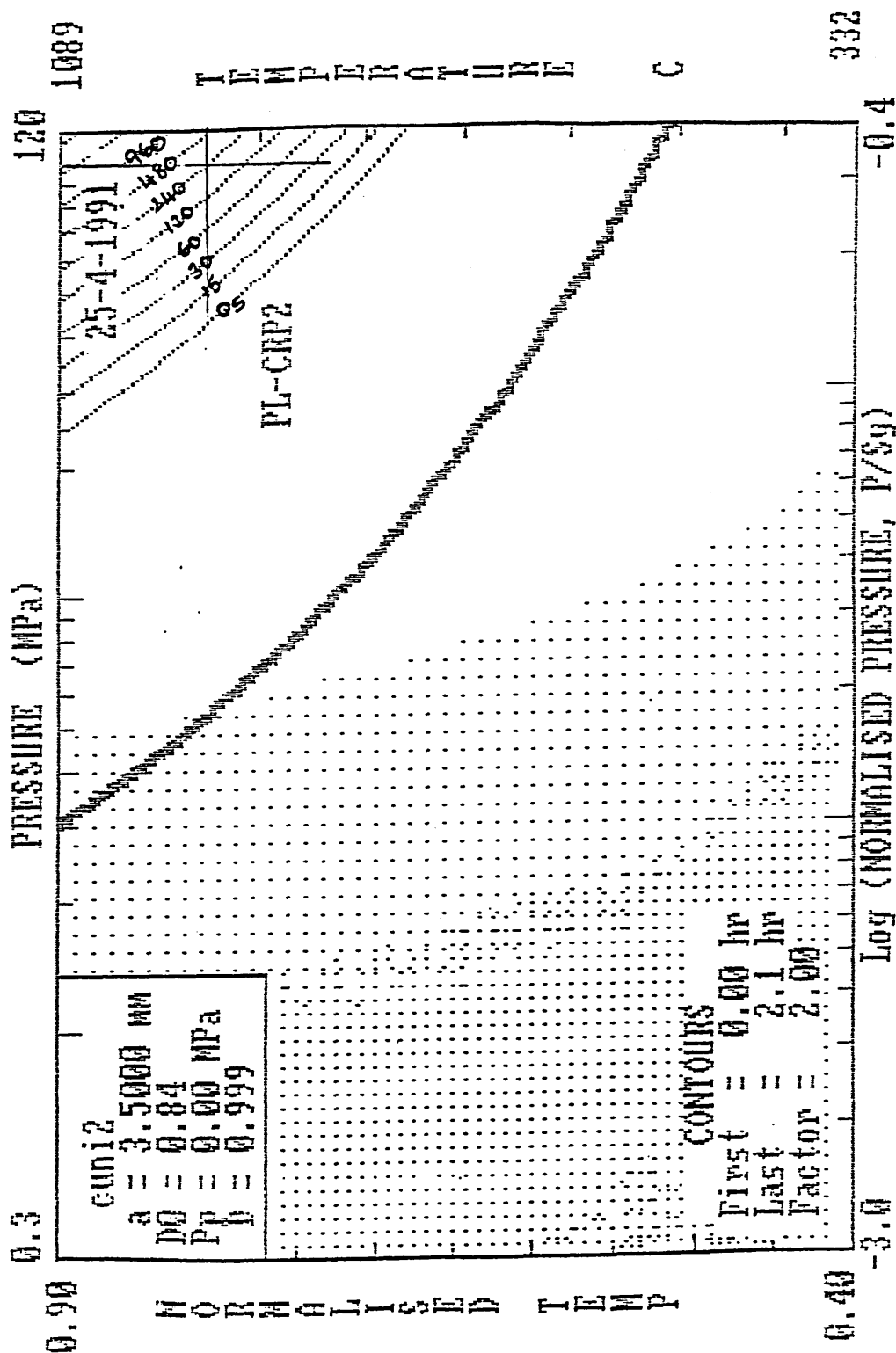
Pressure - temperature HIP map for 70/30 cupronickel:
closure of 16% porosity map type 1.

Figure 192



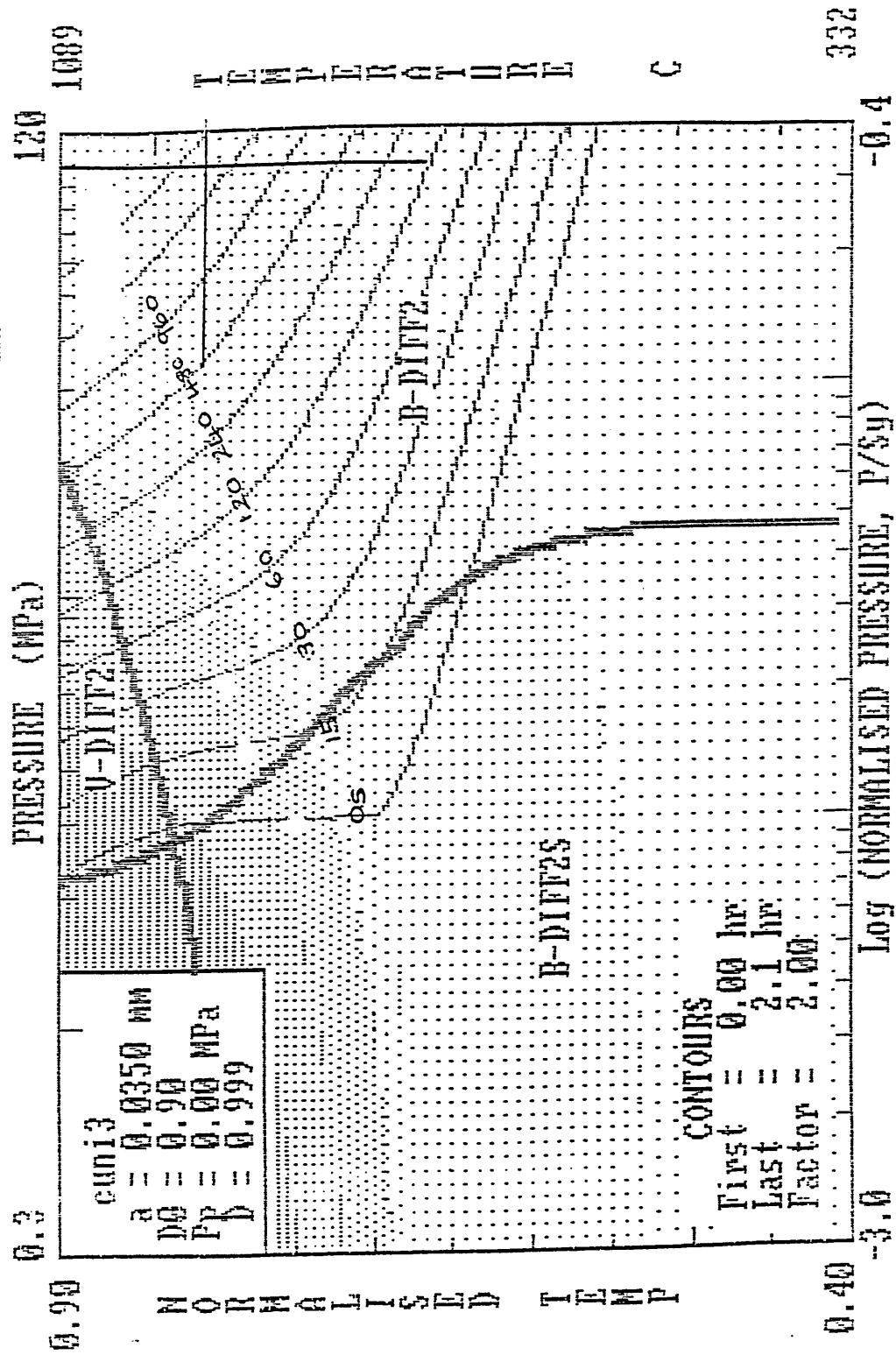
Pressure - temperature HIP map for 70/30 cupronickel:
closure of 10% porosity map type 2.

Figure 193



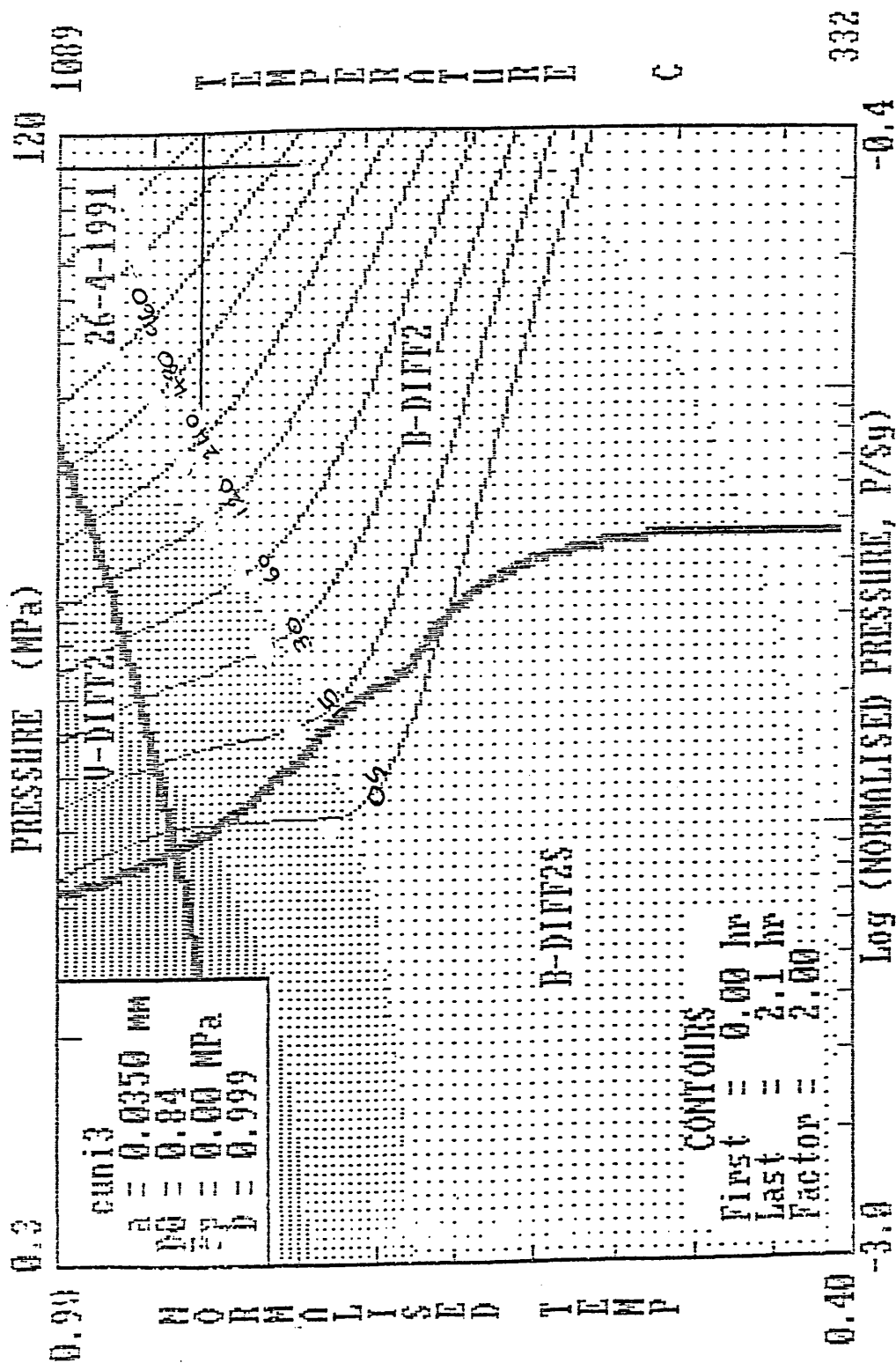
Pressure - temperature HIP map for 70/30 cupronickel:
closure of 16% porosity map type 2.

Figure 194



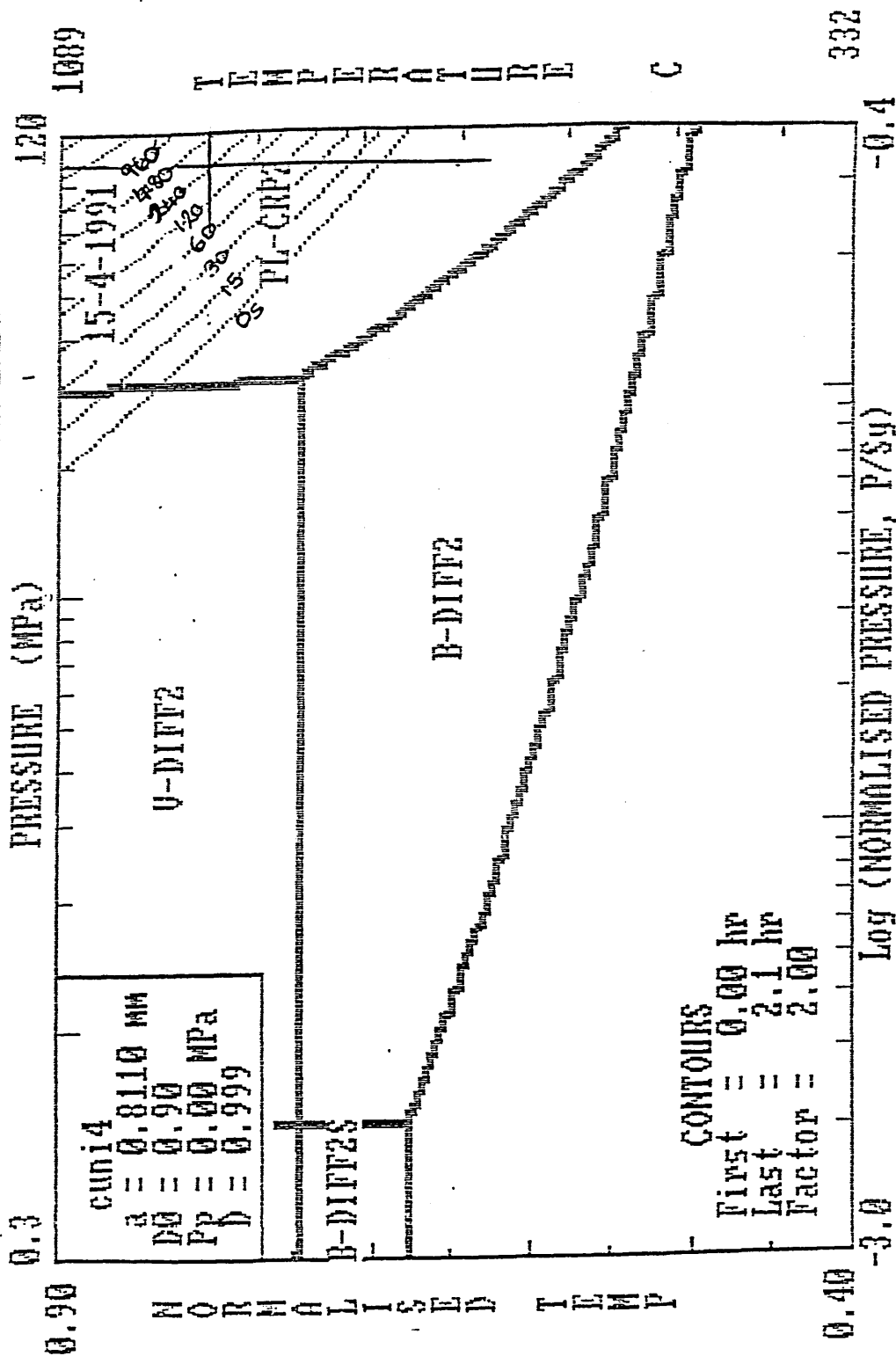
Pressure - temperature HIP map for 70/30 cupronickel:
closure of 10% porosity map type 3.

Figure 195



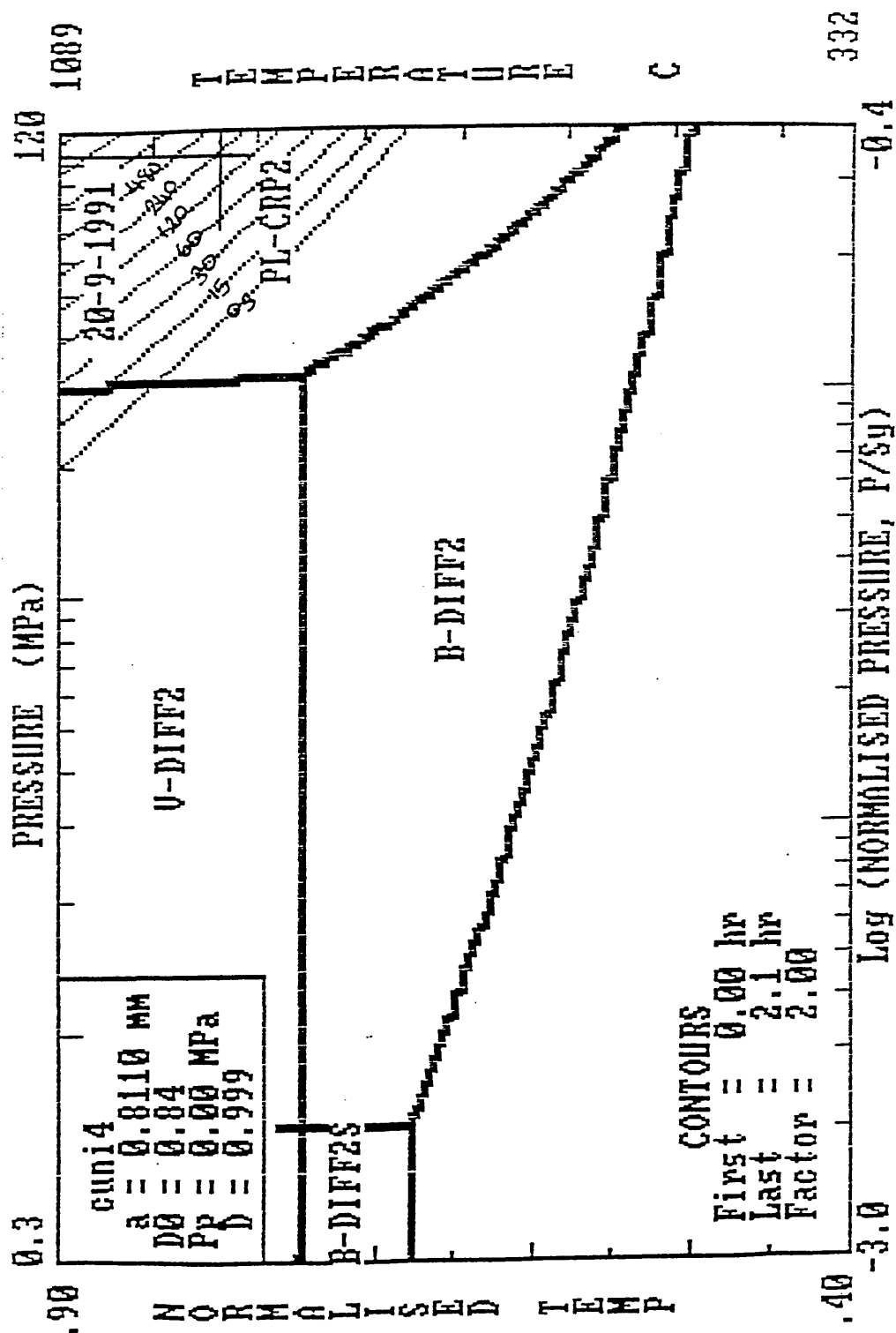
Pressure - temperature HIP map for 70/30 cupronickel:
 closure of 16% porosity map type 3.

Figure 196



Pressure - temperature HIP map for 70/30 cupronickel:
closure of 10% porosity map type 4.

Figure 197



Pressure - temperature HIP map for 70/30 cupronickel:
closure of 16% porosity map type 4.

Figure 198

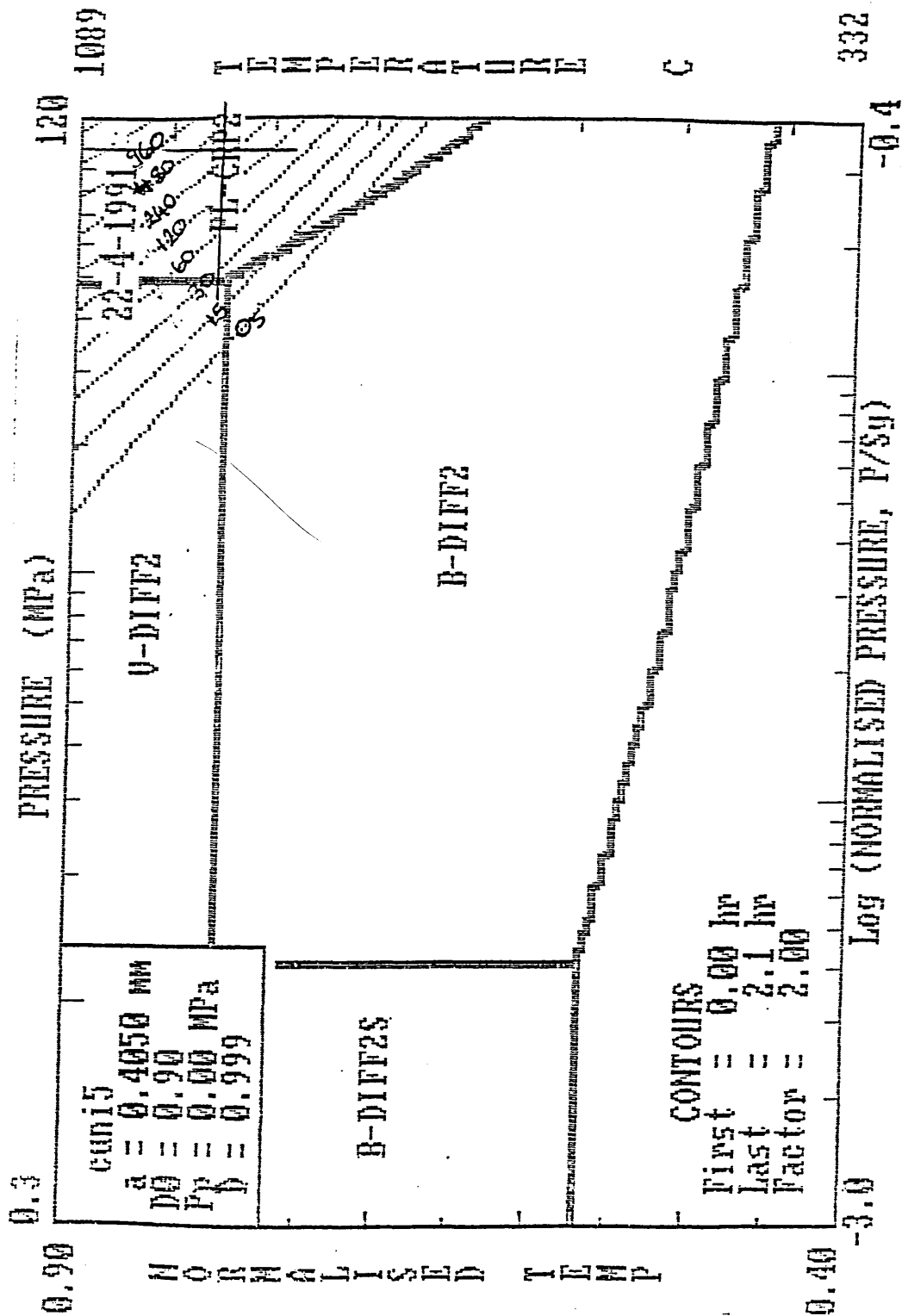
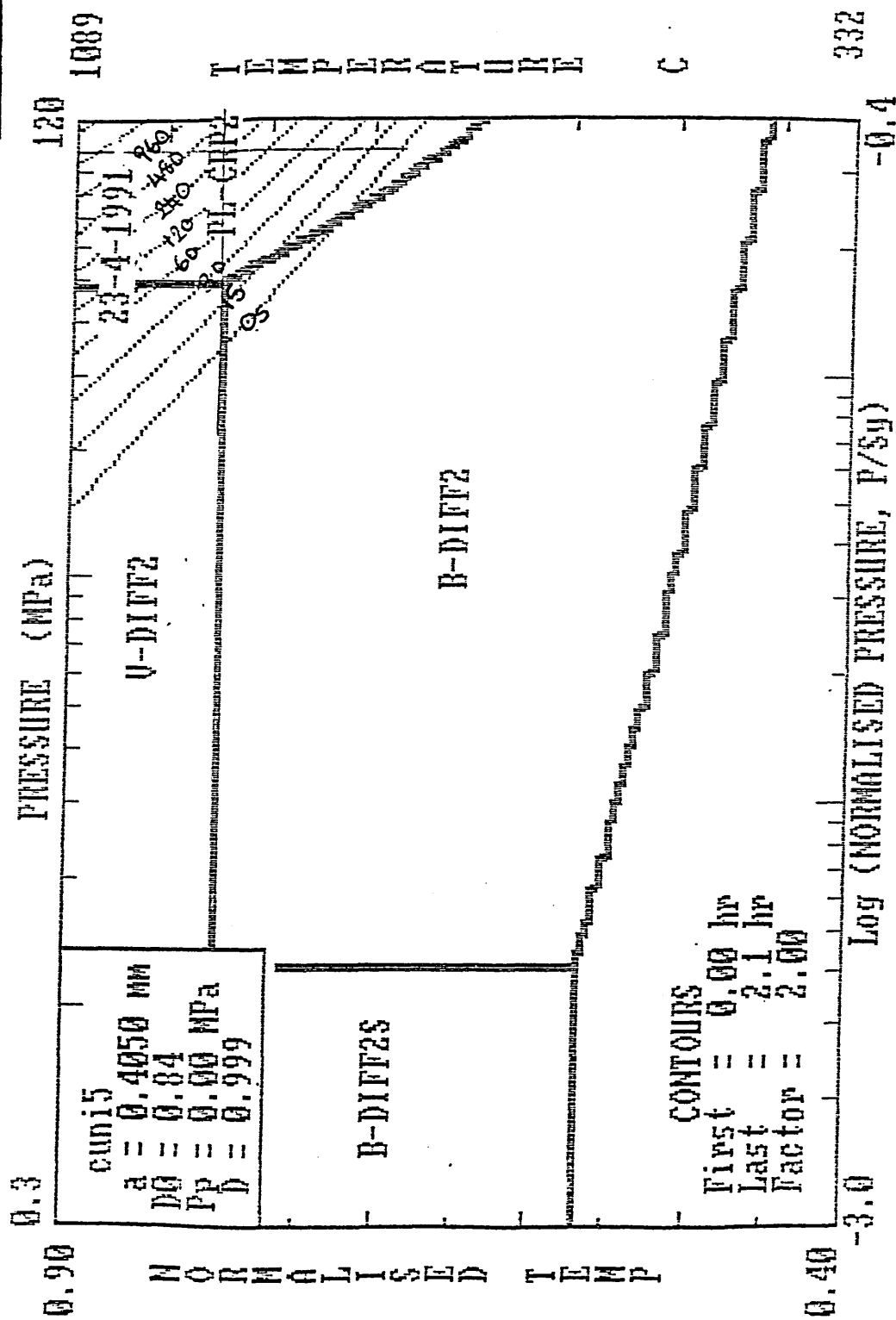
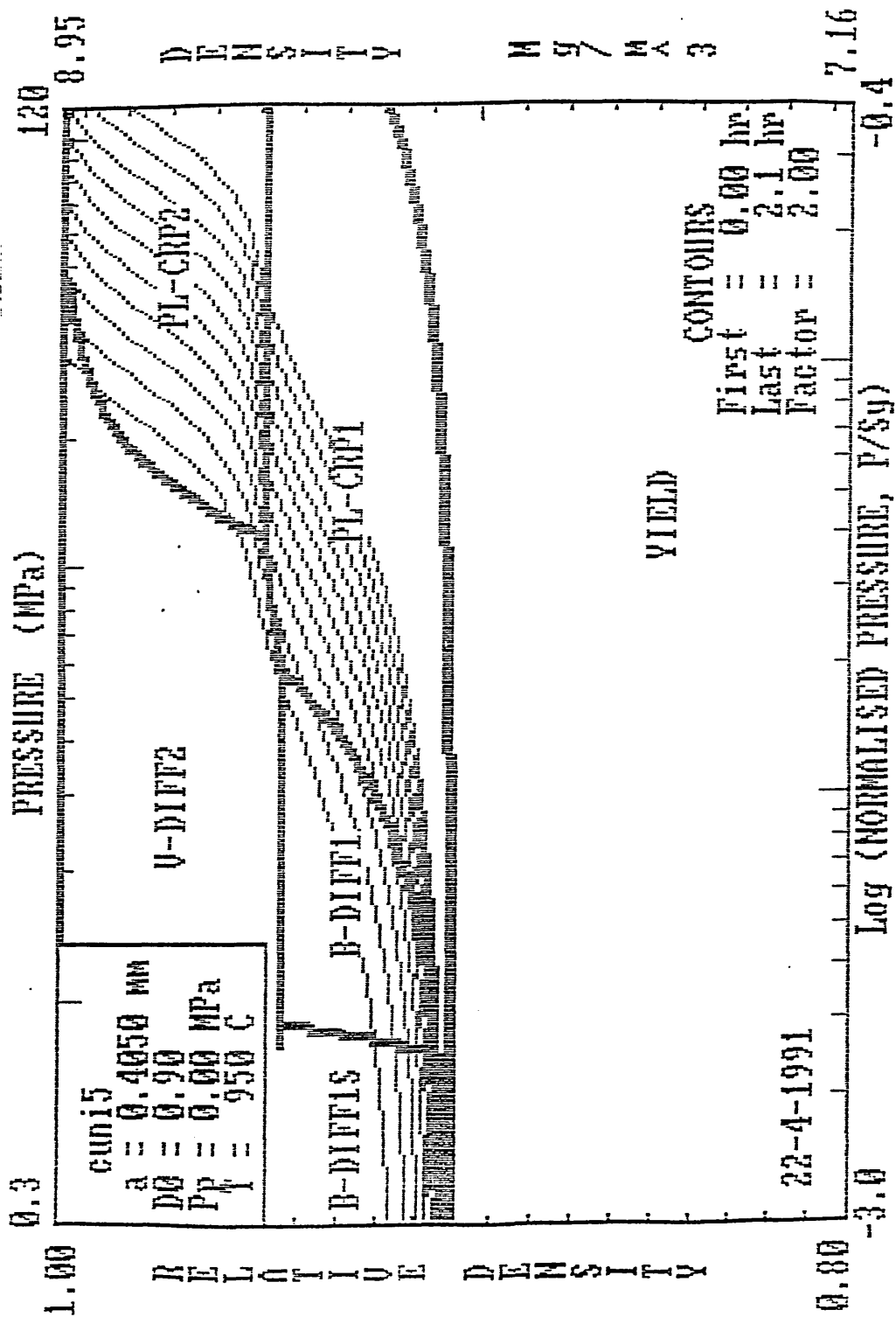


Figure 199



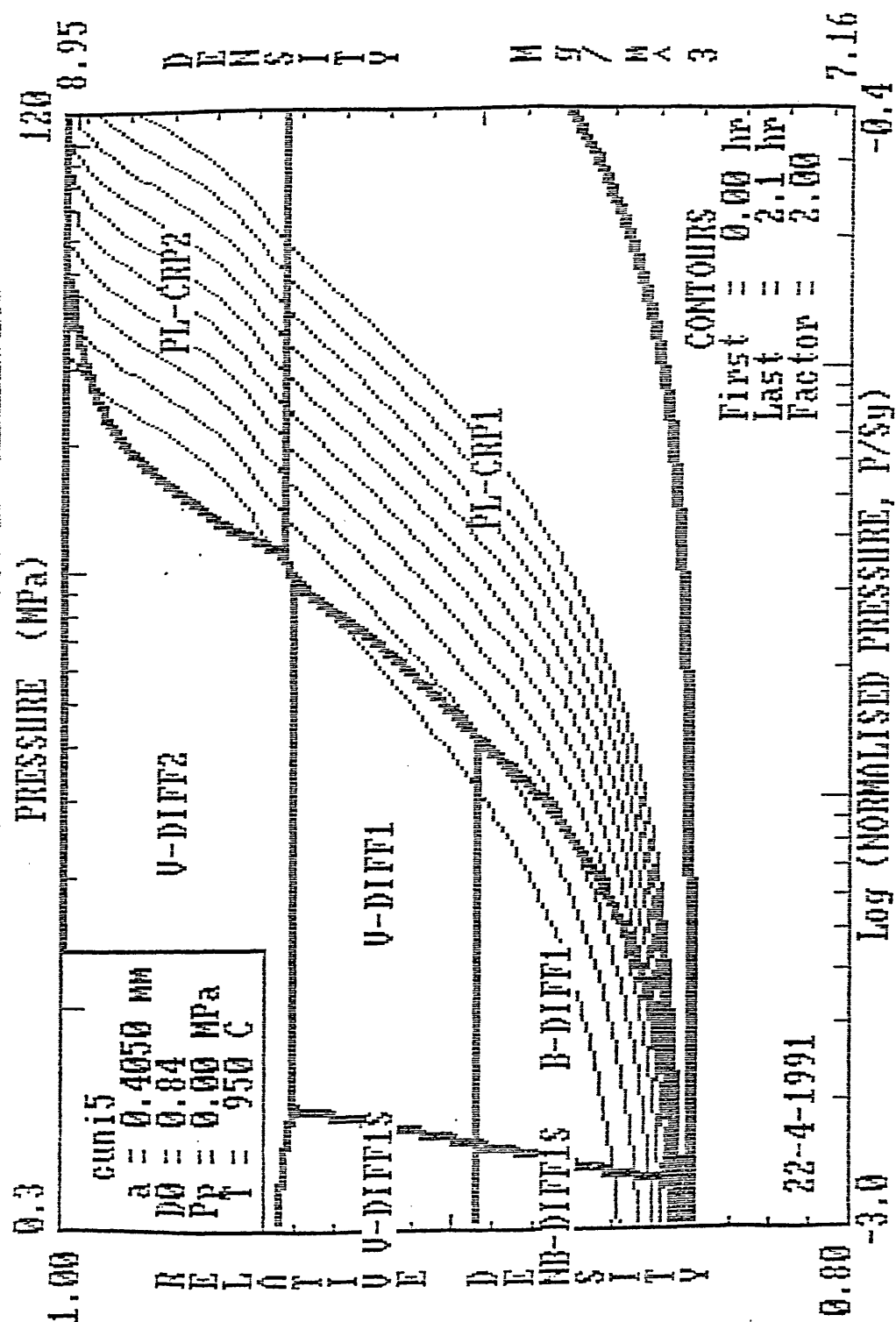
Pressure - temperature HIP map for 70/30 cupronickel:
closure of 16% porosity map type 5.

Figure 200



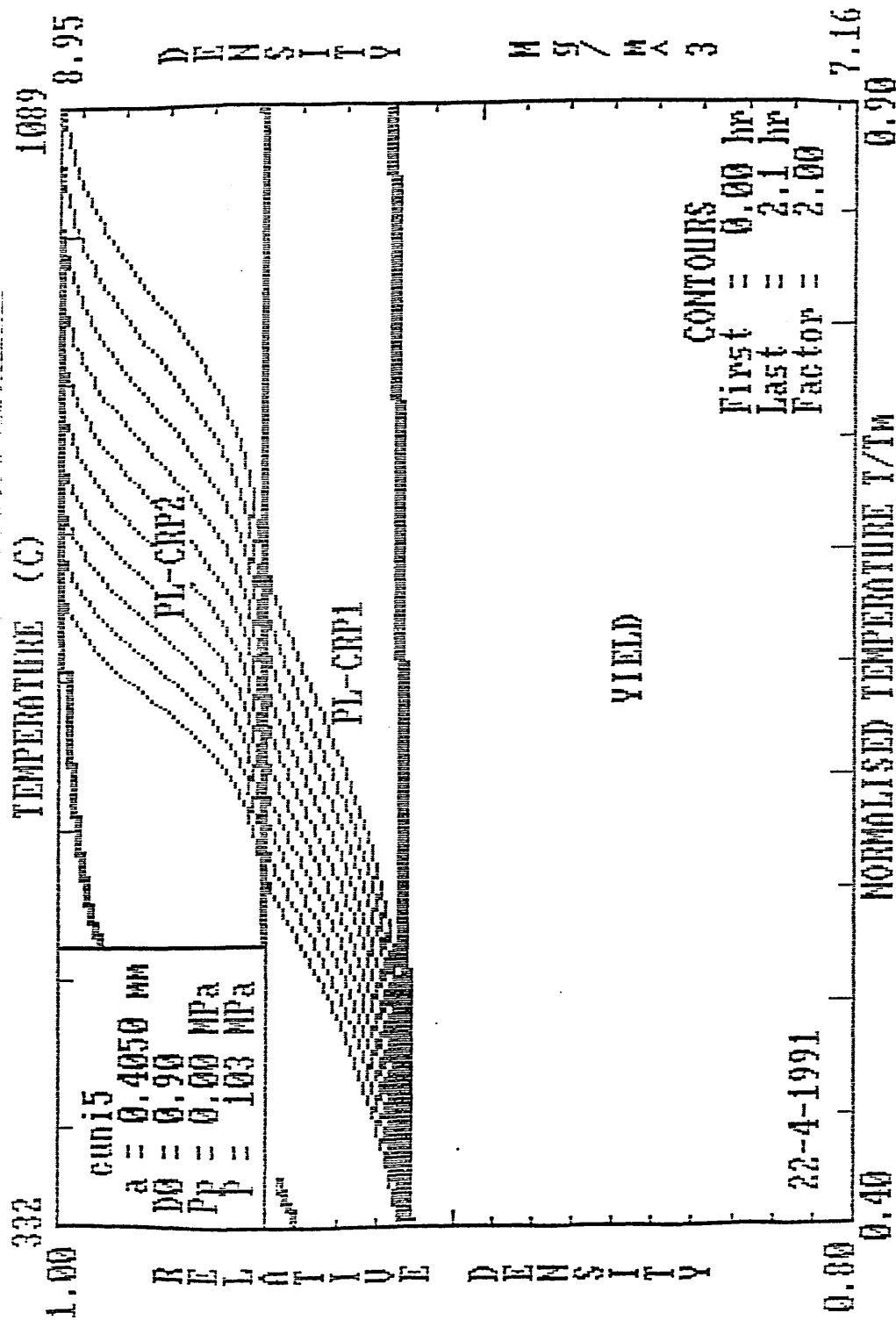
Density - pressure HIP map for 70/30 cupronickel:
closure of 10% porosity map type 5.

Figure 201



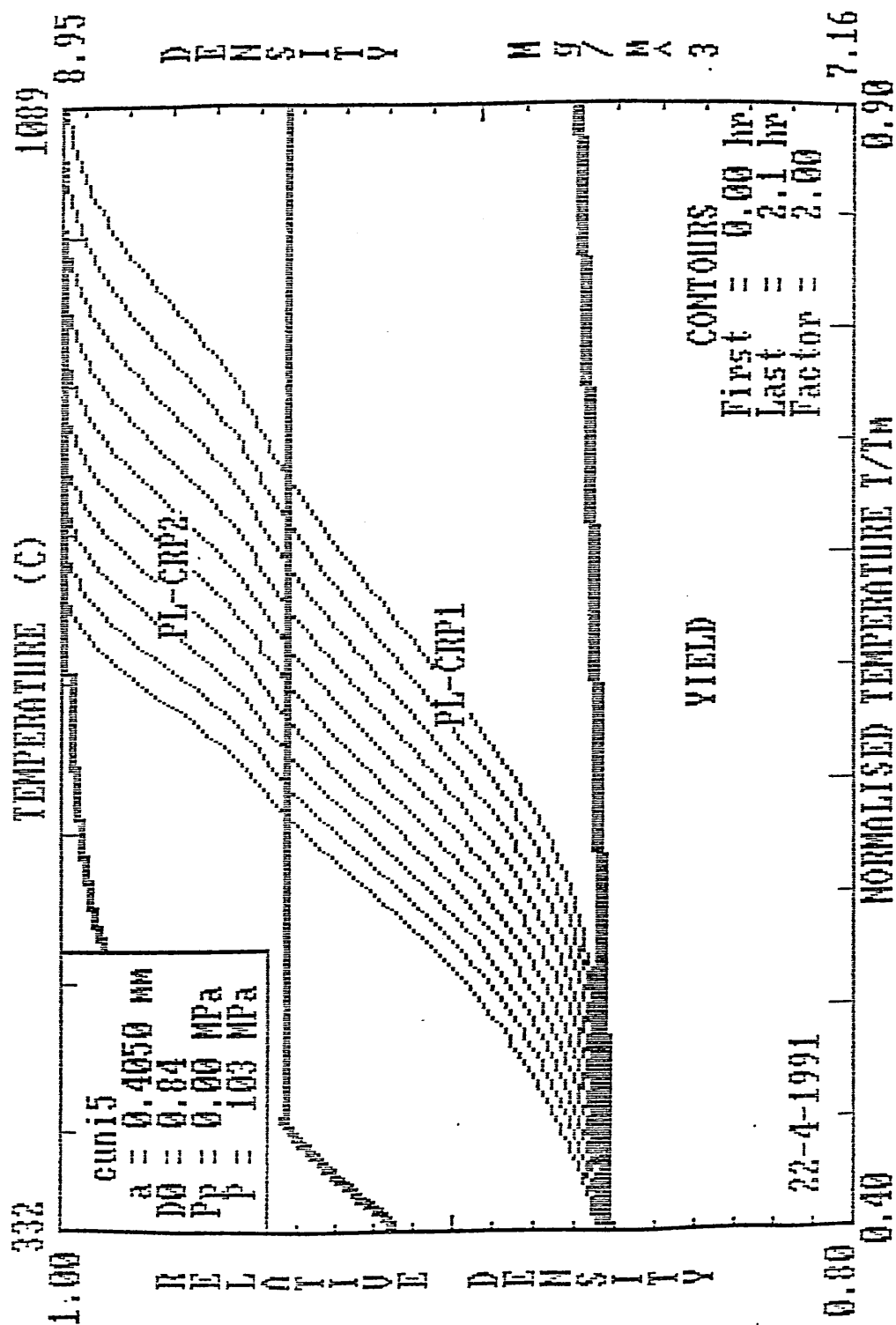
Density - pressure HIP map for 70/30 cupronickel:
closure of 16% porosity map type 5.

Figure 202



Density - temperature HIP map for 70/30 cupronickel:
closure of 10% porosity map type 5.

Figure 203



Density - temperature HIP map for 70/30 cupronickel:
closure of 16% porosity map type 5.

HOT ISOSTATIC PROCESSING CHARACTERISTICS OF 70/30 CUPRONICKEL CASTINGS

H V Atkinson (Sheffield University, Sheffield, UK), A J Fletcher, S King
(Sheffield City Polytechnic, Sheffield, UK), B A Rickinson (HIP Ltd,
Chesterfield, UK)

*4th International Conference
on Isostatic Pressing*

Stratford-upon-Avon (UK), November 5-7, 1990

THE HOT ISOSTATIC PROCESSING CHARACTERISTICS OF

70/30 CUPRONICKEL CASTINGS

H.V. Atkinson*, A.J. Fletcher, S. King, B.A. Rickinson**.

School of Engineering, Sheffield City Polytechnic, Pond Street, Sheffield.

* School of Materials, Sheffield University, Mappin Street, Sheffield.

** H.I.P Limited, Carlisle Close, Sheffield Road, Chesterfield.

ABSTRACT

Hot isostatic pressing is being investigated as a quality enhancement process for particular cast components which are to be used in a marine environment. The aim is to determine the optimum processing conditions for the material.

Hot isostatic pressing trials were carried out, using processing temperatures within the range 850°C to 1025°C and argon gas pressures of 45 to 145MPa, on encapsulated 70/30 (NES 824) cupronickel specimens that contained artificially introduced surface-connected porosity in the form of cylindrical pores. These investigations have revealed that castings containing up to 5% porosity (Class I) can be fully consolidated using much shorter processing times than those previously considered necessary. In addition, successive cycles of short duration were more effective in closing large voids than a single cycle of the same total duration, and elongated pores of small diameter appear to be removed using shorter HIP times than large diameter squat pores of equal volume.

The densification process during hot isostatic pressing involves two stages; plastic flow and viscous flow. For the cupronickel specimens, the first stage predominates and produces high rates of densification within a short period of time at the sustain temperature and pressure, after which further densification occurs at a low rate.

The optimum processing conditions for the successful densification of 70/30 cupronickel castings are sustain times of up to 2 hours, a temperature of 950°C and argon gas pressures within the range of 83-103MPa. Encapsulation techniques may also be required for the removal of surface connected defects.

1. INTRODUCTION

Many of the components used in sea water systems operate in an extremely severe environment both from a mechanical and a corrosion view point. One of the cast alloys presently used in marine applications is nickel-aluminium bronze used primarily for its high strength and shock resistance (1). However, in sea water this alloy can suffer from excessive preferential phase corrosion at crevices and weld-affected areas (2). A replacement material is therefore required. A high strength chromium cupronickel, (70Cu-30Ni alloy containing Cr and Si strengthened by spinodal decomposition (3)), has been chosen for high integrity cast components. This alloy is specified in the Naval Engineering Standard NES 824 (4), which restricts the welding of cupronickel material if it is to be wetted by sea water, due to the risk of premature corrosion failure. This prevents the use of welding to recover castings containing surface defects and porosity. Thus, there is a need to find an alternative recovery process for castings. Hot Isostatic Pressing (HIPping) is a potential alternative.

The use of castings in engineering applications is restricted by the difficulties encountered in producing structural parts of high strength free from defects, such as porosity and microshrinkage. Even if the presence of cavities and internal cracks do not lead to the rejection of castings, they significantly reduce strength, fatigue and creep life in comparison with wrought alloys (5-7). Until 1960 there was no economical method of repairing castings containing internal porosity. Repair consisted of cutting out the defective areas and then fill-welding with weld metal (8). This process is extremely labour intensive, is often prone to failure at the first attempt, and develops an area of material of nominally different grain size and composition at the surface of the component. Such an area can suffer severe galvanic corrosion in sea water. Hence an alternative method of defect repair is required such as HIPping, which has been practised as a recovery process since 1970 (9). The removal of defects by HIPping introduces no new material, and is rapidly proving cost effective particularly for large cast parts. The structure and properties of the cast material are generally improved by the HIP process.

The marine performance of cupronickel castings has been widely investigated (1-3,11-15) and they have been shown to possess excellent corrosion resistance. However, the mechanisms of pore closure via HIPping had received little attention and the optimum process parameters needed to successfully remove defects from such castings had not been determined. Hence an evaluation of the hot isostatic pressing characteristics of 70/30 cupronickel was required.

The effect of the hot isostatic processing variables including time, temperature and pressure on the recovery of 70/30 cupronickel castings containing surface connected porosity is reported here, and the influence of pore geometry and encapsulation techniques on the rate of pore closure discussed. First of all some background on densification via HIPping will be given.

2. BACKGROUND: VOID CLOSURE DURING DENSIFICATION BY HIP

Void closure is a function of temperature, pressure and time. Temperature is the most influential; pressure has relatively little effect once above a critical level (10).

There are two driving forces for pore closure during the compaction of a porous solid body subjected to isostatic pressure (16-18):

- (1) Surface tension
- (2) Externally applied pressure

The surface tension gives an effective pressure (P_s):

$$P_s = \frac{2\gamma}{r}$$

where γ = surface energy per unit area
 r = radius of the pore.

P_s only becomes significant when the pore is small ($r < 100\text{\AA}$).

The total pressure acting on a pore (P) is:

$$P = P_s + P_e - P_i$$

where P_e = externally applied pressure
 P_i = internal pressure in the pores.

If there is any gas contained in the pore, the internal pressure will oppose pore closure since P_i increases with an increase in the density of the component, and can eventually stop densification completely. However, in general as the pore shrinks the gas tends to dissolve in the matrix.

If the pressure P exceeds the yield stress of the material at the HIPping temperature the stresses generated allow densification by instantaneous plastic yielding, dislocation and diffusional creep and by particle sliding (16,19,20).

3. PROCEDURE

The determination of the optimum processing conditions for the HIPping of cupronickel was carried out using artificial porosity specimens. These are cylindrical samples of 70/30 cupronickel 76.2mm long x 12.7mm diameter cut in half with hole(s) of known sizes to represent the porosity. When the two halves of the specimen are reassembled in their original positions an internal pore which is surface-connected is created. The pore geometries include squat pores of large diameter, elongated pores of small diameter and pores of an angular nature as illustrated in Figure 1. In the case of the angular pore the aspect ratio of the elongated pore was maintained while the rectangular section was replaced by sharp acute angles at stages along its length. The angular defect was introduced to determine the effect of stress concentrators around the edge of the pore on the driving force for densification by surface tension effects. As the artificial porosity is surface-connected, encapsulation (ie. forming a gas tight membrane around the component) was required prior to HIPping, as shown in Figure 2. The capsule was evacuated, sealed and subjected to X-ray penetration examination prior to HIPping.

Three types of pressure transmitting media were used during encapsulation:

- (1) A traditional silicious based medium which tends to sinter at the temperatures and pressures associated with HIPping.
- (2) A fine calcined oxide powder.
- (3) Coarse tabular granules.

The latter two were investigated to ascertain the effect of particle shape and size on the densification rates of encapsulated castings. It was thought that the fine calcined powder might improve the densification rate, due to greater resistance to sintering and/or mechanical locking, or by enhanced ease of particle flow under HIPping conditions. The coarse tabular granules were expected to reach a maximum packing density in shorter times for equivalent HIP conditions than the fine powder, and thus impair densification.

The HIP experiments were conducted within a laboratory-sized HIP system. The specimens were heated at $15^{\circ}\text{C}/\text{minute}$ to the treatment temperature under an argon gas pressure that increased progressively during heating to a maximum pressure in the range 41-145MPa (6000-21000psi). The treatment temperatures selected lay in the range 850 - 1025°C . However, previous work (21) had suggested that a temperature of 950°C provided the best combination of strength and ductility whilst inhibiting the grain growth associated with higher HIPping temperatures. Thus, a comparison was made between the rate of pore closure using three types of treatment at this temperature.

(i) Pore closure as a consequence of repeated applications of a HIP cycle that involved holding the specimen for 45 minutes at 950°C with a gas pressure of 103MPa. The specimen was encapsulated heated and pressurised to the sustain conditions, cooled and removed from its capsule, and re-encapsulated with fresh packing material before reapplying the temperature and pressure at the start of the next cycle. Thus each cycle contained a heating and cooling stage as well as the period at 950°C .

(ii) Pore closure when the same conditions were applied as a single continuous cycle. Thus, only involving one heating and cooling stage.

(iii) To separate the effects of the encapsulation process on densification from the effect of the initial heating and holding at temperature during the first HIP cycle, specimens were subjected to repeated cycles without re-encapsulation at the end of each cycle.

The period for which the HIP conditions were held constant is termed the sustain period, and the experiments carried out in (i) indicated that the majority of densification occurred during the first HIP cycle (or within 45 minutes at the sustain conditions). Thus, it was necessary to estimate the amount of densification due to plastic yielding and that due to viscous flow (i.e. creep and diffusion). Plastic yielding occurs instantaneously as the HIP pressure exceeds the yield stress of the material. Therefore densification by plastic yielding should be complete by the time the sustain conditions are reached. HIP experiments to substantiate this assumption were carried out at temperatures of 850°C , 950°C and 1025°C and gas pressures of 103MPa for zero sustain times. Extending the sustain time to 45 minutes allowed the increase in densification due to creep and diffusion to be identified. Hence, the next step was to examine the effect of HIP pressure on densification. Experiments involving 45 minutes at 950°C and gas pressures of 41, 62, 85, 103, 124 and 145 MPa were carried out to predict the pressure required to obtain maximum densification.

On completion of the constant temperature and pressure stage the specimen was cooled at $10^{\circ}\text{C}/\text{minute}$ until ambient was reached.

Finally the dimensions of the pore profile after HIPping were determined by X-ray penetration examination. It should be noted that pore closure as a result of HIPping has been deduced by measuring the absolute porosity remaining in the specimen.

The mechanical properties of as-cast 70/30 cupronickel (NES 824) had been investigated to determine the change in flow stress with temperature within the range 300 - 1025°C . Comparison of the yield strength at temperature with the applied HIP pressure during the heating/pressurisation stage of the HIP cycle allowed the minimum temperature at which plastic yielding will occur to be estimated.

4. RESULTS

On the basis of previous work 950°C was considered to be a reasonable HIPping temperature for the removal of defects from 70/30 cupronickel castings. Hence a comparison was made between the rate of pore closure as a consequence of repeated applications of a HIP cycle that involved holding the specimen for 45 minutes at 950°C with a gas pressure of 103MPa, with that obtained when the same conditions were applied continuously. In comparing the two types of treatments Figure 3 shows that the level of porosity fell continuously as the number of HIP cycles increased with complete removal of 16% porosity after 4 cycles at 950°C , and the complete removal of up to 10% porosity after 2 cycles providing that only the more elongated pore was considered. On the other hand the use of a squat pore generally inhibited pore closure: this was particularly evident in the case of the specimens that initially contained 10% porosity. Figure 4 shows the corresponding reduction in the porosity during the continuous HIPping of specimens containing the more elongated pores. Unlike the situation produced by the successive application of HIP cycles (Figure 3) the continuous process did not produce a steady reduction in the porosity level. Instead a very large reduction in porosity occurred during the first 45 minutes (which corresponds to the application of a single cycle in Figure 3) but the subsequent rate of porosity removal was low: as much as 8 hours was required to remove 10% porosity, while 4% porosity still remained after the specimen that originally contained 16% porosity had been processed for 12 hours at 950°C .

A heating and cooling stage is inevitable in any HIP process and in the case of multiple cycles several such stages are involved. Figure 5 shows the effect on pore closure of heating to and cooling from the working temperature without any sustain period at that temperature. The HIPping pressure was attained simultaneously with the maximum temperature. The same figure shows the increase in densification achieved by holding for short periods of time (45 minutes) at the sustain temperature and pressure. Figures 6 and 7 show the effect of maximum temperature on the porosity level both with and without any sustain period at the maximum temperature. At 950°C (Figure 6), the initial porosity of 5% was reduced to 2.5% by the heating and cooling stage alone and at 1025°C complete densification was achieved. No densification occurred during processing at 850°C . Figure 6 also shows the effect of temperature on the reduction of initially 5% volume porosity when the maximum temperature and pressure were held for 45 minutes. In every case (including 850°C) this period at the HIPping temperature produced some densification. At a temperature of 950°C increasing the sustain period from 0 to 45 minutes increased densification and reduced the porosity present from 2.5% to 1.25%. Figure 7 shows the corresponding results when the initial level of porosity was 16%. Although some porosity remained after completion of the HIP cycle even when 1025°C was employed, the general trends were very similar to those obtained with the specimens that initially contained 5% porosity.

Figure 8 shows the effect of the maximum pressure used in the HIP cycle on the level of porosity in specimens that contained initially 10% porosity in the form of a single elongated pore. The results are given in terms of the number of cycles, each of which involved a period of 45 minutes at the maximum temperature and pressure. An increase in pressure from 41MPa to 124MPa produced a steady increase in the rate of densification although there is a certain amount of scatter in the results. When the pressure used exceeded 103MPa complete densification was achieved by the end of the second cycle.

The shape of the pore had some effect on the densification of the specimen with 10% initial porosity. Thus 3 cycles were required to close squat pores whereas only 2 cycles were needed when the pores were elongated (Figure 3 and 9). The introduction of angularity into the pore (without altering the overall aspect ratio) had little effect on the rate of densification. This

last observation is confirmed by the results in Figure 10, where the continuous application of the hot isostatic pressing conditions produced very similar results with and without the presence of sharp angles along the edges of the elongated pore. The angular pores appeared to reduce in size slightly more slowly in the early stages than the standard elongated pores, but with a slightly higher rate of densification later in their treatment. However, it is doubtful whether these differences are significant and in any case the differences over the whole course of the treatment (8 hours) were negligible.

As far as encapsulation is concerned it is necessary to separate the effects of the encapsulation process from the effect of the initial heating and holding at temperature for the first cycle. Figure 11 shows the effect of subjecting 10% initial porosity specimens to repeated cycles without re-encapsulation at the end of each. Comparison with Figure 3 shows that the absence of re-encapsulation greatly reduced the rate of densification in the second and subsequent cycles. These results indicate the importance of the use of fresh packing material around the specimen for each cycle. This material must be refractory, in order to withstand the temperatures involved. Sintering of the granules of this material might prevent its use as a pressure transmitting medium. Both fine calcined powder and coarse tabular granules were used with re-encapsulation at the end of each cycle. Figure 12 shows that the former produced densification rates very similar to those obtained with the traditional pressure transmitting medium, while the tabular medium produced significantly lower densification rates. However all these types of packing media showed greater rates of densification when repacking was used than was the case when the refractory medium was left in the capsule for extended time continuous cycles, or, as in the case of the traditional medium, was left in the capsule through several cycles.

The properties of as-cast 70/30 cupronickel at elevated temperatures are shown in Figure 13 and indicate that a major reduction in both ultimate tensile and yield strengths occurs at about 700°C. Also at this temperature the difference in value between these properties becomes very small. The same figure shows the relationship between the applied pressure in the HIP operation and the temperature during the heating up stage. Although the stress applied in the HIP process is not uniaxial it is evident that plastic flow will only occur when the temperature exceeds 850°C. However, in practice the packing media used during encapsulation diminishes the HIP pressure transmitted to the specimen, and no significant amount of densification occurs until the HIP temperature exceeds 900°C.

5. DISCUSSION

The results obtained are consistent with the densification process during hot isostatic pressing involving two stages. The first predominantly involves plastic flow and the second viscous flow (ie. creep and diffusion). It is the first stage that predominates in the removal of porosity, as shown by the high rate of densification at short times (Figure 4). Viscous flow is time dependent and therefore cannot be contributing to any significant extent. Figure 4 also shows the importance of the initial plastic flow and subsequent recrystallisation on the removal of porosity. Such a contrast between the early and later stages of the densification process is surprising in view of the high temperatures involved, suggesting that the applied load falls as the pressing operation continues, thus densification does not continue to occur during the later stages of the HIP process. This reduction in the rate of densification is probably an effect of encapsulation rather than a characteristic of cupronickel material. The most probable causes of the loss of applied load would be the mechanical locking and sintering of the refractory particles used as packing around the specimen. For pressing to be effective these particles must be able to move under the applied load as densification continues. Further investigations are planned to find whether the rate of densification in the later stages is consistent with the measured values of the coefficient of viscosity of the component material. However, in the absence of a detailed analysis, consideration has been given to the possibility of sintering of the refractory, and the effect of a change in the type of refractory on the densification process has been examined. Figure 12 shows that a change in the packing material does effect the reduction in porosity during pressing although neither the calcined or tabular medium showed an improvement on the traditional silicious medium. The results referring to the fine calcined powder are contrary to the expectations that it would give improved densification relative to the traditional medium since the former does not sinter under HIPping conditions. However they do confirm that coarse granules reach a maximum packing density in shorter sustain times than fine powders and thus impair densification. Further investigations are required to separate the various effects of packing density, sintering and mechanical locking on the behaviour of the refractory pressure transmitting medium under HIPping conditions. A search for an alternative pressure transmitting medium is continuing. Further work is also in progress to examine HIPping in the absence of encapsulation, which removes the need for any refractory packing and could be used for castings that contain only internal pores.

Previous work suggests that the optimum HIPping temperature for 70/30 cupronickel is 950°C (21). At higher temperatures the ductility is reduced and the grain size increased, while 850°C is the threshold temperature below which plastic flow is not produced during pressing. Consideration of the pressure applied during the processing of encapsulated castings (Figure 8), suggests that a minimum pressure somewhere between 62MPa and 83MPa would be required for HIPping at 950°C , but this would only be effective where the size of the pore is small. The optimum pressure for larger pores would be around 103MPa. For encapsulated castings the pressure involved in closing a large pore is greater than that for a small pore because a higher driving force for plastic flow is required to cause maximum densification in zero sustain time, prior to a reduction in the applied load caused by the sintering and mechanical locking of the refractory packing medium. The shape of the hole is also of importance since Figure 9 indicates that the aspect ratio of the rectangular pores used in this investigation affects the rate of densification. However, this could also be an effect of encapsulation. It should also be noted that the porosity refers to the portion in a specimen of a particular size with a single hole at its centre, so the results only give an indication of the situation likely to be found in a casting with widely distributed porosity with a range of pore sizes, shapes

and distribution.

6. CONCLUSIONS AND SUMMARY

- (1) The optimum processing conditions for the densification of 70/30 cupronickel castings containing surface connected porosity which are encapsulated prior to HIPing are short sustain times of up to 2 hours, a temperature of 950°C and argon gas pressures of 83-103MPa (12000-15000psi).
- (2) A HIP temperature of 850°C is too low to allow plastic flow to occur since the yield stress of cupronickel is not exceeded by the HIP pressure of 103MPa. When the component is encapsulated the packing media diminishes the HIP pressure transmitted to the component and no significant amount of plastic flow occurs until the HIP temperature exceeds 900°C.
- (3) For encapsulated castings successive HIP treatments of short duration combined with the re-encapsulation of the castings prior to each HIP treatment, are more effective in removing pores of greater than 10% porosity than single continuous treatments of the same total HIP time.
- (4) Encapsulated castings containing elongated pores of small diameter can be recovered in shorter HIP times than those containing large diameter squat pores of the same volume porosity. Increasing the angularity of the casting defect has negligible effect on the rate of densification during successive short treatments.
- (5) Results are consistent with the densification process during HIPing involving two stages (i) plastic flow and (ii) viscous flow (creep and diffusion). The suggested interpretation of the results is as follows. Initial densification which occurs during the heating/pressurisation stage of the HIP treatment takes place predominantly by plastic flow, and 2-3% porosity can be recovered irrespective of the starting porosity. Increasing the HIP temperature from 950°C to 1025°C increases the amount of initial densification by 3% to 8% for a pore of initially 16% porosity. The majority of pore closure occurs within a short period of time at the sustain temperature and pressure (45 minutes) after which further densification occurs at a low rate. The densification rate accelerates slightly at extended HIP times of 4 to 12 hours due to viscous flow. The fall off in the rate of densification is thought to be due to the exposure of the refractory pressure transmitting media to high temperatures and pressures causing a maximum packing density, mechanical locking and partial sintering to occur. This reduces the amount of pressure transmitted to the casting during the later stages of the HIP process and hence the rate of densification.

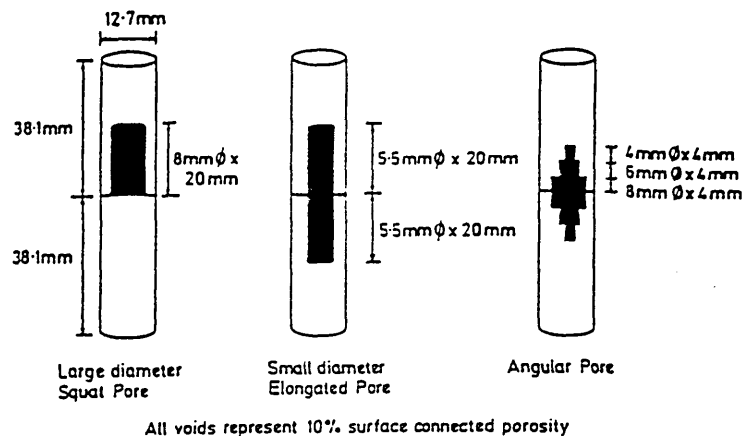
ACKNOWLEDGEMENTS

The authors wish to thank L.E.Tidbury and M.A.Cartlidge of H.I.P Limited for helpful discussions and use of the Autoclave laboratory HIP vessel. One of the authors (S.K) acknowledges the financial support of the Science and Engineering Research Council. The authors are also grateful to Professor D. Tidmarsh, Director of the School of Engineering at Sheffield City Polytechnic for the provision of research facilities.

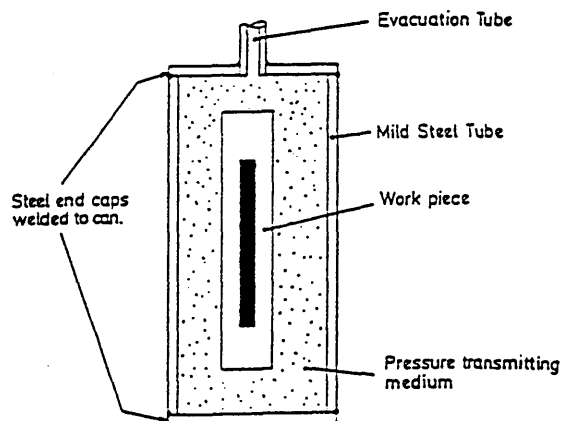
REFERENCES

- (1) Rowlands J.C., Angel B., ARE TM (UMM) 88405 March 1988*.
The Marine Corrosion Performance Of IN678 Cast High Strength Cupronickel.
- (2) Rowlands J.C., 8th Int. Conf. on Metallic Corrosion, Mainz, 6-11th September 1981.
- (3) Ansuini F.J., Badia F.A., Trans American Foundry Society Vol 78, 1970, P165.
- (4) Naval Engineering Standard, NES 824 Part 1, Issue 1.
Requirements For The Production Of High Strength Chromium Cupronickel Sand Castings And Ingots.
- (5) Person C., Ostensson M., Int Conf on HIPing of Materials, Antwerp, 25-27th April 1988, (4.13).
- (6) Strode I., Proc 3rd Int Conf on Isostatic Pressing, London, Vol 1, 1986, (37.1-37.11).
- (7) Strode I., Evans D., Proc Conf on HIPing of Materials, Antwerp 25-27th April 1988, (4.7).
- (8) Poyet P., Cercle Etude Metaux Bull., June - September 1984, (6-8), 11.1-11.4.
- (9) James P.L., Isostatic Pressing Technology (Book)1983.
Applied Science Publishers.
- (10) Wasielewski G.E., Lindblad N.R., Proc 2nd Int Conf Isostatic Pressing. AIME MCIC 72-10.
- (11) Lichtarowicz A., Scott P.J., Proc 5th Int Conf on Erosion by Solid and Liquid Impact, Cambridge, Sept 1979.
- (12) Orava R.N., Proc Corrosion/69, Houston, Texas, March 1969.
- (13) Brown T.R., AMTE (M) TM 78210*.
- (14) Galsworthy J.C., ARE TM (UMM) 88406 March 1988*.
- (15) Anderson D.B., Badia F.A., Trans ASME April 1977, P134-135.
- (16) Balakrishna Bhat, Arunachalam V.S., Conf Isostatic Pressing, 19-21 Sept 1978, Loughborough University of Technology.
- (17) Freeman W.R., Met Progress 1977, 112, 32.
- (18) Swinkels F.B., Ashby M.F., Acta Metallurgy 28, 259, 1981.
- (19) Coble R.L., Journal of Applied Physics 1970, 41, 4789.
- (20) Wilkinson D.S., Ashby M.F., Acta Met 1975, 23, 1277.
- (21) King S., Walker R., Foundry Trade Journal Vol 163, P97, 1989.

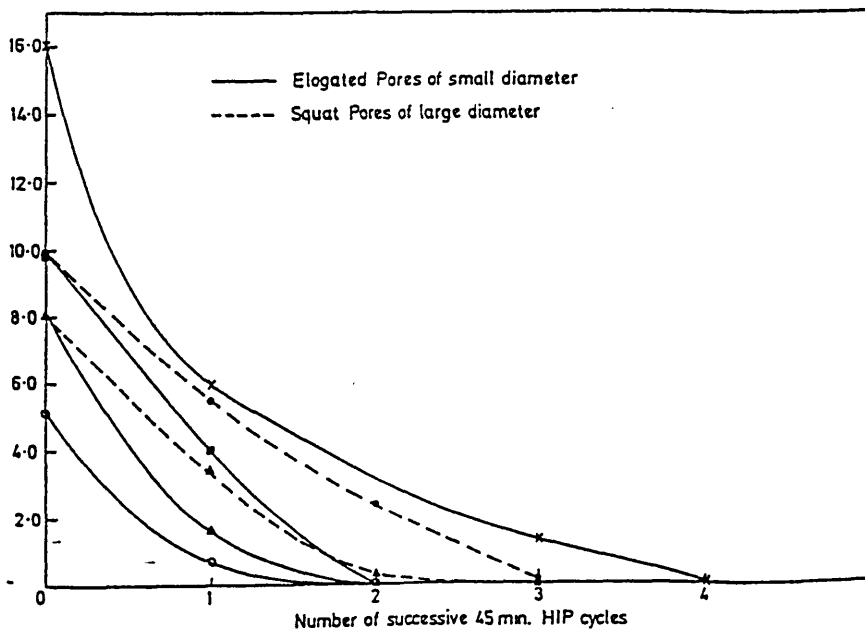
* Available from HMSO.



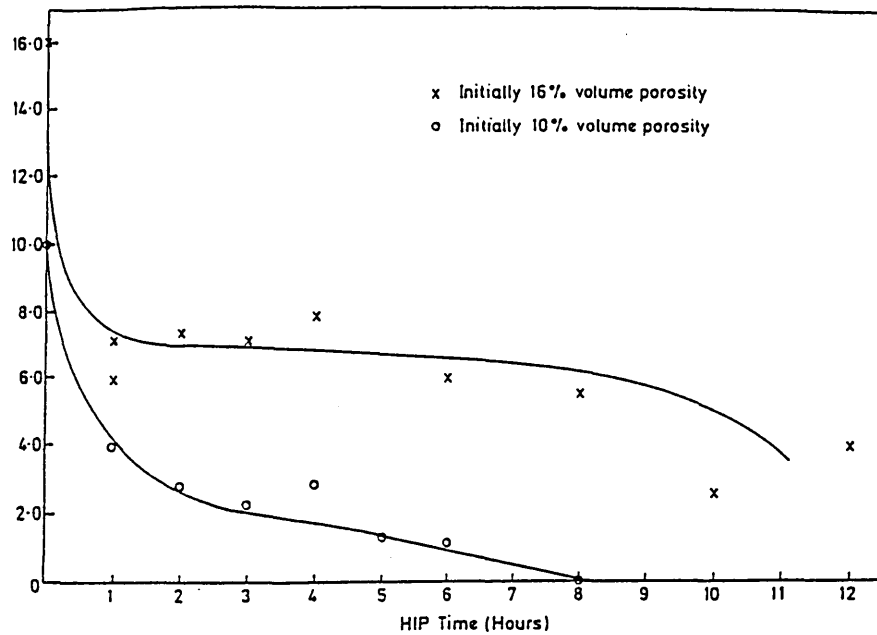
(1) Pore Geometry Of Artificial Porosity Specimens



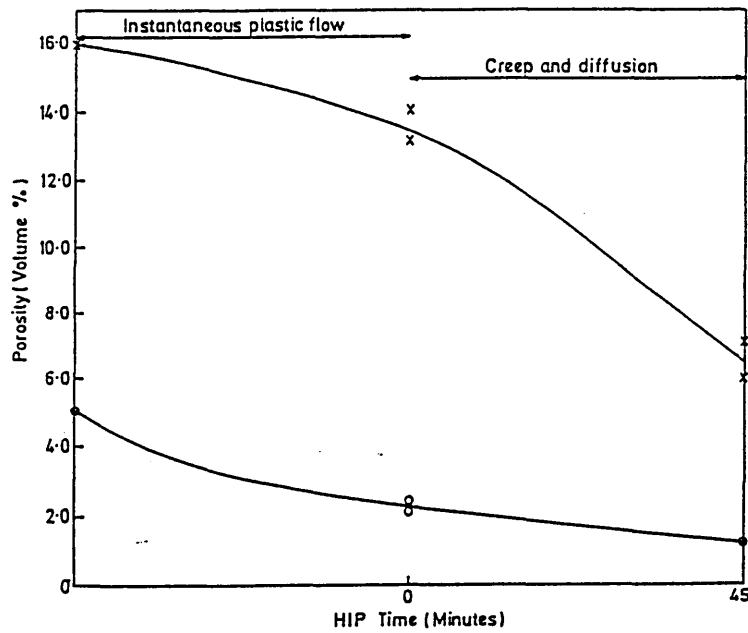
(2) Encapsulation Techniques For Castings Containing Surface Connected Porosity



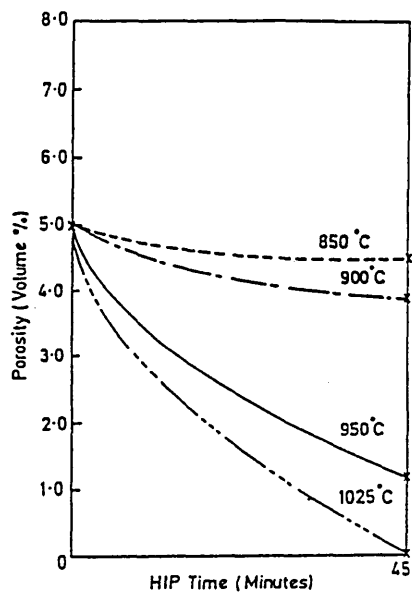
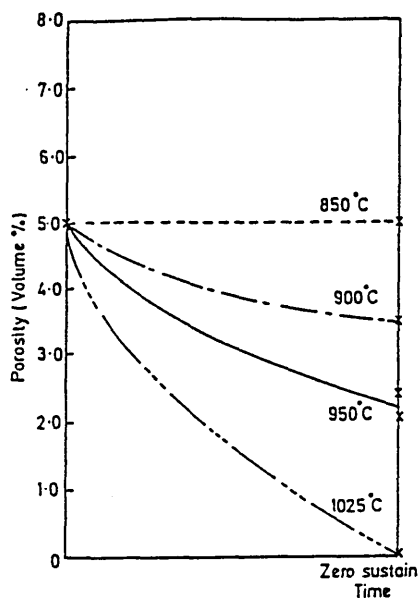
(3) Effect Of 45 Minute Successive HIP Cycles On Densification



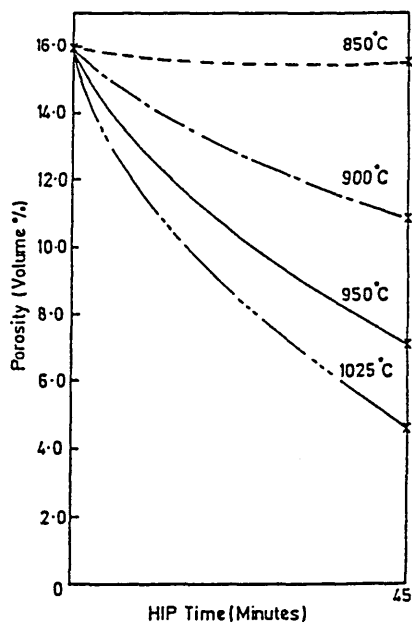
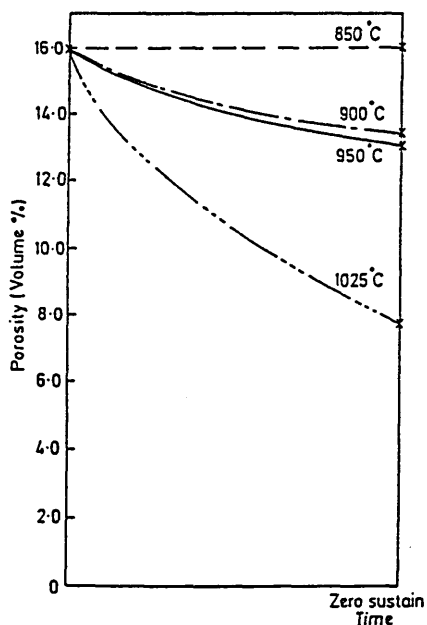
(4) Effect Of Continuous HIP Time On The Closure Of Elongated Pores



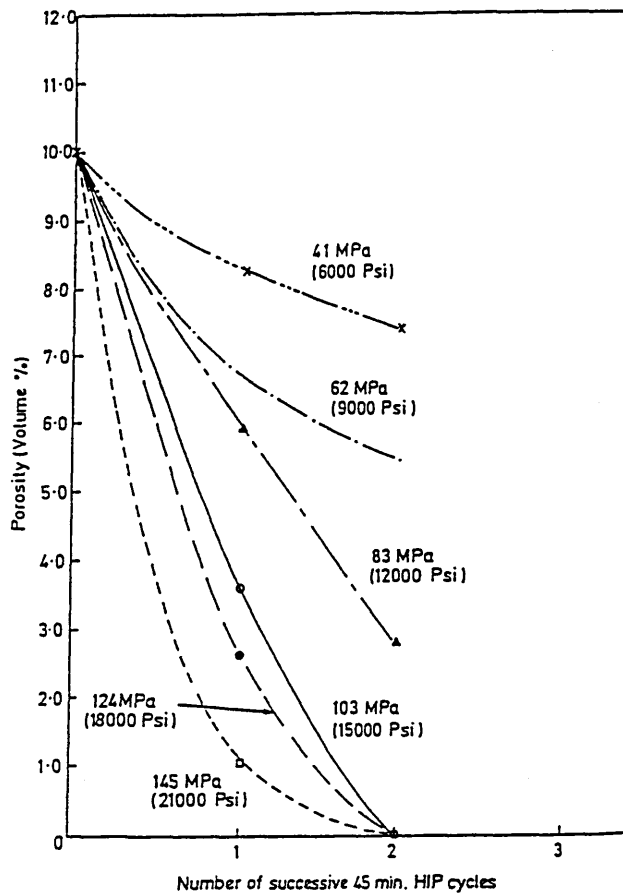
(5) Effect Of HIP Time On Recovery Rate And Densification Mechanisms



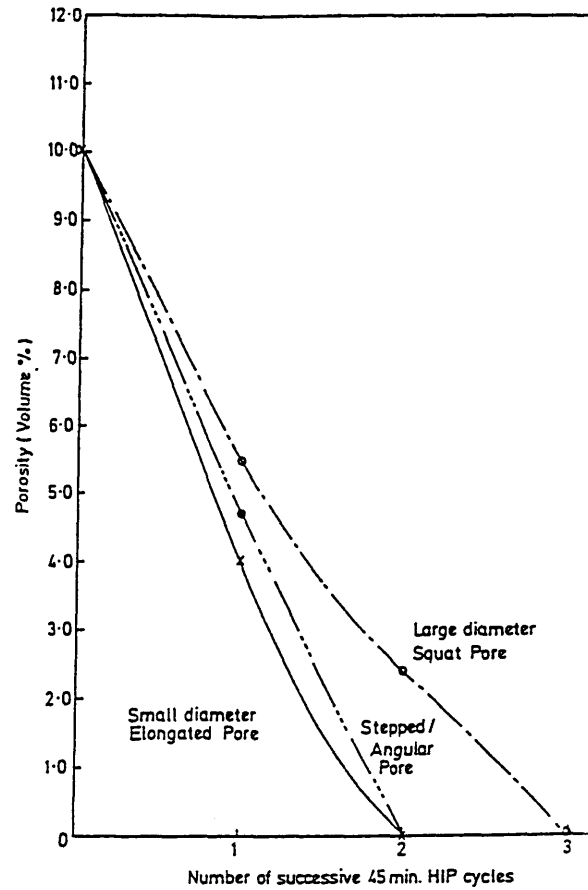
(6) Effect Of HIP Temperature On Pore Closure (5% Porosity)



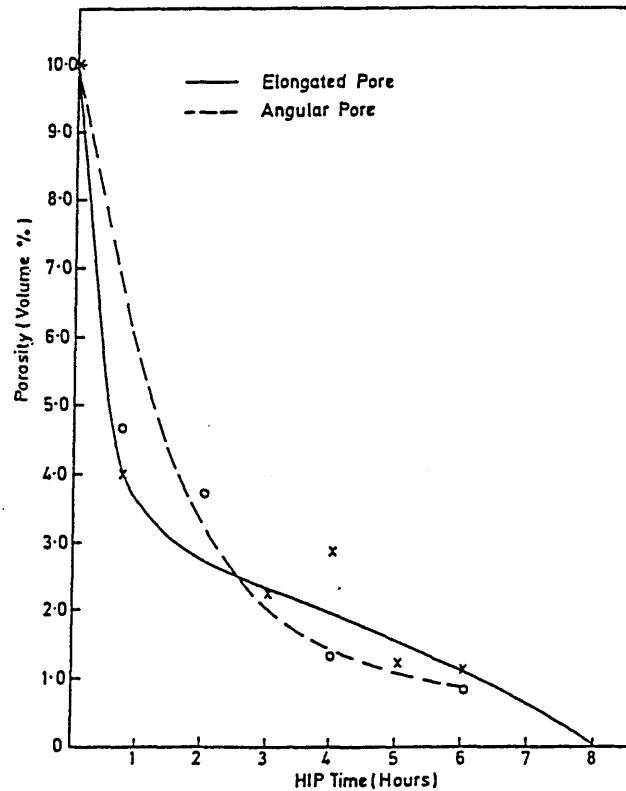
(7) Effect Of HIP Temperature On Pore Closure (16% Porosity)



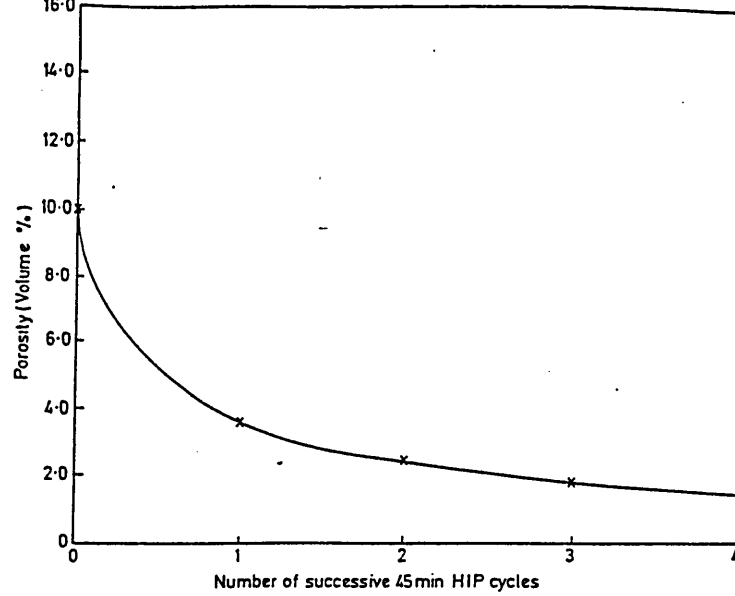
(8) Effect Of HIP Pressure On Pore Closure



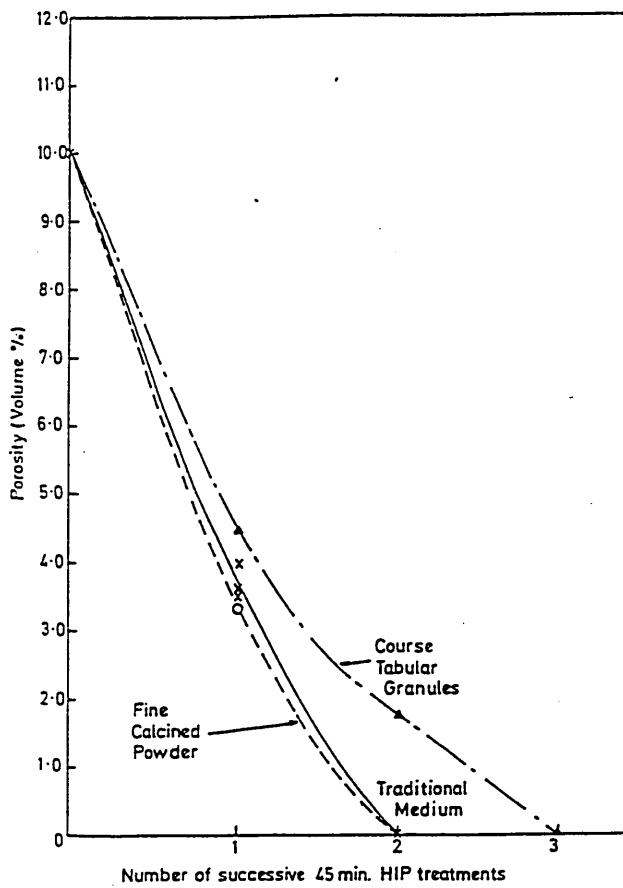
(9) Effect Of Pore Geometry On Densification Via Successive Short HIP Cycles



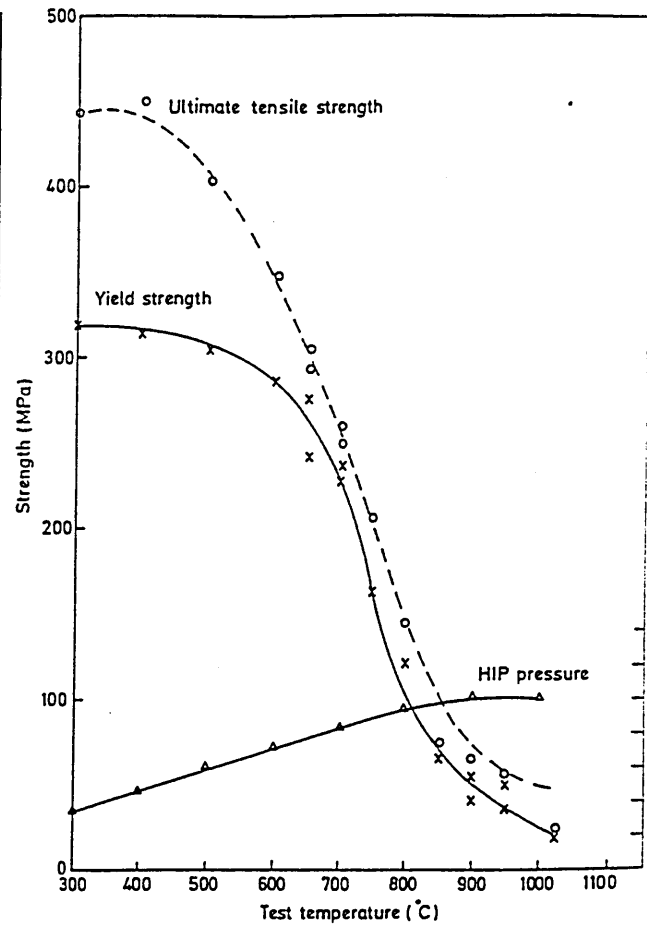
(10) Effect Of Pore Angularity On Densification Via Continuous HIP Cycles



(11) Effect Of Encapsulation On Pore Closure



(12) Effect Of Pressure Transmitting Media On Pore Closure



(13) Hot Strength Of 70/30 Cupronickel

The effect of HIP on cast cupro-nickel alloys

☐ Cupro-nickel castings frequently contain a degree of porosity which may be unacceptable for critical marine applications. Corrosion studies have shown that the technique of weld repair on surfaces in contact with salt water is unacceptable and therefore alternative procedures are being sought to provide defect free castings. Hot Isostatic Pressing (HIP) has been used successfully to reduce the level of porosity in cupro-nickel castings, but there is relatively little information about the mechanism by which defects are removed, or the effect of HIP on the mechanical and metallurgical characteristics of such cast cupro-nickel material. Furthermore, the optimum conditions under which HIP should be carried out are not well established.

Test procedures

As part of this work, a number of interesting observations have been made on the effects of HIP on the metallurgical properties and microstructure of cupro-nickel castings.

Cast test bars of a 70/30 (Cu/Ni) cupro-nickel alloy produced in accordance with current Navy specification (NES 824), were encapsulated and HIPped. The process parameters included argon gas pressures of 103 mPa (15,000psi) sustained for a period of three hours at one of the following temperatures: 850°C, 950°C and 1,025°C.

From previous experience with other copper based alloys, encapsulation (ie, forming a gas tight membrane around the component) has been found to be essential in ensuring that sub-surface porosity connected to the surface by fine passageways is removed.

Mechanical property and microstructural testing indicated a number of interesting features which are considered to be representative of other material cast to more complex shapes.

Mechanical properties

HIPping at 850°C, 950°C or 1,025°C had no detrimental effect on the as-cast properties of the cupro-nickel test bars, since the overall proof stress and tensile strength of the material remained relatively unchanged. However, the ductility of the material significantly improved and all properties were well in excess of the specified requirements. As the temperature at which HIP was conducted was increased, increases in proof and ultimate tensile strength were apparent.

However, this increase in strength was accompanied by a decrease in ductility. The results from the mechanical property evaluation of the cupro-nickel test bars are shown in figs 1-3.

The authors are Susan King, research student Sheffield City Polytechnic and R M Walker, Senior Project Engineer HIP Limited, Chesterfield.

An ongoing investigation into the HIPping of cupro-nickel castings is increasing the understanding of the mechanisms of HIP, and aims to forecast those optimum processing conditions required to remove porosity and achieve desirable microstructures and mechanical properties.

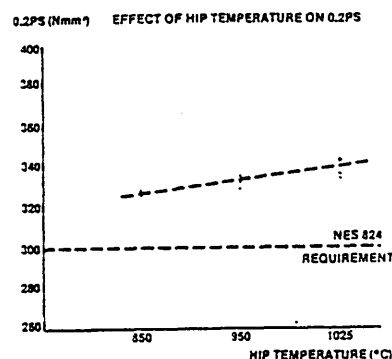


Fig 1. Effect of HIP temperature on 0.2PS.

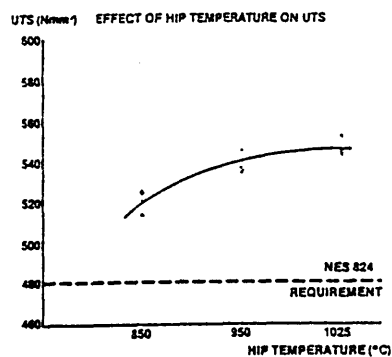


Fig 2. Effect of HIP temperature on UTS.

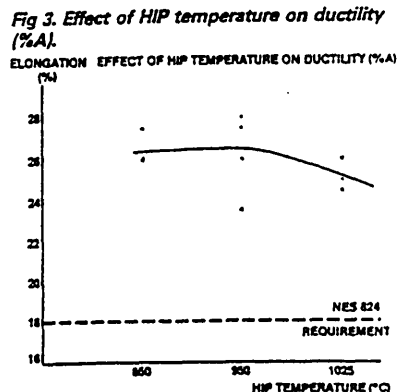


Fig 3. Effect of HIP temperature on ductility (%A).

Metallurgical examination

Optical examination of specimens polished and etched in 10% alcoholic ferric chloride, representing material from test bars HIPped at 850°C, 950°C and 1,025°C, revealed that the grain size of the cast cupro-nickel increased as the HIP temperature increased.

Such an observation would be consistent with expectation, although a quantitative measurement of grain size was not possible. The appearance of a section at low magnification was misleading since examining single grains at higher magnifications revealed an accumulation of smaller sub-grains. Only a qualitative comparison of the change in grain size with increasing HIP temperature can therefore be made, as shown in figs 4 and 5. These results suggest that cast cupro-nickel becomes increasingly homogenised as the HIP temperature increases, ie coring is less extensive.

Fig 4. Effect of HIP temperature on grain size. A = 850°C, B = 950°C, C = 1,025°C. Mag $\times 6$.



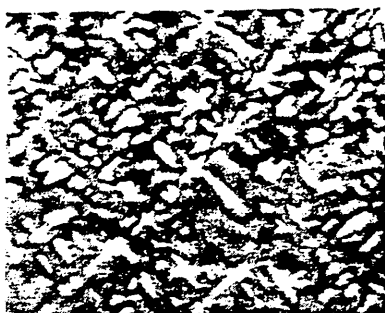
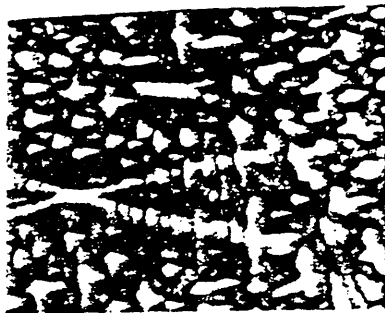


Fig 5. Effect of HIP temperature on microstructure. A = 850°C, B = 950°C, C = 1,025°C. Mag × 50.

Examination using scanning electron microscopy (SEM)

Examination of the tensile fracture surfaces using SEM revealed, for all three HIP temperatures, a ductile matrix containing large, randomly distributed matrix oxides, and small evenly distributed zirconia-based particles. The latter were found in the bottom of the ductile dimples. This observation would suggest that the presence of the

zirconia-based particles may have initiated tensile failure. A typical example of the fracture surface from a test bar HIPped at 850°C is shown in fig 6. The matrix oxides and zirconia-based particles are more clearly identified at higher magnifications as shown in figs 7 and 8 respectively.

Identification of the particles was carried out using EDAX analysis, and fig 9 shows a back scattered electron image where the zirconia-based particles can clearly be distinguished from the matrix material. The analysis of these particles shown in fig 10 indicates an element peak intensity curve appropriate to zirconium and oxygen.

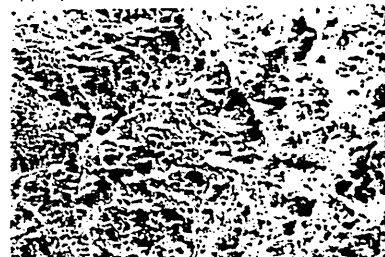


Fig 6. Typical fracture appearance of a test bar HIPped at 850°C. Mag × 60.

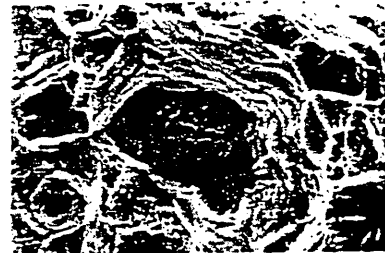


Fig 7. Large, randomly distributed matrix oxides. Mag × 450.

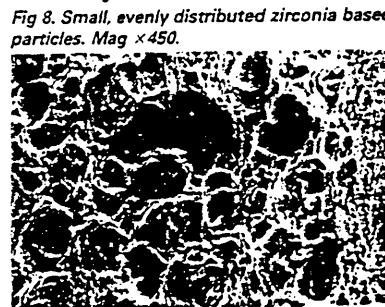
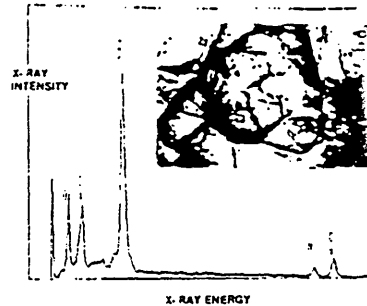


Fig 8. Small, evenly distributed zirconia based particles. Mag × 450.



Figs 9 and 10. Edax analysis of zirconia based particles (peak intensity curve), back scattered electron image of Zirconia based particles found in the matrix mag × 500.

Summary

The practice of encapsulation and Hot Isostatic Pressing (HIP) provides an effective route by which porosity within cast cupro-nickel sections can be removed. With such treatment, defects may be removed from within the body of the casting even when connected to a free surface.

The mechanical properties of cast cupro-nickel material exposed to HIP are not markedly changed. However, an increase in UTS and proof strength with increasing HIP temperature was observed. Grain size and segregation effects are also modified by HIP treatment and these effects are consistent with those expected for such an alloy. Opportunities, therefore, exist in the use of optimised HIP practice to remove casting defects without recourse to weld recovery.

Work is continuing to assess the effect of HIP treatment on impact, fatigue and corrosion behaviour of such materials.

Acknowledgements

All materials used for HIP trials were kindly supplied by Vickers Shipbuilding and Engineering Limited (VSEL), Barrow-in-Furness. The authors would like to thank Infutec Limited for providing the encapsulation samples.

For further information please contact Mr R M Walker or Dr A J Hartley at HIP/INFUTECH Limited, Carlisle Close, Sheffield Rd, Sheepbridge, Chesterfield S41 9ED. Tel: 0246 260999, Fax: 0246 260889, Tx: 574441.



Ministry of Defence
Sea Systems Controllerate

Naval Engineering Standard

NES 824 Part 1 Issue 2 May 1989

COPPER NICKEL CHROMIUM SAND CASTINGS
AND INGOTS

PART 1

PRODUCTION REQUIREMENTS

Defects

1301. Any casting may be rejected for defects when discovered during subsequent machining notwithstanding that the casting had been passed previously as conforming to this NES.

Rectification of Defects

1302. All proposals for weld repair are to be submitted to the contract sponsor for approval.
1303. Prior to any welding being undertaken to rectify casting defects it is mandatory that.
- a. Approved welding procedures in accordance with NES 825 are available.
 - and b. Weldability tests in accordance with Clause 1104-8 and Clause 1203 have been completed and results satisfactory.
1304. The rectification of surface defects by welding is not permitted on any sea water wetted surface.
1305. Weld repair of surface (non-wetted area) and sub-surface defects will only be considered on a concession basis. If approved on a concession, weld repair of sub-surface defects may only be rectified when, after removal of the defect, excavation does not penetrate to within 10 mm of the wetted surface.
1306. All permitted weld repairs are to be carried out in accordance with NES 825.
1307. Weld fabrication or cosmetic repair of Copper Nickel Chromium Castings is not permitted.
1308. All welding is to be undertaken using qualified procedures and welders.
1309. After all weld repairs have been completed the casting is to be re-heat treated in accordance with Clause 0502.
1310. After heat treatment the casting must be Dye-Penetrant tested, Clause 1113, and the welded areas must be re-radiographed, Clause 1114. The requirements of Section 12 must be met.
1311. Unacceptable surface defects may be blended out by an approved process providing the resultant depression does not reduce the designed wall thickness by more than 6mm or 10% whichever is the less. The depression is to be faired out with a minimum radius equal to three times the maximum depth. The remaining wall thickness in way of the depression is to be free from sub surface defects in Critical Test Regions and Test Regions (see Section 8 for definitions). The total area subjected to blending, including the area affected by the fairing is not to exceed 10% of the Critical Test Region or 20% of the Test Region in which the defect is situated.

1312. All proposals for repair by hotisostatic pressing (HIP) are to be submitted to the contract sponsor for approval.
1313. Repair of sub-surface and surface breaking defects by HIP may be considered on a concession basis. If approved by concession, HIP may be permitted for removal of areas of sponge type porosity up to a total of 15% of total casting volume. It may also be permitted for removal of individual voids with maximum dimensions no greater than 9 mm in any direction and orientated such that the defect does not reduce any wall thickness more than 5%.
1314. All HIP repairs must be to an approved HIP procedure, agreed by NA132, to ensure adequate process control. Process control conditions are to be within the following parameters:
- Temperature $960 + 15^{\circ}\text{C}$
 $- 10^{\circ}\text{C}$
- Pressure $103 \pm 10 \text{ MPa}$
- Sustain Time - Up to 240 minutes (dependent on size of component)
- Post HIP Cooling Rate = Less than $10^{\circ}\text{C}/\text{minute}$ (natural cooldown).
1315. All repairs are to be by the encapsulated HIP process utilizing a close fitting, gas tight container filled with ceramic grain to act as a pressure transmitting medium unless otherwise agreed by NA132.
1316. Following encapsulated HIP treatment, castings are to be shot blasted to remove residual pressure transmitting media, prior to inspection.
1317. Prior to further processing and X-ray inspection, castings are to be subjected to dye penetrant and dimensional inspection.

NOTE Closure of very large voids, where massive material movement takes place, may be accompanied by local microstructural changes. Such large metal movements may result in local thinning of cast sections. Closure of near surface porosity may result in surface depressions.